



**BINDING SERVICES**  
Tel +44 (0)29 2087 4949  
Fax +44 (0)29 20371921  
e-mail [bindery@cardiff.ac.uk](mailto:bindery@cardiff.ac.uk)



Declaration

CARDIFF  
UNIVERSITY

PRIFYSGOL  
CAERDYDD

This work has not previously been submitted for any degree and is not being concurrently submitted elsewhere.

Signed: *Richard Lilly* (candidate)

Date: *13<sup>th</sup> Sept 2006*

**The Magmatic Evolution and Crustal Accretion  
of the Northern  
Oman–United Arab Emirates Ophiolite**

This thesis is the result of my own investigations, except where otherwise stated. Other sources are acknowledged by footnotes giving explicit references. A bibliography is appended.

**Richard Mark Lilly**

Signed: *Richard Lilly* (candidate)

Date: *13<sup>th</sup> Sept 2006*

Statement 2

Submitted in partial fulfilment of the requirements for the  
degree of Ph.D.

Cardiff University

Signed: *Richard Lilly* (candidate)

Date: *13<sup>th</sup> Sept* May 2006

UMI Number: U584812

All rights reserved

INFORMATION TO ALL USERS

The quality of this reproduction is dependent upon the quality of the copy submitted.

In the unlikely event that the author did not send a complete manuscript and there are missing pages, these will be noted. Also, if material had to be removed, a note will indicate the deletion.



UMI U584812

Published by ProQuest LLC 2013. Copyright in the Dissertation held by the Author.  
Microform Edition © ProQuest LLC.

All rights reserved. This work is protected against  
unauthorized copying under Title 17, United States Code.



ProQuest LLC  
789 East Eisenhower Parkway  
P.O. Box 1346  
Ann Arbor, MI 48106-1346

## Declaration

This work has not previously been accepted in substance for any degree and is not being concurrently submitted in candidature for any degree.

Signed.....*Richard Lilly*.....(candidate)

Date.....*13<sup>th</sup> Sept 2006*.....

## Statement 1

This thesis is the result of my own investigations, except where otherwise stated. Other sources are acknowledged by footnotes giving explicit references. A bibliography is appended.

Signed.....*Richard Lilly*.....(candidate)

Date.....*13<sup>th</sup> Sept 2006*.....

## Statement 2

I hereby give consent for my thesis, if accepted, to be available for photocopying and for inter-library loan, and for the title and summary to be made available to outside organisations

Signed.....*Richard Lilly*.....(candidate)

Date.....*13<sup>th</sup> Sept 2006*.....

# **Abstract**

## **The Magmatic Evolution and Crustal Accretion of the northern Oman–U.A.E. ophiolite**

The Oman - United Arab Emirates (U.A.E.) ophiolite is the largest and best-preserved ophiolite complex in the world and has assumed critical importance in guiding ideas as to the functioning of mid-ocean ridge magma chambers and accretion of lower crust formed at a fast-spreading ridge. The portion of the ophiolite within the United Arab Emirates has received much less study than that within the Sultanate of Oman, particularly with regard to its magmatic evolution. Fieldwork has been conducted in co-operation with the British Geological Survey on the ophiolite sections in the U.A.E. Geochemical and field characteristics of these plutonic and extrusive units provide important constraints on the influence subduction-related fluids have on crustal accretion processes.

Initial V1 magmatic events exhibit a MORB-like composition and record mid-ocean ridge accretion processes which relate to modern crust, forming from steady-state magma chambers. The Khawr Fakkan Block provides the first 'true' MORB mantle source signature to be documented in the Oman-U.A.E. ophiolite, which represents pre-subduction zone influenced oceanic crust and applies constraints to the mechanisms and timing of subduction initiation and propagation.

These primary events were followed by V2 magmatic events in a supra subduction zone (SSZ) setting, with plutonic magmatism localised predominantly along major faults. Each subsequent magmatic event exhibits an increase in the subduction related component to the mantle source. The V2, SSZ, magmatic period of the northern Oman-U.A.E. ophiolite can be regarded as an embryonic volcanic arc, which ceased magmatism and was obducted before reaching maturity.

The northern Oman-U.A.E. ophiolite records the transition from spreading- to subduction-related volcanism in a SSZ setting within a marginal (fore-arc) basin, representing the change from steady-state to plutonic magmatism. The SSZ signature increases to the north spatially and temporally.

## Acknowledgements

Firstly, thanks must go to Julian Pearce and Chris MacLeod for their hard work to get this project off the ground in the first place and for their occasional supervision. The project has benefited a great deal from the cooperation with the British Geological Survey both in the field and during the follow-up work. I would like to express my thanks to the mapping project leader Mike Styles for his assistance and input throughout and to all the BGS team members I have worked with and learnt from. Special thanks must also go to Bob Thomas for being such an inspiring and capable geologist, Emrys Philips for his thought-provoking scientific input (and legendary cooking skills) and Kathryn Goodenough for our never-ending discussions about gabbros.

This project has relied heavily on the analytical facilities at Cardiff University and indebted thanks go to Iain McDonald for his unfailing determination to get good results out of machines that often seem equally resolute not to produce them. I would also like to thank Eveline DeVos, Pete Fisher and the rest of the technical staff for their assistance.

I would like to thank office mates past and present for their company and friendships. Special thanks must go to Graham Banks and Shaun Lavis for their patience, guidance and invaluable support throughout this project. Cheers also go to Dave Holwell and Alan Hastie for the excellent banter, which has helped to keep me sane. Thanks also to Vicky Peck and Mairi Nelson for putting up with so many of my rants when it was hard to see the wood for the trees. I would like to thank the other members of Prisoners of the Sun; Richard Wild, David Letellier and Samuel Bigot for putting up with a stressed drummer over the last six months. I would also like to thank everyone who I have worked with at Cardiff University who helped make my time here so enjoyable, including the ground staff who keep Alexandria Gardens Park in such nice bloom.

Finally, a heartfelt thank you to Cathy Lilly, my wonderful wife and best friend, for always having confidence in me and for helping in every way you could throughout my return to university. I could not have done this without your unwavering support.

**For Cathy and Matthew**



# List of Contents

## Chapter 1: The Oman-United Arab Emirates Ophiolite

1.1	Introduction	1
1.2	General aims and content of the thesis	2
1.3	The regional setting of the Oman-U.A.E. ophiolite	4
1.4	History of geological investigation	6
1.5	The internal stratigraphy of the Oman-U.A.E. ophiolite	7
1.5.1	The allochthonous units and metamorphic sole	7
1.5.2	The Mantle Sequence	9
1.5.3	The Moho Transition Zone (MTZ)	10
1.5.2	Wehrlites	12
	1.5.5.1 The Crustal gabbro sequence and magma chamber models	13
	1.5.5.2 Upper Gabbros	14
	1.5.5.3 Late Intrusive Gabbros	17
1.5.6	Sheeted Dyke Complex (SDC)	18
1.5.7	Extrusive Sequence	19

## Chapter 2: Geology of the Ophiolite Blocks in the United Arab Emirates

2.1	Introduction	25
2.2	The Geology of the Khawr Fakkan Block	30
2.2.1	The Mantle Section	30
2.2.2	Moho Transition Zone (MTZ)	31

2.2.3	Layered Gabbros	33
2.2.4	Upper Gabbro	34
2.2.5	Late Intrusive Gabbro Units	36
2.2.6	Sheeted Dyke Complex (SDC)	36
2.2.7	Upper Crustal Dykes	37
	2.2.7.1 Early Dykes	37
	2.2.7.2 Common Dykes	39
	2.2.7.3 Irregular Dykes	39
	2.2.7.4 Clinopyroxene-phyric Dykes	40
	2.2.7.5 Late Dykes	40
2.3	Conclusions from the geology of the Khawr Fakkan Block	41
2.4	The Geology of the Aswad Block	42
2.4.1	The Mantle Section	42
2.4.2	Moho Transition Zone (MTZ)	43
2.4.3	Layered Gabbros	43
2.4.4	Kalba Upper Gabbro	44
2.4.5	Sheeted Dyke Complex (SDC)	47
2.4.6	The Extrusive Sequence	50
2.4.7	Intermediate Dykes	52
2.4.8	Wadi Mai Dykes	52
2.4.9	Late Intrusive Gabbro Units	53
	2.4.9.1 Bithna Gabbro	54
	2.4.9.2 Fujairah Gabbro	55
2.4.10	Late Dyke	58
2.5	Conclusions from the geology of the Aswad Block	58
2.6	Summary and comparisons between U.A.E. Blocks	59

## **Chapter 3: Geochemistry of the Dykes and Extrusive Section of the Khawr Fakkan and Aswad Blocks**

3.1	Introduction	61
3.1.1	Major element mobility	62
3.1.2	Trace element mobility	64
3.2	Geochemistry of the Khawr Fakkan Block dykes and extrusives	66
3.2.1	Major elements	66
3.2.2	Rare Earth Element (REE) profiles	69
3.2.3	N-MORB normalised multi-element patterns	71
3.2.4	Trace element discrimination diagrams	74
3.2.5	Conclusions from Khawr Fakkan Block	82
3.3	Geochemistry of the Aswad Block dykes and extrusives	84
3.3.1	Major elements	84
3.3.2	Rare Earth Element (REE) profiles	87
3.3.3	N-MORB normalised multi-element patterns	89
3.3.4	Trace element discrimination diagrams	92
3.3.5	Conclusions from Aswad Block	99
3.4	Comparison between ophiolite blocks	101
3.4.1	Trace element ratio plots	101
3.4.2	Conclusions from comparison between ophiolite blocks	108

## **Chapter 4: LA-ICP-MS Study of Clinopyroxenes from the Plutonic Section**

4.1	Introduction	109
-----	--------------	-----

4.2	Introduction to clinopyroxenes	110
4.3	Clinopyroxene trace element characteristics	110
4.4	Analytical techniques	112
4.5	Clinopyroxene trace element geochemistry of the Khawr Fakkan Block plutonic series	114
4.5.1	Khawr Fakkan Block field observations	114
4.5.2	Chondrite-normalised multi-element patterns	117
4.5.3	Comparison between relative abundances of REE	119
4.5.4	Trace element characteristics	122
4.5.5	Conclusions from Khawr Fakkan Block gabbro clinopyroxene trace element characteristics	127
4.6	Clinopyroxene trace element geochemistry of the Aswad Block plutonic series	128
4.6.1	Aswad Block field observations	128
4.6.2	Chondrite-normalised multi-element patterns	133
4.6.3	Comparison between relative abundances of REE	135
4.6.4	Trace element characteristics	139
4.6.5	Conclusions from Aswad Block gabbro clinopyroxene trace element characteristics	147

## **Chapter 5: Geochemical Modelling of Clinopyroxenes from the Plutonic Section**

5.1	Introduction	149
5.2	Bulk Partition Coefficients	150

5.3	Petrogenetic modelling of clinopyroxenes from the Khawr Fakkan Block crustal gabbro sequence	153
5.3.1	Chondrite-normalised multi-element patterns	154
5.3.2	Comparison between element ratios	159
5.3.3	Conclusions from petrogenetic modelling of clinopyroxenes from the Khawr Fakkan Block crustal gabbro sequence.	162
5.4	Petrogenetic modelling of clinopyroxenes from the Aswad Block crustal gabbro sequence	163
5.4.1	Chondrite-normalised multi-element patterns	165
5.4.2	Petrogenetic modelling of clinopyroxenes from the Aswad Block crustal gabbro sequence	170
5.4.3	Conclusions from petrogenetic modelling of clinopyroxenes from the Aswad Block crustal gabbro sequence	173

## **Chapter 6: Conclusions and Discussion:**

### **The Magmatic Evolution and Crustal Accretion of the Northern Oman-United Arab Emirates Ophiolite**

6.1	Introduction	175
6.2	The crustal accretion history of the Khawr Fakkan Block	177
6.3	The crustal accretion history of the Aswad Block	184
6.4	The magmatic evolution of the northern Oman-U.A.E. ophiolite	193
6.5	The regional palaeotectonic setting of the Oman-U.A.E. Ophiolite	198
6.6	Concluding statements	201

## **Appendix A: Sample preparation for ICP-OES (whole rock major and minor elements) analysis**

A1.1	Preparation of sample powders	<i>i</i>
A1.2	Loss on Ignition (LOI) analysis	<i>i</i>
A2.1	Sample preparation for ICP-OES analysis	<i>i</i>
A2.2	Inductively-Coupled Plasma Optical Emission Spectrometry (ICP-OES)	<i>ii</i>
A3	Calibration and data quality	<i>ii</i>
A4	Use of major element abundances for geochemical discrimination of plutonic gabbros	<i>iii</i>

## **Appendix B: Sample preparation for ICP-MS (trace element) analysis**

B1.1	Sample preparation for ICP-MS analysis	<i>i</i>
B1.2	Calibration and analysis	<i>ii</i>
B1.3	Drift correction	<i>iii</i>
B1.4	Data quality assessment	<i>iii</i>
B2	Alteration related element mobilisation within the Sheeted Dyke Complex (SDC)	<i>v</i>

### **Whole-rock major (ICP-OES) and trace (ICP-MS) element data tables**

## **Appendix C: Data sources for geochemical field generation**

C1	PETDB data sources (MORB, IAT, Boninites, BAB)
----	--

## **Appendix D: Analytical method for LA-ICP-MS analysis**

D1.1	Introduction	<i>i</i>
D1.2	Instrument parameters	<i>i</i>
D1.3	External standards	<i>ii</i>
D1.4	Initial experiments	<i>iii</i>
D1.5	The matrix effect	<i>v</i>
D1.6	CaO correction factor	<i>vi</i>
D2	Ablation Problems: Burn-through	<i>ix</i>
	Ejecta Contamination	<i>x</i>
	Cleavage spalling	<i>xi</i>
D3	Results from Initial experiments	<i>xiii</i>

### **Clinopyroxene major (SEM-EDS) and trace (LA-ICP-MS) element data tables**

## **Appendix E: Partition Coefficient modelling**

E1	Partition coefficient theory	<i>i</i>
E2	Partition coefficient calculation	<i>iii</i>
E3	Calculated partition coefficients	<i>v</i>

### **Calculated partition coefficients (per crystal) tables**

## **References**

# Chapter 1: The Oman-United Arab Emirates

## Ophiolite

### 1.1 Introduction

The Cretaceous Oman-United Arab Emirates (U.A.E.) ophiolite is the largest and best preserved ophiolite complex in the world. Ophiolites are fragments of oceanic lithosphere that have been emplaced on continental crust (Penrose, 1972). The Oman-U.A.E. ophiolite has dimensions of over 600 km in length, up to 150 km in width, between 5 and 10 km in thickness and crops out over an area of around 20,000 km<sup>2</sup> (Lippard et al., 1986). The ophiolite forms rugged mountains with an average elevation of between 500-1500m and a deeply incised relief. The region has a dry desert climate offering little or no vegetation cover and the mountains are frequently cut by antecedent and fault-controlled wadis which provide some of the best sections through the ophiolite sequence. The low degree of emplacement-related deformation and outstanding exposure provides an excellent opportunity to study oceanic lithosphere; consequently the Oman-U.A.E. ophiolite has assumed critical importance in guiding ideas on the functioning of modern oceanic spreading centres.

The tectonic setting of formation of the ophiolite has been a topic of debate since the initial geochemical fingerprinting of the extrusive sequence indicated that their compositions are not everywhere the same as typical mid-ocean ridge basalts (MORB). Pioneering studies, concentrating on the southern Oman portion of the ophiolite, (e.g. Reinhardt, 1969; Glennie et al., 1974) concluded that the ophiolite was formed at a 'normal' mid-ocean ridge. However, geochemical work from more northerly parts of the ophiolite concluded that the ophiolite complex represents not just oceanic crust and mantle, but the intrusive and extrusive products of subsequent arc magmatism, and that at least part of the ophiolite might have formed in a marginal basin above a subduction zone (e.g. Pearce, 1981; Alabaster et al., 1982).



The debate over the tectonic setting of the ophiolite has continued throughout the last 20 years. While early studies relied on the geochemistry of the extrusive sequence for tectonic indicators, modern studies are able to draw on advances in analytical techniques, such as laser ablation (LA-ICP-MS), to analyse compositions of individual mineral phases within the plutonic sequence. Such research can hopefully match individual gabbro units to their extrusive products, providing direct constraints on the timing and associated geological activity during individual magmatic events. With such techniques it is possible to build up a very detailed understanding of the evolution of the crust and the tectonic environment in which it formed.

## **1.2 General aims and content of the thesis**

The aim of this study is to investigate the mid-ocean ridge vs. supra-subduction zone (SSZ) tectonic setting debate by studying magma genesis and crustal accretion processes in the northernmost portion of the ophiolite, which lies within the U.A.E. This area contains the Khawr Fakkan and Aswad Blocks of the ophiolite (Figure 1.2) and has received considerably less study than that within the Sultanate of Oman particularly with regard to its magmatic evolution.

This study will use field evidence and geochemical data to offer direct constraints on the tectonic setting and processes that led to the generation of the (fast-spreading) oceanic crust in the northern Oman-U.A.E. ophiolite, and our understanding of the magmatic evolution of the ophiolite as a whole.

Extensive fieldwork and sample collection was conducted by the author at all stratigraphic levels of the ophiolite within the U.A.E.; from the mantle section to the extrusive basalts. This was completed with the aim of gathering the most complete sample base from which to identify all possible periods of magmatism recorded within the northern blocks of the Oman-U.A.E ophiolite.

This thesis comprises six chapters.

- Chapter one. The geology and setting of the Oman-U.A.E. ophiolite, including the rationale of the project, and an introduction to ophiolite theory
- Chapter two. The geology of the Khawr Fakkan and Aswad Blocks, field observations and general geology of the field areas for this study are described. Multiple magmatic events were identified and constraints have been established for the evolution of the crust and its tectonic setting
- Chapter three. The geochemistry of the extrusive sequence and dykes. ICP-MS analyses were conducted on 100+ samples with the objective to constrain the geochemical characteristics of the major phases of magmatism identified by fieldwork. The two U.A.E. tectonic blocks are interpreted separately to ascertain any differences in the evolution of the mantle source for each block. Once the geochemistry of each magmatic phase has been established, constraints can be placed on the tectonic setting and comparisons can be made between the magmatic histories of each block and the rest of the ophiolite.
- Chapter four. The LA-ICP-MS analysis of clinopyroxene from the plutonic section. This chapter presents the results of a new technique to analyse clinopyroxene mineral chemistry from the plutonic section and aims to describe the variations in the geochemistry of the plutonic section and the probable physio-chemical conditions under which the plutonics were accreted.
- Chapter five. The objective of this chapter is to geochemically match the plutonic rocks described in Chapter four to their extrusive equivalents discriminated in Chapter three through the use of partition coefficient modelling.
- Chapter six. A synthesis and presentation of a preferred model for the crustal accretion and magmatic evolution of the Khawr Fakkan and Aswad Blocks. Comparison will also be made with the rest of the Oman-U.A.E. ophiolite and the implications for its palaeotectonic setting during the Cretaceous.

### 1.3 The regional setting of the Oman-U.A.E. ophiolite

The Oman-U.A.E. ophiolite is the largest and least deformed member of a long, discontinuous, chain of over 30 late Jurassic to late Cretaceous ophiolites of varying chemistry and structure that crop out from the western Mediterranean to the Himalayas (Figure 1.1). Many of the ophiolites have been highly altered by emplacement-related deformation and have therefore lost much of their important structural and geochemical information to overprinting (Lippard et al., 1986).



Figure 1.1, (A) Distribution of Tethyan ophiolites in Europe and Asia (B) Inset map displays the extent of the Oman-U.A.E. ophiolite (dark grey) located at the eastern tip of Arabian peninsula. (Modified from Lippard et al., 1986).

The Oman-U.A.E. ophiolite formed in the Neotethys Ocean, between ~97.9 and 93.5Ma (Tilton et al., 1981). It is believed to have formed by sea-floor spreading, with fast spreading rates of between 50 and 100mm yr<sup>-1</sup>, leading to comparisons between the ophiolite and the modern East Pacific Rise (Figure 1.2) (e.g. Lippard et al., 1986; MacLeod and Rothery, 1992; Girardeau et al., 2002), though the tectonic environment of formation is still a topic of much debate.

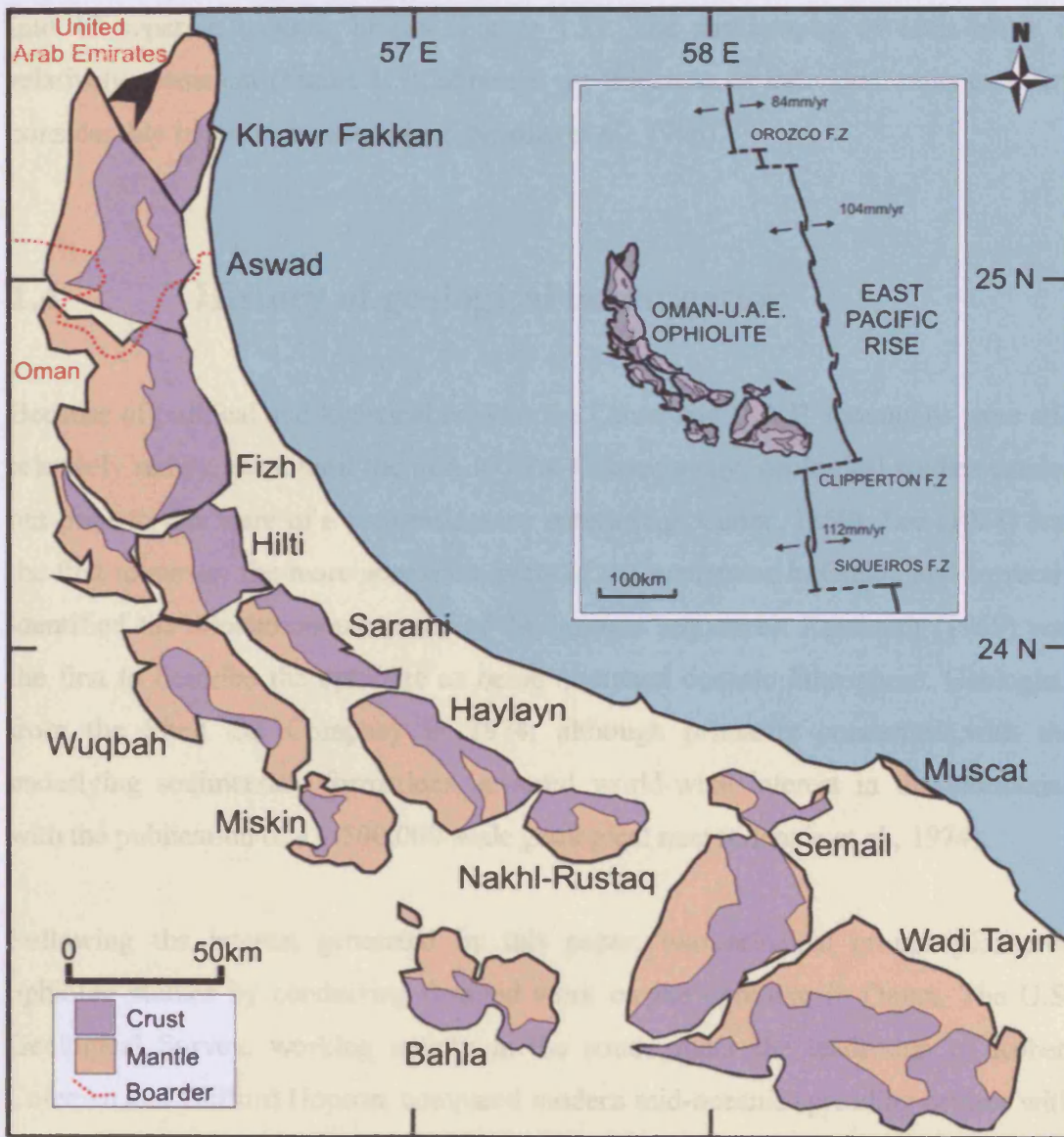


Figure 1.2, Generalised geological map of the Oman-U.A.E. ophiolite. The 12 major ophiolite blocks define the northern coast of the Sultanate of Oman and the United Arab Emirates. Inset map shows the East Pacific Rise and Oman-U.A.E. ophiolite at the same scale. Map modified from Nicolas and Boudier, (2000). Inset modified from Nicolas et al. (1988).

The ophiolite was emplaced in the form of a crescent-shaped thrust sheet onto the Arabian continental margin (Figure 1.2), following south-westward intra-oceanic thrusting within 5Ma of its formation, in the Early Palaeocene (e.g. Searle and Malpas, 1980; Tilton et al., 1981). Paleomagnetic studies have shown that, during the magmatic evolution of the oceanic crust and its subsequent obduction, the crust underwent a 145° clockwise rotation (Perrin et al., 1994 and 2000). During the last

stages of obduction onto the Arabian margin, the Oman-U.A.E. ophiolite was divided into 12 separate tectonic blocks (Figure 1.2). The stratigraphy of each block is relatively consistent (Figure 1.3), although the thickness of individual units can vary considerably between locations (e.g. Nicolas et al., 1996).

## **1.4 History of geological investigation**

Because of political and logistical reasons the Oman and U.A.E. mountains were still relatively remote even until the mid-1970's. Consequently, geological studies carried out prior to this were of a reconnaissance nature (e.g. Carter, 1850). Lee (1928) was the first to survey the more accessible parts of the mountains in Oman, and correctly identified the allochthonous nature of the igneous sequences. Reinhardt (1969) was the first to describe the ophiolite as being obducted oceanic lithosphere. Geologists from the Shell Oil Company in 1974, although primarily concerned with the underlying sedimentary formations, aroused world-wide interest in the mountains with the publication of a 1:500,000-scale geological map (Glennie et al., 1974).

Following the interest generated by this paper, two principal groups pioneered ophiolite studies by conducting detailed work on the ophiolite in Oman. The U.S. Geological Survey, working mainly in the south under the leadership of Robert Coleman and Clifford Hopson, compared modern mid-oceanic spreading centres with the ophiolite. They used their observations to produce a model for magma chambers beneath mid-ocean ridges (Pallister and Hopson, 1981). Their principal findings are published in a Special Volume ("Oman ophiolite", *J. Geophys. Res.*, vol. 86, 1981) and an accompanying 1:100,000-scale geological map.

Another study at the time was by a series of workers from the Open University led by Prof. Ian Gass which culminated in the publication of the book "The Ophiolite of Northern Oman" (Lippard et al., 1986). The principal conclusion from this work was that the ophiolite formed in a back-arc basin related to a hypothetical subduction zone.

Since 1981, groups from the Universities of Nantes and Strasburg, led by Adolphe Nicolas and Thierry Juteau respectively, have conducted 1:400,000-scale structural mapping of the whole ophiolite. Their detailed research has led to a better understanding of magma chamber dynamics (Figure 1.4), mantle diapirs (Figure 1.5), and the mechanics of ophiolite emplacement. Part of their results can be found in “The ophiolite of Oman” (Tectonophysics, vol. 151, 1988), and in Marine Geophysical Researches, vol. 21, (2000).

This thesis forms part of the U.A.E. Geological Mapping Project (2002-2006), based in the United Arab Emirates section of the ophiolite and funded by the Government of the United Arab Emirates Ministry of Petroleum and Mineral Resources. The project involves detailed 1:50,000-scale mapping and geophysical surveying of the Khawr Fakkan and northern Aswad Blocks of the ophiolite. The project is being undertaken by the British Geological Survey, with cooperation with Cardiff University, and will provide the most accurate mapping and sampling of any part of the of the Oman-U.A.E. ophiolite to date.

## **1.5 The internal stratigraphy of the Oman-U.A.E. ophiolite**

The internal structure of the Oman-U.A.E. ophiolite corresponds with that of the classic Penrose Conference (1972) definition of an ophiolite (Figure 1.3). The following sections provide a basic summary of the Units found within, and associated with, the Oman-U.A.E. ophiolite.

### **1.5.1 The allochthonous units and metamorphic sole**

The Oman-U.A.E. ophiolite was emplaced as a complex sequence series of nappes thrust over the Pre-Permian Basement rocks of the Arabian Shield. These include the Sumeini Group, consisting of fine-grained Mesozoic continental slope limestones and the overthrust Mesozoic Hawasina assemblage, composed mostly of sediments of

turbidite origin (Glennie, et al., 1974). Overlying these assemblages is the Haybi Complex, which has diverse origins and includes both pre and syn-nappe emplacement sediments (Glennie et al., 1974). The highest unit below the ophiolite is a highly sheared basal serpentinite mélangé which also contains blocks of the sub-ophiolitic metamorphic sole as well as some of the Haybi Volcanics. The serpentinite and metamorphic sole rocks were derived from the base of the ophiolite during nappe emplacement (Searle and Malpas, 1980).

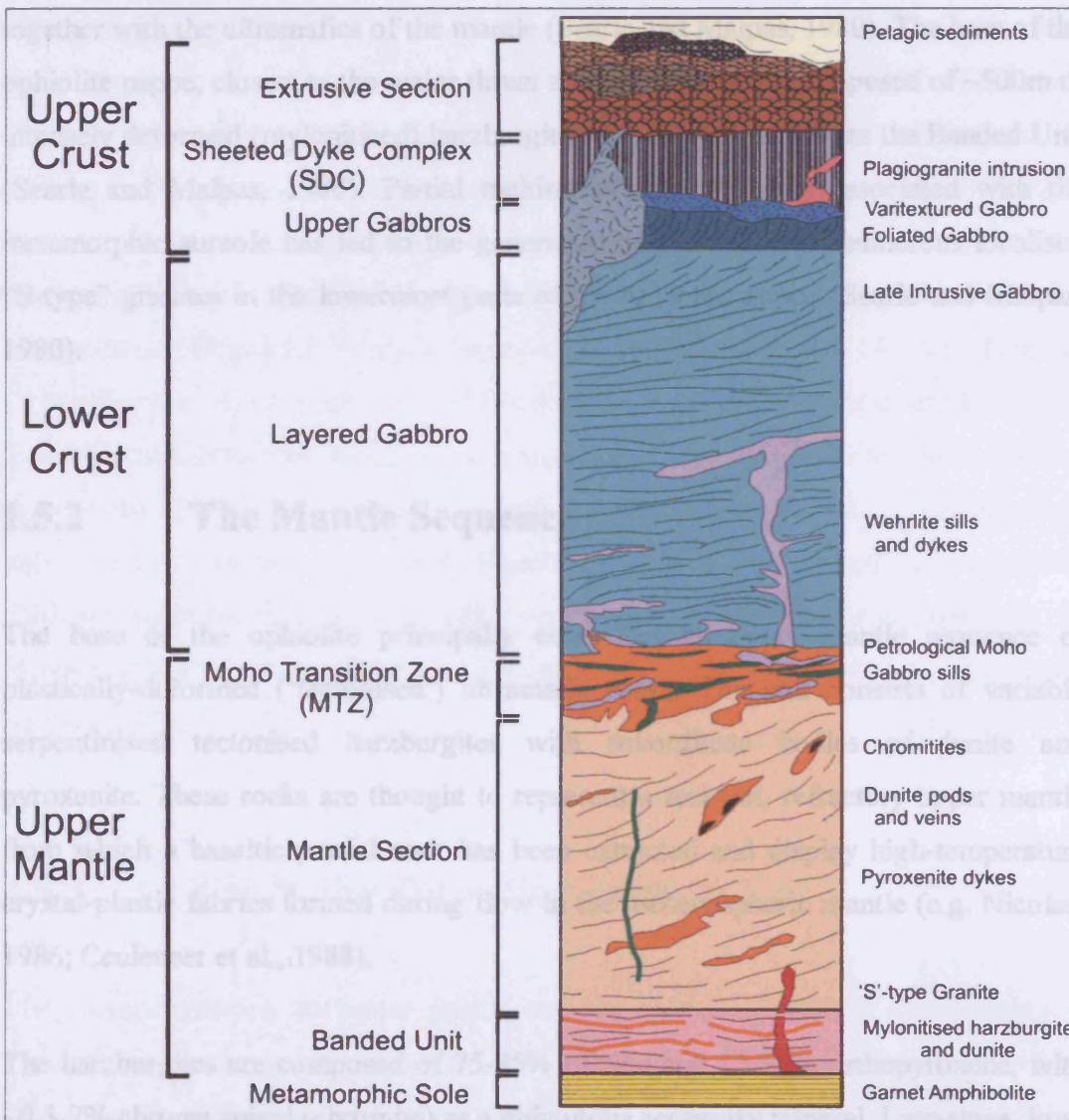


Figure 1.3, Generalised cross-section through the Oman-U.A.E. ophiolite. Structural relations are correct, but units are not to scale. Modified from Nicolas (1989).

The base of the Oman-U.A.E. ophiolite is marked by a thin (<500m), fault-bounded sheet of highly strained amphibolite-grade metamorphic rocks (Searle and Malpas, 1980) (Figure 1.3). This sole unit is believed to have been formed in the very earliest stages of detachment and metamorphic conditions have been estimated at 700-900<sup>o</sup> C and 9-13 kbar (Wakabayashi and Dilek, 2000). As the ophiolite became uncoupled from the surrounding oceanic crust, the base rode over the pelagic and carbonaceous sediments of the sea floor and acted as a kind of bulldozer blade. Some of the sediments were pushed in front of the ophiolite (later to form the Haybi Complex) and some became entrained underneath the moving slab of crust and were metamorphosed together with the ultramafics of the mantle (Searle and Malpas, 1980). The base of the ophiolite nappe, closest to the major thrust zone, is commonly composed of ~500m of intensely deformed (mylonitised) harzburgites and dunites, known as the Banded Unit (Searle and Malpas, 1980). Partial melting of the sediments associated with the metamorphic aureole has led to the generation and intrusion of numerous localised “S-type” granites in the lowermost parts of the ophiolite nappe (Searle and Malpas, 1980).

## 1.5.2 The Mantle Sequence

The base of the ophiolite principally comprises an upper mantle sequence of plastically-deformed (‘tectonised’) ultramafic rocks. The unit consists of variably serpentinised tectonised harzburgites with subordinate bodies of dunite and pyroxenite. These rocks are thought to represent a residual, refractory upper mantle from which a basaltic partial melt has been extracted and display high-temperature crystal-plastic fabrics formed during flow in the asthenospheric mantle (e.g. Nicolas, 1986; Ceuleneer et al., 1988).

The harzburgites are composed of 75-85% olivine and 15-25% orthopyroxene, with ~0.5-2% chrome spinel (chromite) as a ubiquitous accessory mineral. Late-stage, low-temperature (<50°C) alteration (serpentinisation) by post-emplacement exposure to meteoric ground waters has affected between 50-80% of the primary silicate minerals (Dunlop and Fouillac, 1986). Dunites, which constitute ~5-15% of the exposed



mantle section (Brown, 1980), may represent conduits for chemically isolated melt transport through the shallow mantle beneath oceanic spreading centres (Braun and Keleman, 2002). The depleted upper-mantle material is the residue left behind after a harzburgite has partially melted to produce a basaltic melt. Dunite bodies range in size from centimetres to kilometres in length, and can have diffuse or sharp contacts with the host harzburgite (e.g. Browning, 1982; Ceuleneer et al., 1988; Joussetin and Nicolas, 2000). The shape, size, abundance and distribution of dunite bodies vary considerably from place to place, and the shape and deformation of the dunite masses are commonly related to the harzburgite foliation (e.g. Browning, 1982; Ceuleneer et al., 1988).

The pervasive tectonic fabric (foliation) of the harzburgites and dunites is seen in outcrop as the alignment of orthopyroxene and spinel grains and is caused by high-temperature plastic flow (Nicolas et al., 1988). Structural studies have interpreted the steepening of such fabrics to represent the presence of mantle diapirs beneath the ridge axis (see Figure 1.5) (e.g. Ceuleneer et al., 1988; Nicolas et al., 1988). These 10-15 km diameter features are believed to be zones of intense magmatic activity, where focused channels of melt feed the overlying crust (Nicolas et al., 1988). Such features can also be inferred by traces of magmatic activity such as magmatic impregnation, entrapment of melt relicts in dunite, abundance of gabbro dykes and the presence of chromite pods (Nicolas et al., 1988). Such features are also associated with an increase in the thickness of the Moho Transition Zone directly above the diapir (see Section 1.5.3).

### **1.5.3 The Moho Transition Zone (MTZ)**

The contact between the upper mantle and the overlying crust of the ophiolite is marked by an irregular structural and petrological horizon termed the Moho Transition Zone (MTZ) (Benn et al., 1988). Compositionally, the MTZ shows large lateral variations in thickness and composition and consists primarily of residual dunite, a magmatic component present as clinopyroxene or plagioclase impregnations, and gabbro lenses, marking a gradational passage from mantle to crust (Benn et al.,

1988). Structures within the MTZ and near the base of the crust are near-parallel to the Moho. Benn et al. (1988) also noted that plastic flow (ductile deformation in the solid state) dominates in the upper mantle, while viscous flow (magmatic alignment in the presence of melt), resulting in strong magmatic fabrics, dominates at crustal levels. The MTZ contains several important changes in physical and chemical properties of the rocks, and is not a simple contact between mantle and crust, but an intricate, crust generating, mixed system.

Contacts between dunite and gabbro lenses may be sharp or diffuse and chilled margins are not observed (Keleman et al., 1997; Koga et al., 2001). Dunites located close to diffuse contacts with gabbros often exhibit variable enrichment (impregnation) of plagioclase and clinopyroxene for up to several metres (Koga et al., 2001). Gabbroic bodies generally increase in abundance up-section and vary in size from <1m to many tens of metres in thickness and up to hundreds of metres in length. The gabbros within the MTZ also typically have millimetre- to tens of centimetre-scale modal layering, which resembles that of the Layered Gabbro sequence (Korenga and Keleman, 1997). These gabbro lenses have been interpreted as fossilised sills from which residual liquids have been efficiently expelled (e.g. Benn et al., 1988; Keleman et al., 1997; Koga et al., 2001). Such sills have recently been imaged by seismic reflection, at a depth corresponding with the MTZ, of modern fast-spreading centres in the East Pacific. Such evidence supports the hypothesis that the crust is generated by multiple magma bodies and that the MTZ is a vital part of the magma storage and fractionation processes in the lowermost crust (Nedimovic et al., 2005).

The thickness of the MTZ, which ranges from several metres to over 1km, is measured from the uppermost level of harzburgite to the start of the continuous Layered Gabbros. Three grades of MTZ have been identified, resulting in the classification of: *Thin* (<10m), *Intermediate* (~100-300m) and *Thick* (500m+) MTZ's (Boudier and Nicolas, 1995). Areas of *Thick* MTZ's, combined with structural measurements from the mantle section have been interpreted to indicate the presence of ~20-50km areas of mantle upwelling (Figure 1.5), with *Thin* MTZ's distal to such structures (Nicolas and Boudier, 2000).

## 1.5.4 Wehrlites

Wehrlite is a common ultra-basic intrusive rock that can be found irregularly throughout the lower crustal sequence, and has been recorded intruding the pillow lavas (Juteau et al., 1988; and this study). The composition of wehrlites varies, as does their description in the literature. Wehrlites are essentially composed of olivine and clinopyroxene, with accessory chromite and up to 10% plagioclase (Streckeisen, 1976). Because of compositional and textural similarities, the distinction between 'true' wehrlites, melagabbros and impregnated dunites is often difficult; hence all such rocks are often grouped together as 'wehrlites' (Koga et al., 2001).

Wehrlites are observed at a number of scales, from centimetre-thick concordant sills or lenses within the Layered Gabbro sequence, to kilometre-length intrusions crosscutting the MTZ and the crustal gabbros (Browning and Smewing, 1982; Juteau et al., 1988; Koga et al., 2001). No wehrlites have ever been recorded in the mantle harzburgites below the MTZ. This provides evidence that wehrlitic intrusions represent a crystal-melt mixture which is closely related to the origins of gabbroic melt, originating from the MTZ, and has been emplaced into crustal levels. The mode of emplacement of Wehrlites is still a topic of debate and direct links to compaction processes in the immediate vicinity of the ridge axis has been proposed as the most probable physical method of emplacement (e.g. Juteau et al., 1988; Benn et al., 1988; Jousselin and Nicolas, 2000).

Typical MORB crystallisation at crustal pressures will crystallise in the sequence: olivine-plagioclase-clinopyroxene. Wehrlites follow the crystallisation sequence: olivine-clinopyroxene-plagioclase (Koga et al., 2001). This change in the order of crystallisation is directly related to the presence of volatiles, most commonly water (Ernewein et al., 1988). Thus the presence of wehrlites in the lower crust and MTZ can be interpreted as evidence for the existence of a melt that is distinctly different from MORB, such as a subduction-related melt. The presence of wehrlites thus has important implications for the tectonic setting and geochemical evolution of the lower crust (Pearce et al., 1984) in that their formation requires elevated water contents.

## 1.5.5 The Crustal gabbro sequence and magma chamber models

Despite the considerable amount of research conducted on the Oman-U.A.E. ophiolite over the last 30-years there is little consensus on the sub-division of the gabbro sequence, with different terms applied during different studies (Thomas, 2003) (Table 1.1). Although the Layered Gabbro Sequence is common to all parts of the ophiolite, the overlying (non-layered) gabbro sequence exhibits considerable variation in composition and thickness between blocks (e.g. Lippard et al., 1986).

<b>This Study</b>	<b>Lippard et al. (1986)</b>	<b>Nicolas (1989)</b>	<b>Keleman et al. (1997)</b>	<b>MacLeod and Yaouancq (2000)</b>	<b>Thomas (2003)</b>
<b>Upper Gabbros</b>	<b>High-Level Intrusives</b>	<b>Recrystallised or Isotropic Gabbro</b>	<b>Upper Gabbros</b>	<b>Varitextured Gabbros</b>	<b>Varitextured Gabbros</b>
		<b>Foliated Gabbros</b>		<b>Foliated Gabbros</b>	<b>Foliated Gabbros</b>
				<b>Transitional Gabbros</b>	
<b>Layered Gabbros</b>	<b>Layered Gabbros</b>	<b>Lower Gabbros</b>	<b>Layered Gabbros</b>	<b>Layered Gabbros</b>	<b>Layered Gabbros</b>

Table 1.1, Comparison of terminology used in the subdivision of the gabbro sequence of the Oman-U.A.E. ophiolite (after Thomas, 2003).

Figure 1.4 illustrates selected (fast-spreading) mid-ocean ridge magma chamber models. Early models concentrate on the concept of a large, 3-4km thick and up to 30km wide, long-lived magma chamber beneath fast spreading ridges (e.g. Cann, 1974 and Smewing, 1981). Seismic studies over the last twenty years have disproved earlier models by providing evidence of a thin, 20-200m thick and 1-2km wide, narrow lens-shaped magma chamber which grades downward into a wider, poorly constrained, zone of 'crystal mush' (e.g. Sinton and Detrick, 1992 and Singh et al.,

1998), with evidence of multiple gabbroic melt accumulations at the base of the crust close to the MTZ (Nedimovic et al., 2005).

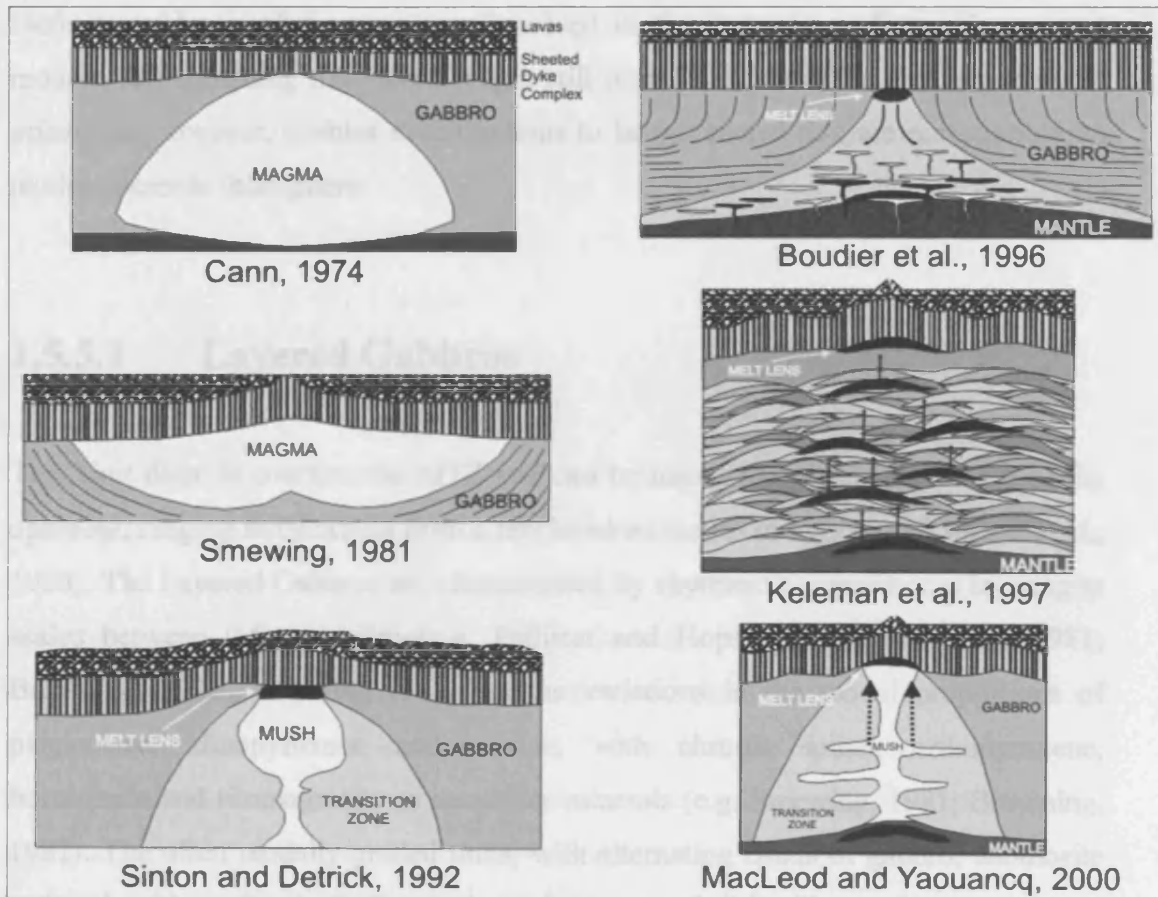


Figure 1.4, Magma chamber models. The crustal sequence is approximately 5km thick in all models, with vertical scale being equal to horizontal scale. The patterns used for sheeted dykes and lavas in Cann, (1974) are the same for all models.

Sinton and Detrick (1992) divided the lower crust into three main parts: a narrow melt lens; a partly solidified crystal mush zone; and hot, but predominantly solid transition to the surrounding rock on either side of the axis. They suggest that the melt lens is replenished by buoyant melt migration through the partly crystalline mush, which acts as a density filter. Boudier et al. (1996), Keleman et al. (1997) and MacLeod and Yaouancq (2000), based on observations from the Oman-U.A.E. ophiolite, incorporated these findings into their own models which propose that a substantial portion of the lower crust forms as injected sills (Figure 1.4). Contrary models, such as those of Phipps-Morgan and Chen (1993), Quick and Denlinger (1993), Henstock et al. (1993) and Thomas (2003) still favour subsidence of crystals from the melt lens

as the primary method of lower crustal accretion, an idea first proposed by Sleep (1975).

Definite evidence of the processes involved in the generation of oceanic crust at modern fast-spreading mid-ocean ridges still remains elusive. The detailed study of ophiolites, however, enables investigations to be completed that are not possible on modern oceanic lithosphere.

### **1.5.5.1 Layered Gabbros**

This Unit directly overlies the MTZ and can be traced throughout the length of the ophiolite, ranging in thickness from a few hundred metres to over 6km (Lippard et al., 1986). The Layered Gabbros are characterised by rhythmic compositional layering at scales between 0.5cm to 2m (e.g. Pallister and Hopson, 1981; Smewing, 1981; Browning, 1982). Layering is defined as variations in the modal proportions of plagioclase, clinopyroxene and olivine, with chrome spinel, orthopyroxene, hornblende and titanomagnetite as accessory minerals (e.g. Smewing, 1981; Browning, 1982). The often modally-graded units, with alternating bands of gabbro, anorthosite and melagabbro often including contemporaneous wehrlitic sills, can be traced for up to several hundred metres along strike but invariably pinch out or are truncated (e.g. Pallister and Hopson, 1981; Smewing, 1981; Browning, 1982).

Layering at the base of the sequence is strongly defined and parallel to the Moho, but these layers become less aligned and less distinct towards the top of unit (e.g. Browning, 1982; MacLeod and Yaouancq, 2000). Grain size is relatively constant within the lower Layered Gabbros (~1-3 mm) with a magmatic foliation and lineation defined by the fabric of plagioclase laths and elongated olivine aggregates. Foliations are parallel or sub-parallel to the layering and lineations can be consistent on a kilometre scale (Browning, 1982; Boudier et al., 1996; MacLeod and Yaouancq, 2000). These planar and linear structures indicate that the whole lower crustal section has been transposed in the magmatic state by simple shear (Nicolas et al., 1988). Dynamic structures such as boudinage, isoclinal folds, overturned folds and shear

bands have been observed disturbing the gabbro layering at various scales (e.g. Pallister and Hopson, 1981; Browning, 1982; Nicolas, 1992; Thomas, 2003). Compositional layering generally decreases up-section and the abundance of ultramafic sills also decreases (Boudier et al., 1996). The upper limit of the sequence is gradual, often over tens to hundreds of metres, and corresponds to the level at which discrete layering cannot be distinguished (Boudier et al., 1996; MacLeod and Yaouancq, 2000)

### **1.5.5.2 Upper Gabbros**

Layered gabbros pass up into a foliated gabbro facies, up to ~1 km in thickness, composed of massive, non-layered gabbros and olivine gabbros with similar geochemical patterns and grain size (typically 1-4 mm) to the Layered Gabbros (e.g. Nicolas et al., 1986; MacLeod and Yaouancq, 2000). Foliated gabbros are characterised by a steep, Moho-perpendicular, foliation, and steep lineation, which tends to become weaker up-section, before becoming indistinguishable at the top of the unit, where they pass (usually gradationally) into a varitextured gabbro facies (MacLeod and Yaouancq, 2000).

Varitextured gabbros are regularly encountered above the foliated gabbros and form a ~150 m thick horizon defined by extreme variability in grain size (doleritic to coarse grained), texture and chemical composition over short distances (MacLeod and Yaouancq, 2000). The transition from foliated to varitextured gabbros may be sharp, spanning only a few metres. Varitextured gabbro represents the horizon at which cumulate crystal residues pass up into basaltic liquids; by analogy with seismic data taken from fast-spreading ridges, the varitextured gabbros are taken to represent the fossilised equivalent of a melt lens (MacLeod and Yaouancq, 2000). Additional primary phases, such as Fe-oxides and amphibole, and secondary replacement minerals, such as actinolite and epidote, are common in this unit (e.g. Pallister and Hopson, 1981; Lippard et al., 1986; Yaouancq, 2001) and testify to the increased presence of water (be it primary magmatic or hydrothermal in origin) in the upper crust.

Continuing up-section, the varitextured gabbros give way to fine-grained gabbros and dolerites of the dyke root zone, where chilled margins are first encountered (MacLeod and Rothery, 1992). The transition from varitextured gabbros to sheeted dykes is gradual and complex, with mutually intrusive contacts between dykes and varitextured gabbro. Felsic trondhjemite and tonalite (both commonly termed 'plagiogranite'), produced by fractionation of a basaltic melt, are widespread in the varitextured gabbros and are observed as veins, dykes or intrusions, occasionally intruding into the extrusive sequence.

### 1.5.5.3 Late Intrusive Gabbros

Late, intrusive, plutonic complexes have been recorded along the length of the ophiolite, although they are generally more common in the northern ophiolite blocks, and can intrude as high as the extrusive sequence (e.g. Browning and Smewing, 1982; Browning, 1982; Umino et al., 1990). Such bodies cross-cut the ophiolite stratigraphy and have been interpreted to represent discrete, high-level, magma chambers feeding upper lava units (e.g. Browning and Smewing, 1982; Browning, 1982). The units are generally petrographically indistinguishable from the upper gabbros of the axis sequence, but intrude into the upper crustal units of the ophiolite (e.g. Browning and Smewing, 1982; Browning, 1982). These authors divided the late intrusives into two groups: an older series of large (1-10km<sup>2</sup>) differentiated gabbro to plagiogranite plutons (Cpx-Series) and a younger group of smaller (<1km diameter) wehrlite-gabbro intrusions (Opx-Series).

The first group, the Cpx-series of Umino et al. (1990), are large intrusions mostly composed of massive gabbros and dolerites with subordinate volumes of plagiogranite, outcropping over areas from 1km<sup>2</sup> to over 10km<sup>2</sup>. The Lasail complex of the Hilti Block is typical and consists of a core of gabbros transitional into dolerites, and overlain by an irregular sheet of tonalite. It is emplaced into the sheeted dykes and the base of the lavas and is faulted against Layered Gabbros of the main axis sequence along its southern margin (Browning and Smewing, 1982; Browning,



1982). These intrusions were interpreted to represent the roof zones of moderately large magma chambers which fed the Lasail Unit extrusives (Alabaster et al., 1980) (section 1.4.7).

The second group, the Opx-series of Umino et al. (1990), mainly consist of younger and smaller (<1km<sup>2</sup>) intrusions that are composed of coarse grained wehrlite with subordinate gabbros, with more differentiated rocks in marginal zones. The intrusions are characterised by the early appearance of orthopyroxene in the crystallisation sequence, contrasting with the axial suite of gabbros, which contain little or no orthopyroxene. The intrusions are generally up to 1.5km long and a few hundreds of metres wide and are mainly elongate; commonly aligned along NW to WNW-trending faults (Browning and Smewing, 1982; Lippard et al., 1986). However, Umino et al. (1990) reported that these Opx-series intrusives are the largest late intrusive bodies in the Fizh Block. The Opx-series intrusions are commonly observed chilling against the axial Layered Gabbros and can contain xenolithic blocks of the axial suite (up to several kilometres in diameter) and have been recorded as high as the lava sequence (Smewing, 1981), sometimes cutting the Cpx-series intrusions. The Opx-series late intrusive gabbros are associated with cone sheets and E-W striking dykes and have been interpreted to represent high-level magma chambers in which late-stage magmas collected and fractionated before feeding the Alley and Clinopyroxene phyric Units (see section 1.4.7).

### **1.5.6 Sheeted Dyke Complex (SDC)**

The SDC is composed of ~95% to 100% steeply dipping, parallel doleritic dykes. They represent extension and form one of the strongest pieces of structural evidence that ophiolites formed at an ocean ridge spreading axis (Gass, 1968; Moores and Vine, 1971). Individual dykes range from <0.1m to over 4m, but most are 0.5-1m thick, with dyke widths generally being related on their position within the SDC. The dykes generally become thicker towards the base (Pallister, 1981; Rothery, 1983). The thickness of the SDC throughout the ophiolite varies from ~600-2000m with an average of around 1500m (Lippard et al., 1986). At the upper and lower contacts of

the SDC the nearly 100% sheeted nature gives way, over a vertical distance of tens of metres, to lavas and gabbros respectively. Dykes of up to 4m in width, which coarsen to isotropic microgabbro in their centres, have been observed 'rooting' in the varitextured gabbros (MacLeod and Rothery, 1992).

The dykes exhibit a wide range of compositions from basalts to andesites, which overlap with the compositions of the overlying basalt lava units (Section 1.5.7) (Pearce et al., 1981 and Lippard et al., 1986). The primary mineralogy of the dykes is calcic plagioclase, clinopyroxene and Fe-Ti oxides (titanomagnetite and ilmenite), but most show almost complete replacement by greenschist facies minerals due to sea-floor hydrothermal metamorphism (Lippard et al., 1986).

Because the SDC is believed to be formed by injection of magma parallel to the ridge axis, the general strike of the SDC throughout the ophiolite has been used by various authors to infer the location and direction of the original ridge axis spreading (i.e. perpendicular to the strike of the SDC) (e.g. Lippard et al., 1986; MacLeod and Rothery, 1992; Nicolas and Boudier, 1995; Nicolas et al., 2000). The sheeted dykes of the Oman-U.A.E. ophiolite typically strike N-S to NW-SE (Figure 1.5).

### **1.5.7 Extrusive Sequence**

The extrusive sequence, the uppermost part of the Oman-U.A.E. ophiolite, consists of up to 2000 m of andesite to rhyolite pillows and massive flows. In a few locations they are intercalated and depositionally overlain by deep water sediments (Glennie et al., 1974). The complex magmatic history of the ophiolite is represented by the presence of several distinct lava units, which are cut by later dykes, sills and occasional high-level intrusions (Alabaster et al., 1982). Feeder dykes of each unit crosscut the previous unit(s). All of the lava groups have been altered by sea-floor hydrothermal alteration to some extent, with several alteration phases related to successive magmatic episodes and off-axis hydrothermal circulations being observed (Einaudi et al., 2000). Secondary minerals (including Fe-hydroxides, quartz, albite, chlorite, zeolite and calcite) replace primary mineral phenocrysts, parts of the

groundmass, and fill vesicles and small fractures. The degree and nature of the alteration is variable and is directly related to the lithostratigraphic location of unit, with lavas from the lower sequences being more intensively altered than those of the upper lavas (Einaudi et al., 2000). A detailed discussion of the low-grade metamorphic history of the lava sequence in the Oman portion of the ophiolite can be found in Pfumino (1991).

Initial analyses of lava samples taken from the southern ophiolite in Oman allowed Pearce et al. (1981) and Alabaster et al. (1980, 1982) to agree on the classification of the extrusive section into 5 Units using both field evidence and geochemical characteristics. They are, starting with the oldest: *Geotimes*, *Lasail*, *Alley*, *Clinopyroxene-phyric* and *Salahi* Units (Figure 1.5). These are the Units that will be referred to in this study. Subsequent work by Ernewein et al. (1988) and Godard et al. (2002) has sought to re-name and re-categorise the lavas into three main magmatic Units, the V1 (*Geotimes*), V2-I (*Lasail*), V2-II (*Alley*) and V3 (*Salahi*). However, the volcanic stratigraphy is spatially variable between blocks with some sections not including all volcanic Units (Figure 1.5) and variable thicknesses of Units (Alabaster et al., 1982). A brief summary of the geochemical characteristics of each unit is displayed in Table 1.2. It is worth noting that no volcanoclastic or ash-bearing pelagic sediments characteristic of back-arc or fore-arc environments have ever been recorded in the sediments associated with the extrusive sequence of the Oman-U.A.E. ophiolite (Ernewein et al., 1988).

The *Geotimes* Unit (or V1) is the stratigraphically lowermost sequence, and represents ~60% of the exposed extrusive rocks in Oman (Nicolas et al., 2000). They are believed to have been erupted between 94 and 96Ma based on hornblende  $^{40}\text{Ar}/^{39}\text{Ar}$  dates (Hacker et al., 1996 and references within). The unit directly overlies the SDC and therefore are thought to have formed by igneous activity at a spreading centre (Alabaster et al., 1982). Throughout the ophiolite the *Geotimes* Unit records a lava thickness of ~300m to a maximum of 1600m (Alabaster et al., 1982). The Unit consists primarily of large and commonly elongate, weakly vesicular, reddish-brown pillow basalts with rare massive lava flows. The composition of the *Geotimes* Unit is close to that of mid-ocean ridge basalt (MORB). The lavas have light rare earth

element to heavy rare earth element (LREE/HREE) ratios that are slightly depleted relative to N-MORB.

Unit (Thickness)	FeO/MgO	TiO <sub>2</sub>	Incompatible trace elements	REE-Chondrite normalisation	Tectonic Setting
<b>Salahi</b> (100m max)	1-3	1.2-1.9	Enriched relative to N-MORB, especially in incompatible elements	LREE –enriched $La_n/Yb_n > 5$ LREE>MREE>HREE	Within-plate basalts, small degrees of melting of undepleted mantle.
<b>Cpx-Ø</b> (50m max)	1	0.2-0.5	Highly depleted relative to N-MORB	LREE –depleted $La_n/Yb_n < 0.3$ LREE<MREE<HREE	IAT suite with strong boninitic affinity. Formed by hydrous melting of very depleted mantle. Associated with high-level intrusive bodies.
<b>Alley</b> (500m max)	1-2.5	0.4-1.1	Depleted relative to N-MORB	LREE –depleted $La_n/Yb_n \sim 0.5$ LREE<MREE<HREE	IAT Suite with boninitic affinity formed by hydrous melting of depleted mantle. Associated with rifting.
<b>Lasail</b> (500m max)	1	0.3-0.9	Depleted relative to N-MORB	LREE –depleted $La_n/Yb_n \sim 0.6$ LREE<MREE=HREE	Transitional MORB to IAT suite, high melting (20-30%) of slightly depleted mantle. Localised, high-level magma chambers.
<b>Geotimes</b> (750-1500m)	1.5-5.0	0.9-2.2	Slightly depleted relative to N-MORB	Slightly LREE –depleted $La_n/Yb_n 0.7-1.0$	Relatively evolved magmas similar to MORB. Steady-state magma chamber.

Table 1.2 Geochemical characteristics and interpreted tectonic settings of the Oman-U.A.E. ophiolite extrusive sequence as defined in Oman (after Lippard et al., 1986).

The Lasail Unit (or V2 type I) outcrops mainly in the northern part of the ophiolite and reaches a maximum thickness of around 750m (Alabaster et al., 1982). It is sometimes separated from the Geotimes Unit by a thin layer (<2.5m) of pelagic sediments indicating a short time interval between the eruption of the two units (Alabaster et al., 1982; Ishikawa et al., 2002). The Lasail pillow lavas are green-grey in colour with small and ‘bun-shaped’ pillows, which contain altered microcrysts of olivine and clinopyroxene (Alabaster et al., 1982). The lavas are associated with localised cone-sheets and dyke swarms, which mark the spatial position of high-level magma chambers, possibly representing ‘seamount’-type volcanism (Figure 1.5), and are now preserved as late intrusive gabbro bodies (Cpx-series) within the crustal sequence (e.g. Alabaster et al., 1980; Pearce, 1981). The Lasail lavas are of tholeiitic affinity and can be distinguished from the Geotimes Unit by a REE signature that is depleted relative to N-MORB and the Geotimes Unit.

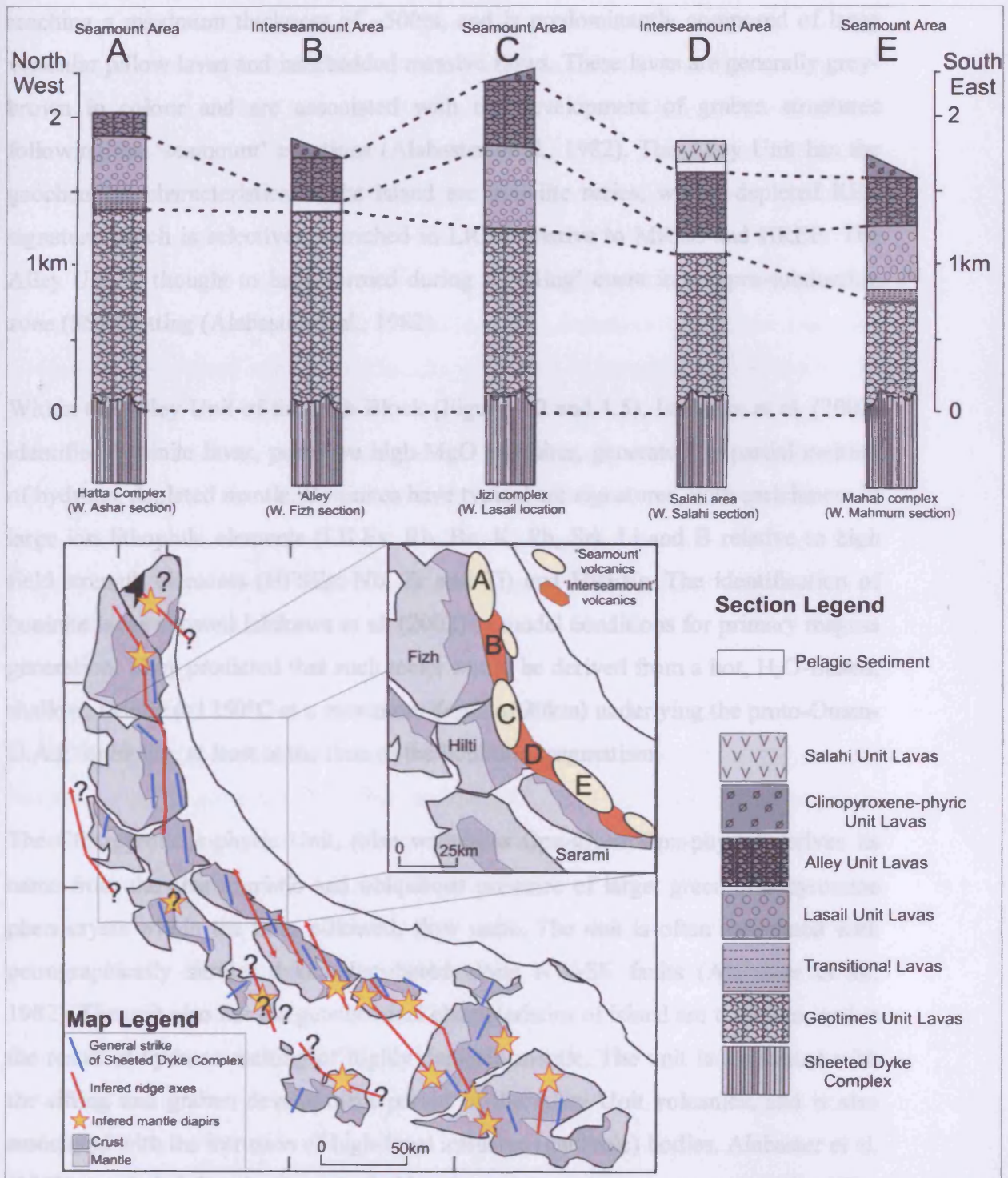


Figure 1.5, Extrusive sequence stratigraphic columns illustrating how some areas can lack more than one lava Unit. Structural map of the Oman-U.A.E. ophiolite, showing inferred strike of ridge axis, and mantle diapirs (After Nicolas and Boudier, 2000). Map inset shows locations of lava Unit sections and the location of 'seamount' areas (those containing the Lasail Unit; areas A-C-E) and 'inter-seamount' areas (where the Lasail Unit is absent; areas B-D). After Alabaster et al. (1982).

The Alley Unit (or V2 type II), is typically thinner than the earlier lava sequences, reaching a maximum thickness of ~500m, and is predominantly composed of large vesicular pillow lavas and interbedded massive flows. These lavas are generally grey-brown in colour and are associated with the development of graben structures following the 'seamount' eruptions (Alabaster et al., 1982). The Alley Unit has the geochemical characteristics of the island arc tholeiite series, with a depleted REE signature which is selectively enriched in LREE relative to MREE and HREE. The Alley Unit is thought to have formed during a 'rifting' event in a supra-subduction zone (SSZ) setting (Alabaster et al., 1982).

Within the Alley Unit of the Fizh Block (Figure 1.2 and 1.5), Ishikawa et al. (2002) identified boninite lavas, primitive high-MgO andesites, generated by partial melting of hydrous, depleted mantle. Boninites have typical arc signatures, with enrichment in large ion lithophile elements (LILEs: Rb, Ba, K, Pb, Sr), Li and B relative to high field strength elements (HFSEs: Nb, Zr and Ti) and HREEs. The identification of boninite lavas allowed Ishikawa et al. (2002) to model conditions for primary magma generation. They predicted that such melts would be derived from a hot, H<sub>2</sub>O-fluxed, shallow, mantle (>1250°C at a maximum depth of 30km) underlying the proto-Oman-U.A.E. ophiolite, at least at the time of the boninitic magmatism.

The Clinopyroxene-phyric Unit, (also written as Cpx-Ø, or Cpx-phyric) derives its name from the characteristic and ubiquitous presence of large, green clinopyroxene phenocrysts within the thin, pillowed, flow units. The unit is often associated with petrographically similar dykes distributed along NW-SE faults (Alabaster et al., 1982). The unit also has the geochemical characteristics of island arc tholeiites, and is the result of hydrous melting of highly depleted mantle. The unit is associated with the rifting and graben development period of the Alley Unit volcanics, and is also associated with the intrusion of high-level intrusive (gabbroic) bodies. Alabaster et al. (1982) concluded that the Cpx-phyric Unit formed from the same magma as the Alley Unit, but reached the surface rapidly, via faults, without undergoing the same segregation and mixing as the Alley Unit. Ishikawa et al. (2002) also identified the Cpx-phyric Unit in the Fizh Block, including it as part of the Alley Unit.

The uppermost lava sequence, the Salahi Unit (or V3), is volumetrically the least significant and (prior to the present study) was only known in a small area of the Hilti massif as localised lavas and feeder dykes. Outcrops consist of up to 20m thickness of small pillow lavas overlain by up to 60m of massive, columnar-jointed flow units, and always have an unconformable contact with the Alley Unit, being separated by up to several metres of oceanic sediments (Alabaster et al., 1982, Ernewein et al., 1988). Trace element analysis by Alabaster et al. (1982) and Godard et al. (2003) of the Salahi Unit lavas showed enrichment relative to MORB of the most incompatible elements, resembling the pattern of within-plate volcanism. The lavas comprise alkaline to transitional within-plate basalts, explained as eruptions that post-date the detachment of a subducted slab (Alabaster et al., 1982) or intraplate seamount volcanism produced after the beginning of oceanic thrusting, but preceding the end of the obduction of the ophiolite onto the Arabian continental margin (Ernewein et al., 1988; Godard et al., 2003). Alabaster et al. (1982) regarded the lavas as products of melting of sub-continental mantle beneath the converging plate during the initial stages of ophiolite obduction.

No definitive dates have been published for the eruption of the Lasail, Alley or Cpx-phyric Units partly due to the limited extent of the units in certain areas (Figure 1.5). Inter-pillow sediments are only able to conclude that the Alley and Cpx-phyric magmatism took place during the Cenomanian to Turonian ages (98.9 to 89Ma) in the late Cretaceous (Tippit et al., 1981). However,  $^{40}\text{Ar}/^{39}\text{Ar}$  dates of Hacker et al. (1996) provide evidence that the ophiolite had cooled to below 550°C by 93.8Ma, constraining the Geotimes, Lasail, Alley and Cpx-phyric magmatism to between 96 and 93.8Ma. Sediments associated with the Salahi Unit are believed to date from the Coniacian to Santonian age (89 to 85.8Ma), just before or during the early stages of obduction (Ernewein et al., 1988) and significantly post-dating the eruption of the earlier units.

Accurate dates for the different lava (and plutonic) units throughout the length of the ophiolite would provide a much stronger framework on which to interpret the magmatic evolution and crustal accretion history of the ophiolite as a whole.

## **Chapter 2: Geology of the Ophiolite Blocks in the United Arab Emirates**

### **2.1 Introduction**

The Khawr Fakkan and Aswad Blocks are the northernmost of the Oman-U.A.E. ophiolite blocks (Figure 1.2). The Khawr Fakkan Block (also spelt Khor Faqqan, and Khor Fakhan) is located entirely within the U.A.E., and the Aswad Block is located mostly within the U.A.E., with some of the southernmost outcrops located in Oman (Figure 1.2 and 2.1). The U.A.E. ophiolite blocks have received considerably less attention than the blocks in the Oman portion of the ophiolite, particularly with regard to their magmatic evolution. It is the aim of this study to use combined fieldwork and geochemical investigation to establish the magmatic history and methods of crustal accretion for these blocks and to compare this with the evolution of the rest of the ophiolite to the south.

The Khawr Fakkan Block is approximately 50km in length and 35km wide and has an area of approximately 870km<sup>2</sup> (Lippard et al., 1986). The block is truncated to the north by the Dibba zone, the northernmost limit of the ophiolite, which is composed of mixed metamorphic rocks and syn-emplacement Units of the Hawasina and Haybi Complex (Section 1.5.1). The block is truncated to the south by the sub-vertical Wadi Ham fault zone (also referred to as the Masafi-Fujairah fault by Nicolas et al., 1988) (Figure 2.1). The Khawr Fakkan Block contains a large thrust-bound slice of sub-ophiolitic metamorphic rocks known as the Beni Hamed metamorphics, separated by E-SE dipping thrust faults (Figure 2.1). The syn-emplacement amphibolite to granulite facies, metasedimentary and metaigneous rocks are dominated by schistose quartzites and gneissose calc-silicate rocks, and have been described in detail by Gnos and Nicolas (1996).

The Khawr Fakkan Block has previously been separated into two sections on the basis of mantle fabrics. An E-SE dipping thrust fault extending north from the northern end of the Beni Hamed metamorphic zone (displayed in Figure 2.1) was inferred by Gnos



and Nicolas (1996) and extrapolated on the basis of mantle foliations by Nicolas et al. (2000). Recent detailed mapping of the Khawr Fakkan Block, however, by the British Geological Survey (U.A.E. Geological Mapping Project, 2002-2006), has not recognised this feature but has instead identified two discrete, crustal-scale, suture zones extending from the Beni Hamed metamorphic zone (Figure 2.1). The north-east trending features separate the northern Khawr Fakkan Block, comprising solely of mantle rocks, and the southern Khawr Fakkan Block, comprising easterly ( $\sim 30\text{-}45^\circ\text{E}$ ) dipping mantle and crustal units. During this (crustal) study the name 'Khawr Fakkan Block' will refer to the *southern* Khawr Fakkan Block, unless otherwise stated.

During emplacement, the Khawr Fakkan Block has been partially thrust over the north-eastern part of the Aswad Block (Figure 2.1), and sheared against it along the Wadi Ham suture (Nicolas et al., 2000). Both of the blocks in contact with the sub vertical, sinistral, Wadi Ham suture zone have outcrops of migmatite, indicating a high temperature role for the suture in the past (Philips, E. Pers. Comm.).

The Aswad Block is the largest ophiolite fragment within the United Arab Emirates, and measures over  $1700\text{km}^2$  in area (Lippard et al., 1986). The Aswad Block has been partly overthrust by the Khawr Fakkan Block, to the north, along the north-west trending Wadi Ham suture. The Wadi Hatta sinistral shear zone, which corresponds approximately to the border between the U.A.E and Oman, forms the boundary with the Fizh Block to the south (Nicolas et al., 2000) (Figure 2.1).

The Aswad Block is considered to have the simplest internal structure of the twelve massifs comprising the Oman-U.A.E ophiolite (Nicolas et al., 2000). It has been proposed that it should therefore represent the best analogue to a ridge segment of a fast-spreading system such as the East-Pacific Rise (Nicolas et al., 2000) (see also Figure 1.2). The block exposes the complete ophiolite sequence from the mantle section in the west, bordering the desert, to extrusive pillow basalts in the eastern coastal outcrops. The Aswad Block is unusual when compared to other blocks in the ophiolite as the Moho lies virtually horizontal in the west of the block, becoming gently easterly-dipping ( $\sim 15^\circ$  to  $25^\circ$ ) towards the coast (Figure 2.2) (Nicolas et al., 2000).

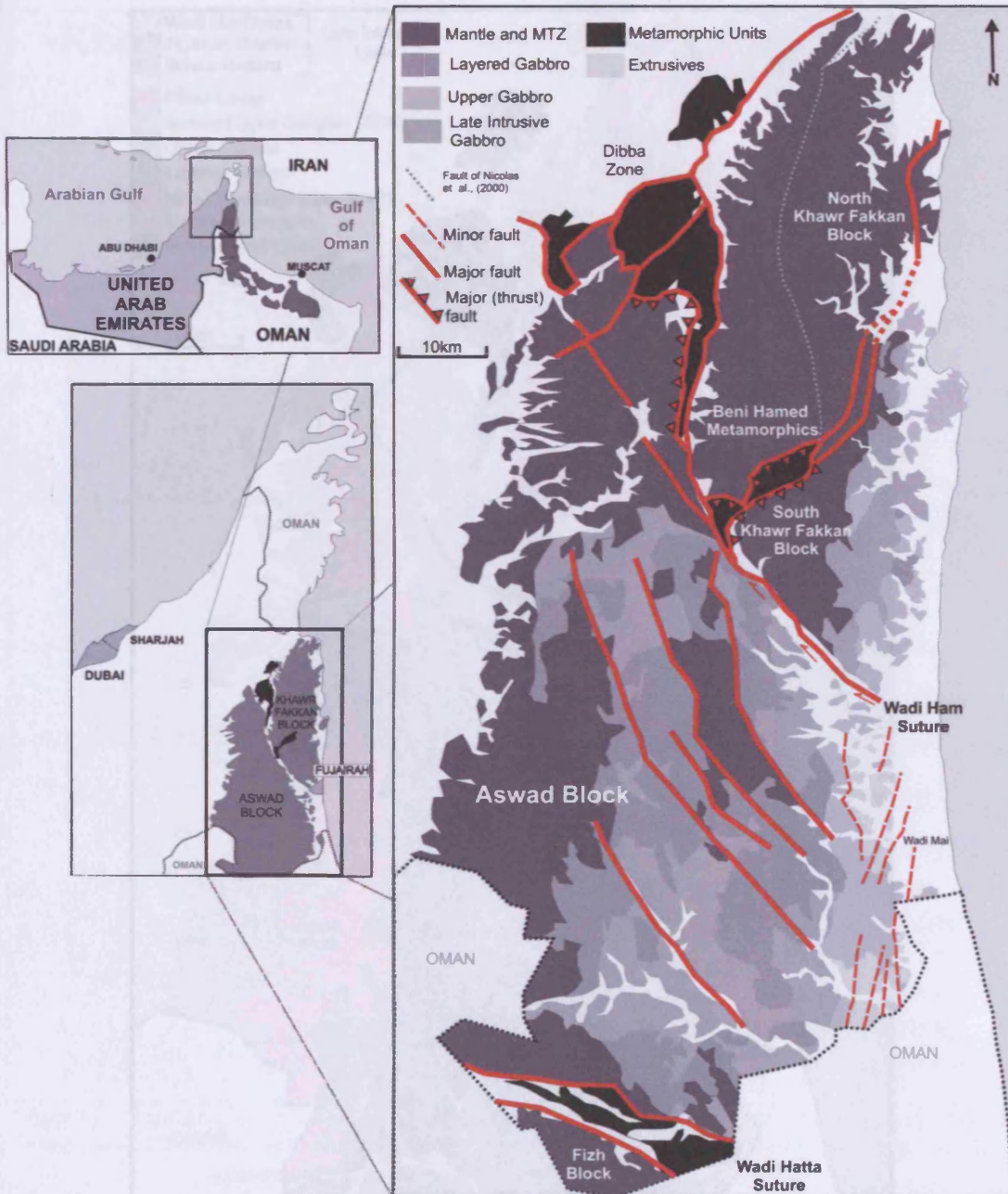


Figure 2.1, Map of location and major structures within the Khawr Fakkan and Aswad Blocks (inset: location of the blocks within the Oman-U.A.E. ophiolite). After BGS (2006); and Hunting (1985).

The Aswad Block is also divided by at least five other major, NW-SE striking, crustal-scale fault structures on ~5-10km scales (Figure 2.1). These normal, extensional, faults form horst and graben features and are associated with the intrusion of late intrusive gabbro bodies (see section 2.4.9). These NW-SE features overprint an earlier N-S system of extensional faults, on scales of 1-3km, which affect the highest stratigraphic units in the east of the block (see section 2.4.4).

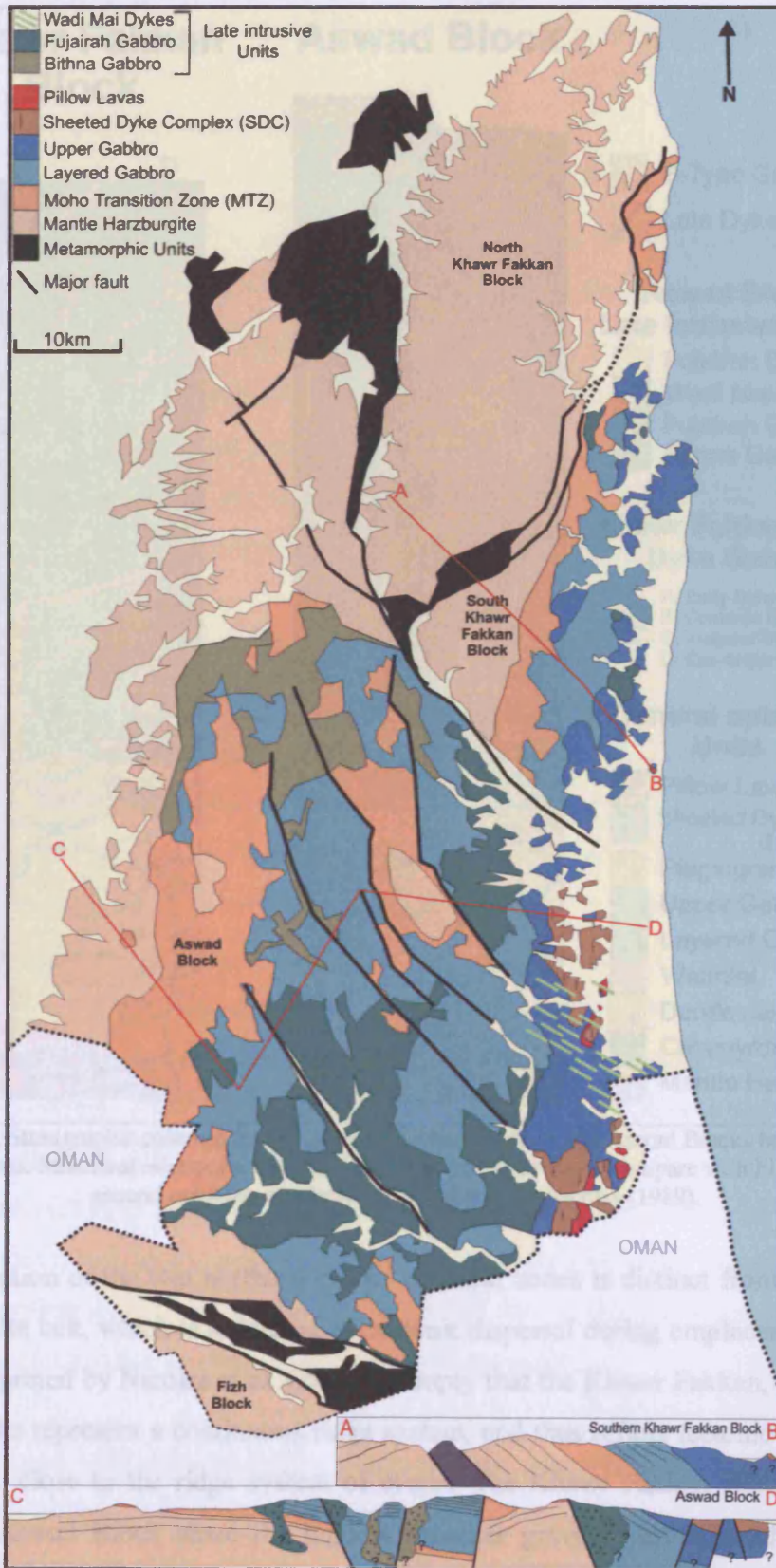


Figure 2.2. Simplified geological map of the southern Khawr Fakkan and Aswad Blocks. Inset: simplified cross-sections (not to scale), (after BGS, 2006; Hunting, 1985; Nicolas et al., 2000).

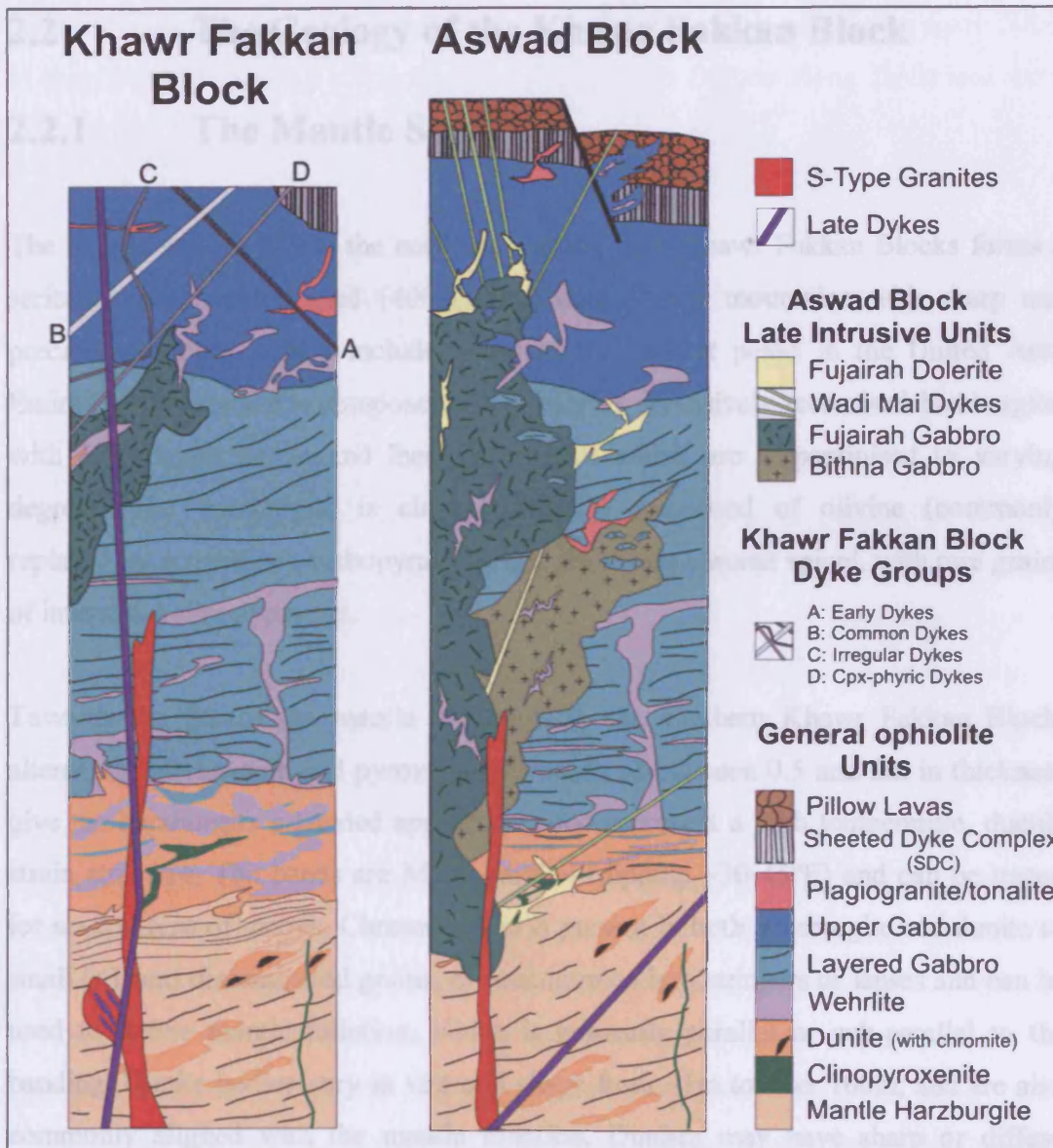


Figure 2.3. Stratigraphic columns for the (southern) Khawr Fakkan and Aswad Blocks based on field observations. Structural relations are correct, but units are not to scale. Compare with Figure 1.3 for general ophiolite stratigraphy. Modified after Nicolas (1989).

The separation of the two northern blocks by shear zones is distinct from the rest of the ophiolite belt, which is separated by tectonic dispersal during emplacement. It has been interpreted by Nicolas et al. (2000) to imply that the Khawr Fakkan, Aswad and Fizh Blocks represent a continuous ridge system, and thus reflect tectonic events that took place close to the ridge system of origin. The Khawr Fakkan Block, together with the Aswad Block share the highest Bouguer gravity anomalies of the entire ophiolite belt, with anomalies exceeding 150mgal (Ravaut et al., 1997). Gravity anomalies of this size have been interpreted to represent an ophiolite nappe thickness of approximately 10km (Nicolas et al., 2000).

## **2.2 The Geology of the Khawr Fakkan Block**

### **2.2.1 The Mantle Section**

The mantle section within the northern and southern Khawr Fakkan Blocks forms a series of steep and rugged (400-1200m) dark brown mountains with sharp and precipitous slopes, which include many of the highest peaks in the United Arab Emirates. The section is composed principally of pervasively tectonised harzburgite, with subordinate dunite and lherzolite, all of which are serpentinitised to varying degrees. The harzburgite is characteristically composed of olivine (commonly replaced by serpentine), orthopyroxene, and accessory chrome spinel, with rare grains of interstitial clinopyroxene.

Towards the top of the mantle sequence, in the southern Khawr Fakkan Block, alternating olivine-rich and pyroxene-rich bands of between 0.5 and 2m in thickness give the harzburgite a banded appearance, and represent a high temperature, ductile strain structure. The bands are Moho-parallel (dipping ~30-45°E) and can be traced for several tens of metres. Chrome spinel is present in both harzburgite and dunite as small (<1mm) disseminated grains, or concentrated into stringers or lenses and can be used to define mantle foliation, which is generally parallel or sub-parallel to the banding. Dunite bodies vary in size and shape from ~1m to over 100m, and are also commonly aligned with the mantle foliation. Dunites may have sharp or diffuse margins, and rarely form anastomosing networks, comprising veins and channels of variable size. Dunites increase in abundance up-section towards the MTZ. Chromite bodies large enough to be economically viable have recently been worked at several locations within dunites of the mantle section of the northern and southern Khawr Fakkan Blocks, though no mining is currently in operation.

The mantle and MTZ are intruded by numerous, but volumetrically insignificant, thin (<1m), undeformed, pyroxenite dykes with sharp, intrusive contacts, which cut the harzburgite foliation. The dykes are usually composed entirely of coarse-grained pyroxene, with occasional olivine and chrome spinel grains and are thought to have intruded into a cooling mantle section (Nicolas et al., 2000). The mantle is also

intruded by numerous, small, emplacement-related 'S' type granite bodies up to 500m in length (S.A.G.S, 2001) (Figure 2.3). The granites intrude along faults and were injected into a cooled mantle.

## **2.2.2 Moho Transition Zone (MTZ)**

The MTZ is particularly well developed in the southern Khawr Fakkan Block, and is up to ~1km thick in places (Figure 2.2 and 2.3). The MTZ is principally composed of mixed dunite, wehrlite and gabbroic lenses, with sharp and gradational contacts between the compositionally similar rocks. Where gradational contacts exist between dunites, wehrlites and gabbro lenses it is common for plagioclase and/or clinopyroxene to have diffuse contacts with the host rock, indicating a certain amount of impregnation of the country rock. Impregnation of different mineral phases leads to areas of undifferentiated and heterogeneous ultramafic rock types (Figure 2.4).

Troctolite is present in the MTZ of the southern Khawr Fakkan Block in the area of Wadi Sahana. The presence of troctolite is noteworthy as its occurrence requires the crystallisation sequence olivine-plagioclase-clinopyroxene, typical of the MORB crystallisation pattern. Wehrlites, part of the crystallisation sequence; olivine-clinopyroxene-plagioclase, are also very common within the MTZ and lower crust, providing evidence for the existence of a melt distinctly different from MORB. Mutually-intrusive relationships between troctolites and wehrlites within the MTZ of the southern Khawr Fakkan Block (e.g. Figure 2.4) provide evidence for the simultaneous presence of at least two distinct melt types.

Dunites are observed principally as pods or lenses of varying size and shape, up to several kilometres in length, with accessory chromite as disseminated crystals or accumulations of up to several metres in length. Gabbroic lenses within the dunites and wehrlites are also a common feature of the MTZ. The commonly cusped lenses are up to 10m in length, and 2m width, and are often plastically-deformed parallel to the Moho. Contacts between the gabbro and surrounding rocks can be sharp or diffuse.

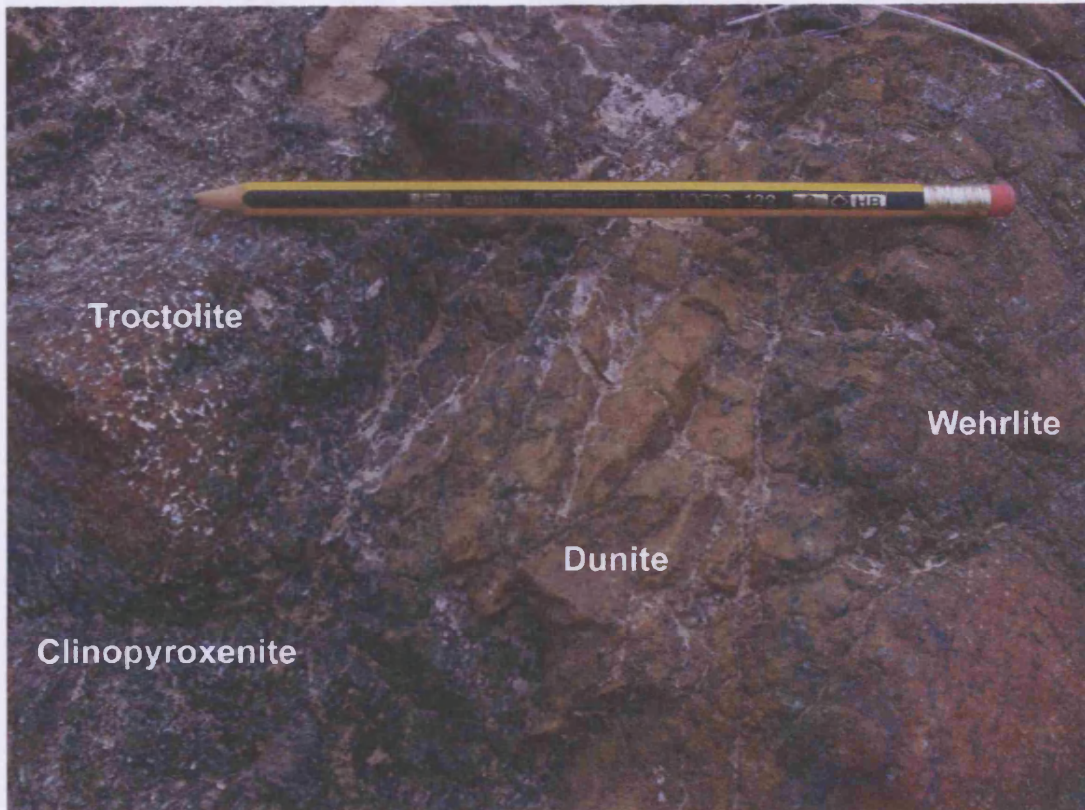


Figure 2.4, Small scale diffuse contacts between different ultramafic rock types within the MTZ of the southern Khawr Fakkan Block indicating the presence of multiple melt groups. (pencil length 15cm).

Following the arguments presented by Nicolas et al. (1988) and Nicolas and Boudier (2000), the 'thick' MTZ of the southern Khawr Fakkan Block is thought to correspond to an area of upwelling mantle. Such thickness combined with steepening foliations and lineation measurements in mantle harzburgites led Nicolas et al. (1988) to propose the presence of a mantle diapir (termed the '*El Sharawaddi*' diapir) within the northern Khawr Fakkan Block (see Figure 1.5). The evidence used by Nicolas et al. (1988) for the presence of a mantle diapir used mantle foliation measurements from both the northern and southern Khawr Fakkan Blocks, and also relied on the presence of a thick MTZ within the southern Khawr Fakkan Block without recognising the faults separating the two blocks. The proposed diapir, sited in the northern Khawr Fakkan Block, is based on invalid evidence. The presence of a thick MTZ in the southern Khawr Fakkan Block, however, indicates the presence of an area of upwelling mantle, but more evidence is required to confirm this as a mantle diapir.

### 2.2.3 Layered Gabbros

Layered Gabbros are only encountered in the southern Khawr Fakkan Block, and reach thicknesses of up to 4km. The series forms rugged mountains of similar height to the mantle sequence. The slopes are generally covered in distinctive, large, rounded blocks of scree that has been termed '*tombstone weathering*' (R.Thomas, pers. comm.). All gabbroic exposures are covered with a 1-3mm thick red/brown oxidation crust ('*desert varnish*'), which can obscure some structural details.

The rhythmically layered gabbros, on scales of ~10cm to 2m, can be distinguished by variations in grain size and/or mineralogy between the principal constituent minerals of plagioclase, clinopyroxene and olivine. Individual layers may be ultramafic to anorthositic in composition and can be traced for between tens of metres and hundreds of metres, though they are invariably truncated or pinch out. Various macroscopic ductile deformation structures, such as folding, cross-bedding and boudinage, have been observed within the Layered Gabbros. Such structures provide evidence for sub-solidus post-formation magmatic deformation of the layers. Layering at the base of the unit is less well developed than in the main part of the unit, and while generally Moho parallel, can vary up to  $\pm 20^\circ$  within short distances. Foliation and lineation are generally weak to moderate and are parallel to the layering.

Ultramafic layers (wehrlite/melagabbro) are very common at the base of the Unit and the frequency of such units lessens up-section. Wehrlites can intrude the Layered Gabbro sequence concordantly, as sill-like intrusions, or discordantly, cross-cutting existing layers. Individual wehrlitic layers have been observed intruding concordantly, before switching between layers and continuing to intrude concordantly, and can also include patches (<10cm to ~10m) of dunitic composition. Layering is less well developed in areas with a greater presence of wehrlitic/ultramafic intrusions, which are thought to root in the MTZ (e.g. Juteau et al., 1988; Benn et al., 1988 and Jousselin and Nicolas, 2000). Such ultramafic intrusions commonly share the 'impregnated' textures common to MTZ rocks. Wehrlites (which constitute the majority of the intrusions) are composed



predominantly of a serpentinised olivine-rich matrix with varying proportions of clinopyroxene, rare interstitial plagioclase, and accessory chrome spinel.

The transition from Layered Gabbro to the Upper Gabbros is gradational over several hundred meters and involves an increasing irregularity of layer orientation before layering ceases, initially interspersed with areas of layer-parallel foliations and continuing up-section to be replaced by irregular, but generally Moho-perpendicular foliation and lineation of the Upper Gabbros.

## 2.2.4 Upper Gabbro

Upper Gabbros only outcrop in the southern Khawr Fakkan Block, and consist of varied foliated, isotropic and varitextured gabbros of the upper crustal sequence. The highest stratigraphic levels are found in the east of the block, close to the town of Mirbah, where they form dark-brown coastal hills. Varitextured gabbros generally weather to form undulating hills covered in dark, rounded boulders, whereas foliated gabbros weather to produce steep hills with pale-brown, angular scree.

The Upper Gabbros are composed largely of medium-grained (1-5mm), equigranular, unaltered zoned plagioclase and clinopyroxene (augite), altered or partly altered to amphibole (actinolite-hornblende). Widespread amphibolisation is especially common in the upper sequence, where clusters of green amphibole form distinctive 'spotty' textures. Olivine-free gabbros predominate higher in the sequence, but olivine gabbros are sometimes present at the highest stratigraphic outcrops, with subhedral olivine grains commonly partially or completely replaced by secondary phases such as serpentinite or magnetite.

Within the uppermost stratigraphic levels of the Upper Gabbro, varitextured, ophitic, gabbro is common. Grain size can vary from microgabbroic to pegmatitic over several centimetres and is commonly associated with leucogabbros and tonalites. Pegmatitic segregation patches are also common in all Upper Gabbros and can have diffuse, gradational or sharp contacts with the host gabbro.

Foliations are distinguished by planar alignment of the constituent minerals, particularly plagioclase, and can be highly pronounced but are typically irregular and discontinuous in orientation. Such foliations are not generally laterally continuous, even across individual outcrops on a sub-metre scale. Patches of isotropic and varitextured gabbro have been observed with foliations contoured around them. Irregular wispy-layering of minor modal variations has been noted in several locations of the Upper Gabbro associated with pegmatite segregations. Such irregular layering takes place on scales of ~2cm to 1m, and is not accompanied by parallel foliations or lineations. Individual layers are not laterally continuous and cannot be traced for more than a maximum distance of 10m, illustrating their localised nature. Such 'wispy-layering' illustrates that there is certainly more than one method of forming 'Layered Gabbro', possibly including physio-chemical reaction processes.

The Upper Gabbro is intruded at all levels by irregularly-shaped wehrlite bodies up to 100m in diameter. Wehrlitic bodies are more common towards the base of the unit and often contain xenoliths of the host gabbro, which sometimes exhibit relic foliation or a variable texture.

Deformation zones have been identified within the Upper Gabbro, normally at ~1m scale, steeply dipping (over 60°) shear bands trending NE-SW. Brittle shear zones have associated chloritisation from circulating hydrothermal fluids. Ductile, mylonitic shear zones display amphibolite- to greenschist-facies alteration assemblages and pre-date the intrusion of most of the dyke phases (see section 2.2.7).

The highest stratigraphic levels of the Upper Gabbro are characterised by dyke swarms constituting up to 50% of outcrop over a 100m section. Several phases of dykes have been identified by cross-cutting relationships (see section 2.2.7). Within the densest dyke swarms rare, mutually-chilled, dyke margins have been observed with thin gabbro screens between dykes indicating the proximal location of the dyke root zone, as observed by MacLeod and Rothery (1992).

### **2.2.5 Late Intrusive Gabbros**

The Layered and Upper Gabbros are intruded in several locations by late intrusive gabbros (Figure 2.2 and 2.3). The intrusive gabbros are generally fine-grained and commonly have an emplacement-related magmatic foliation (vertical to sub-vertical) proximal to the contacts with the Upper Gabbro. A single late intrusive gabbro pegmatite is observed at the base of the Layered Gabbro sequence, close to Khawr Fakkan town, and is associated with wehrlites and intrusive dunite. The contacts between the late intrusive gabbros and the Upper Gabbro can be sharp or diffuse but are rarely chilled. The late intrusive gabbros are associated with, and intruded by, contemporaneous wehrlites and microgabbro dykes. The presence of late intrusive gabbros provides firm evidence for multiple magmatic events in the Khawr Fakkan Block. Petrographically the late intrusive gabbros consist of fine-grained plagioclase laths, with subhedral clinopyroxene almost completely altered to amphibole. Fe-Ti oxide grains are a common accessory phase and no orthopyroxene has been observed; this could be the result of the pervasive alteration to amphibole throughout the intrusions and is consistent with active hydrothermal circulation systems at the time of intrusion. The late gabbro pegmatite does not display evidence of hydrothermal alteration, possibly due to the later timing and depth of its intrusion compared to the other late intrusive gabbros. Due to their limited size and the abundance of wehrlites associated with these intrusions they can be interpreted to correspond to the second group (Opx-series) of late intrusive complexes as identified by Browning and Smewing, (1982), and could represent discrete high-level magma chambers.

### **2.2.6 Sheeted Dyke Complex (SDC)**

A single small outcrop of relic SDC has been identified in the southern Khawr Fakkan Block, close to Fujairah port (although its location in a quarry does not bode well for its continued existence). The lone outcrop consists of a 30m section of parallel, mutually-chilled, near-vertical dykes which strike at  $\sim 106^\circ$ . The relic SDC has been intruded and surrounded by the Upper Gabbro. Contacts with the enclosing gabbro can be sharp or diffuse with stringer veins of varitextured gabbro commonly intruding

the SDC for up to 50cm. The SDC and gabbro are both intruded by a 40cm-thick, pale-coloured clinopyroxene-phyric microgabbro dyke, with well formed chilled margins, striking perpendicular to the SDC dykes.

## **2.2.7 Khawr Fakkan Dyke Groups**

The highest stratigraphic levels of the Upper Gabbro are intruded by dykes that represent distinct magmatic events. Different dyke phases can be identified by cross-cutting relationships and, in the absence of these, strike, width and texture can be used to discriminate dyke groups. Despite these criteria, some dykes cannot be distinguished by field criteria alone and geochemical methods have been used to discriminate the dykes (Chapter 3). Secondary alteration is ubiquitous within the Khawr Fakkan Dyke Groups, with amphibole, epidote and chlorite being the main replacement minerals. Figure 2.5A and B display observed dyke relationships and presents stereonet plots which illustrate the principal (extensional) stress planes present at the time of the injection of each dyke group.

### **2.2.7.1 Early Dykes**

The Early Dykes are the oldest group of dykes in the Upper Gabbro and are cut by all other dyke groups. They are most commonly encountered in the highest exposed stratigraphic levels of the crustal sequence, in the extreme south of the Massif, close to the city of Fujairah. They are easily distinguished by their N-S strike, dark grey/black colour, narrow width (<20cm to ~1m) and generally fine-grained basaltic texture. The dykes consist of plagioclase microlaths and amphibolitised clinopyroxenes, and sometimes contain relic plagioclase phenocrysts up to 5mm in length. The dykes chill against the host gabbro and are the only dyke group that is affected by ductile shear zones that are common in the highest stratigraphic levels of the upper gabbro. Sheared dykes have been observed intruded by later dykes (Figure 2.5A), indicating that the ductile shearing event(s) occurred prior to the intrusion of the subsequent dyke phases.

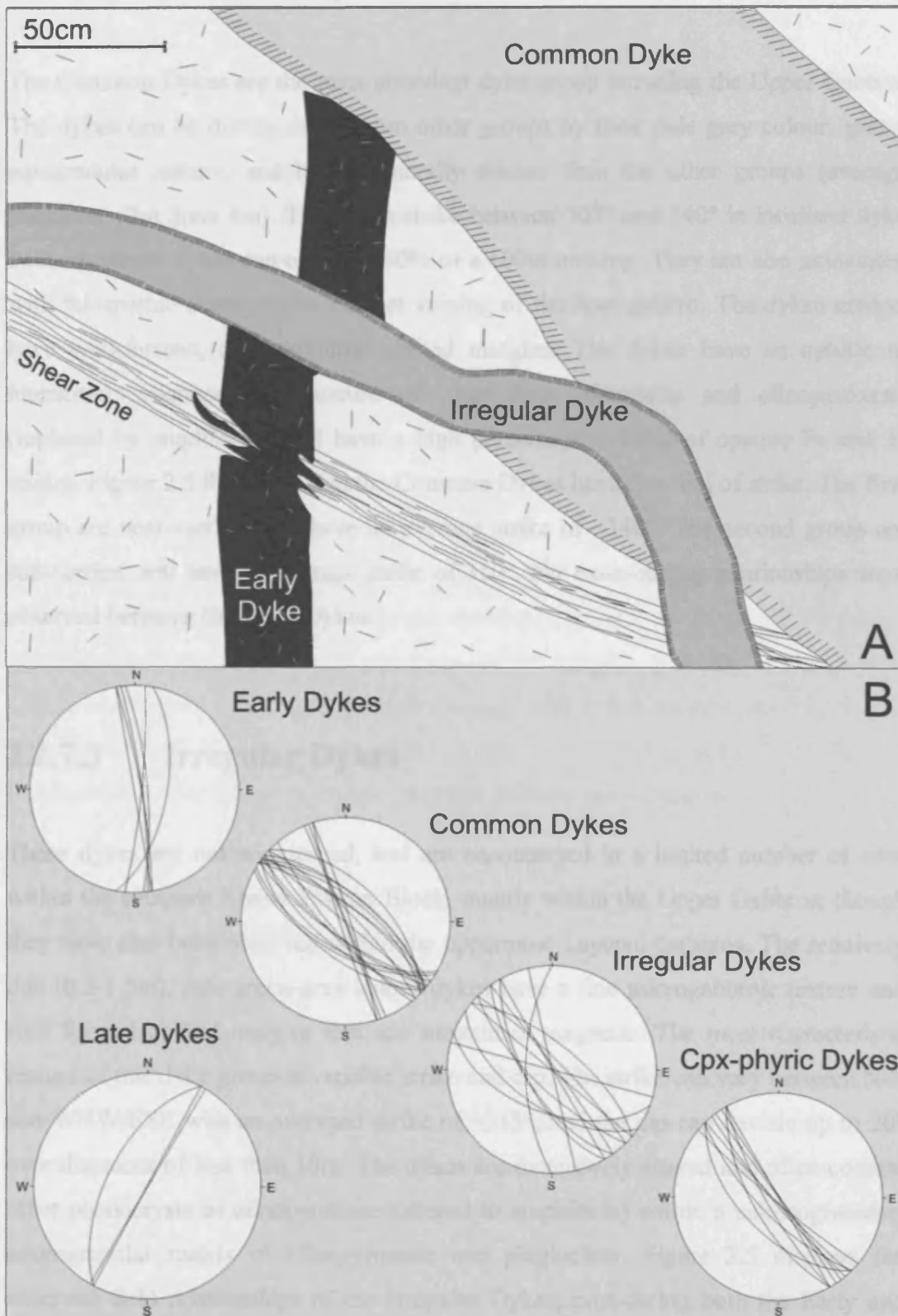


Figure 2.5, A: Field sketch of observed cross-cutting relationships between dykes in the Upper Gabbro of the Khawr Fakkan Block. The sheared, basaltic-textured, Early Dyke is intruded by microgabbro-textured, Common Dyke. All features are then cut by an Irregular Dyke. B: Stereonet diagrams display strike and dip of selected dykes for each dyke group. The data is consistent with dyke intrusion during easterly rotation of the crust (e.g. Perrin et al., 1994, 2000).

### **2.2.7.2 Common Dykes**

The Common Dykes are the most abundant dyke group intruding the Upper Gabbro. The dykes can be distinguished from other groups by their pale grey colour, gritty, equigranular texture, and being generally thicker than the other groups (average thickness ~2m, max 4m). The dykes strike between 305° and 340° in localised dyke swarms, where dykes can occupy ~50% of a 100m outcrop. They are also associated with feldspathic segregations and net veining of the host gabbro. The dykes always have well-formed, dark coloured chilled margins. The dykes have an ophitic to interstitial, microgabbroic texture of plagioclase microlaths and clinopyroxene (replaced by amphibole), and have a high percentage (~10%) of opaque Fe and Ti oxides. Figure 2.5 illustrates that the Common Dykes have two foci of strike. The first group are near-vertical and have an average strike of ~340°. The second group are sub-vertical and have an average strike of 310°. No cross-cutting relationships were observed between Common Dykes.

### **2.2.7.3 Irregular Dykes**

These dykes are not widespread, and are encountered in a limited number of sites within the southern Khawr Fakkan Block, mainly within the Upper Gabbros, though they have also been observed within the uppermost Layered Gabbros. The relatively thin (0.2-1.5m), pale green-grey colour dykes have a fine microgabbroic texture and well formed chilled margins that are sometimes magnetic. The most characteristic feature of this dyke group is variable strike and dip. The strike can vary between N-S and WNW-ESE with an averaged strike of ~315°, and the dip can deviate up to 20° over distances of less than 10m. The dykes are extensively altered and often contain relict phenocrysts of clinopyroxene (altered to amphibole) within a sub-isogranular-microgranular matrix of clinopyroxene and plagioclase. Figure 2.5 displays the observed field relationships of the Irregular Dykes, post-dating both the Early and Common Dykes.

#### **2.2.7.4 Clinopyroxene-phyric Dykes**

The Clinopyroxene-phyric (Cpx-phyric) dykes were initially discriminated in the field by the presence of clinopyroxene phenocrysts in a fine microgabbro matrix, and are present throughout the southern Khawr Fakkan upper crust with a WNW-ESE strike. The 0.7m to 1.8m dykes weather to a distinctive pale green colour and often coarsen in their centre. Occasional small xenoliths of host gabbro can be seen in the dyke margins. Thin (<30cm), basaltic texture stringer veins sourced from the main dykes are a common feature of this dyke group. Some dykes preserve a strong flow fabric of aligned plagioclase laths in an interstitial matrix of amphibolitised clinopyroxene. Secondary carbonate and quartz veins are also common, denoting active hydrothermal systems during their intrusion.

The Cpx-phyric Dykes are associated with the late intrusive gabbros and wehrlites within the Upper Gabbro. The dykes are observed intruding the late intrusive gabbro and associated wehrlites, but do not form chilled margins. Cpx-phyric Dykes have also been recorded intruding contemporaneously with wehrlites, evidenced by ductile deformation and the absence of chilled margins, providing evidence for a time of emplacement close to that of the late intrusive gabbros and wehrlites.

#### **2.2.7.5 Late Dykes**

This final dyke group has been identified by the presence of several near-vertical, E-W striking, 2-3m thick, microgabbro-textured dykes. The fine-grained microgabbro dykes, which can contain up to 40% plagioclase phenocrysts, intrude and chill against all units of the ophiolite from several kilometres into the mantle section, to the Upper Gabbro. This demonstrates that the dykes intruded a cool ophiolite section a significant time period after most crustal accretion processes had ceased. These dykes are volumetrically the least significant and are associated with contemporaneous felsic (granitoid) intrusions (Figure 2.3). Mixing between the basic dykes and felsic bodies has resulted in hybrid intrusions in some locations of the Khawr Fakkan Block. Figure 2.5 displays the strike of the sampled Late Dykes in the Khawr Fakkan Block,

illustrating that the strike of this dyke group is considerably different to the other groups and providing evidence for a time of intrusion unrelated to the other dykes.

### **2.3 Conclusions from the geology of the Khawr Fakkan Block**

- Coexisting troctolite and wehrlite within the MTZ of the southern Khawr Fakkan Block provides evidence for the presence of at least two chemically distinct melts, one MORB-like, and the other distinctly different to MORB, such as a subduction-related melt (Pearce, 1984).
- The thick (~1km) MTZ can be interpreted as evidence for the proximal location of a zone of upwelling mantle, such as a mantle diapir.
- The presence of an SDC demonstrates extension in an oceanic setting.
- The presence of late intrusive gabbros provides evidence for multiple magmatic events in the history of the crust.
- Five dyke groups have been identified, with each group exhibiting a variation in field characteristics and strike. This can be interpreted that the different dyke groups represent distinct magmatic events. The variation in strike is consistent with tectonic rotation of the crust between dyke groups.



## **2.4 The Geology of the Aswad Block**

### **2.4.1 The Mantle Section**

The mantle section of the Aswad Block is exposed predominantly in the west of the block and forms a series of low, dark brown coloured hills on the periphery of the desert, and is known to extend further west under the Quaternary sand dunes for several kilometres (Nicolas et al., 2000). The mantle rocks are also exposed in a fault-bounded window in the centre of the block (Figure 2.1 and 2.2) and together with structural data of mantle foliation, this window has been interpreted by Nicolas et al. (2000) to represent a mantle diapir. However, the mantle window is too small, fault-controlled, and insufficiently eroded to fully support this interpretation. The window is fault-bounded on both sides and when viewed in cross-section (Figure 2.2) simply represents the eroded remains of a NW-SE striking horst structure.

The mantle section is dominantly composed of harzburgite, with minor dunite in the form of discordant veins or lenses. The primary structure comprises alternating olivine-rich and orthopyroxene-rich bands of up to 1m thick. A secondary foliation, defined by the orientation of orthopyroxene crystals and chrome spinels, is also observed, generally parallel or sub-parallel to the banding. The harzburgite is composed of 75-85% variably serpentinised, coarse-grained (2-5mm), equigranular olivine, 15-25% orthopyroxene (often with exsolution lamellae of clinopyroxene), 1-5% anhedral chrome spinel and rare grains of interstitial clinopyroxene. The mantle section is commonly cut by thin (<0.5m) undeformed dykes of coarse-grained, equigranular pyroxenite, or pegmatoidal melagabbro of varying strike. Clinopyroxene impregnations in the form of small, rounded clusters are also a common feature toward the top of the mantle section and are normally aligned parallel to the mantle foliation. Listwaenite, formed by siliceous replacement of serpentinised harzburgite, is a widespread alteration facies in the most westerly exposures and has been related to Tertiary tropical weathering (Nicolas et al., 2000).

## 2.4.2 Moho Transition Zone (MTZ)

The MTZ in the Aswad Block is less than 200m in thickness, and is sometimes as thin as 50m. It is distinguished in the field by a light brown weathering colour and the common occurrence of small caves (due to the presence of preferentially eroded dunites) which often contain bee hives. The Moho in the western part of the Aswad Block is almost flat-lying. As a result, many cuestas of between 150-300m elevations, consist of foliated harzburgite at their base, mixed MTZ rocks in the ascent, and a cap of layered gabbro at the summit; offering an excellent cross-section exposure of the transition from mantle to crust.

The MTZ is composed of heterogeneous ultramafic rocks including dunites, wehrlites and gabbroic sills and lenses. Contacts between dunites, wehrlites and gabbros can be diffuse or sharp, with interfingering and impregnation of mineral phases between rock types being widespread. The gabbro lenses and sills are easily distinguished from the host dunites and wehrlites by their bold colour of dark pyroxene and white plagioclase and their resistance to weathering compared to the more easily weathered, pale red/brown, dunites and wehrlites. The gabbroic lenses are generally thinner than those observed in the MTZ of the Khawr Fakkan Block, possibly indicating greater magmatic transposition of the MTZ in the Aswad Block. The thin ( $\leq 200\text{m}$ ) MTZ also indicates that the setting of the Aswad Block is distal to an area of upwelling mantle (Nicolas and Boudier, 2000).

Towards the top of the MTZ, it is common to see blocks of layered gabbros surrounded by wehrlite. The frequency of wehrlites at and around this stratigraphic level makes it difficult to accurately locate the Moho in most localities.

## 2.4.3 Layered Gabbros

The Layered Gabbro sequence in the Aswad block consists of Moho parallel, modally-layered gabbros marked by rugged hills ~500-700m in height. Some excellent cross-sections through the 2-3km thick sequence are located in the southern

Aswad Block, close to the Oman border. Individual layers, defined by grain size or mineralogical variations, are 0.1m to 2m thick and can be followed laterally for several tens of metres before pinching out. Interlayering of wehrlite and melagabbro sills is ubiquitous throughout the layered sequence but is especially common at the base of the unit. In thin section, the layered gabbros are principally composed of calcic plagioclase, clinopyroxene and olivine with a dominant planar adcumulate or mesocumulate texture. The gabbros followed the crystallisation sequence olivine-plagioclase-clinopyroxene.

Intrusive wehrlite and clinopyroxenite bodies, some of which contain entrained areas of dunite, cross-cut the Layered Gabbro sequence in many forms, from dykes to irregular bosses. The latter vary in size from a few metres to several hundreds of metres in extent and in some areas constitute a significant proportion of the crust. The margins of such bodies have a strong intrusion foliation and lineation. Wehrlites (which constitute the majority of the intrusions), are composed predominantly of a serpentinitised olivine-rich matrix with varying proportions of clinopyroxene (diopside), rare interstitial plagioclase, and accessory chrome spinel. Wehrlites have been recorded intruding as high as the extrusive sequence and relationships between the intrusions and hydrothermal fractures indicate that the wehrlitic mush intruded during hydrothermal alteration when the gabbro unit was at 400-500°C and still close to the ridge axis (Nicolas et al., 2000). The Layered Gabbro sequence is also intruded by at least two late intrusive gabbros (see Section 2.4.9).

The boundary between the Layered Gabbros and the Kalba Upper Gabbro (Section 2.4.4) is diffuse over a distance of several hundred metres, with the layering becoming less prominent and to be replaced with a steepening foliation.

## **2.4.4 Kalba Upper Gabbro**

The Upper Gabbro of the Aswad Block has been termed the Kalba Upper Gabbro after the largest settlement closes to the primary outcrops. The Kalba Upper Gabbro is exposed in a range of 200-300m high hills located within sight of the coast, with

boulders and scree exhibiting a typical rounded character. The Kalba Upper Gabbro consists of isotropic, foliated, and varitextured horizons, and is intruded by wehrlites, Wadi Mai Dykes (Section 2.4.7) and the late intrusive gabbros (Section 2.4.8). Wehrlites are common at the base of the Kalba Upper Gabbro where they cross-cut foliations. As noted earlier wehrlites have also been observed in the highest stratigraphic units of the Kalba Upper Gabbro, intruding as high as the SDC and extrusive sequence.

The foliated horizon is not continuous and foliations are rarely continuous for more than a few tens of metres. Commonly varying considerably on an outcrop scale. No lineations were observed in outcrop. Screens of foliated gabbro have been observed within the varitextured and isotropic gabbros. The foliated horizon is also disrupted by the presence of a late intrusive gabbro; the Fujairah Gabbro (see section 2.4.8.2)

Varitextured areas of Kalba Gabbro are characterised by a major variability in grain size, texture and fabric (Figure 2.6). Grain size can vary from microgabbroic to pegmatitic over several centimetres, exhibiting ophitic to granular texture. The contacts between such coarse and fine gabbros are irregular and can vary from sharp, intrusive contacts to diffuse, interfingering, gradational contacts. There is no evidence of chilled margins between the pegmatitic gabbros and the microgabbroic material. Plagioclase/felsic segregations are relatively common in the varitextured areas of the Kalba Upper Gabbro. Within the varitextured gabbro, clinopyroxene is commonly comprehensively altered to amphibole (actinolite or hornblende).

Cupolas of the Kalba Upper Gabbro intrude the SDC and extrusive sequence along N-S striking, extensional fault structures on 1-2km scales (Figure 2.1 and 2.2). The graben structures, proposed to have formed when extension exceeded melt supply at the ridge axis, juxtapose Kalba Gabbro, SDC and extrusives. The faults acted as the path of least resistance for cupolas of Kalba Upper Gabbro to intrude into the SDC and extrusive sequence.

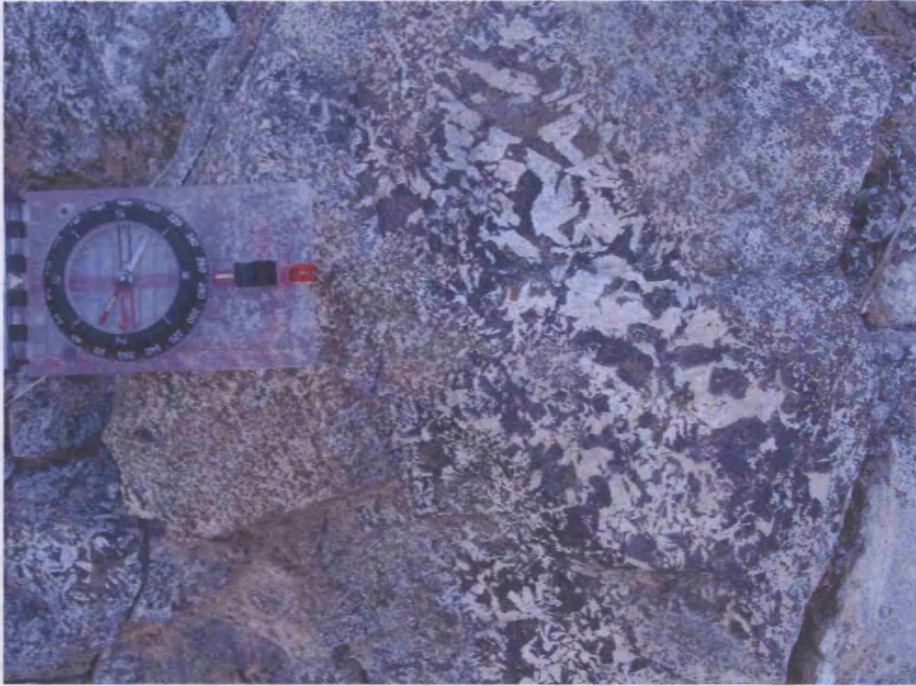


Figure 2.6, Pegmatitic segregation within a varitextured gabbro horizon in the Kalba Gabbro. Note the diffuse contact of the pegmatite and the significant variation in grain size. Compass dial is 5cm in diameter



Figure 2.7, Stringer vein from an intrusive cupola of Kalba Gabbro intruding basaltic to doleritic textured dykes of the SDC. Note the lack of chilled margins at the contact between the units.

The contacts between the cupolas and the SDC/extrusives are sharp and intrusive (see section 2.4.5), with no chilled margins being observed (Figure 2.7), although grain size of the gabbros does infrequently decrease towards the contact.

The intrusive, isotropic sections of the Kalba Upper Gabbro can be characterised by widespread recrystallisation into amphibole bearing gabbros with a typical 'spotty' texture caused by the presence of green amphibole (hornblende) often containing relicts of clinopyroxene. These intrusive sections are composed of medium-grained, ophitic, subhedral gabbro with zoned euhedral plagioclase laths (up to 60mm in length), interstitial poikilitic clinopyroxene crystals, following the crystallisation order of olivine-plagioclase-clinopyroxene. Accessory Fe-Ti oxides can constitute up to 15% of the modal proportion, with other secondary alteration minerals, including epidote and chlorite, also common in areas proximal to the intrusive gabbro and often concentrated along faults (Section 2.4.5). Finger-like pegmatitic stringer veins up to 50cm in width intrude the SDC and lavas for up to 5m away from the main contact (Figure 2.7). The areas of Kalba gabbro that intrude the SDC and extrusive sequence are intruded by Wadi Mai Dykes, which chill on contact with the gabbro, demonstrating that the gabbro was cool at the time of Wadi Mai Dyke injection (Section 2.4.7).

## **2.4.5 Sheeted Dyke Complex (SDC)**

The SDC outcrops discontinuously throughout the eastern Aswad Block, interrupted by numerous faults, and weathers to typically steep-sided hills of very regular height (~50m). The SDC is formed of ~100% near-parallel, mutually intrusive microgabbro dykes of between ~25cm to 1.6m, with an average dyke width of ~1m (Figure 2.9). The dykes are dominantly vertical to sub-vertical and strike N-S (345° to 025°) (Figure 2.12). In general, there is a positive correlation between grain size and dyke thickness. Thin dykes (<0.5m) and stringer veins from larger dykes are dark-grey to black in outcrop, with basaltic textures. Dykes thicker than this tend to be pale grey/green in colour and have a grain size which generally coarsens towards their centres, increasing from basaltic at the margins to microgabbroic textures, with a

grain size of up to 1-2mm, in the centre. Chilled margins are variable and can be up to 5cm thick, but typically average around 2cm, and are defined by a decrease in grain size to a knife-sharp contact.

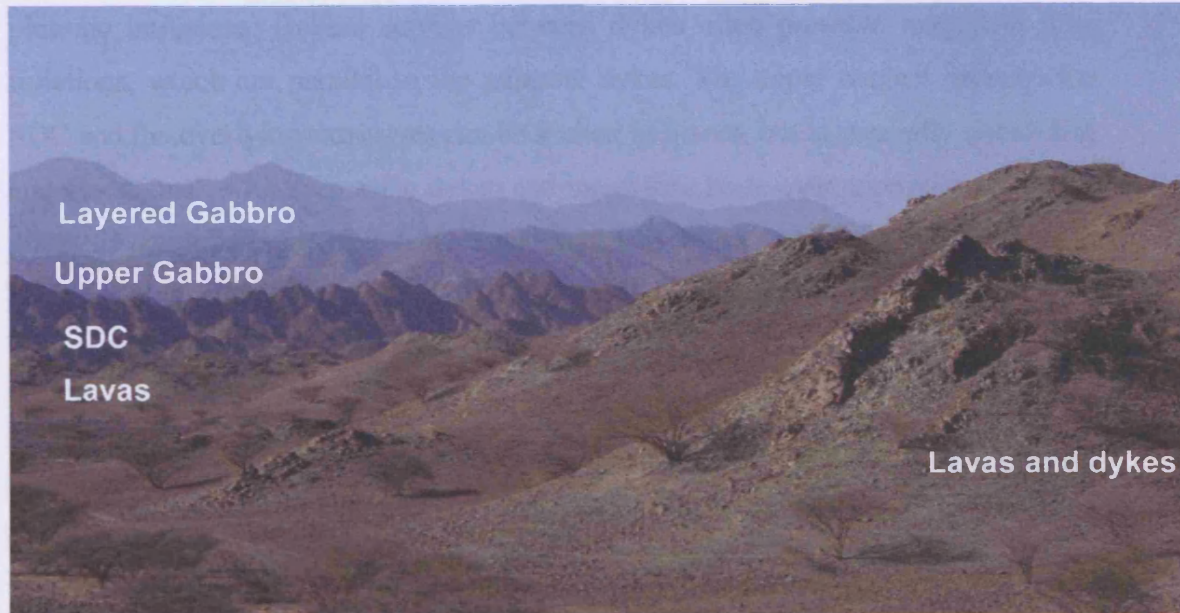


Figure 2.8, View from the Oman border looking NW over the southernmost Aswad Block. Note the distinctive topography of each of the ophiolite units and abundant feeder dykes cutting the lowermost lavas in the foreground.

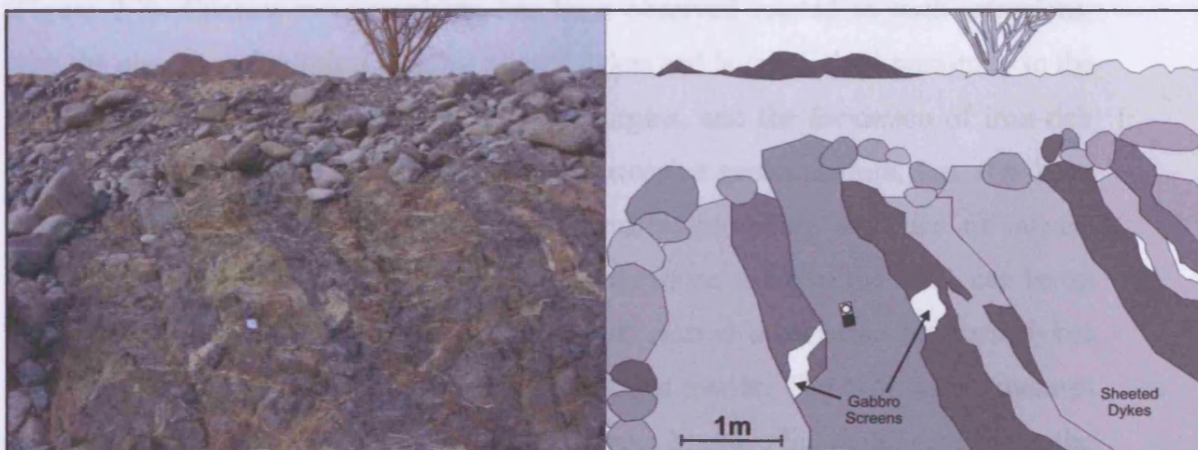


Figure 2.9, Photo and sketch of polished wadi-floor exposure ~100% sheeted dykes. Note the different dyke colours, caused by variations in grain size and degrees of alteration, and the pale gabbroic screens between dykes.

At the upper and lower contacts of the SDC, the nearly 100% sheeted nature gives way to lavas and gabbros respectively. The lower contact between the SDC and the Kalba Upper Gabbro is marked by an increasing frequency of gabbroic screens between dykes. The dyke root zone, as described by MacLeod and Rothery (1992), is not directly observed in the Aswad Block as it is obscured by either faulting or later plutonic intrusions. Gabbro screens between dykes often preserve magmatic flow foliations, which are parallel to the adjacent dykes. The upper contact between the SDC and the overlying extrusives can be faulted in places, but is generally undulating and gradational, with decreasing dykes and increasing lavas over approximately 20 to 100m. Dykes of SDC strike, texture and width have been observed intruding lavas higher than this boundary and are presumed to be feeder dykes for lavas higher in the sequence (Figure 2.8 and 2.11).

Petrographically, the dykes of the SDC have equigranular, medium to fine-grained, ophitic, sub-ophitic and intergranular doleritic textures. The main constituent minerals are plagioclase, as both zoned and unzoned microlaths, interstitial green amphibole (hornblende-actinolite) replacing clinopyroxene, and accessory, opaque Fe-Ti oxides. Hydrothermal alteration of the dykes has led to extensive epidotisation, especially along dyke margins. Other alteration phases include quartz, chlorite and carbonate.

The SDC is intruded by the Kalba Upper Gabbro with sharp, interfingering contacts (Figure 2.7). Contact metamorphism has been observed related to such intrusions, with the presence of hornfels in some altered dykes and lavas in close proximity to the intrusions. Silicification of dykes and dyke margins, and the formation of iron-rich gossans with Cu and Fe oxide staining and extensive green epidote, has also been observed associated with the N-S fault structures, providing evidence of intense hydrothermal circulation. Silicified veins, with the same strike as the SDC, can be up to 1m thick and can preserve evidence of fault related brecciation between dykes producing basaltic-textured fragments in a siliceous matrix. The N-S fault structures offer the best potential for economic (Volcanogenic Massive Sulphide) deposits in the U.A.E.



## 2.4.6 The Extrusive Sequence

The extrusive sequence of the Aswad block consists of pillow lavas and lava flows, and outcrops in several areas as low (<10m), extensively weathered outcrops contained within the gypsiferous sabka plains adjacent to the coast. Individual pillows vary from reddish-brown to light green in colour and are of regular shape, in the order of 1m diameter, and commonly elongate (Figure 2.10). Classic slump-shapes and lobe-forms can be observed, providing evidence for an inclination to the palaeotopography. Pillows are interspersed with 0.5-2m thick sheet flows, with distinctive rubbly textures to their upper surfaces. Devitrified rind structures can clearly be seen on many pillows but no fresh glassy rinds have survived the sea-floor brownstone weathering. Hyaloclastite is a common feature filling inter-pillow spaces together with occasional red jasper and scarce secondary copper minerals. Where alteration has obscured original pillow shapes, the presence of such inter-pillow features is a useful facies indicator.

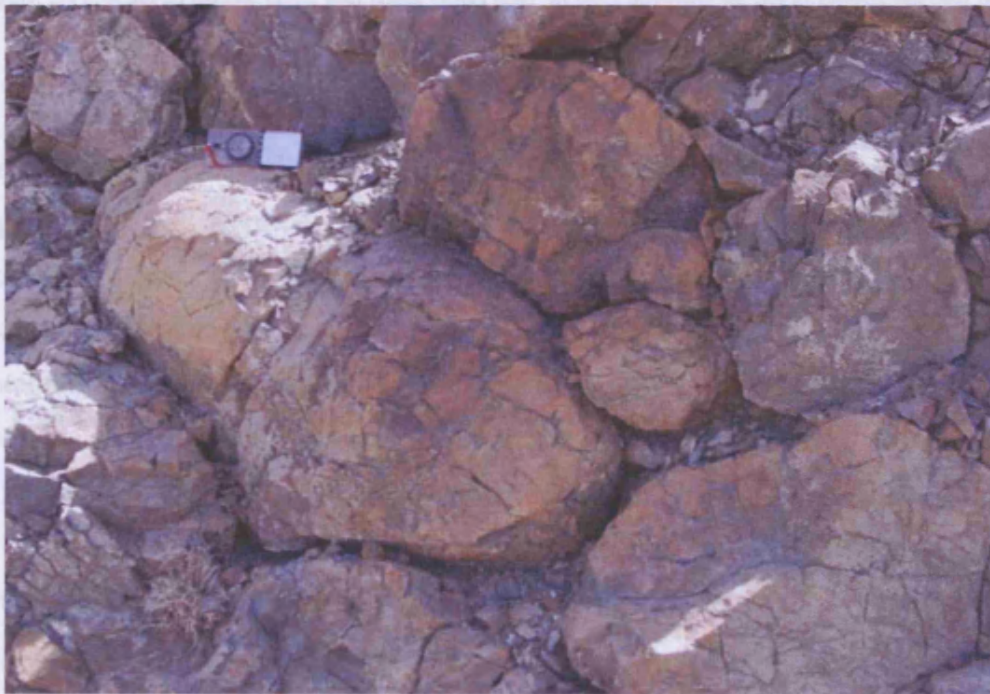


Figure 2.10, Classic pillow lavas (~1m diameter) preserved in the extrusive sequence of the Aswad Block, close to the Oman border. Note the slump-shapes providing a way-up indicator.

In thin section, the lavas have microlitic to microporphyritic textures. The primary minerals consist mainly of plagioclase as albitised microlaths and microphenocrysts and clinopyroxene as amphibolised relict microphenocrysts. The devitrified groundmass consists of an association of clay minerals, chlorite, albite, iron oxide granules (magnetite and/or haematite) as well as quartz, carbonate and zeolite facies minerals.

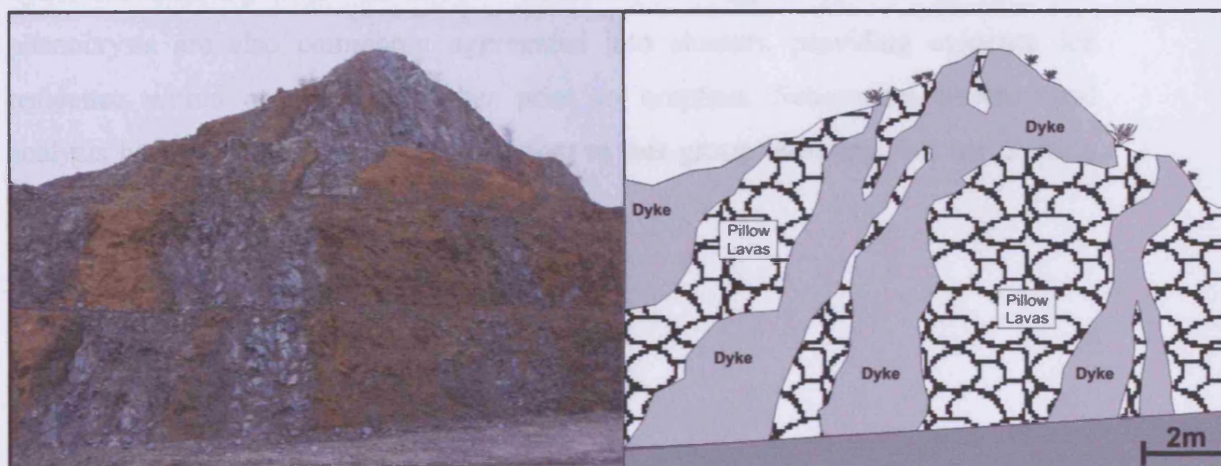


Figure 2.11, Altered pillow lavas and sheet flows (red, at left) intruded by dykes (grey) feeding upper lavas

The extrusive sequence has been intruded in many locations by dykes of the SDC (Figure 2.11) and Wadi Mai Dykes (see Section 2.4.7 and Figure 2.12). The ~1m thick SDC dykes can be distinguished by their fine grain size and N-S strike. The basalts are also intruded in several locations by the Kalba Upper Gabbro, locally containing basaltic xenoliths and scarce chilled margins. Interfingering of both units is common, often making it unclear which unit has intruded the other. The contact is also associated with extensive epidotisation, rare hornfels, and common fracturing of the basalt, with gabbroic to pegmatitic texture stringers intruding the basalt for up to several metres away from the contact (Figure 2.7).

The field evidence from the extrusives observed in the Aswad Block are consistent with the interpretation that they all represent the (lowermost) Geotimes Unit as observed in Oman.

### **2.4.7 Intermediate Dykes**

The Kalba Upper Gabbro, SDC, and extrusive sequence are intruded in several locations by SDC-parallel (N-S striking) dykes with a distinctive dark/black colour and up to 1m in width. The dykes have a fine basaltic texture, and contain abundant pale phenocrysts of plagioclase and clinopyroxene, up to 10mm in diameter. The dykes are relatively fresh with limited alteration of clinopyroxene to amphibole. The phenocrysts are also commonly aggregated into clusters, providing evidence for residence within a magma chamber prior to eruption. Subsequent geochemical analysis has also identified dykes belonging to this group intruding, but not chilling against, the Bithna Gabbro (Section 2.4.9.1).

### **2.4.8 Wadi Mai Dykes**

The Wadi Mai Dyke swarm is concentrated in a NW-SE striking, 2-3km wide, zone centring on Wadi Mai in the central-eastern part of the Aswad Block, forming an eastern extension of one of the main NW-trending crustal scale faults (Figure 2.1 and 2.2). The absence of this phase of dykes from areas away from this fault-controlled area has led to their interpretation as a dyke swarm associated with 'seamount' volcanism. The distinctive dykes are between 2-5m in width and have a granular microgabbro texture with well-formed chilled margins, up to 5cm in thickness. The dykes are more resistant to weathering than the SDC and extrusives, and commonly form pronounced ridges when intruding these units (Figure 2. 8 and 2.12A). In thin section the fine-grained (~1mm) microgabbroic texture is composed of intergranular to sub-ophitic laths of plagioclase, interstitial clinopyroxene (augite), between 5-10% quartz, opaque minerals (including Fe-Ti oxides), and alteration minerals such as epidote and chlorite.

The dykes have a typical, if somewhat variable, NW-SE (strike ~290° to 310°) trend and are steeply dipping (80° ± 10°) (Figure 2.12B). The trend of the dyke swarm becomes more E-W in the southern outcrops and have been observed deflecting strike when intruding wehrlites within the Kalba Gabbro.

The source of the Mai Dykes was not established during fieldwork. The dykes clearly post-date the Kalba Gabbro, but are commonly truncated by the intrusive Fujairah Dolerite (2.4.9.2).

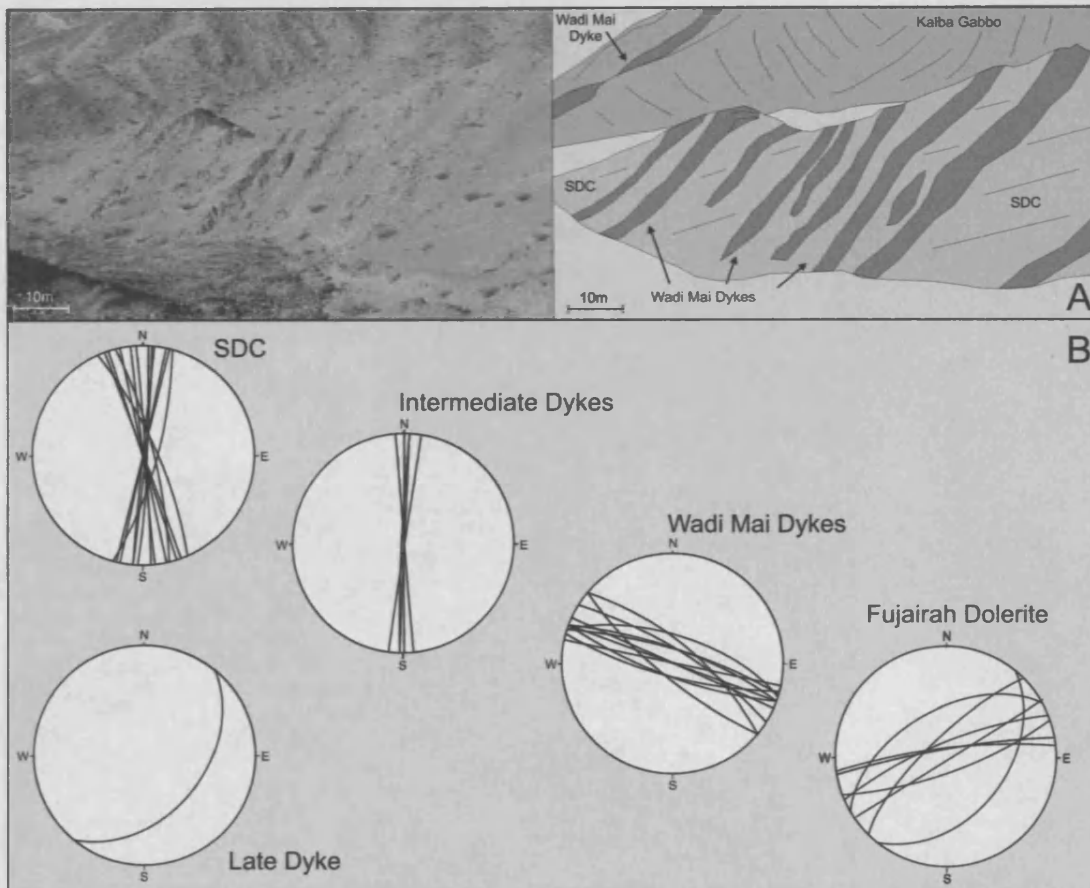


Figure 2.12A, Wadi Mai Dykes intruding SDC and Kalba Gabbro. Note the density of near-parallel dykes on the ridge and the typical resistant nature of the dykes, B: Stereonet plots showing the strike of the SDC, Wadi Mai, Fujairah Dolerite and Late Dyke magmatic phases (compare with Figure 2.5).

## 2.4.9 Late Intrusive Gabbros

Within the crustal section of the Aswad Block, two distinct late intrusive gabbros have been identified. These large plutonic gabbros cross-cut the stratigraphy and represent discrete off-axis melt supply to the crust after 'normal' mid-ocean ridge processes have ceased (e.g. Alabaster et al., 1982). The gabbros are associated with a series of NW-SE striking crustal scale faults (Figure 2.1), which represent horst and graben structures that post-date the initial magmatic period of the crust (which

accreted the Layered Gabbro, Kalba Upper Gabbro, SDC and observed extrusives). The NW-SE structures represent an apparent rotation of the principal (SDC) extension direction anticlockwise by  $\sim 40^\circ$  and correspond to the rifting event of Alabaster et al. (1982).

These plutonic gabbro bodies probably represent off-axis magma chambers that fed upper extrusive units. Both intrusions are associated with, and intruded by, small wehrlitic intrusions that correspond to the second group of intrusions identified by Browning and Smewing, (1982).

### **2.4.9.1 Bithna Gabbro**

The Bithna Gabbro is located in the north-west of the Aswad Block (Figure 2.2) and is associated with NW-SE trending crustal scale faults (Figure 2.2 and 2.3). The Bithna Gabbro predominantly intrudes the Layered Gabbro sequence. The gabbro is typically medium to coarse grained, with grain size commonly varying over short distances, and always includes a fine-microgabbroic phase. The uppermost stratigraphic outcrop of this gabbro commonly includes large ( $\sim 2$  to 20m) xenolith 'rafts' of layered gabbro. Associated with the layered gabbro xenoliths are concentrations of coarse pegmatitic and tonalitic patches, indicating the presence of volatiles, that may have concentrated in the upper levels of a magma chamber. The tonalitic segregations tend to back-vein into the Bithna Gabbro, causing localised (brittle) brecciation. The Bithna Gabbro is intruded in several locations by the Fujairah Gabbro, providing evidence that the Bithna Gabbro pre-dates the Fujairah Gabbro (Figure 2.2 and Section 2.4.9.2). The Bithna Gabbro also preserves some localised ductile shear zones, indicating compressional forces acting on the crust during cooling (Thomas. B, pers. comm.).

The Bithna Gabbro is intruded by at least two different groups of dykes. The first group does not chill against the gabbro, and is considered to be a contemporaneous phase of magmatism, possibly feeding an extrusive unit. These N-S striking dykes are  $\sim 1$ m in thickness and have a microgabbroic texture, with occasional phenocrysts of

plagioclase and clinopyroxene. The dykes have a characteristic 'splintery' appearance and are not associated with felsic segregations. These dykes have undergone extreme hydrothermal alteration with all mineral phases altered to amphibole. Dykes from this group are included in the Intermediate Dyke group. The second group of dykes are ~2m in width, chill at their contact with the host, and have a microgabbro-texture. Subsequent geochemical investigation has revealed that these dykes belong to the Fujairah Dolerite (Section 2.4.9.2), providing evidence that the Bithna Gabbro pre-dates the Fujairah Gabbro.

The Bithna Gabbro corresponds to the Cpx-series of intrusions of Smewing (1981) and the first group of intrusions as defined by Browning and Smewing, (1982), indicating that the Bithna Gabbro could be related to the magmatic events associated with the Lasail Unit as defined in Oman.

### **2.4.9.2 Fujairah Gabbro**

The Fujairah Gabbro is a late intrusive gabbro that intrudes the Layered Gabbro, Kalba Upper Gabbro and Bithna Gabbro units, commonly along NW-SE trending fault structures, and is considerably more extensive in size than the Bithna Gabbro. It has its 'type' exposure in the north-eastern outcrops of the block, close to the city of Fujairah, but is also has extensive outcrops in the south east of the block. The Fujairah Gabbro intrudes all of the upper crustal units of the Aswad Block and commonly contains xenoliths of the Kalba Upper Gabbro, Layered Gabbro and Wadi Mai Dykes. The unit weathers to a pale colour with splintery scree and is less resistant than the host Kalba Upper Gabbro (Figure 2.13), weathering to jagged ridges rather than rounded hills. The unit has a characteristic variable texture and is closely associated with plagioclase-rich separations and impregnations. The Fujairah Gabbro can be observed intruding wehrlites and melagabbroic layers at the base of the Layered Gabbro sequence, where it surrounds large mega-xenoliths (~20m in width) of the host Layered Gabbro.



Figure 2.13, Undulating contact of the Fujairah Gabbro intruding the Kalba Upper Gabbro close to the city of Fujairah in the northernmost Aswad Block. Note the pale colour, and more angular scree characteristics of the Fujairah Gabbro when compared to the Kalba Gabbro. The field of view is approximately 150m left to right.



Figure 2.14, Detail of a typical Fujairah Dolerite 'vinaigrette' intrusion, displaying the unusual rounded magma mixing texture. Note the smooth mafic clasts, aligned with the flow direction of the dyke, within a tonalitic matrix.

The Fujairah Gabbro is predominantly fine-grained with characteristic patches of variable grain size and texture. Petrographically the gabbro is composed of plagioclase, orthopyroxene and clinopyroxene (commonly replaced by amphibole). Southern exposures display a characteristic 'spotty' texture, caused by the clustering of large subhedral amphibole crystals. The presence of orthopyroxene is strong evidence that the Fujairah Gabbro belongs to the second group of younger, Opx-series, intrusions that belong to the subduction-related suite (Browning and Smewing, 1982; Browning, 1982 and Umino, 1990) despite its much larger size than the typical (~1km) younger intrusions.

The Fujairah Gabbro is the source for a series of dykes known as the Fujairah Dolerite (Figure 2.14). The Fujairah Dolerite is commonly composed of a mixed unit of mafic microgabbro and felsic tonalite, similar to the 'net-veined complex' of Browning and Smewing, (1982), and the 'vinaigrette' texture of Juteau et al. (1988). The Fujairah Dolerite roots in the Fujairah Gabbro. It intrudes the whole ophiolite sequence, from the mantle section to the extrusives (Figure 2.3), as NW-SE striking, 1m to 15m thick dykes (Figure 2.14). The Fujairah Dolerite can also take the form of ~2m thick dolerite dykes, which often contain well-formed clinopyroxene phenocrysts.

Where Fujairah Dolerite dykes intrude the mantle sequence, chilled margins are present, demonstrating that the dykes were injected into a cooled or cooling mantle and that 'normal' mid-ocean ridge crustal accretion had probably ceased at the time of their intrusion. The mixed mafic and felsic components of the Fujairah Dolerite vary in their styles of mixing, with sharp (brittle) and gradational contacts both apparent. It is also common to see the mafic component forming rounded inclusions, which are deformed parallel with the flow direction of the dyke (Figure 2.14). The Fujairah Gabbro is the last major magmatic event in the crustal accretion history of the Aswad Block, being observably superseded only by a single Late Dyke and emplacement related granites (Figure 2.3).



### **2.4.10 Late Dyke**

A single Late Dyke was observed and sampled in the north of the Aswad Block. The ~1m thick dyke intrudes serpentinised harzburgites and dunites of the mantle section along a 3-4m wide fault zone (dip 45°SE, strike 040°). The fault zone contains brecciated harzburgite, which has been incorporated into the dyke margins as xenoliths, providing evidence that the fault was active and functioning in a brittle fashion prior to the intrusion of the dyke. The ophitic, plagioclase-phyric dyke has a basaltic to microgabbro texture with individual plagioclase laths measuring up to 10mm. Boulders with the same plagioclase-phyric texture were found in several other unconnected sections of the wadi, indicating that the dyke was probably not unique.

## **2.5 Conclusions from the geology of the Aswad Block**

- The presence of a Sheeted Dyke Complex and extrusive pillow lavas demonstrates extension in an oceanic setting.
- The thin (~50-200m) MTZ indicates that the Aswad Block was distal to an area of upwelling mantle.
- Kalba Upper Gabbros in fault-related and intrusive contact with the SDC and extrusive section can be interpreted as evidence for a period in the history of the early crust where extension exceeded magma supply that was followed by a period of magmatic activity.
- The presence of two, fault-related, late intrusive gabbros provides evidence for multiple magmatic events in the history of the crust and the apparent rotation of stress fields, possibly related to tectonic rotation of the pre-ophiolite crust.

## **2.6 Summary and comparisons between U.A.E. blocks**

- Both ophiolite blocks within the U.A.E. display characteristics consistent with formation at an oceanic spreading centre.
- Both blocks preserve evidence of initial oceanic crustal accretion events to form the SDC and Upper Gabbros.
- Both blocks display evidence of multiple intrusive magmatic events, which post-date the main period of crustal accretion, preserved as discrete gabbro bodies, wehrlites and dykes.
- Intrusive wehrlitic rocks are common in the crustal sequence of both blocks, and can be interpreted to indicate the existence of a melt distinctly different to MORB.
- The crustal gabbro sequence of the Khawr Fakkan Block is intruded by multiple small late intrusive gabbros that correspond to the second group of intrusions as identified by Browning and Smewing, (1982).
- The crustal gabbro sequence of the Aswad Block is intruded by two large late intrusive gabbros that are themselves intruded by multiple smaller intrusions. The Bithna Gabbro corresponds to the first, older (Cpx-series) of intrusions and the Fujairah Gabbro corresponds to the second, younger (Opx-series) of intrusions as identified by Browning and Smewing, (1982).
- The Khawr Fakkan Block preserves at least 5 periods of magmatism, as evidenced by the different dyke groups.

- The Aswad Block preserves at least 4 periods of magmatism, with two major periods of faulting separated by significant rotation of (extensional) stress fields.
- Initial investigation into the rotation of the blocks provides evidence that each block experienced different rotations at different times in their crustal accretion histories (Figure 2.4 and 2.11). This indicates that the blocks may not have always been in their present position in relation to one another. This subject will be discussed further in Chapter 6, after the results of the geochemical investigations have been presented.
- The observations presented in this Chapter illustrate that the Khawr Fakkan and Aswad Blocks have different and individual magmatic histories.

To further investigate and compare the magmatic histories of the Khawr Fakkan and Aswad Blocks it is necessary to examine the possible variations in geochemistry between the identified magmatic events. This will enable constraints to be applied to the tectonic setting of the original crust at the time of the magmatic events identified in the Khawr Fakkan and Aswad Blocks.

## Chapter 3: Geochemistry of the Dykes and Extrusive Section of the Khawr Fakkan and Aswad Blocks

### 3.1.1 Introduction

The tectonic setting of formation of the Oman-U.A.E. ophiolite has been a topic of debate since the initial geochemical fingerprinting of the extrusive sequence indicated that their compositions are not everywhere the same as typical mid-ocean ridge basalts (MORB). Studies on the southern Oman portion of the ophiolite, (e.g. Glennie et al., 1974) concluded that the ophiolite was formed at a 'normal' mid-ocean ridge. However geochemical work from the northern portion concluded that at least part of the ophiolite might have formed in a marginal basin in a Supra Subduction Zone (SSZ) setting (e.g. Pearce, 1981; Alabaster et al., 1982). Figure 3.1 displays the main differences in the geochemical signatures of crust formed in the tectonic settings discussed in this study.

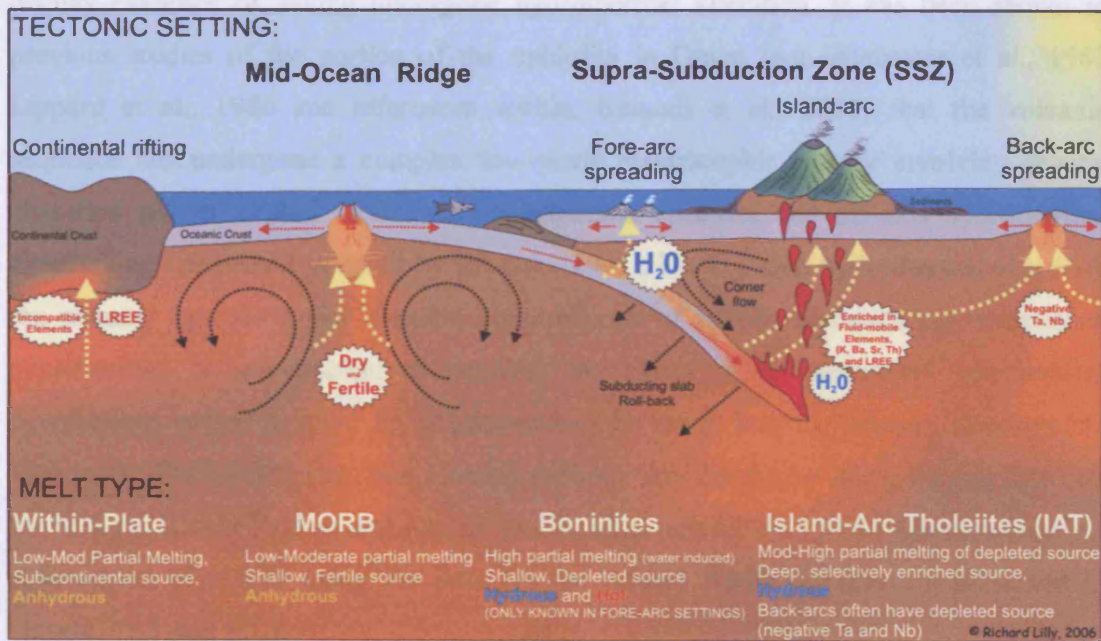


Figure 3.1, Simplified diagram demonstrating the main geochemical variations between different tectonic settings which are relevant to this study.

A geochemical study of the lavas and dykes from the two U.A.E. ophiolite blocks has been conducted to investigate: (1) whether the field classification of the lava and dyke units could be confirmed using geochemical criteria, (2) whether the dykes could be linked geochemically to the lava units described in Oman, (3) the tectonic setting of the U.A.E. lavas, and (4) the petrogenetic history and evolution of the ophiolite complex and its relationship to the generation of modern oceanic crust. Over 300 samples of basalts and dolerites were collected from the Khawr Fakkan and Aswad Massifs in 2003-2004. Of these over 120 were analysed by Inductively-Coupled Plasma Optical Emission Spectrometry (ICP-OES) for major elements and Inductively-Coupled Plasma Mass Spectrometry (ICP-MS) for trace elements at Cardiff University (see Appendix A and B for full laboratory procedures and data sets).

### **3.1.1 Major element mobility**

As discussed in Chapters 1 and 2, hand specimens and thin sections of almost all samples display evidence of having undergone hydrothermal alteration. It has been shown in previous studies of the portion of the ophiolite in Oman (e.g. Alabaster et al., 1982 Lippard et al., 1986 and references within, Einaudi et al., 2000) that the volcanic sequence has undergone a complex low-grade metamorphic history involving several alteration phases related to successive magmatic episodes and off-axis hydrothermal circulations, (described in detail by Pflumio, 1991). During such hydrothermal alteration the primary igneous major element compositions of mobile elements can experience modification. It is important to establish the extent of the secondary geochemical overprinting before detailed investigations can be made into the primary geochemical signatures. The investigation into element mobility was conducted using the full data sets for both the Khawr Fakkan and Aswad Blocks, although for clarity of presentation only a selected set of results using the data for the Aswad Block samples are presented in section 3.1.1 and 3.1.2.

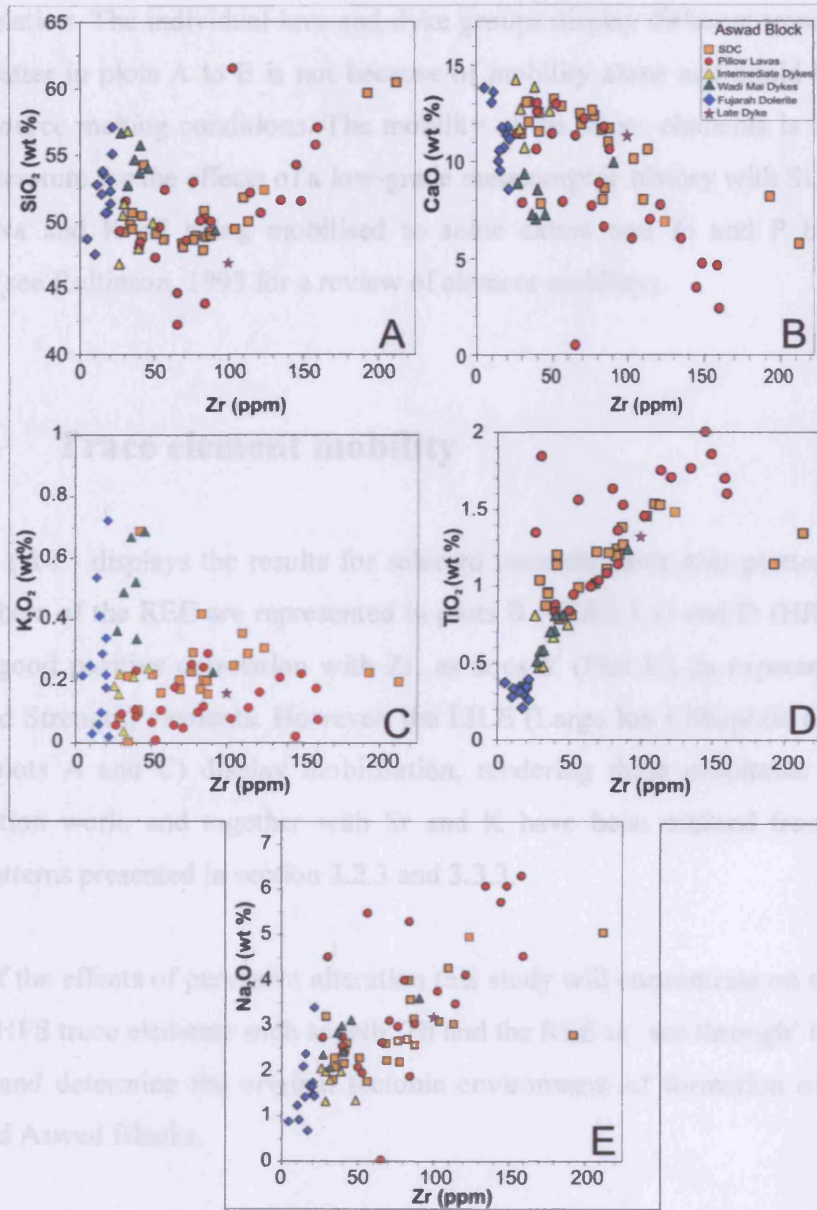


Figure 3.2, Plots of selected major elements versus Zr for the Aswad Block extrusives and dyke samples. The degree of mobility of the element is represented by its correlation with Zr. An immobile element will display a positive correlation.

Figure 3.2 (A-E) displays selected major elements plotted against the immobile element Zr. Immobile elements will display a good positive correlation with Zr. Plots A-C (SiO<sub>2</sub>-CaO-K<sub>2</sub>O<sub>2</sub>) do not display a good linear correlation with Zr when compared to plot D (TiO<sub>2</sub>), which displays a good positive correlation with Zr. Plot E (Na<sub>2</sub>O) displays a fairly

good correlation. The individual lava and dyke groups display different trends indicating that the scatter in plots A to E is not because of mobility alone and could be related to different source melting conditions. The mobility of the major elements is in agreement with the literature for the effects of a low-grade metamorphic history with Si, Al, Fe, Mg, Mn, Ca, Na and K all being mobilised to some extent and Ti and P being largely immobile (see Rollinson, 1993 for a review of element mobility).

### **3.1.2 Trace element mobility**

Figure 3.3 (A-E) displays the results for selected trace elements also plotted against Zr. Two members of the REE are represented in plots B (LREE La) and D (HREE Yb) and display a good positive correlation with Zr, as does Y (Plot E), as expected with HFS (High Field Strength) elements. However, the LILE (Large Ion Lithophile Elements) Ba and Rb (plots A and C) display mobilisation, rendering them unsuitable for detailed discrimination work, and together with Sr and K have been omitted from the multi-element patterns presented in section 3.2.3 and 3.3.3.

Because of the effects of pervasive alteration this study will concentrate on the relatively immobile HFS trace elements such as; Nb, Th and the REE to ‘see through’ the affects of alteration and determine the original tectonic environment of formation of the Khawr Fakkan and Aswad Blocks.

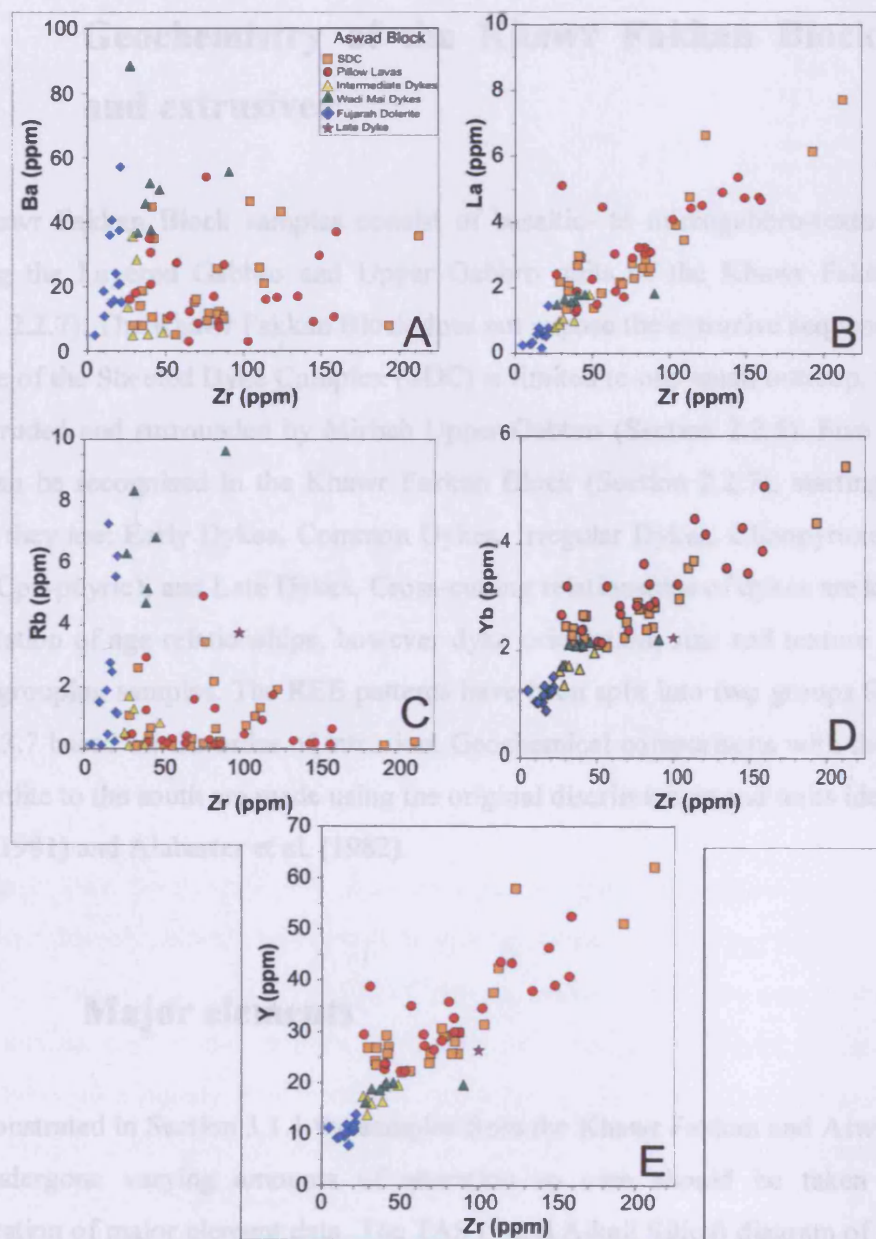


Figure 3.3, Plots of selected trace elements versus Zr. The degree of mobility of the element is represented by its correlation with Zr. An immobile element will display a positive correlation.



## **3.2 Geochemistry of the Khawr Fakkan Block dykes and extrusives**

The Khawr Fakkan Block samples consist of basaltic- to microgabbro-textured dykes intruding the Layered Gabbro and Upper Gabbro units of the Khawr Fakkan Block (Section 2.2.7). The Khawr Fakkan Block does not expose the extrusive sequence and the exposure of the Sheeted Dyke Complex (SDC) is limited to one small outcrop, which has been intruded and surrounded by Mirbah Upper Gabbro (Section 2.2.5). Five phases of dykes can be recognised in the Khawr Fakkan Block (Section 2.2.7), starting with the earliest, they are; Early Dykes, Common Dykes, Irregular Dykes, Clinopyroxene-phyric Dykes (Cpx-phyric), and Late Dykes. Cross-cutting relationships of dykes are key for the interpretation of age relationships, however dyke orientation, size and texture were also used in grouping samples. The REE patterns have been split into two groups for Figures 3.6 and 3.7 based on the order of intrusion. Geochemical comparisons with the rocks of the ophiolite to the south are made using the original discriminants and units identified by Pearce (1981) and Alabaster et al. (1982).

### **3.2.1 Major elements**

As demonstrated in Section 3.1.1 the samples from the Khawr Fakkan and Aswad Blocks have undergone varying amounts of alteration so care should be taken with the interpretation of major element data. The TAS (Total Alkali Silica) diagram of Cox et al. (1979) (with updated fields of Le Maitre et al., 1989) has been used with much success for the classification and discrimination of fresh volcanic rocks. The rocks of the Khawr Fakkan and Aswad Blocks have experienced modification of both Si and K, with Na being fairly immobile (Figure 3.2). While the TAS diagram is not intended to be used for altered rocks it does offer a simple preliminary classification.

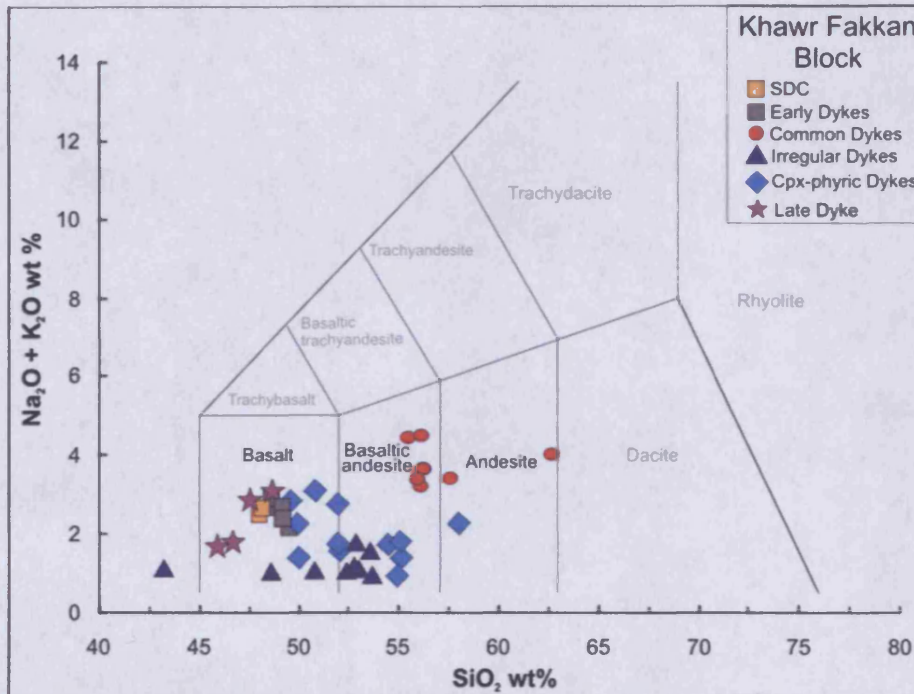


Figure 3.4. TAS (Total Alkali Silica) of Cox et al. (1979) using the updated fields of Le Maitre et al. (1989) for the Khawr Fakkan Block samples

The majority of Khawr Fakkan Block samples plot as basalts or basaltic andesites (Figure 3.4), with relatively minor variations in total alkali concentrations between most groups. The SDC, Early Dykes and Late Dykes plot as basalts. The Common Dykes plot as basaltic andesites, with two samples plotting as andesites. The Irregular Dykes and Cpx-phyric Dykes also mainly plot as basalts and basaltic andesites, with a single (possibly altered) sample plotting as an andesite. These results concur with the proposed oceanic origin for the rocks of the Khawr Fakkan Block.

Figure 3.5 displays selected major elements (A-C) and the incompatible element Zr (D) plotted against MgO, with original fields for the Oman Units as described by Alabaster et al. (1982). The fields have a large degree of overlap, as would be expected of altered rocks from similar tectonic settings. The SiO<sub>2</sub> versus MgO plot (Figure 3.5A) displays a general negative correlation with a large range of scatter because of alteration. The Early Dykes, SDC and Common Dykes all plot within the overlap of the Geotimes, Lasail and Alley fields. However, the Common Dykes are distinguished on all plots by their low

MgO contents (<5%). The Irregular and Cpx-phyrlic Dykes display some association with the field for the Cpx-phyrlic Group, but have higher MgO contents. The Late Dykes display a large degree of overlap between several fields.

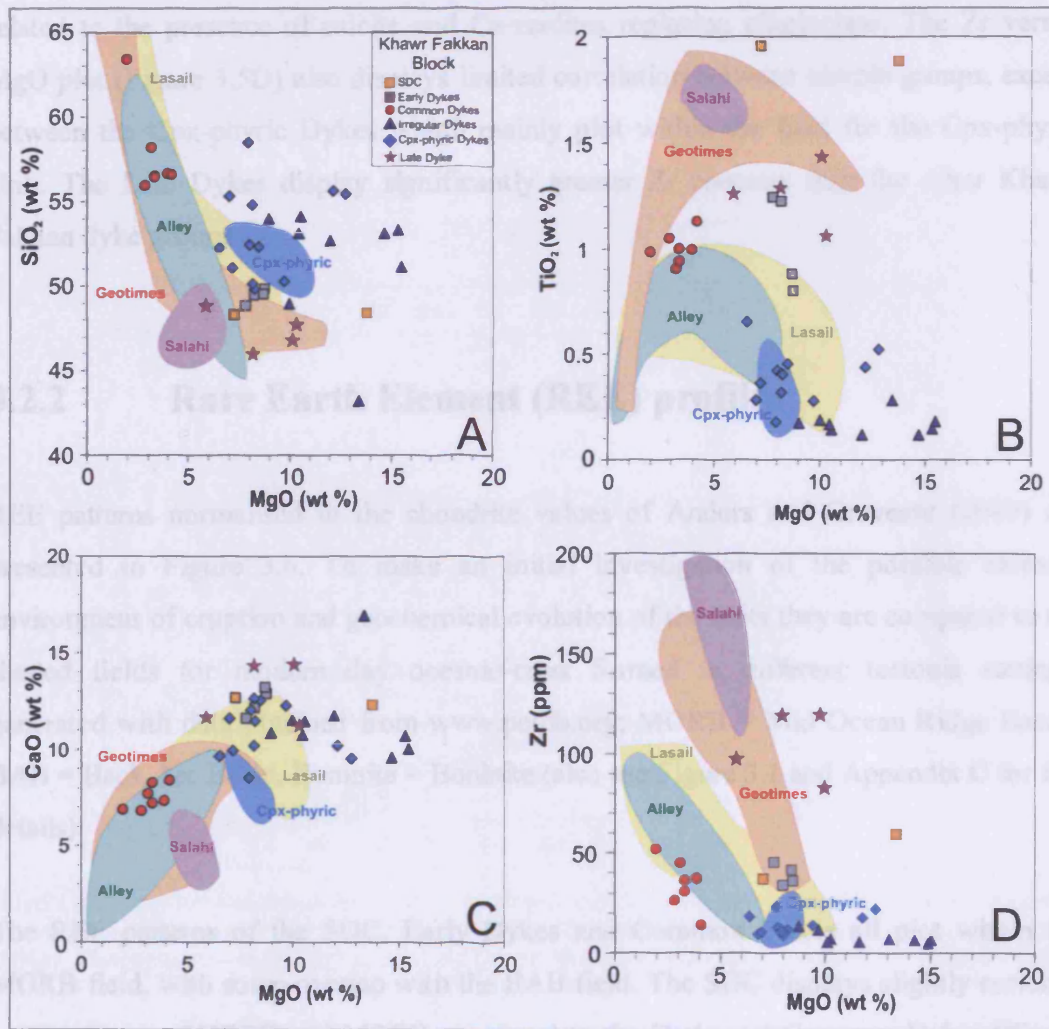


Figure 3.5. Plots of selected major elements and incompatible element Zr versus MgO for the Khawr Fakkan Block samples. Fields for the Geotimes, Lasail, Alley, Cpx-phyrlic and Salahi Units from Alabaster et al. (1982).

The fields of the TiO<sub>2</sub> versus MgO plot (Figure 3.5B) display the differentiation trends observed in the lava units defined in Oman. There is little overlap between the fields for the Geotimes and Alley and Lasail Units as a result of earlier fractionation of oxides in the later lava groups (Alabaster et al., 1982). However, there is little correspondence

between any of the Khawr Fakkan samples and the original fields except between the Cpx-phyric Dykes which mainly plot partly within the field for the Cpx-phyric Unit. The CaO versus MgO plot (Figure 3.5C) displays little correlation between sample groups, with most Khawr Fakkan samples displaying increased CaO values (>10wt.%), possibly related to the presence of calcite and Ca-zeolites replacing plagioclase. The Zr versus MgO plot (Figure 3.5D) also displays limited correlation between sample groups, except between the Cpx-phyric Dykes which mainly plot within the field for the Cpx-phyric Unit. The Late Dykes display significantly greater Zr contents than the other Khawr Fakkan dyke groups.

### **3.2.2 Rare Earth Element (REE) profiles**

REE patterns normalised to the chondrite values of Anders and Grevesse (1989) are presented in Figure 3.6. To make an initial investigation of the possible tectonic environment of eruption and geochemical evolution of the units they are compared to the shaded fields for modern day oceanic-crust formed in different tectonic settings, generated with data obtained from [www.petdb.org](http://www.petdb.org); MORB = Mid Ocean Ridge Basalt, BAB = Back Arc Basin, Boninite = Boninite (also see Figure 3.1 and Appendix C for full details).

The REE patterns of the SDC, Early Dykes and Common Dykes all plot within the MORB field, with some overlap with the BAB field. The SDC displays slightly enriched compositions of HREE and MREE compared to the Early and Common Dykes (Figure 3.6A). The SDC and Early Dyke samples exhibit a slight depletion in LREE compared to MREE and HREE. The Common Dykes have a flatter pattern and are relatively enriched in LREE compared to the SDC and Early Dykes. The REE contents for the samples in Figure 3.6A lie within the range of melts produced at a mid-ocean ridge spreading centre.

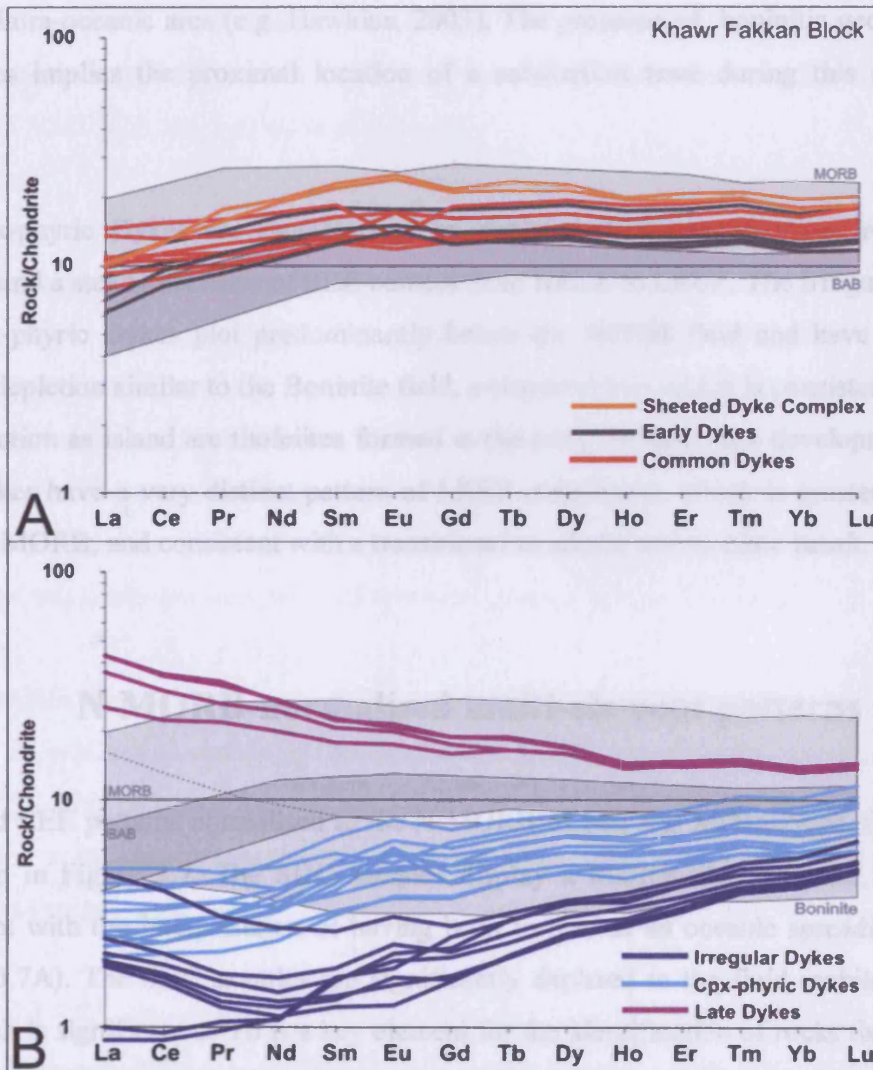


Figure 3.6, Geochemical abundance patterns for Khawr Fakkan dykes normalised to the Chondrite values of Anders and Grevesse (1989). A: Sheeted Dyke Complex, Early Dykes and Common Dykes. B: Irregular Dykes, Clinopyroxene-phyric Dykes and Late Dykes. Shaded MORB, BAB and Boninite fields generated with data from [www.petdb.org](http://www.petdb.org) (for more details see Appendix C).

The Irregular Dykes, which pre-date the Cpx-phyric Dykes, are distinguished by their considerably lower REE concentrations compared to any other group and are characterised by a steady decrease from HREE to MREE, with a relative increase in abundances from MREE to LREE for most samples (Figure 3.6B). This 'U'-shaped pattern is typical of boninites (e.g. Crawford et al., 1989). Boninites are petrographically and geochemically distinctive rocks that are encountered solely in the fore-arc regions of

modern intra-oceanic arcs (e.g. Hawkins, 2003). The presence of boninitic geochemical signatures implies the proximal location of a subduction zone during this magmatic period.

The Cpx-phyric Dykes are characterised by depleted REE concentrations relative to MORB, and a steady decrease of REE content from HREE to LREE. The Irregular Dykes and Cpx-phyric Dykes plot predominantly below the MORB field and have levels of relative depletion similar to the Boninite field, a characteristic which is consistent with an interpretation as island arc tholeiites formed in the early stages of arc development. The Late Dykes have a very distinct pattern of LREE enrichment, which is greater than the range of MORB, and consistent with a transitional to alkalic within-plate basalt.

### **3.2.3 N-MORB-normalised multi-element patterns**

Extended REE patterns normalised to the N-MORB of Sun and McDonough, (1989) are presented in Figure 3.7. The SDC samples display a MORB-like character, which is consistent with the interpretation of having been formed at an oceanic spreading centre (Figure 3.7A). The SDC samples are significantly depleted in the fluid-mobile element Th, which is significant as Th is a key element for the identification of rocks that formed in a SSZ setting. Th is a highly incompatible element that is immobile under hydrothermal alteration conditions, but mobile during source melting readily partitioning into silicate melts (e.g. Keppler, 1999). Th is therefore found in greater concentration in rocks that formed in SSZ environments. The SDC samples (Section 2.2.6) were collected in different field seasons and analysed twelve months apart. They are the only Khawr Fakkan Block samples to display such selective Th depletion. However, the pattern is consistent with those of similarly intruded SDC samples in the Aswad Block, which have had LREE ‘baked’ or ‘sweated’ off by local gabbro intrusions and the associated hydrothermal systems (discussed further in Appendix B). This demonstrates that the Th depletion in the Khawr Fakkan samples could be connected to atypical alteration resulting from local gabbroic intrusion, but more work is required to confirm this

hypothesis. Further study would offer insight into the spatial behaviour of element concentrations associated with hydrothermal alteration, which has implications for the genesis of VMS (Cu, Zn, Au) mineral deposits.

The Early dykes plot within the BAB field, although there is some overlap of the MORB and BAB fields. The characteristic negative Ta and Nb anomaly indicates formation in a back-arc basin setting, possibly within a volcanic arc. Modern-day Indian Ocean MORB also has slight variations in Ta and Nb, and it is possible that the Tethyan mantle source for the ophiolite also had Ta and Nb variations (C. MacLeod, pers. comm.). This geochemical dilemma could be researched further by normalisation with Indian Ocean MORB and comparison with the mantle sources for other Tethyan ophiolites, but for the purpose of this study the standard back-arc basin setting will be discussed.

The Common Dykes have a transitional MORB-BAB character and are relatively enriched in subduction-mobile elements (Th and LREE) compared to the Early Dykes and MORB. This signature demonstrates that a subduction-derived component may have been added to the mantle source of the Common Dykes. The results reveal a transitional-MORB character for the earliest dyke groups of the Khawr Fakkan Block.

Figure 3.7B illustrates that the Irregular Dykes are strongly depleted in all HREE and MREE relative to MORB. The boninitic 'U' shaped pattern is parallel to the field for modern-day boninites and provides firm evidence that the Irregular Dykes were formed from melt formed in a SSZ setting.

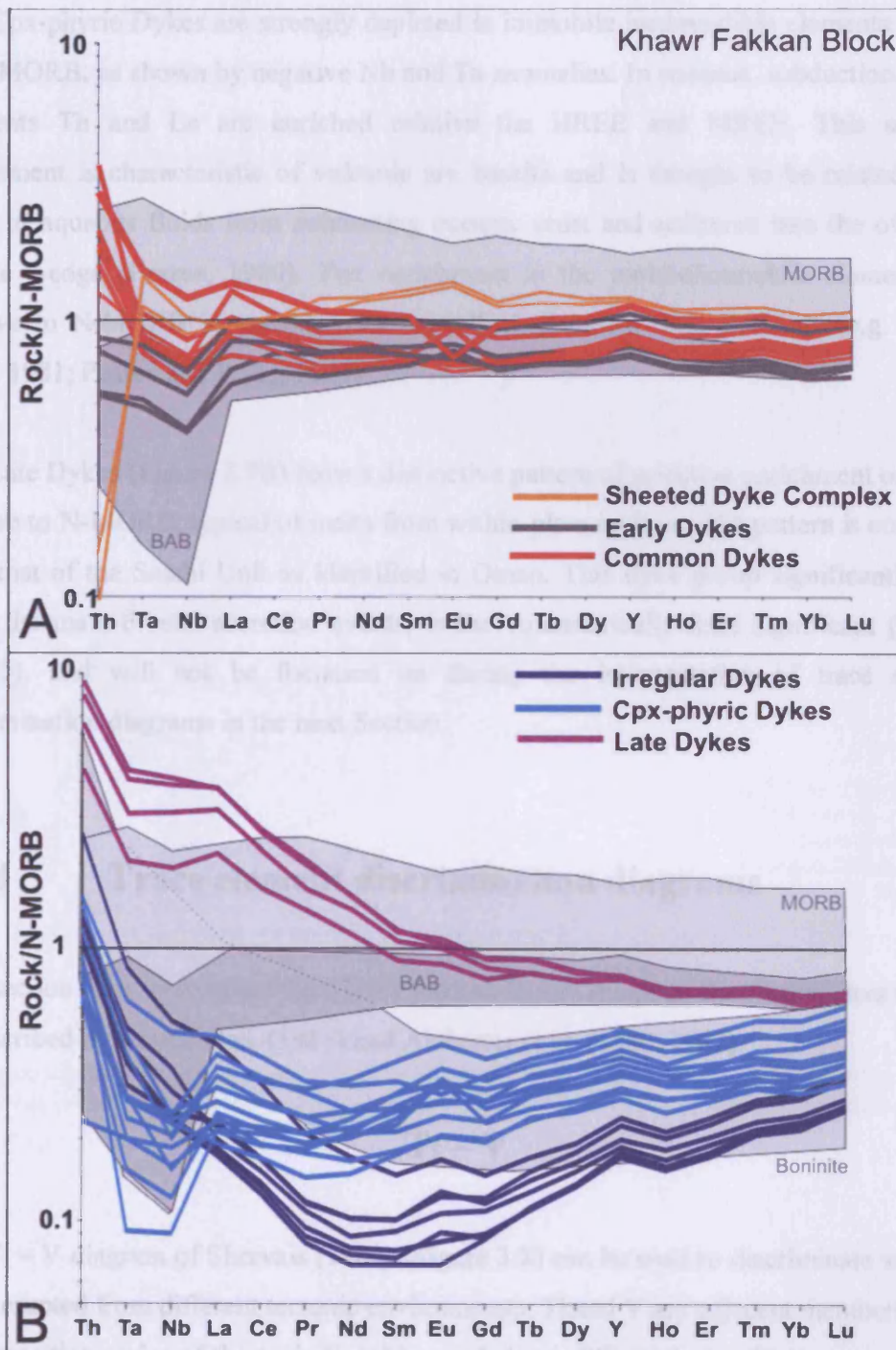


Figure 3.7, N-MORB-normalised multi-element diagrams for Khawr Fakkan dykes normalised to N-MORB values of Sun and McDonough (1989). A: Sheeted Dyke Complex, Early Dykes, and Common Dykes. B: Irregular Dykes, Clinopyroxene-phyric Dykes, and Late Dykes. Shaded MORB, BAB and Boninite fields generated with data from [www.petdb.org](http://www.petdb.org) (fully listed in Appendix C).



The Cpx-phyric Dykes are strongly depleted in immobile incompatible elements relative to N-MORB, as shown by negative Nb and Ta anomalies. In contrast, subduction-mobile elements Th and La are enriched relative the HREE and MREE. This selective enrichment is characteristic of volcanic arc basalts and is thought to be related to the input of aqueous fluids from subducting oceanic crust and sediment into the overlying mantle wedge (Pearce, 1980). The enrichment in the mobile/immobile element ratio relative to N-MORB in oceanic rocks usually indicates a SSZ character (e.g. Pearce, 1980, 1981; Pearce and Peate, 1995).

The Late Dykes (Figure 3.7B) have a distinctive pattern of selective enrichment of LREE relative to N-MORB, typical of melts from within-plate settings. The pattern is consistent with that of the Salahi Unit as identified in Oman. This dyke group significantly post-dates the main crustal accretion events, is the volumetrically least significant (Section 2.2.7.5), and will not be focussed on during the interpretation of trace element discrimination diagrams in the next Section.

### 3.2.4 Trace element discrimination diagrams

This section aims to compare the Khawr Fakkan Dyke Groups to the original lava units as described by Pearce et al. (1981) and Alabaster et al. (1980, 1982).

#### Ti – V

The Ti – V diagram of Shervais (1982) (Figure 3.8) can be used to discriminate volcanic rocks erupted from different tectonic environments. Ti and V are adjacent members of the first transition series of the periodic table, yet behave differently in silicate systems as V can exist in reduced ( $V^{3+}$ ) or oxidised ( $V^{4+}$ ,  $V^{5+}$ ) valency states, whereas Ti only exists as  $Ti^{4+}$ . Therefore variations in V relative to Ti act as a measure of the oxygen fugacity of a magma, as well as fractional crystallisation (Shervais, 1982). Both Ti and V are immobile

under conditions of hydrothermal alteration and at intermediate-to-high grades of metamorphism (e.g. Lavis, 2005).

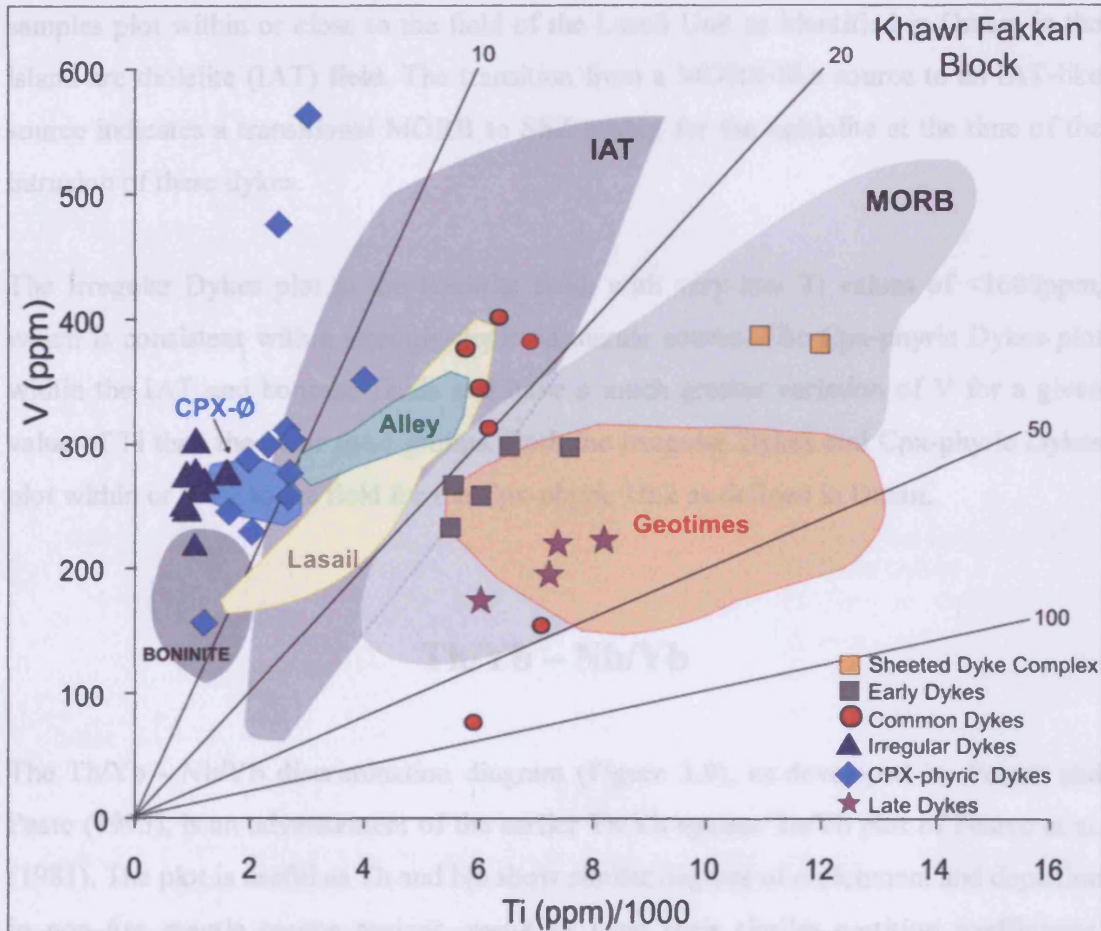


Figure 3.8, Ti-V plot for Khawr Fakkan Block Dyke Groups. Boninite, IAT and MORB fields after Shervais (1982). Fields for Oman lava units, Geotimes, Lasail, Alley and Cpx-Ø from Alabaster et al. (1982).

The fields of the basalt units identified by Pearce et al. (1981) and Alabaster et al. (1980, 1982) are displayed with the original fields Shervais (1982) of lavas from different tectonic settings. The Late Dykes, while plotted on this diagram, are not discussed in detail as their proposed within-plate source plots outside the (oceanic source) compositional fields used.

The SDC and Early Dykes all plot inside the MORB field (Figure 3.8) and the Early Dykes plot within or close to the field of the Geotimes Unit as described in Oman. This concurs with the field evidence that these are the earliest dykes. Most Common Dyke samples plot within or close to the field of the Lasail Unit as identified in Oman, in the island arc tholeiite (IAT) field. The transition from a MORB-like source to an IAT-like source indicates a transitional MORB to SSZ setting for the ophiolite at the time of the intrusion of these dykes.

The Irregular Dykes plot in the boninite field, with very low Ti values of <1600ppm, which is consistent with a strongly-depleted mantle source. The Cpx-phyric Dykes plot within the IAT and boninite fields and have a much greater variation of V for a given value of Ti than the other dyke groups. Both the Irregular Dykes and Cpx-phyric Dykes plot within or close to the field for the Cpx-phyric Unit as defined in Oman.

### **Th/Yb – Nb/Yb**

The Th/Yb - Nb/Yb discrimination diagram (Figure 3.9), as developed by Pearce and Peate (1995), is an advancement of the earlier Th/Yb against Ta/Yb plot of Pearce et al. (1981). The plot is useful as Th and Nb show similar degrees of enrichment and depletion in non-Arc mantle source regions, resulting from their similar partition coefficients. However, Th is more incompatible in the presence of water. Thus Th is enriched in mantle wedges above subduction zones, where it is derived from de-watering of the subducting slab and associated sediment. The REE Yb is used as a normalising factor to eliminate the effects of fractional crystallisation and is chosen because it is not significantly affected by the processes that cause mantle heterogeneity, yet it behaves as an incompatible element during partial melting and fractional crystallisation (Alabaster et al., 1982). Thus the ratios, Th/Yb and Nb/Yb, are close to the ratios in the source regions from which the melts were derived. The fields of the different basalt units identified by Pearce et al. (1981) and Alabaster et al. (1980, 1982) are not displayed as levels of Nb were below detection limits at the time of analysis.

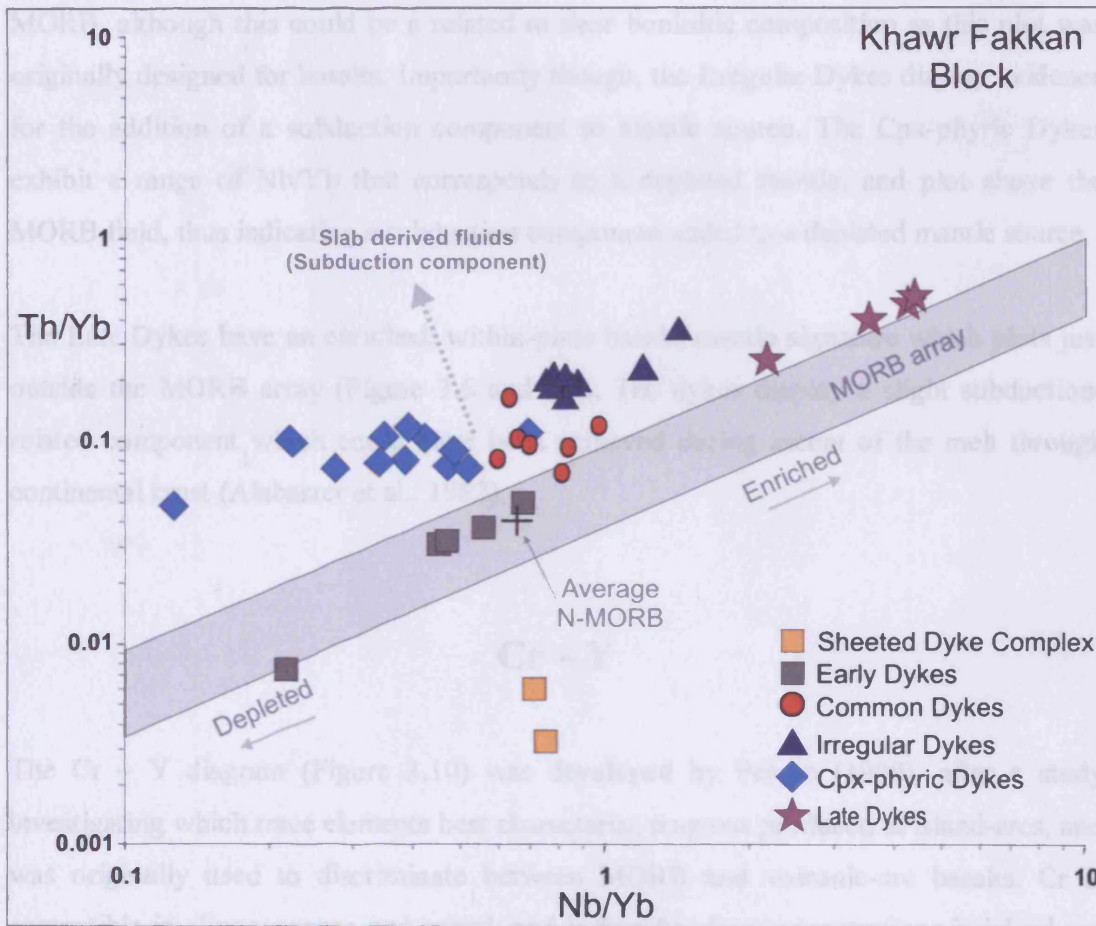


Figure 3.9, Th/Yb-Nb/Yb plot for the Khawr Fakkan Block after Pearce and Peate, (1995). Increasing presence of slab-derived fluids move samples in direction of dashed-arrow.

The Early Dykes plot in the MORB array (Figure 3.9), close to the value of N-MORB. The SDC exhibit very similar Nb/Yb ratios to the Early Dykes and N-MORB, but plot below the MORB array due to their depletion in Th (discussed in Appendix B).

The Common Dykes have higher Th/Yb ratios than the SDC and Early Dykes and plot mostly outside the MORB array, indicating the addition of a subduction-derived fluid component to the mantle source.

The Irregular Dykes display a mantle source that is slightly enriched relative to N-MORB, although this could be related to their boninitic composition as this plot was originally designed for basalts. Importantly though, the Irregular Dykes display evidence for the addition of a subduction component to mantle source. The Cpx-phyric Dykes exhibit a range of Nb/Yb that corresponds to a depleted mantle, and plot above the MORB field, thus indicating a subduction component added to a depleted mantle source.

The Late Dykes have an enriched, within-plate basalt, mantle signature which plots just outside the MORB array (Figure 3.6 and 3.7). The dykes display a slight subduction-related component which could have been achieved during ascent of the melt through continental crust (Alabaster et al., 1982).

### Cr – Y

The Cr – Y diagram (Figure 3.10) was developed by Pearce (1980), after a study investigating which trace elements best characterise magmas produced at island-arcs, and was originally used to discriminate between MORB and volcanic-arc basalts. Cr is compatible in clinopyroxene and spinel, and is found in low concentrations in island-arc basalts relative to other basalt types. Y is incompatible compared to Cr and is also depleted in island-arc basalts relative to other basalt types, for a given degree of fractionation.

Figure 3.10 illustrates that the Early Dykes and SDC plot within the MORB field and do not correspond directly with any of the lava groups identified in Oman. This is significant as the Early Dykes and SDC have plotted within or close to the MORB field on all of the discrimination diagrams used and is the first 'true' MORB to be recorded in the Oman – U.A.E. ophiolite. This places firm constraints on the composition of the original mantle source and tectonic setting of the Khawr Fakkan Block prior to any additional subduction component.

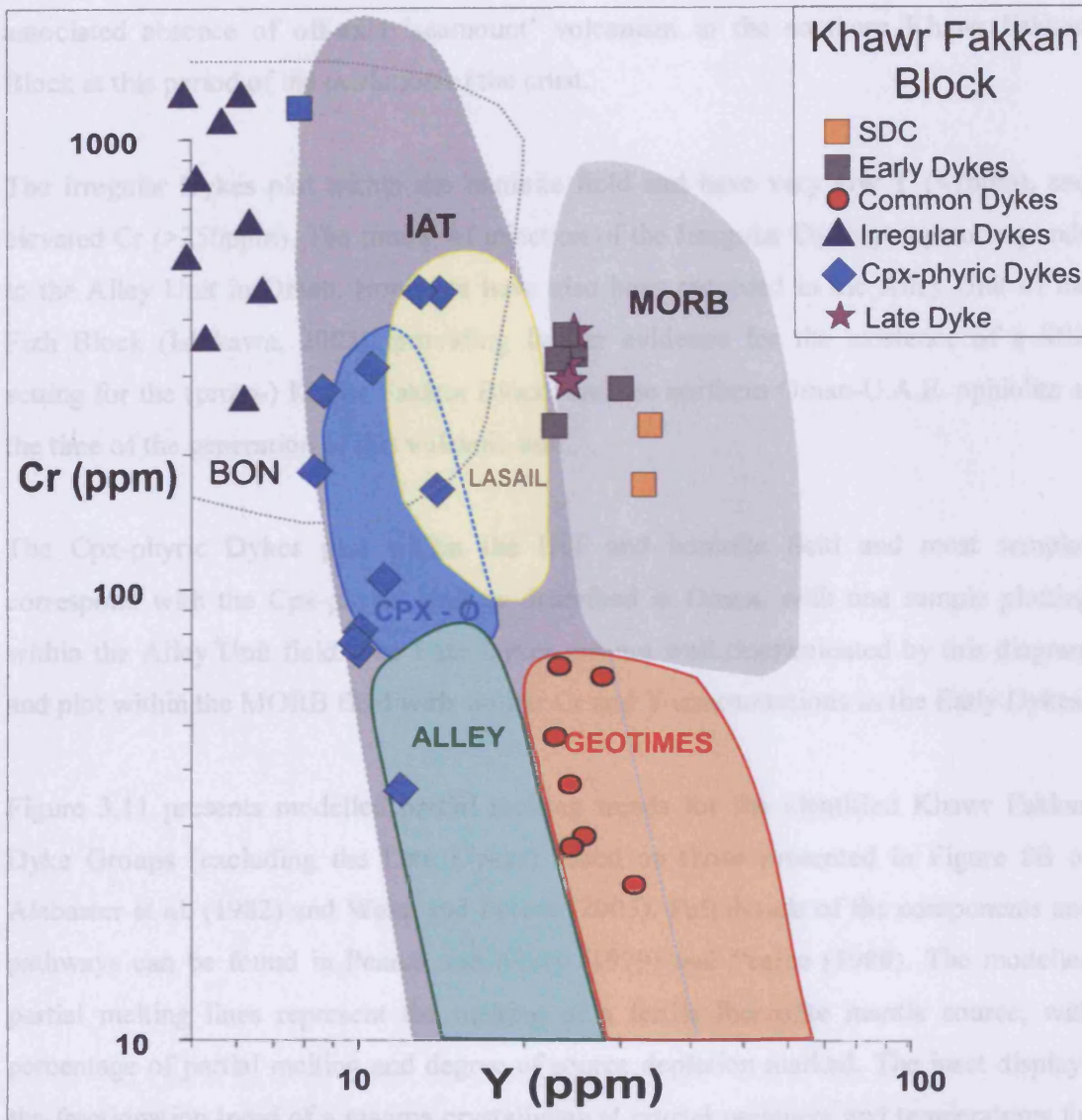


Figure 3.10, Cr/Y plot for the Khawr Fakkan Block Dyke Groups, MORB-IAT fields after Pearce (1980), BON (boninite) field after Pearce (1981), Oman lava groups (Geotimes, Lasail, Alley and Cpx-phyric) after Alabaster et al. (1982).

The Common Dykes plot within the IAT field and within the field of the Geotimes Unit as defined in Oman. No samples from the Khawr Fakkan Block correspond to the Lasail Unit as defined in Oman. Alabaster, (1982) proposed that the Lasail Unit represents discrete volcanism at localised, off-axis, magmatic centres. If this hypothesis is correct the absence of dykes corresponding to the Lasail Unit may be taken as evidence for the

associated absence of off-axis 'seamount' volcanism in the southern Khawr Fakkan Block at this period of the evolution of the crust.

The Irregular Dykes plot within the boninite field and have very low Y (<7ppm), and elevated Cr (>250ppm). The timing of injection of the Irregular Dyke group corresponds to the Alley Unit in Oman. Boninites have also been recorded in the Alley Unit of the Fizh Block (Ishikawa, 2002), providing further evidence for the existence of a SSZ setting for the (proto-) Khawr Fakkan Block, and the northern Oman-U.A.E. ophiolite at the time of the generation of this volcanic unit.

The Cpx-phyric Dykes plot within the IAT and boninite field and most samples correspond with the Cpx-phyric Unit as described in Oman, with one sample plotting within the Alley Unit field. The Late Dykes are not well discriminated by this diagram and plot within the MORB field with similar Cr and Y concentrations as the Early Dykes.

Figure 3.11 presents modelled partial melting trends for the identified Khawr Fakkan Dyke Groups (excluding the Late Dykes) based on those presented in Figure 8B of Alabaster et al. (1982) and Wake and Pearce (2005). Full details of the components and pathways can be found in Pearce and Norry (1979) and Pearce (1980). The modelled partial melting lines represent the melting of a fertile lherzolite mantle source, with percentage of partial melting and degree of source depletion marked. The inset displays the fractionation trend of a magma crystallising at crustal pressures and temperatures for the minerals present in the assemblage. This method allows a general estimation of the percentage of partial melting required of the mantle source to produce the identified dyke groups and is simply a guide to the differences between the relative levels of depletion of the mantle source between units.

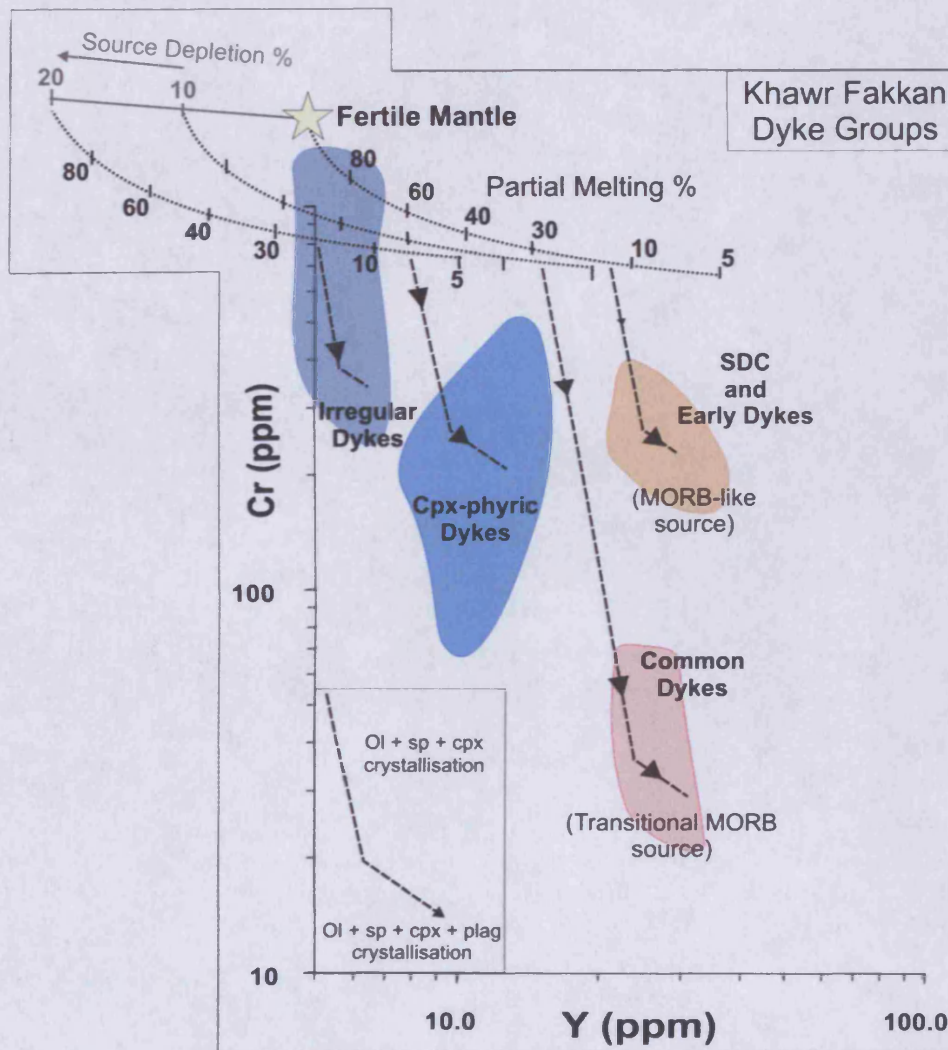


Figure 3.11, Modelled partial melting trends of the identified Khawr Fakkan Dyke Groups. Method of modelling based on the work of Pearce and Norry (1979) and Pearce (1980). Degrees of partial melting based on Alabaster et al. (1982) and Wake and Pearce (2005).

Extrapolation of the fractionation trends for the SDC and Early Dykes corresponds to between 10 and 20% partial melting of a fertile mantle source. The Common Dykes (Geotimes Unit) exhibit a different pathway and are modelled to represent ~30% melting of a fertile mantle source. This is consistent with the modelling by Alabaster et al. (1982), who concluded that the Geotimes Unit (and Lasail Unit) in Oman were produced from ~30% partial melt from a fertile source.



The Irregular Dykes have a very depleted composition and model as being produced from between 10 and 30% partial melting of a 20% depleted source, or a 40-60% partial melt of a 10% depleted source. The genesis of the boninitic Irregular Dykes will be discussed in more detail in Chapter 6.

The Cpx-phyric Dykes (Cpx-phyric Unit), which have a depleted mantle source, model as having been formed from between 5 and 10% partial melting of a 20% depleted source, or from ~30% partial melting from a 10% depleted source. As mentioned before, these values are model dependent and therefore only estimates. However, the method does offer another way for the evolution of the mantle source to be investigated, and charts the evolution from fertile MORB, through transitional MORB, to a depleted SSZ-type mantle source.

### **3.2.5 Conclusions from Khawr Fakkan Block**

- The SDC and Early Dykes, exhibit a MORB-like composition, the first to be documented in the Oman-U.A.E. ophiolite.
- The MORB-like composition of the SDC and Early Dykes provides evidence for formation at a 'normal' oceanic spreading centre, not obviously influenced by subduction, and were formed from between 10 and 20% partial melting.
- The Early Dykes, SDC and Common Dykes (Geotimes Unit) were formed from a MORB-like to transitional MORB mantle source during an initial magmatic period (VI).
- The Common Dykes exhibit a transitional volcanic arc character, and correspond to the Geotimes Unit as defined in Oman, and were formed from ~30% partial melting.

- The Irregular Dykes have a distinctive boninitic signature and their timing of intrusion corresponds with the Alley Unit in Oman. This provides evidence for north-south variation in the volcanic stratigraphy of the ophiolite, and provides firm constraints on the paleotectonic setting of the Khawr Fakkan Block at the time of their generation.
- The Cpx-phyric Dykes contain a subduction zone component and correlate with the Cpx-phyric Unit as identified in Oman.
- The Irregular Dykes and Cpx-phyric Dykes were formed in a SSZ setting during a second major volcanic period (V2).
- The Late Dykes are significantly enriched in incompatible elements, typical of lavas from within-plate settings. These dykes correspond with the Salahi Unit in Oman, and were formed during a third magmatic event (V3) some time after the earlier magmatic events (V1 and V2).
- In summary the Khawr Fakkan Block provides geochemical evidence for the transition from spreading- to subduction-related volcanism.

### **3.3 Geochemistry of the Aswad Block dykes and extrusives**

The Aswad Block exposes a complete ophiolite sequence, preserving multiple magmatic events (Figure 2.3). The initial magmatic events include the N-S striking SDC, the lowermost lavas and the Intermediate Dykes, exposed in the eastern part of the block (Section 2.4.5 to 2.4.7). The Wadi Mai Dykes (section 2.4.8) are a series of NW-SE striking microgabbro dykes which cut the upper crustal gabbros, SDC, lavas and Intermediate Dykes. The Fujairah Gabbro, a late intrusive gabbro, is believed to be the source of the Fujairah Dolerite, which intrudes all of the above units. A single Late Dyke, containing xenoliths of serpentinised harzburgite in its margin, was also recorded intruding along a crustal scale fault within the mantle sequence and is thought to represent the last magmatic phase prior to, or during, the obduction of the ophiolite. As in Section 3.2.2 the REE patterns of the magmatic events identified in the Aswad Block have been split into two groups for Figures 3.14 and 3.15 based on the order of the events.

#### **3.3.1 Major elements**

As described in Section 3.2.1 the TAS diagram (Cox et al., 1979, with fields of Le Maitre et al., 1989) was not intended for use with altered volcanic rocks, it is included here for a preliminary classification of the Aswad Block dykes and extrusive samples.

The majority of the Aswad Block samples plot within the basalt and basaltic andesite field (Figure 3.12). The SDC and Lavas display the greatest range of values, with some samples with elevated alkali concentrations plotting as trachybasalts and basaltic trachyandesites. This is the result of mobilisation of K (and to a lesser extent Na) during hydrothermal alteration (Figure 3.2C and E). Some SDC and lava samples also plot as andesites and this could also be the result of Si enrichment within the groundmass,

vesicles or fractures during hydrothermal alteration. The Intermediate Dykes, Wadi Mai Dykes and Fujairah Dolerite samples all plot within the basalt and basaltic andesite fields with limited variation in the alkali component. The results concur with the proposed oceanic origin for the rocks of the Aswad Block

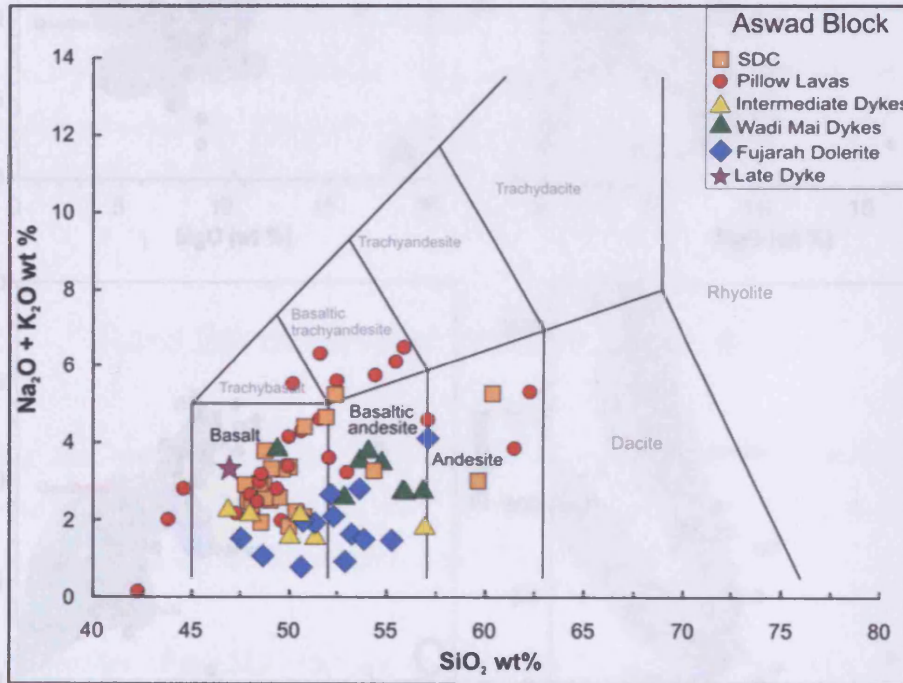


Figure 3.12. TAS (Total Alkali Silica) of Cox et al. (1979) using the updated fields of Le Maitre et al. (1989) for the Aswad Block samples

Figure 3.13 displays selected major elements (A-C) and the incompatible element Zr (D) plotted against MgO, with the fields of the lava units as described by Alabaster et al. (1982). The SiO<sub>2</sub> versus MgO plot (Figure 3.13A) displays a slight negative correlation with a large range of scatter because of alteration. Almost all of the Aswad Block units plot within the overlap of the Geotimes, Lasail and Alley Unit fields, with the Fujairah Dolerite displaying some association with the field for the Cpx-phyric Unit.

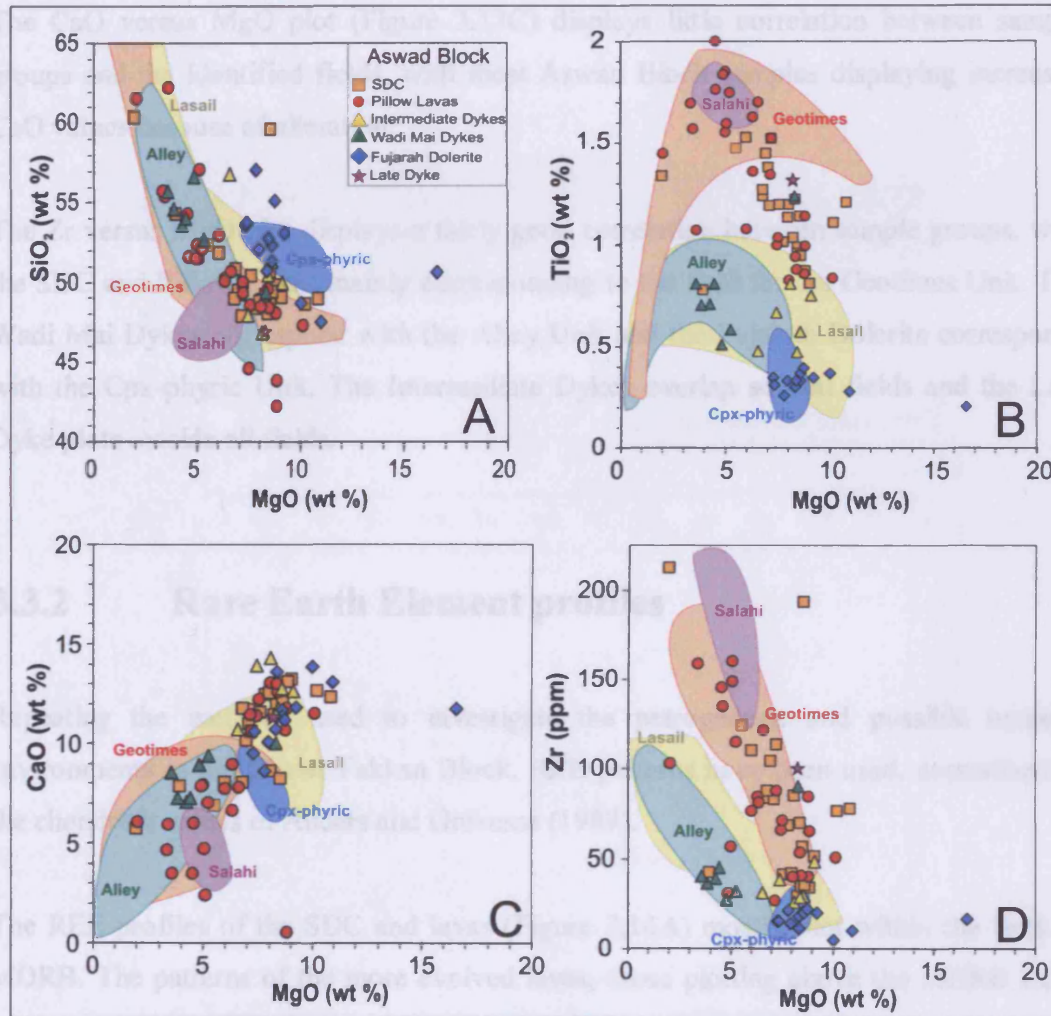


Figure 3.13. Plots of selected major elements and incompatible element Zr versus MgO for the Aswad Block samples. Fields for the Geotimes, Lasail, Alley, Cpx-phyric and Salahi Units from Alabaster et al. (1982).

The TiO<sub>2</sub> versus MgO plot (Figure 3.13B) distinguishes the early magmatic events of the SDC and Pillow Lavas, which correspond to the TiO<sub>2</sub> values of the Geotimes Unit. Later magmatic events, the Intermediate Dykes and the Wadi Mai Dykes, probably correspond to the Lasail and Alley Units respectively as indicated by the earlier fractionation of oxides (Alabaster et al., 1982). The Fujairah Dolerite again corresponds well with the Cpx-phyric Unit.

The CaO versus MgO plot (Figure 3.13C) displays little correlation between sample groups and the identified fields, with most Aswad Block samples displaying increased CaO values because of alteration.

The Zr versus MgO plot displays a fairly good correlation between sample groups, with the SDC and Pillow Lavas mainly corresponding to the field for the Geotimes Unit. The Wadi Mai Dykes correspond with the Alley Unit and the Fujairah Dolerite corresponds with the Cpx-phyric Unit. The Intermediate Dykes overlap several fields and the Late Dyke plots outside all fields.

### **3.3.2 Rare Earth Element profiles**

Repeating the methods used to investigate the petrogenesis and possible tectonic environments in the Khawr Fakkan Block, REE patterns have been used, normalised to the chondritic values of Anders and Grevesse (1989).

The REE profiles of the SDC and lavas (Figure 3.14A) mostly plot within the field of MORB. The patterns of the more evolved lavas, those plotting above the MORB field, correspond well with the Geotimes Unit as defined in Oman. The range of element concentration for the SDC and the lavas they fed, from MORB-like to slightly evolved relative to MORB, is gradual and possibly represents MORB-like melt that has fractionated in a magma chamber. The negative Eu anomaly present in some lava samples indicates Eu removal by significant fractionation and removal of cumulus plagioclase in a magma chamber.

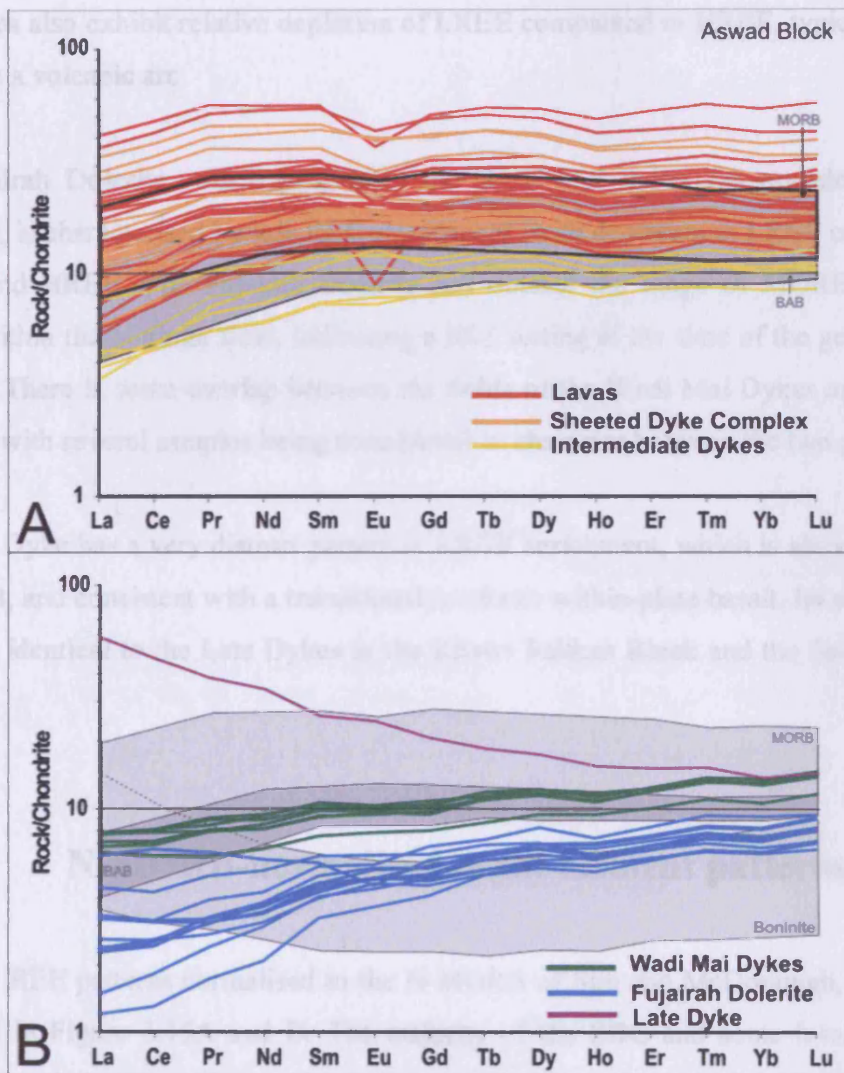


Figure 3.14. Geochemical abundance patterns for Aswad Block samples normalised to Chondrite REE abundances of Anders and Grevesse (1989). A: Sheeted Dyke Complex, Lavas and Intermediate Dykes. B: Wadi Mai Dykes, Fujairah Dolerite and Late Dyke. Shaded MORB, BAB and Boninite fields generated with data from [www.petdb.org](http://www.petdb.org) (See Appendix C).

The Intermediate Dykes (Figure 3.14A) display REE patterns that are parallel, but depleted relative to the SDC and Lavas. The patterns lie mostly within the BAB field, indicating a slightly more depleted source for these dykes than the SDC and lavas.

The Wadi Mai Dykes (Figure 3.14B) are characterised by a lower abundance of REE than the Lavas and SDC, plotting mostly within the range of the BAB field. The Wadi

Mai Dykes also exhibit relative depletion of LREE compared to HREE, typical of melts formed in a volcanic arc

The Fujairah Dolerite, which post-dates the Wadi Mai dykes (as revealed by field relations), is characterised by low REE abundances, with depletion in LREE compared to MREE and HREE. The Fujairah Dolerite lies outside the range of MORB and plots mainly within the boninite field, indicating a SSZ setting at the time of the generation of this unit. There is some overlap between the fields of the Wadi Mai Dykes and Fujairah Dolerite, with several samples being transitional in character between the two groups.

The Late Dyke has a very distinct pattern of LREE enrichment, which is above the range of MORB, and consistent with a transitional to alkalic within-plate basalt. Its composition is almost identical to the Late Dykes in the Khawr Fakkan Block and the Salahi Unit in Oman.

### **3.3.3 N-MORB-normalised multi-element patterns**

Extended REE patterns normalised to the N-MORB of Sun and McDonough, (1989) are presented in Figure 3.15A and B. The majority of the SDC and some lavas exhibit a MORB-like character, with some more depleted samples plotting in the BAB field. All lavas and SDC samples also display variable negative Ta and Nb anomalies typical of transitional volcanic arc settings. Some SDC samples and most lavas display enrichment relative to MORB of the incompatible elements (Figure 3.15A), indicating a transitional MORB character for the earliest stages of crustal accretion of the Aswad Block.



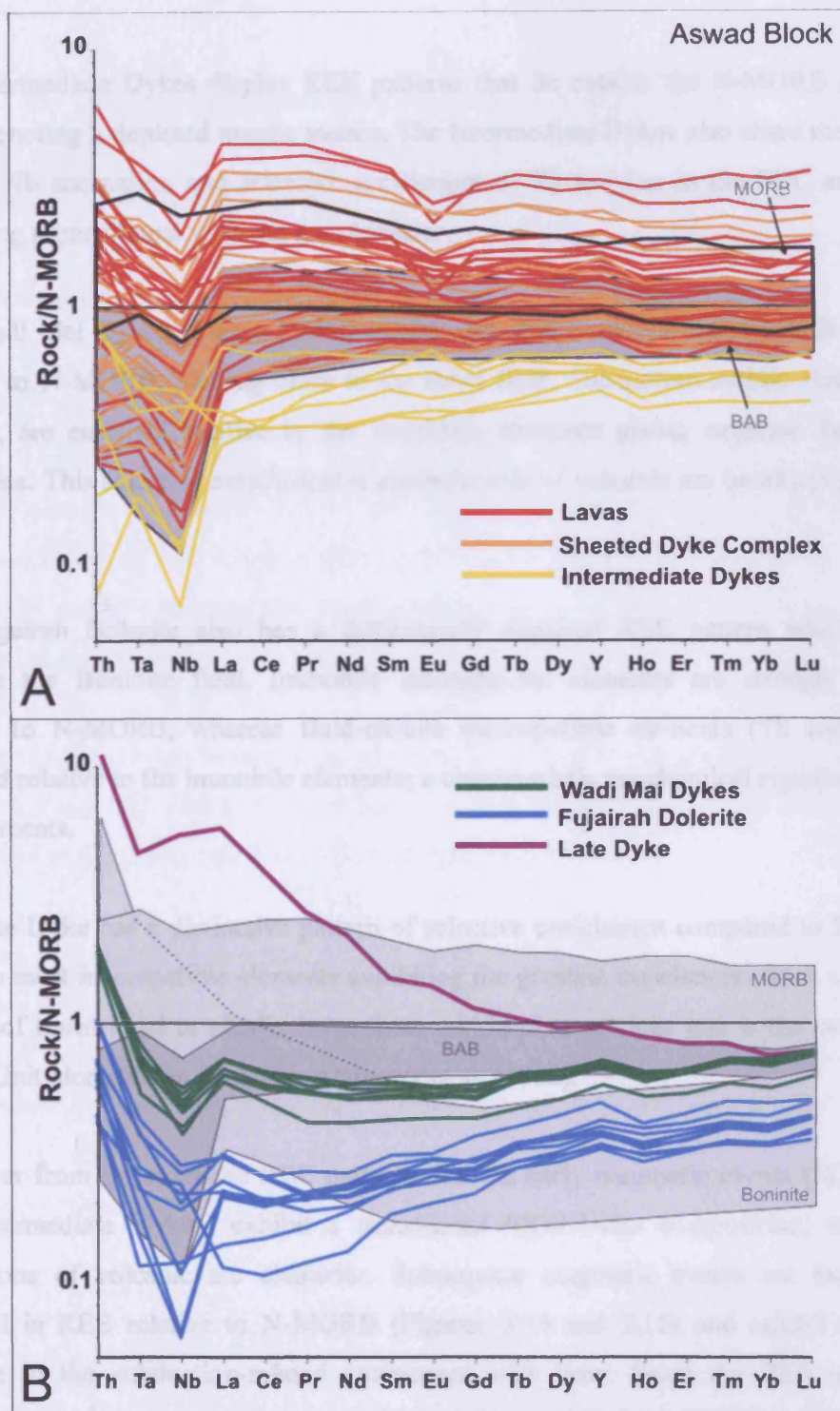


Figure 3.15, N-MORB-normalised multi-element diagrams for Aswad Block samples normalised to N-MORB values of Sun and McDonough (1989). A: Sheeted Dyke Complex, Lavas and Intermediate Dykes, B: Wadi Mai Dykes, Fujairah Dolerite and Late Dyke. Shaded MORB, BAB and Boninite fields generated with data from [www.petdb.org](http://www.petdb.org) (See Appendix C).

The Intermediate Dykes display REE patterns that lie outside the N-MORB and BAB fields denoting a depleted mantle source. The Intermediate Dykes also share the negative Ta and Nb anomalies, and selective enrichment of Th and La, as the SDC and Lavas, indicating a transitional volcanic arc character.

The Wadi Mai Dykes (Figure 3.15B) exhibit depleted immobile incompatible elements relative to N-MORB, plotting close to the BAB field. Subduction-mobile elements, Th and La, are enriched relative to the immobile elements giving negative Ta and Nb anomalies. This selective enrichment is characteristic of volcanic arc basalts (e.g. Pearce, 1980).

The Fujairah Dolerite also has a distinctively depleted REE pattern which closely matches the Boninite field. Immobile incompatible elements are strongly depleted relative to N-MORB, whereas fluid-mobile incompatible elements (Th and La) are enriched relative to the immobile elements; a characteristic geochemical signature of SSZ environments.

The Late Dyke has a distinctive pattern of selective enrichment compared to N-MORB, with the most incompatible elements exhibiting the greatest enrichment. Such a pattern is typical of transitional to alkalic lavas from within-plate settings and is the same as the Salahi Unit identified in Oman by Alabaster et al. (1982).

It is clear from the extended REE patterns that the early magmatic events (SDC, Lavas and Intermediate Dykes) exhibit a transitional MORB-like composition, with some indications of volcanic arc character. Subsequent magmatic events are increasingly depleted in REE relative to N-MORB (Figures 3.14 and 3.15) and exhibit a relative increase in the subduction-related component with time. From the REE patterns it appears that the Aswad and Khawr Fakkan Blocks display a similar (spreading to subduction) magmatic history. The comparison between blocks will be discussed further in Section 3.4.

### 3.3.4 Trace element discrimination diagrams

This section aims to compare the Aswad Block extrusives, dykes and magmatic events to the original lava units as described by Pearce et al. (1981) and Alabaster et al. (1980, 1982) using the same discrimination diagrams introduced in Section 3.2.4.

#### Ti – V

The Ti-V plot for the Aswad Block (Figure 3.16) illustrates that the SDC and lavas from the Aswad Block all plot within or very close to the MORB field. The majority of Aswad Block SDC and lava samples also correspond well with the field of the Geotimes Unit of Alabaster et al. (1982).

The Intermediate Dykes have a range of values for Ti and V that are transitional between the MORB and IAT fields, but plot mainly within the IAT field. Most of the samples correspond to the field of the Lasail Unit as defined in Oman.

The Wadi Mai Dykes plot within the IAT field, with Ti-V ratios of between 10 and 20. The Wadi Mai Dykes mostly plot outside the range of the Alley or Lasail Unit fields as defined by Alabaster et al. (1982), but the increased concentrations of V compared to the Intermediate Dykes is similar to the pattern observed in Oman between the Lasail and Alley units. This provides evidence for variation in the composition of the magmatic stratigraphy within the ophiolite.

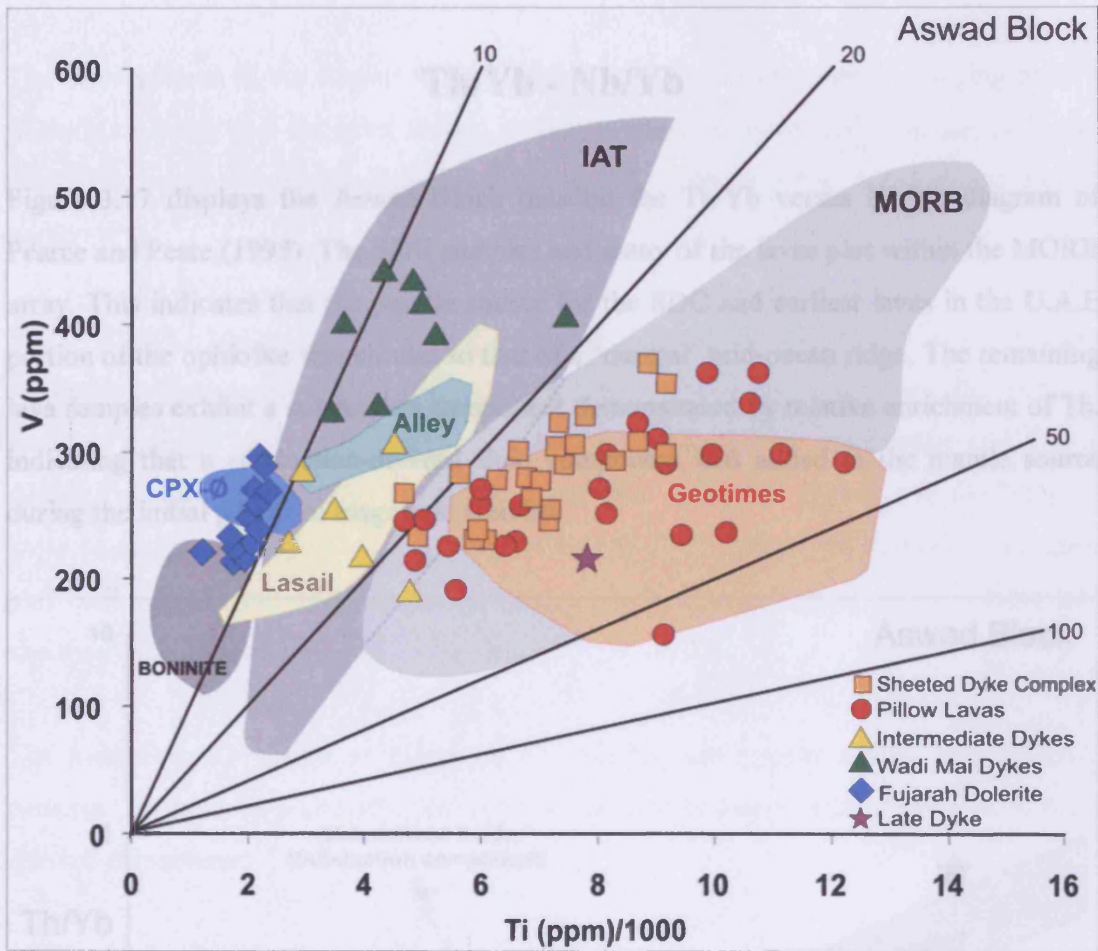


Figure 3.16, Ti-V plot of for Aswad Block samples after Shervais (1982). Boninite, IAT and MORB fields after Shervais (1982). Fields for Oman lava units, Geotimes, Lasail, Alley and Cpx-Ø from Alabaster et al. (1982).

The Fujairah Dolerite samples have boninitic affinity and plot in a tight group overlapping closely with the field of the Cpx-phyrlic Unit as defined in Oman. The Fujairah Dolerite samples have low Ti-V ratios (~10) and lower Ti and V abundances than most arc tholeiites. This pattern is consistent with the proposed origin of the Cpx-phyrlic Unit by fluid-induced melting of a previously depleted mantle source (Alabaster et al., 1982). The Late Dyke plots within the MORB field, but this diagram is not effective at discriminating within-plate sources from oceanic sources (see Figure 3.17).

### Th/Yb - Nb/Yb

Figure 3.17 displays the Aswad Block data on the Th/Yb versus Nb/Yb diagram of Pearce and Peate (1995). The SDC samples and many of the lavas plot within the MORB array. This indicates that the mantle source for the SDC and earliest lavas in the U.A.E portion of the ophiolite was similar to that of a 'normal' mid-ocean ridge. The remaining lava samples exhibit a subduction component demonstrated by relative enrichment of Th, indicating that a subduction-derived fluid component was added to the mantle source during the initial period of magmatic activity.

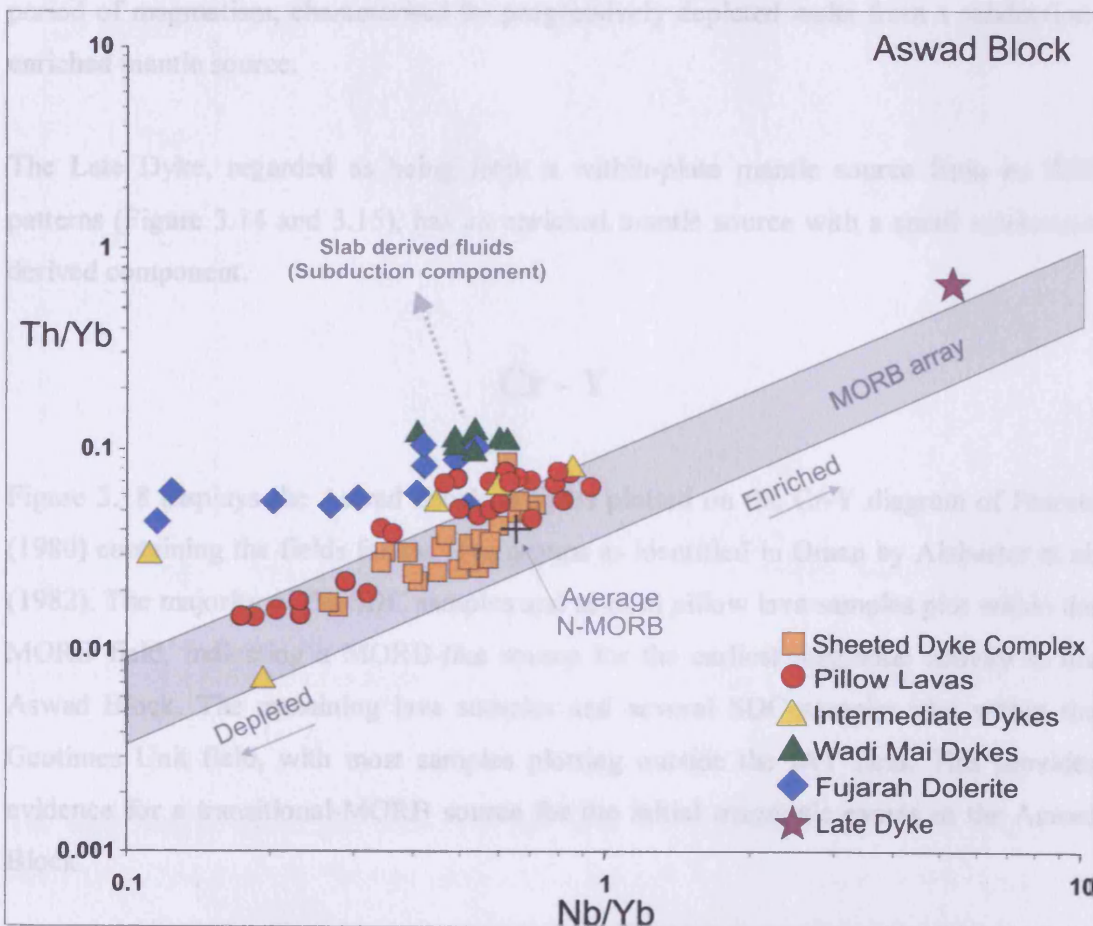


Figure 3.17, Th/Yb-Nb/Yb plot for the Aswad Block after Pearce and Peate, (1995). Increasing presence of slab-derived fluids move samples in direction of dashed-arrow

The Intermediate Dykes display a broad range of Nb/Yb compositions, ranging from a slightly enriched to a depleted mantle source, relative to N-MORB. The samples also display a range of Th/Yb ratios indicating the addition of a variable subduction component.

The Wadi Mai Dykes plot above the MORB field, with the addition of a subduction-derived component to a source mantle with average N-MORB composition. The Fujairah Dolerite samples also show evidence of a subduction derived component added to a depleted mantle source. The overlap between the Wadi Mai Dykes and the Fujairah Dolerite samples provides evidence that these two dyke groups are related to the same period of magmatism, characterised by progressively depleted melts from a subduction-enriched mantle source.

The Late Dyke, regarded as being from a within-plate mantle source from its REE patterns (Figure 3.14 and 3.15), has an enriched mantle source with a small subduction derived component.

### Cr - Y

Figure 3.18 displays the Aswad Block samples plotted on the Cr-Y diagram of Pearce, (1980) containing the fields for the lava groups as identified in Oman by Alabaster et al. (1982). The majority of the SDC samples and several pillow lava samples plot within the MORB field, indicating a MORB-like source for the earliest magmatic activity in the Aswad Block. The remaining lava samples and several SDC samples plot within the Geotimes Unit field, with most samples plotting outside the IAT field. This provides evidence for a transitional-MORB source for the initial magmatic events in the Aswad Block.

The Intermediate Dyke samples all plot within the IAT field and in particular within the Lasail Unit field, providing evidence that the Aswad Block experienced an additional

volcanic period when compared to the Khawr Fakkan Block, corresponding to the localised 'seamount' magmatic period of Alabaster et al. (1982).

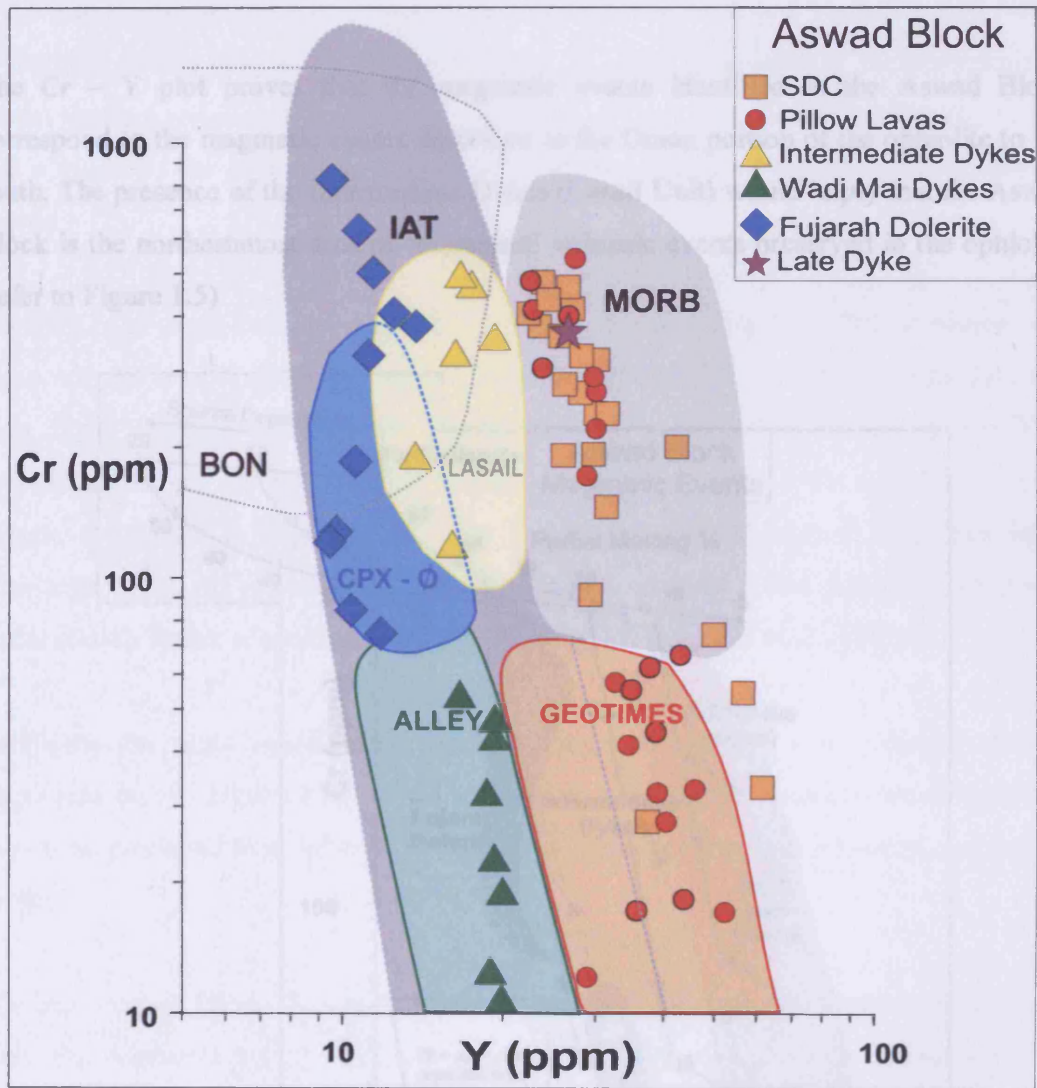


Figure 3.18, Cr/Y plot for the Aswad Block, MORB/IAT fields after Pearce (1980), partial BON field after Pearce (1981). Lava groups after Alabaster et al (1982).

The Wadi Mai Dykes all plot within the IAT field, and specifically within the field of the Alley Unit. The Fujairah Dolerite plots within the IAT field and the majority of samples correspond to the Cpx-phyric Unit as defined in Oman. The remaining Fujairah Dolerite samples plot within an area of overlap between the IAT and boninite fields with Y concentrations equivalent to the Cpx-phyric group, but with increased Cr, indicating

hydrous melting of a depleted mantle source. The Late Dyke is not well discriminated by this diagram and plots within the MORB field with similar Cr and Y concentrations as the SDC and some lavas.

The Cr – Y plot proves that the magmatic events identified in the Aswad Block correspond to the magmatic events described in the Oman portion of the ophiolite to the south. The presence of the Intermediate Dykes (Lasail Unit) would imply that the Aswad Block is the northernmost area of ‘seamount’ volcanic events preserved in the ophiolite (refer to Figure 1.5)

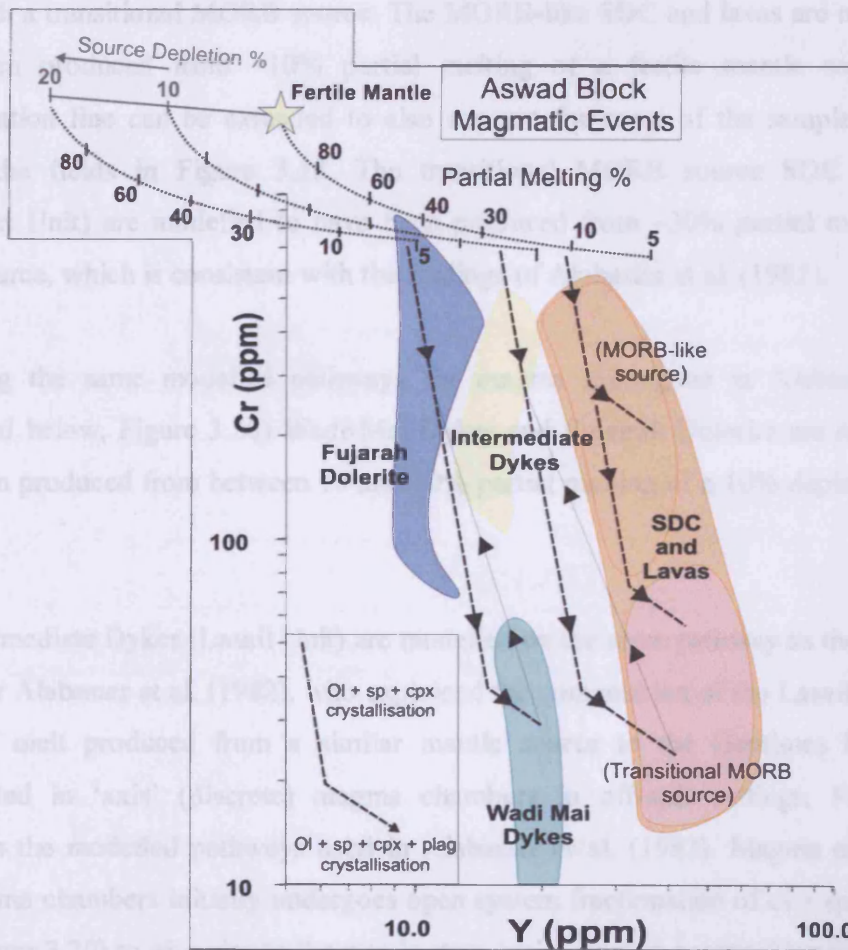


Figure 3.19, Modelled partial melting trends of the identified Khawr Fakkan Dyke Groups. Method of modelling based on the work of Pearce and Norry (1979) and Pearce (1980). Degrees of partial melting based on Alabaster et al. (1982) and Wake and Pearce (2005). Inset A: Highlights the evolution of the Lasail and Geotimes Units (taken from Alabaster et al., 1982). See Figure 3.20 for full explanation of mixing lines.



Figure 3.19 presents the modelled partial melting trends for the identified Aswad Block magmatic events (excluding the Late Dykes) compiled using the same method as section 3.2.4. Full details of the components and pathways can be found in Pearce and Norry (1979) and Pearce (1980). This method allows a general estimation of the percentage of partial melting required of the mantle source to produce the identified magmatic events and a guide to the differences between the relative levels of depletion of the mantle source.

The SDC and lavas can essentially be split into those with a MORB-like source, and those with a transitional MORB source. The MORB-like SDC and lavas are modelled to have been produced from ~10% partial melting of a fertile mantle source. This crystallisation line can be extended to also account for some of the samples that plot outside the fields in Figure 3.18. The transitional MORB source SDC and lavas (Geotimes Unit) are modelled to have been produced from ~30% partial melting of a fertile source, which is consistent with the findings of Alabaster et al. (1982).

Following the same modelled pathways for magma mixing as in Alabaster (1982) (explained below, Figure 3.20) Wadi Mai Dykes and Fujairah Dolerite are modelled to have been produced from between 10 and 30% partial melting of a 10% depleted mantle source.

The Intermediate Dykes (Lasail Unit) are modelled on the same pathway as the Geotimes Unit after Alabaster et al. (1982), who explained the composition of the Lasail Units as a result of melt produced from a similar mantle source to the Geotimes Unit being fractionated in 'axis' (discrete) magma chambers in off-axis settings. Figure 3.20 illustrates the modelled pathways used in Alabaster et al. (1982). Magma entering the axis magma chambers initially undergoes open system fractionation of ol + sp + cpx (B-C, in Figure 3.20) to give rise to the steady state 'axis' magma composition (D), erupted as the Geotimes Unit. Subsequent mixing of (depleted) remnants of this steady state magma and fresh magma entering the reduced axis chambers (D-B) gives rise to transitional lavas and the Lasail Unit (Intermediate Dykes) in the northern ophiolite.

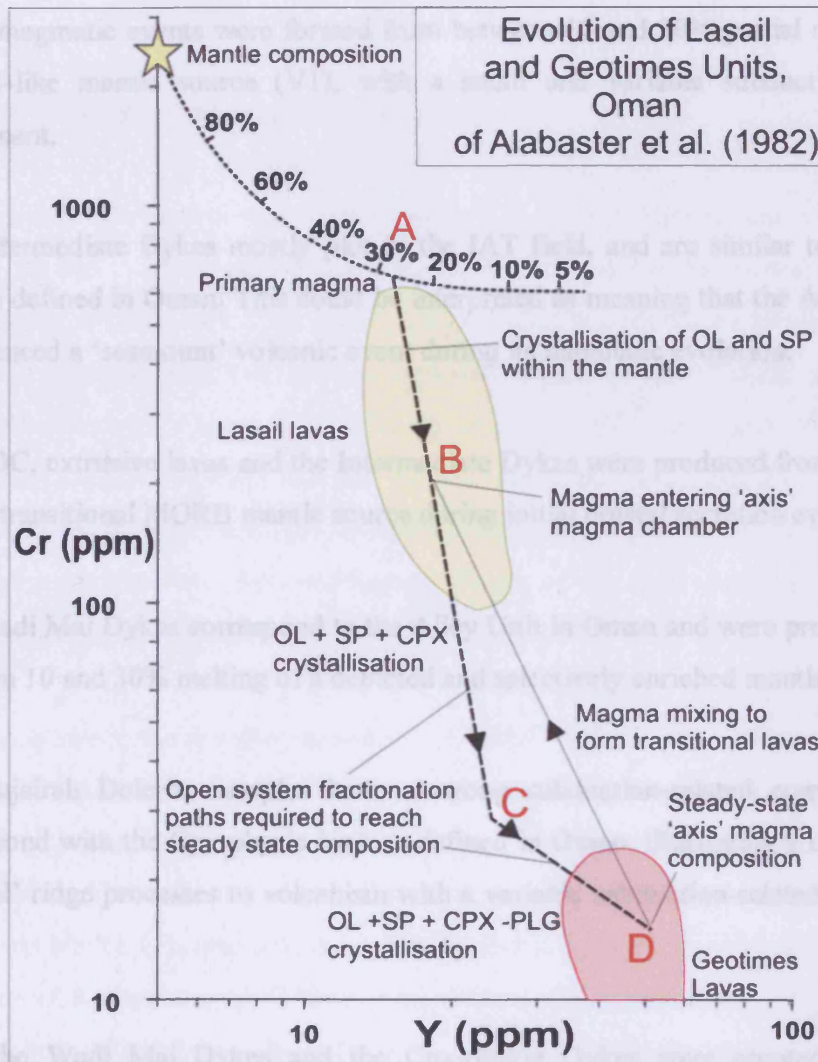


Figure 3.20, Highlighting the evolution of the Lasail and Geotimes lavas from a 30% partial melt to their erupted magma compositions after Alabaster et al. (1982). Method of modelling based on the work of Pearce and Norry (1979) and Pearce (1980). Pathways A-D explained in text.

### 3.3.5 Conclusions from Aswad Block

- The Sheeted Dyke Complex and some lavas exhibit MORB-like signatures, indicating formation at an N-MORB-like oceanic spreading centre not obviously influenced by subduction.

- Most of the extrusive lavas correspond to the Geotimes Unit, as defined in Oman. Initial magmatic events were formed from between 10 and 30% partial melting of a MORB-like mantle source (V1), with a small and variable subduction derived component.
- The Intermediate Dykes mostly plot in the IAT field, and are similar to the Lasail Unit as defined in Oman. This could be interpreted as meaning that the Aswad Block experienced a 'seamount' volcanic event during its magmatic evolution.
- The SDC, extrusive lavas and the Intermediate Dykes were produced from a MORB-like to transitional MORB mantle source during initial crustal accretion events (V1).
- The Wadi Mai Dykes correspond to the Alley Unit in Oman and were produced from between 10 and 30% melting of a depleted and selectively enriched mantle source
- The Fujairah Dolerite samples have a strong subduction-related component and correspond with the Cpx-phyric Unit as defined in Oman, illustrating a change from 'normal' ridge processes to volcanism with a variable subduction-related component (V2).
- Both the Wadi Mai Dykes and the Cpx-phyric Dykes were erupted in a SSZ environment during a second major magmatic period (V2).
- The Late Dyke displays a distinctive pattern of enrichment of incompatible elements typical of lavas from within-plate settings and was erupted during the last magmatic event (V3).
- The Aswad Block provides geochemical evidence for the transition from spreading to subduction-related volcanism (V1-V2), with successive magmatic events displaying an increased role of subduction related fluids.

## 3.4 Comparison between ophiolite blocks

### 3.4.1 Trace element ratio plots

The geochemical evidence presented in Sections 3.2 and 3.3 demonstrates that the lavas and dykes of the Aswad and Khawr Fakkan Blocks exhibit an increasing role for subduction-related fluids with time. Each Unit identified in both blocks displays a distinct geochemical signature and can be discriminated with the use of REE patterns and incompatible elements. Figure 3.21 presents selected REE ratio plots of the Khawr Fakkan and Aswad Block data and the data of Alabaster et al. (1982). This enables comparison to be made between the subduction component present in the northernmost U.A.E. blocks and the Fizh, Hilti and Sarami Blocks of the 1982 study (See Figure 1.5 for lava stratigraphy of Alabaster et al., 1982).

Comparison between the relative abundance of LREE, MREE and HREE illustrates the variation in the subduction-derived component present in the samples. To gauge the amount of depletion of the mantle source, La/Nd and Sm/Yb ratios are used. Other elements that could also be used in similar ratio plots include Ce/Sm versus Gd/Yb and Th/Yb versus Nb/Yb (Figures 3.9 and 3.17). Unfortunately in the original geochemical investigation of Alabaster et al. (1982) some of these elements (namely Nb, Ce and Gd) were either not analysed or were present at levels below detection in most samples, resulting in incomplete fields. Normalised values are used to compare the signatures with N-MORB

Figure 3.21 displays  $La_{(N)}/Nd_{(N)}$  versus  $Sm_{(N)}/Yb_{(N)}$  for the identified units of the Khawr Fakkan and Aswad Blocks and for the data of Alabaster et al. (1982). Depletion (or enrichment) of the mantle source is demonstrated by a decrease (or increase) in the  $Sm_{(N)}/Yb_{(N)}$  value, and subduction influence is recorded by an increase in the  $La_{(N)}/Nd_{(N)}$  value (much the same as the Th/Yb versus Nb/Yb plot). The data are presented with a

MORB array and fields for Boninites and BAB settings generated with data from [www.petdb.org](http://www.petdb.org) (fully listed in Appendix C).

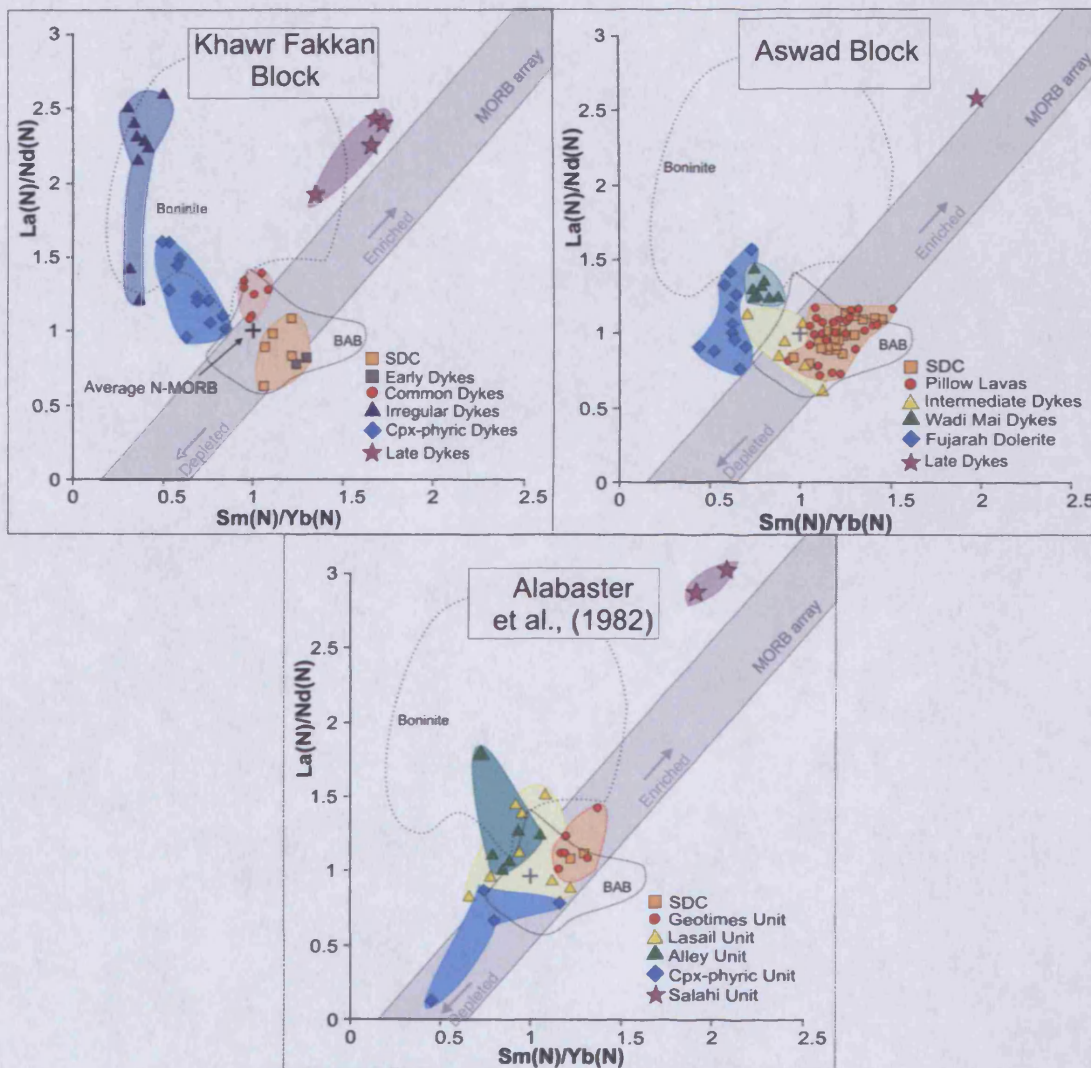


Figure 3.21,  $La_{(N)}/Nd_{(N)}$  versus  $Sm_{(N)}/Yb_{(N)}$  plots displaying regional variation of subduction component within the U.A.E blocks compared to data from Oman of Alabaster et al (1982). Normalised to the N-MORB values of Sun and McDonough (1989). The MORB array and BAB-Boninite fields were generated with data from [www.petdb.org](http://www.petdb.org) (see Appendix C for full list).

The earliest (V1) units present in the northern ophiolite blocks, illustrated in Figure 3.19, (Khawr Fakkan; SDC and Early Dykes. Aswad; SDC and Pillow Lavas. Alabaster; SDC and Geotimes Unit) plot close to the value of N-MORB within the MORB array. The

SDC and Geotimes Unit samples of Alabaster et al. (1982) plot within the MORB array, with a slightly enriched mantle source. The Common Dykes of the Khawr Fakkan Block, which correspond to the Geotimes Unit on the Cr/Y plot (Figure 3.10), plot mostly outside the MORB array. These dykes display an increase in the  $La_{(N)}/Nd_{(N)}$  value compared to the  $Sm_{(N)}/Yb_{(N)}$  value indicating an increase in the subduction component to the mantle source of this magmatic event. This increase demonstrates that the subduction component was present in the Khawr Fakkan Block, the most northerly block of the ophiolite, before it was present in the equivalent magmatic events elsewhere in the ophiolite, or that the Khawr Fakkan ('true' MORB) crust was accreted during an earlier period. This also provides evidence of independent melt supply to the magmatic foci of each block.

The next documented phase of magmatism is the Lasail Unit of Alabaster et al. (1982), most samples of which display a small subduction component added to a mantle source with a composition close to that of N-MORB, overlapping with the BAB field; slightly depleted in relation to the earliest (V1) magmatic events. This unit is also present in the Aswad Block (Intermediate Dykes), which have a similar range of  $La_{(N)}/Nd_{(N)}$  and  $Sm_{(N)}/Yb_{(N)}$  values to the Lasail Unit. The Lasail Unit magmatic event is not recorded in the Khawr Fakkan Block, providing more evidence for the discontinuity of magmatic events along the strike of the ophiolite.

The Alley Unit of Alabaster et al. (1982) is the next magmatic event in the Oman portion of the ophiolite (Figure 3.21). It is represented by  $Sm_{(N)}/Yb_{(N)}$  values close to that of N-MORB, but increased  $La_{(N)}/Nd_{(N)}$  values plotting close to, or within, the Boninite field indicating the addition of a subduction component to the mantle source. This magmatic event is represented in the Aswad Block by the Wadi Mai Dykes, which have generally higher  $La_{(N)}/Nd_{(N)}$  values than the Alley Unit as identified in Oman. Field relationships of dykes in the Khawr Fakkan Block indicate that the Irregular Dykes are the equivalent magmatic event to the Alley Unit in Oman (Section 2.2.7.3). These dykes have significantly higher  $La_{(N)}/Nd_{(N)}$  values than the Alley Unit and plot within the Boninite field. If the Irregular Dykes were emplaced in the Khawr Fakkan Block at the same time

as the Wadi Mai Dykes in the Aswad Block, then this is evidence for a significant difference in melt supply to these blocks, and places tectonic constraints on the setting of the ophiolite at the time of melt generation.

The next magmatic event identified in Oman is the Cpx-phyric Unit. This Unit is formed from the same source magma as the Alley Unit, but is less evolved, because it reached the surface rapidly without undergoing the same mixing (Alabaster et al., 1982). The  $La_{(N)}/Nd_{(N)}$  and  $Sm_{(N)}/Yb_{(N)}$  values for Alabaster et al. (1982) denote formation above a depleted mantle source with little subduction influence. The equivalent Units in the Khawr Fakkan (Cpx-phyric Dykes) and Aswad Blocks (Fujairah Dolerite) were produced from a slightly depleted mantle and contain a greater subduction component than the Units in Oman. The Alley Unit (Wadi Mai Dykes and Irregular Dykes) and Cpx-phyric Unit (Fujairah Dolerite and Cpx-phyric Dykes) were formed in a SSZ environment during a second major magmatic period (V2).

The final magmatic event is the Salahi Unit (Late Dykes). All data display a significantly enriched mantle source with a slight subduction component (Figure 3.21), possibly gained on ascent through continental crust, with some variation in the relative enrichment of the mantle between blocks. This is consistent with the interpretation that the Salahi Unit was produced from the melting of sub-continental mantle, possibly related to the onset of obduction (Alabaster et al., 1982).

The significant difference between the data from the northern Khawr Fakkan and Aswad Blocks and that from the southern ophiolite in Oman is that the subduction influence is stronger in the northernmost blocks (Figure 3.22). This is illustrated well by the presence of boninites in the Khawr Fakkan Block and in some areas of the Alley Unit of the Fizh Block (Ishikawa et al., 2002). Comparison between the Cpx-phyric Unit, Fujairah Dolerite and the Cpx-phyric Dykes also provides evidence that the northernmost Units exhibit an increased subduction signature (Figure 3.22).

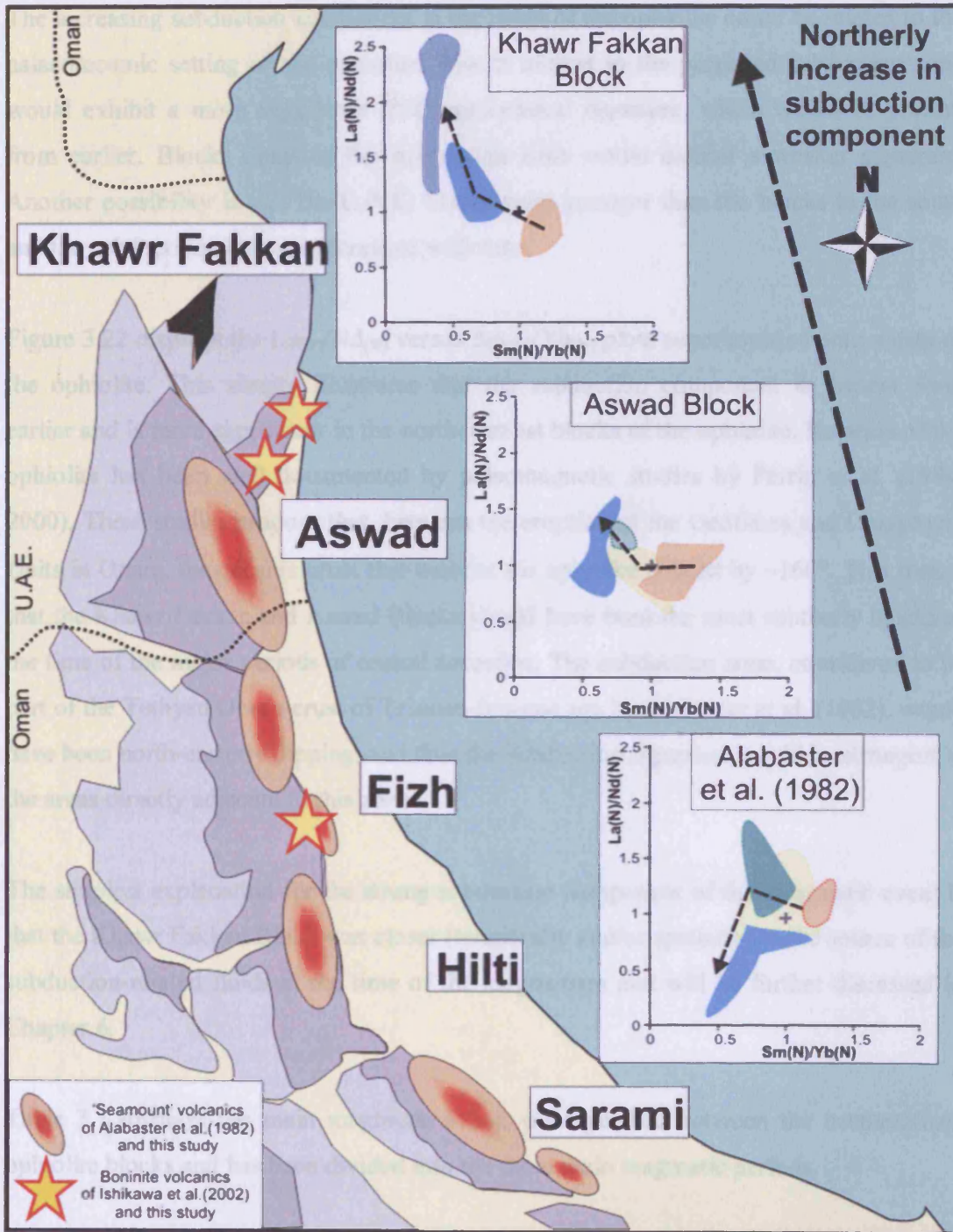


Figure 3.22, Illustrating the northerly increase in subduction component between the data of Alabaster et al. (1982) (Sarami, Hilti and Fizh Blocks) and this study (Aswad and Khawr Fakkan Blocks), illustrated by dotted arrows on the inset plots.



The increasing subduction component in the north of the ophiolite could be related to the palaeotectonic setting of the ophiolite. Blocks closest to the proposed subduction zone would exhibit a more significant SSZ geochemical signature, which would be present from earlier. Blocks distal to the subduction zone would exhibit a weaker signature. Another possibility is that the U.A.E. blocks were younger than the blocks to the south and the subduction signature increased with time.

Figure 3.22 displays the  $La_{(N)}/Nd_{(N)}$  versus  $Sm_{(N)}/Yb_{(N)}$  plots superimposed onto a map of the ophiolite. This simply illustrates that the subduction component is present from earlier and is more significant in the northernmost blocks of the ophiolite. Rotation of the ophiolite has been well documented by paleomagnetic studies by Perrin et al. (1994, 2000). These studies propose that, between the eruption of the Geotimes and Cpx-phyric Units in Oman, the oceanic crust that became the ophiolite rotated by  $\sim 160^\circ$ . This means that the Khawr Fakkan and Aswad Blocks would have been the most southerly blocks at the time of the major periods of crustal accretion. The subduction zone, considered to be part of the Tethyan Ocean crust of Triassic-Jurassic age by Alabaster et al. (1982), would have been north-easterly dipping, and thus the subduction signature would be strongest in the areas directly adjacent to this zone.

The simplest explanation for the strong subduction component of this magmatic event is that the Khawr Fakkan Block was closer (temporally and/or spatially) to the source of the subduction-related fluids at the time of the magmatism and will be further discussed in Chapter 6.

Table 3.1 displays the main magmatic events distinguished between the northernmost ophiolite blocks and has been divided into the three main magmatic periods.



Summary of main magmatic events		This Study		Umino et al, (1990)	Alabaster et al, (1980)
		Khawr Fakkan Block	Aswad Block	Fizh Block	Fizh, Hilti and Sarami Blocks
<b>V3</b> Last Magmatic Events (obduction related?)  Unconformity Increase in subduction component with time	<b>V3 (Salahi Unit)</b> Late Dykes <sup>a</sup>	<b>V3 (Salahi Unit)</b> Late Dyke	<b>Salahi Volcanics</b> Extrusive basalts and dolerite dykes	<b>Salahi Unit</b> Extrusive basalts and dolerite dykes <b>The Collision Event</b>	
	Cooling and rotation		Unconformity - (pelagic sediments)		
	<b>V2-II (Cpx-phyric unit)</b> Cpx-phyric Dykes	<b>V2-II (Cpx-phyric unit)</b> Cpx-phyric Dykes and Vinaigrette Unit sourced from fractionated intrusive Fujairah Gabbro		<b>Cpx-phyric Unit</b> Basalts distributed along NE-SW faults	
<b>V2</b> <b>SSZ source</b>  Unconformity Increase in subduction component with time	<b>V2-I (Alley Unit)</b> Irregular Dykes with boninitic composition	<b>V2-I (Alley Unit)</b> Wadi Mai Dykes	<b>Alley volcanics</b> Alternation of basalt and andesite Dacite at higher levels. Associated with Opx-series intrusive cumulates	<b>Alley Unit</b> Rhyolite, basalt and andesite Located on major NW-SE faults <b>The Rifting Event</b>	
	Rotation of crust		Unconformity (ferrous sediments and volcanic breccia)		
<b>V1</b> <b>MORB-like source</b> Earliest Magmatic Events	<b>V1-II (Geotimes Unit)</b> Common Dykes	<b>V1-III (Lasail Unit)</b> Intermediate Dykes		<b>Lasail Unit</b> Basalt, andesite Sourced from 'late intrusive complexes' (gabbro-diorite-tonalite-trondhjemite) <b>The 'Seamount' Event</b>	
		<b>V1-II (Transitional Geotimes Unit)</b> Intrusive Kalba Gabbro magmatic event		Unconformity <b>Transitional Lavas</b>	
	<b>V1-I (Early Dykes and SDC)</b> (only true-MORB source documented in ophiolite)	<b>V1-I (Geotimes Unit)</b> Extrusive basaltic andesites, feeder dykes and SDC	<b>Geotimes Volcanics</b> Alternation of basalt, andesite and rare dacite. Basalt predominates in higher levels	<b>Geotimes Unit</b> Basalt and andesite 'volcanic basement' <b>Marginal Basin Spreading Event</b>	

Table 3.1, Comparison between magmatic events identified in the Khawr Fakkan and Aswad Blocks and the events in the Fizh, Hilti and Sarami Blocks (Umino et al., 1990 and Alabaster et al., 1982). V1, V2 and V3 subdivisions after Ernewein et al. (1988) and Godard et al. (2002)

### **3.4.2 Conclusions from comparison between ophiolite blocks**

- The Geotimes Unit (SDC, lavas and Early Dykes) and Lasail Unit (Wadi Mai Dykes) were formed during initial magmatic events (V1) from a MORB-like to Transitional MORB mantle source.
- The Alley Unit (Wadi Mai Dykes and Irregular Dykes) and Cpx-phyric Unit (Fujairah Dolerite and Cpx-phyric Dykes) were formed in a SSZ environment during a second major magmatic period (V2).
- Each ophiolite block studied displays a unique magmatic history, with equivalent magmatic events displaying different  $La_{(N)}/Nd_{(N)}$  and  $Sm_{(N)}/Yb_{(N)}$  ratios depending on melt supply and their proximity to the subduction zone.
- The subduction zone signature is stronger in the northernmost ophiolite blocks.
- The Aswad and Khawr Fakkan Blocks were closer to the proposed subduction zone than those studied by Alabaster et al. (1982) from the Fizh, Hilti and Sarami Blocks in Oman.
- Magmatic events can be split into three main periods V1 (MORB-transitional MORB source), V2 (SSZ source) and V3 (Within-plate source).

To further study the crustal evolution of the Aswad and Khawr Fakkan Blocks it is necessary to investigate the possible plutonic sources for the identified magmatic events to establish the order of crustal accretion events represented by the Upper Gabbros and late intrusive gabbros.

## **Chapter 4: LA-ICP-MS Study of Clinopyroxenes from the Plutonic Section**

### **4.1 Introduction**

The aims of this chapter are to investigate the trace element compositions of clinopyroxene mineral phases within the crustal gabbro section and to establish geochemical links between the magmatic events identified in Chapter 3 (Summarised in Table 3.1) and their parental plutonic gabbros. Cumulate gabbro whole-rock chemistry tells us what was mixed and eventually crystallised but, because of compositional variability, there are limits to the interpretation of this data. Individual whole-rock compositions for cumulate rocks will represent a combination of: (1) the composition(s) of the liquid(s) from which the crystals grew (both cumulus and post-cumulus) that reflect both variations in the compositions of melts extracted from the mantle and the compositional evolution of the crust including chemical exchange reactions with percolating interstitial melts; (2) the modal proportions of mineral phases which may reflect both physical and chemical processes, such as mixing of crystal populations; and (3) subsequent compositional modifications during sub-solidus hydrothermal alteration (Coogan et al., 2000). Previous studies of the Oman ophiolite have shown that the composition of gabbros are not equivalent to basaltic liquids, but are representative of cumulate composition (e.g. Browning and Smewing, 1981 and Browning, 1982) and have also provided information about crystal-melt separation during cumulate formation and melt fractionation (Coogan et al., 2001).

The whole-rock and trace element data for the gabbro sequence provides only a small insight into their mode of formation and original melt compositions. Whole-rock data can indicate the relative depth of crystallisation between samples, and the efficiency of the expulsion of trapped melt (Coogan et al., 2001). However, it provides no significant evidence to discriminate between the compositions of the initial melts that crystallised to form these rocks. To gather data of more value it is therefore necessary to analyse compositions of individual mineral phases within the gabbros which will hopefully preserve the initial composition of the source melt.

## 4.2 Introduction to clinopyroxenes

To further study the magma plumbing system beneath the ophiolite blocks (including melt generation, delivery and aggregation), it is necessary to investigate the geochemistry of individual cumulus phases, in this case, by using the silicate mineral clinopyroxene. This rock-forming mineral was chosen as the analyte phase because most trace elements partition into clinopyroxene more readily than plagioclase, leading to higher relative abundances, and therefore better detection limits. Clinopyroxene is also commonly more resistant to alteration than olivine and plagioclase because of the greater energy required to break the strong Si-O bonds in its  $\text{Si}_2\text{O}_6$  chains (Pearce, 2003). Analysis of clinopyroxene REE and trace elements will enable modelling (Chapter 5) to establish primary compositions of the melts supplied to different areas of the crust, and for comparison to be made between each Massif. The ubiquitous presence of clinopyroxene in all stratigraphic units of the ophiolite also permits comparisons across the whole field area.

Normal mid-ocean ridge basalts (N-MORB) crystallise clinopyroxene at a late stage, with the crystallisation order olivine-plagioclase-clinopyroxene. Therefore clinopyroxene crystals from this setting may not record compositional information about the nature of the melt prior to mixing and fractionation (Coogan et al., 2003). Because of the higher oxygen fugacity in SSZ settings, the crystallisation order is changed to olivine-clinopyroxene-plagioclase (Rocci et al., 1975), which offers potential for the preservation of more information about the evolution of the magma.

## 4.3 Clinopyroxene trace element characteristics

Recent research has provided much insight into partitioning of trace elements into clinopyroxene. There are, however, two assumptions that we must make if we are to consider trace element abundance in individual crystals as representing compositions of their parental melts. First we must be sure that the crystals formed in equilibrium

with the surrounding melt, and that the partitioning between melt and crystals was constant during crystal growth. Second we must also be certain that, subsequent to formation, there has been no modification of the crystal composition, for example, by re-equilibration with trapped melt (Coogan et al., 2002).

To investigate the first requirement, experimental studies have shown that surface equilibrium between melt and clinopyroxene is highly probable during crystal growth (Watson, 1996) and disequilibrium growth, even at temperatures of  $>1210^{\circ}\text{C}$ , is unlikely at natural growth rates (Van Orman et al., 2001). It has also been shown by Shimizu (1981) that disequilibrium partitioning leads to an enrichment of high charge-to-mass elements over lower charge-to-mass elements. This means that variation in the extent of disequilibrium will lead to variations in the effective partition coefficient during crystallisation (Coogan et al., 2002) and therefore elements such as Zr and Nd would be fractionated. They instead exhibit a strong positive correlation, as seen in Figure 4.1.

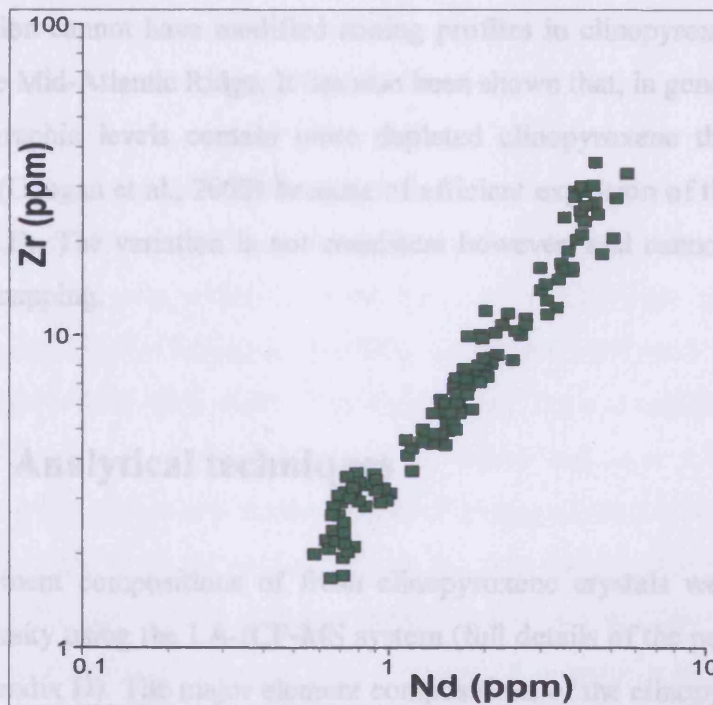


Figure 4.1, Clinopyroxene Zr and Nd values (ppm) gathered by LA-ICP-MS from representative samples used in this study. The strong positive correlation between the elements provides evidence for equilibrium growth of the crystals. Disequilibrium growth would result in a poor correlation.

The recent availability of data from cumulate samples recovered from various Legs of the Ocean Drilling Project (ODP) also permits direct comparison between ophiolite

samples and samples from the slow-spreading Mid-Atlantic Ridge and fast-spreading East Pacific Rise. The comparison is appropriate unless crystallisation rates were substantially different during the formation of the Oman-U.A.E. ophiolite (Coogan et al., 2002). The final argument against disequilibrium growth is that the sampled plutonic rocks are all relatively equigranular, and have similar coarse grain sizes, indicating simultaneous crystallisation. If disequilibrium growth had taken place then one would expect to see varied grain sizes and other evidence of differentiated crystallisation, such as chilled margins (Coogan et al., 2002). Caution should be used when interpreting data from gabbro pegmatite samples, as accessory mineral phases, such as apatite and zircon, are common and can strongly partition certain incompatible elements (L. Coogan, pers comm.).

Post-crystallisation modification by diffusive elemental transport between clinopyroxene crystals is unlikely to have affected the cores of the crystals, as all elements analysed have slow diffusion rates (Sneeringer et al., 1984; Van Orman et al., 2001). Coogan et al. (2000b) also support these findings, demonstrating that sub-solidus diffusion cannot have modified zoning profiles in clinopyroxene in plutonic rocks from the Mid-Atlantic Ridge. It has also been shown that, in general, rocks from deeper stratigraphic levels contain more depleted clinopyroxene than those from higher levels (Coogan et al., 2002) because of efficient expulsion of the trapped melt fraction (T.M.F). The variation is not consistent however, and cannot be applied to fieldwork or mapping.

#### **4.4 Analytical techniques**

The trace element compositions of fresh clinopyroxene crystals were analysed at Cardiff University using the LA-ICP-MS system (full details of the procedure can be found in Appendix D). The major element compositions of the clinopyroxene sample were determined using the Cardiff University SEM-EDS system. Several crystals per slide were chosen for analysis on the basis that they were unaltered and large enough for a line to be ablated (minimum 250 $\mu$ m diameter, preferably ~1-2mm). Initially, a minimum of three crystals were selected per slide and three lines of analysis were

ablated per crystal. After the procedure was established, the number of lines per crystal varied according to the size and level of alteration of the target crystal. Large crystals were chosen to increase the probability that the section represented the centre of the crystal and therefore carried a record of the primary melt composition. It is more likely that crystals will be sectioned obliquely, and therefore the centres of these crystals will not expose the true cores. However, because of the length of the LA-ICP-MS ablation (250-300 $\mu$ m) and the (relatively) very large volume of sample analysed compared to ion-probe techniques, the effects of crystal zoning are minimised (further discussion of the technique and its implications can be found together with the full data set in Appendix D).

Because of the hydrothermal amphibolitisation of clinopyroxenes, only the freshest samples were analysed, specifically ten samples from the Khawr Fakkan Block, and eighteen from the Aswad Block. All samples chosen had low visual alteration and low whole-rock LOI (within the range 0.03 to 3.44 wt %). Although samples were selected for their freshness amphibolitisation was observed in most samples, especially along clinopyroxene cleavage planes. When such alteration was present, an alternative crystal on the section was selected for analysis.

The results are presented with fields of other clinopyroxene analysis from gabbros collected at present-day spreading centres and the Troodos ophiolite in Cyprus. The modern-day samples were collected from the East Pacific Rise (EPR) and Mid Atlantic Ridge (MAR) by Coogan et al (2000a, 2000b and 2002) and are displayed as a combined EPR-MAR data field. The fields have been combined because the individual fields share a very similar range of values and have a large degree of overlap. The similar signature is related to the efficiency of the mixing processes that compositionally diverse partial melt undergoes prior to the eruption of an N-MORB signature melt. The database for clinopyroxene analysis is small, as the technique is still relatively new, with insufficient data available to produce a standard set of N-MORB values for normalisation and comparison of the data. For the comparison of the REE in Figures 4.3 and 4.9 chondrite normalised REE plots are used to avoid any uncertainty that would arise from normalising the data to the available MORB clinopyroxene data.



## **4.5 Clinopyroxene trace element geochemistry of the Khawr Fakkan Block plutonic series**

### **4.5.1 Khawr Fakkan Block field observations**

In this study, ten samples were analysed from the Khawr Fakkan Block: two Mantle Transition Zone Gabbros (MTZ Gabbro), two Layered Gabbros, five Upper Gabbros and one Gabbro Pegmatite. Note that the terms used for these samples reflect only their general stratigraphic position. Although the number of samples is limited, it was considered a sufficient initial sample base from which to establish links between the plutonic units and the Dyke Groups identified in Chapters 2 and 3.

As already stated in Chapter 2, the southern Khawr Fakkan Block crustal section exposes the lower and upper crustal gabbros in a range of coastal hills with summits ranging in height from 100 to 600m. The majority of the western Massif is composed of the mantle sequence and Moho. The overlying crustal gabbro units dip at  $\sim 30^\circ$  to the east (Figure 2.2) in the areas of the Block where gabbroic samples were collected.

The MTZ Gabbro samples (UAE276 and UAE322) are gabbroic sills from within the MTZ. Sample UAE276 is from a 1m thick gabbro sheet, which intrudes a wehrlite, within a lobe of MTZ that intrudes the lowermost Layered Gabbro sequence. Such intrusive areas of the MTZ suite of rocks (dunite, clinopyroxenite, wehrlite and gabbro sills) are observed cross-cutting the Layered Gabbro sequence, and are assumed to be off-axis features related to the intrusion of wehrlites (e.g. Koga et al., 2001). Sample UAE322 is taken from a major sheet of gabbro ( $\sim 10$ m thick) within dunite. The upper contact is diffuse and plagioclase from the gabbro has impregnated the dunite up to 10 cm away from the contact.

Layered Gabbro samples (UAE419 and UAE421) are taken from typical modal layers,  $\sim 15$ cm in thickness, within the layered gabbro sequence. Mineral constituents display layer- (and Moho-) parallel alignment. Sample UAE421 is from a layer associated with ultramafic bands, close to the base of the Layered Gabbro sequence.

Such ultramafic sills have been interpreted in Oman by Boudier et al. (1996) as the relics of contemporaneous wehrlitic sills.

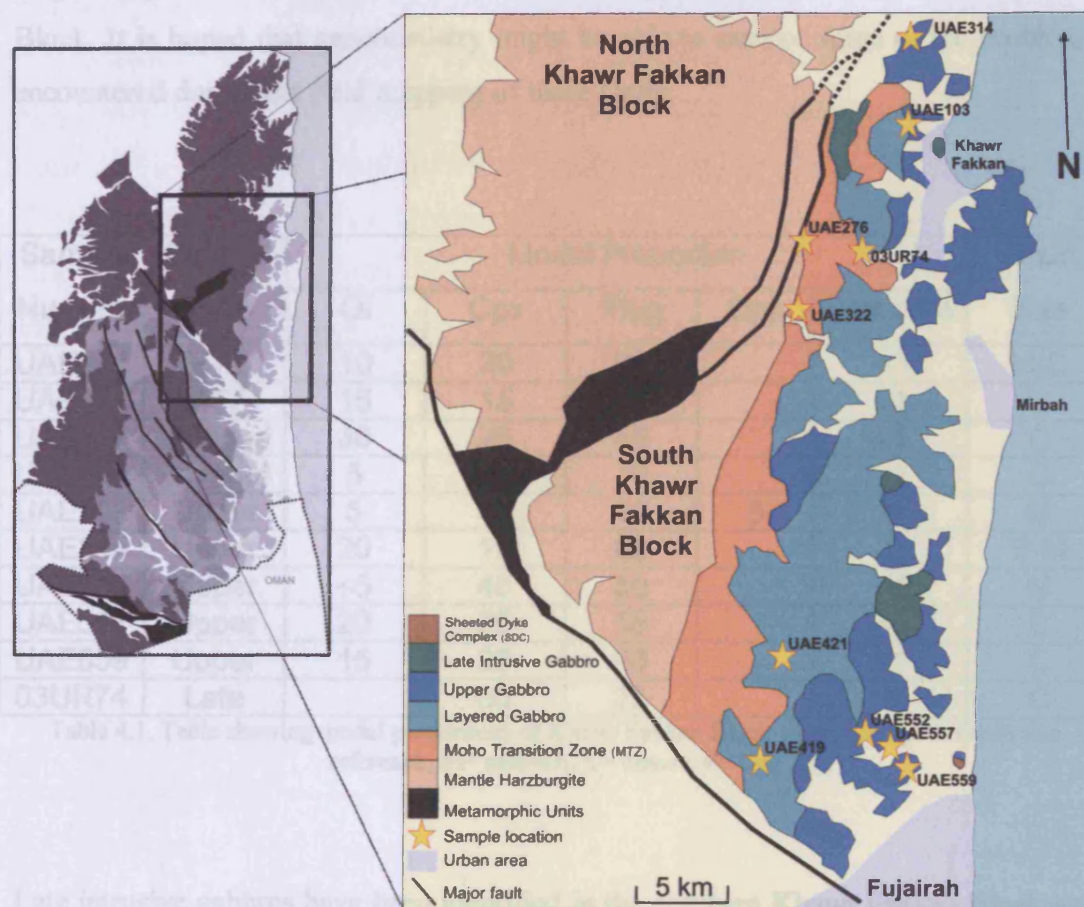


Figure 4.2, Sketch map of the Southern Khawr Fakkan Block. Stars represent the locations of gabbro samples used in LA-ICP-MS study. Sample co-ordinates are fully listed in Appendix D.

Upper Gabbro samples (UAE103, UAE314, UAE552, UAE557 and UAE559) are from a variety of stratigraphic heights, but all are medium- to coarse-grained gabbros. Modal proportions vary between samples (as can be seen in Table 4.1) and all Upper Gabbro samples crystallised in the order olivine-plagioclase-clinopyroxene. Field mapping identified multiple units of gabbro with individual field characteristics, varying in composition between foliated gabbro and olivine melagabbro and were initially interpreted as multiple late intrusive events. Continued field mapping and observation of these units was inconclusive and few firm boundaries could be established because of widespread heterogeneity of the Upper Gabbro units, even on an outcrop scale. This heterogeneity has been interpreted as representing the very earliest stages of crustal gabbro accretion, as all Upper Gabbros sampled for LA-ICP-

MS analysis are cut by dykes of 'Geotimes' composition and all subsequent dyke groups. All dykes chill in contact with the Upper Gabbros, indicating that the main magmatic period of formation was early in the magmatic history of the Khawr Fakkan Block. It is hoped that geochemistry might be able to resolve some of the problems encountered during the field mapping of these Units.

Sample Number	Gabbro Type	Modal Proportion					Grain Size
		OI	Cpx	Plag	Opx	Opaques	
UAE276	MTZ	10	30	60		<1	M-C
UAE322	MTZ	15	15	70		<1	C
UAE419	Layered	30	25	45		<1	C
UAE421	Layered	5	25	70		<1	C
UAE103	Upper	5	45	45	5	5	M
UAE314	Upper	20	19	60		1	F-M
UAE552	Upper	<5	45	50		<1	M
UAE557	Upper	20	25	55		<1	C
UAE559	Upper	15	25	60		<1	C
03UR74	Late		60	35		5	C

Table 4.1, Table showing modal proportions of Khawr Fakkan Block gabbro samples. Grain size reference; M= medium, C= coarse, F= fine

Late intrusive gabbros have been identified in the southern Khawr Fakkan Block and are associated with the Cpx-phyric Dyke Group and contemporaneous wehrlitic intrusions. The former have similar REE patterns to the Clinopyroxene-phyric Unit identified in Oman (Chapter 3). Unfortunately no samples of the late intrusive gabbros identified in the region of Khawr Fakkan (Figure 4.2) were available for LA-ICP-MS analysis because of fieldwork constraints and high levels of alteration. A sample from a late intrusive gabbro pegmatite (03UR74) was collected and found to be suitable for analysis. The pegmatite intrudes Layered Gabbros and is associated with dunites and clinopyroxenites/wehrlites and represents a late intrusive event. The intrusion corresponds to the first group of late intrusions as identified by Browning (1981) and Browning and Smewing (1982). Individual megacrysts of clinopyroxene from this body measured up to 100 mm in diameter. The gabbro pegmatite crystallised with the order olivine-clinopyroxene-plagioclase.

## 4.5.2 Chondrite-normalised multi-element patterns

The fields for Khawr Fakkan Block clinopyroxene compositions can be seen in Figure 4.3 normalised to the chondrite values of Anders and Grevesse (1989). The EPR-MAR data field is characterised by depletion in LREE compared to HREE with negative Ti, Zr and Sr anomalies. The outline of clinopyroxene data collected by Coogan et al. (2003) from the plutonic section of the Troodos ophiolite, which formed in a Supra Subduction Zone (SSZ) setting, are represented as a dotted field. The Troodos data field displays similar patterns to the EPR-MAR field, but with a greater range and generally lower values.

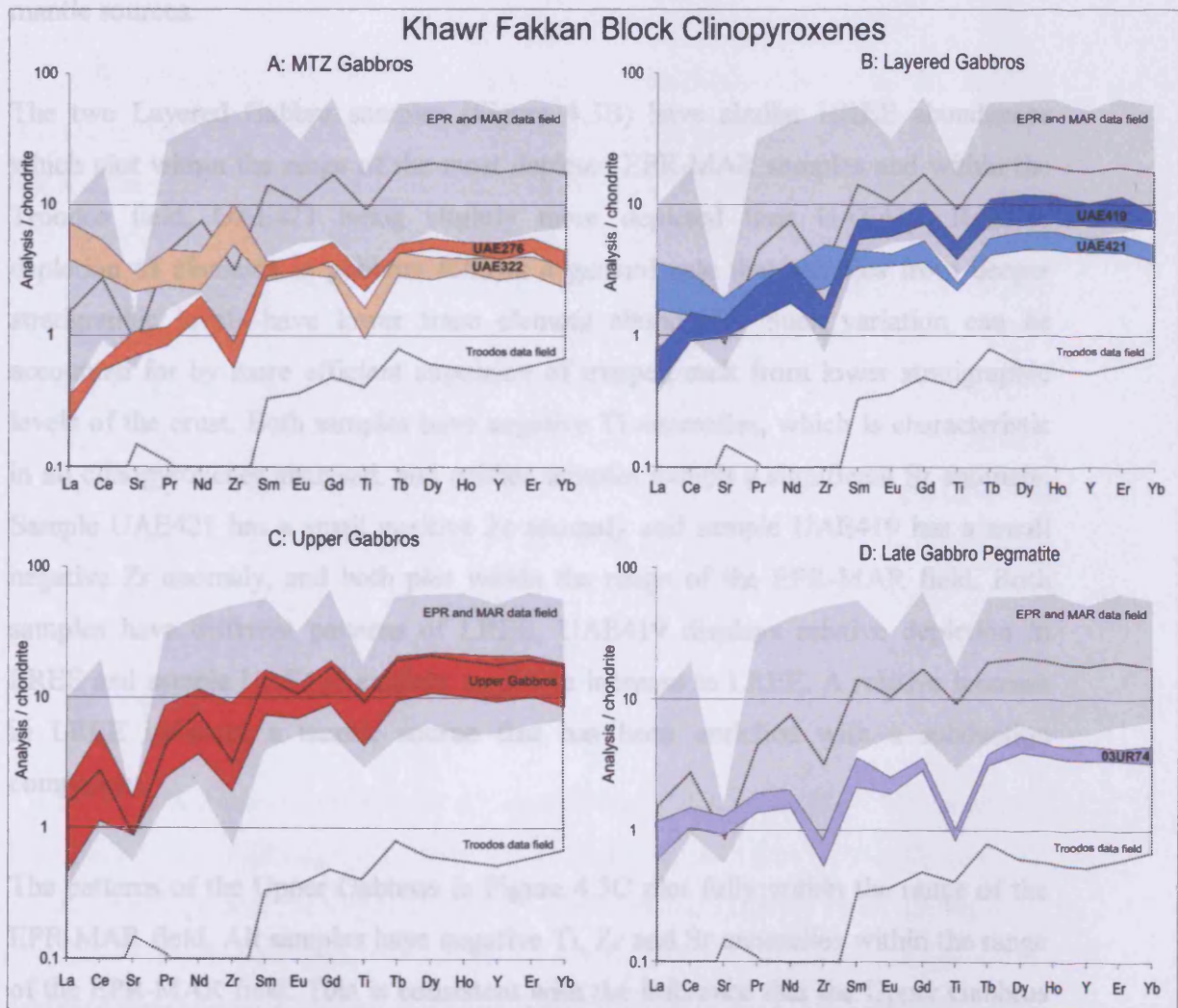


Figure 4.3, Chondrite-normalised (Anders and Grevasse, 1989) extended REE diagrams (with Sr, Zr, Ti and Y) for clinopyroxene of the Khawr Fakkan Block. Composite EPR-MAR and Troodos fields after Coogan et al. (2000a, 2000b, 2002, 2003).

It can be seen in Figure 4.3A that the two MTZ Gabbro clinopyroxene samples have distinctly different patterns. Both samples are depleted in HREE compared to the EPR-MAR field and have distinct negative Ti anomalies that lie within the range of the Troodos field. Sample UAE276 has a negative Zr anomaly and depletion in LREE (including Sr) compared to HREE, which conforms to the pattern of the EPR-MAR and Troodos fields. Sample UAE322 has a positive Zr anomaly and is progressively enriched in LREE (including Sr) compared to HREE indicating an enriched mantle source. This pattern of LREE enrichment is shared by the Late Dykes, which correspond to the Salahi Unit identified in Oman. The different patterns of LREE enrichment demonstrates that the two MTZ Gabbro samples probably have different mantle sources.

The two Layered Gabbro samples (Figure 4.3B) have similar HREE abundances which plot within the range of the most depleted EPR-MAR samples and within the Troodos field, UAE421 being slightly more depleted than UAE419. Relative depletion of elements in gabbros follows a general rule that samples from deeper stratigraphic levels have lower trace element abundance. Such variation can be accounted for by more efficient expulsion of trapped melt from lower stratigraphic levels of the crust. Both samples have negative Ti anomalies, which is characteristic in all clinopyroxenes analysed, and neither samples exhibit a significant Sr anomaly. Sample UAE421 has a small positive Zr anomaly and sample UAE419 has a small negative Zr anomaly, and both plot within the range of the EPR-MAR field. Both samples have different patterns of LREE; UAE419 displays relative depletion in LREE and sample UAE421 exhibits a relative increase in LREE. A relative increase in LREE indicates a mantle source that has been enriched with a subduction component.

The patterns of the Upper Gabbros in Figure 4.3C plot fully within the range of the EPR-MAR field. All samples have negative Ti, Zr and Sr anomalies within the range of the EPR-MAR field. This is consistent with the inference that the Upper Gabbros formed from a mantle source similar to that beneath the present-day EPR and MAR.

The late intrusive gabbro pegmatite (03UR74) has HREE concentrations that plot within the Troodos field. The sample has significant negative Ti and Zr anomalies and a slight negative Sr anomaly. A positive Sr anomaly in samples with the depleted incompatible element abundances has been noted by Coogan et al. (2002) while studying clinopyroxenes from the Troodos ophiolite plutonic sequence. The positive Sr anomaly was shown to be consistent with a model in which the parental melts for these samples were generated from a depleted source into which Sr, and to a lesser extent LREE, were added in a SSZ environment (Coogan et al., 2002).

### 4.5.3 Comparison between relative abundances of REE

As demonstrated in Chapter 3 (Section 3.4.1), comparison between the relative abundance of LREE, MREE and HREE elements can illustrate the variation in the subduction-derived component present in samples. The  $La_{(n)}/Nd_{(n)}$  versus  $Sm_{(n)}/Yb_{(n)}$  plot is especially useful when dealing with clinopyroxenes, which can have large variations in element abundance, essentially seeing-through the effects of varying abundance of REE between samples. As in Section 3.4.1, other REE element ratios could be used to interpret the depletion of the mantle source and the subduction-derived component, such as  $Ce_{(n)}/Sm_{(n)}$  and  $Gd_{(n)}/Yb_{(n)}$ . However, for continuity,  $La_{(n)}/Nd_{(n)}$  versus  $Sm_{(n)}/Yb_{(n)}$  is again used. Chondrite values of Anders and Grevesse (1989) are used to normalise the samples and data for clinopyroxenes gathered from the EPR-MAR (Coogan et al., 2000a, 2000b, 2002) and Troodos (Coogan et al., 2003) are again used to provide fields for modern mid-oceanic spreading centres and SSZ settings respectively.

Figure 4.4 effectively discriminates clinopyroxenes with a subduction component on the basis of their high  $La_{(n)}/Nd_{(n)}$  ratios however, the depletion of the mantle source is not as well displayed. All Upper Gabbros, Layered Gabbro sample UAE419 and MTZ Gabbro UAE276 plot within the combined EPR-MAR field, indicating a LREE depleted mantle source, similar to those of the EPR and MAR. This pattern is similar to that of the initial magmatic phases identified in Section 3.2 and is consistent with

the same mantle source and period of formation as the Early Dykes and SDC. This concurs with the field evidence for these gabbro samples.

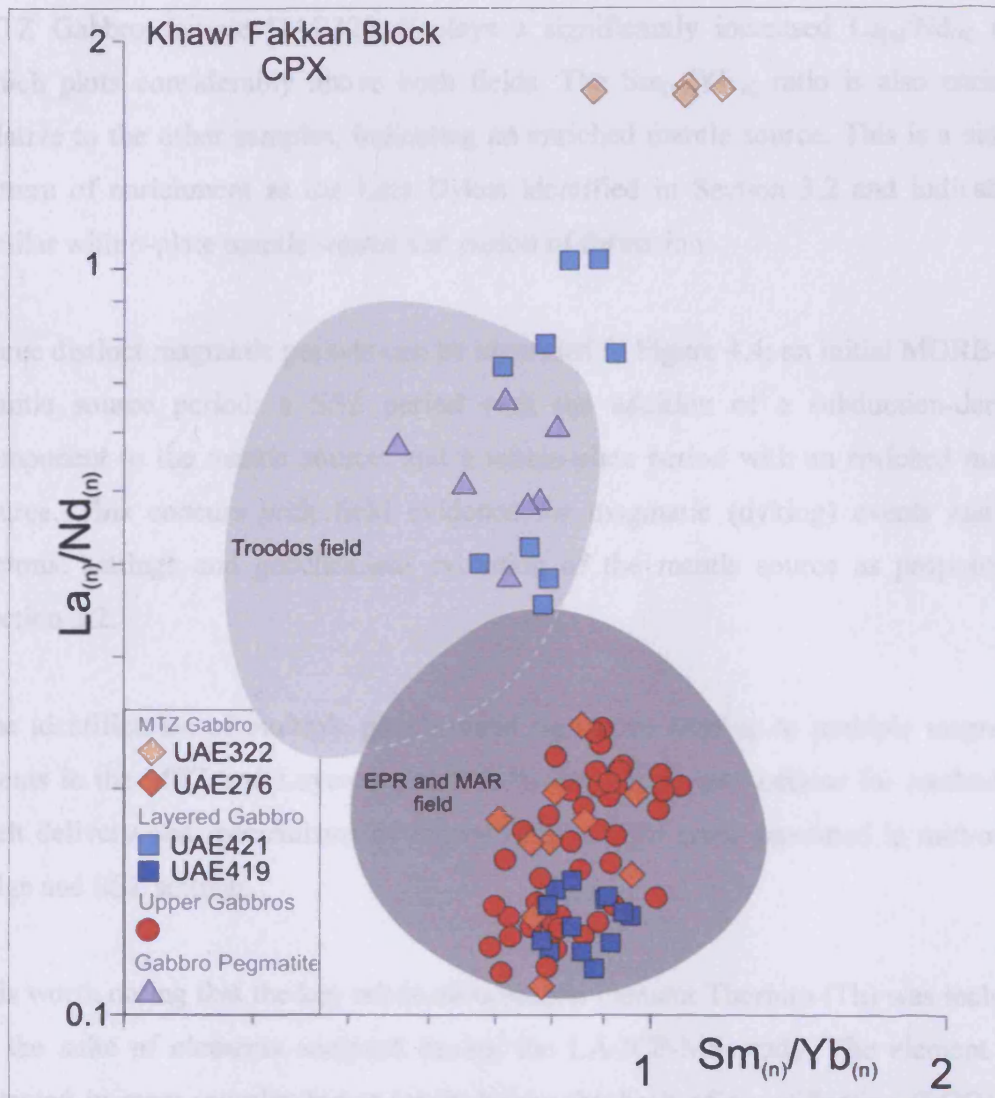


Figure 4.4.  $La_{(n)}/Nd_{(n)}$  versus  $Sm_{(n)}/Yb_{(n)}$  plot displaying results for LA-ICP-MS analysis of Khawr Fakkan Block clinopyroxenes normalised to the chondrite values of Anders and Grevesse (1989). Composite EPR-MAR and Troodos fields after Coogan et al, (2000a, 2000b, 2002, 2003)

Layered Gabbro sample UAE421 and late gabbro pegmatite sample 03UR75 plot within or close to the Troodos field, with an increased  $La_{(n)}/Nd_{(n)}$  ratio demonstrating a mantle source with a subduction-derived component. The gabbro pegmatite has an average  $Sm_{(n)}/Yb_{(n)}$  ratio which is slightly lower than that of the samples that plot within the EPR-MAR field, indicating a more depleted mantle source. This is similar to the pattern of enrichment found in the Irregular Dykes and Cpx-phyric Dykes

identified in Section 3.2 and provides evidence for the same mantle source and period of formation.

MTZ Gabbro sample UAE322 displays a significantly increased  $La_{(n)}/Nd_{(n)}$  ratio which plots considerably above both fields. The  $Sm_{(n)}/Yb_{(n)}$  ratio is also enriched relative to the other samples, indicating an enriched mantle source. This is a similar pattern of enrichment as the Late Dykes identified in Section 3.2 and indicates a similar within-plate mantle source and period of formation.

Three distinct magmatic periods can be identified in Figure 4.4; an initial MORB-like mantle source period; a SSZ period with the addition of a subduction-derived component to the mantle source; and a within-plate period with an enriched mantle source. This concurs with field evidence for magmatic (dyking) events and the tectonic settings and geochemical evolution of the mantle source as proposed in Section 3.2.

The identification of multiple geochemical signatures relating to multiple magmatic events in the MTZ and Layered Gabbros has important implications for methods of melt delivery and mechanisms of crustal accretion for crust generated in mid-ocean ridge and SSZ settings.

It is worth noting that the key subduction-mobile element Thorium (Th) was included in the suite of elements analysed during the LA-ICP-MS study. The element was detected in most samples but at levels below the limit of quantification (LOQ). Th was present in samples UAE322 and UAE421 at quantifiable levels several orders of magnitude greater than other samples. This concurs with the evidence presented in Figure 4.4 that these samples have the most enriched mantle source, and concurs with similar Th enrichment of the Late Dyke Group presented in Section 3.2. Full data tables can be found in Appendix D.



#### 4.5.4 Trace element characteristics

Clinopyroxene REE ratios clearly discriminate between gabbros from the Khawr Fakkan Block containing a subduction-derived (LREE) component, but do not clearly illustrate variations in the relative depletion or enrichment of the mantle source. Further investigation into the composition of the mantle source can be achieved using elements that are unlikely to be significantly affected by the addition of a slab-derived component (e.g. Cr, Y, Ti and V). Data fields for clinopyroxenes from the EPR and MAR (Coogan et al., 2000a, 2000b, 2002) and Troodos (Coogan et al., 2003) are used to generate fields for mid-oceanic and SSZ settings respectively. Overlap is illustrated by a dashed line.

### Ti – V

The Ti/V diagram of Shervais (1982) can be used to investigate the redox conditions, percentage of source melting and amount of source depletion under which the parental melts to the Khawr Fakkan Block formed (illustrated by arrows in Figure 4.5). As described in Chapter 3; the distribution coefficient for V ( $D_V$ ), is a function of the oxidation state of the mantle of the source region. The field for Troodos clinopyroxenes is displaced relative to the EPR and MAR field to lower Ti for a given value of V. This could be explained by an initial depletion of the mantle source under relatively reducing conditions, at a normal mid-ocean ridge, which remelted under more oxidising (SSZ) conditions (Coogan et al., 2002). The plot is displayed in this section with a logarithmic scale on both axes to best display the range of values obtained by this study and those of Coogan et al (2000a, 2000b, 2002 and 2003).

All Khawr Fakkan Upper Gabbros plot within or close to the EPR-MAR field perhaps indicating oxidising conditions, percentage of source melting and source depletion for the parental melt to be similar to those found at a modern day mid-ocean ridge.

Both Layered Gabbro samples plot within the Troodos field or within the overlap between the fields. Sample UAE419 is slightly more depleted than, but overlaps, the

Upper Gabbro samples indicating a similar and MORB-like source and possibly a time of formation similar to that of the Upper Gabbros. Sample UAE421 plots entirely within the Troodos field providing evidence for a more depleted mantle source that has undergone a greater degree of partial melting than the Upper Gabbros and UAE419.

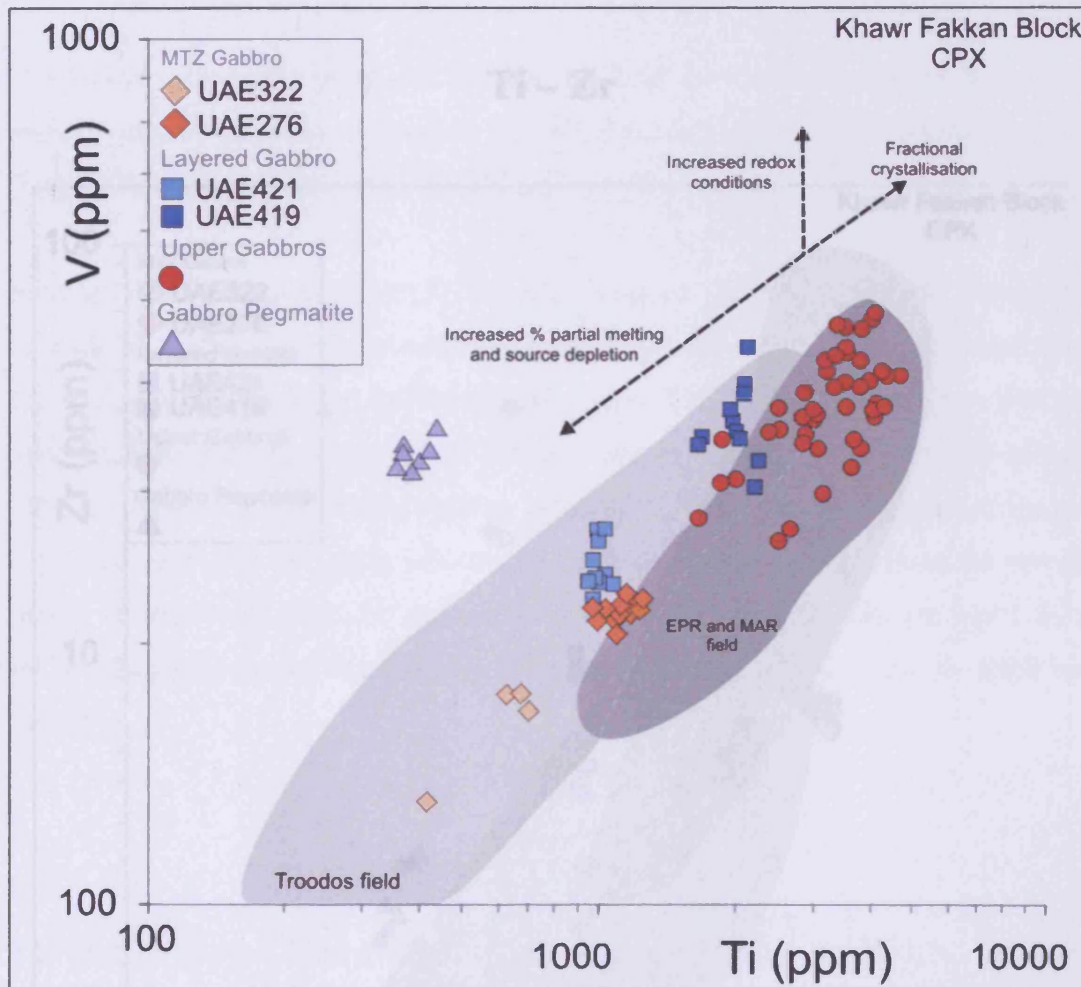


Figure 4.5, The Ti – V diagram of Shervais (1982) displaying results for LA-ICP-MS analysis of Khawr Fakkan Block clinopyroxenes. Composite EPR-MAR and Troodos fields after Coogan et al, (2000a, 2000b, 2002, 2003).

MTZ gabbro sample UAE276 plots close to the values of UAE421, within the overlap of the Troodos and EPR-MAR fields, and UAE322 plots entirely within the Troodos field. This provides evidence for a combination of redox conditions, percentage of melting and mantle source similar to those of the Troodos crust; i.e. in a SSZ environment. It is worth noting that within-plate mantle sources are not well discriminated by the Ti-V diagram.

The Gabbro Pegmatite plots outside both fields, with an increased Ti/V ratio compared to the Troodos clinopyroxenes. This can be interpreted as a product of increased redox conditions and a higher percentage of partial melting from a more depleted mantle source than the other Khawr Fakkan samples. This pattern is similar to that of the Irregular and Cpx-phyric Dykes (as can be seen in Figure 3.8).

### Ti – Zr

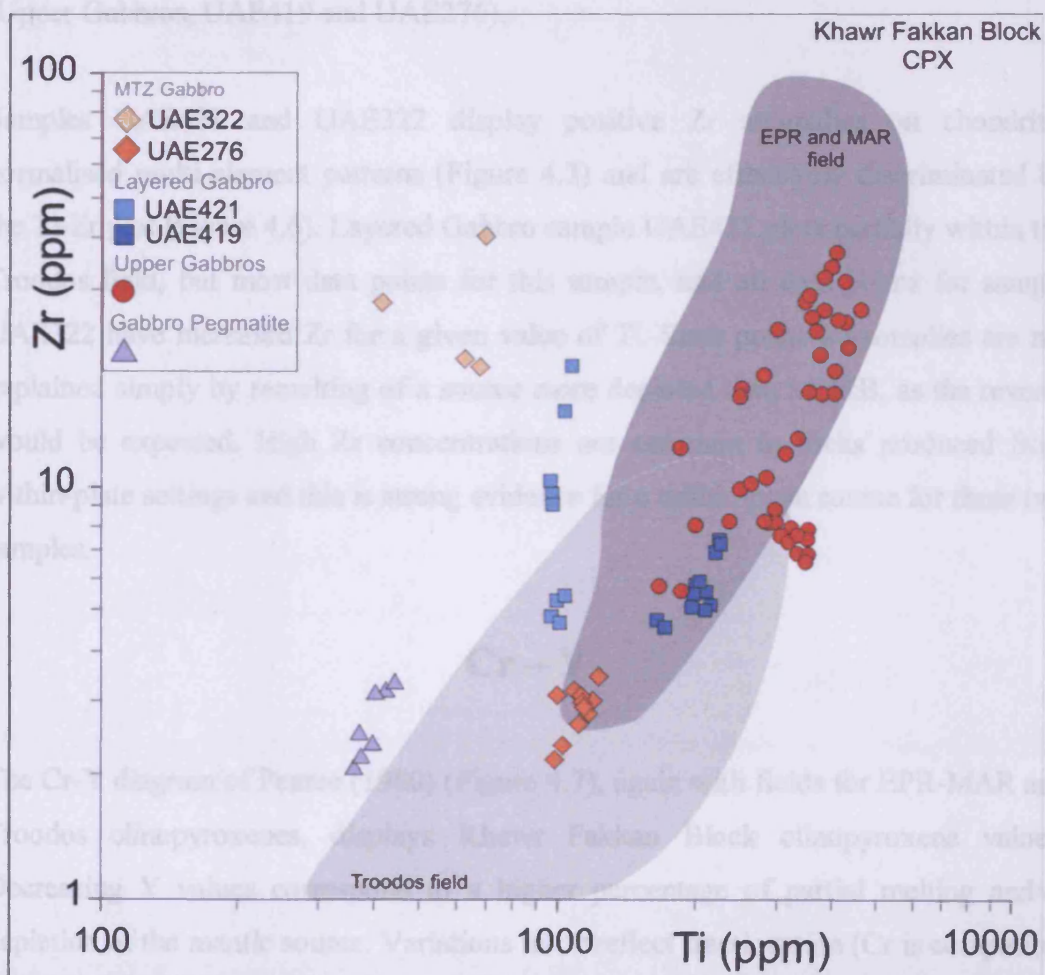


Figure 4.6, Ti – Zr diagram displaying results for LA-ICP-MS analysis of Khawr Fakkan Block clinopyroxenes. Composite EPR-MAR and Troodos fields after Coogan et al, (2000a, 2000b, 2002, 2003).

Figure 4.6 discriminates the Khawr Fakkan samples on the basis of source depletion, using Ti and the incompatible element Zr. Troodos clinopyroxenes are depleted in Zr

and Ti relative to modern oceanic ridges, signifying their more depleted source or greater degree of melting. Khawr Fakkan Upper Gabbros all plot within or close to the EPR-MAR field, indicating a relatively fertile source for these gabbros. Layered Gabbro sample UAE419 and most data points for MTZ Gabbro sample UAE276 plot within the overlap of the Troodos and EPR-MAR fields indicating continued partial melting (and depletion) of the mantle source.

The Gabbro Pegmatite plots just outside the field for Troodos samples denoting a more depleted mantle source for than that of the initial (MORB-like) magmatic period (Upper Gabbros, UAE419 and UAE276).

Samples UAE421 and UAE322 display positive Zr anomalies on chondrite-normalised multi-element patterns (Figure 4.3) and are effectively discriminated by the Ti-Zr plot (Figure 4.6). Layered Gabbro sample UAE421 plots partially within the Troodos field, but most data points for this sample, and all data points for sample UAE322 have increased Zr for a given value of Ti. Such positive anomalies are not explained simply by remelting of a source more depleted than MORB, as the reverse would be expected. High Zr concentrations are common in rocks produced from within-plate settings and this is strong evidence for a within-plate source for these two samples.

## Cr – Y

The Cr-Y diagram of Pearce (1980) (Figure 4.7), again with fields for EPR-MAR and Troodos clinopyroxenes, displays Khawr Fakkan Block clinopyroxene values. Decreasing Y values correspond to a higher percentage of partial melting and/or depletion of the mantle source. Variations in Cr reflect fractionation (Cr is compatible in olivine, clinopyroxene/orthopyroxene and spinel; fractionation trends are illustrated by the dashed arrows) and mantle melting, although as a general rule-of-thumb, clinopyroxenes that crystallise at greater depth within the crust will have higher Cr. Different modal proportions of olivine (Table 4.1) do not obviously affect the level of Cr within clinopyroxenes.

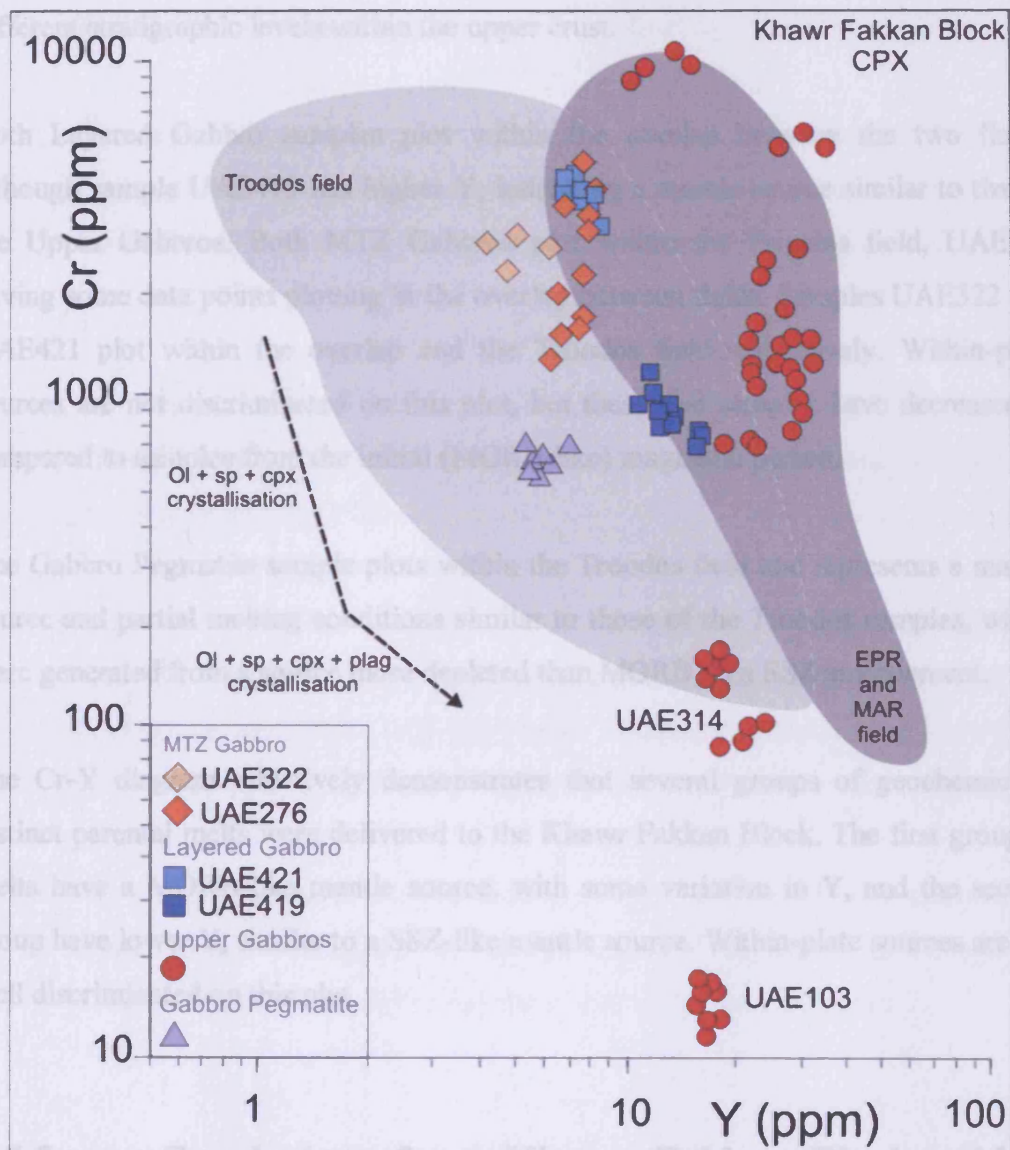


Figure 4.7. Cr-Y projection (Pearce, 1980) of Khawr Fakkan Block clinopyroxenes. Composite EPR-MAR and Troodos fields after Coogan et al, (2000a, 2000b, 2002, 2003).

The Upper Gabbro samples mostly plot within the EPR-MAR field, but vary significantly in concentrations of Y. Modelling of EPR clinopyroxenes by Coogan et al, (2002) concluded that to generate melts with this composition requires up to 30% melting of a fertile source. Two Upper Gabbro samples UAE314 and UAE103 (labelled in Figure 4.7) have low Y values and very low Cr which plot with separate fractionation paths compared to the majority of Upper Gabbro samples. This provides evidence for a variation in the composition of the melt supplied to the Khawr Fakkan upper crust during the initial magmatic period. The two samples possibly represent

separate batches of melt that have had different fractionation histories, possibly at different stratigraphic levels within the upper crust.

Both Layered Gabbro samples plot within the overlap between the two fields, although sample UAE419 has higher Y, indicating a mantle source similar to that of the Upper Gabbros. Both MTZ Gabbros plot within the Troodos field, UAE276 having some data points plotting in the overlap between fields. Samples UAE322 and UAE421 plot within the overlap and the Troodos field respectively. Within-plate sources are not discriminated on this plot, but these two samples have decreased Y compared to samples from the initial (MORB-like) magmatic period.

The Gabbro Pegmatite sample plots within the Troodos field and represents a mantle source and partial melting conditions similar to those of the Troodos samples, which were generated from a source more depleted than MORB, in a SSZ environment.

The Cr-Y diagram effectively demonstrates that several groups of geochemically distinct parental melts were delivered to the Khawr Fakkan Block. The first group of melts have a MORB-like mantle source, with some variation in Y, and the second group have lower Y, similar to a SSZ-like mantle source. Within-plate sources are not well discriminated on this plot.

#### **4.5.5 Conclusions from Khawr Fakkan Block gabbro clinopyroxene trace element characteristics**

- All Upper Gabbro samples plot within or close to the field of EPR-MAR clinopyroxenes on all diagrams, indicating a MORB-like mantle source and accretion during early magmatic events (V1), with comparable amounts of partial melting to modern-day mid-ocean ridge spreading centres.
- MTZ sample UAE276 and Layered Gabbro sample UAE421 display a slightly more depleted signature than the Upper Gabbros, but do not have a significant

subduction component. They are interpreted to have formed during the initial, MORB-like, V1 magmatic period at a time after the Upper Gabbro samples.

- The Gabbro Pegmatite sample plots within or close to the Troodos field in all diagrams, and has a subduction-derived component added to a relatively depleted mantle source, providing evidence for a SSZ setting at the time of its generation (V2).
- MTZ Gabbro sample UAE322 and Layered Gabbro sample UAE421 have increased concentrations of LREE and Zr, representing an enriched within-plate mantle source (V3).
- Gabbro clinopyroxenes from the Khawr Fakkan Block provide evidence for at least three distinct periods of melt generation and supply to the crust. The first period has a variable MORB-like mantle source (V1), the second has a SSZ-like mantle source (V2) and the third has a within-plate mantle source (V3).
- The three magmatic periods distinguished by LA-ICP-MS analysis of clinopyroxenes correspond to the geochemical signatures and magmatic periods identified from dykes and the extrusive section in Chapter 3.

## **4.6 Clinopyroxene trace element geochemistry of the Aswad Block plutonic series**

### **4.6.1 Aswad Block field observations**

The Aswad Block exposes a complete ophiolite sequence dipping at close to the original orientation of the oceanic crust (sub-horizontal). The block offers excellent exposure of the upper crustal gabbros which are characterised by two high-level intrusive gabbros; the Bithna Gabbro and the Fujairah Gabbro (Section 2.4.9). Samples were selected for LA-ICP-MS analysis with the aim of geochemically

discriminating these intrusive events and to, hopefully, match the dyke groups identified in Chapter 3 with their plutonic counterparts.

In this study, eighteen samples were analysed from throughout the Aswad Block: two Layered Gabbros, five Kalba (Upper) Gabbros, four Bithna (late intrusive) Gabbros and four Fujairah (late intrusive) Gabbros (Figure 4.8). Three Microgabbro Dykes with clinopyroxene phenocrysts large enough for LA-ICP-MS analysis were also analysed.

Layered Gabbro samples 04UR44 and UAE644 are both taken from typical fine- to medium-grained modal layers. Sample 04UR44 displays elongate clinopyroxenes that have strong layer- (and Moho-) parallel alignment.

As stated in Section 2.4.4, the Upper Gabbro of the Aswad Block has been termed the Kalba Gabbro. The Kalba Gabbro consists of isotropic, foliated and varitextured horizons which crystallised with the order olivine-plagioclase-clinopyroxene. Cupolas of ophitic Kalba Gabbro intrude into the SDC and extrusive sequence along N-S striking extensional faults. Field observations led to the conclusion that these intrusive events post-dated initial crustal accretion, but preceded the next period of magmatism represented by the Wadi Mai Dykes (Section 2.4.8). To investigate possible variations in the mantle source for different phases of the Kalba Gabbro, five samples that represented both 'Massive' and 'Intrusive' phases of Kalba Gabbro were selected for analysis. Samples 03UR85, 03UR123 and UAE3031 are typical, ophitic 'Massive' Kalba Gabbro that are believed to represent the initial stages of crustal accretion.

Kalba Gabbro samples 03UR140 and 03UR199 are from areas of 'Intrusive' Kalba Gabbro associated with melt transported along the N-S extensional faults. Sample 03UR140 intrudes the extrusive sequence and represents the highest stratigraphic sample of Kalba Gabbro. Sample 03UR199 is from a cupola of Kalba Gabbro which intrudes, but does not chill against, the SDC (similar to the relationship seen in Figure 2.6). All Kalba Gabbro LA-ICP-MS samples are medium- to coarse-grained ophitic gabbros that exhibit some variation in grain size. All samples have undergone extensive hydrothermal alteration (amphibolitisation) because of their high stratigraphic position and association with faults, which would have been a focus for



hydrothermal fluids. Despite this alteration, enough unaltered clinopyroxenes were present for analysis.

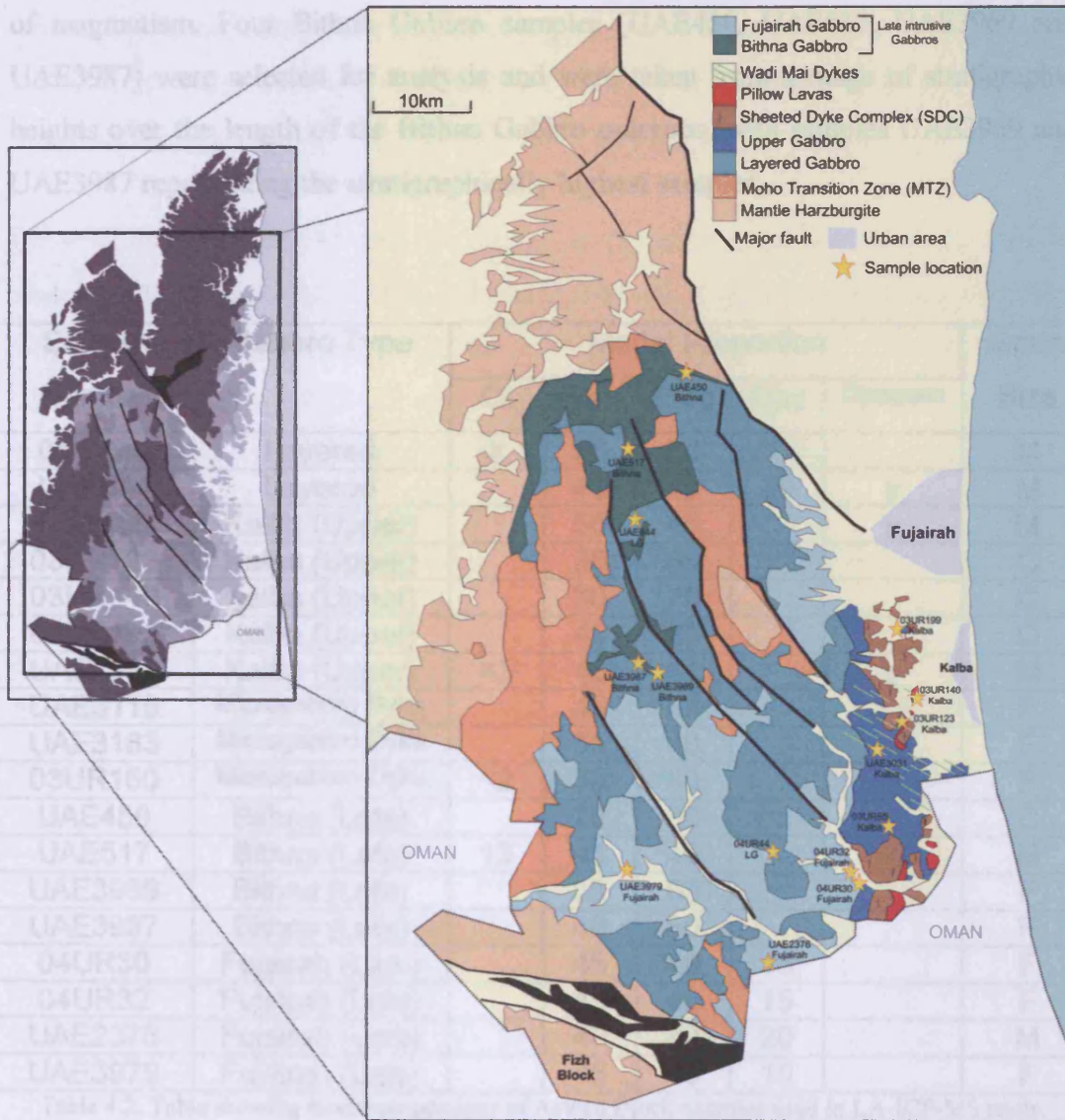


Figure 4.8, Sketch map highlighting the Aswad Block.

Stars represent the locations of samples (with sample number and type) used in LA-ICP-MS study. Sample co-ordinates are fully listed in Appendix D.

The Bithna Gabbro intrudes the lower crust and the Layered Gabbro series of the Aswad Block. It is a typically varitextured gabbro with grain size varying from fine to coarse, often over short distances, and it always includes a characteristic fine-microgabbroic phase. At the uppermost stratigraphic levels of the unit the grain size becomes very coarse, indicating the presence of volatiles and a slow cooling history.

Field observations suggest that the Bithna Gabbro represents an individual pluton that halted in ascent and cooled before it reached the uppermost crust. The Bithna Gabbro is intruded by Fujairah Dolerite dykes, which chill in contact with the gabbro, providing evidence that the Bithna Gabbro pre-dates, and had cooled by, this period of magmatism. Four Bithna Gabbro samples (UAE450, UAE517, UAE3969 and UAE3987) were selected for analysis and were taken from a range of stratigraphic heights over the length of the Bithna Gabbro outcrops, with samples UAE3969 and UAE3987 representing the stratigraphically highest samples.

Sample Number	Gabbro Type	Modal Proportion					Grain Size
		OI	Cpx	Plag	Opx	Opaques	
04UR44	Layered	tr	50	50			M
UAE644	Layered		40	40	20	tr	M
03UR85	Kalba (Upper)		55	45		tr	M
03UR123	Kalba (Upper)		35	65			C
03UR140	Kalba (Upper)		30	70			C
03UR199	Kalba (Upper)		40	60			C
UAE3031	Kalba (Upper)	<3	45	52		tr	M
UAE3115	Microgabbro Dyke		45	45		<5	F
UAE3183	Microgabbro Dyke		55	40		<5	F
03UR150	Microgabbro Dyke	<2	38	60		tr	F
UAE450	Bithna (Late)		70	30		tr	C
UAE517	Bithna (Late)	13	45	40		<2	M
UAE3969	Bithna (Late)		35	65			F
UAE3987	Bithna (Late)		40	60			F
04UR30	Fujairah (Late)		45	40	15		F
04UR32	Fujairah (Late)		45	40	15		F
UAE2376	Fujairah (Late)		40	40	20		M
UAE3979	Fujairah (Late)		45	40	15		F

Table 4.2, Table showing modal proportions of Aswad Block samples used in LA-ICP-MS study. Grain size reference; M= medium, C= coarse, F= fine

The last major phase of magmatism recorded in the Aswad Block is the late intrusive Fujairah Gabbro. This large gabbro pluton intrudes all other units in the crustal sequence and is closely associated with NW-SE trending crustal-scale faults. The Fujairah Gabbro is commonly varitextured and has associated felsic segregations and dolerite dykes. The geochemistry of these dykes corresponds with the Clinopyroxene-phyric Unit identified in Oman. The Fujairah Gabbro has a generally cumulate texture, consists of up to 20 percent orthopyroxene, and has plagioclase as an

interstitial mineral phase, demonstrating that the gabbro crystallised with the order olivine-orthopyroxene-clinopyroxene-plagioclase. Many pyroxenes within the gabbro have undergone considerable alteration to amphibole, with up to 20 percent of samples consisting poikilitic plates of green amphibole (actinolite or hornblende), which may be magmatic in origin. Four representative Fujairah Gabbro samples were selected for analysis (04UR30, 04UR32, UAE2376 and UAE3979) from a range of stratigraphic heights on the basis of their freshness.

Three Microgabbro Dykes with clinopyroxene phenocrysts large enough for analysis were also included in the LA-ICP-MS study. The dykes were sampled from the Kalba Gabbro and SDC horizons and their whole-rock compositions were included in Chapter 3. Samples UAE3115 and UAE3183 are both feeder dykes sampled from within 'Massive' Kalba Gabbro and have a granular microgabbroic texture. The N-S trending, near-vertical dykes both have whole-rock trace element compositions that plot within the fields of the SDC and Pillow lavas in Chapter 3 (and corresponding to the Geotimes Unit as described in Oman). This would indicate that they have been sourced during the initial (V1) spreading-ridge magmatic period of the Aswad Block. They are referred to in the text as the 'Geotimes' Dykes. Sample 03UR150 is a near-vertical, N-S trending, fine microgabbro dyke associated with the N-S trending faults. The dyke intrudes the lower SDC and contains abundant sub-rounded phenocrysts (up to 3mm in diameter) of plagioclase and clinopyroxene. The large phenocrysts form aggregated clusters that denote formation in a magma chamber prior to eruption. The dyke is included in the Intermediate Dyke group (see Section 2.4.7) and has a whole-rock trace element composition that plots within the field for the Lasail Unit as identified in Oman. This indicates formation during the 'seamount' magmatic period of Alabaster et al. (1982), and the sample is termed the 'Lasail' Dyke in the text. Dykes of the Intermediate Group intrude, and sometimes chill against, the Bithna Gabbro, providing field evidence that the Bithna Gabbro was present at this stage of crustal accretion. It is hoped that geochemical constraints from clinopyroxene analysis will clarify such observations and allow the full history of crustal accretion to be established.

## 4.6.2 Chondrite-normalised multi-element patterns

The fields for Aswad Block clinopyroxene compositions can be seen in Figure 4.9, and have again been normalised to the chondrite values of Anders and Grevesse (1989). As in Section 4.5.2 fields for modern-day spreading centres are shown as a combined EPR-MAR field (Coogan et al., 2000a, 2000b and 2002) and are compared to those from the SSZ setting of the Troodos ophiolite (dotted field) from Coogan et al. (2003).

The Layered Gabbro samples (Figure 4.9A) display a REE pattern of relative depletion of LREE and MREE compared to HREE that is very similar to the EPR-MAR field, but with lower overall abundance, which places them within the field of Troodos clinopyroxenes. The samples display typical negative Ti and Zr anomalies, but do not display a significant negative Sr anomaly.

Figure 4.9B displays the results for the five Kalba Gabbro samples. These samples plot almost entirely within the field for modern-day spreading centres with negative Ti, Zr and Sr anomalies of a similar extent. This is evidence for the melts that formed these gabbros to have formed at a 'normal' spreading centre with a MORB-like mantle source.

Bithna Gabbro clinopyroxene samples (Figure 4.9C) also plot almost entirely within the EPR-MAR field, but are slightly more depleted in LREE and do not have the same range of REE abundance as the Kalba Gabbro clinopyroxenes. The lower abundance could be related to the greater depth of crystallisation. The Bithna Gabbro samples also display negative Ti, Zr and Sr anomalies of a similar range to the EPR-MAR field.

The Fujairah Gabbro clinopyroxenes (Figure 4.9D) have a narrow range of values that plot mostly within the area of overlap between the EPR-MAR field and the Troodos field. The samples display negative Ti, Zr and Sr anomalies similar to the EPR-MAR field, but are relatively enriched in LREE compared to the other gabbro samples, indicating a possible subduction influence to the mantle source for these samples.

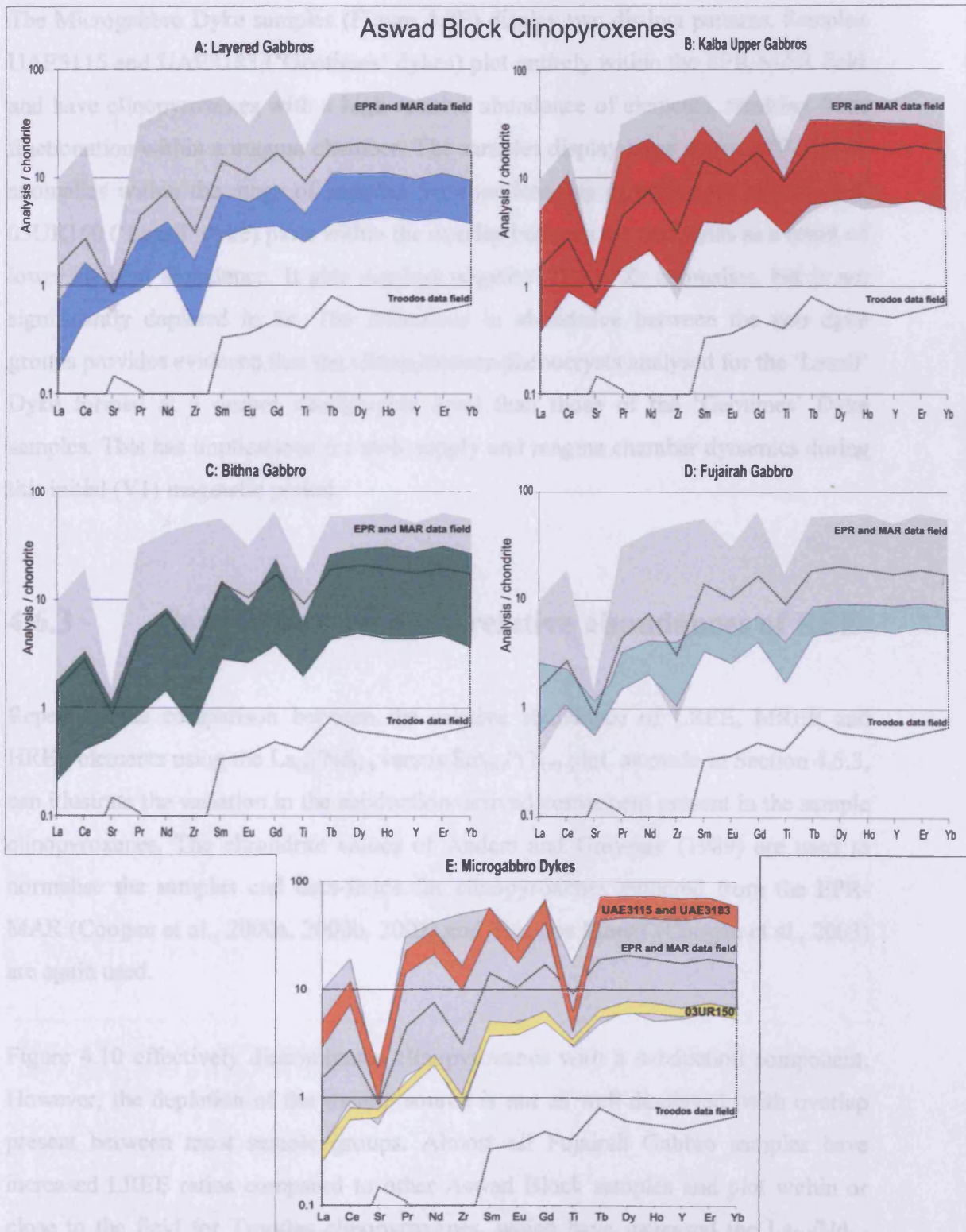


Figure 4.9, Chondrite-normalised (Anders and Grevasse, 1989) extended REE diagrams (with Sr, Zr, Ti and Y) for clinopyroxenes from the Aswad Block. Composite EPR-MAR and Troodos fields after Coogan et al. (2000a, 2000b, 2002, 2003).

The Microgabbro Dyke samples (Figure 4.9E) display two distinct patterns. Samples UAE3115 and UAE3183 ('Geotimes' dykes) plot entirely within the EPR-MAR field and have clinopyroxenes with a high relative abundance of elements, resulting from fractionation within a magma chamber. The samples display large negative Ti and Sr anomalies within the range of samples from modern-day spreading centres. Sample 03UR150 ('Lasail' dyke) plots within the overlap between the two fields as a result of lower element abundance. It also displays negative Ti and Zr anomalies, but is not significantly depleted in Sr. The difference in abundance between the two dyke groups provides evidence that the clinopyroxene phenocrysts analysed for the 'Lasail' Dyke formed at a deeper stratigraphic level than those of the 'Geotimes' Dyke samples. This has implications for melt supply and magma chamber dynamics during this initial (V1) magmatic period.

### 4.6.3 Comparison between relative abundances of REE

Repeating the comparison between the relative abundance of LREE, MREE and HREE elements using the  $La_{(n)}/Nd_{(n)}$  versus  $Sm_{(n)}/Yb_{(n)}$  plot, as made in Section 4.5.3, can illustrate the variation in the subduction-derived component present in the sample clinopyroxenes. The chondrite values of Anders and Grevesse (1989) are used to normalise the samples and data-fields for clinopyroxenes gathered from the EPR-MAR (Coogan et al., 2000a, 2000b, 2002) and Troodos Massif (Coogan et al., 2003) are again used.

Figure 4.10 effectively discriminates clinopyroxenes with a subduction component. However, the depletion of the mantle source is not as well displayed, with overlap present between most sample groups. Almost all Fujairah Gabbro samples have increased LREE ratios compared to other Aswad Block samples and plot within or close to the field for Troodos clinopyroxenes, which have increased the  $La_{(n)}/Nd_{(n)}$  values for a given value of  $Sm_{(n)}/Yb_{(n)}$ . Some Fujairah Gabbro data points plot within the EPR-MAR field, and illustrate variation in the subduction-derived component present in the mantle source for this gabbro (discussed further below).

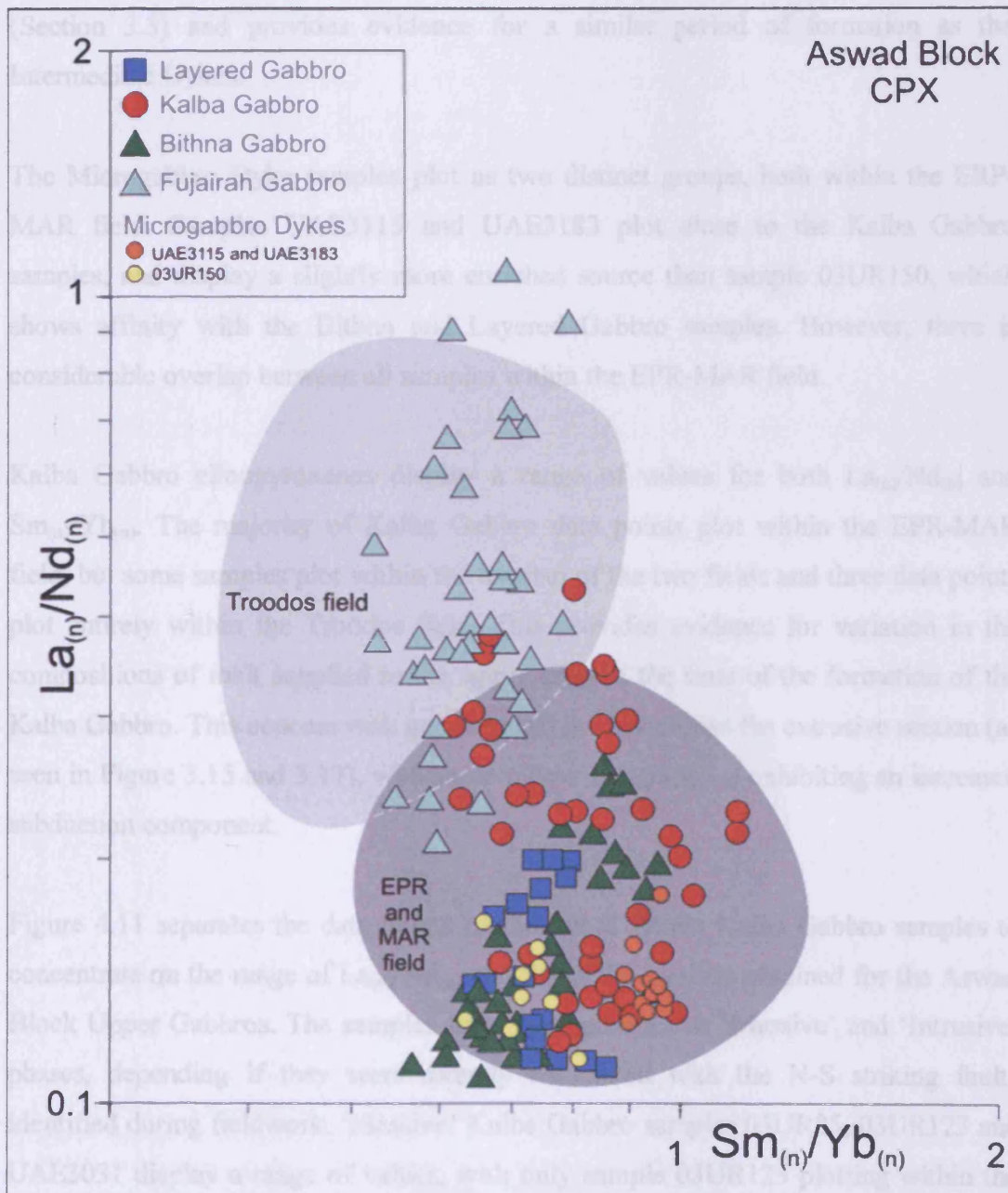


Figure 4.10,  $La_{(n)}/Nd_{(n)}$  versus  $Sm_{(n)}/Yb_{(n)}$  plot displaying results for LA-ICP-MS analysis of Aswad Block clinopyroxenes normalised to the chondrite values of Anders and Grevesse (1989). Composite EPR-MAR and Troodos fields after Coogan et al. (2000a, 2000b, 2002, 2003)

All Bithna Gabbro samples and both Layered Gabbro samples plot within, or close to, the combined EPR-MAR field and display a slightly more depleted mantle source than the majority of Kalba Gabbro samples. This indicates a mantle source of similar composition (that is not relatively enriched in LREE) to those that sourced the EPR and MAR samples, but one that is depleted relative to the majority of Kalba Gabbro

samples. This is a similar pattern as the Intermediate Dykes identified in Chapter 3 (Section 3.3) and provides evidence for a similar period of formation as the Intermediate Dykes.

The Microgabbro Dyke samples plot as two distinct groups, both within the ERP-MAR field. Samples UAE3115 and UAE3183 plot close to the Kalba Gabbro samples, and display a slightly more enriched source than sample 03UR150, which shows affinity with the Bithna and Layered Gabbro samples. However, there is considerable overlap between all samples within the EPR-MAR field.

Kalba Gabbro clinopyroxenes display a range of values for both  $La_{(n)}/Nd_{(n)}$  and  $Sm_{(n)}/Yb_{(n)}$ . The majority of Kalba Gabbro data points plot within the EPR-MAR field, but some samples plot within the overlap of the two fields and three data points plot entirely within the Troodos field. This provides evidence for variation in the compositions of melt supplied to the upper crust at the time of the formation of the Kalba Gabbro. This concurs with geochemical evidence from the extrusive section (as seen in Figure 3.15 and 3.17), with some pillow lava samples exhibiting an increased subduction component.

Figure 4.11 separates the data points of the five different Kalba Gabbro samples to concentrate on the range of  $La_{(n)}/Nd_{(n)}$  and  $Sm_{(n)}/Yb_{(n)}$  values obtained for the Aswad Block Upper Gabbros. The samples have been grouped as 'Massive' and 'Intrusive' phases, depending if they were directly associated with the N-S striking faults identified during fieldwork. 'Massive' Kalba Gabbro samples 03UR85, 03UR123 and UAE3031 display a range of values, with only sample 03UR123 plotting within the EPR-MAR field. The remaining 'Massive' Kalba Gabbro samples have a range of both  $La_{(n)}/Nd_{(n)}$  and  $Sm_{(n)}/Yb_{(n)}$  values, indicating a variation in the subduction component present in the mantle source of these gabbros. The two 'Intrusive' Kalba Gabbro samples (03UR199 and 03UR140) also display a similar range of  $La_{(n)}/Nd_{(n)}$  and  $Sm_{(n)}/Yb_{(n)}$  values which is in turn similar to that of the 'Massive' gabbros. Figure 4.11 also shows the fields for the Microgabbro Dyke samples, which display overlap with both 'Massive' and 'Intrusive' Kalba Gabbro samples, making the specific source of these dykes difficult to determine from this plot.



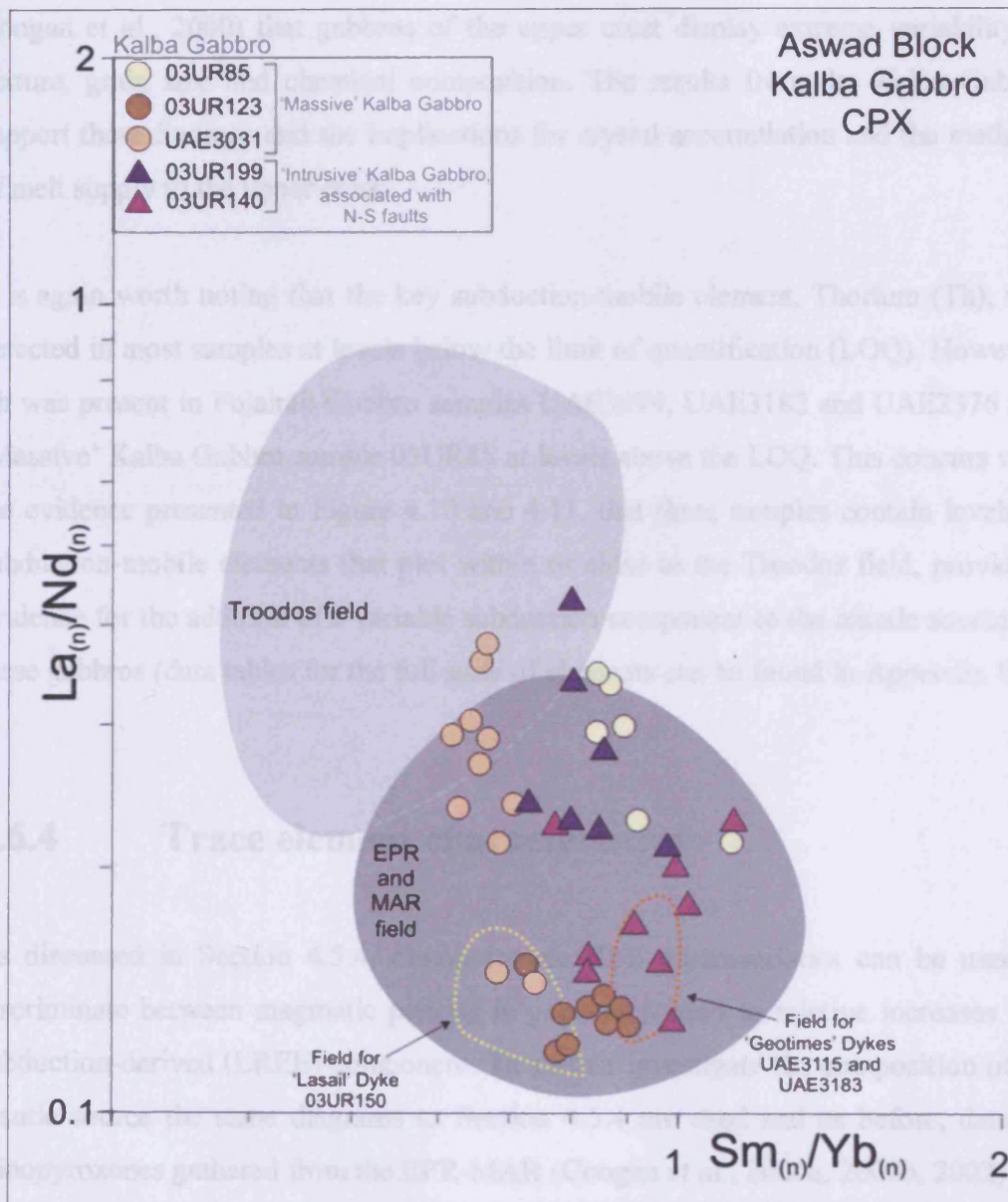


Figure 4.11,  $La_{(n)}/Nd_{(n)}$  versus  $Sm_{(n)}/Yb_{(n)}$  plot displaying results for LA-ICP-MS analysis of clinopyroxenes from the Kalba Gabbro of the Aswad Block normalised to the chondrite values of Anders and Grevesse (1989). Composite EPR-MAR and Troodos fields after Coogan et al. (2000a, 2000b, 2002, 2003).

Figure 4.11 provides evidence that the N-S faulting/rifting event, which happened when extension of the crust exceeded melt supply, does not represent a change in the chemical variability of the mantle source. In other words, the N-S rifting during the initial (MORB-like) magmatic period of the Aswad Block represents a syn-magmatic event that did not affect the 'plumbing' of the upper crust, as post-rifting melts are not chemically distinct from pre-rifting melts. It has been noted in previous ophiolite and crustal gabbro studies (e.g. MacLeod and Yaouancq, 2000; Thomas, 2003 and

Coogan et al., 2000) that gabbros of the upper crust display extreme variability in texture, grain size and chemical composition. The results from the Kalba Gabbro support these findings and the implications for crystal accumulation and the methods of melt supply to the upper crust.

It is again worth noting that the key subduction-mobile element, Thorium (Th), was detected in most samples at levels below the limit of quantification (LOQ). However, Th was present in Fujairah Gabbro samples UAE3979, UAE3182 and UAE2376 and 'Massive' Kalba Gabbro sample 03UR85 at levels above the LOQ. This concurs with the evidence presented in Figure 4.10 and 4.11, that these samples contain levels of subduction-mobile elements that plot within or close to the Troodos field, providing evidence for the addition of a variable subduction component to the mantle source for these gabbros (data tables for the full suite of elements can be found in Appendix D).

#### **4.6.4 Trace element characteristics**

As discussed in Section 4.5.4, clinopyroxene REE characteristics can be used to discriminate between magmatic periods in gabbros related to relative increases in a subduction-derived (LREE) component. To further investigate the composition of the mantle source the same diagrams as Section 4.5.4 are used and as before, data for clinopyroxenes gathered from the EPR-MAR (Coogan et al., 2000a, 2000b, 2002) and Troodos (Coogan et al., 2003) are used to generate fields for mid-oceanic and SSZ settings respectively.

### **Ti - V**

The Ti/V diagram of Shervais (1982) can again be used to investigate the relative variations in redox conditions, percentage of source melting and amount of source depletion under which the parental melts to the Aswad Block formed (Figure 4.12). The plot does not discriminate the Aswad Block clinopyroxenes as clearly as those of the Khawr Fakkan Block (Figure 4.5), although it does illustrate differences between the mantle sources of the two blocks. The Aswad Block samples generally have lower

V and Ti values than the equivalent unit in the Khawr Fakkan Block (Upper Gabbro). This variation provides more evidence for a different mantle source and the original relative position of the two Blocks at the time of the accretion of the Upper crustal gabbros (discussed further in Chapter 5).

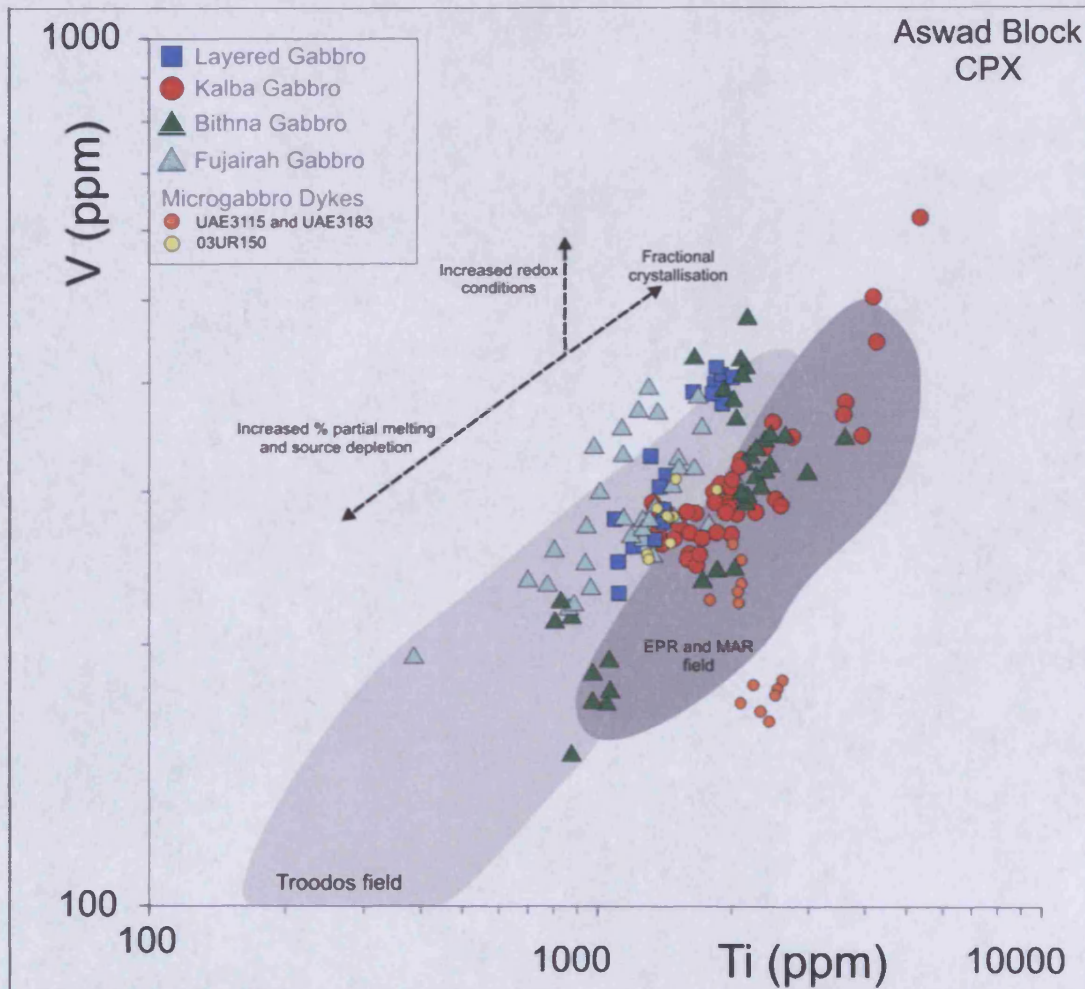


Figure 4.12, The Ti – V diagram of Shervais (1982) displaying results for LA-ICP-MS analysis of Aswad Block clinopyroxenes. Composite EPR-MAR and Troodos fields after Coogan et al. (2000a, 2000b, 2002, 2003).

The majority of Kalba Gabbro samples plot within the overlap between the EPR-MAR and Troodos field, with some data points plotting entirely within each field. This indicates variation in oxidising conditions, percentage of source melting and source depletion for the mantle source of the Kalba Gabbro.

The Microgabbro Dykes are well discriminated by Figure 4.12. Whereas the 'Geotimes' Dykes (UAE3115 and UAE3183) plot partially outside the EPR-MAR field, they display Ti values that are very similar to those of the Kalba and Bithna Gabbros. 'Lasail' Dyke 03UR150 displays slightly reduced Ti, indicating a more depleted mantle source. This is the same pattern that is observed between the Geotimes and Lasail fields in Figure 3.16, and confirms that LA-ICP-MS data for clinopyroxenes give the same tectonic interpretation as data generated from whole-rock trace element analysis of the extrusive series and other fine grained rocks.

The Layered Gabbro samples all plot within or very close to the Troodos field, with lower Ti concentrations and similar V levels to the Kalba Gabbro samples. This is evidence for a slightly more depleted source for the Layered Gabbros than the Kalba Gabbro that has undergone melting in slightly increased redox conditions.

The Bithna Gabbro has a range of values for Ti and V that plot within the EPR-MAR and Troodos fields. Some samples have a similar composition to the Kalba Gabbro, and other samples are more similar to the Fujairah Gabbro. Most Bithna samples plot with similar Ti to the Kalba Gabbro, indicating a similar mantle source. Increased V in some of these samples provides evidence for a variation in redox conditions at the time of emplacement of the Bithna Gabbro. Several data points plot with low Ti-V values providing evidence for melt supplied to the pluton from a more depleted source. The range of values for the Bithna Gabbro is greater than that of the Kalba Gabbro and provides evidence for a variation in the percentage of source melting, degree of source depletion and redox conditions for the mantle source of the Bithna Gabbro.

The Fujairah Gabbro samples also have a range of values for V for a given amount of Ti, and all data points plot within, or close to, the field for Troodos clinopyroxenes. The relatively depleted source and increased ratio of subduction-derived LREE, as illustrated in Figure 4.10, is consistent with the geochemistry of the extrusive section and dykes, that the Fujairah Gabbro post-dates the accretion of the Kalba and Bithna Gabbros, and represents the last major period (V2) of crustal accretion in the Aswad Block.

### Ti – Zr

The Ti-Zr plot (Figure 4.13) displays a very similar pattern to Figure 4.12, and also gives an indication of the relative depletion or enrichment of the mantle source for the Aswad Block clinopyroxenes.

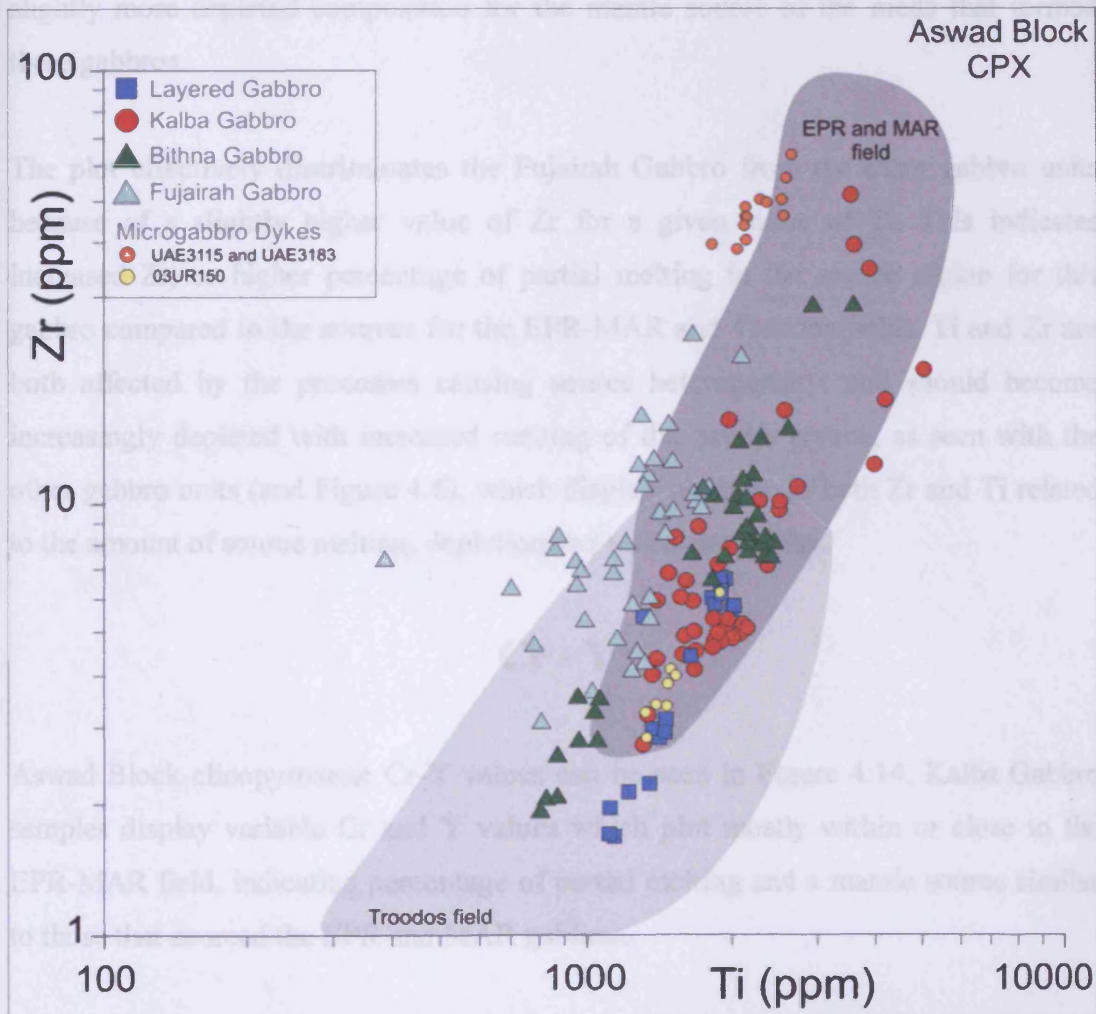


Figure 4.13, Ti – Zr diagram displaying results for LA-ICP-MS analysis of Aswad Block clinopyroxenes. Composite EPR-MAR and Troodos fields after Coogan et al. (2000a, 2000b, 2002, 2003).

All Kalba Gabbro samples plot within or very close to the combined EPR-MAR field, with most data points plotting within the overlap between the two fields. This

provides evidence for similar (fertile) concentrations of Zr and Ti as modern-day mid-ocean ridges. Bithna Gabbro samples have a range of values similar to that of the Kalba Gabbro and plot within both fields. This is evidence for a variation in the composition of the mantle source for this gabbro, and possibly indicates multiple, chemically distinct, melt batches supplied to the crust.

Most data points for the Layered Gabbro samples plot within the overlap between the two fields, with some data points fully within the Troodos field. This denotes a slightly more depleted composition for the mantle source of the melts that formed these gabbros.

The plot effectively discriminates the Fujairah Gabbro from the other gabbro units because of a slightly higher value of Zr for a given value of Ti. This indicates increased Zr, or higher percentage of partial melting in the source region for this gabbro compared to the sources for the EPR-MAR and Troodos fields. Ti and Zr are both affected by the processes causing source heterogeneity, and should become increasingly depleted with increased melting of the mantle source, as seen with the other gabbro units (and Figure 4.6), which display variation in both Zr and Ti related to the amount of source melting, depletion and redox conditions.

## Cr - Y

Aswad Block clinopyroxene Cr-Y values can be seen in Figure 4.14. Kalba Gabbro samples display variable Cr and Y values which plot mostly within or close to the EPR-MAR field, indicating percentage of partial melting and a mantle source similar to those that sourced the EPR and MAR gabbros.

The Kalba Gabbro samples were each gathered from different stratigraphic levels and the variation in Cr should provide some evidence for the crystallisation of this unit at different crustal levels (assuming equilibrium crystallisation), and is investigated further in Figure 4.15.

The Microgabbro Dykes are again discriminated, and plot as two groups. The 'Geotimes' Dykes have low Cr and high Y values and the 'Lasail' Dyke has much higher Cr and lower Y, providing evidence for potential differences in the depth of the magma chamber that fed these samples.

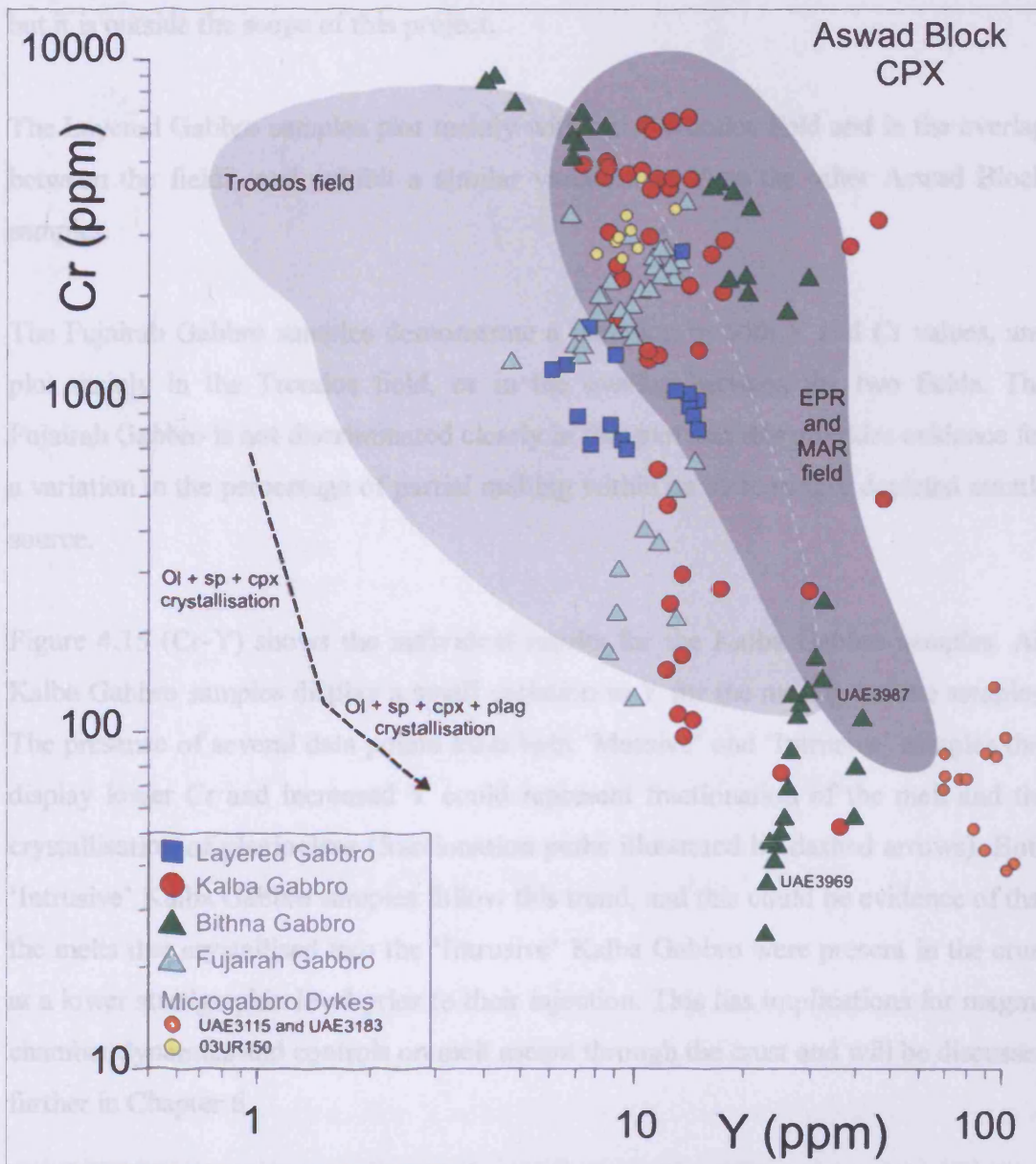


Figure 4.14, Cr-Y projection (Pearce, 1980) of Aswad Block clinopyroxenes. Composite EPR-MAR and Troodos fields after Coogan et al. (2000a, 2000b, 2002, 2003).

Bithna Gabbro samples display variations in Y that are similar to the EPR-MAR field. Samples UAE3969 and UAE3987 (labelled on plot) have very low Cr values and have a fractionation trend similar to that of Khawr Fakkan Upper Gabbro samples

UAE103 and UAE314 (as seen in Figure 4.7). The fractionation trend is noteworthy as Y decreases with Cr, which is the reverse of what would be expected by open-system fractionation. This pattern could be caused by the inadvertent sampling of alteration-related exsolution lamella within the clinopyroxene which have altered to orthopyroxene. Further work is required to constrain the cause of this chemical effect, but it is outside the scope of this project.

The Layered Gabbro samples plot mainly within the Troodos field and in the overlap between the fields, and exhibit a similar variation in Y as the other Aswad Block samples.

The Fujairah Gabbro samples demonstrate a variation in both Y and Cr values, and plot mainly in the Troodos field, or in the overlap between the two fields. The Fujairah Gabbro is not discriminated clearly in this plot and this provides evidence for a variation in the percentage of partial melting within an increasingly depleted mantle source.

Figure 4.15 (Cr-Y) shows the individual results for the Kalba Gabbro samples. All Kalba Gabbro samples display a small variation in Y for the most primitive samples. The presence of several data points from both 'Massive' and 'Intrusive' samples that display lower Cr and increased Y could represent fractionation of the melt and the crystallisation of plagioclase (fractionation paths illustrated by dashed arrows). Both 'Intrusive' Kalba Gabbro samples follow this trend, and this could be evidence of that the melts that crystallised into the 'Intrusive' Kalba Gabbro were present in the crust at a lower stratigraphic level prior to their injection. This has implications for magma chamber dynamics and controls on melt ascent through the crust and will be discussed further in Chapter 6.



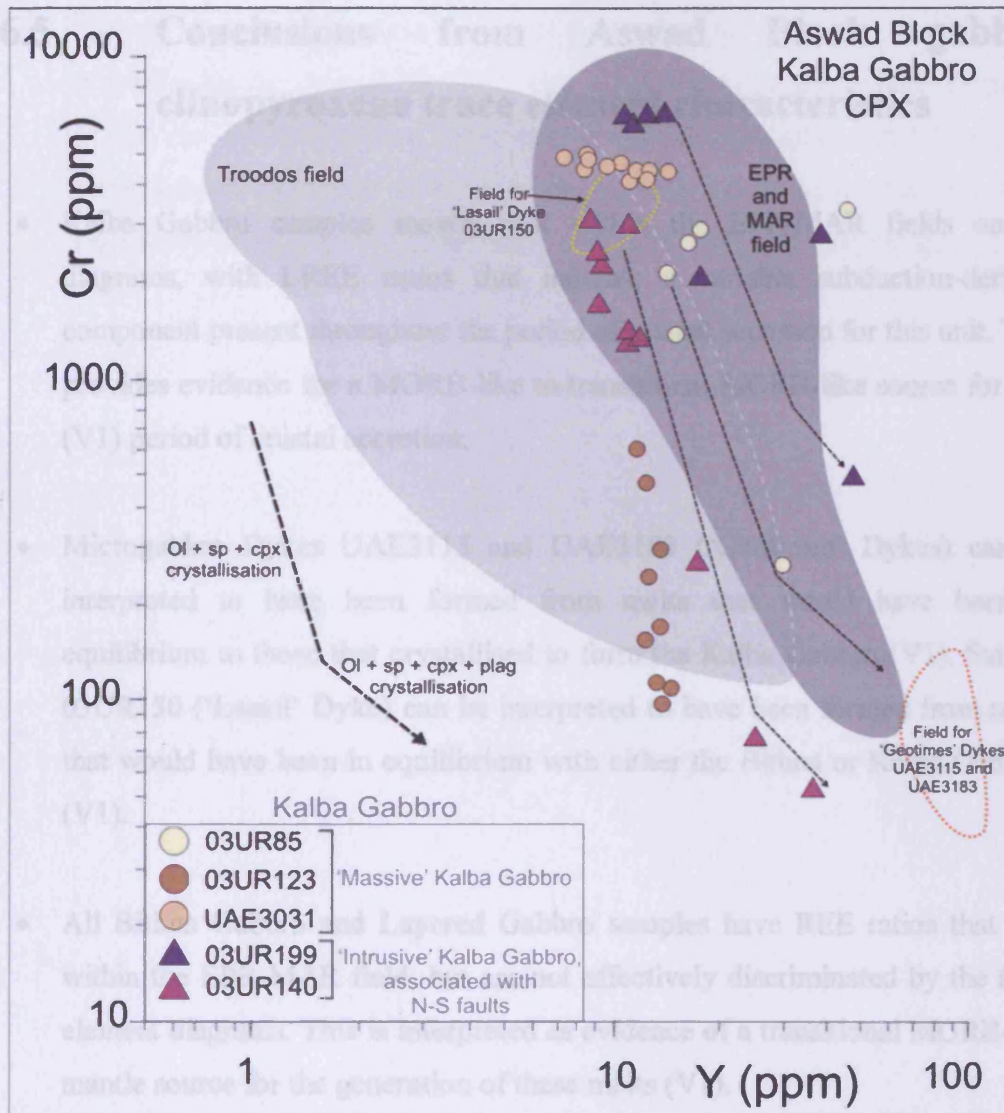


Figure 4.15, Cr-Y projection (Pearce, 1980) of Aswad Block Kalba Gabbro clinopyroxenes. Composite EPR-MAR and Troodos fields after Coogan et al. (2000a, 2000b, 2002, 2003).

The fields for the two Microgabbro Dyke Groups are also illustrated in Figure 4.15. The 'Lasail' Dyke overlaps both 'Massive' and 'Intrusive' Kalba Gabbros. The 'Geotimes' Dykes however, have a composition that can be explained by plagioclase crystallisation from a melt of similar composition to the 'Lasail' Dyke. This pattern of fractionation is parallel to the modelled trend of the evolution of the Geotimes and Lasail Unit in Section 3.3.4, displayed in Figure 3.20.

#### **4.6.5 Conclusions from Aswad Block gabbro clinopyroxene trace element characteristics**

- Kalba Gabbro samples mostly plot within the EPR-MAR fields on all diagrams, with LREE ratios that indicate a variable subduction-derived component present throughout the period of crustal accretion for this unit. This provides evidence for a MORB-like to transitional MORB-like source for this (V1) period of crustal accretion.
- Microgabbro Dykes UAE3115 and UAE3183 ('Geotimes' Dykes) can be interpreted to have been formed from melts that would have been in equilibrium to those that crystallised to form the Kalba Gabbro (V1). Sample 03UR150 ('Lasail' Dyke) can be interpreted to have been formed from melts that would have been in equilibrium with either the Bithna or Kalba Gabbros (V1).
- All Bithna Gabbro and Layered Gabbro samples have REE ratios that plot within the EPR-MAR field, but are not effectively discriminated by the trace element diagrams. This is interpreted as evidence of a transitional MORB-like mantle source for the generation of these melts (V1).
- All Fujairah Gabbro samples have increased LREE ratios that plot within, or very close to, the field of Troodos clinopyroxenes and are discriminated by trace element diagrams as having a more depleted source than other crustal gabbros. The Fujairah Gabbro samples display evidence for formation in a SSZ setting from a mantle source with an additional subduction-derived component (V2).
- The Aswad Block gabbro clinopyroxenes record at least two magmatic periods. The first with a transitional MORB-like character (V1) and the second with a SSZ-like character (V2).

- The apparent crystallisation vector of some samples displayed on the Cr -Y projection for the Aswad Block (Figure 4.14) is the opposite of that expected by 'normal' crystallisation. This trend, which is probably related to post-crystallisation alteration effects within the clinopyroxene crystal structure, deserves to be fully investigated but is outside the scope of this project.

# Chapter 5: Geochemical Modelling of Clinopyroxenes from the Plutonic Section

## 5.1 Introduction

The aim of this chapter is to compare the petrogenetic geochemical data gathered from the clinopyroxene analysis in Chapter 4 to that of the extrusive Units identified in Chapter 3. This will allow extrusive events and dykes to be directly linked to the gabbro source, and enable accurate crustal accretion history processes to be defined for the Khawr Fakkan and Aswad Blocks. The link will be established by using the modelling of clinopyroxene REE compositions, to calculate the composition of the melt from which the crystal formed. These compositions will be compared to the data from the different lava units identified in Chapter 3. It is hoped that the results from this modelling will help to confirm the MORB-like to SSZ variation of the mantle source identified in Chapters 3 and 4. This will make it possible to constraint in more detail the nature of the mantle source and the tectonic setting during the different crustal accretion events in the northern Oman-U.A.E. ophiolite crust.

When interpreting petrogenetic processes through geochemical modelling of trace elements it is vital to understand how elements behave within a system and in particular, how they partition between minerals and melt. The latter is expressed as partition (distribution) coefficients, defined as the distribution of a trace element between a mineral and a melt, and represented by the symbol  $K_{(D)}$ . This definition assumes that two key rules are satisfied: firstly, that the trace element obeys Henry's law (that the partition coefficient of an element is independent of the concentration of the element), and secondly, that crystal-melt interface equilibrium is achieved. Studies of trace element behaviour in natural basaltic systems (e.g. Watson, 1985) and results from experimental partitioning studies (e.g. Beattie, 1993) provide strong evidence that, for the range of REE concentrations attained in this study, Henry's Law is obeyed. The REE modelled in this study exist in parts per million (ppm), orders of magnitude lower than the ~1wt% necessary to exceed Henry's Law (Beattie, 1993).

Disequilibrium partitioning in the crystal-melt system is unlikely at the temperatures and cooling rates of the crustal sections studied; as described in Section 4.3, there is no enrichment of high charge-to-mass elements over lower charge-to-mass elements (Figure 4.1) so it is assumed for the purposes of this study that the two key rules are satisfied.

## 5.2 Bulk Partition Coefficients

Partition coefficients describe the distribution of a trace element between a mineral and a melt. Their values are not fixed and are functions of both external (pressure, temperature) and internal (composition of melt/crystal) conditions (e.g. Blundy and Wood, 1991, 1994; Wood and Blundy, 1997). Separating the different effects is difficult, making the use of suitable values essential (Wood and Blundy, 1997). The range of published mineral-melt partition coefficients for clinopyroxene varies considerably. An example of the wide range of published experimental and calculated partition coefficient values can be found at the GERM Earth Ref website ([www.earthref.org](http://www.earthref.org)).

Petrogenetic modelling requires element partition coefficients to be quantified in terms of its equilibrium with all mineral phases present. This is termed the *bulk partition coefficient* ( $D$ ) which is calculated from the Nernst coefficients weighted according to the relative proportions of coexisting phases in the assemblage. Bédard (1993) demonstrated that the principal potential sources of errors in calculating  $D_i$  are (in decreasing order of importance): analytical error, uncertainty in the  $D$  values, imprecision of modal data and the use of the wrong Trapped Melt Fraction (TMF) stripping modes. Thomas (2003) also noted that neither realistic change to the proportions of the crystallising phases, nor to the Nernst partition coefficients, significantly alter modelled REE profiles for the clinopyroxenes of the southern Oman-U.A.E. ophiolite blocks. Thus it could be argued that, although mineral modes vary considerably between gabbro samples, for the purpose of this study these changes can be ignored. Also, the variations in clinopyroxene major element

composition, the principal control on Nernst partition coefficients (Wood and Blundy, 1997), are minor.

The REE were chosen as the elements to be modelled in this Chapter as it has been demonstrated earlier in this study (Chapter 3) that the variation of relative abundance between these elements (La to Yb) is sufficient to discriminate the different magmatic events identified in each block.

To compare the effects of different partition coefficients,  $D$  were calculated for each clinopyroxene crystal sampled in this study. As mentioned in Section 4.4, several lines were ablated per slide (normally three lines per crystal and three crystals per slide, totalling around 9 analyses per sample). Major element data was collected for each crystal analysed using the Cardiff University SEM-EDS, with a minimum of 5 data points per crystal. The averaged major element compositions per crystal were used to calculate the  $D$ . The method used the calculations and method of Wood and Blundy (1997) with a spreadsheet program generated by Banks (2004), which calculates  $D$  following the Brice equation (the full method together with the full list of calculated partition coefficients can be found in Appendix E). Calculations using these  $D$  are compared to the  $D$  calculated for ophiolitic clinopyroxene based on data from the Bay of Islands ophiolite of Bédard (1994) (Table 5.1).

The results from the  $D$  calculations essentially provide a modelled composition for the melt from which the analysed clinopyroxenes crystallised from. Despite the difference in technique, the results are very similar. The results gained from the  $D$  calculated for this study, on a per sample basis, are generally lower than those calculated using the  $D$  of Bédard, but have comparable patterns and share the same relative enrichment or depletion. All values are presented normalised to the chondrite values of Anders and Grevesse (1989) for continuity with preceding chapters.

Element	Bulk Partition Coefficient (D)		
	Range of D calculated for this Study		D of Bédard (1991 and 1994)
	Low	High	
La	0.050	0.115	0.0536
Ce	0.075	0.167	0.0858
Pr	0.104	0.228	0.124
Nd	0.138	0.294	0.1873
Sm	0.197	0.404	0.291
Eu	0.218	0.440	0.3288
Gd	0.234	0.465	0.367
Tb	0.244	0.477	0.404
Dy	0.247	0.476	0.442
Ho	0.244	0.463	0.4145
Er	0.236	0.442	0.387
Tm	0.226	0.417	0.4085
Yb	0.213	0.390	0.43

Table 5.1, Comparison between the ranges of partition coefficients calculated for this study (0.5 GPa and 1500K crystallisation) and those used to model clinopyroxenes from the Bay of Islands ophiolite by Bédard (1994). The D-values of Bédard are mainly sourced from Hart and Dunn (1993). Full methodology and list of calculated partition coefficients can be found in Appendix E.

The modelled melt compositions (full methodology and equations contained in Appendix E) are compared to fields of composition with basalts from different tectonic settings (MORB, BAB and Boninite, using data from [www.petdb.org](http://www.petdb.org), listed in Appendix C) and the fields for the different dyke groups and magmatic events in each block. This will enable the different plutonic gabbros and magmatic events to be directly linked. The field for MORB and BAB lavas have a large degree of overlap as the mantle source for typical BAB is essentially depleted MORB (Figure 3.1). This means that samples plotting in the BAB field represent a mantle source that is depleted relative to MORB.

### 5.3 Petrogenetic modelling of clinopyroxenes from the Khawr Fakkan Block crustal gabbro sequence

The aim of this section is to constrain as closely as possible the composition of the melt which crystallised to form the clinopyroxenes analysed in Section 4.5 and to see how this compares to dyke groups identified in Section 3.2. A brief recap of the main crustal accretion events identified from the extrusives and dykes is given in Figure 5.1, with magmatic events divided simply into three main periods that can be applied throughout the ophiolite; early events (V1), SSZ events (V2) and a final event (V3) as originally defined by Alabaster et al. (1982) with 'V' groups after Ernewein et al. (1988)

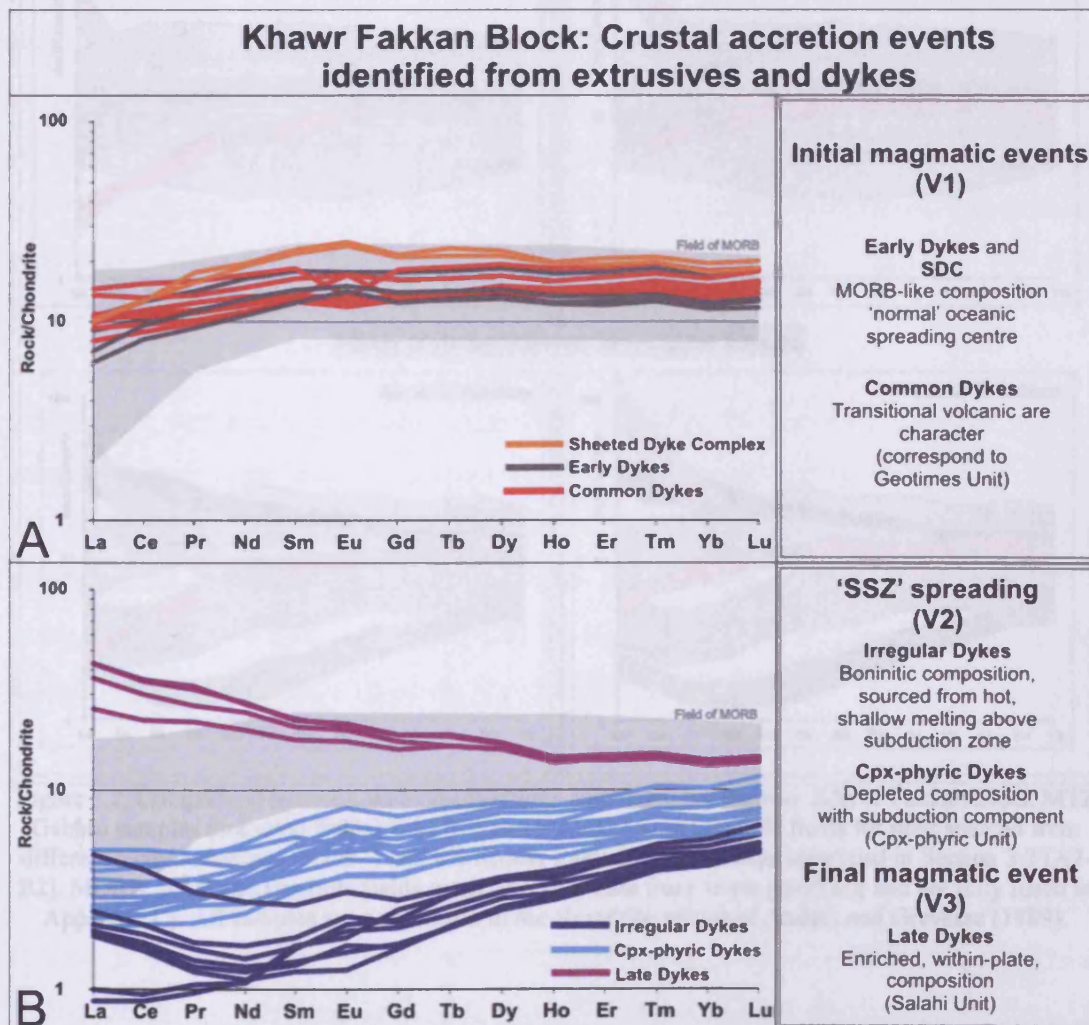


Figure 5.1, Chondrite-normalised REE patterns of the Khawr Fakkan Dyke Groups as identified in Section 3.2. The adjacent table notes some of the key features of the groups in chronological order. All samples are normalised to the chondrite values of Anders and Grevesse (1989).



### 5.3.1 Chondrite-normalised multi-element patterns

The Figures in this section display the REE patterns calculated to be in equilibrium with the clinopyroxenes analysed from the Khawr Fakkan Block. Two different sets of D were used; the first was calculated on a per sample basis using individual major element compositions (details can be found in Appendix E) and the second, fixed, set of D is taken from Bédard (1994) (Table 5.1).

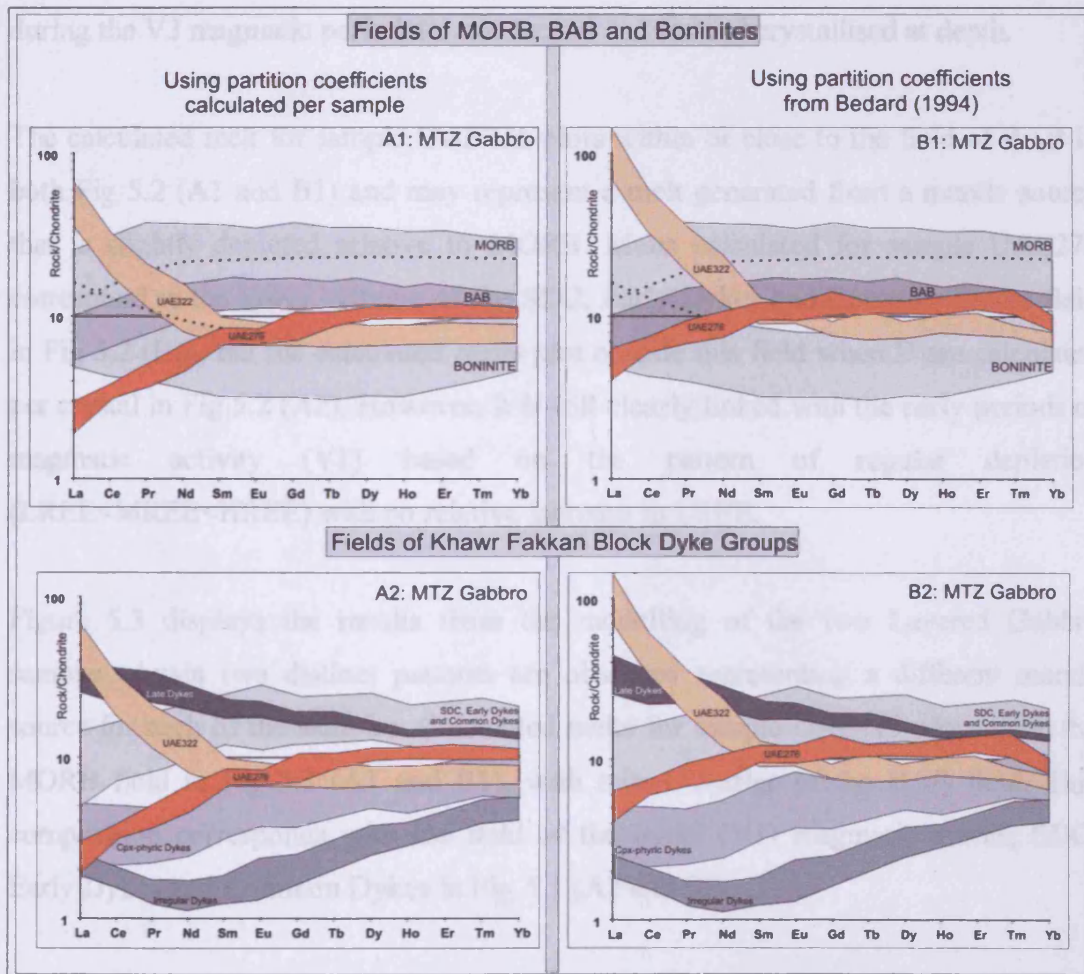


Figure 5.2. Comparison between melt compositions calculated for the two Khawr Fakkan Block MTZ Gabbro samples (coloured fields) UAE276 and UAE322 with (shaded) fields for melt sourced from different tectonic settings (A1-B1) and the Khawr Fakkan Dyke Groups identified in Section 3.2 (A2-B2). MORB, BAB and Boninite fields generated with data from [www.petdb.org](http://www.petdb.org) and are fully listed in Appendix C). All samples are normalised to the chondrite values of Anders and Grevesse (1989).

The calculated results for the two Moho Transition Zone (MTZ) Gabbro samples (UAE276 and UAE322) are compared in Figure 5.2 to the shaded fields of basalts

from different tectonic settings. The bimodal distribution of the MTZ samples observed in Section 4.5.2 (Figure 4.3) is also apparent in Figure 5.2 (A1 and B1). The two samples clearly represent melts generated in different tectonic settings. The key difference is the relative enrichment of LREE in sample UAE322. The pattern is distinctly  $LREE > MREE = HREE$ , and is similar to the field of the Late Dykes (Fig 5.2 A2-B2), although the calculated melts only have a limited overlap with this field because of lower abundance (possibly related to the D values used). The presence of an intrusive gabbro unit within the MTZ which might correspond to the last (within-plate) magmatic period provides evidence that a proportion of the melt supplied during the V3 magmatic period did not ascend and instead crystallised at depth.

The calculated melt for sample UAE276 plots within or close to the field of BAB in both Fig 5.2 (A1 and B1) and may represent a melt generated from a mantle source that is slightly depleted relative to MORB. Melts calculated for sample UAE276 correspond to the lower extreme of the SDC, Early Dykes and Common Dykes field in Fig 5.2 (B2), but the calculated melts plot outside this field when D are calculated per crystal in Fig 5.2 (A2). However, it is still clearly linked with the early periods of magmatic activity (V1) based on the pattern of regular depletion ( $LREE < MREE < HREE$ ) with no relative increase in LREE.

Figure 5.3 displays the results from the modelling of the two Layered Gabbro samples. Again two distinct patterns are observed representing a different mantle source for each of the samples. Calculated melts for sample UAE419 plot within the MORB field in Fig 5.3 (A1 and B1), with minor overlap of the BAB field. This composition corresponds with the field of the initial (V1) magmatic events; SDC, Early Dykes and Common Dykes in Fig 5.3 (A2 and B2).

Sample UAE421 has a pattern of enrichment  $LREE > MREE < HREE$  in Fig 5.2 (A1), which appears to correspond to the upper extreme of the Boninite field. This pattern is not repeated using the D values of Bédard (1994) in Figure 5.3 (B1), where the pattern is flatter in the MREE and the overall pattern is of  $LREE \geq MREE > HREE$ . Such a difference in results is the reason that two sets of bulk distribution coefficients (D) were used for comparison in this study. While the implications for the tectonic setting of sample UAE421 (Fig 5.3 A1 and B1) are not conclusive, the results from Fig

5.3 A2 and B2 indicate that the modelled melt composition is not depleted enough to correspond to the boninitic Irregular Dyke Group. The modelled melts instead plot above the fields for the SSZ-related dyke groups and probably corresponds to the last (V3) magmatic period indicated by the increased levels of LREE compared to the other (still relatively enriched) elements.

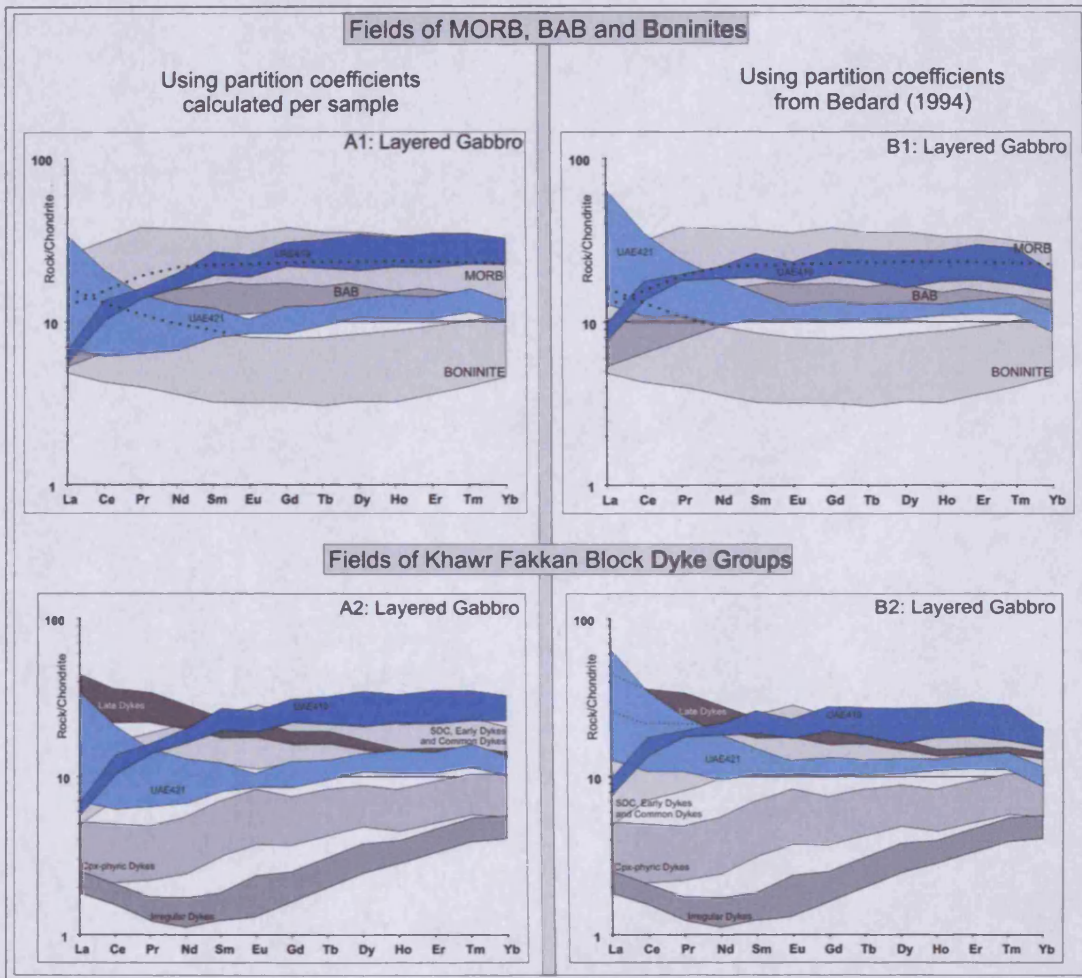


Figure 5.3. Comparison between melt compositions calculated for the two Khawr Fakkan Block Layered Gabbro samples (coloured fields) UAE419 and UAE421 with (shaded) fields for melt sourced from different tectonic settings (A1-B1) and the Khawr Fakkan Dyke Groups identified in Section 3.2 (A2-B2). MORB, BAB and Boninite fields generated with data from [www.petdb.org](http://www.petdb.org). All samples are normalised to the chondrite values of Anders and Grevesse (1989).

The field calculated for the five Khawr Fakkan Upper Gabbro samples is illustrated in Figure 5.4. The modelled compositions, from samples collected over a range of stratigraphic heights within the upper gabbro sequence, all display relatively enriched compositions that correspond to the MORB field in Fig 5.4 (A1 and B1). All of the results have a negative Eu anomaly caused by the primary crystallisation of

plagioclase, typical of a MORB-like system. The field in Fig 5.4 (A2 and B2) is partially more enriched than the field for the SDC, Early Dykes and Common Dykes, and could represent greater fractionation of the melt. This relative enrichment combined with the characteristic MORB-like pattern of LREE depletion is taken as strong evidence that the Upper Gabbros all formed during the initial (V1) period of crustal accretion.

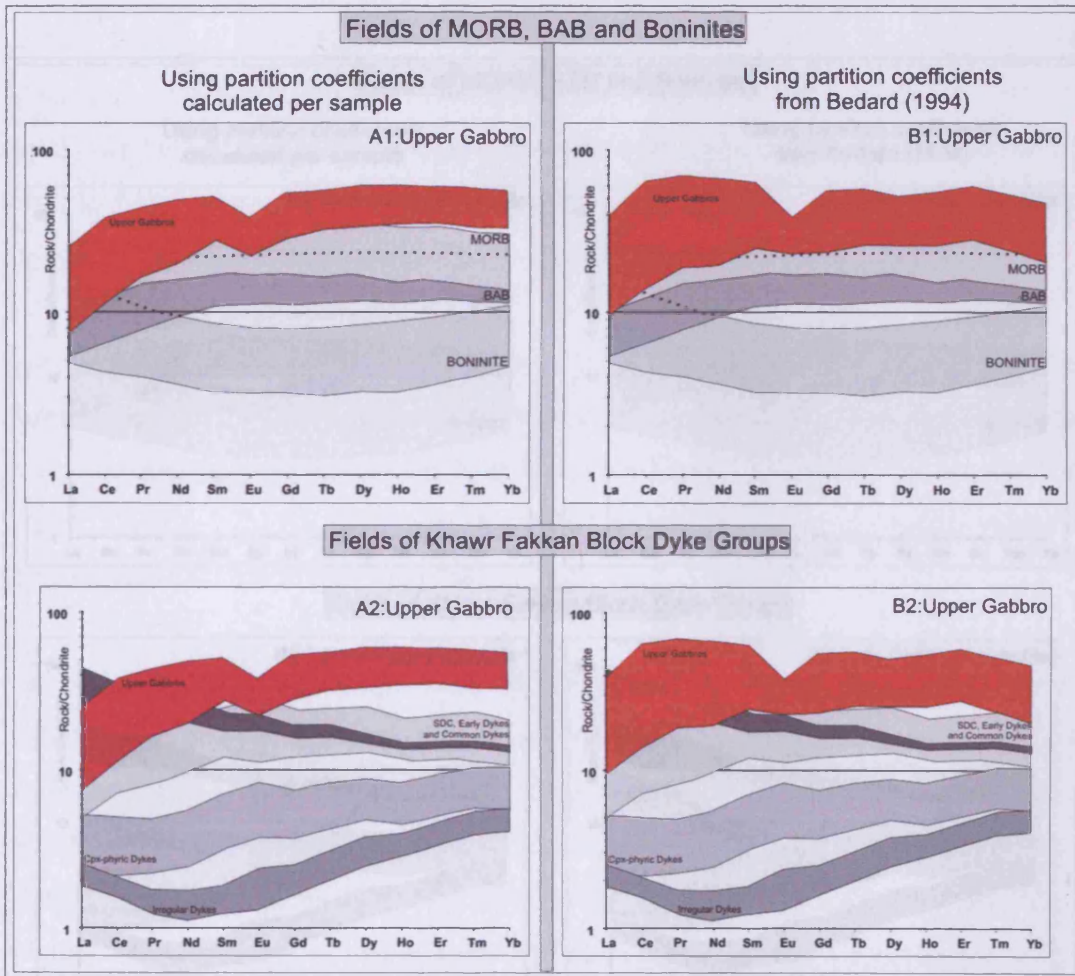


Figure 5.4. Comparison between of melt compositions calculated for the five Khawr Fakkan Block Upper Gabbro samples (coloured field) with (shaded) fields for melt sourced from different tectonic settings (A1-B1) and the Khawr Fakkan Dyke Groups identified in Section 3.2 (A2-B2). MORB, BAB and Boninite fields generated with data from [www.petdb.org](http://www.petdb.org). All samples are normalised to the chondrite values of Anders and Grevesse (1989).

The modelled results for the clinopyroxene phenocrysts from the late gabbro pegmatite (O3UR74) are displayed in Figure 5.5. The gabbro is associated with intrusive dunite bodies and other ultramafic rocks intruding the lower Layered Gabbro sequence. The source melt for the gabbro has a modelled composition which is

enriched in LREE compared to MREE and HREE. The 'U'-shaped pattern is typical of boninites and fits within the Boninite field in Fig 5.5 (B1). When compared to the compositions of the identified Khawr Fakkan Dyke Groups, the results are significantly enriched compared to the field of the boninitic Irregular Dykes. However, the REE patterns are parallel and this may be taken as evidence that the late gabbro pegmatite is associated with melting above a subduction zone during the second (V2) magmatic period.

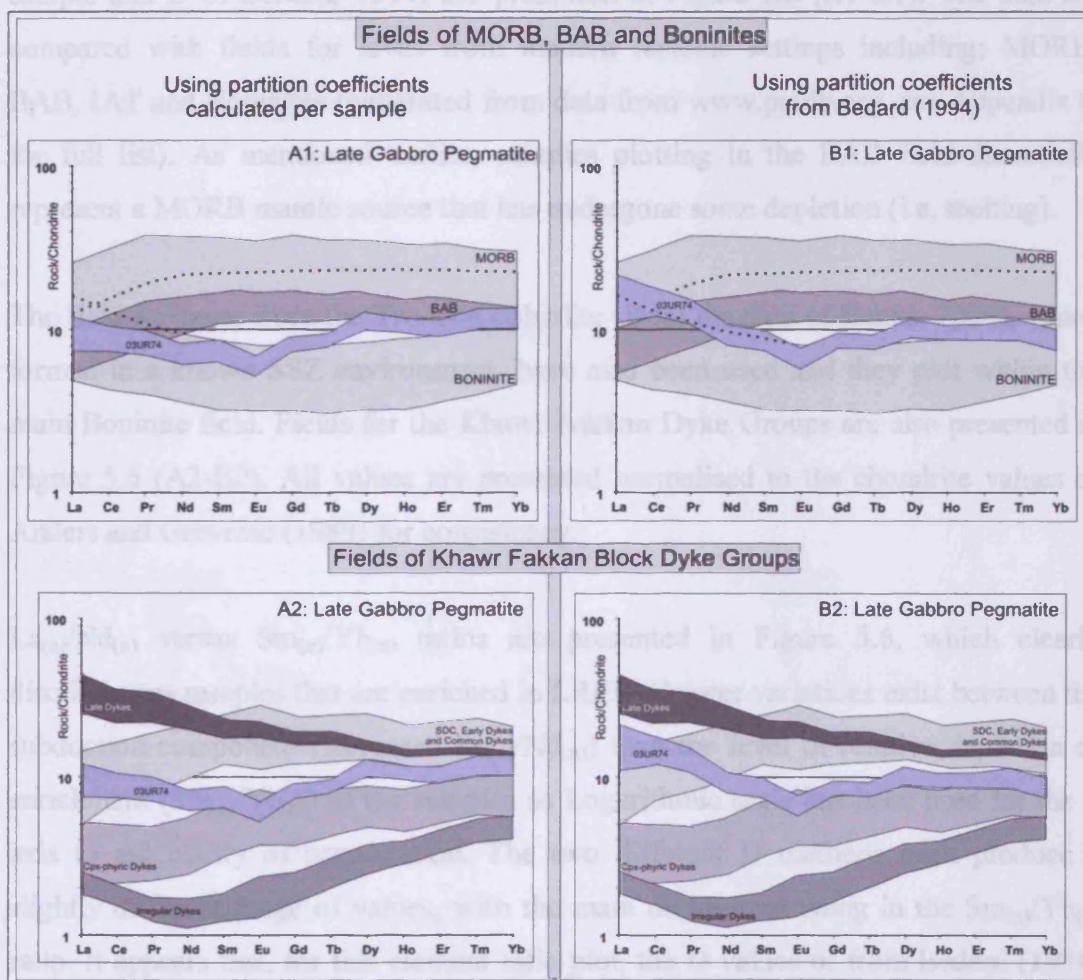


Figure 5.5. Comparison between melt compositions calculated for the Khawr Fakkan Block late gabbro pegmatite sample (coloured field) with (shaded) fields for melt sourced from different tectonic settings (A1-B1) and the Khawr Fakkan Dyke Groups identified in Section 3.2 (A2-B2). MORB, BAB and Boninite fields generated with data from [www.petdb.org](http://www.petdb.org). All samples are normalised to the chondrite values of Anders and Grevesse (1989).

### 5.3.2 Comparison between element ratios

As discussed in Section 3.4.1, comparison between the relative abundance of LREE, MREE and HREE can help to illustrate the variation in the subduction-derived component. This Section aims to compare the chondrite-normalised modelled results, displayed above, as element ratio plots. Partition coefficient-modelled melt composition data generated by both methods used in Section 5.3.1 (D calculated per sample and D of Bédard, 1994) are presented in Figure 5.6 (A1-B1). The data are compared with fields for lavas from modern tectonic settings including; MORB, BAB, IAT and Boninites (generated from data from [www.petdb.org](http://www.petdb.org), see Appendix C for full list). As mentioned earlier, samples plotting in the BAB field essentially represent a MORB mantle source that has undergone some depletion (i.e. melting).

The field for lavas from the Troodos ophiolite (from the data of Banks, 2004), which formed in a known SSZ environment, have also been used and they plot within the main Boninite field. Fields for the Khawr Fakkan Dyke Groups are also presented in Figure 5.6 (A2-B2). All values are presented normalised to the chondrite values of Anders and Grevesse (1989) for consistency.

$La_{(n)}/Nd_{(n)}$  versus  $Sm_{(n)}/Yb_{(n)}$  ratios are presented in Figure 5.6, which clearly discriminates samples that are enriched in LREE. Greater variations exist between the subduction component (increased  $La_{(n)}/Nd_{(n)}$ ) than the level of relative depletion or enrichment ( $Sm_{(n)}/Yb_{(n)}$ ) of the samples so Logarithmic scale has been used for the Y axis to aid clarity of presentation. The two different D methods each produce a slightly different range of values, with the main differences being in the  $Sm_{(n)}/Yb_{(n)}$  ratio. It appears that, for this element ratio plot, the D values of from Bédard (1994) produce a better fit with the data fields (discussed further in Appendix E).

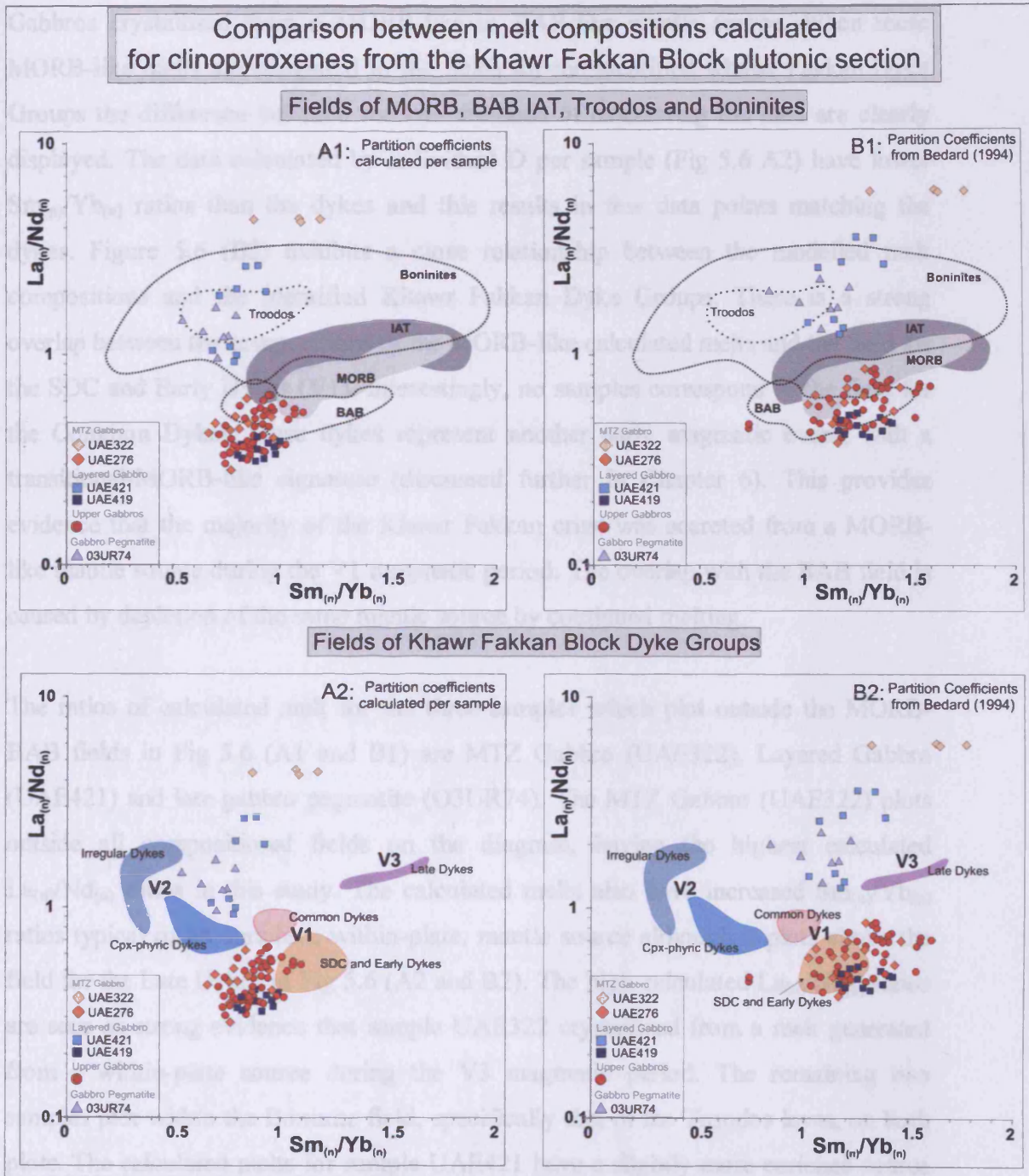


Figure 5.6. Comparison between melt compositions calculated from the clinopyroxenes of the Khawr Fakkan Block plutonic section with fields for melt sourced from different tectonic settings (A1-B1) and the Khawr Fakkan Dyke Groups identified in Section 3.2 (A2-B2). MORB, BAB, IAT and Boninite fields generated with data from [www.petdb.org](http://www.petdb.org) (full list in Appendix C). Troodos field generated with data from Banks (2004). All samples are normalised to the chondrite values of Anders and Grevesse (1989).

Most samples that do not have a subduction component plot within or close to the BAB field in Fig 5.6 (A1), and within the MORB and BAB field in Fig 5.6 (B1). This provides strong evidence that samples UAE276, UAE419 and all of the Upper

Gabbros crystallised from a MORB-like to BAB-like mantle source. When these MORB-like melts are compared to the fields for the identified Khawr Fakkan Dyke Groups the difference between the two methods of calculating the data are clearly displayed. The data calculated by individual D per sample (Fig 5.6 A2) have lower  $Sm_{(n)}/Yb_{(n)}$  ratios than the dykes and this results in few data points matching the dykes. Figure 5.6 (B2) exhibits a close relationship between the modelled melt compositions and the identified Khawr Fakkan Dyke Groups. There is a strong overlap between the compositions of the MORB-like calculated melts and the field for the SDC and Early Dykes (V1). Interestingly, no samples correspond to the field for the Common Dykes; these dykes represent another early magmatic event, with a transitional-MORB-like signature (discussed further in Chapter 6). This provides evidence that the majority of the Khawr Fakkan crust was accreted from a MORB-like mantle source during the V1 magmatic period. The overlap with the BAB field is caused by depletion of the same mantle source by continued melting.

The ratios of calculated melt for the three samples which plot outside the MORB-BAB fields in Fig 5.6 (A1 and B1) are MTZ Gabbro (UAE322), Layered Gabbro (UAE421) and late gabbro pegmatite (O3UR74). The MTZ Gabbro (UAE322) plots outside all compositional fields on the diagram, having the highest calculated  $La_{(n)}/Nd_{(n)}$  ratios in this study. The calculated melts also have increased  $Sm_{(n)}/Yb_{(n)}$  ratios typical of an enriched, within-plate, mantle source although it plots above the field for the Late Dykes in Fig 5.6 (A2 and B2). The high calculated  $La_{(n)}/Nd_{(n)}$  ratios are seen as strong evidence that sample UAE322 crystallised from a melt generated from a within-plate source during the V3 magmatic period. The remaining two samples plot within the Boninite field, specifically that of the Troodos lavas, on both plots. The calculated melts for sample UAE421 have a slightly more enriched source than those of O3UR74, represented by higher average  $Sm_{(n)}/Yb_{(n)}$  and  $La_{(n)}/Nd_{(n)}$  ratios, although these still plot within the Boninite field. When these two samples are compared to the identified dyke groups, there is no overlap between any of the fields. Sample O3UR74 has a similar modelled  $La_{(n)}/Nd_{(n)}$  ratio to that of the Irregular Dykes and is considered by the author to represent a slowly cooled melt produced in the early stages of a SSZ setting (hot, shallow, hydrous melting of a depleted mantle source) during the V2 magmatic period. The  $La_{(n)}/Nd_{(n)}$  and  $Sm_{(n)}/Yb_{(n)}$  ratios compared of UAE421 (Fig 5.6), combined with incompatible element data from



Section 4.5.4 (Figure 4.6) indicate that Layered Gabbro sample UAE421 has an enriched source similar to that of UAE322, and provides evidence for the accretion of the Layered Gabbro sequence during the final (V3) period of magmatism in the Khawr Fakkan Block.

### **5.3.3 Conclusions from petrogenetic modelling of clinopyroxenes from the Khawr Fakkan Block crustal gabbro sequence**

- MTZ Gabbro sample UAE276 was sourced from a slightly depleted MORB-like mantle and corresponds to the initial (V1) magmatic events (SDC and Early Dykes). It does not contain a subduction component.
- MTZ Gabbro sample UAE322 was sourced from a mantle that was selectively enriched in LREE compared to MREE and HREE and corresponds to the Late Dyke Group, which represents the last (V3) magmatic event recorded in the Khawr Fakkan Block.
- Layered Gabbro sample UAE419 corresponds to the initial (V1) magmatic events (SDC and Early Dykes) and has a MORB-like mantle source.
- Layered Gabbro sample UAE421 was sourced from a mantle that was selectively enriched in LREE compared to MREE and HREE and corresponds to the Late Dyke Group (V3).
- All of the Upper Gabbros sampled plot in the field of MORB and formed during the initial magmatic events (V1) from a MORB-like mantle source and correspond to the SDC and Early Dykes.
- Late gabbro pegmatite O3UR74 corresponds to the boninitic Irregular Dyke Group. This is evidence that the gabbro crystallised from a melt produced

from hot, shallow, hydrous melting of a depleted mantle source, during the earliest SSZ magmatic events. Boninites provide firm constraints on the tectonic setting of the Khawr Fakkan crust at the time of melt generation for this magmatic event (early V2).

- The majority of the Khawr Fakkan crust was accreted from a MORB-like mantle source during the initial magmatic period (V1), with relatively minor crustal accretion recorded in the later magmatic periods (V2 and V3).
- The results from the geochemical modelling of clinopyroxene compositions from the plutonic section of the Khawr Fakkan Block confirm the discriminations made in Chapter 4 (Section 4.5) and allow direct links between the gabbros and the dyke groups to be made. This provides firm constraints on the relative timing and methods of crustal accretion of the plutonic section (discussed further in Chapter 6).

## **5.4 Petrogenetic modelling of clinopyroxenes from the Aswad Block crustal gabbro sequence**

The aim of this section is to constrain as closely as possible the composition of the melt which crystallised to form the clinopyroxenes analysed from the Aswad Block plutonic section in Section 4.6 and to compare this to the fields of the dyke groups identified in Section 3.3. A brief recap of the main crustal accretion events identified from the extrusives and dykes is given below in Figure 5.7, with events again divided into the three main magmatic periods (V1, V2 and V3).

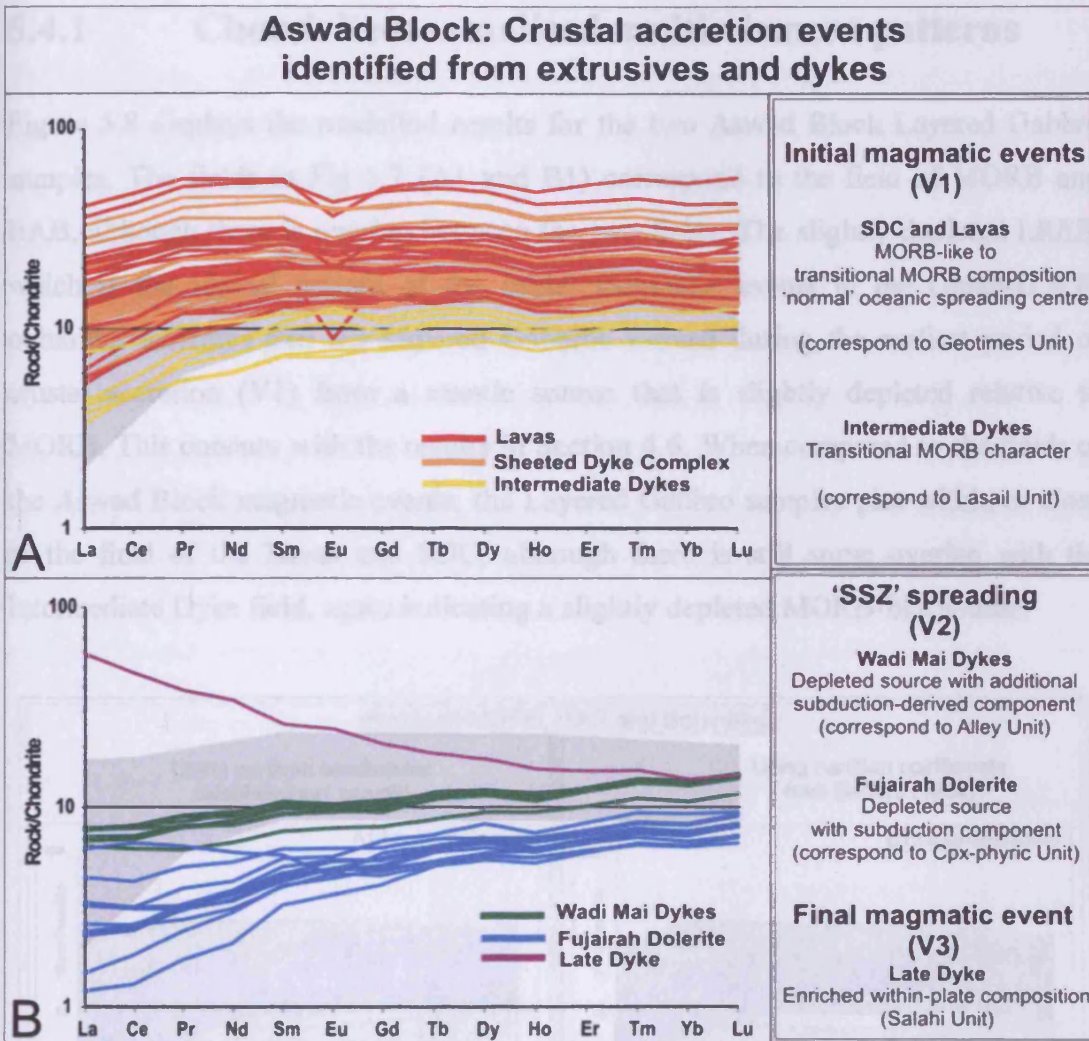


Figure 5.7. Chondrite-normalised REE patterns of the Aswad Block magmatic events identified in Chapter 3 (Section 3.2). The adjacent table notes some of the key features of the groups in chronological order. All samples are normalised to the chondrite values of Anders and Grevesse (1989).

The Figures in this section display the results of bulk partition coefficient (D) modelling of clinopyroxene compositions from the Aswad Block crustal gabbro sequence. The results (using the same two sets of D as Section 5.3) are again compared to fields of known compositions for different tectonic settings (MORB, BAB and Boninites) generated with data from [www.petdb.org](http://www.petdb.org). The fields of the Aswad Block extrusives and dykes as identified in Section 3.3 are also displayed, except the field for the single Late Dyke (V3), which was not included for clarity of presentation. All values are presented normalised to the chondrite values of Anders and Grevesse (1989).

### 5.4.1 Chondrite-normalised multi-element patterns

Figure 5.8 displays the modelled results for the two Aswad Block Layered Gabbro samples. The fields in Fig 5.7 (A1 and B1) correspond to the field of MORB and BAB, although there is overlap between the two fields. The slightly depleted LREE, which is the typical pattern of the initial magmatic events in the Oman-U.A.E. ophiolite, indicates that the Layered Gabbros formed during the earliest period of crustal accretion (V1) from a mantle source that is slightly depleted relative to MORB. This concurs with the results in Section 4.6. When compared to the fields of the Aswad Block magmatic events, the Layered Gabbro samples plot within or close to the field of the Lavas and SDC, although there is still some overlap with the Intermediate Dyke field, again indicating a slightly depleted MORB-like source.

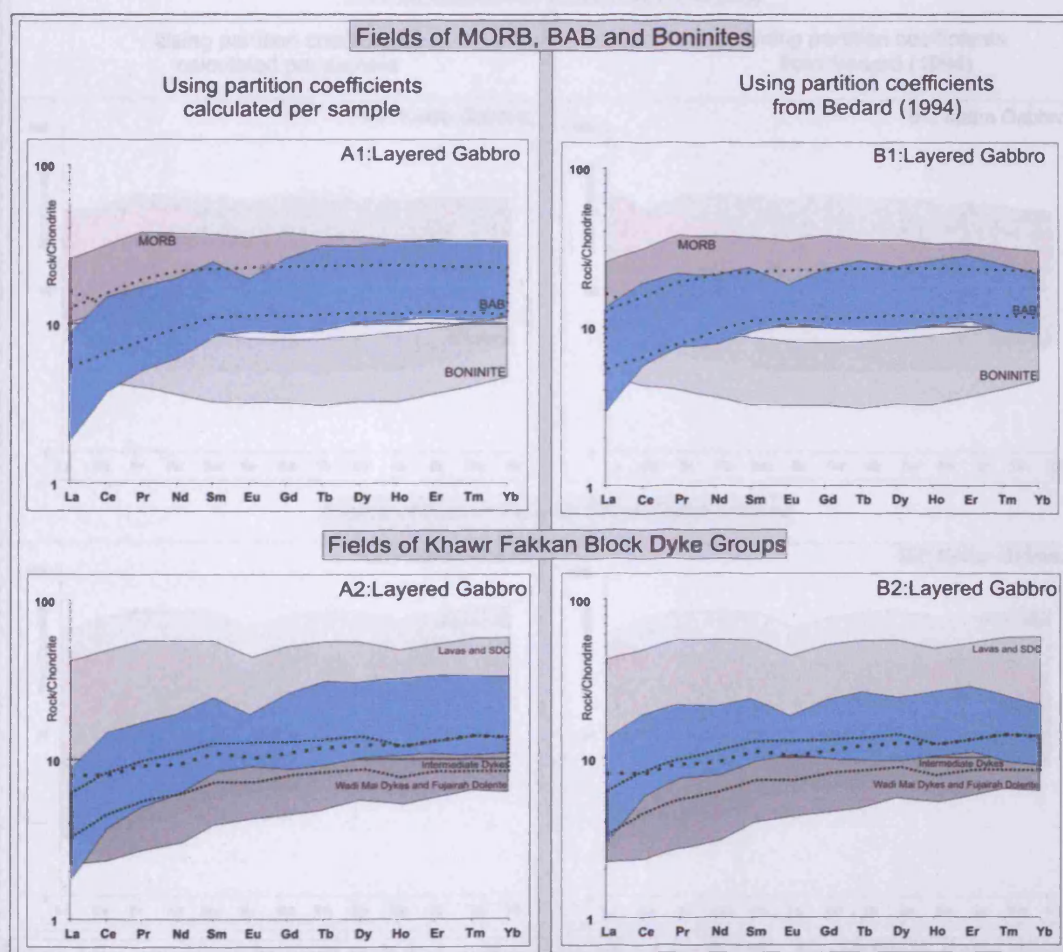


Figure 5.8. Comparison between melt compositions calculated for the two Aswad Block Layered Gabbro samples (coloured field) with (shaded) fields for melt sourced from different tectonic settings (A1-B1) and the Aswad Block magmatic events as identified in Section 3.2 (A2-B2). MORB, BAB and Boninite fields generated with data from [www.petdb.org](http://www.petdb.org) and are fully listed in Appendix C. All samples are normalised to the chondrite values of Anders and Grevesse (1989).

Figure 5.10 displays the results for modelled melts for the Kanawa Basalt Gabbro.

The patterns for melt calculated for the five Kalba (Upper) Gabbro samples, displayed in Figure 5.9 (A1 and B1), have a relatively narrow field that corresponds closely to the MORB field. The most notable characteristic of the modelled data is the MORB-like composition with slightly increased LREE in some samples. This LREE enrichment, which was also observed in Section 4.6 (Figure 4.11), denotes a MORB-like to transitional MORB-like mantle source for the Kalba Gabbro that has an additional, but variable, subduction-related component. The Kalba Gabbro results all plot within the field for the Lavas and SDC in Fig 5.9 (A2 and B2). This relationship is confirmed by field observations (Section 3.4.5) that the Kalba Gabbro is the source for the SDC and lowermost lavas and formed in the V1 magmatic period.

slightly depleted relative to MORB, i.e. within the V1 magmatic period.

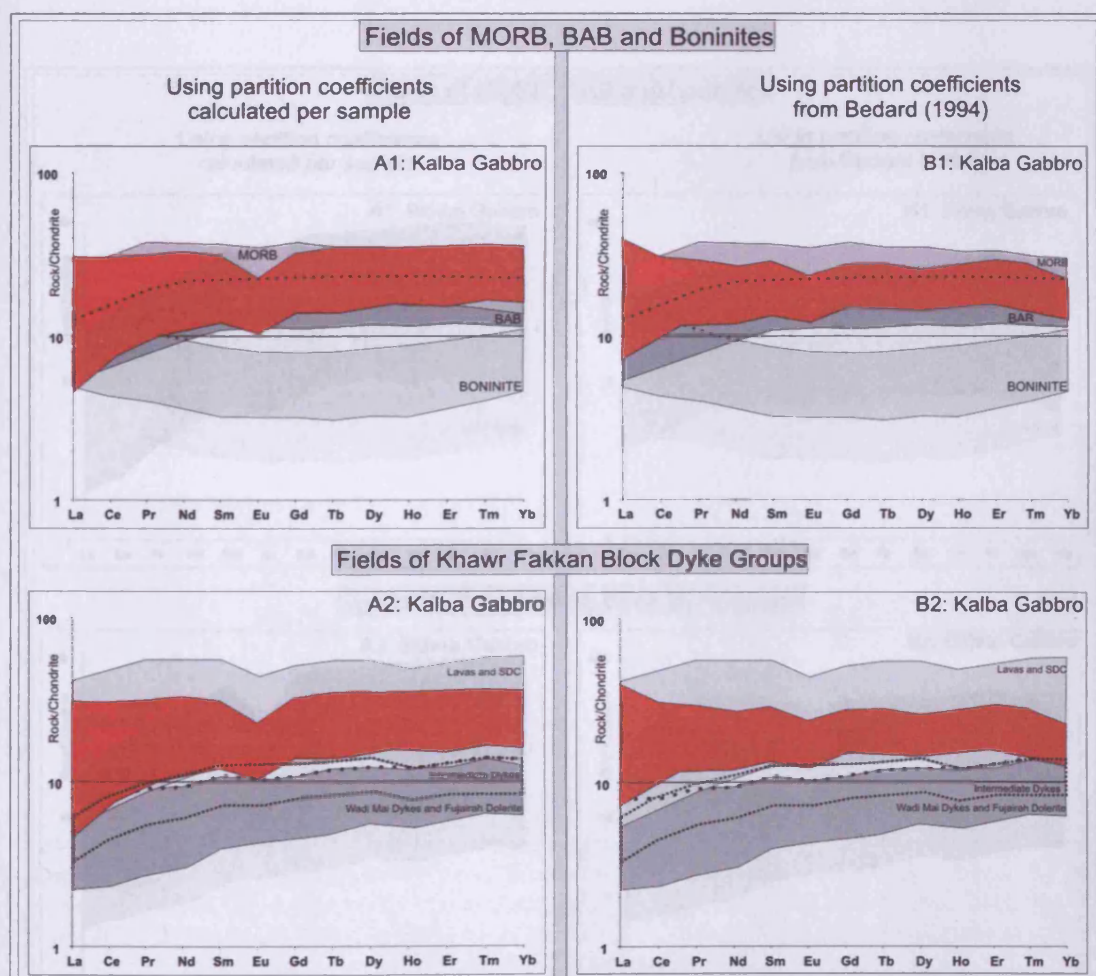


Figure 5.9. Comparison between melt compositions calculated for the five Aswad Block Kalba (Upper) Gabbro samples (coloured field) with (shaded) fields for melt sourced from different tectonic settings (A1-B1) and the Aswad Block magmatic events as identified in Section 3.2 (A2-B2). MORB, BAB and Boninite fields generated with data from [www.petdb.org](http://www.petdb.org). All samples are normalised to the chondrite values of Anders and Grevesse (1989).

Figure 5.10 displays the results for modelled melts for the intrusive Bithna Gabbro. The calculated values have a broad range which overlap both the MORB and BAB fields entirely (Figure 5.10 A1 and B1) with  $LREE < MREE$ . The LREE depletion is more pronounced using individual Di calculated per crystal (Fig 5.10 A1). The melts modelled for the Bithna Gabbro are more depleted than those calculated for the Kalba Gabbro and do not have variable enrichment in LREE. This provides evidence that the Bithna Gabbro was sourced from a relatively depleted mantle source that did not have an additional subduction component. When compared to the fields for the identified magmatic events in the Bithna Gabbro overlaps the fields of the Lavas, SDC and the Intermediate Dykes. This implies that the Bithna Gabbro is the source for the Intermediate Dykes which, as described in Chapter 4, were sourced from a mantle slightly depleted relative to MORB, i.e. within the V1 magmatic period.

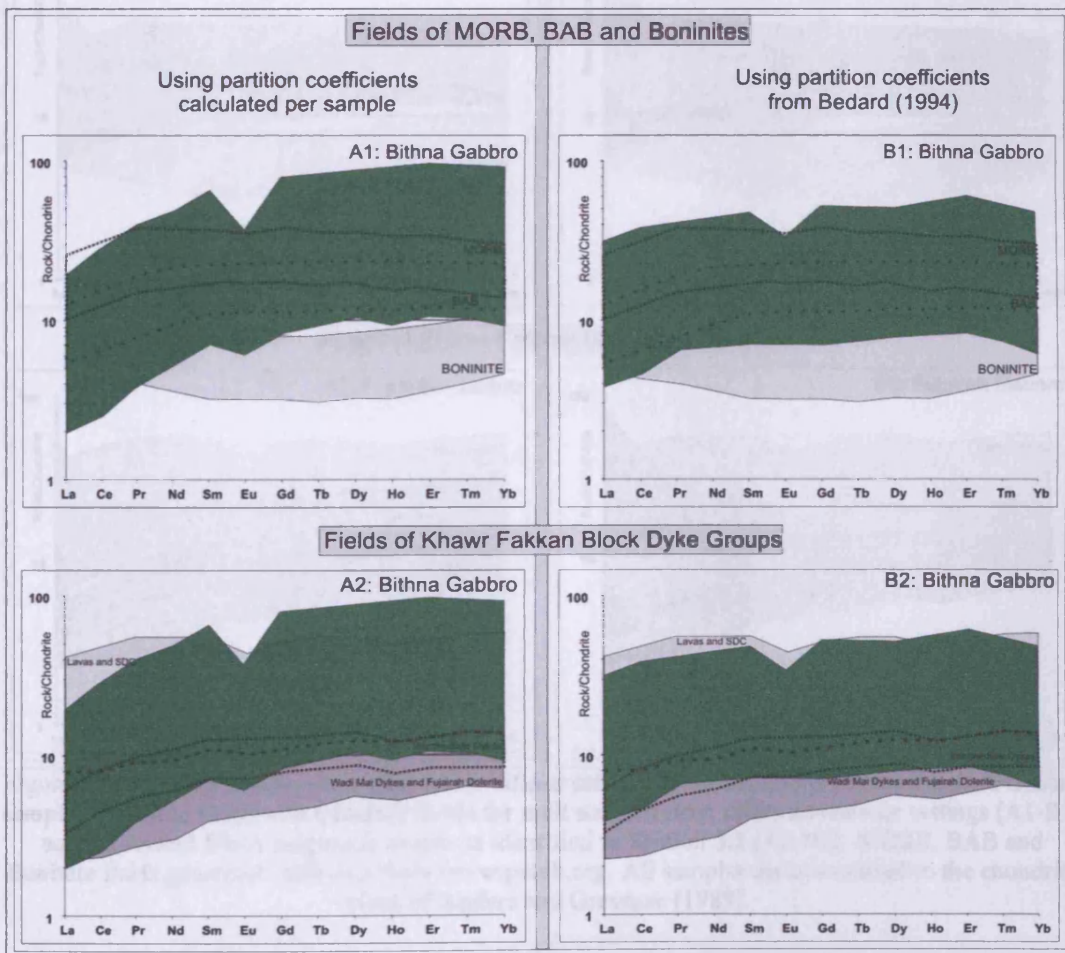


Figure 5.10. Comparison between melt compositions calculated for the Aswad Block Bithna Gabbro samples (coloured field) with (shaded) fields for melt sourced from different tectonic settings (A1-B1) and the Aswad Block magmatic events as identified in Section 3.2 (A2-B2). MORB, BAB and Boninite fields generated with data from [www.petdb.org](http://www.petdb.org). All samples are normalised to the chondrite values of Anders and Grevesse (1989).

The results for the modelled melt compositions of the intrusive Fujairah Gabbro are displayed in Figure 5.11. The results display the characteristic LREE>MREE<HREE pattern of enrichment typical of Boninitic melts (Fig 5.11 B1), although the field plots within with the MORB and BAB fields. The enrichment in the subduction-mobile LREE provides firm evidence that the Fujairah Gabbro was intruded during the SSZ (V2) volcanic period, and post-dates the main period of crustal accretion. This is confirmed in the field by its intrusive relationships, which post-date all magmatic events except the Late Dykes.

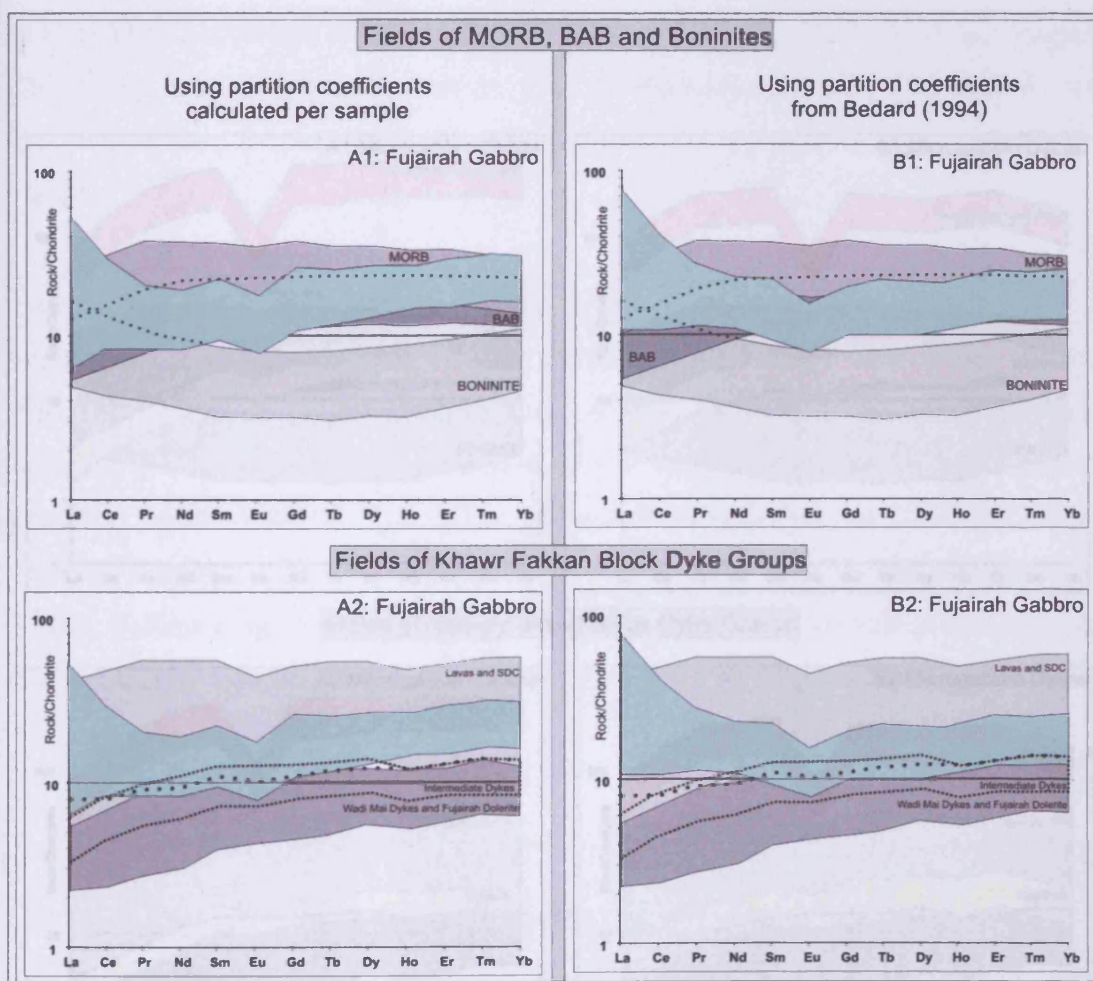


Figure 5.11. Comparison between melt compositions calculated for the Aswad Block Fujairah Gabbro samples (coloured field) with (shaded) fields for melt sourced from different tectonic settings (A1-B1) and the Aswad Block magmatic events as identified in Section 3.2 (A2-B2). MORB, BAB and Boninite fields generated with data from [www.petdb.org](http://www.petdb.org). All samples are normalised to the chondrite values of Anders and Grevesse (1989).

When compared to the identified magmatic events in the Aswad Block the modelled melts for the Fujairah Gabbro plot mainly within the field of the Lavas and SDC, a

consequence of the high REE abundances within the sampled clinopyroxenes, resulting from fractional crystallisation. Element ratio diagrams are able to ‘see-through’ such effects of fractional crystallisation (e.g. Figures 5.6 and 5.13). The significantly LREE enriched pattern of the Fujairah Gabbro in Fig 5.11 is very similar to the pattern of the Wadi Mai Dykes and Fujairah Dolerite (which is observed rooting in the Fujairah Gabbro). The increase in LREE from a relatively depleted mantle source is a key identification factor for the Fujairah Gabbro and other V2 rocks.

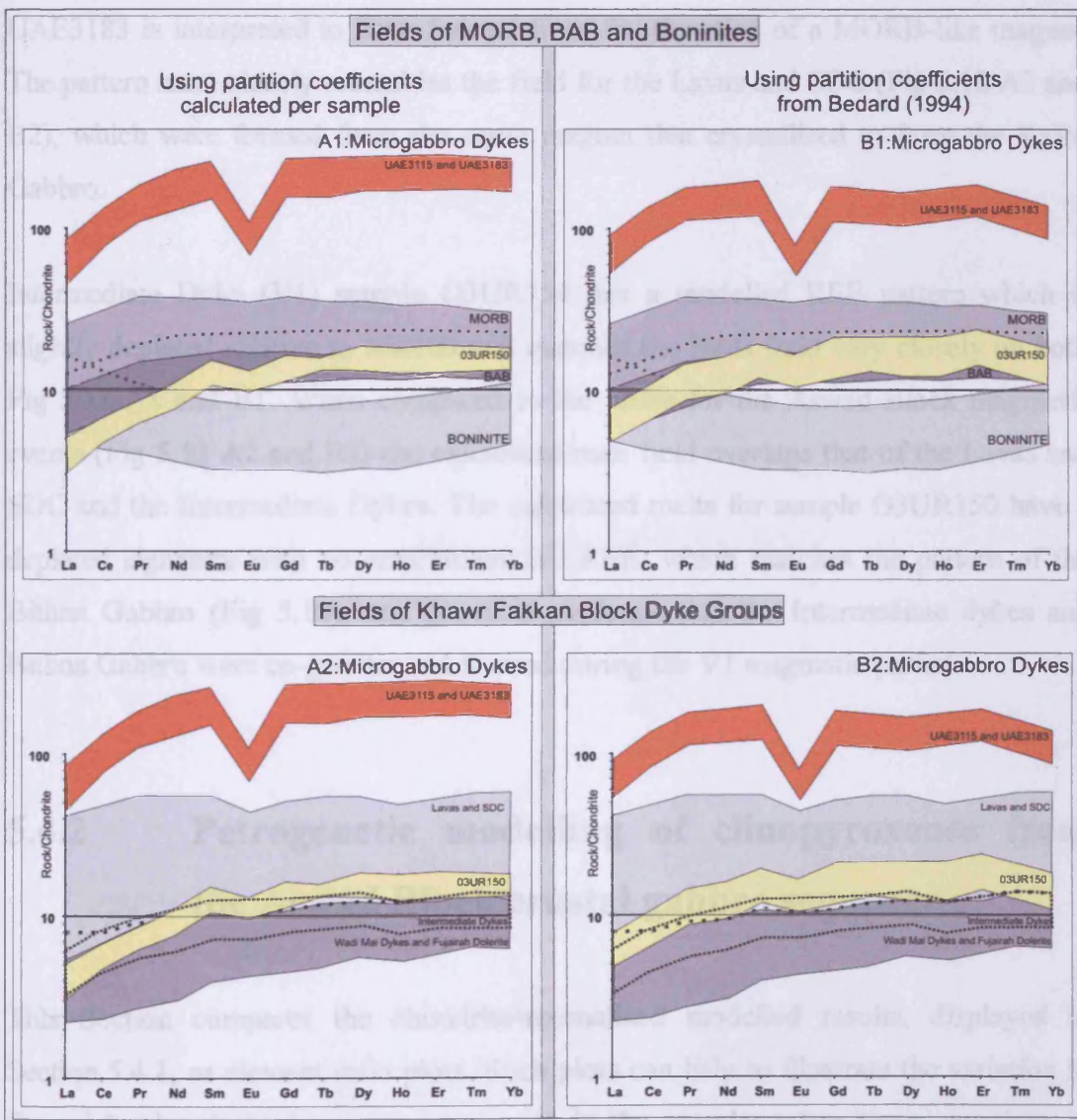


Figure 5.11. Comparison between melt compositions calculated for the Aswad Block Microgabbro Dyke samples (coloured fields) with (shaded) fields for melt sourced from different tectonic settings (A1-B1) and the Aswad Block magmatic events as identified in Section 3.2 (A2-B2). MORB, BAB and Boninite fields generated with data from [www.petdb.org](http://www.petdb.org). All samples are normalised to the chondrite values of Anders and Grevesse (1989).



Figure 5.12 displays the modelled data for the three Microgabbro Dykes from the Aswad Block that have also been discriminated in Chapter 3. The pattern for the calculated melts for dykes UAE3115 and UAE3183, which formed during the MORB-like (V1 period), have an enriched modelled REE pattern (Fig 5.12 A1 and B1), which lies significantly above the field of MORB. However, the pattern is parallel to the MORB field and is only slightly LREE depleted. The samples have a negative Eu anomaly which represents crystallisation of plagioclase from the melt, possibly in a magma chamber. The modelled REE pattern for samples UAE3115 and UAE3183 is interpreted to have formed from fractionation of a MORB-like magma. The pattern most closely resembles the field for the Lavas and SDC (Fig 5.12 A2 and B2), which were formed from the same magma that crystallised to form the Kalba Gabbro.

Intermediate Dyke (V1) sample O3UR150 has a modelled REE pattern which is slightly depleted relative to MORB and matches the BAB field very closely on both Fig 5.12 A1 and B1. When compared to the fields for the Aswad Block magmatic events (Fig 5.12 A2 and B2) the calculated melt field overlaps that of the Lavas and SDC and the Intermediate Dykes. The calculated melts for sample O3UR150 have a depleted signature with no enrichment in LREE, which matches the pattern of the Bithna Gabbro (Fig 5.10), and provides evidence that the Intermediate dykes and Bithna Gabbro were co-genetic and formed during the V1 magmatic period.

## **5.4.2 Petrogenetic modelling of clinopyroxenes from the Aswad Block crustal gabbro sequence**

This Section compares the chondrite-normalised modelled results, displayed in Section 5.4.1, as element ratio plots. Such plots can help to illustrate the variation in the subduction-derived component present in the samples when large variations in elemental abundance exist. The modelled melt compositions, generated by both methods, are compared with fields for different tectonic settings including; MORB, BAB, IAT, Boninites and Troodos lavas (generated from data from [www.petdb.org](http://www.petdb.org))

and Banks, 2004). Fields for the magmatic events identified in the Aswad Block are also presented in Figure 5.13. The D values calculated for this study on a per sample basis again give low  $Sm_{(n)}/Yb_{(n)}$  ratios, resulting in most of the MORB-like samples plotting mostly outside any of the fields in Fig 5.13 (A1) (discussed further in Appendix E).

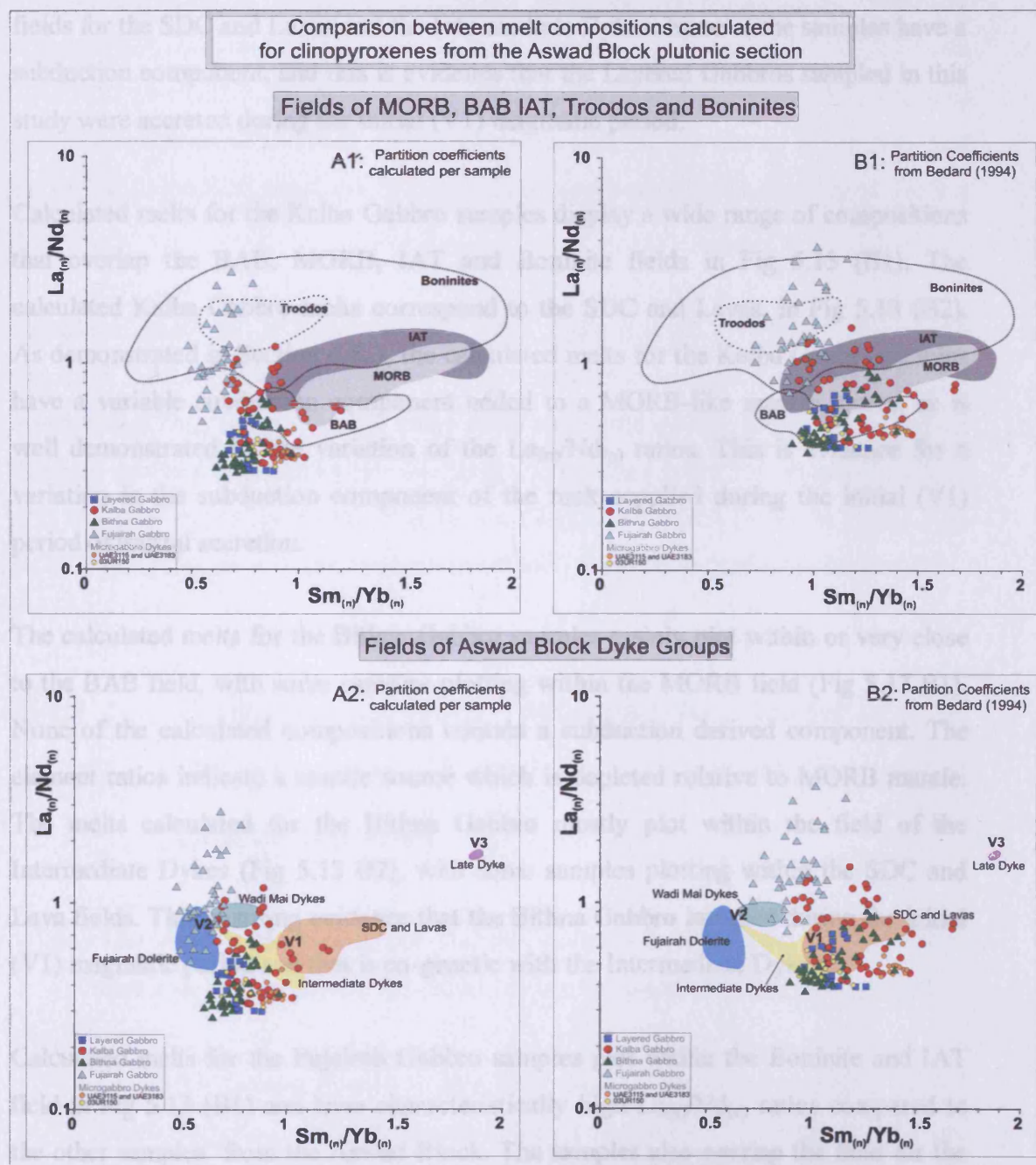


Figure 5.13, Comparison between melt compositions calculated for the clinopyroxenes from the Aswad Block plutonic section with fields for melt sourced from different tectonic settings (A1-B1) and the Aswad Block magmatic events as identified in Section 3.2 (A2-B2). MORB, BAB, IAT and Boninite fields generated with data from [www.petdb.org](http://www.petdb.org) (fully listed in Appendix C). Troodos field generated with data from Banks, (2004). All samples are normalised to the chondrite values of Anders and Grevesse (1989).

The calculated melts for the Layered Gabbro samples plot within the MORB and BAB fields in Fig 5.13 (B1), with samples generally having lower  $Sm_{(n)}/Yb_{(n)}$  and  $La_{(n)}/Nd_{(n)}$  ratios than most of the other samples except some of the melts calculated for the Bithna Gabbro. When compared to the fields for the different magmatic units identified in the Aswad Block (Fig 5.13 B2) the Layered Gabbro samples match the fields for the SDC and Lavas and the Intermediate Dykes. None of the samples have a subduction component, and this is evidence that the Layered Gabbros sampled in this study were accreted during the initial (V1) magmatic period.

Calculated melts for the Kalba Gabbro samples display a wide range of compositions that overlap the BAB, MORB, IAT and Boninite fields in Fig 5.13 (B1). The calculated Kalba Gabbro melts correspond to the SDC and Lavas, in Fig 5.13 (B2). As demonstrated in Section 4.6.3, the calculated melts for the Kalba Gabbro samples have a variable subduction component added to a MORB-like mantle source, as is well demonstrated by the variation of the  $La_{(n)}/Nd_{(n)}$  ratios. This is evidence for a variation in the subduction component of the melt supplied during the initial (V1) period of crustal accretion.

The calculated melts for the Bithna Gabbro samples mainly plot within or very close to the BAB field, with some samples plotting within the MORB field (Fig 5.13 B1). None of the calculated compositions contain a subduction derived component. The element ratios indicate a mantle source which is depleted relative to MORB mantle. The melts calculated for the Bithna Gabbro mostly plot within the field of the Intermediate Dykes (Fig 5.13 B2), with some samples plotting within the SDC and Lava fields. This is strong evidence that the Bithna Gabbro intruded during the initial (V1) magmatic period and that is co-genetic with the Intermediate Dykes.

Calculated melts for the Fujairah Gabbro samples plot within the Boninite and IAT field in Fig 5.13 (B1) and have characteristically high  $La_{(n)}/Nd_{(n)}$  ratios compared to the other samples from the Aswad Block. The samples also overlap the field for the Troodos boninitic lavas and this provides evidence for formation above a subduction zone during the second (V2) magmatic period. When compared to the fields for the magmatic units in the Aswad Block the calculated melts for the Fujairah Gabbro have

some overlap with the (V2) Wadi Mai Dykes in Fig 5.13 (B2) but most samples have higher  $La_{(n)}/Nd_{(n)}$  ratios. The D calculated per sample in Fig 5.13 (A2) display a good match with the Fujairah Dolerite, which concurs with field observations that the Fujairah Gabbro was the source for this unit.

The calculated melts for the Microgabbro 'Geotimes' Dykes are again effectively characterised by element ratio plots. Melts calculated for V1 samples UAE3115 and UAE3183 plot within or just outside the BAB and MORB fields in Fig 5.13 (A1 and B1). When compared to fields for the magmatic units in the Aswad Block they plot very close to the SDC and Lava field, which is consistent with the findings of Section 3.3.

Calculated melts for the Intermediate 'Lasail' Dyke (sample O3UR150) plot within the BAB field and overlaps with the Bithna Gabbro calculated melts, with slightly lower  $Sm_{(n)}/Yb_{(n)}$  ratios than the other early magmatic events, indicating a slightly depleted source compared to MORB mantle. Calculated melts for sample O3UR150 plot within or very close to the field for the (V1) Intermediate Dykes in Figure 5.13 (B2), which is consistent with field evidence and the results presented in Section 3.3.

### **5.4.3 Conclusions from petrogenetic modelling of clinopyroxenes from the Aswad Block crustal gabbro sequence**

- The Aswad Block Layered Gabbro samples formed from a MORB-like mantle source, indicating formation during the initial (V1) magmatic period.
- The Kalba Gabbro formed from a MORB-like mantle source during the V1 magmatic period, and corresponds to the Geotimes Unit as identified in Oman. The Kalba Gabbro records the input of a variable subduction-derived component into the mantle source, providing the earliest evidence for a proximal subduction zone.

- The Kalba Gabbro was co-genetic with the SDC and lavas.
- The Bithna Gabbro formed from a mantle source slightly depleted relative to MORB mantle and has no significant subduction-derived component. The Bithna Gabbro intruded the Kalba Gabbro sometime after its formation and was co-genetic with the Intermediate Dyke Group (during the V1 magmatic event), and corresponds to the Lasail Unit as identified in Oman.
- The Fujairah Gabbro formed above a subduction zone during the V2 magmatic event from a mantle source with an additional subduction-derived component. The Fujairah Gabbro was co-genetic with the Wadi Mai Dykes and the Fujairah Dolerite, which correspond to the Alley and Cpx-phyric Units respectively.
- The modelled data for the clinopyroxenes of the Microgabbro Dykes (UAE3115 and UAE3183) confirms that these dykes were intruded during the V1 magmatic period.
- Microgabbro Dyke sample O3UR150 (V1, Intermediate Dyke Group) is slightly depleted relative to MORB and does not contain a subduction-derived component. Sample O3UR150 is co-genetic with the Bithna Gabbro.
- No gabbro samples collected in the Aswad Block match the pattern of selective enrichment displayed by the Late Dyke from the V3 magmatic event.
- The results displayed in this chapter are significant as they confirm that the relative enrichment or depletion of certain elements within clinopyroxene is a very effective method of discriminating gabbros formed in different tectonic settings. The LA-ICP-MS analytical technique presented in this project has significant future potential for the identification of the tectonic environment of formation of coarse-grained igneous rocks.

## **Chapter 6: Conclusions and Discussion:**

# **The Magmatic Evolution and Crustal Accretion of the Northern Oman-United Arab Emirates Ophiolite**

### **6.1 Introduction**

This Chapter provides a detailed account of the crustal history of the northernmost Oman-U.A.E. ophiolite as revealed from field evidence, geochemical sampling and petrogenetic modelling of the extrusive and plutonic sequence, as presented in the preceding Chapters.

Having established direct links between extrusive units and their co-genetic intrusive counterparts it is possible to arrange the information into chronological order and to establish a detailed crustal accretion history for the Khawr Fakkan and Aswad Blocks. The information obtained about the crustal accretion processes involved in the evolution of the Khawr Fakkan and Aswad Blocks will also offer constraints on mechanisms of crustal accretion both in the rest of the Oman-U.A.E. ophiolite and in modern oceanic crust formed at mid-ocean ridges and marginal basin settings.

The northernmost blocks of the Oman-U.A.E. ophiolite record the strongest SSZ signature and the presence of boninites, which are only recorded in present-day SSZ settings, confirms the SSZ setting of the ophiolite during this magmatic period. The subduction signature also becomes stronger with time in both blocks studied. Detailed information about the evolution of the mantle source allows constraints to be applied to the palaeotectonic setting and evolution of the crust.

The schematic diagrams presented in Sections 6.2 and 6.3 have been drawn with the aim of most clearly displaying the crustal accretion history of the Khawr Fakkan and

Aswad Blocks. Although certain events in the crustal accretion history have been highlighted, the diagrams do not attempt to define every intrusive event; rather they have been created to emphasise the most important magmatic and tectonic events identified by this study. Wehrlites and other ultramafic intrusions are omitted from the diagrams to aid clarity of presentation, but are discussed separately in Section 6.4. It is worth noting that every major period of magmatism recorded in the Khawr Fakkan and Aswad Blocks is also associated with faulting and is accompanied by intrusive wehrlites, or other ultramafic rocks.

Magmatic events have been split into three main episodes V1, V2 and V3 (after Alabaster et al., 1982; Ernewein et al., 1988 and Godard et al., 2002), which are differentiated by the chronology of events and the changing geochemical signature of the mantle source. Although these three main magmatic episodes are recorded throughout the length of the ophiolite, the proposed subdivisions are only applicable to each individual block and should not be used to directly imply associated synchronous volcanism in adjacent crustal blocks or to the ophiolite as a whole (discussed further in Section 6.4). For this reason the evolution of the Khawr Fakkan and Aswad Blocks are summarised separately in Sections 6.2 and 6.3 before a synthesis in Section 6.4. Whereas field relationships in the diagrams are correct, individual units are not to scale. The clockwise rotation of the Khawr Fakkan and Aswad Blocks is also illustrated in Figures 6.1 to 6.11 and is based on observations of faults and intrusive directions of dykes (Chapter 2). Clockwise rotation of the crust has been favoured over the rotation of extension direction in these models, and is supported by palaeomagnetic studies on the northern ophiolite (e.g. Perrin et al., 1994 and 2000). Arrows display the principal direction of (extensional or compressional) stress believed to be acting on the crust during each magmatic episode.

There is no direct evidence within either Block studied that any of the dyke groups, other than the SDC and lowermost extrusive lavas in the Aswad Block, ever reached the surface and fed extrusive pillow lavas and the subaerial seamounts illustrated in Figures 6.1 to 6.11. However, the respective groups have been presented as feeding extrusive units based on observations of unit thicknesses made in other blocks and the lava stratigraphy displayed in Figure 2.4.

## 6.2 The crustal accretion history of the Khawr Fakkan Block

### Khawr Fakkan Block

#### V1-I

The earliest recorded magmatic events in the Khawr Fakkan Block have a MORB mantle source and represent the only 'true' MORB currently recorded in the Oman-U.A.E. ophiolite. The crust was formed by approximately 10% to 20% decompression melting of a fertile mantle source. The extension resulted in 'normal' spreading and the presence of a steady-state magma chamber (Figure 6.1) which formed a typical oceanic crustal sequence (Figure 2.3). The V1-I magmatic period resulted in the formation of the majority of the Khawr Fakkan crust, including the Layered and Upper Gabbros, which have a MORB-like signature. The Early Dyke Group, SDC and lowermost lavas (which are not preserved) were also formed during this period. The Early Dyke Group is geochemically indistinguishable from the sampled SDC and almost certainly represents the 'roots' of the SDC.

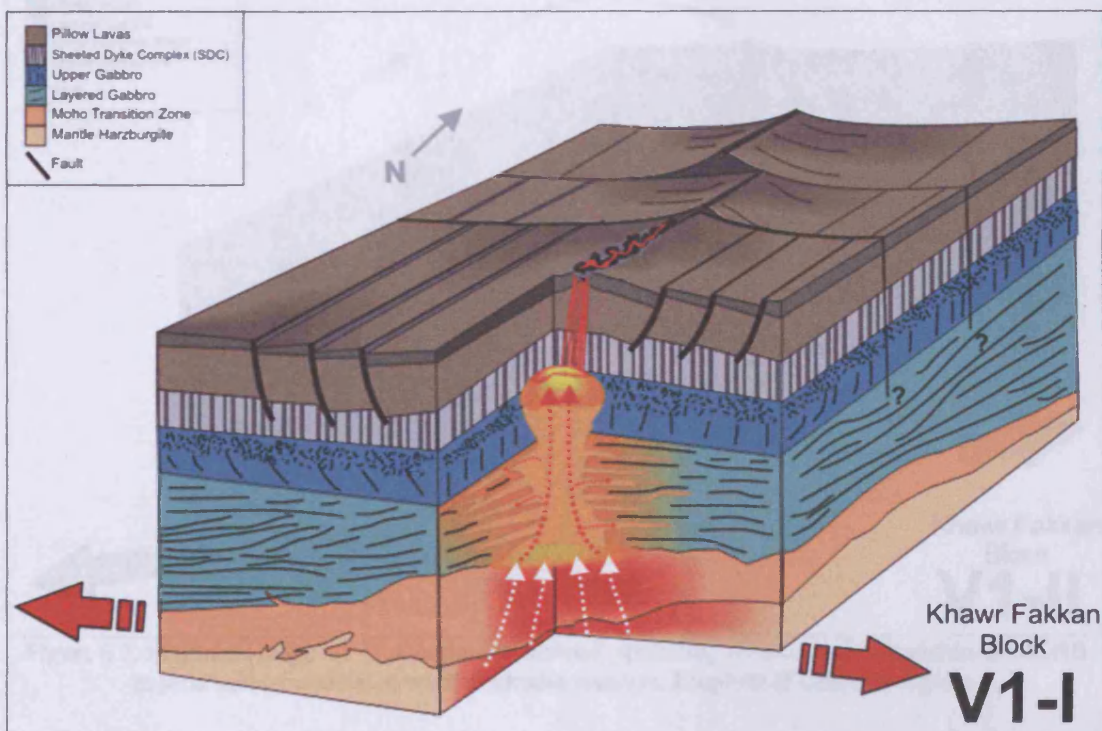


Figure 6.1, Magmatic stage V1-I: Normal spreading at a mid-oceanic ridge. Steady-state magma chamber and continual melt supply from MORB form upper crust and feed SDC and Early Dykes. Main period of crustal accretion in Khawr Fakkan Block.



## Khawr Fakkan Block

## V1-II

The beginning of the V1-II is marked by  $\sim 40^\circ$  clockwise rotation of the crust. The rotation is accompanied by magmatism, which corresponds to the Geotimes Unit (V1) in Oman, and formed the Common Dykes that intruded primarily along faults (Figure 6.2). The Common Dykes represent  $\sim 30\%$  partial melting of a fertile mantle source with the addition of a subduction-derived component to the mantle source. Although no plutonic samples record the V1-II magmatic event, there are no associated major gabbroic intrusions, which is consistent with the presence of a steady-state magma chamber, as recorded during the Geotimes magmatism in the ophiolite blocks to the south. The twin foci of Common Dyke strikes (Figure 2.5B) is consistent with intrusion during the onset of faulting.

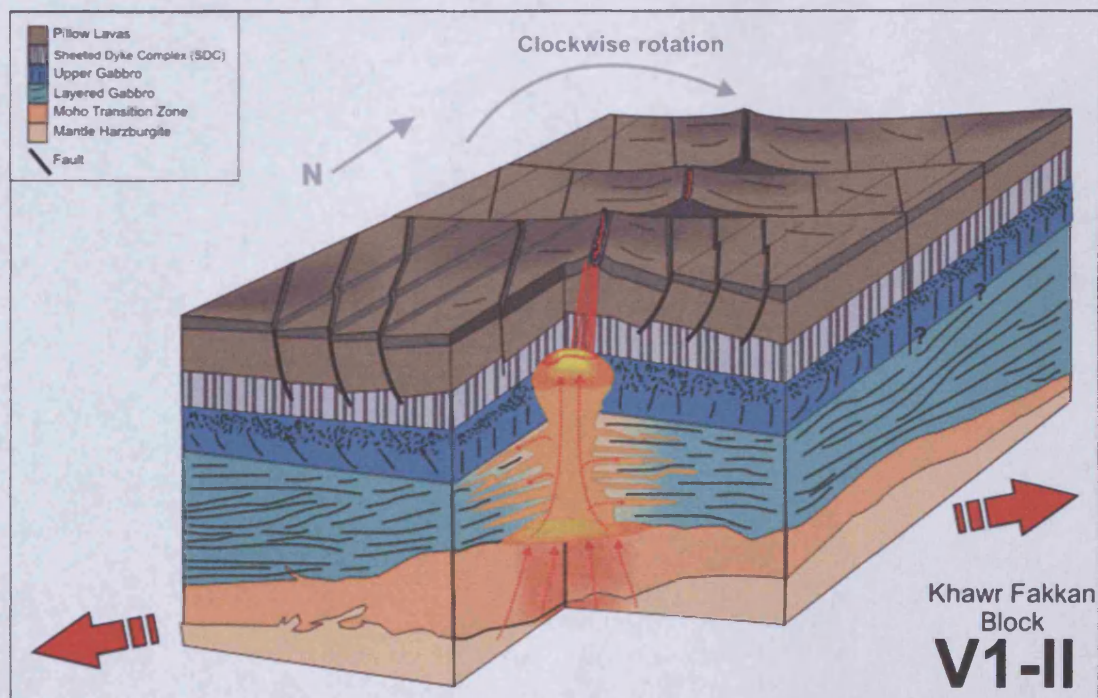


Figure 6.2. Magmatic stage V1-II: Continued 'normal' spreading with change to transitional MORB mantle source associated with clockwise rotation. Eruption of Common Dykes.

## Khawr Fakkan Block

## V2-I

This magmatic period marks the beginning of the Supra Subduction Zone period of magmatism. Whereas a subduction component was present in the Common Dykes, the magmatism of the V2-I period is distinguished by the end of steady-state magmatism and the beginning of more localised volcanics, which are related to the intrusion of off-axis plutonics (Figure 6.3), and sourced from a mantle with a distinctive subduction zone signature. The magmatism of the V2 stage in the Khawr Fakkan Block is also associated with crustal scale NW-SE faulting caused by clockwise rotation within the marginal basin setting (Figure 6.12). All V2-I magmatic events are intrusive, with no samples of the Upper Gabbros preserving a SSZ signature.

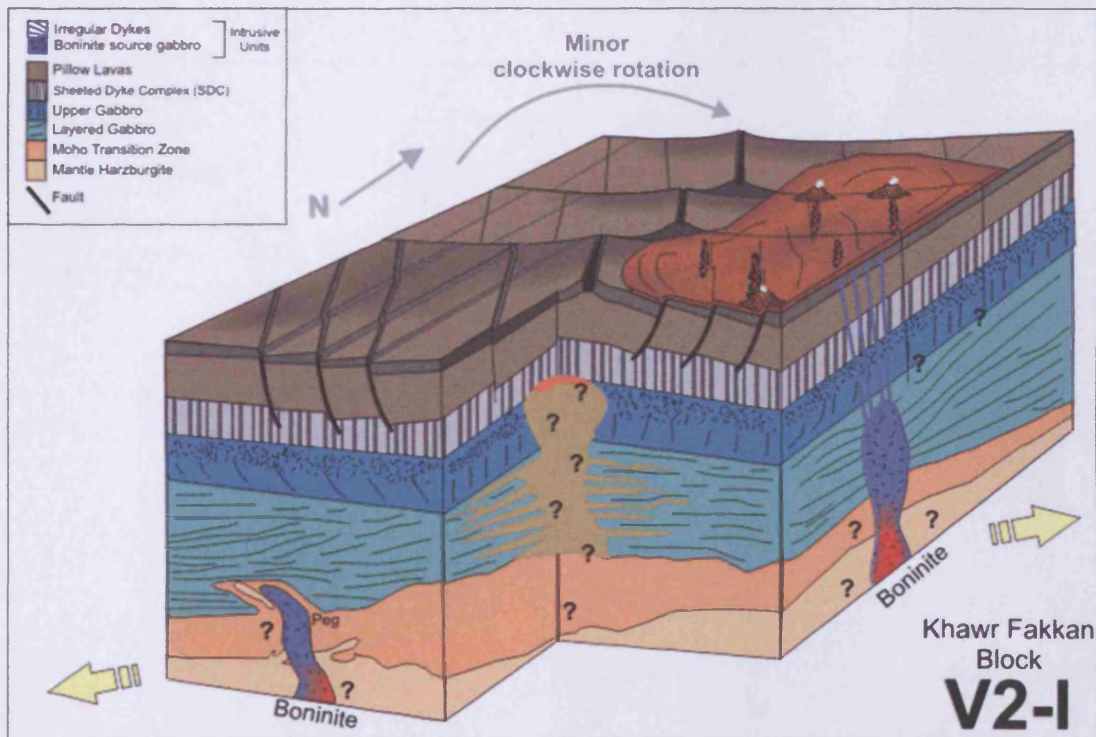


Figure 6.3. Magmatic stage V2-I: Oceanic spreading essentially ceases, with extension of the crust accommodated by faulting. Boninitic melts are generated and ascend through the crust, locally feeding the Irregular Dyke Group. Boninite melts that ascend only as far as the MTZ cool slowly forming pegmatites

The first V2-I magmatic events in the Khawr Fakkan crust are represented by the Irregular Dykes and the intrusion of plutonic gabbro units, some of which cooled at depth to form gabbro pegmatites. These magmatic events have a distinctive boninitic geochemical signature, which can only be formed above a subducting slab and provide strong evidence for the proximal location of the Khawr Fakkan Block to a subduction zone. The boninitic Irregular Dykes correspond to high-Ca boninites according to the definition of Crawford et al. (1989). The generation of this melt requires hot, hydrated shallow mantle ( $>1250^{\circ}\text{C}$  at  $<30\text{km}$  depth in the presence of increased  $\text{H}_2\text{O}$ ) to have underlain the proto-Khawr Fakkan Block at the time of boninite generation (Ishikawa et al., 2002). The resultant 10-30% melting of the highly depleted, shallow mantle-wedge represent the most favourable mechanism for the genesis of the boninitic Irregular Dykes and associated plutonic gabbros.

## Khawr Fakkan Block

## V2-II

The V2-II magmatic period represents the continuation of SSZ magmatism with a progressively depleted mantle source that is selectively enriched in subduction-derived incompatible elements. The magmatic events are represented by the Cpx-phyric Dykes, which are localised along NW-SE faults, and the intrusion of Late intrusive gabbros (Figure 6.4). These intrusive plutonics were recognised in the field, but unfortunately, as a result of hydrothermal alteration, no samples were fresh enough for analysis. The Cpx-phyric Dykes of the V2-II magmatic period were formed from <30% melting from a depleted mantle source.

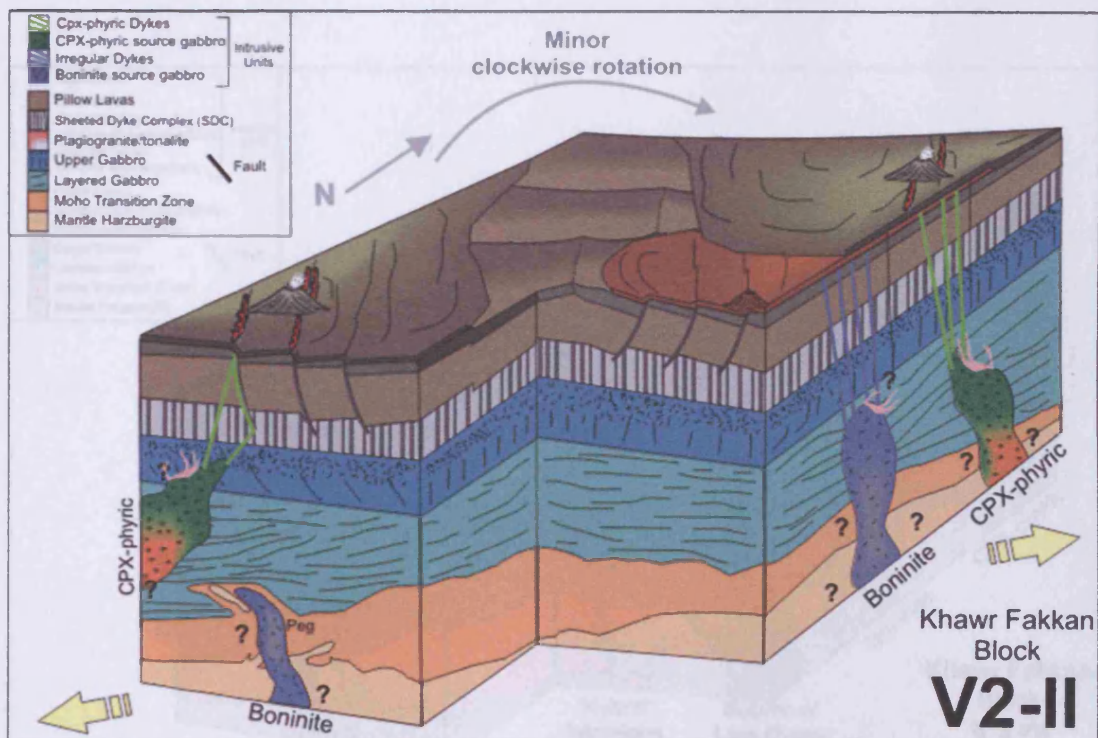


Figure 6.4, Magmatic stage V2-II: Boninitic magmatism ceases and is superseded by the intrusion of Late intrusive gabbros that feed the Cpx-phyric Dyke Group.

## Khawr Fakkan Block

## V3

The last magmatic period in the Khawr Fakkan Block, V3, is represented by the intrusion of the Late Dykes and gabbro sills, with a within-plate signature. The Dykes and gabbros intruded a cooled ophiolite crust, presumed to be during the initial stages of obduction onto the Arabian continental margin (Figure 6.5). The enriched, alkalic, source for the V3 (Salahi Unit in Oman) is a contrast to the depleted nature of the V2-II intrusives. The origin of this signature was proposed by Alabaster et al. (1982) to have been the result of melting of mantle beneath the Arabian margin at the onset of obduction following slab detachment. Pelagic sediments associated with the Salahi Unit in Oman yield radiolarian fossils indicative of Coniacian age (85-89 Ma) (Umino et al., 1990), significantly post-dating the earlier V1 and V2 magmatic periods.

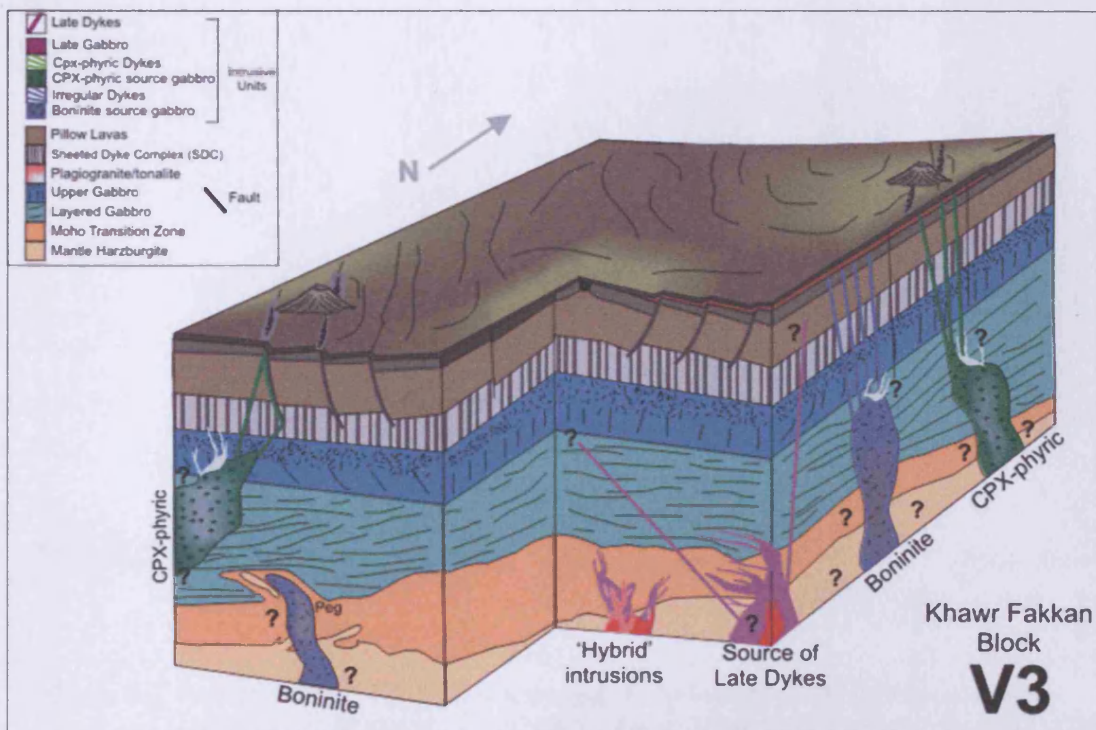


Figure 6.5, Magmatic stage V3: The crust continues to cool and begins to be obducted onto the continental crust of the Arabian Shield. Melting of the sub-continental lithosphere ascends along pre-existing faults and concordantly intrudes the lower crust. Hybrid (felsic-basaltic) intrusions intrude the crust at depth.

The Late Dykes intrude along lithospheric scale faults within a cool, serpentinised mantle, and is accompanied by intrusive plutonic gabbro sills. The sills intrude concordantly within the MTZ and Layered Gabbro sequence, providing evidence that a proportion of the V3 melt did not reach the surface and cooled in situ. The V3 magmatic period is also marked by localised hybrid intrusions, composed of felsic plagiogranites and basaltic melt with a within-plate signature.

The magmatic history and crustal evolution of the Khawr Fakkan Block raises many questions about the evolution of crust formed at mid-ocean ridges and crust formed in an embryonic volcanic arc.

### 6.3 The crustal accretion history of the Aswad Block

This section aims to describe, in detail, the series of major magmatic events that have taken place in the Aswad Block identified through fieldwork and geochemical analysis. The implications to the regional tectonic setting of the crust will be discussed in Section 6.4.

#### Aswad Block V1-I

The initial V1-I magmatic period of the Aswad Block comprised the products of 'normal' oceanic spreading in a marginal basin. During this magmatic period the majority of the Kalba Upper Gabbros, SDC and extrusives were formed from a steady-state magma chamber with ~10-20% melting of a fertile mantle source with a subduction-derived component.

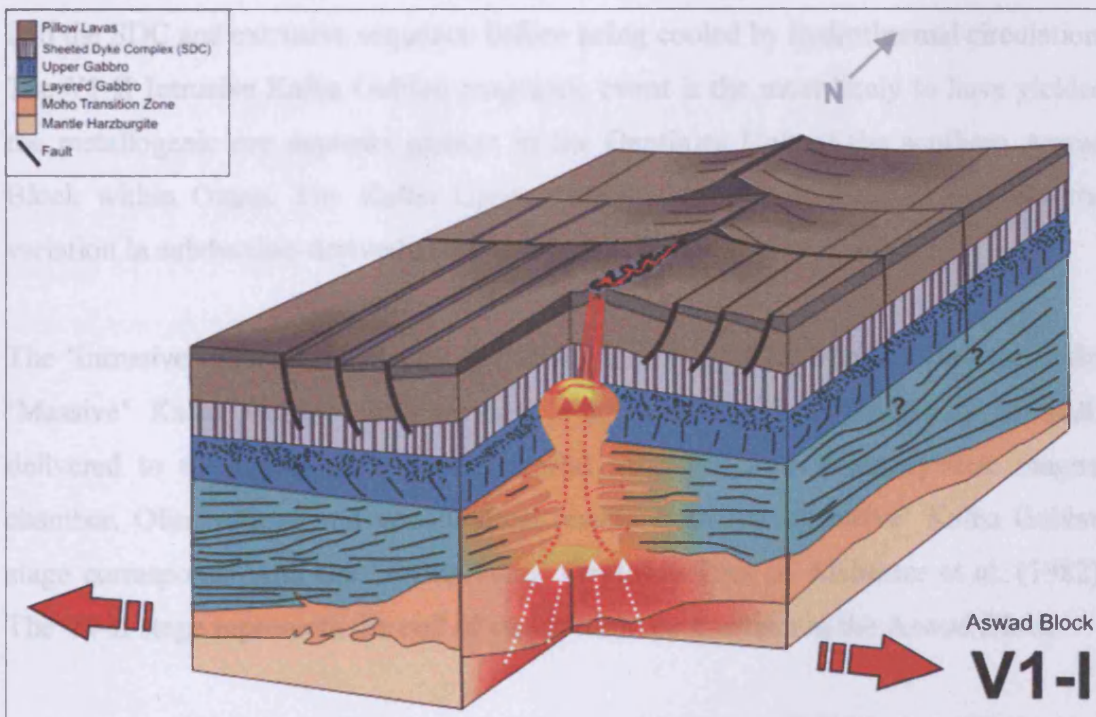


Figure 6.6, Magmatic stage V1-I: Normal spreading at a mid-oceanic ridge Steady-state magma chamber and continual melt supply from transitional-MORB source.

The Aswad Block SDC and lavas correspond to the Geotimes Unit as defined in Oman, which represents the main period of crustal accretion. The mantle source for

the V1 magmatic period is of a MORB- to transitional-MORB-like composition as evidenced by the SDC and extrusive lavas, some of which contain an increased level of subduction-mobile elements. The clinopyroxenes analysed from the Kalba Gabbro also record the delivery and crystallisation of melts with distinct and variable subduction-related components. The implications for the mantle source and melt generation in the mantle are discussed in Section 6.4.

### **Aswad Block**

## **V1-II**

Normal spreading continues until extension of the crust exceeds magma supply, at which point normal faulting becomes dominant, and steady-state magmatism ceases (V1-II, Figure 6.7). Melt supply continues from the same transitional-MORB-like source and, because of increased faulting, the Kalba Upper Gabbro is able to intrude into the SDC and extrusive sequence before being cooled by hydrothermal circulation. The V1-II Intrusive Kalba Gabbro magmatic event is the most likely to have yielded the metallogenic ore deposits present in the Geotimes Unit of the southern Aswad Block within Oman. The Kalba Upper Gabbros, SDC and lavas all preserve the variation in subduction-derived component added to their mantle source.

The 'Intrusive' Kalba Gabbro has the same geochemical variation as the rest of the 'Massive' Kalba Gabbro and provides evidence for the heterogeneity of melts delivered to the upper crust during crustal accretion from a steady-state magma chamber. Observations and geochemical results from the 'Intrusive' Kalba Gabbro stage corresponds with the 'Transitional' Geotimes Unit of Alabaster et al. (1982). The V1-II stage represents the end of steady-state magmatism in the Aswad Block.



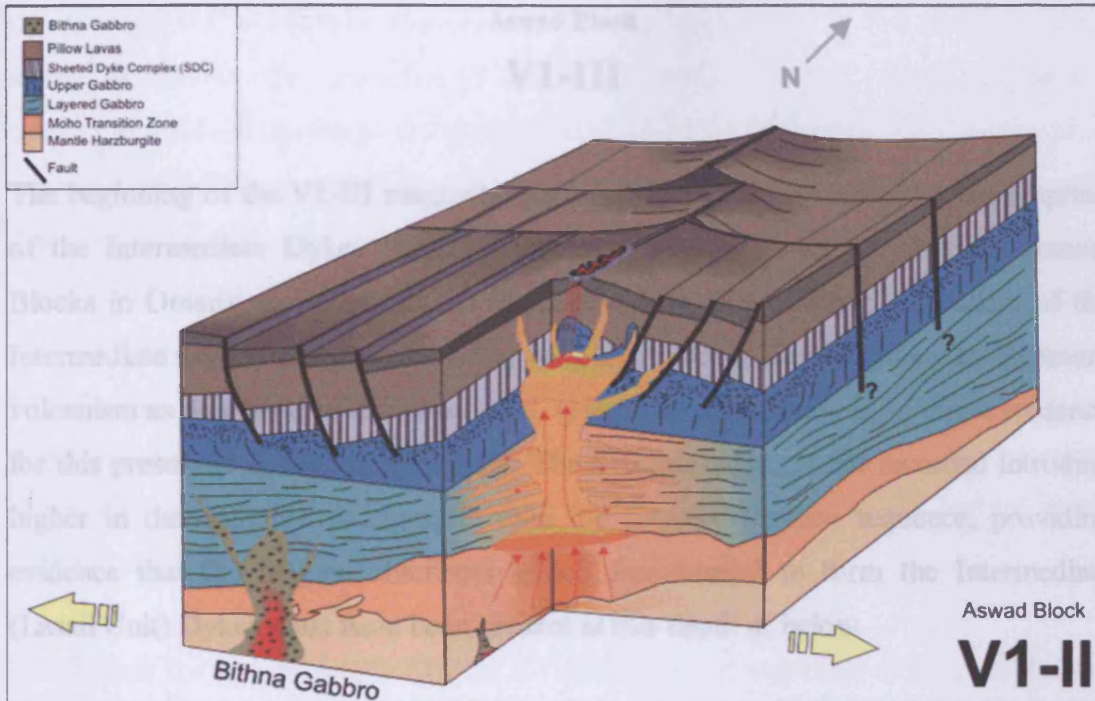


Figure 6.7, Magmatic stage V1-II: Normal spreading continues and magma supply becomes more sporadic, with some extension accommodated by increased N-S normal faulting. Kalba Gabbro intrudes into extrusive sequence primarily along faults. The Bithna Gabbro begins to intrude off axis from a similar, albeit slightly more depleted, Transitional-MORB source.

During (or soon after) the 'Intrusive' Kalba Gabbro magmatic event, the Bithna Gabbro began to ascend off-axis. The Bithna Gabbro was generated from a similar, albeit slightly more depleted, mantle source that has similar levels of depletion to modern day back-arc basins and, significantly, does not have a substantial subduction derived component.

## Aswad Block

## V1-III

The beginning of the V1-III magmatic period (Figure 6.8) is marked by the eruption of the Intermediate Dykes (Lasail Unit in 'seamount' areas of the northernmost Blocks in Oman) sourced from the Bithna Gabbro. The localised volcanism of the Intermediate Dykes along pre-existing N-S faults could have resulted in seamount volcanism as described in Alabaster et al. (1982), although there is no direct evidence for this preserved in the Aswad Block. The Bithna Gabbro is not recorded intruding higher in the ophiolite stratigraphy than the Layered Gabbro sequence, providing evidence that the magma chambers which fractionated to form the Intermediate (Lasail Unit) Dykes must have been present at this depth or below.

The Bithna Gabbro is included in the V1-III magmatic stage based on the following criteria:

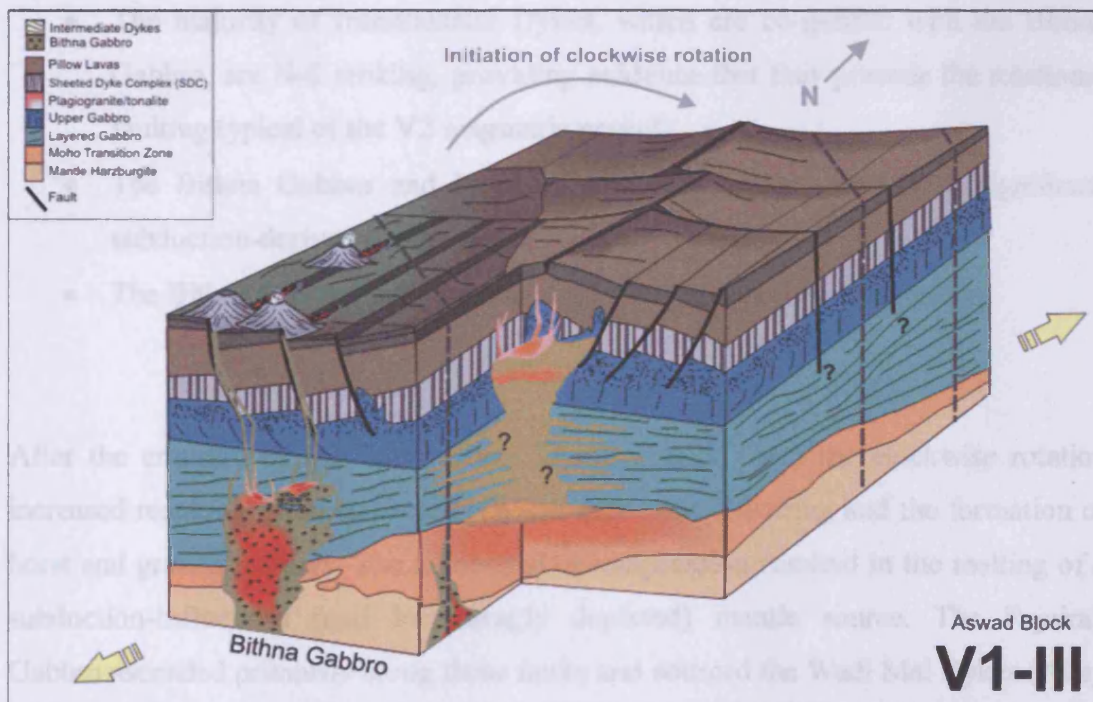


Figure 6.8, Magmatic stage V1-III: Normal spreading ceases and magma supply wanes. The Bithna Gabbro sources the Intermediate Dykes (Lasail Unit) in localised areas from magma chambers at depth primarily along N-S faults, possibly forming sea-mounts. Initiation of clockwise rotation of the crust begins to form major NW-SE crustal-scale faults

The extraction of ~30% partial melt from a fertile mantle followed by accumulation in magma chambers at depth have been demonstrated in Chapter 5 as the likely source of

the geochemical signatures recorded in the clinopyroxenes of Intermediate Dyke sample 03UR150. The initiation of clockwise rotation of the lithosphere and the associated NW-SE faulting could have subjected the Bithna Gabbro to localised compressional forces, which are preserved as small-scale shear zones (Chapter 2). The initiation of such tectonic forces could possibly have contributed to the magmatism of the V1-III period. The Bithna Gabbro is also associated with the NW-SE faults, which provides evidence that the faults were initiated before the Bithna Gabbro had ceased intrusion. During this time, steady-state magmatism had all but stopped, with the magma chamber fractionating as it cooled, resulting in the formation of plagiogranites and tonalities which intruded the Kalba Gabbro, SDC and the lower extrusive sequence.

The Bithna Gabbro is included in the V1-III magmatic stage based on the following criteria:

- The majority of Intermediate Dykes, which are co-genetic with the Bithna Gabbro, are N-S striking, providing evidence that they precede the rotational faulting typical of the V2 magmatic period.
- The Bithna Gabbro and Intermediate Dykes do not contain a significant subduction-derived component.
- The Bithna Gabbro is a member of the (V1) Cpx-series of intrusions.

After the eruption of the Intermediate Dykes (Lasail Unit) the clockwise rotation increased resulting in crustal-scale NW-SE extensional faulting and the formation of horst and graben features. The associated decompression resulted in the melting of a subduction-influenced (and increasingly depleted) mantle source. The Fujairah Gabbro ascended primarily along these faults and sourced the Wadi Mai Dykes (Alley Unit) which are the initial magmatic event in the V2-I magmatic period (Figure 6.4). During the V1-III magmatic period the Bithna Gabbro cooled but continued to fractionate, resulting in the concentration of volatiles at the top of the gabbro, forming tonalites and plagiogranites that intrude locally within the Layered Gabbro sequence.

## Aswad Block

## V2-I

After the eruption of the Intermediate Dykes (Lasail Unit) the clockwise rotation of the crust increased, resulting in major lithospheric NW-SE extensional faulting and the formation of horst and graben features. Subsequent 10-30% melting of a depleted and subduction-influenced mantle source formed the melt for the V2-I magmatic period. The Fujairah Gabbro ascended primarily along the NW-SE faults and sourced the Wadi Mai Dykes (Alley Unit) which are the initial magmatic event in the V2-I magmatic period (Figure 6.9).

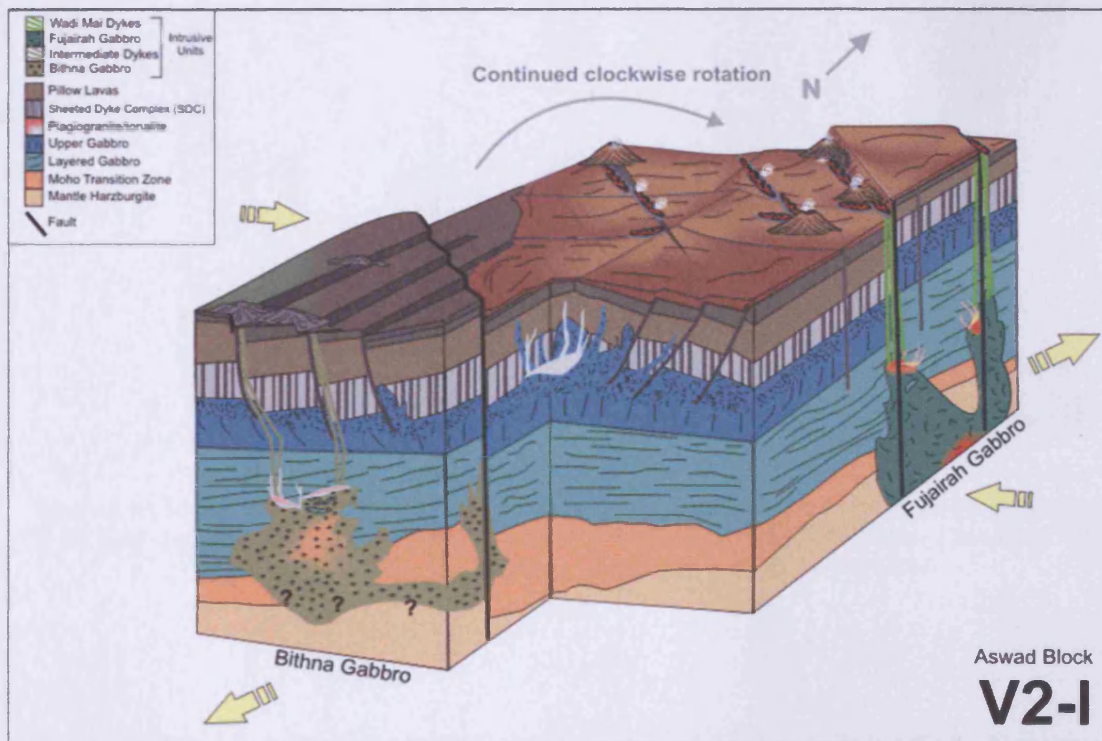


Figure 6.9, Magmatic stage V2-I: Steady-state magmatism essentially ceases with extension accommodated by crustal scale NW-SE faults. The Bithna Gabbro fractionates and cools. The Fujairah Gabbro, sourced from a mantle that is enriched in subduction-mobile elements, ascends through the crust primarily along the NW-SE faults and erupts the Wadi Mai Dykes (Alley Unit)

Numerous locations have been identified where the Bithna Gabbro and Fujairah Gabbro have mutually intrusive relationships, often associated with the NW-SE faults. While the diagrams do not attempt to show this (for clarity of presentation) it is worth noting as it provides evidence that the Bithna and Fujairah Gabbros were both actively intruding, at least in some locations, contemporaneously. This indicates that the time between magmatic periods V1-III and V2-I was not long enough for the Bithna Gabbro to have fully cooled. This will be discussed further in Section 6.4.

## Aswad Block

## V2-II

The V2-II magmatic period is marked by the intrusion of the Fujairah Dolerite and 'Vinaigrette' Units (Section 2.4.9). These units are sourced from the Fujairah Gabbro that has been repeatedly fed by continued melting of an increasingly depleted, subduction-enriched mantle source. The clockwise rotation of the crust continues, causing faulting with a strike closer to E -W.

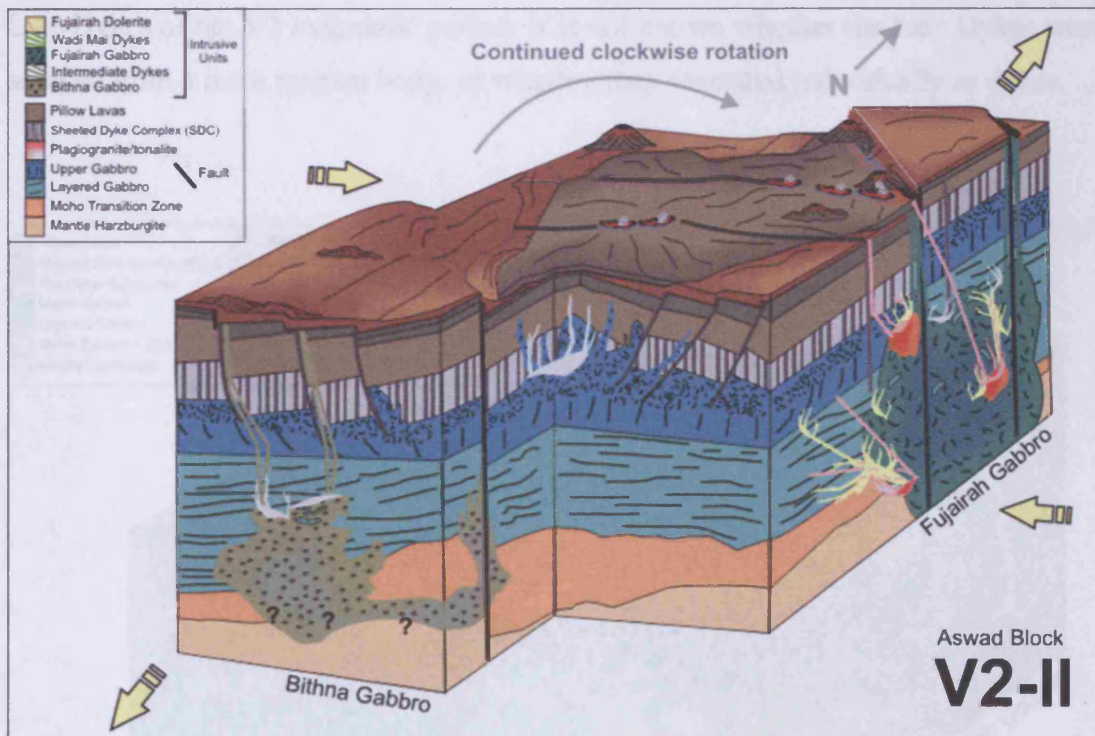


Figure 6.10, Magmatic stage V2-II: The Fujairah Gabbro continues to fractionate and ascend along NW-SE faults leading to the intrusion of the Fujairah Dolerite and 'vinaigrette' units (Cpx-phyric unit). These events mark the last major magmatic events in the Aswad Block.

The Fujairah Gabbro initially erupted the Fujairah Dolerite as dykes along the NW-SE and E-W faults, but continued fractionation resulted in the formation of the 'Vinaigrette' Unit which intruded locally as a mixed mafic and felsic Unit (Figure 2.13) and shares the same mantle source as the Fujairah Dolerite. 'Vinaigrette' Units have been observed in most crustal horizons (MTZ to SDC) associated with the

intrusion of the Fujairah Gabbro. The intrusion of the Fujairah Dolerite and the 'Vinaigrette' Unit mark the last major of oceanic magmatism in the Aswad Block

### Aswad Block

## V3

After a magmatic hiatus, the cooled Aswad Block began to be obducted onto the Arabian Shield continental margin. This caused melting of the sub-continental lithosphere which ascended along pre-existing faults within the crust and sourced the Late Dykes of the V3 magmatic period. It is not known whether the Late Dykes were sourced from a main magma body, or whether they ascended individually as dykes.

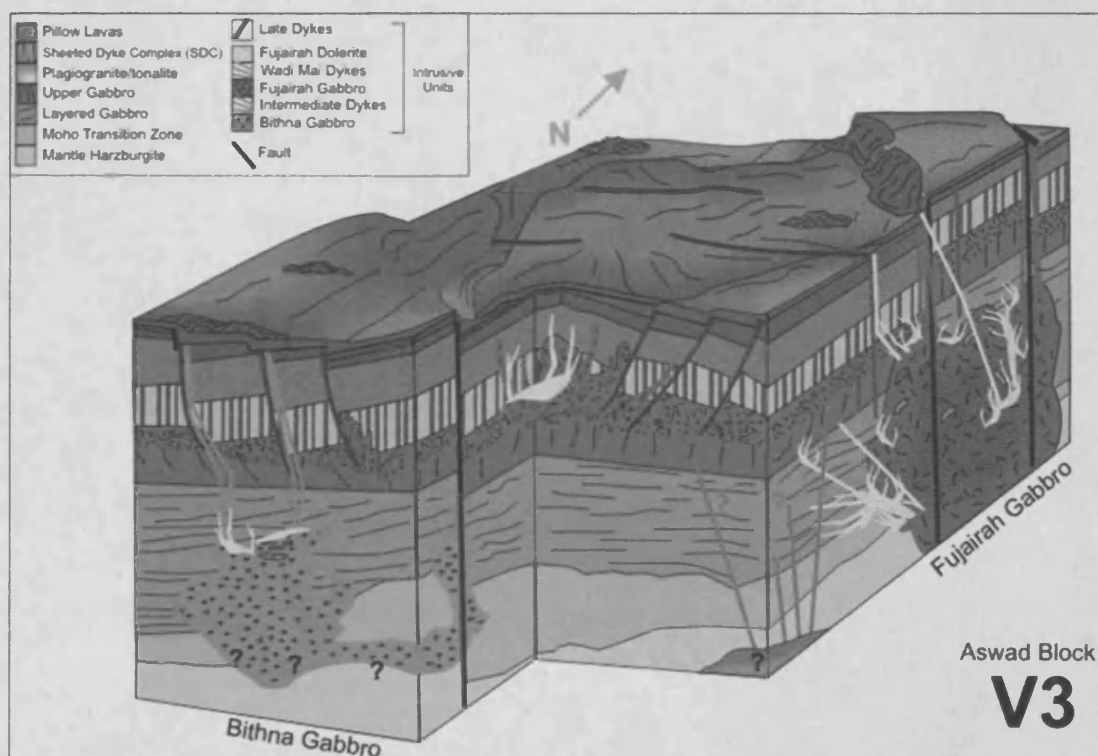


Figure 6.11. Magmatic stage V3: The crust continues to cool and begins to be obducted onto the continental crust of the Arabian Shield. Melting of the sub-continental lithosphere generates melt, which ascends along pre-existing faults.

## **6.4 The magmatic evolution of the northern Oman-U.A.E. ophiolite**

This section will summarise the relationship between the tectonic and petrogenetic evolution of the northernmost blocks of the ophiolite. Table 6.1 displays the main magmatic events distinguished between the northernmost ophiolite blocks, and lists the major extrusive and plutonic magmatic events during each period. Subdivisions between the three main magmatic periods are different for each block, although the events identified in the Aswad Block match closely with the events identified by Alabaster et al. (1982). Without accurate dating of the individual events in each block it is not possible to conclude whether these events were taking place synchronously.

As stated in Chapter 3, the V2 magmatic period plays a more significant role in the evolution of the northern blocks of the ophiolite than in the blocks to the south. The subduction-derived component of the SSZ geochemical signature of both the V1 and V2 magmatic periods is stronger in the northern blocks, and increases both temporally and spatially to the north. The northern blocks of the Oman-U.A.E. ophiolite thus record the change from spreading- to subduction-related volcanism

The different magmatic periods (V1, V2 and V3) are characterised by different methods of crustal accretion, which are directly related to the tectonic setting of the crust. The main mechanism during the V1 magmatic period is accretion through steady-state magma chambers at a spreading ridge, constructing an oceanic crustal sequence typical of the Penrose (1972) description (Figure 1.3). The V2 magmatic period, in a SSZ setting, is distinguished by the intrusion of plutonic gabbro bodies primarily along lithospheric scale faults, feeding localised magmatism, during the first (embryonic) stages of island arc development.

An important finding of this study is the presence of 'true' MORB in the Khawr Fakkan Block. This provides the first pre-subduction influenced crust for the ophiolite and represents oceanic crust formed in a tectonic environment that was not influenced by subduction.



Simplified summary of key magmatic events		This Study		Umino et al, (1990)	Alabaster et al, (1980)
		Khawr Fakkan Block	Aswad Block	Fizh Block	Fizh, Hilti and Sarami Blocks
<p><b>V3</b> Within-plate magmatism Last Magmatic Events (obduction related?)</p> <p>Unconformity</p> <p>Increase in subduction component with time</p> <p><b>V2</b> SUPRA SUBDUCTION ZONE MAGMATISM</p> <p>Associated with NW-SE rifting and intrusive plutonic units</p> <p>Unconformity</p> <p>Increase in subduction component with time</p> <p><b>V1</b> MAIN PERIOD OF CRUSTAL ACCRETION</p> <p>Marginal basin setting (MORB-like source)</p> <p>Earliest Magmatic Events</p>	<p><b>V3 (Salahi Unit)</b> Dolerite Late Dykes and intrusive gabbro units (within Layered Gabbro Sequence and MTZ)</p> <p>Cooling and rotation</p>	<p><b>V3 (Salahi Unit)</b> Single dolerite Late Dyke</p>	<p>Salahi Volcanics Extrusive basalts and dolerite dykes</p>	<p>Salahi Unit Extrusive basalts and dolerite dykes</p> <p><b>The Collision Event</b></p>	
	<p><b>V2-II (Cpx-phyric unit)</b> Cpx-phyric Dykes</p>	<p><b>V2-II (Cpx-phyric unit)</b> Cpx-phyric Dykes and Vinaigrette Unit sourced from fractionated intrusive Fujairah Gabbro</p>		<p>Alley volcanics Alternation of basalt and andesite Dacite at higher levels. Associated with Opx-series intrusive cumulates</p>	<p><b>Cpx-phyric Unit</b> Basalts distributed along NE-SW faults</p> <p><b>Alley Unit</b> Rhyolite, basalt and andesite Located on major NW-SE faults</p> <p><b>The Rifting Event</b></p>
	<p><b>V2-I (Alley Unit)</b> Irregular Dykes with boninitic composition and Intrusive Gabbro Pegmatite</p> <p>Rotation of crust</p>	<p><b>V2-I (Alley Unit)</b> Wadi Mai Dykes sourced from intrusive Fujairah Gabbro (associated with major NW-SE faults)</p>		<p>Unconformity (ferrous sediments and volcanic breccia)</p>	
	<p><b>V1-II (Geotimes Unit)</b> Common Dykes</p> <p><b>V1-I (Early Dykes and SDC)</b> (only true-MORB source documented in ophiolite)</p>	<p><b>V1-III (Lasail Unit)</b> Intermediate Dykes sourced from Bithna Gabbro</p> <p><b>V1-II (Transitional Geotimes Unit)</b> Intrusive Kalba Gabbro magmatic event</p> <p><b>V1-I (Geotimes Unit)</b> Extrusive basaltic andesites, feeder dykes and SDC</p>	<p><b>Geotimes Volcanics</b> Alternation of basalt, andesite and rare dacite. Basalt predominates in higher levels</p>	<p><b>Lasail Unit</b> Basalt, andesite Sourced from 'late intrusive complexes' (gabbro-diorite-tonalite-trondhjemite)</p> <p><b>The 'Seamount' Event</b></p> <p>Unconformity</p> <p><b>Transitional Lavas</b></p> <p><b>Geotimes Unit</b> Basalt and andesite 'volcanic basement'</p> <p><b>Marginal Basin Spreading Event</b></p>	

Table 6.1, Comparison between (extrusive and plutonic) magmatic events identified through field and geochemical investigation in the Khawr Fakkan and Aswad Blocks and the Fizh, Hilti and Sarami Blocks in the Oman portion of the ophiolite (Umino et al., 1990 and Alabaster et al., 1982).

The northerly spatial and temporal increase in the subduction signature has important implications for the palaeotectonic setting of the Khawr Fakkan and Aswad Blocks, and to the spatial orientation of the ophiolite as a whole. Blocks closest to the proposed subduction zone would exhibit a more significant SSZ geochemical signature, which would be present from earlier. Blocks distal to the proposed subduction zone would exhibit a weaker signature.

Despite the amount of data indicating a SSZ setting for the Oman-U.A.E. ophiolite the source of the SSZ geochemical signature, and therefore the tectonic setting of the crust at the time of generation, has several proposed origins. Boudier et al. (1981 and 1988) and Boudier and Coleman (1981) propose that the origin of the subduction-signature is caused by water being transported along lithospheric scale thrust faults into a shallow mantle source region at the onset of intra-oceanic thrusting close to the palaeo-ridge. An alternative model presented by Ishikawa et al. (2005) proposed the origins of the SSZ signature as being the result of amphibolite-facies metamorphic sole-derived fluids entering the mantle source at the onset of intra-oceanic thrusting. Both of these models support the SSZ setting of the Oman-U.A.E. ophiolite as they both require crustal detachment faults to separate the ophiolite from the under thrust, subducting, crust.

It is the conclusion of this study that the Oman-U.A.E. ophiolite was initially formed in an extensional environment within a marginal (fore-arc) basin, close to a propagating subduction zone. An initially MORB-like mantle source became progressively contaminated by a subduction-derived component resulting in embryonic island-arc development prior to obduction onto the Arabian Shield. This palaeotectonic setting was first proposed by the studies of the Open University led by Prof. Ian Gass (culminating in the publication of Lippard et al., 1986). Figure 6.12 displays the proposed palaeotectonic evolution of the Oman-U.A.E. ophiolite during the V1, V2 and V3 magmatic periods.

## The magmatic evolution of the Oman-U.A.E. Ophiolite

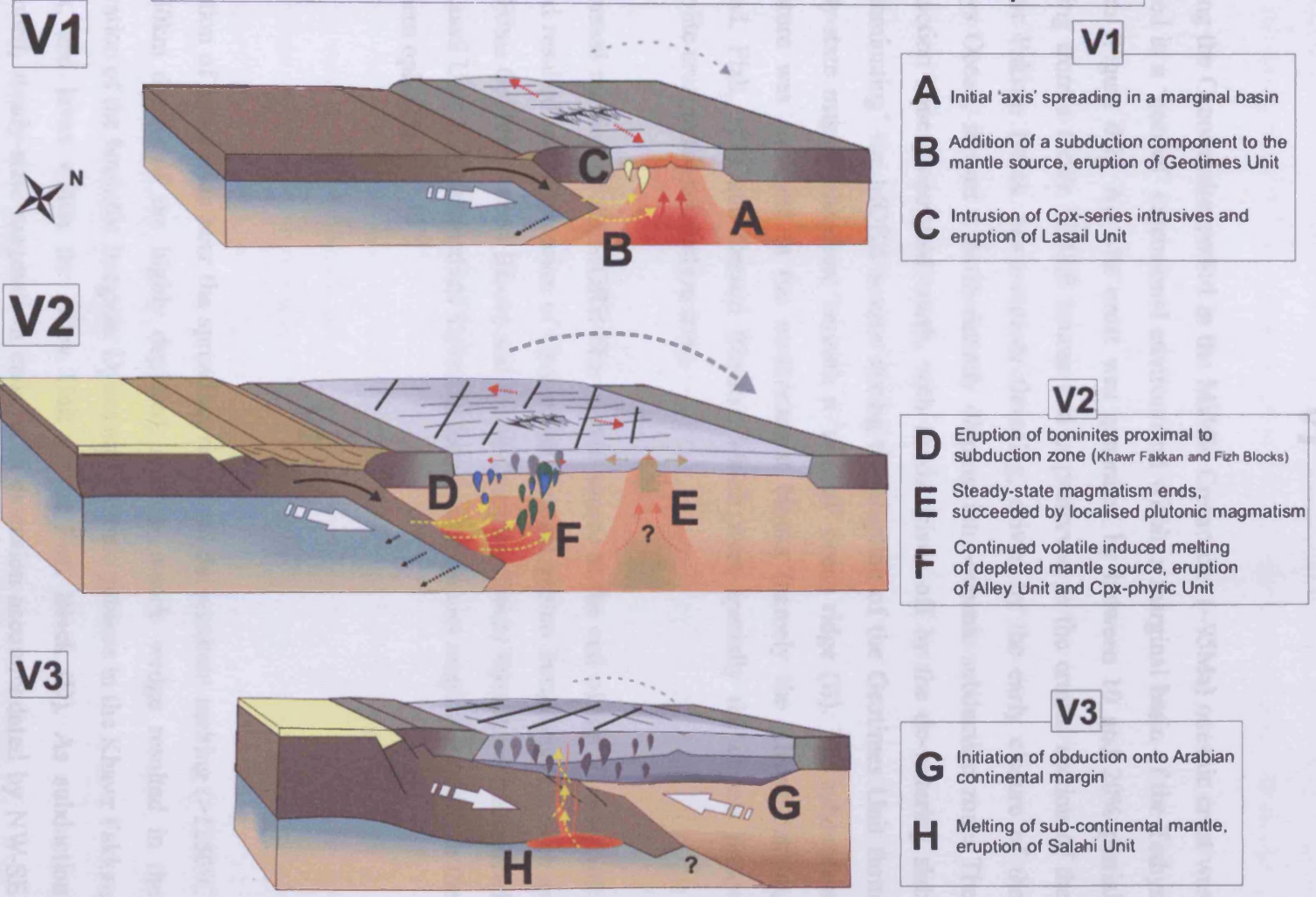


Figure 6.12, The magmatic evolution of the Oman-U.A.E. ophiolite, divided into the main magmatic events, V1: Initial 'axis' spreading, V2: magmatism in a SSZ environment, V3: Syn-collision magmatism. For further explanation see text and Figure 6.13. (Adapted from Alabaster et al., 1982 and Lippard et al., 1986)

## V1

During the Cenomanian period in the Middle Cretaceous (~95Ma) oceanic crust was formed in a 'normal' extensional environment within a marginal basin of the Tethys Ocean (Figure 6.12 A). The crust was generated by between 10 and 20% partial melting from a fertile MORB source and is preserved in the crustal section of the Khawr Fakkan Block. Intra-oceanic thrusting, driven by the early closure of the Tethys Ocean, formed a north-easterly dipping intra-oceanic subduction zone. The subduction zone propagated south, with fluids driven off by the de-watering slab 'contaminating' the MORB source during the eruption of the Geotimes Unit from steady-state magma chambers beneath a 'normal' ocean ridge (B). The subduction signature was strongest in the northernmost blocks (namely the Khawr Fakkan, Aswad, Fizh, Hilti and Sarami Blocks), which were spatially the closest proto-ophiolite crust to the subduction zone.

Continued melting of the MORB-like mantle source at the end of the VI magmatic period resulted in the intrusion of Cpx-series plutonic gabbro intrusions (C), such as the Bithna Gabbro (Aswad Block) and Lasail Complex (Salahi Block), which sourced the Lasail Unit and Intermediate Dykes in localised seamount magmatic events in the northern ophiolite.

## V2

Initiation of subduction near the spreading ridge and the resultant melting (>1250°C at <30km depth) of the highly depleted, shallow mantle wedge resulted in the generation of the boninitic Irregular Dykes and plutonic gabbros in the Khawr Fakkan Block, and lavas within the Alley Unit of the Fizh Block (D). As subduction continued, steady-state magmatism ends, with extension accommodated by NW-SE faulting (E) as the crust begins clockwise rotation. The lithospheric scale faults act as foci for melts formed by ~20% to 30% partial melting of a depleted MORB-like source with an additional subduction-derived component. The melts intrude the cooling upper crust and source the Alley Unit and Wadi Mai Dykes in the northern ophiolite. The magma chambers cooled and fractionated to form the Opx-series

intrusions such the Fujairah Gabbro (F), and source the Cpx-phyrlic Unit and dykes, with the strongest subduction-signature present in the northernmost ophiolite blocks.

### V3

After a magmatic hiatus, during which the cooled ophiolite crust detached from the lithosphere along a basal detachment fault, the beginning of obduction initiated a final magmatic period (G). Obduction onto the Arabian continental margin caused the melting of sub-continental mantle which ascended along pre-existing faults. The resulting magmatism sourced the Salahi Unit, Late Dykes and gabbro intrusions in localised areas in the northern ophiolite (H).

## 6.5 The regional palaeotectonic setting of the Oman-U.A.E. Ophiolite

The magmatic evolution presented in Figure 6.12 provides constraints for the palaeotectonic evolution of the short-lived marginal basin in which the northern Oman-U.A.E. ophiolite formed. Figure 6.13 displays the preferred model for the tectonic setting and evolution of the ophiolite crust during the Late Cretaceous (~95Ma to ~90Ma). The upper inset displays the regional plate tectonic setting of the Eurasian Plate and the Arabian Shield at ~95Ma. Northward motion of the Arabian Shield forms a NE-dipping subduction zone which propagates south during the V1 and V2 magmatic periods (~95 to 96Ma), with associated clockwise rotation of the crust and plutonic magmatism typical of the initial stages of island arc development.

Studies of present day oceanic crust formed in a SSZ setting within marginal basins, such as the Lau Basin and Marianas arc-basin system (Pearce et al., 1995 and 2005), provide firm constraints on the nature and spatial distribution of subduction components. From the results of spatial analysis on the behaviour of subduction components (such as Th and LREE) in present day analogous systems (e.g. Pearce et al., 1995 and 2005) it is proposed that the northern Oman-U.A.E. ophiolite was

located <100km north of the propagating subduction zone during the V1 and V2 magmatic periods.

Subduction is short lived (~1Ma), as evidenced by the lack of any obvious sub-aerial arc volcanism in the ophiolite and the relationship between the V1-III (Bithna gabbro) and V2 (Fujairah gabbro) plutonic gabbros. Subduction ceases when continental crust becomes involved in the subduction zone, effectively choking the subduction process. The end of the V2 period represents the initiation of collision between the Arabian passive continental margin and the young, hot embryonic arc crust, at the beginning of ophiolite emplacement (Alabaster et al., 1982). Over the next ~5Ma the ophiolite overrides the cooler continental crust and clockwise rotation of the crust continues. Syn-collision melting sources the V3 magmatic period at ~90Ma, in localised areas, as the crust continues to be emplaced in the form of an allochthonous nappe.

Palaeotectonic reconstruction of the ophiolite (Figure 6.13), based on the information presented in this study, places the Khawr Fakkan Block closest to the proposed NE-dipping subduction zone (<100km). It is proposed that the Khawr Fakkan Block was the first block of the ophiolite to be emplaced, soon after the end of the V2 magmatic period. The 'welding' of the Khawr Fakkan Blocks amphibolite sole to the Arabian Shield continental margin provides an axis on which the rest of the ophiolite blocks essentially pivot around over the next 20Ma, until the ophiolite blocks achieve the present day assemblage.

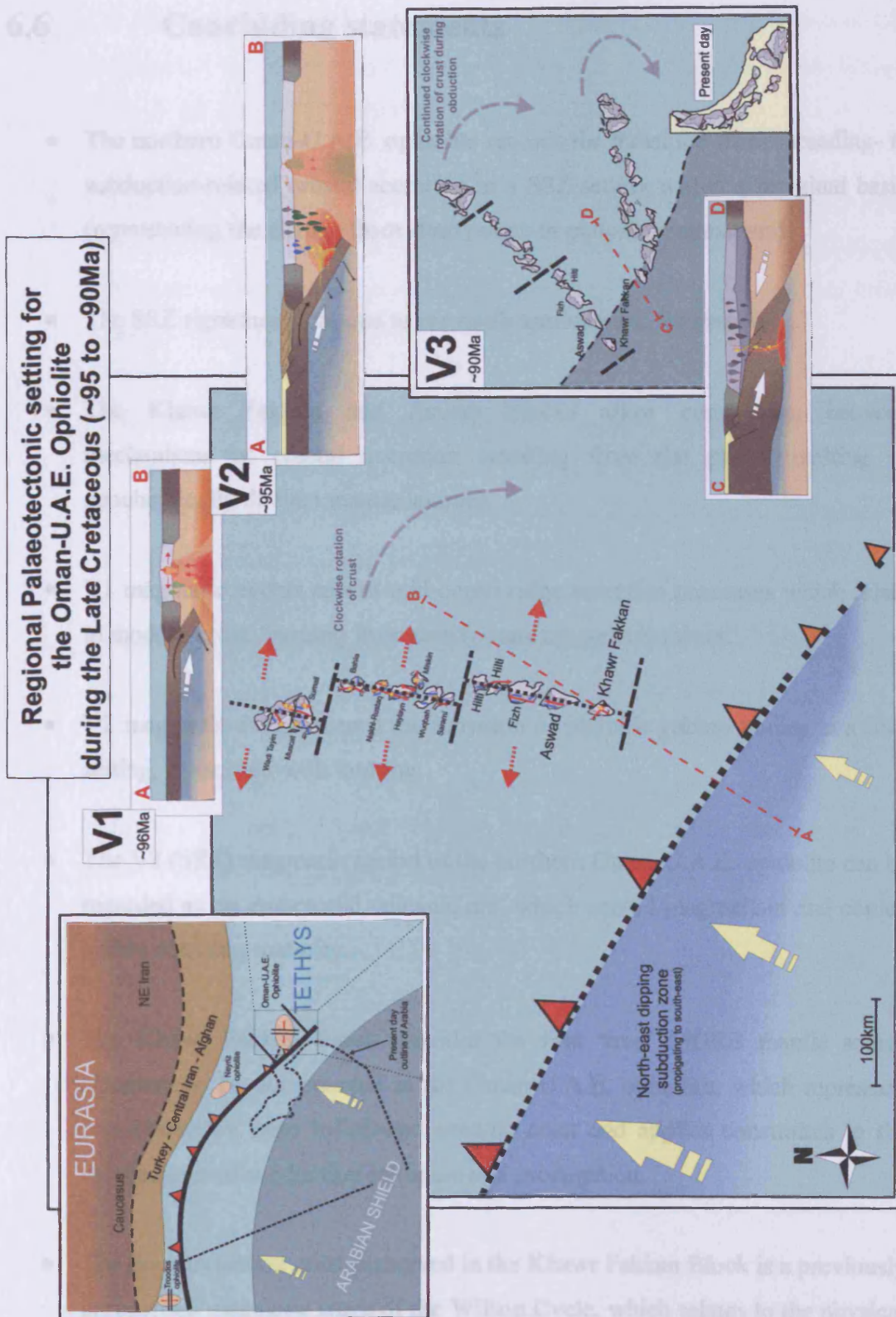


Figure 6.13, The regional palaeotectonic setting of the Oman-U.A.E ophiolite during the Late Cretaceous (~95 to ~90Ma). Upper inset displays the regional plate tectonic setting at the initiation of closure of the Tethys Ocean. V1 and V2 insets display that most magmatism takes place in a SSZ environment. V3 inset displays clockwise emplacement of the ophiolite nappe. For further explanation see text and Figure 6.12. (Adapted from Alabaster et al., 1982 and Lippard et al., 1986).

## 6.6 Concluding statements

- The northern Oman-U.A.E. ophiolite records the transition from spreading- to subduction-related crustal accretion in a SSZ setting within a marginal basin (representing the change from steady-state to plutonic magmatism).
- The SSZ signature increases to the north spatially and temporally
- The Khawr Fakkan and Aswad Blocks allow comparison between mechanisms of crustal accretion resulting from the partial melting of geochemically distinct mantle sources.
- V1 magmatic events record mid-ocean ridge accretion processes which relate to modern crust, forming from steady-state magma chambers.
- V2 magmatic events record the intrusion of plutonic gabbro bodies in a SSZ setting, associated with faulting.
- The V2 (SSZ) magmatic period of the northern Oman-U.A.E. ophiolite can be regarded as an embryonic volcanic arc, which ceased magmatism and cooled before reaching maturity.
- The Khawr Fakkan Block provides the first 'true' MORB mantle source signature to be documented in the Oman-U.A.E. ophiolite, which represents pre-subduction zone influenced oceanic crust and applies constraints to the mechanisms of subduction initiation and propagation.
- The pre-subduction crust preserved in the Khawr Fakkan Block is a previously unrecorded magmatic stage of the Wilson Cycle, which relates to the physical changes in crustal accretion processes at the onset of subduction



- The use of geochronology techniques to investigate subduction initiation and propagation would be of great scientific benefit as this stage of the Wilson Cycle is the least investigated and least understood.
- Future research must focus on the timing and mechanisms of subduction zone propagation in this region at the end Cretaceous, as preserved in other Tethyan ophiolites, such as the Neyriz ophiolite in Iran (Figure 6.13), and other little-studied Turide and Zagros ophiolites.
- Combined studies utilising fieldwork, geochronology and modern geochemical discrimination techniques (such as LA-ICP-MS) in other Tethyan ophiolites offers an excellent tool to establish spatial and temporal constraints on subduction initiation and propagation.
- Generation of an accurate regional tectonic history for the closure of the Tethys Ocean during the Cretaceous period would be of special note, as it is the time period when most of the major oil-bearing structures in the Middle East were formed or initiated, and would provide more insight into the formation of oceanic crust and the preferential tectonic settings for its preservation in the form of ophiolites.

# Appendix

## **Appendix A: Sample preparation for ICP-OES (whole-rock major and minor elements) analysis**

### **A1.1 Preparation of sample powders**

Rock samples collected in the field were prepared following the standard procedures of the geochemistry facilities of the School of Earth, Ocean and planetary sciences, Cardiff University during the duration of the analytical preparations required for this study (Oct 2002-July 2004). Hand specimens were first cut to size and ground on a diamond wheel, to remove saw marks, weathered surfaces and visible veins of alteration minerals. After washing with de-ionised water and air drying the samples were crushed in a clean jaw crusher and powdered using an agate ball mill. Sample handling was kept to a minimum and prepared powders were stored in clean sealable plastic bags or plastic vials for storage.

### **A1.2 Loss on Ignition (LOI) analysis**

Sample powders (~2g) were weighed into clean ceramic vials and placed in a furnace at 900°C for 2 hours. The ignited powders were allowed to cool and then reweighed before calculating the LOI. The cooled samples were stored in sealed plastic bags within a desiccator prior to analysis.

### **A2.1 Sample preparation for ICP-OES analysis**

Samples were analysed in the form of aqueous solutions prepared by the Fluxy method. 0.1g (+/- 0.005g) of each ignited and dried powdered sample and 0.6g (+/- 0.005g) of lithium tetraborate flux were mixed and placed in a platinum crucible. The powders were mixed with a clean spatula and several drops (5-8) of lithium iodide

wetting agent were added and allowed to dry for several minutes. The crucibles were placed, three at a time, into the Fluxy equipment, where the crucibles were heated until the sample powder and flux melted (~700°C). The sample was then poured (in the molten state) into a Teflon beaker filled with 20ml of 10% HNO<sub>3</sub> and 30ml of de-ionised water (18.2MΩ). The quenched sample was then left until completely dissolved in the acid solution. The solution and washings were then decanted into a 100ml nalgene flask and spiked with a 100ppm Rh stock solution before being made up to volume with de-ionised water (18.2MΩ) for long-term storage.

## **A2.2 Inductively-Coupled Plasma Optical Emission Spectrometry (ICP-OES)**

Major elements ( Si, Al, Fe, Mg, Ca, Na, K, Ti, Mn, and P) were analysed for all basalt and dolerite/microgabbro samples by ICP-OES on the Jobin Yvon Ultima 2 instrument at Cardiff University. Three replicates were conducted per isotope and the RF power was 1000W. The samples were analysed over multiple sessions in 2004-5 and the instrument was operated by analytical facility technician Ms. E. De Vos.

## **A3 Calibration and data quality**

A calibration line was generated for each element using the Certified Reference Materials (CRMS) PCC-1, DTS-1, BIR-1, W-2, MRG-1, JA2, JA3, STM-1, and a Total Procedural Blank (TPB); the calibration lines were driven through zero. Calibration lines were generated by the OES software then improved where necessary by re-calculating the line after removal of outliers. Intra-session 'drift' was monitored with the CRM JB-1a. Elements in all samples are above the typical limits of detection on the ICP-OES instrument (calculated by the software). Table A1 displays the values obtained for the CRM JB-1a on the three ICP-OES runs involved in this project.

<b>Wt %</b>	<b>JB-1a Certified values</b>	<b>JB-1a 1st Run</b>	<b>RSD (%)</b>	<b>JB-1a 2nd Run</b>	<b>RSD (%)</b>	<b>JB-1a 3rd Run</b>	<b>RSD (%)</b>
<b>SiO<sub>2</sub></b>	<b>52.16</b>	51.77	0.74	51.50	1.26	52.68	-1.00
<b>TiO<sub>2</sub></b>	<b>1.30</b>	1.26	2.84	1.28	1.45	1.22	6.04
<b>Al<sub>2</sub>O<sub>3</sub></b>	<b>14.51</b>	14.08	2.96	14.23	1.94	14.07	3.05
<b>Fe<sub>2</sub>O<sub>3</sub></b>	<b>7.75</b>	7.91	-2.06	8.01	-3.34	9.20	-18.73
<b>MnO</b>	<b>9.10</b>	8.84	2.88	9.08	0.19	7.90	13.16
<b>MgO</b>	<b>0.15</b>	0.14	5.13	0.14	3.47	0.14	3.75
<b>CaO</b>	<b>9.23</b>	9.42	-2.07	9.46	-2.47	9.47	-2.61
<b>Na<sub>2</sub>O</b>	<b>1.42</b>	1.34	5.64	1.35	5.21	1.54	-8.58
<b>K<sub>2</sub>O</b>	<b>2.74</b>	2.58	5.85	2.65	3.28	2.88	-4.98
<b>P<sub>2</sub>O<sub>5</sub></b>	<b>0.26</b>	0.23	12.98	0.23	11.81	0.27	-4.59
<b>LOI</b>	<b>0.78</b>	0.78		0.78		0.78	
<b>Total</b>	<b>99.40</b>	98.35		98.71		100.16	

Table A1, Displaying the major element values for CRM JB-1a during the three ICP-OES runs conducted during this investigation. The RSD (Relative Standard Deviation) between the individual runs and the certified values display good correlation between runs

## **A4 Use of Major element abundances for geochemical discrimination of plutonic gabbros**

The use of major element abundances to discriminate gabbros and other plutonic igneous rocks is also limited. As mentioned in Section 4.1, gabbro major element concentrations are directly related to the constituent mineral phases. Different modal proportions of minerals will significantly alter the major and trace element abundances within any given sample. To gather as much information from this technique a detailed petrological investigation must also be conducted on the sample gabbros. Such petrological studies are outside the scope of this project. Thus to obtain

a 'true' geochemical signature of the gabbro it is essential to study the trace element compositions of the individual mineral phases (Chapter 4).

A more detailed study of the major element compositions of the Khawr Fakkan and Aswad Blocks can be found within the U.A.E. Geological Mapping Project (2002-2006) published by the British Geological Survey. A rigorous study of the major element compositions of the lower crust of the Nakhl-Rustaq Block in the Oman portion of the ophiolite can be found in Thomas (2003)\*.

(\*if that doesn't put you off gabbro major element geochemistry forever, then nothing will)

## **Appendix B: Sample preparation for ICP-MS (trace element) analysis**

### **B1.1 Sample preparation for ICP-MS analysis**

Whole rock minor and trace element analysis were carried out on the Cardiff University Inductively-Coupled Plasma Mass Spectrometry (X7 series Thermo-Elemental spectrometer) in 2004-2005 operated by Dr. Iain MacDonald. Powdered rock samples (Appendix A, Section A1.1) were dissolved into solution using the standard acid digestion method of Cardiff University Earth Science Department (detailed below).

1. Take 30 clean Savellex vials, add 2 x 0.5ml aliquots of concentrated HNO<sub>3</sub> and leave for 1 hour on hot-plate at 125°C. Discard the acid, rinse twice with de-ionised water and allow to dry.
2. Carefully weigh out 0.1000g (+/- 0.0001g) of each dried sample powder into each clean Savellex vial.
3. Dispense 0.5ml of concentrated HNO<sub>3</sub> onto each sample. Wait until any vigorous reaction stops and replace cap.
4. Dispense 2.0ml of HF twice (a total of 4.0ml) into each vial and replace cap
5. Arrange vials on hot-plate so that overheating does not occur. Set at 125°C and leave for a minimum of 24 hours.
6. Turn off hot-plate and allow samples to cool, and then remove vials from the hot-plate.
7. Remove caps and carefully tap vial to return any droplets that have condensed on the cap to the main solution. Place the vial and cap on the hot-plate. Repeat for all vials. Turn the hot-plate back to 125°C.
8. After evaporation, remove the vials before they are totally dry, giving them a translucent, resinous appearance.
9. Dispense one aliquot of 0.5ml HNO<sub>3</sub> into the first vial, then a second aliquot into the cap and swill carefully to dissolve any evaporate that may have

formed in the lid. Decant this acid into the vial, making 1.0ml in total. Replace vial on hotplate and place cap in tray.

10. Allow to evaporate to a translucent, resinous appearance, which should take around 2 hours at 125°C, then add another 1.0ml of concentrated HNO<sub>3</sub> (2 x 0.5ml) and repeat the evaporation. As each sample is finished, replace its correct cap and place in tray
11. To each vial add 5ml of 5M HNO<sub>3</sub>, reseal the vial and warm the solutions at 125°C for 1-2 hours on the hot-plate.
12. Remove from hot-plate and allow to cool. The solutions should be clear.
13. Spike each solution with 1.0ml of 2500ppb Rh-Re internal standard solution.
14. Transfer the solution to a clean 50ml volumetric flask using a clean plastic funnel and dilute the solution accurately to volume with de-ionised water (18.2Ω), making a 0.5M or (~3% vol.) nitric acid solution that will keep the dissolved ions in solution.
15. Transfer to a new 60ml polypropylene bottle for long-term storage.

Prior to running the solutions on the ICP-MS, the bottles were shaken and 1ml of each sample was extracted and placed in a sample tube. To this 1ml of In/Tl solution was added (naturally low abundance metals used as internal standards for each sample). The samples were then diluted with 8ml 2% HNO<sub>3</sub> to form the 10ml sample aliquot. Solutions of Certified Reference Materials (CRM's) and Total Procedural Blanks (TPB's) were prepared simultaneously by the same method.

## **B1.2 Calibration and analysis**

Prior to this studies samples being run, solutions of CRM's and a TPB were analysed and a best-fit calibration line (acquired count rate versus certified recommended concentrations and 'driven' through blank by the Thermo-Elemental software) was constructed for each element. CRM element concentrations that fell significantly off the calibration line were removed. All element concentrations were then derived from the acquired number of counts using the calibration lines. A number of CRM's (notably JB-1a) were run as unknown samples within the run as calibration



independent standards, permitting data accuracy to be checked after data reduction checks. Multiple U.A.E. samples were analysed in every session for inter-session comparisons. The instrument settings are shown in table B1.

Repetition time	1200ms
Dwell Time	240ms
Number of Sweeps	5
Readings per repetition	1
Number of repetitions	4

Table B1, ICP-MS Instrument parameters

### **B1.3 Drift correction**

During the course of a sample run it is normal for the measured concentrations of some elements to 'drift' to lower than their actual values. To compensate for this instrument drift a drift monitor, chosen as CRM W-2, was analysed after every 8-10 unknowns. The drift for each element in W-2 was then calculated and for elements that drifted more than +/- 5% a drift correction factor was applied.

### **B1.4 Data quality assessment**

Two ICP-MS runs were used during this study. The results for the international standard JB-1a are presented in Table B2, with two duplicate samples analysed in the first run and three duplicate samples analysed in the second batch. The RSD value has been calculated compared to the certified values for JB-1a. The results display excellent correlation between the certified values and the values obtained in this study, with only a few elements displaying a variation in excess of 5%.

Appendix B: Sample preparation for ICP-MS (trace element) analysis

	JB-1a Certified Values	1st run				2nd run					
		JB-1a (i)	RSD	JB-1a (ii)	RSD	JB-1a (i)	RSD	JB-1a (ii)	RSD	JB-1a (iii)	RSD
V	220	192.50	12.50	203.00	7.73	196.10	10.86	207.70	5.59	197.71	10.13
Cr	415	415.70	-0.17	413.90	0.27	423.62	-2.08	415.14	-0.03	408.92	1.46
Co	39.5	35.56	9.97	37.81	4.28	37.50	5.07	38.48	2.58	37.74	4.46
Zn	82	69.90	14.76	70.75	13.72	78.04	4.83	79.59	2.94	77.59	5.38
Ga	18	17.48	2.89	16.79	6.72	17.17	4.60	17.45	3.08	17.26	4.11
Rb	41	41.82	-2.00	42.44	-3.51	39.38	3.96	40.98	0.05	40.16	2.06
Sr	443	456.10	-2.96	487.20	-9.98	427.21	3.56	444.13	-0.26	432.09	2.46
Y	24	23.53	1.96	24.00	0.00	23.76	0.98	23.79	0.88	23.44	2.34
Zr	146	142.20	2.60	134.90	7.60	145.09	0.62	148.41	-1.65	147.51	-1.03
Nb	27	27.79	-2.93	26.71	1.07	27.85	-3.14	28.31	-4.85	27.98	-3.62
Cs	1.2	1.19	0.92	1.23	-2.25	1.15	4.13	1.19	0.95	1.17	2.74
Ba	497	504.10	-1.43	501.40	-0.89	536.84	-8.02	535.60	-7.77	528.20	-6.28
La	38.1	38.09	0.03	39.40	-3.41	38.11	-0.02	38.71	-1.61	37.18	2.42
Ce	66.1	65.87	0.35	68.68	-3.90	66.23	-0.19	66.83	-1.11	64.51	2.41
Pr	7.2	7.27	-0.99	7.59	-5.35	6.71	6.85	6.81	5.36	6.56	8.89
Nd	25.5	26.60	-4.31	27.42	-7.53	26.12	-2.42	26.42	-3.60	25.52	-0.08
Sm	5.07	5.13	-1.18	5.19	-2.27	5.07	-0.09	5.14	-1.33	5.01	1.26
Eu	1.47	1.53	-4.08	1.56	-6.12	1.49	-1.63	1.49	-1.63	1.46	0.58
Gd	4.54	4.81	-5.90	4.89	-7.64	4.65	-2.50	4.62	-1.69	4.52	0.55
Tb	0.69	0.73	-6.25	0.74	-7.42	0.68	0.91	0.69	0.65	0.67	2.18
Dy	4.19	4.04	3.48	4.11	1.96	3.98	5.03	3.97	5.18	3.87	7.60
Ho	0.78	0.75	3.32	0.76	2.90	0.78	0.15	0.78	0.39	0.76	2.79
Er	2.18	2.17	0.41	2.18	0.18	2.16	1.14	2.15	1.15	2.12	2.94
Tm	0.31	0.33	-7.06	0.34	-8.13	0.33	-6.24	0.33	-4.84	0.32	-2.35
Yb	2.10	2.08	1.00	2.12	-1.05	2.02	3.86	2.02	3.88	1.98	5.60
Lu	0.32	0.32	-0.97	0.32	-0.50	0.32	1.30	0.31	2.50	0.31	3.84
Hf	3.48	3.44	1.15	3.20	8.10	3.54	-1.79	3.55	-1.88	3.48	0.01
Ta	1.76	1.79	-1.76	1.71	2.73	1.69	4.07	1.68	4.57	1.64	6.75
Th	8.80	8.46	3.90	8.29	5.78	8.63	1.94	8.23	6.52	8.45	4.01
U	1.60	1.50	6.13	1.41	11.88	1.61	-0.62	1.53	4.12	1.59	0.43

Table B2, Displaying the results for CRM JB-1a from the two ICP-MS runs involved in this project. The RSD (Relative Standard Deviation) for each sample compared to the certified values are also presented

Table B3 displays the results of three unknown samples that were also run in both batches. In the case of the unknown samples the values obtained from the first run were used in this study. The samples display a good correlation between the two runs, with the exception of the values of Sr in samples 03UR138 and 03UR184. The analysis was considered acceptable as Sr values were not used to discriminate units in this study.

	1st run	2nd run	1st run	2nd run	1st run	2nd run
	03UR138	03UR138	03UR143	03UR143	03UR184	03UR184
<b>V</b>	297.52	293.73	232.26	239.95	237.99	238.56
<b>Cr</b>	32.36	28.25	470.65	437.98	178.56	161.37
<b>Co</b>	33.33	36.71	35.89	37.94	35.97	38.21
<b>Zn</b>	56.36	62.96	32.00	36.14	16.94	19.26
<b>Ga</b>	12.22	12.39	14.93	15.05	12.53	12.72
<b>Rb</b>	0.19	0.20	0.09	0.10	0.25	0.25
<b>Sr</b>	199.00	67.24	151.00	154.80	352.00	122.70
<b>Y</b>	38.85	38.89	23.68	23.77	10.60	10.82
<b>Zr</b>	148.98	87.31	68.51	26.42	19.80	16.09
<b>Nb</b>	2.44	2.65	1.14	1.21	0.14	0.28
<b>Cs</b>	0.00	0.00	0.00	0.00	0.01	0.01
<b>Ba</b>	29.50	31.78	15.20	16.28	20.61	22.43
<b>La</b>	4.72	4.85	2.16	2.31	0.53	0.53
<b>Ce</b>	14.07	14.34	6.57	6.92	1.53	1.49
<b>Pr</b>	2.51	2.30	1.24	1.15	0.29	0.27
<b>Nd</b>	12.95	12.57	6.53	6.53	1.73	1.67
<b>Sm</b>	4.19	4.11	2.28	2.30	0.74	0.71
<b>Eu</b>	1.49	1.45	0.86	0.85	0.31	0.30
<b>Gd</b>	5.04	4.98	2.90	2.90	1.07	1.05
<b>Tb</b>	0.98	0.91	0.58	0.55	0.23	0.21
<b>Dy</b>	6.26	6.08	3.79	3.69	1.63	1.55
<b>Ho</b>	1.24	1.27	0.75	0.79	0.35	0.35
<b>Er</b>	3.66	3.57	2.25	2.24	1.10	1.06
<b>Tm</b>	0.57	0.55	0.36	0.35	0.18	0.17
<b>Yb</b>	3.44	3.32	2.23	2.11	1.21	1.12
<b>Lu</b>	0.49	0.49	0.34	0.33	0.19	0.18
<b>Hf</b>	3.43	2.03	1.63	1.01	0.57	0.54
<b>Ta</b>	0.20	0.18	0.09	0.08	0.02	0.02
<b>Th</b>	0.16	0.18	0.06	0.06	0.05	0.05
<b>U</b>	0.07	0.10	0.02	0.02	0.05	0.05

Table B3, Displaying the results for three repeat samples analysed in both ICP-MS runs involved in this project. The results from the first run were used in this study.

## **B2 Alteration related element mobilisation within the Sheeted Dyke Complex (SDC)**

During the course of this study several samples of SDC were noted to have unusual depletions in certain LREE and incompatible elements. The samples were all associated with intrusion of Upper Gabbros. SDC Samples from the area of Al Ghel, associated with the N-S horst and Graben features in the Aswad Block, were noted to

associated with the N-S horst and Graben features in the Aswad Block, were noted to have been intruded by the 'Intrusive' Kalba Gabbro (Section 4.6.1) and have been subjected to localised high temperature hydrothermal alteration as evidenced by pervasive alteration of all mineral phases to hornblende. The two SDC samples from the Khawr Fakkan Block were also intruded and surrounded by the Upper Gabbro. Figure B1 displays the N-MORB normalised multi element patterns for the altered samples (two Khawr Fakkan Block SDC samples and five Aswad Block SDC samples). Hydrothermal systems operating in modern oceanic crust are responsible for the transport of a significant fraction of the Earth's heat budget, and makes a major contribution to geochemical fluxes both into and out of the oceans (e.g. Bickle and Teagle, 1992)

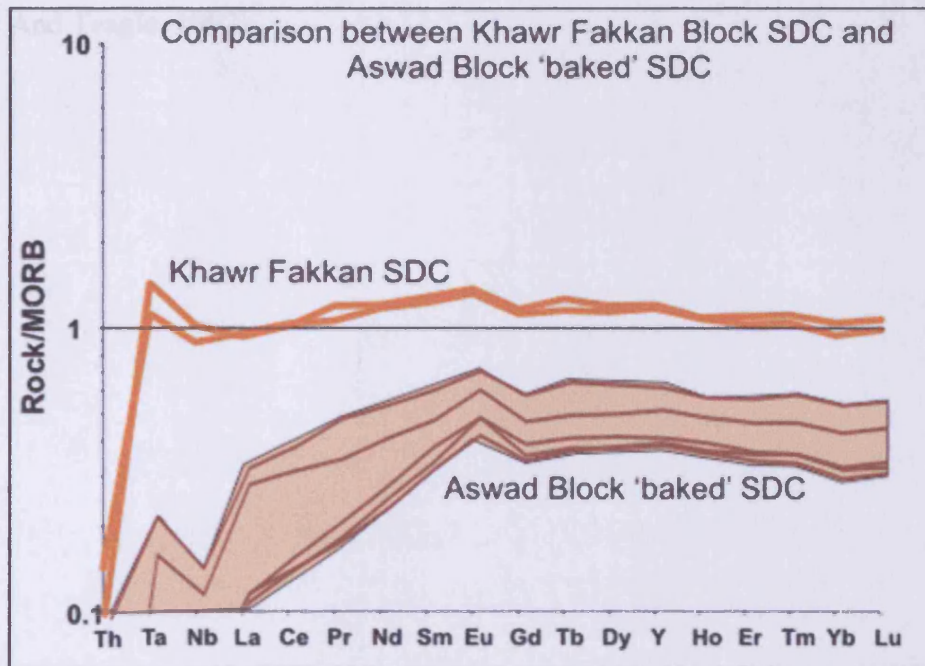


Figure B1, Comparison between the two Khawr Fakkan Block SDC samples and data for similarly intruded and 'baked' SDC outcrops in the Aswad Block. Normalised to the N-MORB values of Sun and McDonough (1989). Proximity to intrusive gabbro units appears to 'sweat off' LREE and other relatively immobile elements although further work is required to confirm this hypothesis.

The 'baked' Aswad Block SDC samples were not included in the main data set used in Section 3.3, as they demonstrate increasing relative depletion of LREE compared to HREE and depletion of selected incompatible elements including Th, Ta and Nb. The Khawr Fakkan SDC samples do not display obvious depletion in any other elements apart from Th. This is unusual as Th is a highly incompatible element that is

the two sets of data are similar for most HREE and MREE, despite the differences in abundance. The ‘baking’ effects are most dramatic for the LREE, and the hydrothermal alteration essentially appears to ‘sweat off’ the LREE and incompatible elements.

It is the conclusion of this study that hydrothermal alteration associated with the localised intrusion of Upper Gabbros into the SDC is the cause of the selective depletion seen in Figure B1. It is not clear why only Th was mobilised by the hydrothermal alteration in the Khawr Fakkan Block. To fully investigate this effect is outside the scope of this project. Further, more detailed work, would offer insight into the spatial behaviour of elements during hydrothermal alteration, and has implications for the genesis (and exploration) of VMS (Cu, Au, Zn, Pb, Sn) mineral deposits (e.g. Bickle And Teagle, 1992).

Block	Khawr Fakkan	Khawr Fakkan	Khawr Fakkan	Khawr Fakkan	Khawr Fakkan	Khawr Fakkan	Khawr Fakkan	Khawr Fakkan	Khawr Fakkan	Khawr Fakkan	Khawr Fakkan	Khawr Fakkan	Khawr Fakkan	Khawr Fakkan	Khawr Fakkan	Khawr Fakkan	Khawr Fakkan	Khawr Fakkan
Sample No:	03UR109	O4UR92	O4UR29	O4UR48	O4UR49	O4UR60	O4UR35	O4UR37	O4UR38	O4UR48	O4UR47	O4UR50	O4UR82	03UR214	O4UR4	O4UR10	O4UR13	O4UR24
Sample type and Geochemical signature	V1-I SDC MORB	V1-I SDC MORB	V1-I Early Dyke MORB	V1-I Early Dyke MORB	V1-I Early Dyke MORB	V1-I Early Dyke MORB	V1-II Common Dyke	V1-II Common Dyke	V1-II Common Dyke	V1-II Common Dyke	V1-II Common Dyke	V1-II Common Dyke	V1-II Common Dyke	V2-I Irregular Dyke	V2-I Irregular Dyke	V2-I Irregular Dyke	V2-I Irregular Dyke	V2-I Irregular Dyke
Location X	0434733	0434705	0434290	0432608	0432507	0432356	0431292	0431497	0431497	0433053	0432813	0432507	0431720	0434758	0429533	0430853	0431174	0431952
Location Y	2785600	2785411	2787653	2781974	2781814	2781050	2782610	2781819	2781819	2781202	2782014	2781814	2780654	2798747	2783129	2784991	2783443	2791355
wt%																		
SiO2	48.22	48.09	48.59	49.57	49.20	49.29	56.04	56.16	55.49	62.62	57.62	55.99	56.11	43.21	53.59	53.71	52.77	52.95
TiO2	1.82	1.89	1.20	0.77	1.18	0.85	0.96	0.96	1.01	0.95	0.87	0.91	1.09	0.27	0.17	0.14	0.12	0.15
Al2O3	14.09	13.74	14.38	15.25	14.90	16.26	14.58	14.48	13.97	14.27	14.38	14.67	14.68	12.24	14.73	12.12	9.44	11.15
Fe2O3	7.86	13.43	11.75	10.09	11.22	8.98	12.08	10.99	13.85	7.18	12.05	12.13	11.60	11.07	9.29	9.18	9.53	9.23
MnO	0.22	0.20	0.17	0.11	0.14	0.10	0.19	0.09	0.23	0.05	0.12	0.11	0.11	0.23	0.17	0.17	0.16	0.17
MgO	13.38	7.07	7.81	8.50	7.99	8.45	3.29	3.96	2.83	1.98	3.11	3.28	4.08	13.02	8.74	10.25	14.23	14.88
CaO	12.45	12.79	11.75	12.98	12.28	13.31	7.48	7.59	7.13	7.19	8.00	6.52	8.83	16.92	11.06	11.68	9.83	10.87
Na2O	2.43	2.48	2.76	2.04	2.54	2.30	3.11	4.36	4.12	3.90	3.31	3.23	3.54	0.82	1.46	0.89	1.16	1.06
K2O	0.20	0.08	0.09	0.05	0.09	0.01	0.08	0.18	0.31	0.13	0.12	0.15	0.09	0.34	0.15	0.06	0.03	0.04
P2O5	0.15	0.13	0.07	0.06	0.06	0.08	0.08	0.07	0.23	0.18	0.07	0.08	0.08	0.09	0.01	0.00	0.00	0.00
LOI	0.23	0.56	0.42	0.74	0.79	0.50	0.62	0.72	0.40	0.57	0.80	0.85	0.82	0.56	0.81	1.34	1.72	0.98
Total	101.07	100.47	98.80	100.15	100.09	100.09	98.42	99.45	99.56	99.00	100.48	99.91	100.63	98.77	100.17	99.53	99.00	101.47
(ppm)																		
V	386.58	379.87	296.60	287.01	259.39	233.01	312.23	375.47	181.92	73.80	343.54	400.87	381.87	276.38	266.12	265.14	248.74	247.83
Cr	232.36	171.60	276.98	330.02	362.65	321.03	36.92	46.83	63.54	22.12	27.99	26.20	67.30	258.54	447.45	639.62	1096.04	1205.68
Co	45.20	46.93	48.16	55.16	55.13	50.69	34.24	31.99	32.18	24.56	37.43	37.03	35.97	39.36	45.03	44.86	56.76	55.25
Cu	15.69	22.87	7.12	9.48	30.19	195.20	26.51	8.69	9.01	2.97	2.87	26.39	9.69	142.40	6.88	62.87	70.01	142.60
Zn	73.13	77.01	34.38	31.01	32.61	22.16	39.24	21.89	76.24	9.84	16.40	24.74	35.08	53.41	54.13	60.08	58.39	54.15
Ga	18.02	17.76	16.61	14.56	15.20	13.75	17.06	15.53	17.23	15.70	16.29	17.09	17.15	11.19	13.10	10.46	8.07	6.85
Rb	0.05	0.11	0.36	0.23	0.36	0.40	0.95	0.79	2.07	1.34	0.87	0.66	0.87	1.97	5.50	0.57	0.63	0.24
Sr	168.50	156.80	121.30	117.40	158.20	170.30	119.50	148.90	216.30	211.80	385.80	115.80	123.80	165.00	88.22	56.58	51.90	36.87
Y	33.63	32.69	29.63	21.11	22.42	20.62	24.13	22.64	27.47	31.46	24.81	23.45	22.94	6.22	6.72	6.28	5.63	4.85
Zr	59.65	36.81	44.94	35.66	33.43	41.59	30.53	36.71	26.02	51.63	44.68	35.58	13.66	7.00	12.99	7.27	6.64	4.85
Nb	2.37	2.06	1.52	0.92	0.94	1.26	1.98	1.37	1.67	2.80	1.59	1.55	1.73	0.11	1.26	0.89	0.58	0.56
Ce	0.00	0.00	0.00	0.01	0.01	0.01	0.03	0.01	0.03	0.05	0.02	0.02	0.02	0.08	0.30	0.02	0.03	0.02
Ba	7.02	7.78	9.24	4.89	16.22	9.50	31.69	19.87	68.79	14.09	35.31	25.20	18.24	15.38	21.35	22.53	13.83	9.57
La	2.33	2.40	2.46	1.47	1.66	2.10	2.55	2.29	3.18	3.40	2.43	1.87	2.16	0.24	1.11	0.55	0.57	0.48
Ce	7.65	7.71	7.80	4.89	5.70	6.21	6.71	6.81	7.91	9.25	6.34	5.34	5.80	0.58	2.39	1.26	1.28	1.04
Pr	1.67	1.39	1.26	0.83	1.00	1.01	1.01	1.10	1.19	1.42	0.98	0.87	0.90	0.09	0.28	0.15	0.16	0.13
Nd	8.77	8.55	7.34	4.80	5.81	5.66	5.55	6.00	6.65	7.76	5.40	5.02	5.04	0.49	1.25	0.75	0.75	0.59
Sm	3.36	3.22	2.83	1.81	2.10	1.97	1.95	1.97	2.39	2.70	1.98	1.90	1.65	0.24	0.39	0.27	0.27	0.21
Eu	1.40	1.34	0.99	0.79	0.83	0.74	0.74	0.95	0.96	0.75	0.72	0.70	0.66	0.12	0.17	0.13	0.13	0.09
Gd	4.26	4.12	3.43	2.42	2.72	2.48	2.59	2.51	3.18	3.53	2.83	2.57	2.49	0.44	0.55	0.45	0.43	0.33
Tb	0.84	0.77	0.65	0.47	0.51	0.46	0.50	0.48	0.59	0.67	0.51	0.50	0.48	0.11	0.12	0.10	0.10	0.07
Dy	5.44	5.16	4.47	3.22	3.45	3.16	3.53	3.33	4.05	4.64	3.62	3.49	3.35	0.87	0.89	0.82	0.76	0.62
Ho	1.09	1.09	0.97	0.69	0.74	0.68	0.77	0.75	0.89	1.02	0.81	0.77	0.74	0.20	0.22	0.20	0.19	0.16
Er	3.25	3.06	2.80	2.00	2.10	1.92	2.32	2.23	2.62	2.97	2.38	2.26	2.15	0.67	0.71	0.68	0.60	0.52
Tm	0.50	0.48	0.44	0.31	0.33	0.30	0.37	0.36	0.42	0.47	0.39	0.36	0.34	0.12	0.13	0.12	0.11	0.10
Yb	3.15	2.87	2.75	1.94	2.00	1.87	2.38	2.30	2.65	2.89	2.42	2.23	2.14	0.85	0.90	0.86	0.75	0.67
Lu	0.49	0.45	0.44	0.31	0.31	0.28	0.38	0.37	0.43	0.44	0.38	0.35	0.33	0.14	0.16	0.15	0.13	0.12
Hf	1.86	1.32	1.55	1.16	1.26	1.26	1.11	1.17	1.07	1.64	1.37	1.14	0.67	0.15	0.36	0.23	0.21	0.16
Ta	0.19	0.15	0.11	0.06	0.07	0.08	0.14	0.10	0.11	0.20	0.11	0.11	0.12	0.02	0.11	0.06	0.04	0.05
Pb	0.09	0.09	0.21	0.15	0.12	0.05	0.43	0.21	1.08	0.13	0.31	0.41	0.23	0.21	0.79	0.82	0.43	0.87
Th	0.01	0.02	0.10	0.06	0.07	0.09	0.23	0.19	0.44	0.35	0.25	0.22	0.15	0.04	0.31	0.15	0.15	0.13
U	0.01	0.01	0.04	0.04	0.04	0.05	0.13	0.19	0.26	0.18	0.20	0.12	0.07	0.02	0.27	0.16	0.12	0.14

Whole rock major (ICP-OES) and trace (ICP-MS) element data for the Khawr Fakkan and Aswad Block samples analysed in this study

Block	Khawr Fakkan	Khawr Fakkan	Khawr Fakkan	Khawr Fakkan	Khawr Fakkan	Khawr Fakkan	Khawr Fakkan	Khawr Fakkan	Khawr Fakkan	Khawr Fakkan	Khawr Fakkan	Khawr Fakkan	Khawr Fakkan	Khawr Fakkan	Khawr Fakkan	Khawr Fakkan	Khawr Fakkan	Khawr Fakkan	Khawr Fakkan	Khawr Fakkan	Khawr Fakkan	Khawr Fakkan
Sample No:	O4UR36	O4UR51	UAE104	UAE556	03UR93	03UR95	03UR110	O4UR6	O4UR8	O4UR21	O4UR22	O4UR23	O4UR25	O4UR28	O4UR27	O4UR58	03UR53	03UR54	03UR73	O4UR94		
Sample type and Geochemical signature	V2-I Irregular Dyke	V2-I Irregular Dyke	V2-I Irregular Dyke	V2-I Irregular Dyke	V2-II Cpx-phyrhic Dyke	V2-II Cpx-phyrhic Dyke	V2-II Cpx-phyrhic Dyke	V2-II Cpx-phyrhic Dyke	V2-II Cpx-phyrhic Dyke	V2-II Cpx-phyrhic Dyke	V2-II Cpx-phyrhic Dyke	V2-II Cpx-phyrhic Dyke	V2-II Cpx-phyrhic Dyke	V2-II Cpx-phyrhic Dyke	V2-II Cpx-phyrhic Dyke	V2-II Cpx-phyrhic Dyke	V3 Late Dyke	V3 Late Dyke	V3 Late Dyke	V3 Late Dyke		
Location X	0431322	0432507	0433138	0433308	0433451	0433228	0434733	0430108	0430128	0433883	0432258	0432258	0433641	0434091	0433120	0434295	0433495	0433478	0435882	0433254		
Location Y	2781947	2781814	2807363	2781899	2805589	2806350	2785800	2778998	2780448	2789587	2791803	2791803	2791088	2788919	2788648	2805308	2817682	2817683	2817334	2789481		
wt%																						
SiO2	52.80	52.35	50.81	48.75	55.18	55.01	49.97	54.91	57.95	52.12	50.78	54.42	51.94	51.98	49.59	49.85	46.81	45.83	47.50	48.83		
TiO2	0.16	0.12	0.18	0.19	0.42	0.51	0.27	0.28	0.17	0.41	0.35	0.39	0.63	0.44	0.39	0.31	1.38	1.24	1.02	1.22		
Al2O3	13.70	11.82	10.17	15.40	14.66	14.67	11.81	13.89	13.00	15.34	15.42	13.56	15.91	14.85	15.10	16.35	16.71	17.19	17.34	17.52		
Fe2O3	8.49	8.59	9.10	9.48	5.18	4.29	11.27	8.65	7.60	9.95	10.02	10.00	11.82	9.11	9.01	9.47	7.99	8.21	8.01	9.73		
MnO	0.15	0.16	0.18	0.15	0.17	0.16	0.16	0.14	0.15	0.16	0.17	0.20	0.13	0.11	0.16	0.14	0.12	0.18	0.18	0.14		
MgO	10.13	11.84	16.02	9.89	11.77	12.41	9.40	8.78	7.70	7.78	8.95	7.92	6.36	8.23	8.00	7.93	9.81	7.96	10.02	5.76		
CaO	10.94	11.91	10.27	11.71	10.38	9.77	12.42	11.76	8.76	12.20	10.11	10.38	9.86	12.65	11.65	12.75	14.48	14.42	11.44	11.86		
Na2O	1.68	1.01	1.04	1.02	1.06	1.46	1.21	0.96	2.18	1.61	3.04	1.66	2.61	1.64	2.71	2.14	1.64	1.10	2.62	2.95		
K2O	0.09	0.04	0.02	0.04	0.31	0.33	0.21	0.00	0.08	0.01	0.10	0.06	0.18	0.03	0.12	0.05	0.27	0.59	0.35	0.14		
P2O5	0.00	0.00	0.03	0.03	0.06	0.06	0.05	0.01	0.01	0.02	0.01	0.02	0.02	0.02	0.00	0.00	0.18	0.16	0.14	0.14		
LOI	2.51	2.22	1.88	2.09	0.84	0.46	1.12	0.93	1.31	0.50	0.97	0.44	1.09	0.48	1.47	0.68	3.19	1.28	1.13	1.09		
Total	100.85	99.87	98.87	98.56	99.82	99.03	97.89	98.32	98.91	100.07	97.91	99.00	100.43	99.58	98.18	99.71	102.30	98.07	99.84	99.18		
(ppm)																						
V	274.14	248.15	218.30	298.75	474.70	563.10	245.86	287.36	156.83	258.80	298.09	278.08	354.23	305.56	310.11	229.45	222.20	219.40	174.28	194.94		
Cr	558.08	818.84	1250.00	352.72	80.35	34.08	1183.47	187.23	451.40	103.61	72.83	452.79	187.04	308.95	276.40	72.20	287.41	372.49	315.41	285.45		
Co	44.88	45.29	59.00	35.00	37.58	36.60	47.18	44.87	33.26	44.91	42.15	44.63	45.44	42.89	50.91	44.37	35.92	38.42	42.86	37.28		
Cu	31.12	115.80	35.00	60.00	188.80	226.20	4.17	6.29	63.28	73.95	31.81	54.63	28.57	80.22	7.84	55.83	11.38	8.22	105.50	81.54		
Zn	62.41	53.73			73.47	38.44	50.04	30.48	58.88	23.07	42.27	71.02	52.97	26.58	24.57	38.99	54.35	31.87	59.71	67.39		
Ga	10.54	8.98	8.03	11.34	13.60	13.87	9.89	12.86	11.06	13.03	13.01	13.81	15.81	12.78	13.03	12.97	15.89	15.52	15.33	16.81		
Rb	1.60	0.18	0.31	0.73	1.08	3.54	0.11	0.52	3.31	0.31	0.42	0.69	2.35	0.24	1.13	0.23	0.85	16.82	4.83	1.00		
Sr	123.20	45.80	42.09	85.11	182.00	313.90	287.80	90.42	99.85	94.24	142.50	89.70	135.50	105.80	183.30	113.70	334.50	433.70	231.00	255.40		
Y	4.84	5.01	6.20	5.28	10.03	11.93	7.87	8.37	14.18	11.14	9.82	12.96	13.87	10.67	8.64	9.80	24.25	24.81	23.81	24.22		
Zr	5.55	5.54	6.38	11.59	17.71	22.22	13.91	9.26	23.23	12.90	10.25	11.35	18.16	11.62	8.65	10.58	119.50	119.16	82.53	97.11		
Nb	0.55	0.53	0.38	0.84	0.46	0.57	0.36	0.53	1.15	0.58	0.29	0.43	0.48	0.55	0.37	0.21	10.12	9.61	4.88	7.67		
Ca	0.03	0.01	0.01	0.01	0.04	0.13	0.00	0.02	0.16	0.00	0.01	0.00	0.02	0.01	0.08	0.00	0.02	0.78	0.21	0.03		
Ba	17.15	10.12	20.59	14.93	24.91	18.85	6.02	8.65	21.98	12.65	16.33	14.34	23.82	13.65	28.49	11.04	18.67	85.72	22.85	43.01		
La	0.46	0.44	0.21	0.50	0.85	1.02	0.60	0.48	1.18	0.77	0.62	0.57	0.92	0.68	0.54	0.53	10.03	10.05	5.89	8.43		
Ce	1.00	0.95	0.53	1.15	2.07	2.52	1.44	1.28	2.98	2.00	1.82	1.65	2.44	1.78	1.57	1.43	21.31	20.87	13.38	18.11		
Pr	0.12	0.11	0.09	0.14	0.32	0.39	0.23	0.19	0.43	0.32	0.25	0.28	0.40	0.28	0.26	0.24	2.93	2.83	1.95	2.32		
Nd	0.66	0.51	0.50	0.64	1.53	1.85	1.22	1.09	2.31	1.86	1.48	1.74	2.41	1.61	1.49	1.53	12.14	12.25	8.94	10.93		
Sm	0.19	0.18	0.25	0.24	0.58	0.88	0.48	0.48	0.88	0.78	0.63	0.77	1.01	0.67	0.59	0.70	3.33	3.27	2.61	3.04		
Eu	0.09	0.07	0.10	0.11	0.25	0.28	0.21	0.21	0.30	0.33	0.34	0.37	0.45	0.28	0.33	0.32	1.15	1.20	0.98	1.11		
Gd	0.32	0.32	0.49	0.40	0.88	1.02	0.72	0.74	1.27	1.12	0.95	1.20	1.45	1.01	0.85	1.01	3.71	3.70	3.12	3.44		
Tb	0.07	0.08	0.11	0.09	0.19	0.23	0.16	0.16	0.26	0.23	0.20	0.25	0.29	0.21	0.17	0.20	0.67	0.67	0.60	0.60		
Dy	0.81	0.63	0.85	0.89	1.44	1.69	1.18	1.19	1.97	1.65	1.42	1.86	2.07	1.52	1.26	1.44	4.15	4.09	3.81	3.85		
Ho	0.16	0.16	0.21	0.17	0.33	0.38	0.25	0.28	0.46	0.37	0.32	0.43	0.48	0.35	0.29	0.32	8.80	0.79	0.76	0.79		
Er	0.52	0.54	0.67	0.57	1.09	1.25	0.82	0.88	1.45	1.12	0.97	1.30	1.37	1.06	0.88	0.94	2.34	2.31	2.24	2.22		
Tm	0.10	0.10	0.11	0.10	0.19	0.22	0.14	0.15	0.25	0.18	0.16	0.22	0.22	0.18	0.14	0.15	0.38	0.38	0.35	0.35		
Yb	0.67	0.69	0.78	0.71	1.33	1.50	0.96	1.01	1.66	1.18	1.04	1.43	1.42	1.13	0.90	0.96	2.28	2.20	2.25	2.12		
Lu	0.12	0.12	0.13	0.12	0.22	0.25	0.16	0.17	0.28	0.19	0.17	0.24	0.23	0.18	0.15	0.16	0.34	0.33	0.36	0.33		
Hf	0.17	0.16	0.22	0.28	0.41	0.55	0.34	0.31	0.71	0.51	0.38	0.46	0.65	0.47	0.35	0.43	2.49	2.53	1.67	2.09		
Ta	0.05	0.05	0.02	0.07	0.05	0.06	0.04	0.04	0.08	0.04	0.02	0.03	0.03	0.04	0.03	0.01	0.80	0.58	0.29	0.43		
Pb	1.66	0.71	0.50	0.22	0.38	0.25	0.11	0.20	0.89	0.19	0.18	0.82	0.35	0.46	0.32	0.17	0.18	0.78	1.53	0.71		
Th	0.13	0.12	0.03	0.18	0.14	0.17	0.08	0.08	0.18	0.10	0.08	0.03	0.11	0.09	0.09	0.10	1.15	1.03	0.58	0.82		
U	0.13	0.13	0.02	0.15	0.07	0.08	0.07	0.06	0.17	0.08	0.03	0.02	0.08	0.07	0.10	0.08	0.28	0.31	0.14	0.21		

Block	Aswad	Aswad	Aswad	Aswad	Aswad	Aswad	Aswad	Aswad	Aswad	Aswad	Aswad	Aswad	Aswad	Aswad	Aswad	Aswad	Aswad	Aswad	Aswad	Aswad
Sample No:	03UR76	03UR77	03UR80	03UR118	03UR128	03UR129	03UR138	03UR139	04UR16	04UR17	04UR53	04UR54	04UR78	UAE2893	UAE3079	UAE3102	UAE3115	UAE3125	UAE3132	UAE3196
Sample type and Geochemical signature	V1-Lavas	V1-Lavas	V1-Lavas	V1-Lavas	V1-Lavas	V1-Lavas	V1-Lavas	V1-Lavas	V1-Lavas	V1-Lavas	V1-Lavas	V1-Lavas	V1-Lavas	V1-Lavas	V1-Lavas	V1-Lavas	V1-Lavas	V1-Lavas	V1-Lavas	V1-Lavas
Location X	0430116	0430118	0430108	0430582	0431517	0431539	0431352	0431395	0430997	0430311	0429940	0430769	0430267	0409883	0432520	0430602	0430228	0429903	0431175	0429777
Location Y	2754839	2754839	2754397	2785324	2788082	2788808	2787795	2787702	2788441	2784714	2752388	2783280	2785158	2821871	2788227	2785487	2789048	2786244	2783935	2784187
wt%																				
SiO <sub>2</sub>	44.59	62.21	50.18	55.39	51.54	55.74	51.50	49.98	54.24	52.35	48.53	48.05	51.50	42.20	43.80	57.04	49.29	50.81	47.27	61.50
TiO <sub>2</sub>	1.00	1.07	1.38	1.57	1.78	1.70	1.85	1.52	2.00	1.58	1.03	0.88	1.84	0.99	1.14	1.80	1.35	1.70	0.84	1.45
Al <sub>2</sub> O <sub>3</sub>	14.53	14.47	15.41	16.08	15.42	15.30	14.82	15.31	13.72	14.80	15.44	18.20	15.19	15.35	16.36	14.11	16.19	14.34	16.39	13.77
Fe <sub>2</sub> O <sub>3</sub>	9.74	9.16	11.77	11.30	12.58	11.34	13.11	12.02	13.32	12.01	9.58	10.02	14.25	27.41	10.08	11.72	10.14	12.16	8.87	7.58
MnO	0.16	0.15	0.18	0.21	0.17	0.14	0.15	0.20	0.17	0.23	0.15	0.16	0.22	0.24	0.16	0.28	0.18	0.17	0.18	0.08
MgO	7.48	3.83	6.32	3.48	4.58	3.38	5.05	7.20	4.55	5.02	7.54	8.81	4.92	8.84	8.83	5.09	7.16	6.82	10.14	2.05
CaO	11.34	3.47	6.60	5.93	5.99	4.61	4.69	10.80	3.49	7.90	12.21	10.83	7.84	0.49	11.74	2.38	11.43	7.78	11.46	8.01
Na <sub>2</sub> O	2.80	5.11	5.28	5.87	6.07	6.29	6.08	3.03	5.72	5.47	3.10	2.53	4.49	0.02	1.87	4.51	2.73	4.10	2.06	3.74
K <sub>2</sub> O	0.18	0.17	0.25	0.22	0.21	0.18	0.22	0.29	0.02	0.10	0.05	0.10	0.09	0.06	0.12	0.07	0.06	0.17	0.07	0.08
P <sub>2</sub> O <sub>5</sub>	0.08	0.16	0.12	0.30	0.16	0.18	0.17	0.15	0.19	0.15	0.08	0.05	0.18	0.08	0.11	0.22	0.15	0.18	0.08	0.16
LOI	7.05	2.11	2.27	0.44	1.82	1.59	1.53	0.85	2.38	0.43	2.40	1.72	0.35	5.51	4.98	2.98	0.16	1.70	1.73	2.38
Total (ppm)	98.74	101.70	89.74	100.75	100.32	100.41	99.15	101.15	99.81	100.03	100.07	99.13	100.87	101.18	99.17	99.94	98.82	99.49	99.04	98.76
V	258.77	225.98	297.19	233.83	337.03	236.32	297.52	284.45	280.79	308.56	228.37	225.37	360.19	275.15	259.47	155.82	270.15	297.24	214.14	251.31
Cr	546.44	71.88	56.55	204.12	62.53	27.71	32.38	222.54	32.88	55.93	411.06	414.98	44.55	290.20	275.85	17.12	169.21	87.03	392.49	41.60
Co	45.38	19.20	38.10	22.02	32.13	20.96	33.33	38.07	41.78	30.25	45.84	43.72	38.04	122.34	48.86	15.86	39.00	40.51	45.23	21.55
Zn	64.75	104.70	90.52	57.02	73.79	68.34	58.38	40.33	140.10	127.40	61.11	47.51	88.20	42.63	37.77	90.81	22.44	35.37	38.22	65.78
Ga	15.99	17.60	17.10	22.89	15.72	15.52	12.22	15.91	15.00	18.36	14.45	14.55	18.31	17.70	15.59	17.82	16.51	18.33	14.28	18.96
Rb	0.42	0.15	0.13	0.34	0.25	0.16	0.19	0.15	0.18	0.32	1.80	1.24	0.45	0.18	1.30	0.83	0.41	1.74	0.27	0.45
Sr	181.20	274.30	360.20	185.70	242.90	225.30	199.00	187.20	55.09	120.10	213.50	183.30	165.50	12.08	189.31	53.29	147.82	154.85	144.48	83.14
Y	27.18	79.33	32.59	74.77	37.83	40.80	38.85	29.83	48.22	34.89	28.34	22.47	38.71	29.38	29.85	52.48	29.25	43.18	22.06	34.58
Zr	65.80	324.82	84.26	268.84	134.90	158.58	148.98	87.84	145.16	56.75	71.05	39.75	30.45	65.01	84.34	159.81	28.74	121.83	50.33	102.99
Nb	0.84	4.28	1.82	5.78	2.23	2.42	2.44	1.58	3.41	2.28	0.55	0.42	2.84	0.98	2.68	3.33	1.10	3.37	0.62	1.89
Ce	0.02	0.00	0.00	0.00	0.01	0.00	0.00	0.00	0.01	0.01	0.08	0.04	0.01	0.02	0.04	0.03	0.08	0.07	0.03	0.01
Ba	12.09	4.84	8.78	31.88	16.81	10.41	29.80	26.79	8.99	27.34	8.52	34.83	17.85	2.78	7.32	38.93	18.06	16.58	183.22	3.03
La	1.89	9.68	3.01	8.52	4.89	4.75	4.72	3.07	5.35	4.45	1.70	1.25	5.09	3.03	3.21	4.67	2.39	4.50	2.24	4.07
Ce	8.49	28.89	9.18	25.71	14.08	14.12	14.07	9.37	15.78	12.71	8.24	4.47	14.77	9.29	9.50	14.34	8.81	13.58	5.98	12.45
Pr	1.28	5.03	1.88	4.82	2.41	2.47	2.51	1.71	2.53	2.01	1.15	0.83	2.32	1.88	1.84	2.51	1.35	2.34	1.07	2.20
Nd	7.07	25.42	9.08	24.31	12.18	12.63	12.95	8.81	14.00	11.05	6.88	5.07	12.88	8.81	8.49	12.80	7.81	12.12	5.50	11.20
Sm	2.53	8.26	3.19	7.99	3.88	4.16	4.19	2.99	4.88	3.81	2.50	1.98	4.14	3.01	2.95	4.59	2.99	4.25	2.00	3.90
Eu	0.95	2.05	1.07	2.41	1.49	1.17	1.49	1.13	1.13	1.31	0.95	0.75	1.45	0.60	1.08	1.51	1.15	1.29	0.77	1.38
Gd	3.21	9.98	3.98	9.61	4.65	5.06	5.04	3.74	5.77	4.48	3.14	2.59	5.04	3.78	3.77	6.29	3.93	5.44	2.68	4.98
Tb	0.65	1.99	0.80	1.85	0.91	0.99	0.98	0.74	1.07	0.82	0.59	0.50	0.92	0.68	0.69	1.17	0.70	0.99	0.49	0.87
Dy	4.33	13.08	5.32	11.88	5.88	6.38	6.28	4.85	7.24	5.49	4.00	3.39	6.09	4.73	4.72	8.09	4.82	6.83	3.45	5.87
Ho	0.88	2.71	1.07	2.38	1.19	1.28	1.24	0.97	1.54	1.17	0.68	0.73	1.28	0.93	0.95	1.64	0.95	1.36	0.71	1.13
Er	2.85	8.38	3.22	8.93	3.57	3.86	3.68	2.89	4.44	3.34	2.45	2.10	3.52	2.82	2.82	5.03	2.78	4.12	2.14	3.33
Tm	0.42	1.38	0.52	1.09	0.58	0.62	0.57	0.48	0.70	0.52	0.39	0.33	0.54	0.45	0.45	0.81	0.43	0.88	0.34	0.51
Yb	2.68	8.78	3.23	8.84	3.53	3.86	3.44	2.90	4.28	3.18	2.37	2.06	3.20	2.82	2.83	5.07	2.68	4.17	2.16	3.24
Lu	0.41	1.40	0.50	1.03	0.54	0.59	0.49	0.43	0.66	0.48	0.37	0.32	0.47	0.43	0.44	0.78	0.42	0.70	0.32	0.47
Hf	1.70	8.12	2.09	6.47	3.12	3.82	3.43	2.19	3.73	1.92	1.80	1.28	1.32	1.87	2.18	4.38	0.90	3.19	1.22	3.09
Ta	0.06	0.39	0.13	0.43	0.18	0.19	0.20	0.12	0.24	0.15	0.04	0.03	0.18	0.09	0.15	0.21	0.09	0.22	0.07	0.13
Th	0.05	0.63	0.18	0.50	0.22	0.27	0.18	0.13	0.32	0.20	0.04	0.03	0.18	0.12	0.18	0.34	0.01	0.27	0.05	0.21
U	0.02	0.25	0.11	0.15	0.13	0.15	0.07	0.09	0.19	0.10	0.02	0.03	0.05	0.11	0.09	0.28	0.01	0.12	0.04	0.18



Block	Aswad	Aswad	Aswad	Aswad	Aswad	Aswad	Aswad	Aswad	Aswad	Aswad	Aswad	Aswad	Aswad	Aswad	Aswad	Aswad	Aswad	Aswad	Aswad	Aswad	Aswad
Sample No:	UAE3137	UAE3148	UAE3164	UAE3167	UAE 4843	UAE3180	03UR63B	03UR83C	03UR84	03UR114	03UR127	03UR132	03UR133	03UR134	03UR137	03UR142	03UR143	03UR146	03UR147	03UR148	03UR152
Sample type and Geochemical signature	V1-Lavas	V1-Lavas	V1-Lavas	V1-Lavas	V1-Lavas	V1-Lavas	V1-SDC	V1-SDC	V1-SDC	V1-SDC	V1-SDC	V1-SDC	V1-SDC	V1-SDC	V1-SDC	V1-SDC	V1-SDC	V1-SDC	V1-SDC	V1-SDC	V1-SDC
Location X	0429598	0427137	0430078	0429209	0430435	0428362	0429050	0429050	0429372	0431263	0431517	0431480	0429173	0429173	0431341	0430749	0430982	0430026	0429140	0428122	0427528
Location Y	2754012	2758235	2752998	2752566	2762026	2752032	2754254	2754254	2756228	2765855	2798082	2799414	2798944	2798944	2787861	2787504	2772784	2771838	2770061	2770156	2770813
wt%																					
SiO2	50.04	48.38	48.43	52.91	49.55	52.11	52.35	50.80	51.80	48.87	54.24	49.22	60.37	48.82	49.44	49.98	48.35	47.84	48.93	48.04	49.04
TiO2	1.63	0.88	0.83	1.08	0.94	1.75	1.48	1.24	1.53	1.20	0.78	1.38	1.34	0.99	1.45	1.52	1.01	1.19	1.27	1.22	0.81
Al2O3	14.97	16.12	15.08	15.98	17.46	14.91	14.98	15.06	15.19	14.38	14.69	15.58	15.07	16.18	15.46	15.31	16.83	15.84	15.27	14.99	16.11
Fe2O3	12.46	8.91	9.84	10.10	8.13	13.31	11.05	10.99	12.28	10.84	12.35	12.05	8.65	9.74	11.97	12.02	9.21	10.32	11.81	10.59	8.22
MnO	0.24	0.18	0.18	0.14	0.15	0.37	0.12	0.15	0.13	0.13	0.17	0.24	0.11	0.19	0.19	0.20	0.15	0.20	0.18	0.16	0.17
MgO	6.33	8.45	8.08	6.01	8.40	5.23	5.54	6.83	6.01	8.08	3.95	7.08	1.98	8.49	6.98	7.20	7.83	7.11	6.79	8.37	9.07
CaO	8.88	12.55	12.99	7.67	12.92	7.01	6.89	8.02	8.03	8.62	7.81	10.99	5.73	12.83	10.15	10.60	12.46	11.67	11.71	11.94	13.21
Na2O	4.00	2.39	2.74	2.97	1.94	3.47	4.94	3.99	4.25	3.57	2.59	3.14	5.03	1.78	3.09	3.03	2.60	2.69	2.56	2.22	2.27
K2O	0.10	0.08	0.23	0.28	0.01	0.11	0.31	0.42	0.35	0.20	0.69	0.20	0.20	0.18	0.25	0.29	0.20	0.17	0.16	0.17	0.22
P2O5	0.13	0.07	0.08	0.10	0.07	0.18	0.15	0.11	0.14	0.11	0.07	0.10	0.35	0.08	0.13	0.15	0.09	0.10	0.11	0.09	0.08
LOI	2.05	1.99	3.44	2.99	0.71	2.28	1.58	1.77	1.47	2.27	2.43	1.31	0.12	0.51	1.44	0.85	0.79	1.11	0.88	0.86	1.07
Total	100.82	99.99	101.86	100.17	100.27	100.73	99.34	99.38	101.19	98.24	99.86	101.30	98.94	99.55	100.53	101.15	99.51	98.25	99.86	98.95	100.27
(ppm)																					
V	321.82	248.88	247.65	269.87	190.58	360.31	368.43	288.60	351.91	249.92	287.34	292.59	107.41	236.18	306.50	298.70	232.26	247.24	304.90	321.29	237.47
Cr	17.31	311.57	381.87	11.96	484.47	18.38	55.43	92.01	27.72	317.97	273.98	188.21	34.11	394.01	146.83	205.80	470.65	369.83	242.45	456.40	392.76
Co	38.19	39.26	42.81	35.55	37.47	37.67	51.19	34.88	36.96	40.82	38.45	36.39	11.72	40.43	38.83	38.44	35.89	35.11	43.88	42.16	39.70
Zn	41.40	57.29	49.91	78.75	68.74	87.86	52.01	25.52	31.73	37.51	56.29	45.94	17.96	22.17	69.46	71.74	32.00	21.94	43.03	24.20	32.73
Ga	17.07	14.13	13.73	17.11	15.15	18.99	25.25	16.19	19.36	14.69	14.51	14.71	20.23	14.32	16.37	16.97	14.93	14.71	16.71	15.42	14.45
Rb	0.29	0.21	2.95	4.93	0.16	0.94	1.92	2.18	1.04	0.64	0.68	0.24	0.22	0.10	0.78	1.33	0.09	0.12	0.23	0.31	0.11
Sr	385.74	147.59	165.08	200.59	122.10	135.24	309.50	183.90	196.50	203.40	150.40	182.10	188.50	381.00	188.60	189.16	151.00	168.20	380.20	378.20	329.00
Y	35.70	23.47	23.50	28.11	22.15	43.57	57.81	29.14	37.41	27.86	26.91	25.44	62.04	22.08	31.23	42.23	23.88	25.43	29.84	25.82	21.87
Zr	80.92	40.25	40.09	76.46	52.96	114.58	124.39	83.81	110.17	84.79	42.73	87.10	212.87	58.46	104.31	113.43	68.51	82.94	87.83	69.44	51.14
Nb	2.07	0.86	0.54	1.33	0.37	2.68	3.21	1.30	1.99	1.63	1.78	1.32	3.65	0.83	2.07	2.55	1.14	1.36	0.96	0.98	0.56
Ce	0.00	0.01	0.02	0.10	0.08	0.02	0.05	0.07	0.02	0.01	0.01	0.01	0.00	0.00	0.01	0.03	0.00	0.01	0.00	0.01	0.00
Ba	16.89	20.57	30.44	53.89	10.67	15.88	43.18	25.80	26.68	12.21	34.87	10.77	35.63	4.95	48.25	20.94	15.20	11.36	9.78	18.01	9.80
La	3.22	1.88	1.34	2.91	1.47	4.41	6.62	2.58	3.46	2.81	2.90	2.48	7.73	1.81	3.91	4.75	2.16	2.60	2.58	2.10	1.36
Ce	9.91	8.00	4.34	8.54	5.37	13.83	20.11	8.08	10.69	8.77	8.45	7.44	22.82	5.70	11.22	13.81	6.57	7.81	8.12	6.53	4.57
Pr	1.78	1.11	0.85	1.51	1.07	2.43	3.60	1.50	1.98	1.57	1.51	1.37	4.04	1.10	1.99	2.34	1.24	1.47	1.53	1.24	0.90
Nd	9.41	5.96	4.77	7.90	5.84	12.74	18.92	8.14	10.58	8.01	7.89	7.28	20.87	5.89	10.22	12.17	6.53	7.66	8.19	6.73	5.09
Sm	3.34	2.17	1.90	2.74	2.17	4.32	6.41	2.85	3.68	2.68	2.70	2.58	6.77	2.12	3.31	3.97	2.28	2.65	2.85	2.43	1.90
Eu	1.22	0.83	0.77	1.00	0.84	1.50	2.24	1.05	1.25	1.04	1.00	0.99	2.18	0.82	1.21	1.38	0.88	0.99	1.08	0.94	0.73
Gd	4.51	2.93	2.76	3.58	2.78	5.72	7.93	3.56	4.73	3.43	3.40	3.25	8.19	2.69	4.12	4.83	2.90	3.27	3.59	3.15	2.53
Tb	0.83	0.54	0.53	0.66	0.51	1.07	1.57	0.71	0.94	0.68	0.67	0.63	1.58	0.55	0.80	0.95	0.58	0.64	0.72	0.63	0.51
Dy	5.79	3.79	3.77	4.59	3.53	7.25	10.14	4.59	6.09	4.53	4.37	4.16	9.82	3.50	5.10	6.12	3.79	4.13	4.70	4.17	3.40
Ho	1.13	0.74	0.74	0.89	0.69	1.41	2.02	0.92	1.23	0.91	0.87	0.84	1.95	0.71	1.03	1.23	0.75	0.83	0.95	0.84	0.69
Er	3.44	2.29	2.31	2.71	1.95	4.27	6.05	2.79	3.65	2.71	2.64	2.50	5.71	2.11	3.03	3.68	2.25	2.45	2.84	2.50	2.10
Tm	0.55	0.37	0.37	0.43	0.33	0.68	0.98	0.44	0.57	0.43	0.42	0.39	0.88	0.33	0.47	0.58	0.38	0.38	0.44	0.40	0.33
Yb	3.80	2.38	2.37	2.84	2.14	4.45	6.11	2.77	3.54	2.70	2.64	2.42	5.43	2.07	2.96	3.67	2.23	2.38	2.81	2.51	2.11
Lu	0.64	0.35	0.35	0.42	0.29	0.84	0.95	0.43	0.55	0.41	0.40	0.37	0.81	0.32	0.48	0.55	0.34	0.38	0.43	0.39	0.32
Hf	2.45	1.43	1.26	2.18	1.40	3.33	3.16	2.10	2.79	2.08	1.22	2.11	5.31	1.47	2.45	2.85	1.63	1.96	2.13	1.77	1.28
Ta	0.15	0.07	0.05	0.10	0.04	0.19	0.26	0.10	0.15	0.13	0.13	0.10	0.28	0.07	0.16	0.19	0.09	0.11	0.08	0.08	0.05
Th	0.17	0.09	0.04	0.20	0.03	0.23	0.21	0.10	0.13	0.12	0.15	0.09	0.28	0.05	0.18	0.18	0.08	0.08	0.09	0.08	0.04
U	0.10	0.05	0.04	0.12	0.02	0.10	0.10	0.05	0.05	0.05	0.05	0.02	0.08	0.01	0.08	0.05	0.02	0.02	0.03	0.02	0.01

Block	Aswad	Aswad	Aswad	Aswad	Aswad	Aswad	Aswad	Aswad	Aswad	Aswad	Aswad	Aswad	Aswad	Aswad	Aswad	Aswad	Aswad	Aswad	Aswad	Aswad	Aswad																																																																																																																																																																																																																																																																																																																																																																																																																																																																																																																																																																																																																																																																																																																																																																																																																																																																																																																																																																																				
Sample No:	03UR166	03UR177	03UR205	04UR56	04UR57	04UR71	04UR77	04UR80	04UR95	03UR122	03UR150	03UR203	03UR202	UAE3092	UAE 3971	03UR115	03UR117	03UR119	03UR125	03UR128	04UR72																																																																																																																																																																																																																																																																																																																																																																																																																																																																																																																																																																																																																																																																																																																																																																																																																																																																																																																																																																																				
Sample type and Geochemical signature	V1-SDC	V1-SDC	V1-SDC	V1-SDC	V1-SDC	V1-SDC	V1-SDC	V1-SDC	V1-SDC	V1-III Intermediate Dykes	V1-III Intermediate Dykes	V1-III Intermediate Dykes	V1-III Intermediate Dykes	V1-III Intermediate Dykes	V1-III Intermediate Dykes	V2-I Wadi Mal Dykes	V2-I Wadi Mal Dykes	V2-I Wadi Mal Dykes	V2-I Wadi Mal Dykes	V2-I Wadi Mal Dykes	V2-I Wadi Mal Dykes																																																																																																																																																																																																																																																																																																																																																																																																																																																																																																																																																																																																																																																																																																																																																																																																																																																																																																																																																																																				
Location X	0428836	0429116	0429314	0430956	0431523	0432188	0429813	0432321	0425993	0430259	0427736	0427440	0428685	0432289	0411794	0431329	0430903	0430230	0430541	0430657	0432119																																																																																																																																																																																																																																																																																																																																																																																																																																																																																																																																																																																																																																																																																																																																																																																																																																																																																																																																																																																				
Location Y	2777534	2777373	2774037	2753962	2753824	2759705	2764831	2761678	2775551	2765384	2770545	2774402	2778758	2754944	2764119	2766144	2765532	2765267	2765594	2765156	2760432																																																																																																																																																																																																																																																																																																																																																																																																																																																																																																																																																																																																																																																																																																																																																																																																																																																																																																																																																																																				
wt%																							SiO <sub>2</sub>	48.92	48.60	59.62	49.18	50.39	48.81	50.64	49.78	49.40	46.88	47.98	51.38	49.94	50.47	56.78	53.64	52.69	54.02	49.35	54.63	54.69	TiO <sub>2</sub>	1.21	1.11	1.14	1.03	1.20	1.13	0.95	0.87	0.95	0.81	0.67	0.57	0.75	0.47	0.48	0.71	0.68	0.81	1.24	0.70	0.83	Al <sub>2</sub> O <sub>3</sub>	14.75	14.59	14.29	14.61	13.84	14.62	14.77	14.28	15.04	16.06	19.38	14.61	15.60	16.12	15.24	14.48	15.35	15.05	15.27	14.60	14.65	Fe <sub>2</sub> O <sub>3</sub>	7.66	7.94	2.78	10.27	12.32	10.50	10.80	11.00	9.80	8.40	6.45	9.41	8.29	8.57	8.72	11.74	10.37	11.99	10.58	11.83	11.50	MnO	0.18	0.12	0.11	0.18	0.23	0.18	0.18	0.17	0.17	0.17	0.12	0.16	0.16	0.21	0.15	0.17	0.18	0.16	0.17	0.17	0.10	MgO	10.85	10.21	8.56	8.25	7.80	8.00	8.48	8.87	8.64	8.10	7.42	8.58	9.11	8.42	8.55	4.25	5.28	4.43	8.30	3.84	4.39	CaO	12.33	12.63	8.18	11.44	11.53	12.49	13.04	13.08	12.03	14.28	13.89	12.74	12.64	11.70	10.74	7.05	9.35	7.25	9.99	7.25	7.56	Na <sub>2</sub> O	2.19	2.64	2.79	3.19	2.15	2.44	2.08	1.78	2.27	2.05	1.99	1.32	1.35	1.99	1.79	2.99	2.08	3.11	3.60	2.83	3.18	K <sub>2</sub> O	0.29	0.23	0.23	0.08	0.10	0.11	0.00	0.00	0.22	0.18	0.21	0.22	0.24	0.16	0.04	0.52	0.49	0.69	0.23	0.67	0.23	P <sub>2</sub> O <sub>5</sub>	0.13	0.11	0.23	0.07	0.10	0.07	0.05	0.07	0.06	0.07	0.07	0.08	0.04	0.02	0.07	0.06	0.07	0.12	0.07	0.07	0.05	LOI	0.91	0.61	1.88	2.03	1.81	0.88	0.59	0.39	0.74	0.84	0.73	0.68	0.66	2.14	0.45	2.54	1.92	1.81	1.11	1.49	1.87	Total	99.44	98.79	99.80	100.34	101.08	99.03	101.59	100.26	99.32	99.79	99.90	99.73	99.02	100.29	100.96	98.15	98.34	99.29	99.95	98.07	99.05	(ppm)																							V	300.98	299.53	278.84	278.17	328.70	262.48	278.79	286.02	231.08	187.82	214.37	256.03	308.81	231.67	285.00	439.31	402.27	431.29	403.74	334.58	390.32	Cr	311.73	240.35	74.72	479.70	189.14	267.54	424.43	437.82	380.08	456.02	314.83	469.47	338.56	183.20	114.02	22.74	12.03	10.37	42.54	32.47	46.04	Co	43.00	42.27	17.03	44.83	48.54	43.60	41.27	49.38	47.00	37.79	31.72	36.39	37.83	35.67	37.60	34.98	40.00	35.12	32.40	31.15	36.93	Zn	56.84	24.06	41.93	71.50	110.30	63.02	64.12	54.25	40.93	71.98	24.14	31.98	61.87	125.28	41.69	75.92	63.89	69.68	55.50	47.52	11.60	Ga	16.45	16.56	19.01	15.44	16.33	15.34	15.39	14.82	13.93	13.59	14.82	12.28	13.95	12.99	14.40	15.66	17.79	15.58	15.36	15.15	15.28	Rb	3.44	0.18	0.12	1.07	0.41	0.22	0.11	0.09	2.62	0.52	0.14	0.12	0.84	1.71	1.31	4.73	8.36	8.85	9.64	10.58	1.88	Sr	365.60	369.10	177.60	189.00	103.20	152.90	88.82	76.98	128.00	387.80	336.00	363.80	342.90	98.15	89.14	174.10	373.90	324.80	312.90	387.20	164.00	Y	28.95	30.51	50.99	26.70	29.07	25.54	26.72	24.13	23.31	17.27	16.29	16.78	19.58	13.84	15.97	19.28	18.82	19.93	19.50	18.51	20.15	Zr	77.81	76.56	193.18	29.47	41.25	41.59	34.69	33.89	34.89	25.84	38.58	28.94	48.25	28.74	31.46	39.34	31.57	45.34	90.39	36.34	39.15	Nb	1.26	1.57	2.77	1.00	1.43	1.13	1.10	0.64	0.72	0.32	0.30	0.19	0.88	1.17	1.03	1.05	1.12	1.16	1.08	0.86	1.30	Ca	0.06	0.00	0.00	0.02	0.01	0.01	0.01	0.00	0.02	0.01	0.00	0.00	0.05	0.05	0.05	0.05	0.14	0.06	0.05	0.07	0.04	Ba	11.54	9.22	7.81	7.73	10.39	44.58	7.83	14.04	18.41	13.48	5.07	4.84	5.84	36.71	28.28	52.27	36.91	50.14	55.77	45.90	20.94	La	2.28	2.72	6.14	2.16	2.67	2.97	2.04	1.35	1.67	0.79	1.01	0.98	1.79	0.88	1.05	1.59	1.65	1.79	1.83	1.58	1.82	Ce	7.07	8.27	17.99	6.74	8.14	9.06	6.45	4.50	6.29	2.83	3.43	2.94	5.06	2.73	2.75	4.27	4.32	4.65	4.78	4.16	4.86	Pr	1.40	1.53	3.21	1.18	1.35	1.45	1.08	0.79	1.09	0.62	0.70	0.58	0.91	0.49	0.49	0.71	0.72	0.81	0.80	0.70	0.75	Nd	7.44	8.10	16.10	6.77	7.71	7.93	6.21	4.76	6.29	3.87	3.80	3.32	4.89	2.73	2.69	3.68	3.69	4.24	4.04	3.67	4.20	Sm	2.76	2.85	5.29	2.49	2.74	2.58	2.27	1.88	2.23	1.58	1.47	1.32	1.74	1.08	1.06	1.38	1.35	1.52	1.46	1.36	1.56	Eu	1.04	1.07	1.59	0.94	0.97	0.98	0.83	0.70	0.84	0.71	0.60	0.47	0.67	0.43	0.40	0.53	0.54	0.57	0.56	0.53	0.58	Gd	3.48	3.59	6.48	3.24	3.51	3.19	3.04	2.59	2.78	2.12	1.91	1.83	2.28	1.63	1.58	1.91	1.85	2.05	2.01	1.90	2.13	Tb	0.69	0.72	1.28	0.62	0.66	0.59	0.58	0.51	0.52	0.43	0.39	0.38	0.46	0.29	0.31	0.40	0.40	0.43	0.43	0.41	0.41	Dy	4.56	4.80	8.08	4.17	4.50	3.96	4.00	3.59	3.53	2.84	2.63	2.59	3.04	2.10	2.31	2.80	2.78	2.97	2.93	2.82	2.94	Ho	0.92	0.97	1.81	0.89	0.96	0.83	0.87	0.79	0.75	0.57	0.54	0.54	0.62	0.43	0.47	0.61	0.60	0.63	0.62	0.61	0.65	Er	2.75	2.89	4.73	2.49	2.73	2.36	2.47	2.29	2.18	1.67	1.64	1.63	1.89	1.34	1.53	1.91	1.90	1.98	1.97	1.91	1.95	Tm	0.43	0.46	0.73	0.39	0.43	0.36	0.39	0.36	0.35	0.26	0.26	0.27	0.30	0.21	0.26	0.32	0.32	0.33	0.33	0.32	0.32	Yb	2.78	2.88	4.38	2.44	2.68	2.22	2.41	2.28	2.11	1.63	1.66	1.71	1.96	1.36	1.72	2.12	2.12	2.17	2.21	2.11	2.08	Lu	0.43	0.44	0.64	0.37	0.42	0.34	0.37	0.36	0.33	0.25	0.26	0.27	0.31	0.21	0.26	0.34	0.34	0.35	0.36	0.34	0.34	Hf	1.92	1.77	4.54	1.11	1.35	1.28	1.23	1.13	1.18	0.86	0.95	0.77	1.22	0.87	0.89	1.11	0.90	1.24	2.19	1.08	1.20	Ta	0.10	0.12	0.23	0.07	0.10	0.08	0.08	0.04	0.05	0.03	0.03	0.02	0.07	0.07	0.06	0.09	0.10	0.11	0.10	0.09	0.10	Th	0.07	0.10	0.35	0.05	0.07	0.06	0.06	0.04	0.06	0.01	0.02	0.05	0.10	0.10	0.11	0.22	0.23	0.22	0.24	0.23	0.23	U	0.02	0.03	0.18	0.03	0.02	0.03	0.03	0.02	0.03	0.01	0.01	0.03	0.05	0.07	0.11	0.17	0.17	0.18	0.17	0.17	0.18
SiO <sub>2</sub>	48.92	48.60	59.62	49.18	50.39	48.81	50.64	49.78	49.40	46.88	47.98	51.38	49.94	50.47	56.78	53.64	52.69	54.02	49.35	54.63	54.69	TiO <sub>2</sub>	1.21	1.11	1.14	1.03	1.20	1.13	0.95	0.87	0.95	0.81	0.67	0.57	0.75	0.47	0.48	0.71	0.68	0.81	1.24	0.70	0.83	Al <sub>2</sub> O <sub>3</sub>	14.75	14.59	14.29	14.61	13.84	14.62	14.77	14.28	15.04	16.06	19.38	14.61	15.60	16.12	15.24	14.48	15.35	15.05	15.27	14.60	14.65	Fe <sub>2</sub> O <sub>3</sub>	7.66	7.94	2.78	10.27	12.32	10.50	10.80	11.00	9.80	8.40	6.45	9.41	8.29	8.57	8.72	11.74	10.37	11.99	10.58	11.83	11.50	MnO	0.18	0.12	0.11	0.18	0.23	0.18	0.18	0.17	0.17	0.17	0.12	0.16	0.16	0.21	0.15	0.17	0.18	0.16	0.17	0.17	0.10	MgO	10.85	10.21	8.56	8.25	7.80	8.00	8.48	8.87	8.64	8.10	7.42	8.58	9.11	8.42	8.55	4.25	5.28	4.43	8.30	3.84	4.39	CaO	12.33	12.63	8.18	11.44	11.53	12.49	13.04	13.08	12.03	14.28	13.89	12.74	12.64	11.70	10.74	7.05	9.35	7.25	9.99	7.25	7.56	Na <sub>2</sub> O	2.19	2.64	2.79	3.19	2.15	2.44	2.08	1.78	2.27	2.05	1.99	1.32	1.35	1.99	1.79	2.99	2.08	3.11	3.60	2.83	3.18	K <sub>2</sub> O	0.29	0.23	0.23	0.08	0.10	0.11	0.00	0.00	0.22	0.18	0.21	0.22	0.24	0.16	0.04	0.52	0.49	0.69	0.23	0.67	0.23	P <sub>2</sub> O <sub>5</sub>	0.13	0.11	0.23	0.07	0.10	0.07	0.05	0.07	0.06	0.07	0.07	0.08	0.04	0.02	0.07	0.06	0.07	0.12	0.07	0.07	0.05	LOI	0.91	0.61	1.88	2.03	1.81	0.88	0.59	0.39	0.74	0.84	0.73	0.68	0.66	2.14	0.45	2.54	1.92	1.81	1.11	1.49	1.87	Total	99.44	98.79	99.80	100.34	101.08	99.03	101.59	100.26	99.32	99.79	99.90	99.73	99.02	100.29	100.96	98.15	98.34	99.29	99.95	98.07	99.05	(ppm)																							V	300.98	299.53	278.84	278.17	328.70	262.48	278.79	286.02	231.08	187.82	214.37	256.03	308.81	231.67	285.00	439.31	402.27	431.29	403.74	334.58	390.32	Cr	311.73	240.35	74.72	479.70	189.14	267.54	424.43	437.82	380.08	456.02	314.83	469.47	338.56	183.20	114.02	22.74	12.03	10.37	42.54	32.47	46.04	Co	43.00	42.27	17.03	44.83	48.54	43.60	41.27	49.38	47.00	37.79	31.72	36.39	37.83	35.67	37.60	34.98	40.00	35.12	32.40	31.15	36.93	Zn	56.84	24.06	41.93	71.50	110.30	63.02	64.12	54.25	40.93	71.98	24.14	31.98	61.87	125.28	41.69	75.92	63.89	69.68	55.50	47.52	11.60	Ga	16.45	16.56	19.01	15.44	16.33	15.34	15.39	14.82	13.93	13.59	14.82	12.28	13.95	12.99	14.40	15.66	17.79	15.58	15.36	15.15	15.28	Rb	3.44	0.18	0.12	1.07	0.41	0.22	0.11	0.09	2.62	0.52	0.14	0.12	0.84	1.71	1.31	4.73	8.36	8.85	9.64	10.58	1.88	Sr	365.60	369.10	177.60	189.00	103.20	152.90	88.82	76.98	128.00	387.80	336.00	363.80	342.90	98.15	89.14	174.10	373.90	324.80	312.90	387.20	164.00	Y	28.95	30.51	50.99	26.70	29.07	25.54	26.72	24.13	23.31	17.27	16.29	16.78	19.58	13.84	15.97	19.28	18.82	19.93	19.50	18.51	20.15	Zr	77.81	76.56	193.18	29.47	41.25	41.59	34.69	33.89	34.89	25.84	38.58	28.94	48.25	28.74	31.46	39.34	31.57	45.34	90.39	36.34	39.15	Nb	1.26	1.57	2.77	1.00	1.43	1.13	1.10	0.64	0.72	0.32	0.30	0.19	0.88	1.17	1.03	1.05	1.12	1.16	1.08	0.86	1.30	Ca	0.06	0.00	0.00	0.02	0.01	0.01	0.01	0.00	0.02	0.01	0.00	0.00	0.05	0.05	0.05	0.05	0.14	0.06	0.05	0.07	0.04	Ba	11.54	9.22	7.81	7.73	10.39	44.58	7.83	14.04	18.41	13.48	5.07	4.84	5.84	36.71	28.28	52.27	36.91	50.14	55.77	45.90	20.94	La	2.28	2.72	6.14	2.16	2.67	2.97	2.04	1.35	1.67	0.79	1.01	0.98	1.79	0.88	1.05	1.59	1.65	1.79	1.83	1.58	1.82	Ce	7.07	8.27	17.99	6.74	8.14	9.06	6.45	4.50	6.29	2.83	3.43	2.94	5.06	2.73	2.75	4.27	4.32	4.65	4.78	4.16	4.86	Pr	1.40	1.53	3.21	1.18	1.35	1.45	1.08	0.79	1.09	0.62	0.70	0.58	0.91	0.49	0.49	0.71	0.72	0.81	0.80	0.70	0.75	Nd	7.44	8.10	16.10	6.77	7.71	7.93	6.21	4.76	6.29	3.87	3.80	3.32	4.89	2.73	2.69	3.68	3.69	4.24	4.04	3.67	4.20	Sm	2.76	2.85	5.29	2.49	2.74	2.58	2.27	1.88	2.23	1.58	1.47	1.32	1.74	1.08	1.06	1.38	1.35	1.52	1.46	1.36	1.56	Eu	1.04	1.07	1.59	0.94	0.97	0.98	0.83	0.70	0.84	0.71	0.60	0.47	0.67	0.43	0.40	0.53	0.54	0.57	0.56	0.53	0.58	Gd	3.48	3.59	6.48	3.24	3.51	3.19	3.04	2.59	2.78	2.12	1.91	1.83	2.28	1.63	1.58	1.91	1.85	2.05	2.01	1.90	2.13	Tb	0.69	0.72	1.28	0.62	0.66	0.59	0.58	0.51	0.52	0.43	0.39	0.38	0.46	0.29	0.31	0.40	0.40	0.43	0.43	0.41	0.41	Dy	4.56	4.80	8.08	4.17	4.50	3.96	4.00	3.59	3.53	2.84	2.63	2.59	3.04	2.10	2.31	2.80	2.78	2.97	2.93	2.82	2.94	Ho	0.92	0.97	1.81	0.89	0.96	0.83	0.87	0.79	0.75	0.57	0.54	0.54	0.62	0.43	0.47	0.61	0.60	0.63	0.62	0.61	0.65	Er	2.75	2.89	4.73	2.49	2.73	2.36	2.47	2.29	2.18	1.67	1.64	1.63	1.89	1.34	1.53	1.91	1.90	1.98	1.97	1.91	1.95	Tm	0.43	0.46	0.73	0.39	0.43	0.36	0.39	0.36	0.35	0.26	0.26	0.27	0.30	0.21	0.26	0.32	0.32	0.33	0.33	0.32	0.32	Yb	2.78	2.88	4.38	2.44	2.68	2.22	2.41	2.28	2.11	1.63	1.66	1.71	1.96	1.36	1.72	2.12	2.12	2.17	2.21	2.11	2.08	Lu	0.43	0.44	0.64	0.37	0.42	0.34	0.37	0.36	0.33	0.25	0.26	0.27	0.31	0.21	0.26	0.34	0.34	0.35	0.36	0.34	0.34	Hf	1.92	1.77	4.54	1.11	1.35	1.28	1.23	1.13	1.18	0.86	0.95	0.77	1.22	0.87	0.89	1.11	0.90	1.24	2.19	1.08	1.20	Ta	0.10	0.12	0.23	0.07	0.10	0.08	0.08	0.04	0.05	0.03	0.03	0.02	0.07	0.07	0.06	0.09	0.10	0.11	0.10	0.09	0.10	Th	0.07	0.10	0.35	0.05	0.07	0.06	0.06	0.04	0.06	0.01	0.02	0.05	0.10	0.10	0.11	0.22	0.23	0.22	0.24	0.23	0.23	U	0.02	0.03	0.18	0.03	0.02	0.03	0.03	0.02	0.03	0.01	0.01	0.03	0.05	0.07	0.11	0.17	0.17	0.18	0.17	0.17	0.18																							
TiO <sub>2</sub>	1.21	1.11	1.14	1.03	1.20	1.13	0.95	0.87	0.95	0.81	0.67	0.57	0.75	0.47	0.48	0.71	0.68	0.81	1.24	0.70	0.83	Al <sub>2</sub> O <sub>3</sub>	14.75	14.59	14.29	14.61	13.84	14.62	14.77	14.28	15.04	16.06	19.38	14.61	15.60	16.12	15.24	14.48	15.35	15.05	15.27	14.60	14.65	Fe <sub>2</sub> O <sub>3</sub>	7.66	7.94	2.78	10.27	12.32	10.50	10.80	11.00	9.80	8.40	6.45	9.41	8.29	8.57	8.72	11.74	10.37	11.99	10.58	11.83	11.50	MnO	0.18	0.12	0.11	0.18	0.23	0.18	0.18	0.17	0.17	0.17	0.12	0.16	0.16	0.21	0.15	0.17	0.18	0.16	0.17	0.17	0.10	MgO	10.85	10.21	8.56	8.25	7.80	8.00	8.48	8.87	8.64	8.10	7.42	8.58	9.11	8.42	8.55	4.25	5.28	4.43	8.30	3.84	4.39	CaO	12.33	12.63	8.18	11.44	11.53	12.49	13.04	13.08	12.03	14.28	13.89	12.74	12.64	11.70	10.74	7.05	9.35	7.25	9.99	7.25	7.56	Na <sub>2</sub> O	2.19	2.64	2.79	3.19	2.15	2.44	2.08	1.78	2.27	2.05	1.99	1.32	1.35	1.99	1.79	2.99	2.08	3.11	3.60	2.83	3.18	K <sub>2</sub> O	0.29	0.23	0.23	0.08	0.10	0.11	0.00	0.00	0.22	0.18	0.21	0.22	0.24	0.16	0.04	0.52	0.49	0.69	0.23	0.67	0.23	P <sub>2</sub> O <sub>5</sub>	0.13	0.11	0.23	0.07	0.10	0.07	0.05	0.07	0.06	0.07	0.07	0.08	0.04	0.02	0.07	0.06	0.07	0.12	0.07	0.07	0.05	LOI	0.91	0.61	1.88	2.03	1.81	0.88	0.59	0.39	0.74	0.84	0.73	0.68	0.66	2.14	0.45	2.54	1.92	1.81	1.11	1.49	1.87	Total	99.44	98.79	99.80	100.34	101.08	99.03	101.59	100.26	99.32	99.79	99.90	99.73	99.02	100.29	100.96	98.15	98.34	99.29	99.95	98.07	99.05	(ppm)																							V	300.98	299.53	278.84	278.17	328.70	262.48	278.79	286.02	231.08	187.82	214.37	256.03	308.81	231.67	285.00	439.31	402.27	431.29	403.74	334.58	390.32	Cr	311.73	240.35	74.72	479.70	189.14	267.54	424.43	437.82	380.08	456.02	314.83	469.47	338.56	183.20	114.02	22.74	12.03	10.37	42.54	32.47	46.04	Co	43.00	42.27	17.03	44.83	48.54	43.60	41.27	49.38	47.00	37.79	31.72	36.39	37.83	35.67	37.60	34.98	40.00	35.12	32.40	31.15	36.93	Zn	56.84	24.06	41.93	71.50	110.30	63.02	64.12	54.25	40.93	71.98	24.14	31.98	61.87	125.28	41.69	75.92	63.89	69.68	55.50	47.52	11.60	Ga	16.45	16.56	19.01	15.44	16.33	15.34	15.39	14.82	13.93	13.59	14.82	12.28	13.95	12.99	14.40	15.66	17.79	15.58	15.36	15.15	15.28	Rb	3.44	0.18	0.12	1.07	0.41	0.22	0.11	0.09	2.62	0.52	0.14	0.12	0.84	1.71	1.31	4.73	8.36	8.85	9.64	10.58	1.88	Sr	365.60	369.10	177.60	189.00	103.20	152.90	88.82	76.98	128.00	387.80	336.00	363.80	342.90	98.15	89.14	174.10	373.90	324.80	312.90	387.20	164.00	Y	28.95	30.51	50.99	26.70	29.07	25.54	26.72	24.13	23.31	17.27	16.29	16.78	19.58	13.84	15.97	19.28	18.82	19.93	19.50	18.51	20.15	Zr	77.81	76.56	193.18	29.47	41.25	41.59	34.69	33.89	34.89	25.84	38.58	28.94	48.25	28.74	31.46	39.34	31.57	45.34	90.39	36.34	39.15	Nb	1.26	1.57	2.77	1.00	1.43	1.13	1.10	0.64	0.72	0.32	0.30	0.19	0.88	1.17	1.03	1.05	1.12	1.16	1.08	0.86	1.30	Ca	0.06	0.00	0.00	0.02	0.01	0.01	0.01	0.00	0.02	0.01	0.00	0.00	0.05	0.05	0.05	0.05	0.14	0.06	0.05	0.07	0.04	Ba	11.54	9.22	7.81	7.73	10.39	44.58	7.83	14.04	18.41	13.48	5.07	4.84	5.84	36.71	28.28	52.27	36.91	50.14	55.77	45.90	20.94	La	2.28	2.72	6.14	2.16	2.67	2.97	2.04	1.35	1.67	0.79	1.01	0.98	1.79	0.88	1.05	1.59	1.65	1.79	1.83	1.58	1.82	Ce	7.07	8.27	17.99	6.74	8.14	9.06	6.45	4.50	6.29	2.83	3.43	2.94	5.06	2.73	2.75	4.27	4.32	4.65	4.78	4.16	4.86	Pr	1.40	1.53	3.21	1.18	1.35	1.45	1.08	0.79	1.09	0.62	0.70	0.58	0.91	0.49	0.49	0.71	0.72	0.81	0.80	0.70	0.75	Nd	7.44	8.10	16.10	6.77	7.71	7.93	6.21	4.76	6.29	3.87	3.80	3.32	4.89	2.73	2.69	3.68	3.69	4.24	4.04	3.67	4.20	Sm	2.76	2.85	5.29	2.49	2.74	2.58	2.27	1.88	2.23	1.58	1.47	1.32	1.74	1.08	1.06	1.38	1.35	1.52	1.46	1.36	1.56	Eu	1.04	1.07	1.59	0.94	0.97	0.98	0.83	0.70	0.84	0.71	0.60	0.47	0.67	0.43	0.40	0.53	0.54	0.57	0.56	0.53	0.58	Gd	3.48	3.59	6.48	3.24	3.51	3.19	3.04	2.59	2.78	2.12	1.91	1.83	2.28	1.63	1.58	1.91	1.85	2.05	2.01	1.90	2.13	Tb	0.69	0.72	1.28	0.62	0.66	0.59	0.58	0.51	0.52	0.43	0.39	0.38	0.46	0.29	0.31	0.40	0.40	0.43	0.43	0.41	0.41	Dy	4.56	4.80	8.08	4.17	4.50	3.96	4.00	3.59	3.53	2.84	2.63	2.59	3.04	2.10	2.31	2.80	2.78	2.97	2.93	2.82	2.94	Ho	0.92	0.97	1.81	0.89	0.96	0.83	0.87	0.79	0.75	0.57	0.54	0.54	0.62	0.43	0.47	0.61	0.60	0.63	0.62	0.61	0.65	Er	2.75	2.89	4.73	2.49	2.73	2.36	2.47	2.29	2.18	1.67	1.64	1.63	1.89	1.34	1.53	1.91	1.90	1.98	1.97	1.91	1.95	Tm	0.43	0.46	0.73	0.39	0.43	0.36	0.39	0.36	0.35	0.26	0.26	0.27	0.30	0.21	0.26	0.32	0.32	0.33	0.33	0.32	0.32	Yb	2.78	2.88	4.38	2.44	2.68	2.22	2.41	2.28	2.11	1.63	1.66	1.71	1.96	1.36	1.72	2.12	2.12	2.17	2.21	2.11	2.08	Lu	0.43	0.44	0.64	0.37	0.42	0.34	0.37	0.36	0.33	0.25	0.26	0.27	0.31	0.21	0.26	0.34	0.34	0.35	0.36	0.34	0.34	Hf	1.92	1.77	4.54	1.11	1.35	1.28	1.23	1.13	1.18	0.86	0.95	0.77	1.22	0.87	0.89	1.11	0.90	1.24	2.19	1.08	1.20	Ta	0.10	0.12	0.23	0.07	0.10	0.08	0.08	0.04	0.05	0.03	0.03	0.02	0.07	0.07	0.06	0.09	0.10	0.11	0.10	0.09	0.10	Th	0.07	0.10	0.35	0.05	0.07	0.06	0.06	0.04	0.06	0.01	0.02	0.05	0.10	0.10	0.11	0.22	0.23	0.22	0.24	0.23	0.23	U	0.02	0.03	0.18	0.03	0.02	0.03	0.03	0.02	0.03	0.01	0.01	0.03	0.05	0.07	0.11	0.17	0.17	0.18	0.17	0.17	0.18																																													
Al <sub>2</sub> O <sub>3</sub>	14.75	14.59	14.29	14.61	13.84	14.62	14.77	14.28	15.04	16.06	19.38	14.61	15.60	16.12	15.24	14.48	15.35	15.05	15.27	14.60	14.65	Fe <sub>2</sub> O <sub>3</sub>	7.66	7.94	2.78	10.27	12.32	10.50	10.80	11.00	9.80	8.40	6.45	9.41	8.29	8.57	8.72	11.74	10.37	11.99	10.58	11.83	11.50	MnO	0.18	0.12	0.11	0.18	0.23	0.18	0.18	0.17	0.17	0.17	0.12	0.16	0.16	0.21	0.15	0.17	0.18	0.16	0.17	0.17	0.10	MgO	10.85	10.21	8.56	8.25	7.80	8.00	8.48	8.87	8.64	8.10	7.42	8.58	9.11	8.42	8.55	4.25	5.28	4.43	8.30	3.84	4.39	CaO	12.33	12.63	8.18	11.44	11.53	12.49	13.04	13.08	12.03	14.28	13.89	12.74	12.64	11.70	10.74	7.05	9.35	7.25	9.99	7.25	7.56	Na <sub>2</sub> O	2.19	2.64	2.79	3.19	2.15	2.44	2.08	1.78	2.27	2.05	1.99	1.32	1.35	1.99	1.79	2.99	2.08	3.11	3.60	2.83	3.18	K <sub>2</sub> O	0.29	0.23	0.23	0.08	0.10	0.11	0.00	0.00	0.22	0.18	0.21	0.22	0.24	0.16	0.04	0.52	0.49	0.69	0.23	0.67	0.23	P <sub>2</sub> O <sub>5</sub>	0.13	0.11	0.23	0.07	0.10	0.07	0.05	0.07	0.06	0.07	0.07	0.08	0.04	0.02	0.07	0.06	0.07	0.12	0.07	0.07	0.05	LOI	0.91	0.61	1.88	2.03	1.81	0.88	0.59	0.39	0.74	0.84	0.73	0.68	0.66	2.14	0.45	2.54	1.92	1.81	1.11	1.49	1.87	Total	99.44	98.79	99.80	100.34	101.08	99.03	101.59	100.26	99.32	99.79	99.90	99.73	99.02	100.29	100.96	98.15	98.34	99.29	99.95	98.07	99.05	(ppm)																							V	300.98	299.53	278.84	278.17	328.70	262.48	278.79	286.02	231.08	187.82	214.37	256.03	308.81	231.67	285.00	439.31	402.27	431.29	403.74	334.58	390.32	Cr	311.73	240.35	74.72	479.70	189.14	267.54	424.43	437.82	380.08	456.02	314.83	469.47	338.56	183.20	114.02	22.74	12.03	10.37	42.54	32.47	46.04	Co	43.00	42.27	17.03	44.83	48.54	43.60	41.27	49.38	47.00	37.79	31.72	36.39	37.83	35.67	37.60	34.98	40.00	35.12	32.40	31.15	36.93	Zn	56.84	24.06	41.93	71.50	110.30	63.02	64.12	54.25	40.93	71.98	24.14	31.98	61.87	125.28	41.69	75.92	63.89	69.68	55.50	47.52	11.60	Ga	16.45	16.56	19.01	15.44	16.33	15.34	15.39	14.82	13.93	13.59	14.82	12.28	13.95	12.99	14.40	15.66	17.79	15.58	15.36	15.15	15.28	Rb	3.44	0.18	0.12	1.07	0.41	0.22	0.11	0.09	2.62	0.52	0.14	0.12	0.84	1.71	1.31	4.73	8.36	8.85	9.64	10.58	1.88	Sr	365.60	369.10	177.60	189.00	103.20	152.90	88.82	76.98	128.00	387.80	336.00	363.80	342.90	98.15	89.14	174.10	373.90	324.80	312.90	387.20	164.00	Y	28.95	30.51	50.99	26.70	29.07	25.54	26.72	24.13	23.31	17.27	16.29	16.78	19.58	13.84	15.97	19.28	18.82	19.93	19.50	18.51	20.15	Zr	77.81	76.56	193.18	29.47	41.25	41.59	34.69	33.89	34.89	25.84	38.58	28.94	48.25	28.74	31.46	39.34	31.57	45.34	90.39	36.34	39.15	Nb	1.26	1.57	2.77	1.00	1.43	1.13	1.10	0.64	0.72	0.32	0.30	0.19	0.88	1.17	1.03	1.05	1.12	1.16	1.08	0.86	1.30	Ca	0.06	0.00	0.00	0.02	0.01	0.01	0.01	0.00	0.02	0.01	0.00	0.00	0.05	0.05	0.05	0.05	0.14	0.06	0.05	0.07	0.04	Ba	11.54	9.22	7.81	7.73	10.39	44.58	7.83	14.04	18.41	13.48	5.07	4.84	5.84	36.71	28.28	52.27	36.91	50.14	55.77	45.90	20.94	La	2.28	2.72	6.14	2.16	2.67	2.97	2.04	1.35	1.67	0.79	1.01	0.98	1.79	0.88	1.05	1.59	1.65	1.79	1.83	1.58	1.82	Ce	7.07	8.27	17.99	6.74	8.14	9.06	6.45	4.50	6.29	2.83	3.43	2.94	5.06	2.73	2.75	4.27	4.32	4.65	4.78	4.16	4.86	Pr	1.40	1.53	3.21	1.18	1.35	1.45	1.08	0.79	1.09	0.62	0.70	0.58	0.91	0.49	0.49	0.71	0.72	0.81	0.80	0.70	0.75	Nd	7.44	8.10	16.10	6.77	7.71	7.93	6.21	4.76	6.29	3.87	3.80	3.32	4.89	2.73	2.69	3.68	3.69	4.24	4.04	3.67	4.20	Sm	2.76	2.85	5.29	2.49	2.74	2.58	2.27	1.88	2.23	1.58	1.47	1.32	1.74	1.08	1.06	1.38	1.35	1.52	1.46	1.36	1.56	Eu	1.04	1.07	1.59	0.94	0.97	0.98	0.83	0.70	0.84	0.71	0.60	0.47	0.67	0.43	0.40	0.53	0.54	0.57	0.56	0.53	0.58	Gd	3.48	3.59	6.48	3.24	3.51	3.19	3.04	2.59	2.78	2.12	1.91	1.83	2.28	1.63	1.58	1.91	1.85	2.05	2.01	1.90	2.13	Tb	0.69	0.72	1.28	0.62	0.66	0.59	0.58	0.51	0.52	0.43	0.39	0.38	0.46	0.29	0.31	0.40	0.40	0.43	0.43	0.41	0.41	Dy	4.56	4.80	8.08	4.17	4.50	3.96	4.00	3.59	3.53	2.84	2.63	2.59	3.04	2.10	2.31	2.80	2.78	2.97	2.93	2.82	2.94	Ho	0.92	0.97	1.81	0.89	0.96	0.83	0.87	0.79	0.75	0.57	0.54	0.54	0.62	0.43	0.47	0.61	0.60	0.63	0.62	0.61	0.65	Er	2.75	2.89	4.73	2.49	2.73	2.36	2.47	2.29	2.18	1.67	1.64	1.63	1.89	1.34	1.53	1.91	1.90	1.98	1.97	1.91	1.95	Tm	0.43	0.46	0.73	0.39	0.43	0.36	0.39	0.36	0.35	0.26	0.26	0.27	0.30	0.21	0.26	0.32	0.32	0.33	0.33	0.32	0.32	Yb	2.78	2.88	4.38	2.44	2.68	2.22	2.41	2.28	2.11	1.63	1.66	1.71	1.96	1.36	1.72	2.12	2.12	2.17	2.21	2.11	2.08	Lu	0.43	0.44	0.64	0.37	0.42	0.34	0.37	0.36	0.33	0.25	0.26	0.27	0.31	0.21	0.26	0.34	0.34	0.35	0.36	0.34	0.34	Hf	1.92	1.77	4.54	1.11	1.35	1.28	1.23	1.13	1.18	0.86	0.95	0.77	1.22	0.87	0.89	1.11	0.90	1.24	2.19	1.08	1.20	Ta	0.10	0.12	0.23	0.07	0.10	0.08	0.08	0.04	0.05	0.03	0.03	0.02	0.07	0.07	0.06	0.09	0.10	0.11	0.10	0.09	0.10	Th	0.07	0.10	0.35	0.05	0.07	0.06	0.06	0.04	0.06	0.01	0.02	0.05	0.10	0.10	0.11	0.22	0.23	0.22	0.24	0.23	0.23	U	0.02	0.03	0.18	0.03	0.02	0.03	0.03	0.02	0.03	0.01	0.01	0.03	0.05	0.07	0.11	0.17	0.17	0.18	0.17	0.17	0.18																																																																			
Fe <sub>2</sub> O <sub>3</sub>	7.66	7.94	2.78	10.27	12.32	10.50	10.80	11.00	9.80	8.40	6.45	9.41	8.29	8.57	8.72	11.74	10.37	11.99	10.58	11.83	11.50	MnO	0.18	0.12	0.11	0.18	0.23	0.18	0.18	0.17	0.17	0.17	0.12	0.16	0.16	0.21	0.15	0.17	0.18	0.16	0.17	0.17	0.10	MgO	10.85	10.21	8.56	8.25	7.80	8.00	8.48	8.87	8.64	8.10	7.42	8.58	9.11	8.42	8.55	4.25	5.28	4.43	8.30	3.84	4.39	CaO	12.33	12.63	8.18	11.44	11.53	12.49	13.04	13.08	12.03	14.28	13.89	12.74	12.64	11.70	10.74	7.05	9.35	7.25	9.99	7.25	7.56	Na <sub>2</sub> O	2.19	2.64	2.79	3.19	2.15	2.44	2.08	1.78	2.27	2.05	1.99	1.32	1.35	1.99	1.79	2.99	2.08	3.11	3.60	2.83	3.18	K <sub>2</sub> O	0.29	0.23	0.23	0.08	0.10	0.11	0.00	0.00	0.22	0.18	0.21	0.22	0.24	0.16	0.04	0.52	0.49	0.69	0.23	0.67	0.23	P <sub>2</sub> O <sub>5</sub>	0.13	0.11	0.23	0.07	0.10	0.07	0.05	0.07	0.06	0.07	0.07	0.08	0.04	0.02	0.07	0.06	0.07	0.12	0.07	0.07	0.05	LOI	0.91	0.61	1.88	2.03	1.81	0.88	0.59	0.39	0.74	0.84	0.73	0.68	0.66	2.14	0.45	2.54	1.92	1.81	1.11	1.49	1.87	Total	99.44	98.79	99.80	100.34	101.08	99.03	101.59	100.26	99.32	99.79	99.90	99.73	99.02	100.29	100.96	98.15	98.34	99.29	99.95	98.07	99.05	(ppm)																							V	300.98	299.53	278.84	278.17	328.70	262.48	278.79	286.02	231.08	187.82	214.37	256.03	308.81	231.67	285.00	439.31	402.27	431.29	403.74	334.58	390.32	Cr	311.73	240.35	74.72	479.70	189.14	267.54	424.43	437.82	380.08	456.02	314.83	469.47	338.56	183.20	114.02	22.74	12.03	10.37	42.54	32.47	46.04	Co	43.00	42.27	17.03	44.83	48.54	43.60	41.27	49.38	47.00	37.79	31.72	36.39	37.83	35.67	37.60	34.98	40.00	35.12	32.40	31.15	36.93	Zn	56.84	24.06	41.93	71.50	110.30	63.02	64.12	54.25	40.93	71.98	24.14	31.98	61.87	125.28	41.69	75.92	63.89	69.68	55.50	47.52	11.60	Ga	16.45	16.56	19.01	15.44	16.33	15.34	15.39	14.82	13.93	13.59	14.82	12.28	13.95	12.99	14.40	15.66	17.79	15.58	15.36	15.15	15.28	Rb	3.44	0.18	0.12	1.07	0.41	0.22	0.11	0.09	2.62	0.52	0.14	0.12	0.84	1.71	1.31	4.73	8.36	8.85	9.64	10.58	1.88	Sr	365.60	369.10	177.60	189.00	103.20	152.90	88.82	76.98	128.00	387.80	336.00	363.80	342.90	98.15	89.14	174.10	373.90	324.80	312.90	387.20	164.00	Y	28.95	30.51	50.99	26.70	29.07	25.54	26.72	24.13	23.31	17.27	16.29	16.78	19.58	13.84	15.97	19.28	18.82	19.93	19.50	18.51	20.15	Zr	77.81	76.56	193.18	29.47	41.25	41.59	34.69	33.89	34.89	25.84	38.58	28.94	48.25	28.74	31.46	39.34	31.57	45.34	90.39	36.34	39.15	Nb	1.26	1.57	2.77	1.00	1.43	1.13	1.10	0.64	0.72	0.32	0.30	0.19	0.88	1.17	1.03	1.05	1.12	1.16	1.08	0.86	1.30	Ca	0.06	0.00	0.00	0.02	0.01	0.01	0.01	0.00	0.02	0.01	0.00	0.00	0.05	0.05	0.05	0.05	0.14	0.06	0.05	0.07	0.04	Ba	11.54	9.22	7.81	7.73	10.39	44.58	7.83	14.04	18.41	13.48	5.07	4.84	5.84	36.71	28.28	52.27	36.91	50.14	55.77	45.90	20.94	La	2.28	2.72	6.14	2.16	2.67	2.97	2.04	1.35	1.67	0.79	1.01	0.98	1.79	0.88	1.05	1.59	1.65	1.79	1.83	1.58	1.82	Ce	7.07	8.27	17.99	6.74	8.14	9.06	6.45	4.50	6.29	2.83	3.43	2.94	5.06	2.73	2.75	4.27	4.32	4.65	4.78	4.16	4.86	Pr	1.40	1.53	3.21	1.18	1.35	1.45	1.08	0.79	1.09	0.62	0.70	0.58	0.91	0.49	0.49	0.71	0.72	0.81	0.80	0.70	0.75	Nd	7.44	8.10	16.10	6.77	7.71	7.93	6.21	4.76	6.29	3.87	3.80	3.32	4.89	2.73	2.69	3.68	3.69	4.24	4.04	3.67	4.20	Sm	2.76	2.85	5.29	2.49	2.74	2.58	2.27	1.88	2.23	1.58	1.47	1.32	1.74	1.08	1.06	1.38	1.35	1.52	1.46	1.36	1.56	Eu	1.04	1.07	1.59	0.94	0.97	0.98	0.83	0.70	0.84	0.71	0.60	0.47	0.67	0.43	0.40	0.53	0.54	0.57	0.56	0.53	0.58	Gd	3.48	3.59	6.48	3.24	3.51	3.19	3.04	2.59	2.78	2.12	1.91	1.83	2.28	1.63	1.58	1.91	1.85	2.05	2.01	1.90	2.13	Tb	0.69	0.72	1.28	0.62	0.66	0.59	0.58	0.51	0.52	0.43	0.39	0.38	0.46	0.29	0.31	0.40	0.40	0.43	0.43	0.41	0.41	Dy	4.56	4.80	8.08	4.17	4.50	3.96	4.00	3.59	3.53	2.84	2.63	2.59	3.04	2.10	2.31	2.80	2.78	2.97	2.93	2.82	2.94	Ho	0.92	0.97	1.81	0.89	0.96	0.83	0.87	0.79	0.75	0.57	0.54	0.54	0.62	0.43	0.47	0.61	0.60	0.63	0.62	0.61	0.65	Er	2.75	2.89	4.73	2.49	2.73	2.36	2.47	2.29	2.18	1.67	1.64	1.63	1.89	1.34	1.53	1.91	1.90	1.98	1.97	1.91	1.95	Tm	0.43	0.46	0.73	0.39	0.43	0.36	0.39	0.36	0.35	0.26	0.26	0.27	0.30	0.21	0.26	0.32	0.32	0.33	0.33	0.32	0.32	Yb	2.78	2.88	4.38	2.44	2.68	2.22	2.41	2.28	2.11	1.63	1.66	1.71	1.96	1.36	1.72	2.12	2.12	2.17	2.21	2.11	2.08	Lu	0.43	0.44	0.64	0.37	0.42	0.34	0.37	0.36	0.33	0.25	0.26	0.27	0.31	0.21	0.26	0.34	0.34	0.35	0.36	0.34	0.34	Hf	1.92	1.77	4.54	1.11	1.35	1.28	1.23	1.13	1.18	0.86	0.95	0.77	1.22	0.87	0.89	1.11	0.90	1.24	2.19	1.08	1.20	Ta	0.10	0.12	0.23	0.07	0.10	0.08	0.08	0.04	0.05	0.03	0.03	0.02	0.07	0.07	0.06	0.09	0.10	0.11	0.10	0.09	0.10	Th	0.07	0.10	0.35	0.05	0.07	0.06	0.06	0.04	0.06	0.01	0.02	0.05	0.10	0.10	0.11	0.22	0.23	0.22	0.24	0.23	0.23	U	0.02	0.03	0.18	0.03	0.02	0.03	0.03	0.02	0.03	0.01	0.01	0.03	0.05	0.07	0.11	0.17	0.17	0.18	0.17	0.17	0.18																																																																																									
MnO	0.18	0.12	0.11	0.18	0.23	0.18	0.18	0.17	0.17	0.17	0.12	0.16	0.16	0.21	0.15	0.17	0.18	0.16	0.17	0.17	0.10	MgO	10.85	10.21	8.56	8.25	7.80	8.00	8.48	8.87	8.64	8.10	7.42	8.58	9.11	8.42	8.55	4.25	5.28	4.43	8.30	3.84	4.39	CaO	12.33	12.63	8.18	11.44	11.53	12.49	13.04	13.08	12.03	14.28	13.89	12.74	12.64	11.70	10.74	7.05	9.35	7.25	9.99	7.25	7.56	Na <sub>2</sub> O	2.19	2.64	2.79	3.19	2.15	2.44	2.08	1.78	2.27	2.05	1.99	1.32	1.35	1.99	1.79	2.99	2.08	3.11	3.60	2.83	3.18	K <sub>2</sub> O	0.29	0.23	0.23	0.08	0.10	0.11	0.00	0.00	0.22	0.18	0.21	0.22	0.24	0.16	0.04	0.52	0.49	0.69	0.23	0.67	0.23	P <sub>2</sub> O <sub>5</sub>	0.13	0.11	0.23	0.07	0.10	0.07	0.05	0.07	0.06	0.07	0.07	0.08	0.04	0.02	0.07	0.06	0.07	0.12	0.07	0.07	0.05	LOI	0.91	0.61	1.88	2.03	1.81	0.88	0.59	0.39	0.74	0.84	0.73	0.68	0.66	2.14	0.45	2.54	1.92	1.81	1.11	1.49	1.87	Total	99.44	98.79	99.80	100.34	101.08	99.03	101.59	100.26	99.32	99.79	99.90	99.73	99.02	100.29	100.96	98.15	98.34	99.29	99.95	98.07	99.05	(ppm)																							V	300.98	299.53	278.84	278.17	328.70	262.48	278.79	286.02	231.08	187.82	214.37	256.03	308.81	231.67	285.00	439.31	402.27	431.29	403.74	334.58	390.32	Cr	311.73	240.35	74.72	479.70	189.14	267.54	424.43	437.82	380.08	456.02	314.83	469.47	338.56	183.20	114.02	22.74	12.03	10.37	42.54	32.47	46.04	Co	43.00	42.27	17.03	44.83	48.54	43.60	41.27	49.38	47.00	37.79	31.72	36.39	37.83	35.67	37.60	34.98	40.00	35.12	32.40	31.15	36.93	Zn	56.84	24.06	41.93	71.50	110.30	63.02	64.12	54.25	40.93	71.98	24.14	31.98	61.87	125.28	41.69	75.92	63.89	69.68	55.50	47.52	11.60	Ga	16.45	16.56	19.01	15.44	16.33	15.34	15.39	14.82	13.93	13.59	14.82	12.28	13.95	12.99	14.40	15.66	17.79	15.58	15.36	15.15	15.28	Rb	3.44	0.18	0.12	1.07	0.41	0.22	0.11	0.09	2.62	0.52	0.14	0.12	0.84	1.71	1.31	4.73	8.36	8.85	9.64	10.58	1.88	Sr	365.60	369.10	177.60	189.00	103.20	152.90	88.82	76.98	128.00	387.80	336.00	363.80	342.90	98.15	89.14	174.10	373.90	324.80	312.90	387.20	164.00	Y	28.95	30.51	50.99	26.70	29.07	25.54	26.72	24.13	23.31	17.27	16.29	16.78	19.58	13.84	15.97	19.28	18.82	19.93	19.50	18.51	20.15	Zr	77.81	76.56	193.18	29.47	41.25	41.59	34.69	33.89	34.89	25.84	38.58	28.94	48.25	28.74	31.46	39.34	31.57	45.34	90.39	36.34	39.15	Nb	1.26	1.57	2.77	1.00	1.43	1.13	1.10	0.64	0.72	0.32	0.30	0.19	0.88	1.17	1.03	1.05	1.12	1.16	1.08	0.86	1.30	Ca	0.06	0.00	0.00	0.02	0.01	0.01	0.01	0.00	0.02	0.01	0.00	0.00	0.05	0.05	0.05	0.05	0.14	0.06	0.05	0.07	0.04	Ba	11.54	9.22	7.81	7.73	10.39	44.58	7.83	14.04	18.41	13.48	5.07	4.84	5.84	36.71	28.28	52.27	36.91	50.14	55.77	45.90	20.94	La	2.28	2.72	6.14	2.16	2.67	2.97	2.04	1.35	1.67	0.79	1.01	0.98	1.79	0.88	1.05	1.59	1.65	1.79	1.83	1.58	1.82	Ce	7.07	8.27	17.99	6.74	8.14	9.06	6.45	4.50	6.29	2.83	3.43	2.94	5.06	2.73	2.75	4.27	4.32	4.65	4.78	4.16	4.86	Pr	1.40	1.53	3.21	1.18	1.35	1.45	1.08	0.79	1.09	0.62	0.70	0.58	0.91	0.49	0.49	0.71	0.72	0.81	0.80	0.70	0.75	Nd	7.44	8.10	16.10	6.77	7.71	7.93	6.21	4.76	6.29	3.87	3.80	3.32	4.89	2.73	2.69	3.68	3.69	4.24	4.04	3.67	4.20	Sm	2.76	2.85	5.29	2.49	2.74	2.58	2.27	1.88	2.23	1.58	1.47	1.32	1.74	1.08	1.06	1.38	1.35	1.52	1.46	1.36	1.56	Eu	1.04	1.07	1.59	0.94	0.97	0.98	0.83	0.70	0.84	0.71	0.60	0.47	0.67	0.43	0.40	0.53	0.54	0.57	0.56	0.53	0.58	Gd	3.48	3.59	6.48	3.24	3.51	3.19	3.04	2.59	2.78	2.12	1.91	1.83	2.28	1.63	1.58	1.91	1.85	2.05	2.01	1.90	2.13	Tb	0.69	0.72	1.28	0.62	0.66	0.59	0.58	0.51	0.52	0.43	0.39	0.38	0.46	0.29	0.31	0.40	0.40	0.43	0.43	0.41	0.41	Dy	4.56	4.80	8.08	4.17	4.50	3.96	4.00	3.59	3.53	2.84	2.63	2.59	3.04	2.10	2.31	2.80	2.78	2.97	2.93	2.82	2.94	Ho	0.92	0.97	1.81	0.89	0.96	0.83	0.87	0.79	0.75	0.57	0.54	0.54	0.62	0.43	0.47	0.61	0.60	0.63	0.62	0.61	0.65	Er	2.75	2.89	4.73	2.49	2.73	2.36	2.47	2.29	2.18	1.67	1.64	1.63	1.89	1.34	1.53	1.91	1.90	1.98	1.97	1.91	1.95	Tm	0.43	0.46	0.73	0.39	0.43	0.36	0.39	0.36	0.35	0.26	0.26	0.27	0.30	0.21	0.26	0.32	0.32	0.33	0.33	0.32	0.32	Yb	2.78	2.88	4.38	2.44	2.68	2.22	2.41	2.28	2.11	1.63	1.66	1.71	1.96	1.36	1.72	2.12	2.12	2.17	2.21	2.11	2.08	Lu	0.43	0.44	0.64	0.37	0.42	0.34	0.37	0.36	0.33	0.25	0.26	0.27	0.31	0.21	0.26	0.34	0.34	0.35	0.36	0.34	0.34	Hf	1.92	1.77	4.54	1.11	1.35	1.28	1.23	1.13	1.18	0.86	0.95	0.77	1.22	0.87	0.89	1.11	0.90	1.24	2.19	1.08	1.20	Ta	0.10	0.12	0.23	0.07	0.10	0.08	0.08	0.04	0.05	0.03	0.03	0.02	0.07	0.07	0.06	0.09	0.10	0.11	0.10	0.09	0.10	Th	0.07	0.10	0.35	0.05	0.07	0.06	0.06	0.04	0.06	0.01	0.02	0.05	0.10	0.10	0.11	0.22	0.23	0.22	0.24	0.23	0.23	U	0.02	0.03	0.18	0.03	0.02	0.03	0.03	0.02	0.03	0.01	0.01	0.03	0.05	0.07	0.11	0.17	0.17	0.18	0.17	0.17	0.18																																																																																																															
MgO	10.85	10.21	8.56	8.25	7.80	8.00	8.48	8.87	8.64	8.10	7.42	8.58	9.11	8.42	8.55	4.25	5.28	4.43	8.30	3.84	4.39	CaO	12.33	12.63	8.18	11.44	11.53	12.49	13.04	13.08	12.03	14.28	13.89	12.74	12.64	11.70	10.74	7.05	9.35	7.25	9.99	7.25	7.56	Na <sub>2</sub> O	2.19	2.64	2.79	3.19	2.15	2.44	2.08	1.78	2.27	2.05	1.99	1.32	1.35	1.99	1.79	2.99	2.08	3.11	3.60	2.83	3.18	K <sub>2</sub> O	0.29	0.23	0.23	0.08	0.10	0.11	0.00	0.00	0.22	0.18	0.21	0.22	0.24	0.16	0.04	0.52	0.49	0.69	0.23	0.67	0.23	P <sub>2</sub> O <sub>5</sub>	0.13	0.11	0.23	0.07	0.10	0.07	0.05	0.07	0.06	0.07	0.07	0.08	0.04	0.02	0.07	0.06	0.07	0.12	0.07	0.07	0.05	LOI	0.91	0.61	1.88	2.03	1.81	0.88	0.59	0.39	0.74	0.84	0.73	0.68	0.66	2.14	0.45	2.54	1.92	1.81	1.11	1.49	1.87	Total	99.44	98.79	99.80	100.34	101.08	99.03	101.59	100.26	99.32	99.79	99.90	99.73	99.02	100.29	100.96	98.15	98.34	99.29	99.95	98.07	99.05	(ppm)																							V	300.98	299.53	278.84	278.17	328.70	262.48	278.79	286.02	231.08	187.82	214.37	256.03	308.81	231.67	285.00	439.31	402.27	431.29	403.74	334.58	390.32	Cr	311.73	240.35	74.72	479.70	189.14	267.54	424.43	437.82	380.08	456.02	314.83	469.47	338.56	183.20	114.02	22.74	12.03	10.37	42.54	32.47	46.04	Co	43.00	42.27	17.03	44.83	48.54	43.60	41.27	49.38	47.00	37.79	31.72	36.39	37.83	35.67	37.60	34.98	40.00	35.12	32.40	31.15	36.93	Zn	56.84	24.06	41.93	71.50	110.30	63.02	64.12	54.25	40.93	71.98	24.14	31.98	61.87	125.28	41.69	75.92	63.89	69.68	55.50	47.52	11.60	Ga	16.45	16.56	19.01	15.44	16.33	15.34	15.39	14.82	13.93	13.59	14.82	12.28	13.95	12.99	14.40	15.66	17.79	15.58	15.36	15.15	15.28	Rb	3.44	0.18	0.12	1.07	0.41	0.22	0.11	0.09	2.62	0.52	0.14	0.12	0.84	1.71	1.31	4.73	8.36	8.85	9.64	10.58	1.88	Sr	365.60	369.10	177.60	189.00	103.20	152.90	88.82	76.98	128.00	387.80	336.00	363.80	342.90	98.15	89.14	174.10	373.90	324.80	312.90	387.20	164.00	Y	28.95	30.51	50.99	26.70	29.07	25.54	26.72	24.13	23.31	17.27	16.29	16.78	19.58	13.84	15.97	19.28	18.82	19.93	19.50	18.51	20.15	Zr	77.81	76.56	193.18	29.47	41.25	41.59	34.69	33.89	34.89	25.84	38.58	28.94	48.25	28.74	31.46	39.34	31.57	45.34	90.39	36.34	39.15	Nb	1.26	1.57	2.77	1.00	1.43	1.13	1.10	0.64	0.72	0.32	0.30	0.19	0.88	1.17	1.03	1.05	1.12	1.16	1.08	0.86	1.30	Ca	0.06	0.00	0.00	0.02	0.01	0.01	0.01	0.00	0.02	0.01	0.00	0.00	0.05	0.05	0.05	0.05	0.14	0.06	0.05	0.07	0.04	Ba	11.54	9.22	7.81	7.73	10.39	44.58	7.83	14.04	18.41	13.48	5.07	4.84	5.84	36.71	28.28	52.27	36.91	50.14	55.77	45.90	20.94	La	2.28	2.72	6.14	2.16	2.67	2.97	2.04	1.35	1.67	0.79	1.01	0.98	1.79	0.88	1.05	1.59	1.65	1.79	1.83	1.58	1.82	Ce	7.07	8.27	17.99	6.74	8.14	9.06	6.45	4.50	6.29	2.83	3.43	2.94	5.06	2.73	2.75	4.27	4.32	4.65	4.78	4.16	4.86	Pr	1.40	1.53	3.21	1.18	1.35	1.45	1.08	0.79	1.09	0.62	0.70	0.58	0.91	0.49	0.49	0.71	0.72	0.81	0.80	0.70	0.75	Nd	7.44	8.10	16.10	6.77	7.71	7.93	6.21	4.76	6.29	3.87	3.80	3.32	4.89	2.73	2.69	3.68	3.69	4.24	4.04	3.67	4.20	Sm	2.76	2.85	5.29	2.49	2.74	2.58	2.27	1.88	2.23	1.58	1.47	1.32	1.74	1.08	1.06	1.38	1.35	1.52	1.46	1.36	1.56	Eu	1.04	1.07	1.59	0.94	0.97	0.98	0.83	0.70	0.84	0.71	0.60	0.47	0.67	0.43	0.40	0.53	0.54	0.57	0.56	0.53	0.58	Gd	3.48	3.59	6.48	3.24	3.51	3.19	3.04	2.59	2.78	2.12	1.91	1.83	2.28	1.63	1.58	1.91	1.85	2.05	2.01	1.90	2.13	Tb	0.69	0.72	1.28	0.62	0.66	0.59	0.58	0.51	0.52	0.43	0.39	0.38	0.46	0.29	0.31	0.40	0.40	0.43	0.43	0.41	0.41	Dy	4.56	4.80	8.08	4.17	4.50	3.96	4.00	3.59	3.53	2.84	2.63	2.59	3.04	2.10	2.31	2.80	2.78	2.97	2.93	2.82	2.94	Ho	0.92	0.97	1.81	0.89	0.96	0.83	0.87	0.79	0.75	0.57	0.54	0.54	0.62	0.43	0.47	0.61	0.60	0.63	0.62	0.61	0.65	Er	2.75	2.89	4.73	2.49	2.73	2.36	2.47	2.29	2.18	1.67	1.64	1.63	1.89	1.34	1.53	1.91	1.90	1.98	1.97	1.91	1.95	Tm	0.43	0.46	0.73	0.39	0.43	0.36	0.39	0.36	0.35	0.26	0.26	0.27	0.30	0.21	0.26	0.32	0.32	0.33	0.33	0.32	0.32	Yb	2.78	2.88	4.38	2.44	2.68	2.22	2.41	2.28	2.11	1.63	1.66	1.71	1.96	1.36	1.72	2.12	2.12	2.17	2.21	2.11	2.08	Lu	0.43	0.44	0.64	0.37	0.42	0.34	0.37	0.36	0.33	0.25	0.26	0.27	0.31	0.21	0.26	0.34	0.34	0.35	0.36	0.34	0.34	Hf	1.92	1.77	4.54	1.11	1.35	1.28	1.23	1.13	1.18	0.86	0.95	0.77	1.22	0.87	0.89	1.11	0.90	1.24	2.19	1.08	1.20	Ta	0.10	0.12	0.23	0.07	0.10	0.08	0.08	0.04	0.05	0.03	0.03	0.02	0.07	0.07	0.06	0.09	0.10	0.11	0.10	0.09	0.10	Th	0.07	0.10	0.35	0.05	0.07	0.06	0.06	0.04	0.06	0.01	0.02	0.05	0.10	0.10	0.11	0.22	0.23	0.22	0.24	0.23	0.23	U	0.02	0.03	0.18	0.03	0.02	0.03	0.03	0.02	0.03	0.01	0.01	0.03	0.05	0.07	0.11	0.17	0.17	0.18	0.17	0.17	0.18																																																																																																																																					
CaO	12.33	12.63	8.18	11.44	11.53	12.49	13.04	13.08	12.03	14.28	13.89	12.74	12.64	11.70	10.74	7.05	9.35	7.25	9.99	7.25	7.56	Na <sub>2</sub> O	2.19	2.64	2.79	3.19	2.15	2.44	2.08	1.78	2.27	2.05	1.99	1.32	1.35	1.99	1.79	2.99	2.08	3.11	3.60	2.83	3.18	K <sub>2</sub> O	0.29	0.23	0.23	0.08	0.10	0.11	0.00	0.00	0.22	0.18	0.21	0.22	0.24	0.16	0.04	0.52	0.49	0.69	0.23	0.67	0.23	P <sub>2</sub> O <sub>5</sub>	0.13	0.11	0.23	0.07	0.10	0.07	0.05	0.07	0.06	0.07	0.07	0.08	0.04	0.02	0.07	0.06	0.07	0.12	0.07	0.07	0.05	LOI	0.91	0.61	1.88	2.03	1.81	0.88	0.59	0.39	0.74	0.84	0.73	0.68	0.66	2.14	0.45	2.54	1.92	1.81	1.11	1.49	1.87	Total	99.44	98.79	99.80	100.34	101.08	99.03	101.59	100.26	99.32	99.79	99.90	99.73	99.02	100.29	100.96	98.15	98.34	99.29	99.95	98.07	99.05	(ppm)																							V	300.98	299.53	278.84	278.17	328.70	262.48	278.79	286.02	231.08	187.82	214.37	256.03	308.81	231.67	285.00	439.31	402.27	431.29	403.74	334.58	390.32	Cr	311.73	240.35	74.72	479.70	189.14	267.54	424.43	437.82	380.08	456.02	314.83	469.47	338.56	183.20	114.02	22.74	12.03	10.37	42.54	32.47	46.04	Co	43.00	42.27	17.03	44.83	48.54	43.60	41.27	49.38	47.00	37.79	31.72	36.39	37.83	35.67	37.60	34.98	40.00	35.12	32.40	31.15	36.93	Zn	56.84	24.06	41.93	71.50	110.30	63.02	64.12	54.25	40.93	71.98	24.14	31.98	61.87	125.28	41.69	75.92	63.89	69.68	55.50	47.52	11.60	Ga	16.45	16.56	19.01	15.44	16.33	15.34	15.39	14.82	13.93	13.59	14.82	12.28	13.95	12.99	14.40	15.66	17.79	15.58	15.36	15.15	15.28	Rb	3.44	0.18	0.12	1.07	0.41	0.22	0.11	0.09	2.62	0.52	0.14	0.12	0.84	1.71	1.31	4.73	8.36	8.85	9.64	10.58	1.88	Sr	365.60	369.10	177.60	189.00	103.20	152.90	88.82	76.98	128.00	387.80	336.00	363.80	342.90	98.15	89.14	174.10	373.90	324.80	312.90	387.20	164.00	Y	28.95	30.51	50.99	26.70	29.07	25.54	26.72	24.13	23.31	17.27	16.29	16.78	19.58	13.84	15.97	19.28	18.82	19.93	19.50	18.51	20.15	Zr	77.81	76.56	193.18	29.47	41.25	41.59	34.69	33.89	34.89	25.84	38.58	28.94	48.25	28.74	31.46	39.34	31.57	45.34	90.39	36.34	39.15	Nb	1.26	1.57	2.77	1.00	1.43	1.13	1.10	0.64	0.72	0.32	0.30	0.19	0.88	1.17	1.03	1.05	1.12	1.16	1.08	0.86	1.30	Ca	0.06	0.00	0.00	0.02	0.01	0.01	0.01	0.00	0.02	0.01	0.00	0.00	0.05	0.05	0.05	0.05	0.14	0.06	0.05	0.07	0.04	Ba	11.54	9.22	7.81	7.73	10.39	44.58	7.83	14.04	18.41	13.48	5.07	4.84	5.84	36.71	28.28	52.27	36.91	50.14	55.77	45.90	20.94	La	2.28	2.72	6.14	2.16	2.67	2.97	2.04	1.35	1.67	0.79	1.01	0.98	1.79	0.88	1.05	1.59	1.65	1.79	1.83	1.58	1.82	Ce	7.07	8.27	17.99	6.74	8.14	9.06	6.45	4.50	6.29	2.83	3.43	2.94	5.06	2.73	2.75	4.27	4.32	4.65	4.78	4.16	4.86	Pr	1.40	1.53	3.21	1.18	1.35	1.45	1.08	0.79	1.09	0.62	0.70	0.58	0.91	0.49	0.49	0.71	0.72	0.81	0.80	0.70	0.75	Nd	7.44	8.10	16.10	6.77	7.71	7.93	6.21	4.76	6.29	3.87	3.80	3.32	4.89	2.73	2.69	3.68	3.69	4.24	4.04	3.67	4.20	Sm	2.76	2.85	5.29	2.49	2.74	2.58	2.27	1.88	2.23	1.58	1.47	1.32	1.74	1.08	1.06	1.38	1.35	1.52	1.46	1.36	1.56	Eu	1.04	1.07	1.59	0.94	0.97	0.98	0.83	0.70	0.84	0.71	0.60	0.47	0.67	0.43	0.40	0.53	0.54	0.57	0.56	0.53	0.58	Gd	3.48	3.59	6.48	3.24	3.51	3.19	3.04	2.59	2.78	2.12	1.91	1.83	2.28	1.63	1.58	1.91	1.85	2.05	2.01	1.90	2.13	Tb	0.69	0.72	1.28	0.62	0.66	0.59	0.58	0.51	0.52	0.43	0.39	0.38	0.46	0.29	0.31	0.40	0.40	0.43	0.43	0.41	0.41	Dy	4.56	4.80	8.08	4.17	4.50	3.96	4.00	3.59	3.53	2.84	2.63	2.59	3.04	2.10	2.31	2.80	2.78	2.97	2.93	2.82	2.94	Ho	0.92	0.97	1.81	0.89	0.96	0.83	0.87	0.79	0.75	0.57	0.54	0.54	0.62	0.43	0.47	0.61	0.60	0.63	0.62	0.61	0.65	Er	2.75	2.89	4.73	2.49	2.73	2.36	2.47	2.29	2.18	1.67	1.64	1.63	1.89	1.34	1.53	1.91	1.90	1.98	1.97	1.91	1.95	Tm	0.43	0.46	0.73	0.39	0.43	0.36	0.39	0.36	0.35	0.26	0.26	0.27	0.30	0.21	0.26	0.32	0.32	0.33	0.33	0.32	0.32	Yb	2.78	2.88	4.38	2.44	2.68	2.22	2.41	2.28	2.11	1.63	1.66	1.71	1.96	1.36	1.72	2.12	2.12	2.17	2.21	2.11	2.08	Lu	0.43	0.44	0.64	0.37	0.42	0.34	0.37	0.36	0.33	0.25	0.26	0.27	0.31	0.21	0.26	0.34	0.34	0.35	0.36	0.34	0.34	Hf	1.92	1.77	4.54	1.11	1.35	1.28	1.23	1.13	1.18	0.86	0.95	0.77	1.22	0.87	0.89	1.11	0.90	1.24	2.19	1.08	1.20	Ta	0.10	0.12	0.23	0.07	0.10	0.08	0.08	0.04	0.05	0.03	0.03	0.02	0.07	0.07	0.06	0.09	0.10	0.11	0.10	0.09	0.10	Th	0.07	0.10	0.35	0.05	0.07	0.06	0.06	0.04	0.06	0.01	0.02	0.05	0.10	0.10	0.11	0.22	0.23	0.22	0.24	0.23	0.23	U	0.02	0.03	0.18	0.03	0.02	0.03	0.03	0.02	0.03	0.01	0.01	0.03	0.05	0.07	0.11	0.17	0.17	0.18	0.17	0.17	0.18																																																																																																																																																											
Na <sub>2</sub> O	2.19	2.64	2.79	3.19	2.15	2.44	2.08	1.78	2.27	2.05	1.99	1.32	1.35	1.99	1.79	2.99	2.08	3.11	3.60	2.83	3.18	K <sub>2</sub> O	0.29	0.23	0.23	0.08	0.10	0.11	0.00	0.00	0.22	0.18	0.21	0.22	0.24	0.16	0.04	0.52	0.49	0.69	0.23	0.67	0.23	P <sub>2</sub> O <sub>5</sub>	0.13	0.11	0.23	0.07	0.10	0.07	0.05	0.07	0.06	0.07	0.07	0.08	0.04	0.02	0.07	0.06	0.07	0.12	0.07	0.07	0.05	LOI	0.91	0.61	1.88	2.03	1.81	0.88	0.59	0.39	0.74	0.84	0.73	0.68	0.66	2.14	0.45	2.54	1.92	1.81	1.11	1.49	1.87	Total	99.44	98.79	99.80	100.34	101.08	99.03	101.59	100.26	99.32	99.79	99.90	99.73	99.02	100.29	100.96	98.15	98.34	99.29	99.95	98.07	99.05	(ppm)																							V	300.98	299.53	278.84	278.17	328.70	262.48	278.79	286.02	231.08	187.82	214.37	256.03	308.81	231.67	285.00	439.31	402.27	431.29	403.74	334.58	390.32	Cr	311.73	240.35	74.72	479.70	189.14	267.54	424.43	437.82	380.08	456.02	314.83	469.47	338.56	183.20	114.02	22.74	12.03	10.37	42.54	32.47	46.04	Co	43.00	42.27	17.03	44.83	48.54	43.60	41.27	49.38	47.00	37.79	31.72	36.39	37.83	35.67	37.60	34.98	40.00	35.12	32.40	31.15	36.93	Zn	56.84	24.06	41.93	71.50	110.30	63.02	64.12	54.25	40.93	71.98	24.14	31.98	61.87	125.28	41.69	75.92	63.89	69.68	55.50	47.52	11.60	Ga	16.45	16.56	19.01	15.44	16.33	15.34	15.39	14.82	13.93	13.59	14.82	12.28	13.95	12.99	14.40	15.66	17.79	15.58	15.36	15.15	15.28	Rb	3.44	0.18	0.12	1.07	0.41	0.22	0.11	0.09	2.62	0.52	0.14	0.12	0.84	1.71	1.31	4.73	8.36	8.85	9.64	10.58	1.88	Sr	365.60	369.10	177.60	189.00	103.20	152.90	88.82	76.98	128.00	387.80	336.00	363.80	342.90	98.15	89.14	174.10	373.90	324.80	312.90	387.20	164.00	Y	28.95	30.51	50.99	26.70	29.07	25.54	26.72	24.13	23.31	17.27	16.29	16.78	19.58	13.84	15.97	19.28	18.82	19.93	19.50	18.51	20.15	Zr	77.81	76.56	193.18	29.47	41.25	41.59	34.69	33.89	34.89	25.84	38.58	28.94	48.25	28.74	31.46	39.34	31.57	45.34	90.39	36.34	39.15	Nb	1.26	1.57	2.77	1.00	1.43	1.13	1.10	0.64	0.72	0.32	0.30	0.19	0.88	1.17	1.03	1.05	1.12	1.16	1.08	0.86	1.30	Ca	0.06	0.00	0.00	0.02	0.01	0.01	0.01	0.00	0.02	0.01	0.00	0.00	0.05	0.05	0.05	0.05	0.14	0.06	0.05	0.07	0.04	Ba	11.54	9.22	7.81	7.73	10.39	44.58	7.83	14.04	18.41	13.48	5.07	4.84	5.84	36.71	28.28	52.27	36.91	50.14	55.77	45.90	20.94	La	2.28	2.72	6.14	2.16	2.67	2.97	2.04	1.35	1.67	0.79	1.01	0.98	1.79	0.88	1.05	1.59	1.65	1.79	1.83	1.58	1.82	Ce	7.07	8.27	17.99	6.74	8.14	9.06	6.45	4.50	6.29	2.83	3.43	2.94	5.06	2.73	2.75	4.27	4.32	4.65	4.78	4.16	4.86	Pr	1.40	1.53	3.21	1.18	1.35	1.45	1.08	0.79	1.09	0.62	0.70	0.58	0.91	0.49	0.49	0.71	0.72	0.81	0.80	0.70	0.75	Nd	7.44	8.10	16.10	6.77	7.71	7.93	6.21	4.76	6.29	3.87	3.80	3.32	4.89	2.73	2.69	3.68	3.69	4.24	4.04	3.67	4.20	Sm	2.76	2.85	5.29	2.49	2.74	2.58	2.27	1.88	2.23	1.58	1.47	1.32	1.74	1.08	1.06	1.38	1.35	1.52	1.46	1.36	1.56	Eu	1.04	1.07	1.59	0.94	0.97	0.98	0.83	0.70	0.84	0.71	0.60	0.47	0.67	0.43	0.40	0.53	0.54	0.57	0.56	0.53	0.58	Gd	3.48	3.59	6.48	3.24	3.51	3.19	3.04	2.59	2.78	2.12	1.91	1.83	2.28	1.63	1.58	1.91	1.85	2.05	2.01	1.90	2.13	Tb	0.69	0.72	1.28	0.62	0.66	0.59	0.58	0.51	0.52	0.43	0.39	0.38	0.46	0.29	0.31	0.40	0.40	0.43	0.43	0.41	0.41	Dy	4.56	4.80	8.08	4.17	4.50	3.96	4.00	3.59	3.53	2.84	2.63	2.59	3.04	2.10	2.31	2.80	2.78	2.97	2.93	2.82	2.94	Ho	0.92	0.97	1.81	0.89	0.96	0.83	0.87	0.79	0.75	0.57	0.54	0.54	0.62	0.43	0.47	0.61	0.60	0.63	0.62	0.61	0.65	Er	2.75	2.89	4.73	2.49	2.73	2.36	2.47	2.29	2.18	1.67	1.64	1.63	1.89	1.34	1.53	1.91	1.90	1.98	1.97	1.91	1.95	Tm	0.43	0.46	0.73	0.39	0.43	0.36	0.39	0.36	0.35	0.26	0.26	0.27	0.30	0.21	0.26	0.32	0.32	0.33	0.33	0.32	0.32	Yb	2.78	2.88	4.38	2.44	2.68	2.22	2.41	2.28	2.11	1.63	1.66	1.71	1.96	1.36	1.72	2.12	2.12	2.17	2.21	2.11	2.08	Lu	0.43	0.44	0.64	0.37	0.42	0.34	0.37	0.36	0.33	0.25	0.26	0.27	0.31	0.21	0.26	0.34	0.34	0.35	0.36	0.34	0.34	Hf	1.92	1.77	4.54	1.11	1.35	1.28	1.23	1.13	1.18	0.86	0.95	0.77	1.22	0.87	0.89	1.11	0.90	1.24	2.19	1.08	1.20	Ta	0.10	0.12	0.23	0.07	0.10	0.08	0.08	0.04	0.05	0.03	0.03	0.02	0.07	0.07	0.06	0.09	0.10	0.11	0.10	0.09	0.10	Th	0.07	0.10	0.35	0.05	0.07	0.06	0.06	0.04	0.06	0.01	0.02	0.05	0.10	0.10	0.11	0.22	0.23	0.22	0.24	0.23	0.23	U	0.02	0.03	0.18	0.03	0.02	0.03	0.03	0.02	0.03	0.01	0.01	0.03	0.05	0.07	0.11	0.17	0.17	0.18	0.17	0.17	0.18																																																																																																																																																																																	
K <sub>2</sub> O	0.29	0.23	0.23	0.08	0.10	0.11	0.00	0.00	0.22	0.18	0.21	0.22	0.24	0.16	0.04	0.52	0.49	0.69	0.23	0.67	0.23	P <sub>2</sub> O <sub>5</sub>	0.13	0.11	0.23	0.07	0.10	0.07	0.05	0.07	0.06	0.07	0.07	0.08	0.04	0.02	0.07	0.06	0.07	0.12	0.07	0.07	0.05	LOI	0.91	0.61	1.88	2.03	1.81	0.88	0.59	0.39	0.74	0.84	0.73	0.68	0.66	2.14	0.45	2.54	1.92	1.81	1.11	1.49	1.87	Total	99.44	98.79	99.80	100.34	101.08	99.03	101.59	100.26	99.32	99.79	99.90	99.73	99.02	100.29	100.96	98.15	98.34	99.29	99.95	98.07	99.05	(ppm)																							V	300.98	299.53	278.84	278.17	328.70	262.48	278.79	286.02	231.08	187.82	214.37	256.03	308.81	231.67	285.00	439.31	402.27	431.29	403.74	334.58	390.32	Cr	311.73	240.35	74.72	479.70	189.14	267.54	424.43	437.82	380.08	456.02	314.83	469.47	338.56	183.20	114.02	22.74	12.03	10.37	42.54	32.47	46.04	Co	43.00	42.27	17.03	44.83	48.54	43.60	41.27	49.38	47.00	37.79	31.72	36.39	37.83	35.67	37.60	34.98	40.00	35.12	32.40	31.15	36.93	Zn	56.84	24.06	41.93	71.50	110.30	63.02	64.12	54.25	40.93	71.98	24.14	31.98	61.87	125.28	41.69	75.92	63.89	69.68	55.50	47.52	11.60	Ga	16.45	16.56	19.01	15.44	16.33	15.34	15.39	14.82	13.93	13.59	14.82	12.28	13.95	12.99	14.40	15.66	17.79	15.58	15.36	15.15	15.28	Rb	3.44	0.18	0.12	1.07	0.41	0.22	0.11	0.09	2.62	0.52	0.14	0.12	0.84	1.71	1.31	4.73	8.36	8.85	9.64	10.58	1.88	Sr	365.60	369.10	177.60	189.00	103.20	152.90	88.82	76.98	128.00	387.80	336.00	363.80	342.90	98.15	89.14	174.10	373.90	324.80	312.90	387.20	164.00	Y	28.95	30.51	50.99	26.70	29.07	25.54	26.72	24.13	23.31	17.27	16.29	16.78	19.58	13.84	15.97	19.28	18.82	19.93	19.50	18.51	20.15	Zr	77.81	76.56	193.18	29.47	41.25	41.59	34.69	33.89	34.89	25.84	38.58	28.94	48.25	28.74	31.46	39.34	31.57	45.34	90.39	36.34	39.15	Nb	1.26	1.57	2.77	1.00	1.43	1.13	1.10	0.64	0.72	0.32	0.30	0.19	0.88	1.17	1.03	1.05	1.12	1.16	1.08	0.86	1.30	Ca	0.06	0.00	0.00	0.02	0.01	0.01	0.01	0.00	0.02	0.01	0.00	0.00	0.05	0.05	0.05	0.05	0.14	0.06	0.05	0.07	0.04	Ba	11.54	9.22	7.81	7.73	10.39	44.58	7.83	14.04	18.41	13.48	5.07	4.84	5.84	36.71	28.28	52.27	36.91	50.14	55.77	45.90	20.94	La	2.28	2.72	6.14	2.16	2.67	2.97	2.04	1.35	1.67	0.79	1.01	0.98	1.79	0.88	1.05	1.59	1.65	1.79	1.83	1.58	1.82	Ce	7.07	8.27	17.99	6.74	8.14	9.06	6.45	4.50	6.29	2.83	3.43	2.94	5.06	2.73	2.75	4.27	4.32	4.65	4.78	4.16	4.86	Pr	1.40	1.53	3.21	1.18	1.35	1.45	1.08	0.79	1.09	0.62	0.70	0.58	0.91	0.49	0.49	0.71	0.72	0.81	0.80	0.70	0.75	Nd	7.44	8.10	16.10	6.77	7.71	7.93	6.21	4.76	6.29	3.87	3.80	3.32	4.89	2.73	2.69	3.68	3.69	4.24	4.04	3.67	4.20	Sm	2.76	2.85	5.29	2.49	2.74	2.58	2.27	1.88	2.23	1.58	1.47	1.32	1.74	1.08	1.06	1.38	1.35	1.52	1.46	1.36	1.56	Eu	1.04	1.07	1.59	0.94	0.97	0.98	0.83	0.70	0.84	0.71	0.60	0.47	0.67	0.43	0.40	0.53	0.54	0.57	0.56	0.53	0.58	Gd	3.48	3.59	6.48	3.24	3.51	3.19	3.04	2.59	2.78	2.12	1.91	1.83	2.28	1.63	1.58	1.91	1.85	2.05	2.01	1.90	2.13	Tb	0.69	0.72	1.28	0.62	0.66	0.59	0.58	0.51	0.52	0.43	0.39	0.38	0.46	0.29	0.31	0.40	0.40	0.43	0.43	0.41	0.41	Dy	4.56	4.80	8.08	4.17	4.50	3.96	4.00	3.59	3.53	2.84	2.63	2.59	3.04	2.10	2.31	2.80	2.78	2.97	2.93	2.82	2.94	Ho	0.92	0.97	1.81	0.89	0.96	0.83	0.87	0.79	0.75	0.57	0.54	0.54	0.62	0.43	0.47	0.61	0.60	0.63	0.62	0.61	0.65	Er	2.75	2.89	4.73	2.49	2.73	2.36	2.47	2.29	2.18	1.67	1.64	1.63	1.89	1.34	1.53	1.91	1.90	1.98	1.97	1.91	1.95	Tm	0.43	0.46	0.73	0.39	0.43	0.36	0.39	0.36	0.35	0.26	0.26	0.27	0.30	0.21	0.26	0.32	0.32	0.33	0.33	0.32	0.32	Yb	2.78	2.88	4.38	2.44	2.68	2.22	2.41	2.28	2.11	1.63	1.66	1.71	1.96	1.36	1.72	2.12	2.12	2.17	2.21	2.11	2.08	Lu	0.43	0.44	0.64	0.37	0.42	0.34	0.37	0.36	0.33	0.25	0.26	0.27	0.31	0.21	0.26	0.34	0.34	0.35	0.36	0.34	0.34	Hf	1.92	1.77	4.54	1.11	1.35	1.28	1.23	1.13	1.18	0.86	0.95	0.77	1.22	0.87	0.89	1.11	0.90	1.24	2.19	1.08	1.20	Ta	0.10	0.12	0.23	0.07	0.10	0.08	0.08	0.04	0.05	0.03	0.03	0.02	0.07	0.07	0.06	0.09	0.10	0.11	0.10	0.09	0.10	Th	0.07	0.10	0.35	0.05	0.07	0.06	0.06	0.04	0.06	0.01	0.02	0.05	0.10	0.10	0.11	0.22	0.23	0.22	0.24	0.23	0.23	U	0.02	0.03	0.18	0.03	0.02	0.03	0.03	0.02	0.03	0.01	0.01	0.03	0.05	0.07	0.11	0.17	0.17	0.18	0.17	0.17	0.18																																																																																																																																																																																																							
P <sub>2</sub> O <sub>5</sub>	0.13	0.11	0.23	0.07	0.10	0.07	0.05	0.07	0.06	0.07	0.07	0.08	0.04	0.02	0.07	0.06	0.07	0.12	0.07	0.07	0.05	LOI	0.91	0.61	1.88	2.03	1.81	0.88	0.59	0.39	0.74	0.84	0.73	0.68	0.66	2.14	0.45	2.54	1.92	1.81	1.11	1.49	1.87	Total	99.44	98.79	99.80	100.34	101.08	99.03	101.59	100.26	99.32	99.79	99.90	99.73	99.02	100.29	100.96	98.15	98.34	99.29	99.95	98.07	99.05	(ppm)																							V	300.98	299.53	278.84	278.17	328.70	262.48	278.79	286.02	231.08	187.82	214.37	256.03	308.81	231.67	285.00	439.31	402.27	431.29	403.74	334.58	390.32	Cr	311.73	240.35	74.72	479.70	189.14	267.54	424.43	437.82	380.08	456.02	314.83	469.47	338.56	183.20	114.02	22.74	12.03	10.37	42.54	32.47	46.04	Co	43.00	42.27	17.03	44.83	48.54	43.60	41.27	49.38	47.00	37.79	31.72	36.39	37.83	35.67	37.60	34.98	40.00	35.12	32.40	31.15	36.93	Zn	56.84	24.06	41.93	71.50	110.30	63.02	64.12	54.25	40.93	71.98	24.14	31.98	61.87	125.28	41.69	75.92	63.89	69.68	55.50	47.52	11.60	Ga	16.45	16.56	19.01	15.44	16.33	15.34	15.39	14.82	13.93	13.59	14.82	12.28	13.95	12.99	14.40	15.66	17.79	15.58	15.36	15.15	15.28	Rb	3.44	0.18	0.12	1.07	0.41	0.22	0.11	0.09	2.62	0.52	0.14	0.12	0.84	1.71	1.31	4.73	8.36	8.85	9.64	10.58	1.88	Sr	365.60	369.10	177.60	189.00	103.20	152.90	88.82	76.98	128.00	387.80	336.00	363.80	342.90	98.15	89.14	174.10	373.90	324.80	312.90	387.20	164.00	Y	28.95	30.51	50.99	26.70	29.07	25.54	26.72	24.13	23.31	17.27	16.29	16.78	19.58	13.84	15.97	19.28	18.82	19.93	19.50	18.51	20.15	Zr	77.81	76.56	193.18	29.47	41.25	41.59	34.69	33.89	34.89	25.84	38.58	28.94	48.25	28.74	31.46	39.34	31.57	45.34	90.39	36.34	39.15	Nb	1.26	1.57	2.77	1.00	1.43	1.13	1.10	0.64	0.72	0.32	0.30	0.19	0.88	1.17	1.03	1.05	1.12	1.16	1.08	0.86	1.30	Ca	0.06	0.00	0.00	0.02	0.01	0.01	0.01	0.00	0.02	0.01	0.00	0.00	0.05	0.05	0.05	0.05	0.14	0.06	0.05	0.07	0.04	Ba	11.54	9.22	7.81	7.73	10.39	44.58	7.83	14.04	18.41	13.48	5.07	4.84	5.84	36.71	28.28	52.27	36.91	50.14	55.77	45.90	20.94	La	2.28	2.72	6.14	2.16	2.67	2.97	2.04	1.35	1.67	0.79	1.01	0.98	1.79	0.88	1.05	1.59	1.65	1.79	1.83	1.58	1.82	Ce	7.07	8.27	17.99	6.74	8.14	9.06	6.45	4.50	6.29	2.83	3.43	2.94	5.06	2.73	2.75	4.27	4.32	4.65	4.78	4.16	4.86	Pr	1.40	1.53	3.21	1.18	1.35	1.45	1.08	0.79	1.09	0.62	0.70	0.58	0.91	0.49	0.49	0.71	0.72	0.81	0.80	0.70	0.75	Nd	7.44	8.10	16.10	6.77	7.71	7.93	6.21	4.76	6.29	3.87	3.80	3.32	4.89	2.73	2.69	3.68	3.69	4.24	4.04	3.67	4.20	Sm	2.76	2.85	5.29	2.49	2.74	2.58	2.27	1.88	2.23	1.58	1.47	1.32	1.74	1.08	1.06	1.38	1.35	1.52	1.46	1.36	1.56	Eu	1.04	1.07	1.59	0.94	0.97	0.98	0.83	0.70	0.84	0.71	0.60	0.47	0.67	0.43	0.40	0.53	0.54	0.57	0.56	0.53	0.58	Gd	3.48	3.59	6.48	3.24	3.51	3.19	3.04	2.59	2.78	2.12	1.91	1.83	2.28	1.63	1.58	1.91	1.85	2.05	2.01	1.90	2.13	Tb	0.69	0.72	1.28	0.62	0.66	0.59	0.58	0.51	0.52	0.43	0.39	0.38	0.46	0.29	0.31	0.40	0.40	0.43	0.43	0.41	0.41	Dy	4.56	4.80	8.08	4.17	4.50	3.96	4.00	3.59	3.53	2.84	2.63	2.59	3.04	2.10	2.31	2.80	2.78	2.97	2.93	2.82	2.94	Ho	0.92	0.97	1.81	0.89	0.96	0.83	0.87	0.79	0.75	0.57	0.54	0.54	0.62	0.43	0.47	0.61	0.60	0.63	0.62	0.61	0.65	Er	2.75	2.89	4.73	2.49	2.73	2.36	2.47	2.29	2.18	1.67	1.64	1.63	1.89	1.34	1.53	1.91	1.90	1.98	1.97	1.91	1.95	Tm	0.43	0.46	0.73	0.39	0.43	0.36	0.39	0.36	0.35	0.26	0.26	0.27	0.30	0.21	0.26	0.32	0.32	0.33	0.33	0.32	0.32	Yb	2.78	2.88	4.38	2.44	2.68	2.22	2.41	2.28	2.11	1.63	1.66	1.71	1.96	1.36	1.72	2.12	2.12	2.17	2.21	2.11	2.08	Lu	0.43	0.44	0.64	0.37	0.42	0.34	0.37	0.36	0.33	0.25	0.26	0.27	0.31	0.21	0.26	0.34	0.34	0.35	0.36	0.34	0.34	Hf	1.92	1.77	4.54	1.11	1.35	1.28	1.23	1.13	1.18	0.86	0.95	0.77	1.22	0.87	0.89	1.11	0.90	1.24	2.19	1.08	1.20	Ta	0.10	0.12	0.23	0.07	0.10	0.08	0.08	0.04	0.05	0.03	0.03	0.02	0.07	0.07	0.06	0.09	0.10	0.11	0.10	0.09	0.10	Th	0.07	0.10	0.35	0.05	0.07	0.06	0.06	0.04	0.06	0.01	0.02	0.05	0.10	0.10	0.11	0.22	0.23	0.22	0.24	0.23	0.23	U	0.02	0.03	0.18	0.03	0.02	0.03	0.03	0.02	0.03	0.01	0.01	0.03	0.05	0.07	0.11	0.17	0.17	0.18	0.17	0.17	0.18																																																																																																																																																																																																																													
LOI	0.91	0.61	1.88	2.03	1.81	0.88	0.59	0.39	0.74	0.84	0.73	0.68	0.66	2.14	0.45	2.54	1.92	1.81	1.11	1.49	1.87	Total	99.44	98.79	99.80	100.34	101.08	99.03	101.59	100.26	99.32	99.79	99.90	99.73	99.02	100.29	100.96	98.15	98.34	99.29	99.95	98.07	99.05	(ppm)																							V	300.98	299.53	278.84	278.17	328.70	262.48	278.79	286.02	231.08	187.82	214.37	256.03	308.81	231.67	285.00	439.31	402.27	431.29	403.74	334.58	390.32	Cr	311.73	240.35	74.72	479.70	189.14	267.54	424.43	437.82	380.08	456.02	314.83	469.47	338.56	183.20	114.02	22.74	12.03	10.37	42.54	32.47	46.04	Co	43.00	42.27	17.03	44.83	48.54	43.60	41.27	49.38	47.00	37.79	31.72	36.39	37.83	35.67	37.60	34.98	40.00	35.12	32.40	31.15	36.93	Zn	56.84	24.06	41.93	71.50	110.30	63.02	64.12	54.25	40.93	71.98	24.14	31.98	61.87	125.28	41.69	75.92	63.89	69.68	55.50	47.52	11.60	Ga	16.45	16.56	19.01	15.44	16.33	15.34	15.39	14.82	13.93	13.59	14.82	12.28	13.95	12.99	14.40	15.66	17.79	15.58	15.36	15.15	15.28	Rb	3.44	0.18	0.12	1.07	0.41	0.22	0.11	0.09	2.62	0.52	0.14	0.12	0.84	1.71	1.31	4.73	8.36	8.85	9.64	10.58	1.88	Sr	365.60	369.10	177.60	189.00	103.20	152.90	88.82	76.98	128.00	387.80	336.00	363.80	342.90	98.15	89.14	174.10	373.90	324.80	312.90	387.20	164.00	Y	28.95	30.51	50.99	26.70	29.07	25.54	26.72	24.13	23.31	17.27	16.29	16.78	19.58	13.84	15.97	19.28	18.82	19.93	19.50	18.51	20.15	Zr	77.81	76.56	193.18	29.47	41.25	41.59	34.69	33.89	34.89	25.84	38.58	28.94	48.25	28.74	31.46	39.34	31.57	45.34	90.39	36.34	39.15	Nb	1.26	1.57	2.77	1.00	1.43	1.13	1.10	0.64	0.72	0.32	0.30	0.19	0.88	1.17	1.03	1.05	1.12	1.16	1.08	0.86	1.30	Ca	0.06	0.00	0.00	0.02	0.01	0.01	0.01	0.00	0.02	0.01	0.00	0.00	0.05	0.05	0.05	0.05	0.14	0.06	0.05	0.07	0.04	Ba	11.54	9.22	7.81	7.73	10.39	44.58	7.83	14.04	18.41	13.48	5.07	4.84	5.84	36.71	28.28	52.27	36.91	50.14	55.77	45.90	20.94	La	2.28	2.72	6.14	2.16	2.67	2.97	2.04	1.35	1.67	0.79	1.01	0.98	1.79	0.88	1.05	1.59	1.65	1.79	1.83	1.58	1.82	Ce	7.07	8.27	17.99	6.74	8.14	9.06	6.45	4.50	6.29	2.83	3.43	2.94	5.06	2.73	2.75	4.27	4.32	4.65	4.78	4.16	4.86	Pr	1.40	1.53	3.21	1.18	1.35	1.45	1.08	0.79	1.09	0.62	0.70	0.58	0.91	0.49	0.49	0.71	0.72	0.81	0.80	0.70	0.75	Nd	7.44	8.10	16.10	6.77	7.71	7.93	6.21	4.76	6.29	3.87	3.80	3.32	4.89	2.73	2.69	3.68	3.69	4.24	4.04	3.67	4.20	Sm	2.76	2.85	5.29	2.49	2.74	2.58	2.27	1.88	2.23	1.58	1.47	1.32	1.74	1.08	1.06	1.38	1.35	1.52	1.46	1.36	1.56	Eu	1.04	1.07	1.59	0.94	0.97	0.98	0.83	0.70	0.84	0.71	0.60	0.47	0.67	0.43	0.40	0.53	0.54	0.57	0.56	0.53	0.58	Gd	3.48	3.59	6.48	3.24	3.51	3.19	3.04	2.59	2.78	2.12	1.91	1.83	2.28	1.63	1.58	1.91	1.85	2.05	2.01	1.90	2.13	Tb	0.69	0.72	1.28	0.62	0.66	0.59	0.58	0.51	0.52	0.43	0.39	0.38	0.46	0.29	0.31	0.40	0.40	0.43	0.43	0.41	0.41	Dy	4.56	4.80	8.08	4.17	4.50	3.96	4.00	3.59	3.53	2.84	2.63	2.59	3.04	2.10	2.31	2.80	2.78	2.97	2.93	2.82	2.94	Ho	0.92	0.97	1.81	0.89	0.96	0.83	0.87	0.79	0.75	0.57	0.54	0.54	0.62	0.43	0.47	0.61	0.60	0.63	0.62	0.61	0.65	Er	2.75	2.89	4.73	2.49	2.73	2.36	2.47	2.29	2.18	1.67	1.64	1.63	1.89	1.34	1.53	1.91	1.90	1.98	1.97	1.91	1.95	Tm	0.43	0.46	0.73	0.39	0.43	0.36	0.39	0.36	0.35	0.26	0.26	0.27	0.30	0.21	0.26	0.32	0.32	0.33	0.33	0.32	0.32	Yb	2.78	2.88	4.38	2.44	2.68	2.22	2.41	2.28	2.11	1.63	1.66	1.71	1.96	1.36	1.72	2.12	2.12	2.17	2.21	2.11	2.08	Lu	0.43	0.44	0.64	0.37	0.42	0.34	0.37	0.36	0.33	0.25	0.26	0.27	0.31	0.21	0.26	0.34	0.34	0.35	0.36	0.34	0.34	Hf	1.92	1.77	4.54	1.11	1.35	1.28	1.23	1.13	1.18	0.86	0.95	0.77	1.22	0.87	0.89	1.11	0.90	1.24	2.19	1.08	1.20	Ta	0.10	0.12	0.23	0.07	0.10	0.08	0.08	0.04	0.05	0.03	0.03	0.02	0.07	0.07	0.06	0.09	0.10	0.11	0.10	0.09	0.10	Th	0.07	0.10	0.35	0.05	0.07	0.06	0.06	0.04	0.06	0.01	0.02	0.05	0.10	0.10	0.11	0.22	0.23	0.22	0.24	0.23	0.23	U	0.02	0.03	0.18	0.03	0.02	0.03	0.03	0.02	0.03	0.01	0.01	0.03	0.05	0.07	0.11	0.17	0.17	0.18	0.17	0.17	0.18																																																																																																																																																																																																																																																			
Total	99.44	98.79	99.80	100.34	101.08	99.03	101.59	100.26	99.32	99.79	99.90	99.73	99.02	100.29	100.96	98.15	98.34	99.29	99.95	98.07	99.05	(ppm)																							V	300.98	299.53	278.84	278.17	328.70	262.48	278.79	286.02	231.08	187.82	214.37	256.03	308.81	231.67	285.00	439.31	402.27	431.29	403.74	334.58	390.32	Cr	311.73	240.35	74.72	479.70	189.14	267.54	424.43	437.82	380.08	456.02	314.83	469.47	338.56	183.20	114.02	22.74	12.03	10.37	42.54	32.47	46.04	Co	43.00	42.27	17.03	44.83	48.54	43.60	41.27	49.38	47.00	37.79	31.72	36.39	37.83	35.67	37.60	34.98	40.00	35.12	32.40	31.15	36.93	Zn	56.84	24.06	41.93	71.50	110.30	63.02	64.12	54.25	40.93	71.98	24.14	31.98	61.87	125.28	41.69	75.92	63.89	69.68	55.50	47.52	11.60	Ga	16.45	16.56	19.01	15.44	16.33	15.34	15.39	14.82	13.93	13.59	14.82	12.28	13.95	12.99	14.40	15.66	17.79	15.58	15.36	15.15	15.28	Rb	3.44	0.18	0.12	1.07	0.41	0.22	0.11	0.09	2.62	0.52	0.14	0.12	0.84	1.71	1.31	4.73	8.36	8.85	9.64	10.58	1.88	Sr	365.60	369.10	177.60	189.00	103.20	152.90	88.82	76.98	128.00	387.80	336.00	363.80	342.90	98.15	89.14	174.10	373.90	324.80	312.90	387.20	164.00	Y	28.95	30.51	50.99	26.70	29.07	25.54	26.72	24.13	23.31	17.27	16.29	16.78	19.58	13.84	15.97	19.28	18.82	19.93	19.50	18.51	20.15	Zr	77.81	76.56	193.18	29.47	41.25	41.59	34.69	33.89	34.89	25.84	38.58	28.94	48.25	28.74	31.46	39.34	31.57	45.34	90.39	36.34	39.15	Nb	1.26	1.57	2.77	1.00	1.43	1.13	1.10	0.64	0.72	0.32	0.30	0.19	0.88	1.17	1.03	1.05	1.12	1.16	1.08	0.86	1.30	Ca	0.06	0.00	0.00	0.02	0.01	0.01	0.01	0.00	0.02	0.01	0.00	0.00	0.05	0.05	0.05	0.05	0.14	0.06	0.05	0.07	0.04	Ba	11.54	9.22	7.81	7.73	10.39	44.58	7.83	14.04	18.41	13.48	5.07	4.84	5.84	36.71	28.28	52.27	36.91	50.14	55.77	45.90	20.94	La	2.28	2.72	6.14	2.16	2.67	2.97	2.04	1.35	1.67	0.79	1.01	0.98	1.79	0.88	1.05	1.59	1.65	1.79	1.83	1.58	1.82	Ce	7.07	8.27	17.99	6.74	8.14	9.06	6.45	4.50	6.29	2.83	3.43	2.94	5.06	2.73	2.75	4.27	4.32	4.65	4.78	4.16	4.86	Pr	1.40	1.53	3.21	1.18	1.35	1.45	1.08	0.79	1.09	0.62	0.70	0.58	0.91	0.49	0.49	0.71	0.72	0.81	0.80	0.70	0.75	Nd	7.44	8.10	16.10	6.77	7.71	7.93	6.21	4.76	6.29	3.87	3.80	3.32	4.89	2.73	2.69	3.68	3.69	4.24	4.04	3.67	4.20	Sm	2.76	2.85	5.29	2.49	2.74	2.58	2.27	1.88	2.23	1.58	1.47	1.32	1.74	1.08	1.06	1.38	1.35	1.52	1.46	1.36	1.56	Eu	1.04	1.07	1.59	0.94	0.97	0.98	0.83	0.70	0.84	0.71	0.60	0.47	0.67	0.43	0.40	0.53	0.54	0.57	0.56	0.53	0.58	Gd	3.48	3.59	6.48	3.24	3.51	3.19	3.04	2.59	2.78	2.12	1.91	1.83	2.28	1.63	1.58	1.91	1.85	2.05	2.01	1.90	2.13	Tb	0.69	0.72	1.28	0.62	0.66	0.59	0.58	0.51	0.52	0.43	0.39	0.38	0.46	0.29	0.31	0.40	0.40	0.43	0.43	0.41	0.41	Dy	4.56	4.80	8.08	4.17	4.50	3.96	4.00	3.59	3.53	2.84	2.63	2.59	3.04	2.10	2.31	2.80	2.78	2.97	2.93	2.82	2.94	Ho	0.92	0.97	1.81	0.89	0.96	0.83	0.87	0.79	0.75	0.57	0.54	0.54	0.62	0.43	0.47	0.61	0.60	0.63	0.62	0.61	0.65	Er	2.75	2.89	4.73	2.49	2.73	2.36	2.47	2.29	2.18	1.67	1.64	1.63	1.89	1.34	1.53	1.91	1.90	1.98	1.97	1.91	1.95	Tm	0.43	0.46	0.73	0.39	0.43	0.36	0.39	0.36	0.35	0.26	0.26	0.27	0.30	0.21	0.26	0.32	0.32	0.33	0.33	0.32	0.32	Yb	2.78	2.88	4.38	2.44	2.68	2.22	2.41	2.28	2.11	1.63	1.66	1.71	1.96	1.36	1.72	2.12	2.12	2.17	2.21	2.11	2.08	Lu	0.43	0.44	0.64	0.37	0.42	0.34	0.37	0.36	0.33	0.25	0.26	0.27	0.31	0.21	0.26	0.34	0.34	0.35	0.36	0.34	0.34	Hf	1.92	1.77	4.54	1.11	1.35	1.28	1.23	1.13	1.18	0.86	0.95	0.77	1.22	0.87	0.89	1.11	0.90	1.24	2.19	1.08	1.20	Ta	0.10	0.12	0.23	0.07	0.10	0.08	0.08	0.04	0.05	0.03	0.03	0.02	0.07	0.07	0.06	0.09	0.10	0.11	0.10	0.09	0.10	Th	0.07	0.10	0.35	0.05	0.07	0.06	0.06	0.04	0.06	0.01	0.02	0.05	0.10	0.10	0.11	0.22	0.23	0.22	0.24	0.23	0.23	U	0.02	0.03	0.18	0.03	0.02	0.03	0.03	0.02	0.03	0.01	0.01	0.03	0.05	0.07	0.11	0.17	0.17	0.18	0.17	0.17	0.18																																																																																																																																																																																																																																																																									
(ppm)																							V	300.98	299.53	278.84	278.17	328.70	262.48	278.79	286.02	231.08	187.82	214.37	256.03	308.81	231.67	285.00	439.31	402.27	431.29	403.74	334.58	390.32	Cr	311.73	240.35	74.72	479.70	189.14	267.54	424.43	437.82	380.08	456.02	314.83	469.47	338.56	183.20	114.02	22.74	12.03	10.37	42.54	32.47	46.04	Co	43.00	42.27	17.03	44.83	48.54	43.60	41.27	49.38	47.00	37.79	31.72	36.39	37.83	35.67	37.60	34.98	40.00	35.12	32.40	31.15	36.93	Zn	56.84	24.06	41.93	71.50	110.30	63.02	64.12	54.25	40.93	71.98	24.14	31.98	61.87	125.28	41.69	75.92	63.89	69.68	55.50	47.52	11.60	Ga	16.45	16.56	19.01	15.44	16.33	15.34	15.39	14.82	13.93	13.59	14.82	12.28	13.95	12.99	14.40	15.66	17.79	15.58	15.36	15.15	15.28	Rb	3.44	0.18	0.12	1.07	0.41	0.22	0.11	0.09	2.62	0.52	0.14	0.12	0.84	1.71	1.31	4.73	8.36	8.85	9.64	10.58	1.88	Sr	365.60	369.10	177.60	189.00	103.20	152.90	88.82	76.98	128.00	387.80	336.00	363.80	342.90	98.15	89.14	174.10	373.90	324.80	312.90	387.20	164.00	Y	28.95	30.51	50.99	26.70	29.07	25.54	26.72	24.13	23.31	17.27	16.29	16.78	19.58	13.84	15.97	19.28	18.82	19.93	19.50	18.51	20.15	Zr	77.81	76.56	193.18	29.47	41.25	41.59	34.69	33.89	34.89	25.84	38.58	28.94	48.25	28.74	31.46	39.34	31.57	45.34	90.39	36.34	39.15	Nb	1.26	1.57	2.77	1.00	1.43	1.13	1.10	0.64	0.72	0.32	0.30	0.19	0.88	1.17	1.03	1.05	1.12	1.16	1.08	0.86	1.30	Ca	0.06	0.00	0.00	0.02	0.01	0.01	0.01	0.00	0.02	0.01	0.00	0.00	0.05	0.05	0.05	0.05	0.14	0.06	0.05	0.07	0.04	Ba	11.54	9.22	7.81	7.73	10.39	44.58	7.83	14.04	18.41	13.48	5.07	4.84	5.84	36.71	28.28	52.27	36.91	50.14	55.77	45.90	20.94	La	2.28	2.72	6.14	2.16	2.67	2.97	2.04	1.35	1.67	0.79	1.01	0.98	1.79	0.88	1.05	1.59	1.65	1.79	1.83	1.58	1.82	Ce	7.07	8.27	17.99	6.74	8.14	9.06	6.45	4.50	6.29	2.83	3.43	2.94	5.06	2.73	2.75	4.27	4.32	4.65	4.78	4.16	4.86	Pr	1.40	1.53	3.21	1.18	1.35	1.45	1.08	0.79	1.09	0.62	0.70	0.58	0.91	0.49	0.49	0.71	0.72	0.81	0.80	0.70	0.75	Nd	7.44	8.10	16.10	6.77	7.71	7.93	6.21	4.76	6.29	3.87	3.80	3.32	4.89	2.73	2.69	3.68	3.69	4.24	4.04	3.67	4.20	Sm	2.76	2.85	5.29	2.49	2.74	2.58	2.27	1.88	2.23	1.58	1.47	1.32	1.74	1.08	1.06	1.38	1.35	1.52	1.46	1.36	1.56	Eu	1.04	1.07	1.59	0.94	0.97	0.98	0.83	0.70	0.84	0.71	0.60	0.47	0.67	0.43	0.40	0.53	0.54	0.57	0.56	0.53	0.58	Gd	3.48	3.59	6.48	3.24	3.51	3.19	3.04	2.59	2.78	2.12	1.91	1.83	2.28	1.63	1.58	1.91	1.85	2.05	2.01	1.90	2.13	Tb	0.69	0.72	1.28	0.62	0.66	0.59	0.58	0.51	0.52	0.43	0.39	0.38	0.46	0.29	0.31	0.40	0.40	0.43	0.43	0.41	0.41	Dy	4.56	4.80	8.08	4.17	4.50	3.96	4.00	3.59	3.53	2.84	2.63	2.59	3.04	2.10	2.31	2.80	2.78	2.97	2.93	2.82	2.94	Ho	0.92	0.97	1.81	0.89	0.96	0.83	0.87	0.79	0.75	0.57	0.54	0.54	0.62	0.43	0.47	0.61	0.60	0.63	0.62	0.61	0.65	Er	2.75	2.89	4.73	2.49	2.73	2.36	2.47	2.29	2.18	1.67	1.64	1.63	1.89	1.34	1.53	1.91	1.90	1.98	1.97	1.91	1.95	Tm	0.43	0.46	0.73	0.39	0.43	0.36	0.39	0.36	0.35	0.26	0.26	0.27	0.30	0.21	0.26	0.32	0.32	0.33	0.33	0.32	0.32	Yb	2.78	2.88	4.38	2.44	2.68	2.22	2.41	2.28	2.11	1.63	1.66	1.71	1.96	1.36	1.72	2.12	2.12	2.17	2.21	2.11	2.08	Lu	0.43	0.44	0.64	0.37	0.42	0.34	0.37	0.36	0.33	0.25	0.26	0.27	0.31	0.21	0.26	0.34	0.34	0.35	0.36	0.34	0.34	Hf	1.92	1.77	4.54	1.11	1.35	1.28	1.23	1.13	1.18	0.86	0.95	0.77	1.22	0.87	0.89	1.11	0.90	1.24	2.19	1.08	1.20	Ta	0.10	0.12	0.23	0.07	0.10	0.08	0.08	0.04	0.05	0.03	0.03	0.02	0.07	0.07	0.06	0.09	0.10	0.11	0.10	0.09	0.10	Th	0.07	0.10	0.35	0.05	0.07	0.06	0.06	0.04	0.06	0.01	0.02	0.05	0.10	0.10	0.11	0.22	0.23	0.22	0.24	0.23	0.23	U	0.02	0.03	0.18	0.03	0.02	0.03	0.03	0.02	0.03	0.01	0.01	0.03	0.05	0.07	0.11	0.17	0.17	0.18	0.17	0.17	0.18																																																																																																																																																																																																																																																																																															
V	300.98	299.53	278.84	278.17	328.70	262.48	278.79	286.02	231.08	187.82	214.37	256.03	308.81	231.67	285.00	439.31	402.27	431.29	403.74	334.58	390.32	Cr	311.73	240.35	74.72	479.70	189.14	267.54	424.43	437.82	380.08	456.02	314.83	469.47	338.56	183.20	114.02	22.74	12.03	10.37	42.54	32.47	46.04	Co	43.00	42.27	17.03	44.83	48.54	43.60	41.27	49.38	47.00	37.79	31.72	36.39	37.83	35.67	37.60	34.98	40.00	35.12	32.40	31.15	36.93	Zn	56.84	24.06	41.93	71.50	110.30	63.02	64.12	54.25	40.93	71.98	24.14	31.98	61.87	125.28	41.69	75.92	63.89	69.68	55.50	47.52	11.60	Ga	16.45	16.56	19.01	15.44	16.33	15.34	15.39	14.82	13.93	13.59	14.82	12.28	13.95	12.99	14.40	15.66	17.79	15.58	15.36	15.15	15.28	Rb	3.44	0.18	0.12	1.07	0.41	0.22	0.11	0.09	2.62	0.52	0.14	0.12	0.84	1.71	1.31	4.73	8.36	8.85	9.64	10.58	1.88	Sr	365.60	369.10	177.60	189.00	103.20	152.90	88.82	76.98	128.00	387.80	336.00	363.80	342.90	98.15	89.14	174.10	373.90	324.80	312.90	387.20	164.00	Y	28.95	30.51	50.99	26.70	29.07	25.54	26.72	24.13	23.31	17.27	16.29	16.78	19.58	13.84	15.97	19.28	18.82	19.93	19.50	18.51	20.15	Zr	77.81	76.56	193.18	29.47	41.25	41.59	34.69	33.89	34.89	25.84	38.58	28.94	48.25	28.74	31.46	39.34	31.57	45.34	90.39	36.34	39.15	Nb	1.26	1.57	2.77	1.00	1.43	1.13	1.10	0.64	0.72	0.32	0.30	0.19	0.88	1.17	1.03	1.05	1.12	1.16	1.08	0.86	1.30	Ca	0.06	0.00	0.00	0.02	0.01	0.01	0.01	0.00	0.02	0.01	0.00	0.00	0.05	0.05	0.05	0.05	0.14	0.06	0.05	0.07	0.04	Ba	11.54	9.22	7.81	7.73	10.39	44.58	7.83	14.04	18.41	13.48	5.07	4.84	5.84	36.71	28.28	52.27	36.91	50.14	55.77	45.90	20.94	La	2.28	2.72	6.14	2.16	2.67	2.97	2.04	1.35	1.67	0.79	1.01	0.98	1.79	0.88	1.05	1.59	1.65	1.79	1.83	1.58	1.82	Ce	7.07	8.27	17.99	6.74	8.14	9.06	6.45	4.50	6.29	2.83	3.43	2.94	5.06	2.73	2.75	4.27	4.32	4.65	4.78	4.16	4.86	Pr	1.40	1.53	3.21	1.18	1.35	1.45	1.08	0.79	1.09	0.62	0.70	0.58	0.91	0.49	0.49	0.71	0.72	0.81	0.80	0.70	0.75	Nd	7.44	8.10	16.10	6.77	7.71	7.93	6.21	4.76	6.29	3.87	3.80	3.32	4.89	2.73	2.69	3.68	3.69	4.24	4.04	3.67	4.20	Sm	2.76	2.85	5.29	2.49	2.74	2.58	2.27	1.88	2.23	1.58	1.47	1.32	1.74	1.08	1.06	1.38	1.35	1.52	1.46	1.36	1.56	Eu	1.04	1.07	1.59	0.94	0.97	0.98	0.83	0.70	0.84	0.71	0.60	0.47	0.67	0.43	0.40	0.53	0.54	0.57	0.56	0.53	0.58	Gd	3.48	3.59	6.48	3.24	3.51	3.19	3.04	2.59	2.78	2.12	1.91	1.83	2.28	1.63	1.58	1.91	1.85	2.05	2.01	1.90	2.13	Tb	0.69	0.72	1.28	0.62	0.66	0.59	0.58	0.51	0.52	0.43	0.39	0.38	0.46	0.29	0.31	0.40	0.40	0.43	0.43	0.41	0.41	Dy	4.56	4.80	8.08	4.17	4.50	3.96	4.00	3.59	3.53	2.84	2.63	2.59	3.04	2.10	2.31	2.80	2.78	2.97	2.93	2.82	2.94	Ho	0.92	0.97	1.81	0.89	0.96	0.83	0.87	0.79	0.75	0.57	0.54	0.54	0.62	0.43	0.47	0.61	0.60	0.63	0.62	0.61	0.65	Er	2.75	2.89	4.73	2.49	2.73	2.36	2.47	2.29	2.18	1.67	1.64	1.63	1.89	1.34	1.53	1.91	1.90	1.98	1.97	1.91	1.95	Tm	0.43	0.46	0.73	0.39	0.43	0.36	0.39	0.36	0.35	0.26	0.26	0.27	0.30	0.21	0.26	0.32	0.32	0.33	0.33	0.32	0.32	Yb	2.78	2.88	4.38	2.44	2.68	2.22	2.41	2.28	2.11	1.63	1.66	1.71	1.96	1.36	1.72	2.12	2.12	2.17	2.21	2.11	2.08	Lu	0.43	0.44	0.64	0.37	0.42	0.34	0.37	0.36	0.33	0.25	0.26	0.27	0.31	0.21	0.26	0.34	0.34	0.35	0.36	0.34	0.34	Hf	1.92	1.77	4.54	1.11	1.35	1.28	1.23	1.13	1.18	0.86	0.95	0.77	1.22	0.87	0.89	1.11	0.90	1.24	2.19	1.08	1.20	Ta	0.10	0.12	0.23	0.07	0.10	0.08	0.08	0.04	0.05	0.03	0.03	0.02	0.07	0.07	0.06	0.09	0.10	0.11	0.10	0.09	0.10	Th	0.07	0.10	0.35	0.05	0.07	0.06	0.06	0.04	0.06	0.01	0.02	0.05	0.10	0.10	0.11	0.22	0.23	0.22	0.24	0.23	0.23	U	0.02	0.03	0.18	0.03	0.02	0.03	0.03	0.02	0.03	0.01	0.01	0.03	0.05	0.07	0.11	0.17	0.17	0.18	0.17	0.17	0.18																																																																																																																																																																																																																																																																																																																						
Cr	311.73	240.35	74.72	479.70	189.14	267.54	424.43	437.82	380.08	456.02	314.83	469.47	338.56	183.20	114.02	22.74	12.03	10.37	42.54	32.47	46.04	Co	43.00	42.27	17.03	44.83	48.54	43.60	41.27	49.38	47.00	37.79	31.72	36.39	37.83	35.67	37.60	34.98	40.00	35.12	32.40	31.15	36.93	Zn	56.84	24.06	41.93	71.50	110.30	63.02	64.12	54.25	40.93	71.98	24.14	31.98	61.87	125.28	41.69	75.92	63.89	69.68	55.50	47.52	11.60	Ga	16.45	16.56	19.01	15.44	16.33	15.34	15.39	14.82	13.93	13.59	14.82	12.28	13.95	12.99	14.40	15.66	17.79	15.58	15.36	15.15	15.28	Rb	3.44	0.18	0.12	1.07	0.41	0.22	0.11	0.09	2.62	0.52	0.14	0.12	0.84	1.71	1.31	4.73	8.36	8.85	9.64	10.58	1.88	Sr	365.60	369.10	177.60	189.00	103.20	152.90	88.82	76.98	128.00	387.80	336.00	363.80	342.90	98.15	89.14	174.10	373.90	324.80	312.90	387.20	164.00	Y	28.95	30.51	50.99	26.70	29.07	25.54	26.72	24.13	23.31	17.27	16.29	16.78	19.58	13.84	15.97	19.28	18.82	19.93	19.50	18.51	20.15	Zr	77.81	76.56	193.18	29.47	41.25	41.59	34.69	33.89	34.89	25.84	38.58	28.94	48.25	28.74	31.46	39.34	31.57	45.34	90.39	36.34	39.15	Nb	1.26	1.57	2.77	1.00	1.43	1.13	1.10	0.64	0.72	0.32	0.30	0.19	0.88	1.17	1.03	1.05	1.12	1.16	1.08	0.86	1.30	Ca	0.06	0.00	0.00	0.02	0.01	0.01	0.01	0.00	0.02	0.01	0.00	0.00	0.05	0.05	0.05	0.05	0.14	0.06	0.05	0.07	0.04	Ba	11.54	9.22	7.81	7.73	10.39	44.58	7.83	14.04	18.41	13.48	5.07	4.84	5.84	36.71	28.28	52.27	36.91	50.14	55.77	45.90	20.94	La	2.28	2.72	6.14	2.16	2.67	2.97	2.04	1.35	1.67	0.79	1.01	0.98	1.79	0.88	1.05	1.59	1.65	1.79	1.83	1.58	1.82	Ce	7.07	8.27	17.99	6.74	8.14	9.06	6.45	4.50	6.29	2.83	3.43	2.94	5.06	2.73	2.75	4.27	4.32	4.65	4.78	4.16	4.86	Pr	1.40	1.53	3.21	1.18	1.35	1.45	1.08	0.79	1.09	0.62	0.70	0.58	0.91	0.49	0.49	0.71	0.72	0.81	0.80	0.70	0.75	Nd	7.44	8.10	16.10	6.77	7.71	7.93	6.21	4.76	6.29	3.87	3.80	3.32	4.89	2.73	2.69	3.68	3.69	4.24	4.04	3.67	4.20	Sm	2.76	2.85	5.29	2.49	2.74	2.58	2.27	1.88	2.23	1.58	1.47	1.32	1.74	1.08	1.06	1.38	1.35	1.52	1.46	1.36	1.56	Eu	1.04	1.07	1.59	0.94	0.97	0.98	0.83	0.70	0.84	0.71	0.60	0.47	0.67	0.43	0.40	0.53	0.54	0.57	0.56	0.53	0.58	Gd	3.48	3.59	6.48	3.24	3.51	3.19	3.04	2.59	2.78	2.12	1.91	1.83	2.28	1.63	1.58	1.91	1.85	2.05	2.01	1.90	2.13	Tb	0.69	0.72	1.28	0.62	0.66	0.59	0.58	0.51	0.52	0.43	0.39	0.38	0.46	0.29	0.31	0.40	0.40	0.43	0.43	0.41	0.41	Dy	4.56	4.80	8.08	4.17	4.50	3.96	4.00	3.59	3.53	2.84	2.63	2.59	3.04	2.10	2.31	2.80	2.78	2.97	2.93	2.82	2.94	Ho	0.92	0.97	1.81	0.89	0.96	0.83	0.87	0.79	0.75	0.57	0.54	0.54	0.62	0.43	0.47	0.61	0.60	0.63	0.62	0.61	0.65	Er	2.75	2.89	4.73	2.49	2.73	2.36	2.47	2.29	2.18	1.67	1.64	1.63	1.89	1.34	1.53	1.91	1.90	1.98	1.97	1.91	1.95	Tm	0.43	0.46	0.73	0.39	0.43	0.36	0.39	0.36	0.35	0.26	0.26	0.27	0.30	0.21	0.26	0.32	0.32	0.33	0.33	0.32	0.32	Yb	2.78	2.88	4.38	2.44	2.68	2.22	2.41	2.28	2.11	1.63	1.66	1.71	1.96	1.36	1.72	2.12	2.12	2.17	2.21	2.11	2.08	Lu	0.43	0.44	0.64	0.37	0.42	0.34	0.37	0.36	0.33	0.25	0.26	0.27	0.31	0.21	0.26	0.34	0.34	0.35	0.36	0.34	0.34	Hf	1.92	1.77	4.54	1.11	1.35	1.28	1.23	1.13	1.18	0.86	0.95	0.77	1.22	0.87	0.89	1.11	0.90	1.24	2.19	1.08	1.20	Ta	0.10	0.12	0.23	0.07	0.10	0.08	0.08	0.04	0.05	0.03	0.03	0.02	0.07	0.07	0.06	0.09	0.10	0.11	0.10	0.09	0.10	Th	0.07	0.10	0.35	0.05	0.07	0.06	0.06	0.04	0.06	0.01	0.02	0.05	0.10	0.10	0.11	0.22	0.23	0.22	0.24	0.23	0.23	U	0.02	0.03	0.18	0.03	0.02	0.03	0.03	0.02	0.03	0.01	0.01	0.03	0.05	0.07	0.11	0.17	0.17	0.18	0.17	0.17	0.18																																																																																																																																																																																																																																																																																																																																												
Co	43.00	42.27	17.03	44.83	48.54	43.60	41.27	49.38	47.00	37.79	31.72	36.39	37.83	35.67	37.60	34.98	40.00	35.12	32.40	31.15	36.93	Zn	56.84	24.06	41.93	71.50	110.30	63.02	64.12	54.25	40.93	71.98	24.14	31.98	61.87	125.28	41.69	75.92	63.89	69.68	55.50	47.52	11.60	Ga	16.45	16.56	19.01	15.44	16.33	15.34	15.39	14.82	13.93	13.59	14.82	12.28	13.95	12.99	14.40	15.66	17.79	15.58	15.36	15.15	15.28	Rb	3.44	0.18	0.12	1.07	0.41	0.22	0.11	0.09	2.62	0.52	0.14	0.12	0.84	1.71	1.31	4.73	8.36	8.85	9.64	10.58	1.88	Sr	365.60	369.10	177.60	189.00	103.20	152.90	88.82	76.98	128.00	387.80	336.00	363.80	342.90	98.15	89.14	174.10	373.90	324.80	312.90	387.20	164.00	Y	28.95	30.51	50.99	26.70	29.07	25.54	26.72	24.13	23.31	17.27	16.29	16.78	19.58	13.84	15.97	19.28	18.82	19.93	19.50	18.51	20.15	Zr	77.81	76.56	193.18	29.47	41.25	41.59	34.69	33.89	34.89	25.84	38.58	28.94	48.25	28.74	31.46	39.34	31.57	45.34	90.39	36.34	39.15	Nb	1.26	1.57	2.77	1.00	1.43	1.13	1.10	0.64	0.72	0.32	0.30	0.19	0.88	1.17	1.03	1.05	1.12	1.16	1.08	0.86	1.30	Ca	0.06	0.00	0.00	0.02	0.01	0.01	0.01	0.00	0.02	0.01	0.00	0.00	0.05	0.05	0.05	0.05	0.14	0.06	0.05	0.07	0.04	Ba	11.54	9.22	7.81	7.73	10.39	44.58	7.83	14.04	18.41	13.48	5.07	4.84	5.84	36.71	28.28	52.27	36.91	50.14	55.77	45.90	20.94	La	2.28	2.72	6.14	2.16	2.67	2.97	2.04	1.35	1.67	0.79	1.01	0.98	1.79	0.88	1.05	1.59	1.65	1.79	1.83	1.58	1.82	Ce	7.07	8.27	17.99	6.74	8.14	9.06	6.45	4.50	6.29	2.83	3.43	2.94	5.06	2.73	2.75	4.27	4.32	4.65	4.78	4.16	4.86	Pr	1.40	1.53	3.21	1.18	1.35	1.45	1.08	0.79	1.09	0.62	0.70	0.58	0.91	0.49	0.49	0.71	0.72	0.81	0.80	0.70	0.75	Nd	7.44	8.10	16.10	6.77	7.71	7.93	6.21	4.76	6.29	3.87	3.80	3.32	4.89	2.73	2.69	3.68	3.69	4.24	4.04	3.67	4.20	Sm	2.76	2.85	5.29	2.49	2.74	2.58	2.27	1.88	2.23	1.58	1.47	1.32	1.74	1.08	1.06	1.38	1.35	1.52	1.46	1.36	1.56	Eu	1.04	1.07	1.59	0.94	0.97	0.98	0.83	0.70	0.84	0.71	0.60	0.47	0.67	0.43	0.40	0.53	0.54	0.57	0.56	0.53	0.58	Gd	3.48	3.59	6.48	3.24	3.51	3.19	3.04	2.59	2.78	2.12	1.91	1.83	2.28	1.63	1.58	1.91	1.85	2.05	2.01	1.90	2.13	Tb	0.69	0.72	1.28	0.62	0.66	0.59	0.58	0.51	0.52	0.43	0.39	0.38	0.46	0.29	0.31	0.40	0.40	0.43	0.43	0.41	0.41	Dy	4.56	4.80	8.08	4.17	4.50	3.96	4.00	3.59	3.53	2.84	2.63	2.59	3.04	2.10	2.31	2.80	2.78	2.97	2.93	2.82	2.94	Ho	0.92	0.97	1.81	0.89	0.96	0.83	0.87	0.79	0.75	0.57	0.54	0.54	0.62	0.43	0.47	0.61	0.60	0.63	0.62	0.61	0.65	Er	2.75	2.89	4.73	2.49	2.73	2.36	2.47	2.29	2.18	1.67	1.64	1.63	1.89	1.34	1.53	1.91	1.90	1.98	1.97	1.91	1.95	Tm	0.43	0.46	0.73	0.39	0.43	0.36	0.39	0.36	0.35	0.26	0.26	0.27	0.30	0.21	0.26	0.32	0.32	0.33	0.33	0.32	0.32	Yb	2.78	2.88	4.38	2.44	2.68	2.22	2.41	2.28	2.11	1.63	1.66	1.71	1.96	1.36	1.72	2.12	2.12	2.17	2.21	2.11	2.08	Lu	0.43	0.44	0.64	0.37	0.42	0.34	0.37	0.36	0.33	0.25	0.26	0.27	0.31	0.21	0.26	0.34	0.34	0.35	0.36	0.34	0.34	Hf	1.92	1.77	4.54	1.11	1.35	1.28	1.23	1.13	1.18	0.86	0.95	0.77	1.22	0.87	0.89	1.11	0.90	1.24	2.19	1.08	1.20	Ta	0.10	0.12	0.23	0.07	0.10	0.08	0.08	0.04	0.05	0.03	0.03	0.02	0.07	0.07	0.06	0.09	0.10	0.11	0.10	0.09	0.10	Th	0.07	0.10	0.35	0.05	0.07	0.06	0.06	0.04	0.06	0.01	0.02	0.05	0.10	0.10	0.11	0.22	0.23	0.22	0.24	0.23	0.23	U	0.02	0.03	0.18	0.03	0.02	0.03	0.03	0.02	0.03	0.01	0.01	0.03	0.05	0.07	0.11	0.17	0.17	0.18	0.17	0.17	0.18																																																																																																																																																																																																																																																																																																																																																																		
Zn	56.84	24.06	41.93	71.50	110.30	63.02	64.12	54.25	40.93	71.98	24.14	31.98	61.87	125.28	41.69	75.92	63.89	69.68	55.50	47.52	11.60	Ga	16.45	16.56	19.01	15.44	16.33	15.34	15.39	14.82	13.93	13.59	14.82	12.28	13.95	12.99	14.40	15.66	17.79	15.58	15.36	15.15	15.28	Rb	3.44	0.18	0.12	1.07	0.41	0.22	0.11	0.09	2.62	0.52	0.14	0.12	0.84	1.71	1.31	4.73	8.36	8.85	9.64	10.58	1.88	Sr	365.60	369.10	177.60	189.00	103.20	152.90	88.82	76.98	128.00	387.80	336.00	363.80	342.90	98.15	89.14	174.10	373.90	324.80	312.90	387.20	164.00	Y	28.95	30.51	50.99	26.70	29.07	25.54	26.72	24.13	23.31	17.27	16.29	16.78	19.58	13.84	15.97	19.28	18.82	19.93	19.50	18.51	20.15	Zr	77.81	76.56	193.18	29.47	41.25	41.59	34.69	33.89	34.89	25.84	38.58	28.94	48.25	28.74	31.46	39.34	31.57	45.34	90.39	36.34	39.15	Nb	1.26	1.57	2.77	1.00	1.43	1.13	1.10	0.64	0.72	0.32	0.30	0.19	0.88	1.17	1.03	1.05	1.12	1.16	1.08	0.86	1.30	Ca	0.06	0.00	0.00	0.02	0.01	0.01	0.01	0.00	0.02	0.01	0.00	0.00	0.05	0.05	0.05	0.05	0.14	0.06	0.05	0.07	0.04	Ba	11.54	9.22	7.81	7.73	10.39	44.58	7.83	14.04	18.41	13.48	5.07	4.84	5.84	36.71	28.28	52.27	36.91	50.14	55.77	45.90	20.94	La	2.28	2.72	6.14	2.16	2.67	2.97	2.04	1.35	1.67	0.79	1.01	0.98	1.79	0.88	1.05	1.59	1.65	1.79	1.83	1.58	1.82	Ce	7.07	8.27	17.99	6.74	8.14	9.06	6.45	4.50	6.29	2.83	3.43	2.94	5.06	2.73	2.75	4.27	4.32	4.65	4.78	4.16	4.86	Pr	1.40	1.53	3.21	1.18	1.35	1.45	1.08	0.79	1.09	0.62	0.70	0.58	0.91	0.49	0.49	0.71	0.72	0.81	0.80	0.70	0.75	Nd	7.44	8.10	16.10	6.77	7.71	7.93	6.21	4.76	6.29	3.87	3.80	3.32	4.89	2.73	2.69	3.68	3.69	4.24	4.04	3.67	4.20	Sm	2.76	2.85	5.29	2.49	2.74	2.58	2.27	1.88	2.23	1.58	1.47	1.32	1.74	1.08	1.06	1.38	1.35	1.52	1.46	1.36	1.56	Eu	1.04	1.07	1.59	0.94	0.97	0.98	0.83	0.70	0.84	0.71	0.60	0.47	0.67	0.43	0.40	0.53	0.54	0.57	0.56	0.53	0.58	Gd	3.48	3.59	6.48	3.24	3.51	3.19	3.04	2.59	2.78	2.12	1.91	1.83	2.28	1.63	1.58	1.91	1.85	2.05	2.01	1.90	2.13	Tb	0.69	0.72	1.28	0.62	0.66	0.59	0.58	0.51	0.52	0.43	0.39	0.38	0.46	0.29	0.31	0.40	0.40	0.43	0.43	0.41	0.41	Dy	4.56	4.80	8.08	4.17	4.50	3.96	4.00	3.59	3.53	2.84	2.63	2.59	3.04	2.10	2.31	2.80	2.78	2.97	2.93	2.82	2.94	Ho	0.92	0.97	1.81	0.89	0.96	0.83	0.87	0.79	0.75	0.57	0.54	0.54	0.62	0.43	0.47	0.61	0.60	0.63	0.62	0.61	0.65	Er	2.75	2.89	4.73	2.49	2.73	2.36	2.47	2.29	2.18	1.67	1.64	1.63	1.89	1.34	1.53	1.91	1.90	1.98	1.97	1.91	1.95	Tm	0.43	0.46	0.73	0.39	0.43	0.36	0.39	0.36	0.35	0.26	0.26	0.27	0.30	0.21	0.26	0.32	0.32	0.33	0.33	0.32	0.32	Yb	2.78	2.88	4.38	2.44	2.68	2.22	2.41	2.28	2.11	1.63	1.66	1.71	1.96	1.36	1.72	2.12	2.12	2.17	2.21	2.11	2.08	Lu	0.43	0.44	0.64	0.37	0.42	0.34	0.37	0.36	0.33	0.25	0.26	0.27	0.31	0.21	0.26	0.34	0.34	0.35	0.36	0.34	0.34	Hf	1.92	1.77	4.54	1.11	1.35	1.28	1.23	1.13	1.18	0.86	0.95	0.77	1.22	0.87	0.89	1.11	0.90	1.24	2.19	1.08	1.20	Ta	0.10	0.12	0.23	0.07	0.10	0.08	0.08	0.04	0.05	0.03	0.03	0.02	0.07	0.07	0.06	0.09	0.10	0.11	0.10	0.09	0.10	Th	0.07	0.10	0.35	0.05	0.07	0.06	0.06	0.04	0.06	0.01	0.02	0.05	0.10	0.10	0.11	0.22	0.23	0.22	0.24	0.23	0.23	U	0.02	0.03	0.18	0.03	0.02	0.03	0.03	0.02	0.03	0.01	0.01	0.03	0.05	0.07	0.11	0.17	0.17	0.18	0.17	0.17	0.18																																																																																																																																																																																																																																																																																																																																																																																								
Ga	16.45	16.56	19.01	15.44	16.33	15.34	15.39	14.82	13.93	13.59	14.82	12.28	13.95	12.99	14.40	15.66	17.79	15.58	15.36	15.15	15.28	Rb	3.44	0.18	0.12	1.07	0.41	0.22	0.11	0.09	2.62	0.52	0.14	0.12	0.84	1.71	1.31	4.73	8.36	8.85	9.64	10.58	1.88	Sr	365.60	369.10	177.60	189.00	103.20	152.90	88.82	76.98	128.00	387.80	336.00	363.80	342.90	98.15	89.14	174.10	373.90	324.80	312.90	387.20	164.00	Y	28.95	30.51	50.99	26.70	29.07	25.54	26.72	24.13	23.31	17.27	16.29	16.78	19.58	13.84	15.97	19.28	18.82	19.93	19.50	18.51	20.15	Zr	77.81	76.56	193.18	29.47	41.25	41.59	34.69	33.89	34.89	25.84	38.58	28.94	48.25	28.74	31.46	39.34	31.57	45.34	90.39	36.34	39.15	Nb	1.26	1.57	2.77	1.00	1.43	1.13	1.10	0.64	0.72	0.32	0.30	0.19	0.88	1.17	1.03	1.05	1.12	1.16	1.08	0.86	1.30	Ca	0.06	0.00	0.00	0.02	0.01	0.01	0.01	0.00	0.02	0.01	0.00	0.00	0.05	0.05	0.05	0.05	0.14	0.06	0.05	0.07	0.04	Ba	11.54	9.22	7.81	7.73	10.39	44.58	7.83	14.04	18.41	13.48	5.07	4.84	5.84	36.71	28.28	52.27	36.91	50.14	55.77	45.90	20.94	La	2.28	2.72	6.14	2.16	2.67	2.97	2.04	1.35	1.67	0.79	1.01	0.98	1.79	0.88	1.05	1.59	1.65	1.79	1.83	1.58	1.82	Ce	7.07	8.27	17.99	6.74	8.14	9.06	6.45	4.50	6.29	2.83	3.43	2.94	5.06	2.73	2.75	4.27	4.32	4.65	4.78	4.16	4.86	Pr	1.40	1.53	3.21	1.18	1.35	1.45	1.08	0.79	1.09	0.62	0.70	0.58	0.91	0.49	0.49	0.71	0.72	0.81	0.80	0.70	0.75	Nd	7.44	8.10	16.10	6.77	7.71	7.93	6.21	4.76	6.29	3.87	3.80	3.32	4.89	2.73	2.69	3.68	3.69	4.24	4.04	3.67	4.20	Sm	2.76	2.85	5.29	2.49	2.74	2.58	2.27	1.88	2.23	1.58	1.47	1.32	1.74	1.08	1.06	1.38	1.35	1.52	1.46	1.36	1.56	Eu	1.04	1.07	1.59	0.94	0.97	0.98	0.83	0.70	0.84	0.71	0.60	0.47	0.67	0.43	0.40	0.53	0.54	0.57	0.56	0.53	0.58	Gd	3.48	3.59	6.48	3.24	3.51	3.19	3.04	2.59	2.78	2.12	1.91	1.83	2.28	1.63	1.58	1.91	1.85	2.05	2.01	1.90	2.13	Tb	0.69	0.72	1.28	0.62	0.66	0.59	0.58	0.51	0.52	0.43	0.39	0.38	0.46	0.29	0.31	0.40	0.40	0.43	0.43	0.41	0.41	Dy	4.56	4.80	8.08	4.17	4.50	3.96	4.00	3.59	3.53	2.84	2.63	2.59	3.04	2.10	2.31	2.80	2.78	2.97	2.93	2.82	2.94	Ho	0.92	0.97	1.81	0.89	0.96	0.83	0.87	0.79	0.75	0.57	0.54	0.54	0.62	0.43	0.47	0.61	0.60	0.63	0.62	0.61	0.65	Er	2.75	2.89	4.73	2.49	2.73	2.36	2.47	2.29	2.18	1.67	1.64	1.63	1.89	1.34	1.53	1.91	1.90	1.98	1.97	1.91	1.95	Tm	0.43	0.46	0.73	0.39	0.43	0.36	0.39	0.36	0.35	0.26	0.26	0.27	0.30	0.21	0.26	0.32	0.32	0.33	0.33	0.32	0.32	Yb	2.78	2.88	4.38	2.44	2.68	2.22	2.41	2.28	2.11	1.63	1.66	1.71	1.96	1.36	1.72	2.12	2.12	2.17	2.21	2.11	2.08	Lu	0.43	0.44	0.64	0.37	0.42	0.34	0.37	0.36	0.33	0.25	0.26	0.27	0.31	0.21	0.26	0.34	0.34	0.35	0.36	0.34	0.34	Hf	1.92	1.77	4.54	1.11	1.35	1.28	1.23	1.13	1.18	0.86	0.95	0.77	1.22	0.87	0.89	1.11	0.90	1.24	2.19	1.08	1.20	Ta	0.10	0.12	0.23	0.07	0.10	0.08	0.08	0.04	0.05	0.03	0.03	0.02	0.07	0.07	0.06	0.09	0.10	0.11	0.10	0.09	0.10	Th	0.07	0.10	0.35	0.05	0.07	0.06	0.06	0.04	0.06	0.01	0.02	0.05	0.10	0.10	0.11	0.22	0.23	0.22	0.24	0.23	0.23	U	0.02	0.03	0.18	0.03	0.02	0.03	0.03	0.02	0.03	0.01	0.01	0.03	0.05	0.07	0.11	0.17	0.17	0.18	0.17	0.17	0.18																																																																																																																																																																																																																																																																																																																																																																																																														
Rb	3.44	0.18	0.12	1.07	0.41	0.22	0.11	0.09	2.62	0.52	0.14	0.12	0.84	1.71	1.31	4.73	8.36	8.85	9.64	10.58	1.88	Sr	365.60	369.10	177.60	189.00	103.20	152.90	88.82	76.98	128.00	387.80	336.00	363.80	342.90	98.15	89.14	174.10	373.90	324.80	312.90	387.20	164.00	Y	28.95	30.51	50.99	26.70	29.07	25.54	26.72	24.13	23.31	17.27	16.29	16.78	19.58	13.84	15.97	19.28	18.82	19.93	19.50	18.51	20.15	Zr	77.81	76.56	193.18	29.47	41.25	41.59	34.69	33.89	34.89	25.84	38.58	28.94	48.25	28.74	31.46	39.34	31.57	45.34	90.39	36.34	39.15	Nb	1.26	1.57	2.77	1.00	1.43	1.13	1.10	0.64	0.72	0.32	0.30	0.19	0.88	1.17	1.03	1.05	1.12	1.16	1.08	0.86	1.30	Ca	0.06	0.00	0.00	0.02	0.01	0.01	0.01	0.00	0.02	0.01	0.00	0.00	0.05	0.05	0.05	0.05	0.14	0.06	0.05	0.07	0.04	Ba	11.54	9.22	7.81	7.73	10.39	44.58	7.83	14.04	18.41	13.48	5.07	4.84	5.84	36.71	28.28	52.27	36.91	50.14	55.77	45.90	20.94	La	2.28	2.72	6.14	2.16	2.67	2.97	2.04	1.35	1.67	0.79	1.01	0.98	1.79	0.88	1.05	1.59	1.65	1.79	1.83	1.58	1.82	Ce	7.07	8.27	17.99	6.74	8.14	9.06	6.45	4.50	6.29	2.83	3.43	2.94	5.06	2.73	2.75	4.27	4.32	4.65	4.78	4.16	4.86	Pr	1.40	1.53	3.21	1.18	1.35	1.45	1.08	0.79	1.09	0.62	0.70	0.58	0.91	0.49	0.49	0.71	0.72	0.81	0.80	0.70	0.75	Nd	7.44	8.10	16.10	6.77	7.71	7.93	6.21	4.76	6.29	3.87	3.80	3.32	4.89	2.73	2.69	3.68	3.69	4.24	4.04	3.67	4.20	Sm	2.76	2.85	5.29	2.49	2.74	2.58	2.27	1.88	2.23	1.58	1.47	1.32	1.74	1.08	1.06	1.38	1.35	1.52	1.46	1.36	1.56	Eu	1.04	1.07	1.59	0.94	0.97	0.98	0.83	0.70	0.84	0.71	0.60	0.47	0.67	0.43	0.40	0.53	0.54	0.57	0.56	0.53	0.58	Gd	3.48	3.59	6.48	3.24	3.51	3.19	3.04	2.59	2.78	2.12	1.91	1.83	2.28	1.63	1.58	1.91	1.85	2.05	2.01	1.90	2.13	Tb	0.69	0.72	1.28	0.62	0.66	0.59	0.58	0.51	0.52	0.43	0.39	0.38	0.46	0.29	0.31	0.40	0.40	0.43	0.43	0.41	0.41	Dy	4.56	4.80	8.08	4.17	4.50	3.96	4.00	3.59	3.53	2.84	2.63	2.59	3.04	2.10	2.31	2.80	2.78	2.97	2.93	2.82	2.94	Ho	0.92	0.97	1.81	0.89	0.96	0.83	0.87	0.79	0.75	0.57	0.54	0.54	0.62	0.43	0.47	0.61	0.60	0.63	0.62	0.61	0.65	Er	2.75	2.89	4.73	2.49	2.73	2.36	2.47	2.29	2.18	1.67	1.64	1.63	1.89	1.34	1.53	1.91	1.90	1.98	1.97	1.91	1.95	Tm	0.43	0.46	0.73	0.39	0.43	0.36	0.39	0.36	0.35	0.26	0.26	0.27	0.30	0.21	0.26	0.32	0.32	0.33	0.33	0.32	0.32	Yb	2.78	2.88	4.38	2.44	2.68	2.22	2.41	2.28	2.11	1.63	1.66	1.71	1.96	1.36	1.72	2.12	2.12	2.17	2.21	2.11	2.08	Lu	0.43	0.44	0.64	0.37	0.42	0.34	0.37	0.36	0.33	0.25	0.26	0.27	0.31	0.21	0.26	0.34	0.34	0.35	0.36	0.34	0.34	Hf	1.92	1.77	4.54	1.11	1.35	1.28	1.23	1.13	1.18	0.86	0.95	0.77	1.22	0.87	0.89	1.11	0.90	1.24	2.19	1.08	1.20	Ta	0.10	0.12	0.23	0.07	0.10	0.08	0.08	0.04	0.05	0.03	0.03	0.02	0.07	0.07	0.06	0.09	0.10	0.11	0.10	0.09	0.10	Th	0.07	0.10	0.35	0.05	0.07	0.06	0.06	0.04	0.06	0.01	0.02	0.05	0.10	0.10	0.11	0.22	0.23	0.22	0.24	0.23	0.23	U	0.02	0.03	0.18	0.03	0.02	0.03	0.03	0.02	0.03	0.01	0.01	0.03	0.05	0.07	0.11	0.17	0.17	0.18	0.17	0.17	0.18																																																																																																																																																																																																																																																																																																																																																																																																																																				
Sr	365.60	369.10	177.60	189.00	103.20	152.90	88.82	76.98	128.00	387.80	336.00	363.80	342.90	98.15	89.14	174.10	373.90	324.80	312.90	387.20	164.00	Y	28.95	30.51	50.99	26.70	29.07	25.54	26.72	24.13	23.31	17.27	16.29	16.78	19.58	13.84	15.97	19.28	18.82	19.93	19.50	18.51	20.15	Zr	77.81	76.56	193.18	29.47	41.25	41.59	34.69	33.89	34.89	25.84	38.58	28.94	48.25	28.74	31.46	39.34	31.57	45.34	90.39	36.34	39.15	Nb	1.26	1.57	2.77	1.00	1.43	1.13	1.10	0.64	0.72	0.32	0.30	0.19	0.88	1.17	1.03	1.05	1.12	1.16	1.08	0.86	1.30	Ca	0.06	0.00	0.00	0.02	0.01	0.01	0.01	0.00	0.02	0.01	0.00	0.00	0.05	0.05	0.05	0.05	0.14	0.06	0.05	0.07	0.04	Ba	11.54	9.22	7.81	7.73	10.39	44.58	7.83	14.04	18.41	13.48	5.07	4.84	5.84	36.71	28.28	52.27	36.91	50.14	55.77	45.90	20.94	La	2.28	2.72	6.14	2.16	2.67	2.97	2.04	1.35	1.67	0.79	1.01	0.98	1.79	0.88	1.05	1.59	1.65	1.79	1.83	1.58	1.82	Ce	7.07	8.27	17.99	6.74	8.14	9.06	6.45	4.50	6.29	2.83	3.43	2.94	5.06	2.73	2.75	4.27	4.32	4.65	4.78	4.16	4.86	Pr	1.40	1.53	3.21	1.18	1.35	1.45	1.08	0.79	1.09	0.62	0.70	0.58	0.91	0.49	0.49	0.71	0.72	0.81	0.80	0.70	0.75	Nd	7.44	8.10	16.10	6.77	7.71	7.93	6.21	4.76	6.29	3.87	3.80	3.32	4.89	2.73	2.69	3.68	3.69	4.24	4.04	3.67	4.20	Sm	2.76	2.85	5.29	2.49	2.74	2.58	2.27	1.88	2.23	1.58	1.47	1.32	1.74	1.08	1.06	1.38	1.35	1.52	1.46	1.36	1.56	Eu	1.04	1.07	1.59	0.94	0.97	0.98	0.83	0.70	0.84	0.71	0.60	0.47	0.67	0.43	0.40	0.53	0.54	0.57	0.56	0.53	0.58	Gd	3.48	3.59	6.48	3.24	3.51	3.19	3.04	2.59	2.78	2.12	1.91	1.83	2.28	1.63	1.58	1.91	1.85	2.05	2.01	1.90	2.13	Tb	0.69	0.72	1.28	0.62	0.66	0.59	0.58	0.51	0.52	0.43	0.39	0.38	0.46	0.29	0.31	0.40	0.40	0.43	0.43	0.41	0.41	Dy	4.56	4.80	8.08	4.17	4.50	3.96	4.00	3.59	3.53	2.84	2.63	2.59	3.04	2.10	2.31	2.80	2.78	2.97	2.93	2.82	2.94	Ho	0.92	0.97	1.81	0.89	0.96	0.83	0.87	0.79	0.75	0.57	0.54	0.54	0.62	0.43	0.47	0.61	0.60	0.63	0.62	0.61	0.65	Er	2.75	2.89	4.73	2.49	2.73	2.36	2.47	2.29	2.18	1.67	1.64	1.63	1.89	1.34	1.53	1.91	1.90	1.98	1.97	1.91	1.95	Tm	0.43	0.46	0.73	0.39	0.43	0.36	0.39	0.36	0.35	0.26	0.26	0.27	0.30	0.21	0.26	0.32	0.32	0.33	0.33	0.32	0.32	Yb	2.78	2.88	4.38	2.44	2.68	2.22	2.41	2.28	2.11	1.63	1.66	1.71	1.96	1.36	1.72	2.12	2.12	2.17	2.21	2.11	2.08	Lu	0.43	0.44	0.64	0.37	0.42	0.34	0.37	0.36	0.33	0.25	0.26	0.27	0.31	0.21	0.26	0.34	0.34	0.35	0.36	0.34	0.34	Hf	1.92	1.77	4.54	1.11	1.35	1.28	1.23	1.13	1.18	0.86	0.95	0.77	1.22	0.87	0.89	1.11	0.90	1.24	2.19	1.08	1.20	Ta	0.10	0.12	0.23	0.07	0.10	0.08	0.08	0.04	0.05	0.03	0.03	0.02	0.07	0.07	0.06	0.09	0.10	0.11	0.10	0.09	0.10	Th	0.07	0.10	0.35	0.05	0.07	0.06	0.06	0.04	0.06	0.01	0.02	0.05	0.10	0.10	0.11	0.22	0.23	0.22	0.24	0.23	0.23	U	0.02	0.03	0.18	0.03	0.02	0.03	0.03	0.02	0.03	0.01	0.01	0.03	0.05	0.07	0.11	0.17	0.17	0.18	0.17	0.17	0.18																																																																																																																																																																																																																																																																																																																																																																																																																																																										
Y	28.95	30.51	50.99	26.70	29.07	25.54	26.72	24.13	23.31	17.27	16.29	16.78	19.58	13.84	15.97	19.28	18.82	19.93	19.50	18.51	20.15	Zr	77.81	76.56	193.18	29.47	41.25	41.59	34.69	33.89	34.89	25.84	38.58	28.94	48.25	28.74	31.46	39.34	31.57	45.34	90.39	36.34	39.15	Nb	1.26	1.57	2.77	1.00	1.43	1.13	1.10	0.64	0.72	0.32	0.30	0.19	0.88	1.17	1.03	1.05	1.12	1.16	1.08	0.86	1.30	Ca	0.06	0.00	0.00	0.02	0.01	0.01	0.01	0.00	0.02	0.01	0.00	0.00	0.05	0.05	0.05	0.05	0.14	0.06	0.05	0.07	0.04	Ba	11.54	9.22	7.81	7.73	10.39	44.58	7.83	14.04	18.41	13.48	5.07	4.84	5.84	36.71	28.28	52.27	36.91	50.14	55.77	45.90	20.94	La	2.28	2.72	6.14	2.16	2.67	2.97	2.04	1.35	1.67	0.79	1.01	0.98	1.79	0.88	1.05	1.59	1.65	1.79	1.83	1.58	1.82	Ce	7.07	8.27	17.99	6.74	8.14	9.06	6.45	4.50	6.29	2.83	3.43	2.94	5.06	2.73	2.75	4.27	4.32	4.65	4.78	4.16	4.86	Pr	1.40	1.53	3.21	1.18	1.35	1.45	1.08	0.79	1.09	0.62	0.70	0.58	0.91	0.49	0.49	0.71	0.72	0.81	0.80	0.70	0.75	Nd	7.44	8.10	16.10	6.77	7.71	7.93	6.21	4.76	6.29	3.87	3.80	3.32	4.89	2.73	2.69	3.68	3.69	4.24	4.04	3.67	4.20	Sm	2.76	2.85	5.29	2.49	2.74	2.58	2.27	1.88	2.23	1.58	1.47	1.32	1.74	1.08	1.06	1.38	1.35	1.52	1.46	1.36	1.56	Eu	1.04	1.07	1.59	0.94	0.97	0.98	0.83	0.70	0.84	0.71	0.60	0.47	0.67	0.43	0.40	0.53	0.54	0.57	0.56	0.53	0.58	Gd	3.48	3.59	6.48	3.24	3.51	3.19	3.04	2.59	2.78	2.12	1.91	1.83	2.28	1.63	1.58	1.91	1.85	2.05	2.01	1.90	2.13	Tb	0.69	0.72	1.28	0.62	0.66	0.59	0.58	0.51	0.52	0.43	0.39	0.38	0.46	0.29	0.31	0.40	0.40	0.43	0.43	0.41	0.41	Dy	4.56	4.80	8.08	4.17	4.50	3.96	4.00	3.59	3.53	2.84	2.63	2.59	3.04	2.10	2.31	2.80	2.78	2.97	2.93	2.82	2.94	Ho	0.92	0.97	1.81	0.89	0.96	0.83	0.87	0.79	0.75	0.57	0.54	0.54	0.62	0.43	0.47	0.61	0.60	0.63	0.62	0.61	0.65	Er	2.75	2.89	4.73	2.49	2.73	2.36	2.47	2.29	2.18	1.67	1.64	1.63	1.89	1.34	1.53	1.91	1.90	1.98	1.97	1.91	1.95	Tm	0.43	0.46	0.73	0.39	0.43	0.36	0.39	0.36	0.35	0.26	0.26	0.27	0.30	0.21	0.26	0.32	0.32	0.33	0.33	0.32	0.32	Yb	2.78	2.88	4.38	2.44	2.68	2.22	2.41	2.28	2.11	1.63	1.66	1.71	1.96	1.36	1.72	2.12	2.12	2.17	2.21	2.11	2.08	Lu	0.43	0.44	0.64	0.37	0.42	0.34	0.37	0.36	0.33	0.25	0.26	0.27	0.31	0.21	0.26	0.34	0.34	0.35	0.36	0.34	0.34	Hf	1.92	1.77	4.54	1.11	1.35	1.28	1.23	1.13	1.18	0.86	0.95	0.77	1.22	0.87	0.89	1.11	0.90	1.24	2.19	1.08	1.20	Ta	0.10	0.12	0.23	0.07	0.10	0.08	0.08	0.04	0.05	0.03	0.03	0.02	0.07	0.07	0.06	0.09	0.10	0.11	0.10	0.09	0.10	Th	0.07	0.10	0.35	0.05	0.07	0.06	0.06	0.04	0.06	0.01	0.02	0.05	0.10	0.10	0.11	0.22	0.23	0.22	0.24	0.23	0.23	U	0.02	0.03	0.18	0.03	0.02	0.03	0.03	0.02	0.03	0.01	0.01	0.03	0.05	0.07	0.11	0.17	0.17	0.18	0.17	0.17	0.18																																																																																																																																																																																																																																																																																																																																																																																																																																																																																
Zr	77.81	76.56	193.18	29.47	41.25	41.59	34.69	33.89	34.89	25.84	38.58	28.94	48.25	28.74	31.46	39.34	31.57	45.34	90.39	36.34	39.15	Nb	1.26	1.57	2.77	1.00	1.43	1.13	1.10	0.64	0.72	0.32	0.30	0.19	0.88	1.17	1.03	1.05	1.12	1.16	1.08	0.86	1.30	Ca	0.06	0.00	0.00	0.02	0.01	0.01	0.01	0.00	0.02	0.01	0.00	0.00	0.05	0.05	0.05	0.05	0.14	0.06	0.05	0.07	0.04	Ba	11.54	9.22	7.81	7.73	10.39	44.58	7.83	14.04	18.41	13.48	5.07	4.84	5.84	36.71	28.28	52.27	36.91	50.14	55.77	45.90	20.94	La	2.28	2.72	6.14	2.16	2.67	2.97	2.04	1.35	1.67	0.79	1.01	0.98	1.79	0.88	1.05	1.59	1.65	1.79	1.83	1.58	1.82	Ce	7.07	8.27	17.99	6.74	8.14	9.06	6.45	4.50	6.29	2.83	3.43	2.94	5.06	2.73	2.75	4.27	4.32	4.65	4.78	4.16	4.86	Pr	1.40	1.53	3.21	1.18	1.35	1.45	1.08	0.79	1.09	0.62	0.70	0.58	0.91	0.49	0.49	0.71	0.72	0.81	0.80	0.70	0.75	Nd	7.44	8.10	16.10	6.77	7.71	7.93	6.21	4.76	6.29	3.87	3.80	3.32	4.89	2.73	2.69	3.68	3.69	4.24	4.04	3.67	4.20	Sm	2.76	2.85	5.29	2.49	2.74	2.58	2.27	1.88	2.23	1.58	1.47	1.32	1.74	1.08	1.06	1.38	1.35	1.52	1.46	1.36	1.56	Eu	1.04	1.07	1.59	0.94	0.97	0.98	0.83	0.70	0.84	0.71	0.60	0.47	0.67	0.43	0.40	0.53	0.54	0.57	0.56	0.53	0.58	Gd	3.48	3.59	6.48	3.24	3.51	3.19	3.04	2.59	2.78	2.12	1.91	1.83	2.28	1.63	1.58	1.91	1.85	2.05	2.01	1.90	2.13	Tb	0.69	0.72	1.28	0.62	0.66	0.59	0.58	0.51	0.52	0.43	0.39	0.38	0.46	0.29	0.31	0.40	0.40	0.43	0.43	0.41	0.41	Dy	4.56	4.80	8.08	4.17	4.50	3.96	4.00	3.59	3.53	2.84	2.63	2.59	3.04	2.10	2.31	2.80	2.78	2.97	2.93	2.82	2.94	Ho	0.92	0.97	1.81	0.89	0.96	0.83	0.87	0.79	0.75	0.57	0.54	0.54	0.62	0.43	0.47	0.61	0.60	0.63	0.62	0.61	0.65	Er	2.75	2.89	4.73	2.49	2.73	2.36	2.47	2.29	2.18	1.67	1.64	1.63	1.89	1.34	1.53	1.91	1.90	1.98	1.97	1.91	1.95	Tm	0.43	0.46	0.73	0.39	0.43	0.36	0.39	0.36	0.35	0.26	0.26	0.27	0.30	0.21	0.26	0.32	0.32	0.33	0.33	0.32	0.32	Yb	2.78	2.88	4.38	2.44	2.68	2.22	2.41	2.28	2.11	1.63	1.66	1.71	1.96	1.36	1.72	2.12	2.12	2.17	2.21	2.11	2.08	Lu	0.43	0.44	0.64	0.37	0.42	0.34	0.37	0.36	0.33	0.25	0.26	0.27	0.31	0.21	0.26	0.34	0.34	0.35	0.36	0.34	0.34	Hf	1.92	1.77	4.54	1.11	1.35	1.28	1.23	1.13	1.18	0.86	0.95	0.77	1.22	0.87	0.89	1.11	0.90	1.24	2.19	1.08	1.20	Ta	0.10	0.12	0.23	0.07	0.10	0.08	0.08	0.04	0.05	0.03	0.03	0.02	0.07	0.07	0.06	0.09	0.10	0.11	0.10	0.09	0.10	Th	0.07	0.10	0.35	0.05	0.07	0.06	0.06	0.04	0.06	0.01	0.02	0.05	0.10	0.10	0.11	0.22	0.23	0.22	0.24	0.23	0.23	U	0.02	0.03	0.18	0.03	0.02	0.03	0.03	0.02	0.03	0.01	0.01	0.03	0.05	0.07	0.11	0.17	0.17	0.18	0.17	0.17	0.18																																																																																																																																																																																																																																																																																																																																																																																																																																																																																																						
Nb	1.26	1.57	2.77	1.00	1.43	1.13	1.10	0.64	0.72	0.32	0.30	0.19	0.88	1.17	1.03	1.05	1.12	1.16	1.08	0.86	1.30	Ca	0.06	0.00	0.00	0.02	0.01	0.01	0.01	0.00	0.02	0.01	0.00	0.00	0.05	0.05	0.05	0.05	0.14	0.06	0.05	0.07	0.04	Ba	11.54	9.22	7.81	7.73	10.39	44.58	7.83	14.04	18.41	13.48	5.07	4.84	5.84	36.71	28.28	52.27	36.91	50.14	55.77	45.90	20.94	La	2.28	2.72	6.14	2.16	2.67	2.97	2.04	1.35	1.67	0.79	1.01	0.98	1.79	0.88	1.05	1.59	1.65	1.79	1.83	1.58	1.82	Ce	7.07	8.27	17.99	6.74	8.14	9.06	6.45	4.50	6.29	2.83	3.43	2.94	5.06	2.73	2.75	4.27	4.32	4.65	4.78	4.16	4.86	Pr	1.40	1.53	3.21	1.18	1.35	1.45	1.08	0.79	1.09	0.62	0.70	0.58	0.91	0.49	0.49	0.71	0.72	0.81	0.80	0.70	0.75	Nd	7.44	8.10	16.10	6.77	7.71	7.93	6.21	4.76	6.29	3.87	3.80	3.32	4.89	2.73	2.69	3.68	3.69	4.24	4.04	3.67	4.20	Sm	2.76	2.85	5.29	2.49	2.74	2.58	2.27	1.88	2.23	1.58	1.47	1.32	1.74	1.08	1.06	1.38	1.35	1.52	1.46	1.36	1.56	Eu	1.04	1.07	1.59	0.94	0.97	0.98	0.83	0.70	0.84	0.71	0.60	0.47	0.67	0.43	0.40	0.53	0.54	0.57	0.56	0.53	0.58	Gd	3.48	3.59	6.48	3.24	3.51	3.19	3.04	2.59	2.78	2.12	1.91	1.83	2.28	1.63	1.58	1.91	1.85	2.05	2.01	1.90	2.13	Tb	0.69	0.72	1.28	0.62	0.66	0.59	0.58	0.51	0.52	0.43	0.39	0.38	0.46	0.29	0.31	0.40	0.40	0.43	0.43	0.41	0.41	Dy	4.56	4.80	8.08	4.17	4.50	3.96	4.00	3.59	3.53	2.84	2.63	2.59	3.04	2.10	2.31	2.80	2.78	2.97	2.93	2.82	2.94	Ho	0.92	0.97	1.81	0.89	0.96	0.83	0.87	0.79	0.75	0.57	0.54	0.54	0.62	0.43	0.47	0.61	0.60	0.63	0.62	0.61	0.65	Er	2.75	2.89	4.73	2.49	2.73	2.36	2.47	2.29	2.18	1.67	1.64	1.63	1.89	1.34	1.53	1.91	1.90	1.98	1.97	1.91	1.95	Tm	0.43	0.46	0.73	0.39	0.43	0.36	0.39	0.36	0.35	0.26	0.26	0.27	0.30	0.21	0.26	0.32	0.32	0.33	0.33	0.32	0.32	Yb	2.78	2.88	4.38	2.44	2.68	2.22	2.41	2.28	2.11	1.63	1.66	1.71	1.96	1.36	1.72	2.12	2.12	2.17	2.21	2.11	2.08	Lu	0.43	0.44	0.64	0.37	0.42	0.34	0.37	0.36	0.33	0.25	0.26	0.27	0.31	0.21	0.26	0.34	0.34	0.35	0.36	0.34	0.34	Hf	1.92	1.77	4.54	1.11	1.35	1.28	1.23	1.13	1.18	0.86	0.95	0.77	1.22	0.87	0.89	1.11	0.90	1.24	2.19	1.08	1.20	Ta	0.10	0.12	0.23	0.07	0.10	0.08	0.08	0.04	0.05	0.03	0.03	0.02	0.07	0.07	0.06	0.09	0.10	0.11	0.10	0.09	0.10	Th	0.07	0.10	0.35	0.05	0.07	0.06	0.06	0.04	0.06	0.01	0.02	0.05	0.10	0.10	0.11	0.22	0.23	0.22	0.24	0.23	0.23	U	0.02	0.03	0.18	0.03	0.02	0.03	0.03	0.02	0.03	0.01	0.01	0.03	0.05	0.07	0.11	0.17	0.17	0.18	0.17	0.17	0.18																																																																																																																																																																																																																																																																																																																																																																																																																																																																																																																												
Ca	0.06	0.00	0.00	0.02	0.01	0.01	0.01	0.00	0.02	0.01	0.00	0.00	0.05	0.05	0.05	0.05	0.14	0.06	0.05	0.07	0.04	Ba	11.54	9.22	7.81	7.73	10.39	44.58	7.83	14.04	18.41	13.48	5.07	4.84	5.84	36.71	28.28	52.27	36.91	50.14	55.77	45.90	20.94	La	2.28	2.72	6.14	2.16	2.67	2.97	2.04	1.35	1.67	0.79	1.01	0.98	1.79	0.88	1.05	1.59	1.65	1.79	1.83	1.58	1.82	Ce	7.07	8.27	17.99	6.74	8.14	9.06	6.45	4.50	6.29	2.83	3.43	2.94	5.06	2.73	2.75	4.27	4.32	4.65	4.78	4.16	4.86	Pr	1.40	1.53	3.21	1.18	1.35	1.45	1.08	0.79	1.09	0.62	0.70	0.58	0.91	0.49	0.49	0.71	0.72	0.81	0.80	0.70	0.75	Nd	7.44	8.10	16.10	6.77	7.71	7.93	6.21	4.76	6.29	3.87	3.80	3.32	4.89	2.73	2.69	3.68	3.69	4.24	4.04	3.67	4.20	Sm	2.76	2.85	5.29	2.49	2.74	2.58	2.27	1.88	2.23	1.58	1.47	1.32	1.74	1.08	1.06	1.38	1.35	1.52	1.46	1.36	1.56	Eu	1.04	1.07	1.59	0.94	0.97	0.98	0.83	0.70	0.84	0.71	0.60	0.47	0.67	0.43	0.40	0.53	0.54	0.57	0.56	0.53	0.58	Gd	3.48	3.59	6.48	3.24	3.51	3.19	3.04	2.59	2.78	2.12	1.91	1.83	2.28	1.63	1.58	1.91	1.85	2.05	2.01	1.90	2.13	Tb	0.69	0.72	1.28	0.62	0.66	0.59	0.58	0.51	0.52	0.43	0.39	0.38	0.46	0.29	0.31	0.40	0.40	0.43	0.43	0.41	0.41	Dy	4.56	4.80	8.08	4.17	4.50	3.96	4.00	3.59	3.53	2.84	2.63	2.59	3.04	2.10	2.31	2.80	2.78	2.97	2.93	2.82	2.94	Ho	0.92	0.97	1.81	0.89	0.96	0.83	0.87	0.79	0.75	0.57	0.54	0.54	0.62	0.43	0.47	0.61	0.60	0.63	0.62	0.61	0.65	Er	2.75	2.89	4.73	2.49	2.73	2.36	2.47	2.29	2.18	1.67	1.64	1.63	1.89	1.34	1.53	1.91	1.90	1.98	1.97	1.91	1.95	Tm	0.43	0.46	0.73	0.39	0.43	0.36	0.39	0.36	0.35	0.26	0.26	0.27	0.30	0.21	0.26	0.32	0.32	0.33	0.33	0.32	0.32	Yb	2.78	2.88	4.38	2.44	2.68	2.22	2.41	2.28	2.11	1.63	1.66	1.71	1.96	1.36	1.72	2.12	2.12	2.17	2.21	2.11	2.08	Lu	0.43	0.44	0.64	0.37	0.42	0.34	0.37	0.36	0.33	0.25	0.26	0.27	0.31	0.21	0.26	0.34	0.34	0.35	0.36	0.34	0.34	Hf	1.92	1.77	4.54	1.11	1.35	1.28	1.23	1.13	1.18	0.86	0.95	0.77	1.22	0.87	0.89	1.11	0.90	1.24	2.19	1.08	1.20	Ta	0.10	0.12	0.23	0.07	0.10	0.08	0.08	0.04	0.05	0.03	0.03	0.02	0.07	0.07	0.06	0.09	0.10	0.11	0.10	0.09	0.10	Th	0.07	0.10	0.35	0.05	0.07	0.06	0.06	0.04	0.06	0.01	0.02	0.05	0.10	0.10	0.11	0.22	0.23	0.22	0.24	0.23	0.23	U	0.02	0.03	0.18	0.03	0.02	0.03	0.03	0.02	0.03	0.01	0.01	0.03	0.05	0.07	0.11	0.17	0.17	0.18	0.17	0.17	0.18																																																																																																																																																																																																																																																																																																																																																																																																																																																																																																																																																		
Ba	11.54	9.22	7.81	7.73	10.39	44.58	7.83	14.04	18.41	13.48	5.07	4.84	5.84	36.71	28.28	52.27	36.91	50.14	55.77	45.90	20.94	La	2.28	2.72	6.14	2.16	2.67	2.97	2.04	1.35	1.67	0.79	1.01	0.98	1.79	0.88	1.05	1.59	1.65	1.79	1.83	1.58	1.82	Ce	7.07	8.27	17.99	6.74	8.14	9.06	6.45	4.50	6.29	2.83	3.43	2.94	5.06	2.73	2.75	4.27	4.32	4.65	4.78	4.16	4.86	Pr	1.40	1.53	3.21	1.18	1.35	1.45	1.08	0.79	1.09	0.62	0.70	0.58	0.91	0.49	0.49	0.71	0.72	0.81	0.80	0.70	0.75	Nd	7.44	8.10	16.10	6.77	7.71	7.93	6.21	4.76	6.29	3.87	3.80	3.32	4.89	2.73	2.69	3.68	3.69	4.24	4.04	3.67	4.20	Sm	2.76	2.85	5.29	2.49	2.74	2.58	2.27	1.88	2.23	1.58	1.47	1.32	1.74	1.08	1.06	1.38	1.35	1.52	1.46	1.36	1.56	Eu	1.04	1.07	1.59	0.94	0.97	0.98	0.83	0.70	0.84	0.71	0.60	0.47	0.67	0.43	0.40	0.53	0.54	0.57	0.56	0.53	0.58	Gd	3.48	3.59	6.48	3.24	3.51	3.19	3.04	2.59	2.78	2.12	1.91	1.83	2.28	1.63	1.58	1.91	1.85	2.05	2.01	1.90	2.13	Tb	0.69	0.72	1.28	0.62	0.66	0.59	0.58	0.51	0.52	0.43	0.39	0.38	0.46	0.29	0.31	0.40	0.40	0.43	0.43	0.41	0.41	Dy	4.56	4.80	8.08	4.17	4.50	3.96	4.00	3.59	3.53	2.84	2.63	2.59	3.04	2.10	2.31	2.80	2.78	2.97	2.93	2.82	2.94	Ho	0.92	0.97	1.81	0.89	0.96	0.83	0.87	0.79	0.75	0.57	0.54	0.54	0.62	0.43	0.47	0.61	0.60	0.63	0.62	0.61	0.65	Er	2.75	2.89	4.73	2.49	2.73	2.36	2.47	2.29	2.18	1.67	1.64	1.63	1.89	1.34	1.53	1.91	1.90	1.98	1.97	1.91	1.95	Tm	0.43	0.46	0.73	0.39	0.43	0.36	0.39	0.36	0.35	0.26	0.26	0.27	0.30	0.21	0.26	0.32	0.32	0.33	0.33	0.32	0.32	Yb	2.78	2.88	4.38	2.44	2.68	2.22	2.41	2.28	2.11	1.63	1.66	1.71	1.96	1.36	1.72	2.12	2.12	2.17	2.21	2.11	2.08	Lu	0.43	0.44	0.64	0.37	0.42	0.34	0.37	0.36	0.33	0.25	0.26	0.27	0.31	0.21	0.26	0.34	0.34	0.35	0.36	0.34	0.34	Hf	1.92	1.77	4.54	1.11	1.35	1.28	1.23	1.13	1.18	0.86	0.95	0.77	1.22	0.87	0.89	1.11	0.90	1.24	2.19	1.08	1.20	Ta	0.10	0.12	0.23	0.07	0.10	0.08	0.08	0.04	0.05	0.03	0.03	0.02	0.07	0.07	0.06	0.09	0.10	0.11	0.10	0.09	0.10	Th	0.07	0.10	0.35	0.05	0.07	0.06	0.06	0.04	0.06	0.01	0.02	0.05	0.10	0.10	0.11	0.22	0.23	0.22	0.24	0.23	0.23	U	0.02	0.03	0.18	0.03	0.02	0.03	0.03	0.02	0.03	0.01	0.01	0.03	0.05	0.07	0.11	0.17	0.17	0.18	0.17	0.17	0.18																																																																																																																																																																																																																																																																																																																																																																																																																																																																																																																																																																								
La	2.28	2.72	6.14	2.16	2.67	2.97	2.04	1.35	1.67	0.79	1.01	0.98	1.79	0.88	1.05	1.59	1.65	1.79	1.83	1.58	1.82	Ce	7.07	8.27	17.99	6.74	8.14	9.06	6.45	4.50	6.29	2.83	3.43	2.94	5.06	2.73	2.75	4.27	4.32	4.65	4.78	4.16	4.86	Pr	1.40	1.53	3.21	1.18	1.35	1.45	1.08	0.79	1.09	0.62	0.70	0.58	0.91	0.49	0.49	0.71	0.72	0.81	0.80	0.70	0.75	Nd	7.44	8.10	16.10	6.77	7.71	7.93	6.21	4.76	6.29	3.87	3.80	3.32	4.89	2.73	2.69	3.68	3.69	4.24	4.04	3.67	4.20	Sm	2.76	2.85	5.29	2.49	2.74	2.58	2.27	1.88	2.23	1.58	1.47	1.32	1.74	1.08	1.06	1.38	1.35	1.52	1.46	1.36	1.56	Eu	1.04	1.07	1.59	0.94	0.97	0.98	0.83	0.70	0.84	0.71	0.60	0.47	0.67	0.43	0.40	0.53	0.54	0.57	0.56	0.53	0.58	Gd	3.48	3.59	6.48	3.24	3.51	3.19	3.04	2.59	2.78	2.12	1.91	1.83	2.28	1.63	1.58	1.91	1.85	2.05	2.01	1.90	2.13	Tb	0.69	0.72	1.28	0.62	0.66	0.59	0.58	0.51	0.52	0.43	0.39	0.38	0.46	0.29	0.31	0.40	0.40	0.43	0.43	0.41	0.41	Dy	4.56	4.80	8.08	4.17	4.50	3.96	4.00	3.59	3.53	2.84	2.63	2.59	3.04	2.10	2.31	2.80	2.78	2.97	2.93	2.82	2.94	Ho	0.92	0.97	1.81	0.89	0.96	0.83	0.87	0.79	0.75	0.57	0.54	0.54	0.62	0.43	0.47	0.61	0.60	0.63	0.62	0.61	0.65	Er	2.75	2.89	4.73	2.49	2.73	2.36	2.47	2.29	2.18	1.67	1.64	1.63	1.89	1.34	1.53	1.91	1.90	1.98	1.97	1.91	1.95	Tm	0.43	0.46	0.73	0.39	0.43	0.36	0.39	0.36	0.35	0.26	0.26	0.27	0.30	0.21	0.26	0.32	0.32	0.33	0.33	0.32	0.32	Yb	2.78	2.88	4.38	2.44	2.68	2.22	2.41	2.28	2.11	1.63	1.66	1.71	1.96	1.36	1.72	2.12	2.12	2.17	2.21	2.11	2.08	Lu	0.43	0.44	0.64	0.37	0.42	0.34	0.37	0.36	0.33	0.25	0.26	0.27	0.31	0.21	0.26	0.34	0.34	0.35	0.36	0.34	0.34	Hf	1.92	1.77	4.54	1.11	1.35	1.28	1.23	1.13	1.18	0.86	0.95	0.77	1.22	0.87	0.89	1.11	0.90	1.24	2.19	1.08	1.20	Ta	0.10	0.12	0.23	0.07	0.10	0.08	0.08	0.04	0.05	0.03	0.03	0.02	0.07	0.07	0.06	0.09	0.10	0.11	0.10	0.09	0.10	Th	0.07	0.10	0.35	0.05	0.07	0.06	0.06	0.04	0.06	0.01	0.02	0.05	0.10	0.10	0.11	0.22	0.23	0.22	0.24	0.23	0.23	U	0.02	0.03	0.18	0.03	0.02	0.03	0.03	0.02	0.03	0.01	0.01	0.03	0.05	0.07	0.11	0.17	0.17	0.18	0.17	0.17	0.18																																																																																																																																																																																																																																																																																																																																																																																																																																																																																																																																																																																														
Ce	7.07	8.27	17.99	6.74	8.14	9.06	6.45	4.50	6.29	2.83	3.43	2.94	5.06	2.73	2.75	4.27	4.32	4.65	4.78	4.16	4.86	Pr	1.40	1.53	3.21	1.18	1.35	1.45	1.08	0.79	1.09	0.62	0.70	0.58	0.91	0.49	0.49	0.71	0.72	0.81	0.80	0.70	0.75	Nd	7.44	8.10	16.10	6.77	7.71	7.93	6.21	4.76	6.29	3.87	3.80	3.32	4.89	2.73	2.69	3.68	3.69	4.24	4.04	3.67	4.20	Sm	2.76	2.85	5.29	2.49	2.74	2.58	2.27	1.88	2.23	1.58	1.47	1.32	1.74	1.08	1.06	1.38	1.35	1.52	1.46	1.36	1.56	Eu	1.04	1.07	1.59	0.94	0.97	0.98	0.83	0.70	0.84	0.71	0.60	0.47	0.67	0.43	0.40	0.53	0.54	0.57	0.56	0.53	0.58	Gd	3.48	3.59	6.48	3.24	3.51	3.19	3.04	2.59	2.78	2.12	1.91	1.83	2.28	1.63	1.58	1.91	1.85	2.05	2.01	1.90	2.13	Tb	0.69	0.72	1.28	0.62	0.66	0.59	0.58	0.51	0.52	0.43	0.39	0.38	0.46	0.29	0.31	0.40	0.40	0.43	0.43	0.41	0.41	Dy	4.56	4.80	8.08	4.17	4.50	3.96	4.00	3.59	3.53	2.84	2.63	2.59	3.04	2.10	2.31	2.80	2.78	2.97	2.93	2.82	2.94	Ho	0.92	0.97	1.81	0.89	0.96	0.83	0.87	0.79	0.75	0.57	0.54	0.54	0.62	0.43	0.47	0.61	0.60	0.63	0.62	0.61	0.65	Er	2.75	2.89	4.73	2.49	2.73	2.36	2.47	2.29	2.18	1.67	1.64	1.63	1.89	1.34	1.53	1.91	1.90	1.98	1.97	1.91	1.95	Tm	0.43	0.46	0.73	0.39	0.43	0.36	0.39	0.36	0.35	0.26	0.26	0.27	0.30	0.21	0.26	0.32	0.32	0.33	0.33	0.32	0.32	Yb	2.78	2.88	4.38	2.44	2.68	2.22	2.41	2.28	2.11	1.63	1.66	1.71	1.96	1.36	1.72	2.12	2.12	2.17	2.21	2.11	2.08	Lu	0.43	0.44	0.64	0.37	0.42	0.34	0.37	0.36	0.33	0.25	0.26	0.27	0.31	0.21	0.26	0.34	0.34	0.35	0.36	0.34	0.34	Hf	1.92	1.77	4.54	1.11	1.35	1.28	1.23	1.13	1.18	0.86	0.95	0.77	1.22	0.87	0.89	1.11	0.90	1.24	2.19	1.08	1.20	Ta	0.10	0.12	0.23	0.07	0.10	0.08	0.08	0.04	0.05	0.03	0.03	0.02	0.07	0.07	0.06	0.09	0.10	0.11	0.10	0.09	0.10	Th	0.07	0.10	0.35	0.05	0.07	0.06	0.06	0.04	0.06	0.01	0.02	0.05	0.10	0.10	0.11	0.22	0.23	0.22	0.24	0.23	0.23	U	0.02	0.03	0.18	0.03	0.02	0.03	0.03	0.02	0.03	0.01	0.01	0.03	0.05	0.07	0.11	0.17	0.17	0.18	0.17	0.17	0.18																																																																																																																																																																																																																																																																																																																																																																																																																																																																																																																																																																																																																				
Pr	1.40	1.53	3.21	1.18	1.35	1.45	1.08	0.79	1.09	0.62	0.70	0.58	0.91	0.49	0.49	0.71	0.72	0.81	0.80	0.70	0.75	Nd	7.44	8.10	16.10	6.77	7.71	7.93	6.21	4.76	6.29	3.87	3.80	3.32	4.89	2.73	2.69	3.68	3.69	4.24	4.04	3.67	4.20	Sm	2.76	2.85	5.29	2.49	2.74	2.58	2.27	1.88	2.23	1.58	1.47	1.32	1.74	1.08	1.06	1.38	1.35	1.52	1.46	1.36	1.56	Eu	1.04	1.07	1.59	0.94	0.97	0.98	0.83	0.70	0.84	0.71	0.60	0.47	0.67	0.43	0.40	0.53	0.54	0.57	0.56	0.53	0.58	Gd	3.48	3.59	6.48	3.24	3.51	3.19	3.04	2.59	2.78	2.12	1.91	1.83	2.28	1.63	1.58	1.91	1.85	2.05	2.01	1.90	2.13	Tb	0.69	0.72	1.28	0.62	0.66	0.59	0.58	0.51	0.52	0.43	0.39	0.38	0.46	0.29	0.31	0.40	0.40	0.43	0.43	0.41	0.41	Dy	4.56	4.80	8.08	4.17	4.50	3.96	4.00	3.59	3.53	2.84	2.63	2.59	3.04	2.10	2.31	2.80	2.78	2.97	2.93	2.82	2.94	Ho	0.92	0.97	1.81	0.89	0.96	0.83	0.87	0.79	0.75	0.57	0.54	0.54	0.62	0.43	0.47	0.61	0.60	0.63	0.62	0.61	0.65	Er	2.75	2.89	4.73	2.49	2.73	2.36	2.47	2.29	2.18	1.67	1.64	1.63	1.89	1.34	1.53	1.91	1.90	1.98	1.97	1.91	1.95	Tm	0.43	0.46	0.73	0.39	0.43	0.36	0.39	0.36	0.35	0.26	0.26	0.27	0.30	0.21	0.26	0.32	0.32	0.33	0.33	0.32	0.32	Yb	2.78	2.88	4.38	2.44	2.68	2.22	2.41	2.28	2.11	1.63	1.66	1.71	1.96	1.36	1.72	2.12	2.12	2.17	2.21	2.11	2.08	Lu	0.43	0.44	0.64	0.37	0.42	0.34	0.37	0.36	0.33	0.25	0.26	0.27	0.31	0.21	0.26	0.34	0.34	0.35	0.36	0.34	0.34	Hf	1.92	1.77	4.54	1.11	1.35	1.28	1.23	1.13	1.18	0.86	0.95	0.77	1.22	0.87	0.89	1.11	0.90	1.24	2.19	1.08	1.20	Ta	0.10	0.12	0.23	0.07	0.10	0.08	0.08	0.04	0.05	0.03	0.03	0.02	0.07	0.07	0.06	0.09	0.10	0.11	0.10	0.09	0.10	Th	0.07	0.10	0.35	0.05	0.07	0.06	0.06	0.04	0.06	0.01	0.02	0.05	0.10	0.10	0.11	0.22	0.23	0.22	0.24	0.23	0.23	U	0.02	0.03	0.18	0.03	0.02	0.03	0.03	0.02	0.03	0.01	0.01	0.03	0.05	0.07	0.11	0.17	0.17	0.18	0.17	0.17	0.18																																																																																																																																																																																																																																																																																																																																																																																																																																																																																																																																																																																																																																										
Nd	7.44	8.10	16.10	6.77	7.71	7.93	6.21	4.76	6.29	3.87	3.80	3.32	4.89	2.73	2.69	3.68	3.69	4.24	4.04	3.67	4.20	Sm	2.76	2.85	5.29	2.49	2.74	2.58	2.27	1.88	2.23	1.58	1.47	1.32	1.74	1.08	1.06	1.38	1.35	1.52	1.46	1.36	1.56	Eu	1.04	1.07	1.59	0.94	0.97	0.98	0.83	0.70	0.84	0.71	0.60	0.47	0.67	0.43	0.40	0.53	0.54	0.57	0.56	0.53	0.58	Gd	3.48	3.59	6.48	3.24	3.51	3.19	3.04	2.59	2.78	2.12	1.91	1.83	2.28	1.63	1.58	1.91	1.85	2.05	2.01	1.90	2.13	Tb	0.69	0.72	1.28	0.62	0.66	0.59	0.58	0.51	0.52	0.43	0.39	0.38	0.46	0.29	0.31	0.40	0.40	0.43	0.43	0.41	0.41	Dy	4.56	4.80	8.08	4.17	4.50	3.96	4.00	3.59	3.53	2.84	2.63	2.59	3.04	2.10	2.31	2.80	2.78	2.97	2.93	2.82	2.94	Ho	0.92	0.97	1.81	0.89	0.96	0.83	0.87	0.79	0.75	0.57	0.54	0.54	0.62	0.43	0.47	0.61	0.60	0.63	0.62	0.61	0.65	Er	2.75	2.89	4.73	2.49	2.73	2.36	2.47	2.29	2.18	1.67	1.64	1.63	1.89	1.34	1.53	1.91	1.90	1.98	1.97	1.91	1.95	Tm	0.43	0.46	0.73	0.39	0.43	0.36	0.39	0.36	0.35	0.26	0.26	0.27	0.30	0.21	0.26	0.32	0.32	0.33	0.33	0.32	0.32	Yb	2.78	2.88	4.38	2.44	2.68	2.22	2.41	2.28	2.11	1.63	1.66	1.71	1.96	1.36	1.72	2.12	2.12	2.17	2.21	2.11	2.08	Lu	0.43	0.44	0.64	0.37	0.42	0.34	0.37	0.36	0.33	0.25	0.26	0.27	0.31	0.21	0.26	0.34	0.34	0.35	0.36	0.34	0.34	Hf	1.92	1.77	4.54	1.11	1.35	1.28	1.23	1.13	1.18	0.86	0.95	0.77	1.22	0.87	0.89	1.11	0.90	1.24	2.19	1.08	1.20	Ta	0.10	0.12	0.23	0.07	0.10	0.08	0.08	0.04	0.05	0.03	0.03	0.02	0.07	0.07	0.06	0.09	0.10	0.11	0.10	0.09	0.10	Th	0.07	0.10	0.35	0.05	0.07	0.06	0.06	0.04	0.06	0.01	0.02	0.05	0.10	0.10	0.11	0.22	0.23	0.22	0.24	0.23	0.23	U	0.02	0.03	0.18	0.03	0.02	0.03	0.03	0.02	0.03	0.01	0.01	0.03	0.05	0.07	0.11	0.17	0.17	0.18	0.17	0.17	0.18																																																																																																																																																																																																																																																																																																																																																																																																																																																																																																																																																																																																																																																																
Sm	2.76	2.85	5.29	2.49	2.74	2.58	2.27	1.88	2.23	1.58	1.47	1.32	1.74	1.08	1.06	1.38	1.35	1.52	1.46	1.36	1.56	Eu	1.04	1.07	1.59	0.94	0.97	0.98	0.83	0.70	0.84	0.71	0.60	0.47	0.67	0.43	0.40	0.53	0.54	0.57	0.56	0.53	0.58	Gd	3.48	3.59	6.48	3.24	3.51	3.19	3.04	2.59	2.78	2.12	1.91	1.83	2.28	1.63	1.58	1.91	1.85	2.05	2.01	1.90	2.13	Tb	0.69	0.72	1.28	0.62	0.66	0.59	0.58	0.51	0.52	0.43	0.39	0.38	0.46	0.29	0.31	0.40	0.40	0.43	0.43	0.41	0.41	Dy	4.56	4.80	8.08	4.17	4.50	3.96	4.00	3.59	3.53	2.84	2.63	2.59	3.04	2.10	2.31	2.80	2.78	2.97	2.93	2.82	2.94	Ho	0.92	0.97	1.81	0.89	0.96	0.83	0.87	0.79	0.75	0.57	0.54	0.54	0.62	0.43	0.47	0.61	0.60	0.63	0.62	0.61	0.65	Er	2.75	2.89	4.73	2.49	2.73	2.36	2.47	2.29	2.18	1.67	1.64	1.63	1.89	1.34	1.53	1.91	1.90	1.98	1.97	1.91	1.95	Tm	0.43	0.46	0.73	0.39	0.43	0.36	0.39	0.36	0.35	0.26	0.26	0.27	0.30	0.21	0.26	0.32	0.32	0.33	0.33	0.32	0.32	Yb	2.78	2.88	4.38	2.44	2.68	2.22	2.41	2.28	2.11	1.63	1.66	1.71	1.96	1.36	1.72	2.12	2.12	2.17	2.21	2.11	2.08	Lu	0.43	0.44	0.64	0.37	0.42	0.34	0.37	0.36	0.33	0.25	0.26	0.27	0.31	0.21	0.26	0.34	0.34	0.35	0.36	0.34	0.34	Hf	1.92	1.77	4.54	1.11	1.35	1.28	1.23	1.13	1.18	0.86	0.95	0.77	1.22	0.87	0.89	1.11	0.90	1.24	2.19	1.08	1.20	Ta	0.10	0.12	0.23	0.07	0.10	0.08	0.08	0.04	0.05	0.03	0.03	0.02	0.07	0.07	0.06	0.09	0.10	0.11	0.10	0.09	0.10	Th	0.07	0.10	0.35	0.05	0.07	0.06	0.06	0.04	0.06	0.01	0.02	0.05	0.10	0.10	0.11	0.22	0.23	0.22	0.24	0.23	0.23	U	0.02	0.03	0.18	0.03	0.02	0.03	0.03	0.02	0.03	0.01	0.01	0.03	0.05	0.07	0.11	0.17	0.17	0.18	0.17	0.17	0.18																																																																																																																																																																																																																																																																																																																																																																																																																																																																																																																																																																																																																																																																																						
Eu	1.04	1.07	1.59	0.94	0.97	0.98	0.83	0.70	0.84	0.71	0.60	0.47	0.67	0.43	0.40	0.53	0.54	0.57	0.56	0.53	0.58	Gd	3.48	3.59	6.48	3.24	3.51	3.19	3.04	2.59	2.78	2.12	1.91	1.83	2.28	1.63	1.58	1.91	1.85	2.05	2.01	1.90	2.13	Tb	0.69	0.72	1.28	0.62	0.66	0.59	0.58	0.51	0.52	0.43	0.39	0.38	0.46	0.29	0.31	0.40	0.40	0.43	0.43	0.41	0.41	Dy	4.56	4.80	8.08	4.17	4.50	3.96	4.00	3.59	3.53	2.84	2.63	2.59	3.04	2.10	2.31	2.80	2.78	2.97	2.93	2.82	2.94	Ho	0.92	0.97	1.81	0.89	0.96	0.83	0.87	0.79	0.75	0.57	0.54	0.54	0.62	0.43	0.47	0.61	0.60	0.63	0.62	0.61	0.65	Er	2.75	2.89	4.73	2.49	2.73	2.36	2.47	2.29	2.18	1.67	1.64	1.63	1.89	1.34	1.53	1.91	1.90	1.98	1.97	1.91	1.95	Tm	0.43	0.46	0.73	0.39	0.43	0.36	0.39	0.36	0.35	0.26	0.26	0.27	0.30	0.21	0.26	0.32	0.32	0.33	0.33	0.32	0.32	Yb	2.78	2.88	4.38	2.44	2.68	2.22	2.41	2.28	2.11	1.63	1.66	1.71	1.96	1.36	1.72	2.12	2.12	2.17	2.21	2.11	2.08	Lu	0.43	0.44	0.64	0.37	0.42	0.34	0.37	0.36	0.33	0.25	0.26	0.27	0.31	0.21	0.26	0.34	0.34	0.35	0.36	0.34	0.34	Hf	1.92	1.77	4.54	1.11	1.35	1.28	1.23	1.13	1.18	0.86	0.95	0.77	1.22	0.87	0.89	1.11	0.90	1.24	2.19	1.08	1.20	Ta	0.10	0.12	0.23	0.07	0.10	0.08	0.08	0.04	0.05	0.03	0.03	0.02	0.07	0.07	0.06	0.09	0.10	0.11	0.10	0.09	0.10	Th	0.07	0.10	0.35	0.05	0.07	0.06	0.06	0.04	0.06	0.01	0.02	0.05	0.10	0.10	0.11	0.22	0.23	0.22	0.24	0.23	0.23	U	0.02	0.03	0.18	0.03	0.02	0.03	0.03	0.02	0.03	0.01	0.01	0.03	0.05	0.07	0.11	0.17	0.17	0.18	0.17	0.17	0.18																																																																																																																																																																																																																																																																																																																																																																																																																																																																																																																																																																																																																																																																																																												
Gd	3.48	3.59	6.48	3.24	3.51	3.19	3.04	2.59	2.78	2.12	1.91	1.83	2.28	1.63	1.58	1.91	1.85	2.05	2.01	1.90	2.13	Tb	0.69	0.72	1.28	0.62	0.66	0.59	0.58	0.51	0.52	0.43	0.39	0.38	0.46	0.29	0.31	0.40	0.40	0.43	0.43	0.41	0.41	Dy	4.56	4.80	8.08	4.17	4.50	3.96	4.00	3.59	3.53	2.84	2.63	2.59	3.04	2.10	2.31	2.80	2.78	2.97	2.93	2.82	2.94	Ho	0.92	0.97	1.81	0.89	0.96	0.83	0.87	0.79	0.75	0.57	0.54	0.54	0.62	0.43	0.47	0.61	0.60	0.63	0.62	0.61	0.65	Er	2.75	2.89	4.73	2.49	2.73	2.36	2.47	2.29	2.18	1.67	1.64	1.63	1.89	1.34	1.53	1.91	1.90	1.98	1.97	1.91	1.95	Tm	0.43	0.46	0.73	0.39	0.43	0.36	0.39	0.36	0.35	0.26	0.26	0.27	0.30	0.21	0.26	0.32	0.32	0.33	0.33	0.32	0.32	Yb	2.78	2.88	4.38	2.44	2.68	2.22	2.41	2.28	2.11	1.63	1.66	1.71	1.96	1.36	1.72	2.12	2.12	2.17	2.21	2.11	2.08	Lu	0.43	0.44	0.64	0.37	0.42	0.34	0.37	0.36	0.33	0.25	0.26	0.27	0.31	0.21	0.26	0.34	0.34	0.35	0.36	0.34	0.34	Hf	1.92	1.77	4.54	1.11	1.35	1.28	1.23	1.13	1.18	0.86	0.95	0.77	1.22	0.87	0.89	1.11	0.90	1.24	2.19	1.08	1.20	Ta	0.10	0.12	0.23	0.07	0.10	0.08	0.08	0.04	0.05	0.03	0.03	0.02	0.07	0.07	0.06	0.09	0.10	0.11	0.10	0.09	0.10	Th	0.07	0.10	0.35	0.05	0.07	0.06	0.06	0.04	0.06	0.01	0.02	0.05	0.10	0.10	0.11	0.22	0.23	0.22	0.24	0.23	0.23	U	0.02	0.03	0.18	0.03	0.02	0.03	0.03	0.02	0.03	0.01	0.01	0.03	0.05	0.07	0.11	0.17	0.17	0.18	0.17	0.17	0.18																																																																																																																																																																																																																																																																																																																																																																																																																																																																																																																																																																																																																																																																																																																																		
Tb	0.69	0.72	1.28	0.62	0.66	0.59	0.58	0.51	0.52	0.43	0.39	0.38	0.46	0.29	0.31	0.40	0.40	0.43	0.43	0.41	0.41	Dy	4.56	4.80	8.08	4.17	4.50	3.96	4.00	3.59	3.53	2.84	2.63	2.59	3.04	2.10	2.31	2.80	2.78	2.97	2.93	2.82	2.94	Ho	0.92	0.97	1.81	0.89	0.96	0.83	0.87	0.79	0.75	0.57	0.54	0.54	0.62	0.43	0.47	0.61	0.60	0.63	0.62	0.61	0.65	Er	2.75	2.89	4.73	2.49	2.73	2.36	2.47	2.29	2.18	1.67	1.64	1.63	1.89	1.34	1.53	1.91	1.90	1.98	1.97	1.91	1.95	Tm	0.43	0.46	0.73	0.39	0.43	0.36	0.39	0.36	0.35	0.26	0.26	0.27	0.30	0.21	0.26	0.32	0.32	0.33	0.33	0.32	0.32	Yb	2.78	2.88	4.38	2.44	2.68	2.22	2.41	2.28	2.11	1.63	1.66	1.71	1.96	1.36	1.72	2.12	2.12	2.17	2.21	2.11	2.08	Lu	0.43	0.44	0.64	0.37	0.42	0.34	0.37	0.36	0.33	0.25	0.26	0.27	0.31	0.21	0.26	0.34	0.34	0.35	0.36	0.34	0.34	Hf	1.92	1.77	4.54	1.11	1.35	1.28	1.23	1.13	1.18	0.86	0.95	0.77	1.22	0.87	0.89	1.11	0.90	1.24	2.19	1.08	1.20	Ta	0.10	0.12	0.23	0.07	0.10	0.08	0.08	0.04	0.05	0.03	0.03	0.02	0.07	0.07	0.06	0.09	0.10	0.11	0.10	0.09	0.10	Th	0.07	0.10	0.35	0.05	0.07	0.06	0.06	0.04	0.06	0.01	0.02	0.05	0.10	0.10	0.11	0.22	0.23	0.22	0.24	0.23	0.23	U	0.02	0.03	0.18	0.03	0.02	0.03	0.03	0.02	0.03	0.01	0.01	0.03	0.05	0.07	0.11	0.17	0.17	0.18	0.17	0.17	0.18																																																																																																																																																																																																																																																																																																																																																																																																																																																																																																																																																																																																																																																																																																																																																								
Dy	4.56	4.80	8.08	4.17	4.50	3.96	4.00	3.59	3.53	2.84	2.63	2.59	3.04	2.10	2.31	2.80	2.78	2.97	2.93	2.82	2.94	Ho	0.92	0.97	1.81	0.89	0.96	0.83	0.87	0.79	0.75	0.57	0.54	0.54	0.62	0.43	0.47	0.61	0.60	0.63	0.62	0.61	0.65	Er	2.75	2.89	4.73	2.49	2.73	2.36	2.47	2.29	2.18	1.67	1.64	1.63	1.89	1.34	1.53	1.91	1.90	1.98	1.97	1.91	1.95	Tm	0.43	0.46	0.73	0.39	0.43	0.36	0.39	0.36	0.35	0.26	0.26	0.27	0.30	0.21	0.26	0.32	0.32	0.33	0.33	0.32	0.32	Yb	2.78	2.88	4.38	2.44	2.68	2.22	2.41	2.28	2.11	1.63	1.66	1.71	1.96	1.36	1.72	2.12	2.12	2.17	2.21	2.11	2.08	Lu	0.43	0.44	0.64	0.37	0.42	0.34	0.37	0.36	0.33	0.25	0.26	0.27	0.31	0.21	0.26	0.34	0.34	0.35	0.36	0.34	0.34	Hf	1.92	1.77	4.54	1.11	1.35	1.28	1.23	1.13	1.18	0.86	0.95	0.77	1.22	0.87	0.89	1.11	0.90	1.24	2.19	1.08	1.20	Ta	0.10	0.12	0.23	0.07	0.10	0.08	0.08	0.04	0.05	0.03	0.03	0.02	0.07	0.07	0.06	0.09	0.10	0.11	0.10	0.09	0.10	Th	0.07	0.10	0.35	0.05	0.07	0.06	0.06	0.04	0.06	0.01	0.02	0.05	0.10	0.10	0.11	0.22	0.23	0.22	0.24	0.23	0.23	U	0.02	0.03	0.18	0.03	0.02	0.03	0.03	0.02	0.03	0.01	0.01	0.03	0.05	0.07	0.11	0.17	0.17	0.18	0.17	0.17	0.18																																																																																																																																																																																																																																																																																																																																																																																																																																																																																																																																																																																																																																																																																																																																																																														
Ho	0.92	0.97	1.81	0.89	0.96	0.83	0.87	0.79	0.75	0.57	0.54	0.54	0.62	0.43	0.47	0.61	0.60	0.63	0.62	0.61	0.65	Er	2.75	2.89	4.73	2.49	2.73	2.36	2.47	2.29	2.18	1.67	1.64	1.63	1.89	1.34	1.53	1.91	1.90	1.98	1.97	1.91	1.95	Tm	0.43	0.46	0.73	0.39	0.43	0.36	0.39	0.36	0.35	0.26	0.26	0.27	0.30	0.21	0.26	0.32	0.32	0.33	0.33	0.32	0.32	Yb	2.78	2.88	4.38	2.44	2.68	2.22	2.41	2.28	2.11	1.63	1.66	1.71	1.96	1.36	1.72	2.12	2.12	2.17	2.21	2.11	2.08	Lu	0.43	0.44	0.64	0.37	0.42	0.34	0.37	0.36	0.33	0.25	0.26	0.27	0.31	0.21	0.26	0.34	0.34	0.35	0.36	0.34	0.34	Hf	1.92	1.77	4.54	1.11	1.35	1.28	1.23	1.13	1.18	0.86	0.95	0.77	1.22	0.87	0.89	1.11	0.90	1.24	2.19	1.08	1.20	Ta	0.10	0.12	0.23	0.07	0.10	0.08	0.08	0.04	0.05	0.03	0.03	0.02	0.07	0.07	0.06	0.09	0.10	0.11	0.10	0.09	0.10	Th	0.07	0.10	0.35	0.05	0.07	0.06	0.06	0.04	0.06	0.01	0.02	0.05	0.10	0.10	0.11	0.22	0.23	0.22	0.24	0.23	0.23	U	0.02	0.03	0.18	0.03	0.02	0.03	0.03	0.02	0.03	0.01	0.01	0.03	0.05	0.07	0.11	0.17	0.17	0.18	0.17	0.17	0.18																																																																																																																																																																																																																																																																																																																																																																																																																																																																																																																																																																																																																																																																																																																																																																																																				
Er	2.75	2.89	4.73	2.49	2.73	2.36	2.47	2.29	2.18	1.67	1.64	1.63	1.89	1.34	1.53	1.91	1.90	1.98	1.97	1.91	1.95	Tm	0.43	0.46	0.73	0.39	0.43	0.36	0.39	0.36	0.35	0.26	0.26	0.27	0.30	0.21	0.26	0.32	0.32	0.33	0.33	0.32	0.32	Yb	2.78	2.88	4.38	2.44	2.68	2.22	2.41	2.28	2.11	1.63	1.66	1.71	1.96	1.36	1.72	2.12	2.12	2.17	2.21	2.11	2.08	Lu	0.43	0.44	0.64	0.37	0.42	0.34	0.37	0.36	0.33	0.25	0.26	0.27	0.31	0.21	0.26	0.34	0.34	0.35	0.36	0.34	0.34	Hf	1.92	1.77	4.54	1.11	1.35	1.28	1.23	1.13	1.18	0.86	0.95	0.77	1.22	0.87	0.89	1.11	0.90	1.24	2.19	1.08	1.20	Ta	0.10	0.12	0.23	0.07	0.10	0.08	0.08	0.04	0.05	0.03	0.03	0.02	0.07	0.07	0.06	0.09	0.10	0.11	0.10	0.09	0.10	Th	0.07	0.10	0.35	0.05	0.07	0.06	0.06	0.04	0.06	0.01	0.02	0.05	0.10	0.10	0.11	0.22	0.23	0.22	0.24	0.23	0.23	U	0.02	0.03	0.18	0.03	0.02	0.03	0.03	0.02	0.03	0.01	0.01	0.03	0.05	0.07	0.11	0.17	0.17	0.18	0.17	0.17	0.18																																																																																																																																																																																																																																																																																																																																																																																																																																																																																																																																																																																																																																																																																																																																																																																																																										
Tm	0.43	0.46	0.73	0.39	0.43	0.36	0.39	0.36	0.35	0.26	0.26	0.27	0.30	0.21	0.26	0.32	0.32	0.33	0.33	0.32	0.32	Yb	2.78	2.88	4.38	2.44	2.68	2.22	2.41	2.28	2.11	1.63	1.66	1.71	1.96	1.36	1.72	2.12	2.12	2.17	2.21	2.11	2.08	Lu	0.43	0.44	0.64	0.37	0.42	0.34	0.37	0.36	0.33	0.25	0.26	0.27	0.31	0.21	0.26	0.34	0.34	0.35	0.36	0.34	0.34	Hf	1.92	1.77	4.54	1.11	1.35	1.28	1.23	1.13	1.18	0.86	0.95	0.77	1.22	0.87	0.89	1.11	0.90	1.24	2.19	1.08	1.20	Ta	0.10	0.12	0.23	0.07	0.10	0.08	0.08	0.04	0.05	0.03	0.03	0.02	0.07	0.07	0.06	0.09	0.10	0.11	0.10	0.09	0.10	Th	0.07	0.10	0.35	0.05	0.07	0.06	0.06	0.04	0.06	0.01	0.02	0.05	0.10	0.10	0.11	0.22	0.23	0.22	0.24	0.23	0.23	U	0.02	0.03	0.18	0.03	0.02	0.03	0.03	0.02	0.03	0.01	0.01	0.03	0.05	0.07	0.11	0.17	0.17	0.18	0.17	0.17	0.18																																																																																																																																																																																																																																																																																																																																																																																																																																																																																																																																																																																																																																																																																																																																																																																																																																																
Yb	2.78	2.88	4.38	2.44	2.68	2.22	2.41	2.28	2.11	1.63	1.66	1.71	1.96	1.36	1.72	2.12	2.12	2.17	2.21	2.11	2.08	Lu	0.43	0.44	0.64	0.37	0.42	0.34	0.37	0.36	0.33	0.25	0.26	0.27	0.31	0.21	0.26	0.34	0.34	0.35	0.36	0.34	0.34	Hf	1.92	1.77	4.54	1.11	1.35	1.28	1.23	1.13	1.18	0.86	0.95	0.77	1.22	0.87	0.89	1.11	0.90	1.24	2.19	1.08	1.20	Ta	0.10	0.12	0.23	0.07	0.10	0.08	0.08	0.04	0.05	0.03	0.03	0.02	0.07	0.07	0.06	0.09	0.10	0.11	0.10	0.09	0.10	Th	0.07	0.10	0.35	0.05	0.07	0.06	0.06	0.04	0.06	0.01	0.02	0.05	0.10	0.10	0.11	0.22	0.23	0.22	0.24	0.23	0.23	U	0.02	0.03	0.18	0.03	0.02	0.03	0.03	0.02	0.03	0.01	0.01	0.03	0.05	0.07	0.11	0.17	0.17	0.18	0.17	0.17	0.18																																																																																																																																																																																																																																																																																																																																																																																																																																																																																																																																																																																																																																																																																																																																																																																																																																																																						
Lu	0.43	0.44	0.64	0.37	0.42	0.34	0.37	0.36	0.33	0.25	0.26	0.27	0.31	0.21	0.26	0.34	0.34	0.35	0.36	0.34	0.34	Hf	1.92	1.77	4.54	1.11	1.35	1.28	1.23	1.13	1.18	0.86	0.95	0.77	1.22	0.87	0.89	1.11	0.90	1.24	2.19	1.08	1.20	Ta	0.10	0.12	0.23	0.07	0.10	0.08	0.08	0.04	0.05	0.03	0.03	0.02	0.07	0.07	0.06	0.09	0.10	0.11	0.10	0.09	0.10	Th	0.07	0.10	0.35	0.05	0.07	0.06	0.06	0.04	0.06	0.01	0.02	0.05	0.10	0.10	0.11	0.22	0.23	0.22	0.24	0.23	0.23	U	0.02	0.03	0.18	0.03	0.02	0.03	0.03	0.02	0.03	0.01	0.01	0.03	0.05	0.07	0.11	0.17	0.17	0.18	0.17	0.17	0.18																																																																																																																																																																																																																																																																																																																																																																																																																																																																																																																																																																																																																																																																																																																																																																																																																																																																																												
Hf	1.92	1.77	4.54	1.11	1.35	1.28	1.23	1.13	1.18	0.86	0.95	0.77	1.22	0.87	0.89	1.11	0.90	1.24	2.19	1.08	1.20	Ta	0.10	0.12	0.23	0.07	0.10	0.08	0.08	0.04	0.05	0.03	0.03	0.02	0.07	0.07	0.06	0.09	0.10	0.11	0.10	0.09	0.10	Th	0.07	0.10	0.35	0.05	0.07	0.06	0.06	0.04	0.06	0.01	0.02	0.05	0.10	0.10	0.11	0.22	0.23	0.22	0.24	0.23	0.23	U	0.02	0.03	0.18	0.03	0.02	0.03	0.03	0.02	0.03	0.01	0.01	0.03	0.05	0.07	0.11	0.17	0.17	0.18	0.17	0.17	0.18																																																																																																																																																																																																																																																																																																																																																																																																																																																																																																																																																																																																																																																																																																																																																																																																																																																																																																																		
Ta	0.10	0.12	0.23	0.07	0.10	0.08	0.08	0.04	0.05	0.03	0.03	0.02	0.07	0.07	0.06	0.09	0.10	0.11	0.10	0.09	0.10	Th	0.07	0.10	0.35	0.05	0.07	0.06	0.06	0.04	0.06	0.01	0.02	0.05	0.10	0.10	0.11	0.22	0.23	0.22	0.24	0.23	0.23	U	0.02	0.03	0.18	0.03	0.02	0.03	0.03	0.02	0.03	0.01	0.01	0.03	0.05	0.07	0.11	0.17	0.17	0.18	0.17	0.17	0.18																																																																																																																																																																																																																																																																																																																																																																																																																																																																																																																																																																																																																																																																																																																																																																																																																																																																																																																																								
Th	0.07	0.10	0.35	0.05	0.07	0.06	0.06	0.04	0.06	0.01	0.02	0.05	0.10	0.10	0.11	0.22	0.23	0.22	0.24	0.23	0.23	U	0.02	0.03	0.18	0.03	0.02	0.03	0.03	0.02	0.03	0.01	0.01	0.03	0.05	0.07	0.11	0.17	0.17	0.18	0.17	0.17	0.18																																																																																																																																																																																																																																																																																																																																																																																																																																																																																																																																																																																																																																																																																																																																																																																																																																																																																																																																																														
U	0.02	0.03	0.18	0.03	0.02	0.03	0.03	0.02	0.03	0.01	0.01	0.03	0.05	0.07	0.11	0.17	0.17	0.18	0.17	0.17	0.18																																																																																																																																																																																																																																																																																																																																																																																																																																																																																																																																																																																																																																																																																																																																																																																																																																																																																																																																																																																				

Block	Aswad	Aswad	Aswad	Aswad	Aswad	Aswad	Aswad	Aswad	Aswad	Aswad	Aswad	Aswad	Aswad	Aswad	Aswad	Aswad	Aswad
Sample No:	O4UR84	O4UR91	O3UR42	O3UR55	O3UR106	O3UR180	O3UR184	O4UR18	O4UR42	O4UR45	O4UR68	UAE468	UAE496	UAE 4334	UAE 3975	O4UR33	
Sample type and Geochemical signature	V2-I Wadi Mal Dykes	V2-I Wadi Mal Dykes	V2-II Fujairah Dolerite	V2-II Fujairah Dolerite	V2-II Fujairah Dolerite	V2-II Fujairah Dolerite	V2-II Fujairah Dolerite	V2-II Fujairah Dolerite	V2-II Fujairah Dolerite	V2-II Fujairah Dolerite	V2-II Fujairah Dolerite	V2-II Fujairah Dolerite	V2-II Fujairah Dolerite	V2-II Fujairah Dolerite	V2-II Fujairah Dolerite	V2-II Fujairah Dolerite	V3 Late Dyke
Location X	0433853	0430020	0420536	0409117	0423710	0413238	0413099	0430311	0423096	0432870	0433241	0412945	0407867	0411720	0407794	0407428	
Location Y	2782152	2765915	2779992	2779886	2781071	2790015	2786052	2784714	2786530	2755825	2758017	2789140	2779364	2765168	2783737	2804852	
wt%																	
SiO <sub>2</sub>	58.67	55.73	50.72	47.54	52.30	48.66	51.34	53.58	57.09	52.10	53.79	52.78	53.09	50.63	55.11	48.88	
TiO <sub>2</sub>	0.51	0.81	0.30	0.28	0.33	0.37	0.37	0.35	0.28	0.33	0.31	0.33	0.35	0.20	0.39	1.32	
Al <sub>2</sub> O <sub>3</sub>	14.64	14.30	12.03	14.39	13.30	14.99	15.67	14.88	13.27	15.20	14.10	15.83	14.50	10.18	14.68	15.63	
Fe <sub>2</sub> O <sub>3</sub>	11.16	13.01	12.20	8.17	9.64	10.17	7.84	9.81	7.08	9.72	10.23	8.14	8.87	7.89	8.49	10.09	
MnO	0.17	0.19	0.15	0.13	0.16	0.17	0.15	0.19	0.12	0.18	0.19	0.09	0.15	0.14	0.16	0.16	
MgO	4.80	3.54	8.33	10.98	8.58	10.01	8.58	7.27	7.81	7.96	7.33	8.36	9.22	18.59	8.74	8.28	
CaO	8.90	8.55	10.72	13.07	11.68	13.84	11.37	9.51	8.57	10.03	10.58	13.80	11.79	11.75	11.14	11.32	
Na <sub>2</sub> O	2.38	2.41	1.66	1.23	1.74	0.87	1.65	2.37	3.39	2.09	1.41	0.92	1.48	0.67	1.44	3.16	
K <sub>2</sub> O	0.37	0.34	0.29	0.25	0.34	0.22	0.22	0.41	0.72	0.54	0.06	0.03	0.18	0.10	0.02	0.16	
P <sub>2</sub> O <sub>5</sub>	0.03	0.04	0.05	0.04	0.05	0.05	0.05	0.01	0.01	0.01	0.01	0.04	0.04	0.01	0.01	0.21	
LOI	1.01	0.41	1.38	2.07	0.88	0.34	1.34	1.57	0.71	2.55	2.52	0.56	0.53	1.10	0.77	2.84	
Total	100.83	99.33	97.84	98.12	98.99	99.68	98.39	99.95	99.02	100.69	100.52	100.68	100.17	99.26	100.94	100.04	
(ppm)																	
V	328.22	414.89	223.19	231.88	246.91	285.41	237.99	288.66	212.97	257.70	291.64	214.47	227.89	220.43	266.48	216.36	
Cr	53.27	19.21	1016.78	801.54	820.67	493.38	178.56	71.20	399.50	122.82	81.87	121.00	318.19	1393.72	389.57	372.13	
Co	38.43	39.20	48.21	45.99	38.52	46.41	35.97	41.76	33.84	42.83	41.52	37.96	40.81	58.19	43.88	42.77	
Zn	21.26	88.81	49.05	38.28	60.12	54.57	16.94	38.25	27.39	55.10	121.20			52.43	67.38	72.85	
Ga	14.58	18.20	10.18	11.19	10.53	13.19	12.53	12.96	11.46	12.82	12.53	12.19	11.84	9.38	13.71	14.53	
Rb	6.33	5.18	2.49	1.50	1.19	0.14	0.25	7.27	6.23	1.89	0.48	0.13	5.58	2.78	1.13	3.73	
Sr	159.70	99.32	190.40	416.60	264.10	278.50	352.00	119.70	101.60	130.30	87.35	215.96	89.97	55.36	90.08	364.10	
Y	18.09	19.87	10.48	9.16	10.52	11.22	10.80	11.81	12.25	9.58	10.23	9.29	11.17	7.82	13.71	26.40	
Zr	27.16	40.33	17.84	9.98	20.33	4.77	19.80	15.52	21.14	14.23	15.15	11.06	20.22	16.92	21.81	99.89	
Nb	0.93	1.25	0.15	0.55	0.25	0.04	0.14	0.66	0.55	0.44	0.62	0.28	0.51	1.66	0.46	11.95	
Cs	0.04	0.08	0.10	0.27	0.02	0.00	0.01	0.06	0.09	0.07	0.03	0.00	0.14	0.09	0.02	8.71	
Ba	88.50	37.73	24.12	18.57	20.99	4.94	20.81	40.53	57.10	35.83	14.76	10.78	37.33	15.59	15.06	435.20	
La	1.49	1.80	0.56	0.28	0.53	0.25	0.53	0.78	1.45	0.61	0.76	0.35	0.55	0.18	0.78	13.66	
Ce	3.70	4.71	1.48	0.79	1.48	0.82	1.53	1.92	4.01	1.56	1.88	1.11	1.57	0.51	1.90	28.19	
Pr	0.54	0.71	0.28	0.15	0.28	0.20	0.29	0.29	0.57	0.25	0.28	0.21	0.27	0.09	0.35	3.42	
Nd	2.99	3.86	1.55	0.95	1.57	2.95	1.73	1.65	2.68	1.41	1.55	1.35	1.70	0.57	1.93	15.49	
Sm	1.11	1.44	0.65	0.48	0.67	0.71	0.74	0.68	0.84	0.59	0.62	0.60	0.69	0.33	0.81	3.62	
Eu	0.44	0.55	0.27	0.20	0.27	0.31	0.31	0.30	0.26	0.28	0.28	0.25	0.27	0.14	0.32	1.37	
Gd	1.57	1.97	0.98	0.81	1.01	1.12	1.07	1.07	1.16	0.90	0.94	0.96	1.10	0.62	1.34	4.07	
Tb	0.32	0.40	0.22	0.18	0.22	0.25	0.23	0.23	0.23	0.19	0.19	0.19	0.22	0.14	0.26	0.67	
Dy	2.30	2.83	1.52	1.33	1.60	1.79	1.63	1.69	1.68	1.37	1.44	1.40	1.63	1.10	2.00	4.22	
Ho	0.52	0.65	0.33	0.29	0.34	0.38	0.35	0.39	0.39	0.31	0.34	0.31	0.37	0.23	0.41	0.87	
Er	1.59	1.98	1.06	0.94	1.09	1.18	1.10	1.21	1.19	0.96	1.04	0.96	1.15	0.75	1.32	2.41	
Tm	0.27	0.32	0.16	0.16	0.19	0.19	0.18	0.20	0.20	0.16	0.18	0.16	0.19	0.13	0.23	0.37	
Yb	1.72	2.09	1.19	1.05	1.23	1.26	1.21	1.34	1.32	1.04	1.16	1.03	1.23	0.88	1.51	2.24	
Lu	0.28	0.35	0.19	0.17	0.20	0.20	0.19	0.22	0.22	0.18	0.20	0.16	0.20	0.13	0.23	0.35	
Hf	0.87	1.19	0.50	0.33	0.54	0.16	0.57	0.52	0.73	0.46	0.49	0.44	0.61	0.44	0.70	2.16	
Ta	0.07	0.09	0.02	0.03	0.03	0.01	0.02	0.06	0.04	0.03	0.05	0.02	0.04	0.09	0.05	0.58	
Th	0.20	0.23	0.07	0.05	0.07	0.00	0.05	0.12	0.14	0.08	0.12	0.05	0.08	0.05	0.09	1.45	
U	0.15	0.18	0.07	0.05	0.06	0.00	0.05	0.13	0.10	0.06	0.13	0.03	0.07	0.08	0.10	0.33	

## **Appendix C: Data sources for geochemical field generation**

### **C1 PETDB data sources**

For this study MORB, BAB, IAT and Boninite arrays were generated for geochemical data plots in Chapter 3, 4 and 5 from the references listed below. The trace element data for different modern tectonic environments was gathered from the PETDB website ([www.petdb.org](http://www.petdb.org)). PETDB is an archive of analytical data for whole rocks, glasses, minerals and melt inclusions. Data is available in the form of major and trace elements, radiogenic and stable isotopes, U-series and noble gases from a range of modern geographical settings including; mid-ocean ridges, back-arc basins, young near ridge seamounts, and old oceanic crust.

### **MORB**

Chauvel, C; Blichert-Toft, J, 2001, A Hafnium Isotope And Trace Element Perspective On Melting Of The Depleted Mantle, *Earth Planet Sci Lett*, 190, 137 – 151

Hannigan, R E; Basu, A R; Teichmann, F, 2001, Mantle Reservoir Geochemistry From Statistical Analysis Of Icp-MS Trace Element Data Of Equatorial Mid-Atlantic Morb Glasses, *Chem Geol*, 175, 397 - 428

Lawson, K; Searle, R C; Pearce, J A; Browning, P; Kempton, P D, 1996, Detailed Volcanic Geology And Geochemistry Of The Marnock Area (Mid-Atlantic Ridge North Of Kane Transform), *Geol Soc Spec Pub 1118*, Eds: Macleod-C-J, Taylor-P-A, Walker-C-L, 61 – 102, Tectonic, Magmatic, Hydrothermal And Biological Segmentation Of Mid-Ocean Ridges

Pyle, D G; Christie, David M; Mahoney, J J; Duncan, R A, 1995, Geochemistry And Geochronology Of Ancient Southeast Pacific Seafloor, *J Geophys Res*, 100, 22261 - 22282

Regelous, M; Niu, Y; Wendt, J I; Batiza, Rodey; Greig, A.; Collerson, K D, 1999, Variations In The Geochemistry Of Magmatism On The East Pacific Rise At 10 Deg 30 N Since 800 Ka, *Earth Planet Sci Lett*, 168, 45 - 63

Robinson, C-J; Bickle, M-J; Minshull, T A; White, R S; Nichols, A, 2001, Low Degree Melting Under The Southwest Indian Ridge: The Roles Of Mantle Temperature, Conductive Cooling And Wet Melting, *Earth Planet Sci Lett*, 188, 383 - 398

## IAT

Ewart A., Hergt J. M., Hawkins J. W. Jr. ; Major Element, Trace Element, And Isotope (Pb, Sr, And Nd) Geochemistry Of Site 839 Basalts And Basaltic Andesites: Implications For Arc Volcanism ; Proc. Ocean Drill. Program, Scient. Results 135 [1994] 519-531

Jones G., Valsami-Jones E., Sano H. ; Nature And Tectonic Setting Of Accreted Basalts From The Mino Terrane, Central Japan ; J. Geol. Soc. London 150 [1993] 1167-1181

Kerr A. C., Aspden J. A., Tarney J., Pilatasig L. F. ; The Nature And Provenance Of Accreted Oceanic Terranes In Western Ecuador: Geochemical And Tectonic Constraints ; J. Geol. Soc. London 159 [2002] 577-594

Masuda A. ; Geochemistry Of Lanthanides In Basalts Of Central Japan ; Earth Planet. Sci. Lett. 4 [1968] 284-292

Nakamura E., McCulloch M. T., Campbell I. H. ; Chemical Geodynamics In The Back-Arc Region Of Japan Based On The Trace Element And Sr-Nd Isotopic Compositions ; Tectonophysics 174 [1990] 207-233

Thirlwall M. F., Smith T. E., Graham A. M., Theodorou N., Hollings P., Davidson J. P., Arculus R. J. ; High Field Strength Element Anomalies In Arc Lavas: Source Or Process? ; J. Petrol. 35 [1994] 819-838

Yokoyama T., Kobayashi K., Kuritani T., Nakamura E. ; Mantle Metasomatism And Rapid Ascent Of Slab Components Beneath Island Arcs: Evidence From 238u-230th-226ra Disequilibria Of Miyakejima Volcano, Izu Arc, Japan ; J. Geophys. Res. B108 (7) [2003] Ecv 1-1-Ecv 1-25

## Boninite

Arculus R. J., Pearce J. A., Murton B. J., Van Der Laan S. R. ; Igneous Stratigraphy And Major-Element Geochemistry Of Holes 786a And 786b ; Proc. Ocean Drill. Program, Scient. Results 125 [1992] 143-169

Manikyamba C., Naqvi S. M., Subba Rao D. V., Ram Mohan M., Khanna T. C., Rao T. G., Reddy G. L. N. ; Boninites From The Neoproterozoic Gadwal Greenstone Belt, Eastern Dharwar Craton, India: Implications For Archaean Subduction Processes ; Earth Planet. Sci. Lett. 230 [2005] 65-83

Münker C. ; The Isotope And Trace Element Budget Of The Cambrian Devil River Arc System, New Zealand: Identification Of Four Source Components ; J. Petrol. 41 [2000] 759-788

Murton B. J., Peate D. W., Arculus R. J., Pearce J. A., Van Der Laan S. R. ; Trace-Element Geochemistry Of Volcanic Rocks From Site 786: The Izu-Bonin Forearc ; Proc. Ocean Drill. Program, Scient. Results 125 [1992] 211-235

Pearce J. A., Thirlwall M. F., Imgram G., Murton B. J., Arculus R. J., Van Der Laan S. R. ; Isotopic Evidence For The Origin Of Boninites And Related Rocks Drilled In The Izu-Bonin (Ogasawara) Forearc, Leg 125 ; Proc. Ocean Drill. Program, Scient. Results 125 [1992] 237-261

Pearce J. A., Van Der Laan S. R., Arculus R. J., Murton B. J., Ishii T., Peate D. W., Parkinson I. J. ; Boninite And Harzburgite From Leg 125 (Bonin-Mariana Forearc): A Case Study Of Magma Genesis During The Initial Stages Of Subduction ; Proc. Ocean Drill. Program, Scient. Results 125 [1992] 623-659

Pearce J. A., Kempton P. D., Nowell G. M., Noble S. R. ; Hf-Nd Element And Isotope Perspective On The Nature And Provenance Of Mantle And Subduction Components In Western Pacific Arc-Basin Systems ; J. Petrol. 40 [1999] 1579-1611

## **BAB**

Hergt, J M; Nilsson Farley, K, 1994, Major Element, Trace Element, And Isotope (Pb, Sr, And Nd) Variations In Site 834 Basalts: Implications For The Initiation Of Backarc Opening, Proc Odp, Sci Results, 135, 471 – 485

Pearce, J A; Ernewein, M; Bloomer, S H; Parson, L M; Murton, B J; Johnson, L E, 1995, Geochemistry Of Lau Basin Volcanic Rocks: Influence Of Ridge Segmentation And Arc Proximity, Geol Soc London Spec Publ, 81, Volcanism Associated With Extension At Consumed Plate Margins, 53 – 75, Smellie-J-L

Peate, D W; Kokfelt, T F; Hawkesworth, C J; Van Calsteren, P W; Hergt, J M; Pearce, J A, 2001, U-Series Isotope Data On Lau Basin Glasses: The Role Of Subduction-Related Fluids During Melt Generation In Back-Arc Basins, J Petrol, 42, 1449 - 1470

## **Appendix D: Analytical method for LA-ICP-MS analysis**

### **D1.1 Introduction**

Experimental work was carried out in November and December 2004 on the Cardiff University LA-ICP-MS facility to establish a procedure for measuring trace element values of cumulate clinopyroxenes. The instruments comprise a 213 nm (ultra violet) laser by New Wave Industries, coupled to an X-series mass spectrometer supplied by Thermo Elemental. The procedure was selected to maximise the quality of the data. For these experiments, 40µm thick polished thin-sections of medium to coarse grained gabbroic samples were used.

Initial experimental work was based on sample 95OC14, a coarse-grained layered gabbro from the Wadi Abyad lower crustal section in Oman (1520 m above Moho). The sample contained a number of large clinopyroxene (cpx) crystals, one of which had been analysed by Dr. Richard Thomas by ion probe for major and trace elements (procedure and data contained in Thomas, 2003). Because this fresh clinopyroxene sample had known concentrations of key elements it was chosen as the test crystal in a series of short experiments to determine the best analytical procedure for line analysis clinopyroxenes on the Cardiff University LA-ICP-MS.

### **D1.2 Instrument parameters**

The samples to be analysed were first placed into the ablation cell with the selected reference materials and then into a sealed unit below the laser. The equipment is linked to the operator via a video monitoring system, enabling real-time visual evaluation of the ablation in progress, which is crucial for controlled sample ablation.

Laser ablation aerosols are transported to the ICP-MS by an Argon (Ar) or Helium (He) carrier gas. The Cardiff facility uses He as the carrier gas as it has been proven by previous studies (e.g. Sylvester et al., 2001; Horn and Günther, 2003; Jones, 2005)

to produce higher sensitivity in the ICP-MS, and is therefore preferable to pure Ar. Helium has higher thermal conductivity allowing a faster spread of thermal energy away from the sampling position, leading to a more rapid end of condensation growth. This in turn leads to a greater amount of smaller particles, increased transport efficiency and thus enhanced ICP-MS count rates in all materials (Horn and Günther, 2003).

### **D1.3 External standards**

The laser was tuned at the beginning of each day using the certified glass standard SRM 612, from NIST (hereafter NIST 612). Several lines of at least 1500 $\mu$ m were ablated on NIST 612 to allow minor adjustments to the ICP-MS operating parameters and to establish the most stable signal with the highest elemental count rate. A further line was then ablated on NIST 612 under experimental conditions. The data were saved and the relative standard deviation (RSD) established with  $\sim$ 5% as the maximum acceptable value. If this value was exceeded the ICP-MS was re-tuned and the experiment was repeated until the signal was stable ( $<$ 5% RSD).

Calibration was completed using United States Geological Survey (USGS) artificial basalt glass standards BIR-1, BHVO-2 and BCR-2 (Table D2 and current certified values for a full elemental suite can be found at [www.usgs.gov](http://www.usgs.gov)). These glass standards were chosen as their concentrations of key elements are closer to those of pyroxenes than NIST glasses. Three adjacent lines of between 250 and 300 $\mu$ m were ablated on each standard and the results were used in conjunction with the recommended values to establish a calibration curve for the ICP-MS instrument. This process was repeated at the beginning of each experiment, and would remain stable for around 3-4 hours, which was used as the approximate duration for each experiment and provided enough time to sample between 10 and 20 unknown values. A new calibration curve was established per experiment by ablating three fresh lines to maximise accuracy and minimise instrument drift, with a maximum of 4 experiments carried out in any one day. This allows analysis of a maximum of approximately 100 unknown values in a single day; a high-speed analysis method.



Instrument drift was also monitored by ablating a single line (250-300 $\mu$ m) on the standard BCR-2 at the start of each experiment and at intervals of between 3 and 5 unknown samples. This enabled instrument drift to be calculated and a drift correction to be applied to the data if RSD of the BCR-2 standard exceeded ~5%, to ensure optimum precision. BCR-2 was chosen as the drift monitor as it has the highest concentrations of trace elements of the three standard glasses and therefore produces a strong signal with all concentrations well above detection limits for all required elements.

## **D1.4 Initial Experiments**

After calibration and the ablation of a drift monitor, initial experiments were concerned with sample 95OC14, a large, previously ion-probed, clinopyroxene (augite). The crystal was located and suitable areas for laser ablation were determined visually. The crystal had two existing ion-probe sample sites, a *core* and *rim* site. Each existing sample pit was approximately 5  $\mu$ m in diameter (located using the Cardiff University SEM). LA-ICP-MS lines are 40  $\mu$ m in diameter and each line is 250-300 $\mu$ m in length. It was necessary to locate the lines as close as possible to the sample sites to take the best advantage of the pre-existing data. The natural heterogeneity of clinopyroxenes means some variation of composition is expected across a crystal. Figure A1 shows the general location of the sample sites. Because of alteration, regular surface areas large enough for a complete line analysis were limited to areas ~50 to 100 $\mu$ m from the original probe sites.

Initial lines were analysed for a limited suite of elements. The purpose of these primary test lines was to check the precision of the instrument and the repeatability of data. After ablation, the counts for each line were checked (per element) for stability and for the presence of inclusions which may have been ablated and included in the data (Figure D2).

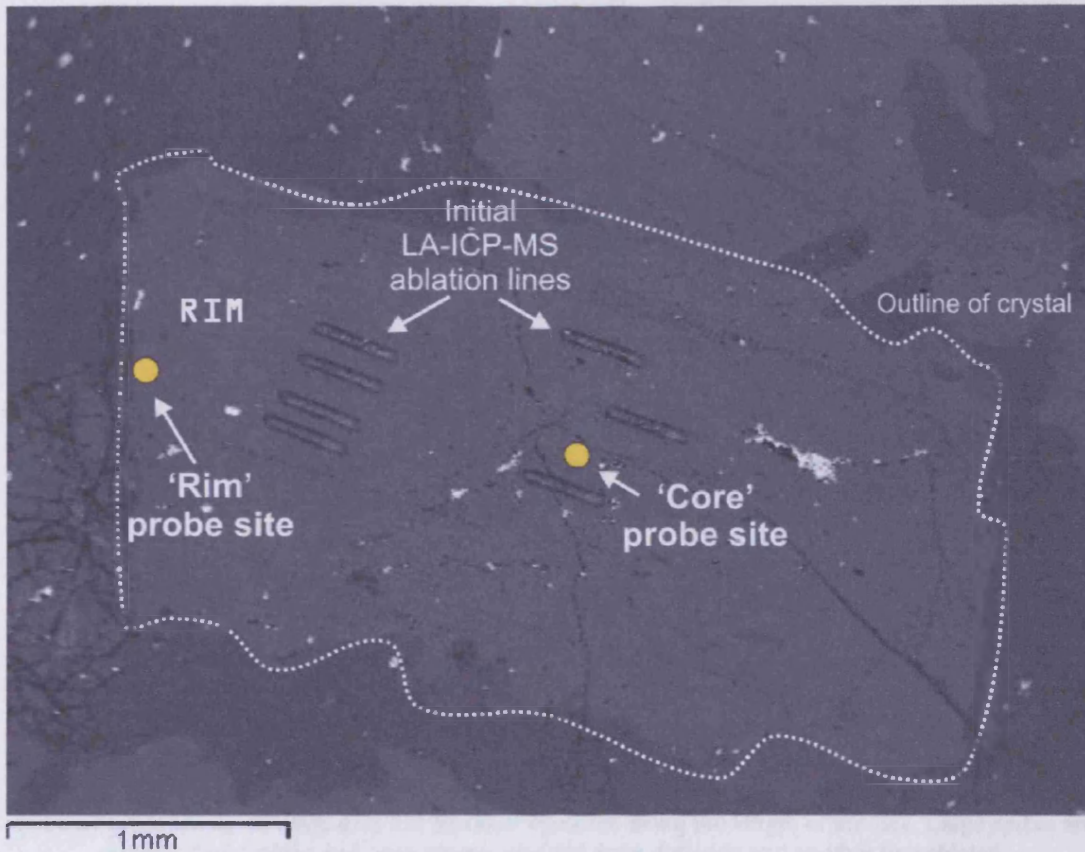


Figure D1, Early SEM photograph of 'test' clinopyroxene crystal from sample 95OC14. Location of previous 'rim' and 'core' ion probe sites are indicated by small circles. LA-ICP-MS lines are 40  $\mu\text{m}$  wide and 250  $\mu\text{m}$  in length

Data was selected after viewing time-slice profiles of the element counts. This enabled good, stable data profiles to be selected over poor, variable profiles. Inclusions are easy to identify as they appear as large positive or negative spikes in the data line. In cases where an inclusion had been included, the affected portion of the line could either be excluded from the final data or the line could be deleted and a fresh line ablated in its place. Initial experiments were concerned with the repeatability of analysis and concentrated on abundant elements. Later experiments focused on detection limits for various key elements, such as Th and Nb. These elements are present in very low abundances in the clinopyroxene samples and are close to the detection limit of the equipment. Their residence time on the ICP-MS was therefore increased relative to other more abundant elements to increase sensitivity and accuracy of these key elements.

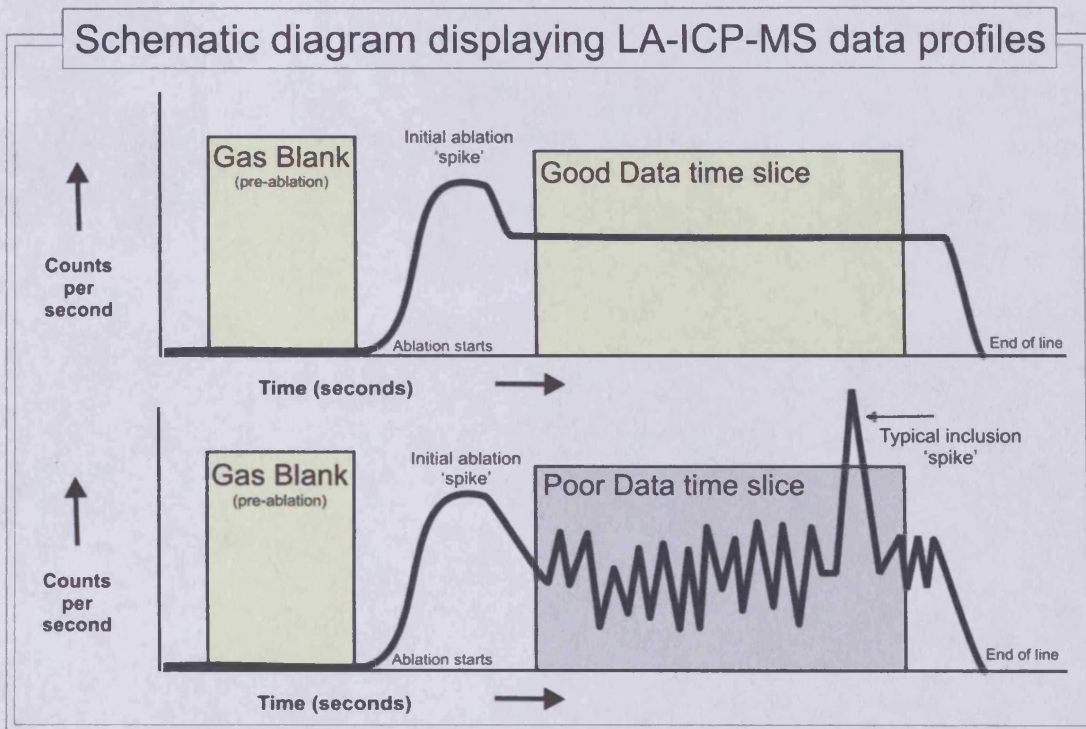


Figure D2, Schematic diagram displaying a typical good data time slice (shaded yellow) and a typical poor data time slice (shaded grey). The data time slice is preceded by a gas blank and an initial ablation spike which is not used. Good data has minimal variation along the length of the line. Large spikes are typical of inclusions and were always omitted from data sets and another line ablated.

Finally, after ablation was complete for each experiment, a time slice was chosen which provided the most stable counts for all standards and unknowns. Data was then exported to Excel and drift-corrected (if required). A CaO correction was then performed as described in Section D1.5.

## D1.5 The matrix effect

It is necessary in every LA-ICP-MS experiment to ablate a clinopyroxene standard to compensate for the different ablation characteristics between clinopyroxene and the glass standards. Clinopyroxene will ablate at a different rate than the glass standard and have different 'fallback' rates. Finding a homogeneous clinopyroxene with known characteristics has proved to be difficult as freshness, size and the number of inclusions all contribute to heterogeneity. However, after initial experiments yielded repeatable data with a low standard variation Test-Crystal 95OC14, which has been

ion probed and extensively probed by SEM-EDS was chosen as a suitable matrix-matched standard.

## D1.6 CaO correction factor

It has been shown by numerous experiments that individual elements fractionate differently under ablation conditions but that Rare Earth Elements (REE) have the same fractionation index as Calcium (Ca) (Figure D3)(e.g. Jackson et al., 1992, Sylvester et al., 2001).

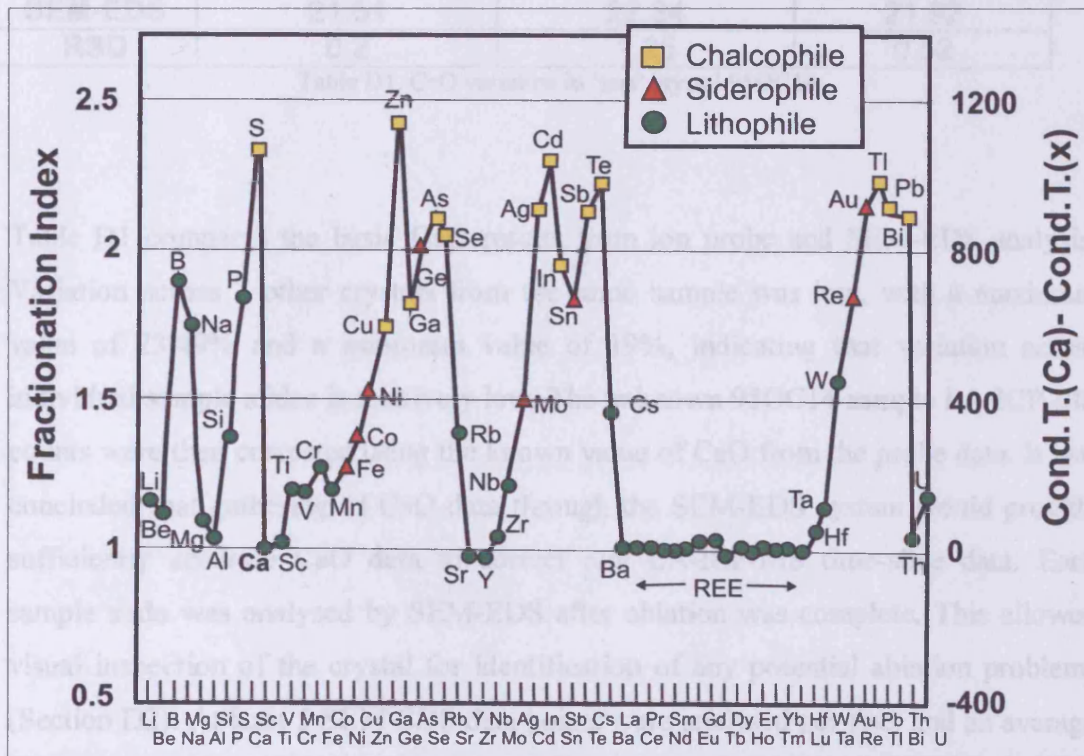


Figure D3, Displaying the fractionation indices for 62 elements relative to Ca. Symbols categorise elements according to the classification of the elements. Note how the REE (and other incompatible elements such as Th, Hf, Ta and Y) have a very similar fractionation index to Ca (after Sylvester et al., 2001 and references within).

Thus Ca should behave in the same way as the REE under ablation conditions. Ca is also abundant in clinopyroxene in the form of CaO, and is therefore easy to detect. To correct the raw ablation data, it is necessary to have accurate CaO data from as close as possible to the ablated area of crystal. This was completed after the initial ablation

so that the lines could be easily visually identified and checked for data quality (inclusions) and other ablation problems (Section D2).

The CaO measurement was carried out using the Cardiff University SEM-EDS system. Test-Crystal 95OC14 was analysed for CaO and other whole rock data and over 45 points across the whole crystal were gathered. The average CaO for the ‘test’ crystal from this method was 21.92%, with a maximum of 23.85% and a minimum of 19.27% with a standard variation of 1.05% (Table D1).

	<b>Average ‘rim’ CaO</b>	<b>Average ‘core’ CaO</b>	<b>Average CaO</b>
<b>Ion Probe</b>	21.57	21.95	21.76
<b>SEM-EDS</b>	21.51	22.34	21.92
<b>RSD</b>	0.2	1.25	0.52

Table D1, CaO variation in ‘test’ crystal 95OC14

Table D1 compares the basic CaO results from ion probe and SEM-EDS analysis. Variation across 7 other crystals from the same sample was low, with a maximum value of 23.49% and a minimum value of 19%, indicating that variation across individual sample slides is relatively low. The unknown 95OC14 sample LA-ICP-MS counts were then corrected using the known value of CaO from the probe data. It was concluded that gathering of CaO data through the SEM-EDS system would provide sufficiently accurate CaO data to correct raw LA-ICP-MS time-slice data. Each sample slide was analysed by SEM-EDS after ablation was complete. This allowed visual inspection of the crystal for identification of any potential ablation problems (Section D2). At least 5 SEM-EDS data points were analysed per line, and an average CaO was calculated for each sample crystal. The LA-ICP-MS data was then corrected using the averaged figure. The SEM-EDS measurements were also used to calculate the  $D_i$  for partition coefficient modelling (Appendix E). An alternative way of CaO correcting the LA-ICP-MS data involves simply using a constant value for CaO as used by Jones (2005) in his study of olivine-hosted melt inclusions where  $\text{SiO}_2$  and  $\text{Al}_2\text{O}_3$  were given constant mass factors despite minor variations between individual samples. As it was deemed necessary to individually investigate each sample slide in this study on the SEM after LA-ICP-MS analysis, to check for ablation problems, it

was considered appropriate to also gather individual CaO data per line/crystal for this study. Future studies may decide to use a CaO constant of around 21.5% to save time.

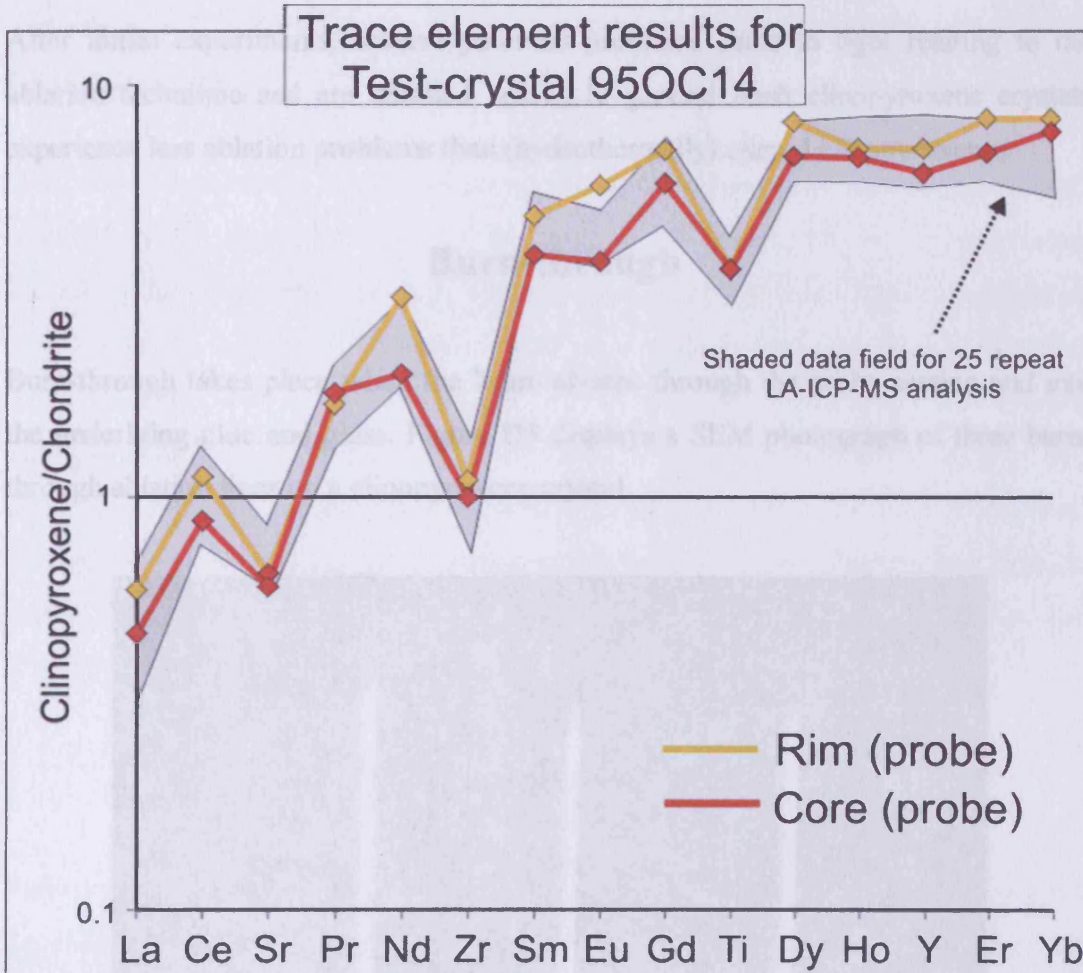


Figure D4. Chondrite normalised multi-element patterns for test-crystal 95OC14. Rim and Core results from Thomas (2003), obtained by ion probe analysis (bold lines), compared to a shaded field for the results of 25 LA-ICP-MS ablations on test crystal 95OC14.

Figure D4 displays the results of the original ion probe data for test-crystal 95OC14 of Thomas (2003) compared to a shaded field for the results of 25 LA-ICP-MS ablations on the same crystal gathered during experiments in 2005-2006 after instrument drift correction and the CaO correction. The variation between the ion probe analysis and the LA-ICP-MS analysis is small (even smaller than the original core to rim variation for some elements) and the small variation was considered good evidence that the LA-ICP-MS technique described above was accurate and repeatable. See Sections 4.1 to 4.4 for further information on the effects of element partitioning between core and rim sample sites.

## D2 Ablation Problems

After initial experiments, several potential problems came to light relating to the ablation technique and are detailed below. In general fresh clinopyroxene crystals experience less ablation problems than (hydrothermally) altered clinopyroxenes

### Burn-through

Burn-through takes place when the beam ablates through the probe section and into the underlying glue and glass. Figure D5 displays a SEM photograph of three burn-through ablation lines on a clinopyroxene crystal.

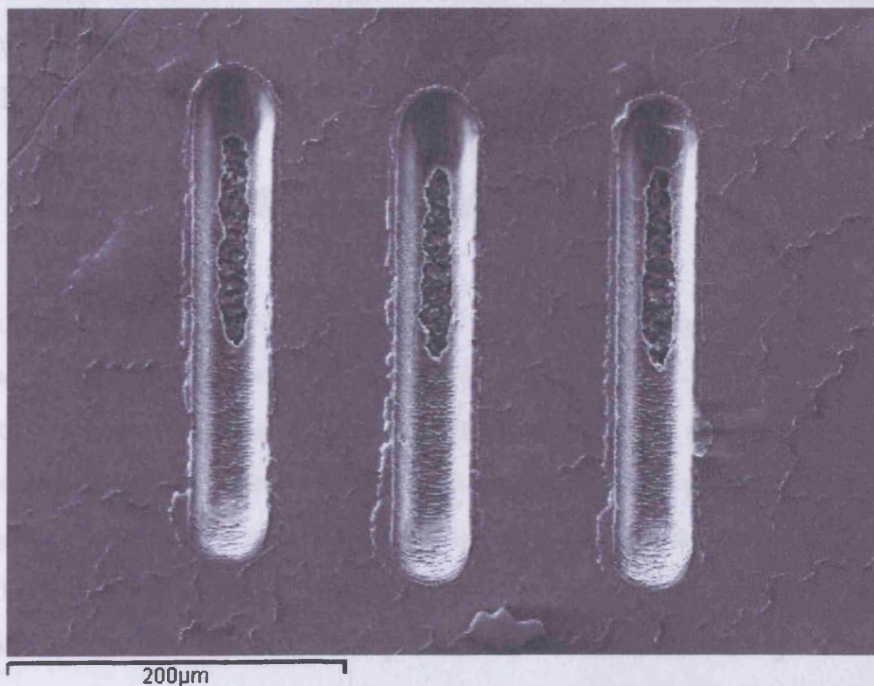


Figure D5, Burn-through in a 30  $\mu\text{m}$  probe section. Ablation lines are 40  $\mu\text{m}$  wide and 250  $\mu\text{m}$  in length. These results would be discarded. Note the ejecta rim around the left perimeter of each line.

All three lines in Figure D5 display burn-through for around half their length. Such an effect has been noticed on several slides, and is most common in crystals that are located close to the edges of the slides, indicating that burn-through could be a result of uneven thickness of a slide resulting from poor quality polishing (a speciality of

the Cardiff University, School of Earth Ocean and Planetary Science technical staff). The effects of ablating through the crystal are to include aerosols of the glue used to attach the sample and silicone from the glass mount. The contribution of these aerosols would be to dilute the sample aerosols by an unknown factor, resulting in poor quality data.

Burn-through cannot be confirmed simply using the video-optics on the LA-ICP-MS, although bright transmitted light at the base of the ablated line is a characteristic indicator. To verify burn-through, the use of a SEM (or other high magnification microscope) to inspect the ablated slide(s) after work is complete is very effective. The use of the SEM after LA-ICP-MS work is necessary to analyse CaO variation across crystals, and provides ample opportunity to inspect lines at the same time. Any data for a line that has suffered from burn-through is discarded. In cases where burn-through is very minor, it is sometimes possible to exclude the affected area from the results by selecting a time-slice of data to exclude the contaminated portion of the line (Figure D2).

## **Ejecta Contamination**

Fallout of ejecta from ablated lines (material which is not fully vaporised) can become deposited around the perimeter of the line to a distance of ~5 to 20 $\mu$ m (Figure D6). The fallout is caused because the ICP-MS is an atmospheric pressure ion source, and therefore ablation must also be carried out in atmospheric pressure ambient gas to ensure contamination-free transport of the ablation products to the ICP-MS (Sylvester et al., 2001). It is this pressure of the small volume of ambient gas within the ablation cell which forces the laser-induced plasma above the ablation region to redeposit ablated material onto the sample surface or the ablation pit-walls. Redeposition can be helped by reducing the volume of carrier gas in the ablation cell by reducing its size (K. Jones pers. comm.).



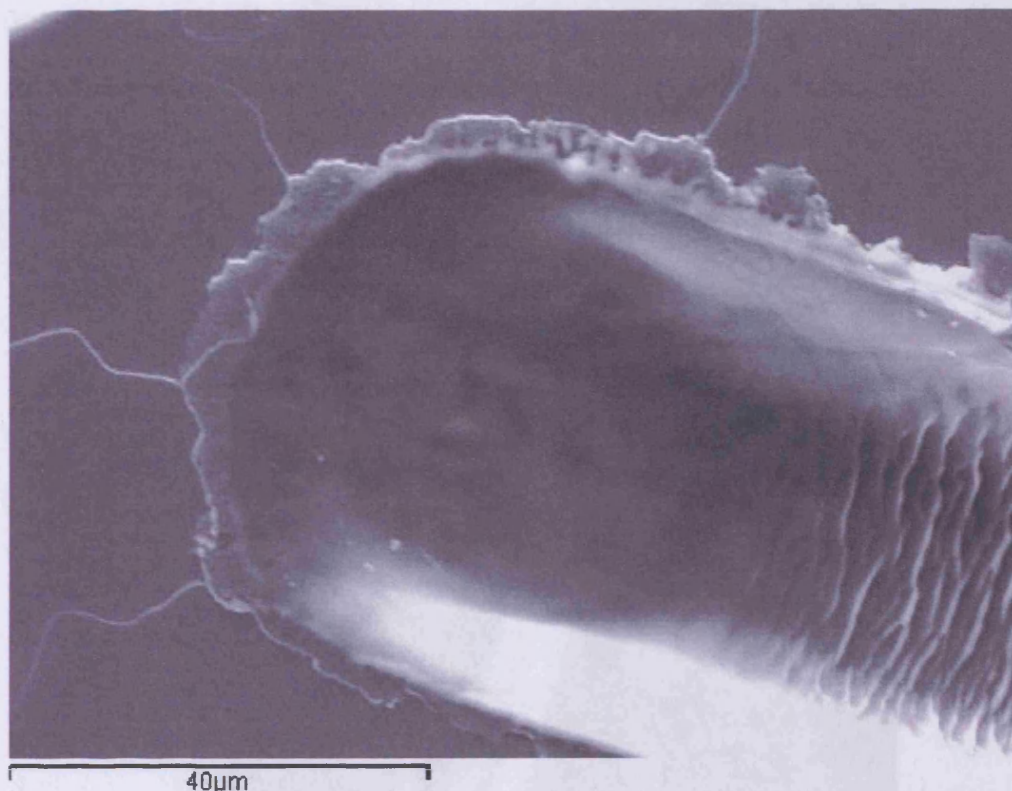


Figure D6, Close up of fallback contamination of ejecta around perimeter of ablated line on clinopyroxene. Such unavoidable redeposition offers a small risk of contamination to subsequent analyses.

While ejecta rims are not unexpected, such redeposition reduces the ablation yield and may influence measured elemental concentrations because of fractionation trends (Sylvester et al., 2001). Redeposition on the sample surface also presents a risk of contamination for subsequent ablation lines where space is limited, as two ablation lines close together could lead to the second line ablating redeposited material. Another potential risk when gathering CaO data on SEM-EDS is if a probe site is located on the fallback ejecta, this could lead to incorrect CaO data. Care was taken at all times to avoid sampling from the fallback ejecta.

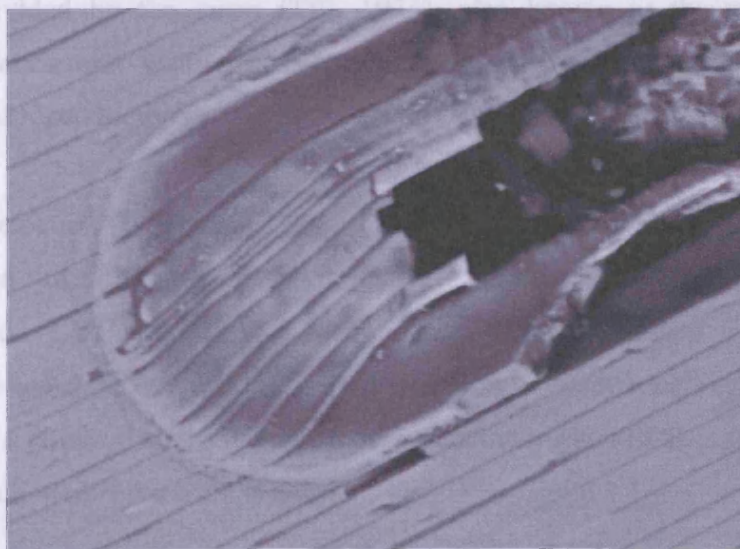
### Cleavage spalling

This problem is not common as most samples used for this study were fresh with good quality polished surfaces. However, in several early experiments the energy

from the laser caused catastrophic break-up of the crystal surface, poor ablation and low count rates, leading to the abandonment of a line (Figure D7 A and B).



A



B

Figure D7, A, Cleavage spalling causing destruction of a sample crystal. B, Close-up of cleavage spalling and burn-through, caused by perpendicular cleavage. Sample sites must be chosen carefully, preferably on fresh crystals, to lower the likelihood of such events

Cleavage spalling arises under several possible conditions; when the sample clinopyroxene crystal has cleavage exposed perpendicular to the surface to be probed (Figure D6 B); when the crystal has been strongly altered prior to collection; and when the sample has been damaged during the polishing process (Figure D6 A). Care must be taken to choose suitable sites that have a low risk of spalling. This can be achieved simply by ablating the freshest areas of a sample crystal.

### **D3 Results from initial experiments**

After taking into account ablation problems and CaO correction factors, it is necessary to ensure that the data are of acceptable quality. Data quality can be measured using three key factors; precision, accuracy and detection limit.

Precision refers to the reproducibility of a measurement. It is determined by making replicate measurements on the same sample (Rollinson, 1993). Precision can be defined more precisely as the coefficient of variation which is 100 times the standard deviation divided by the mean (Till, 1974), also known as the relative standard deviation (Jarvis and Williams, 1989). ICP-MS studies are known for their good precision and reproducibility.

Limits of Detection (LOD) and Limits of Quantification (LOQ) are defined as three times and ten times the standard deviation of the blanks respectively. Element values lower than the LOD are below detection and not used. Element values above the LOD, but below the LOQ can be utilised but must be treated with caution. Table D2 displays the relative standard deviation of drift monitor glass BCR-2 and the LOQ and LOD of the element suite used in this study

After initial experiments several elements (including Lu) were removed from the element suite because of repeatedly poor count rates, possibly related to variations in the fractionation index (Figure D3).

		<b>Standard Glass BIR</b>	<b>Standard Glass BHVO-2</b>	<b>Standard Glass BCR-2</b>	<b>Dwell time (ms)</b>	<b>LOD (ppm)</b>	<b>LOQ (ppm)</b>
<b>Ca</b>	%	13.3	11.4	7.12	2.00	0.16	0.54
<b>Sc</b>	ppm	44	32	33.3	6.00	1.84	6.14
<b>Ti</b>	%	0.96	2.73	2.26	2.00	0.04	0.14
<b>V</b>	ppm	310	317	416	8.00	0.52	1.74
<b>Cr</b>	ppm	370	280	18	8.00	4.58	15.26
<b>Mn</b>	%	0.175	0.17	0.2	5.00	1.78	5.93
<b>Sr</b>	ppm	110	389	346	10.00	0.36	1.19
<b>Y</b>	ppm	16	25.8	37	15.00	0.03	0.10
<b>Zr</b>	ppm	18	172	193	15.00	0.04	0.14
<b>Nb</b>	ppm	0.6	18.2	13.1	15.00	0.12	0.38
<b>La</b>	ppm	0.63	15.1	24.4	25.00	0.10	0.35
<b>Ce</b>	ppm	1.95	37.6	51.9	25.00	0.06	0.19
<b>Pr</b>	ppm	0.38	5.13	6.48	26.00	0.08	0.27
<b>Nd</b>	ppm	2.5	25.1	28.4	25.00	0.00	0.01
<b>Sm</b>	ppm	1.1	6.31	6.58	30.00	0.01	0.02
<b>Eu</b>	ppm	0.54	1.94	1.82	30.00	0.05	0.17
<b>Gd</b>	ppm	1.85	5.8	6.67	30.00	0.01	0.03
<b>Tb</b>	ppm	0.36	0.9	1.07	30.00	0.01	0.02
<b>Dy</b>	ppm	2.5	5.3	6.33	30.00	0.00	0.01
<b>Ho</b>	ppm	0.57	1.05	1.32	30.00	0.01	0.04
<b>Er</b>	ppm	1.7	2.68	3.66	30.00	0.00	0.01
<b>Tm</b>	ppm	0.26	0.35	0.54	30.00	0.01	0.02
<b>Yb</b>	ppm	1.65	2.2	3.4	30.00	0.00	0.00
<b>Lu</b>	ppm	0.26	0.28	0.5	30.00	0.03	0.10
<b>Hf</b>	ppm	0.6	4.1	4.9	30.00	0.00	0.02
<b>Ta</b>	ppm	0.04	1.35	0.81	30.00	0.01	0.04
<b>Pb</b>	ppm	4.12	n.a.	10.3	30.00	0.69	2.30
<b>Th</b>	ppm	0.29	1.2	6.03	30.00	0.01	0.05
<b>U</b>	ppm	0.018	0.45	1.69	30.00	0.00	0.00

Table D2, Displaying the suite of elements analysed by LA-ICP-MS during this study, the elemental concentrations of the three standard glasses used for calibration, the Dwell time of the ICP-MS for each element (dwell time increases for low abundance elements to obtain optimum count rates), and the LOD and LOQ for the elements analysed.

Sample Number	Gabbro Type	Location X	Location Y
UAE276	MTZ	0429102	2795818
UAE322	MTZ	0430855	2800670
UAE419	Layered	0427960	2785850
UAE421	Layered	0426444	2783217
UAE103	Upper	0433146	2807735
UAE314	Upper	0431610	2805620
UAE552	Upper	0430266	2784447
UAE557	Upper	0432547	2782662
UAE559	Upper	0431990	2782990
03UR74	Late	0431480	2803495

Table D3, Displaying the locations of the Khawr Fakkan Block gabbro samples

Sample Number	Gabbro Type	Location X	Location Y
04UR44	Layered	0420636	2756402
UAE644	Layered	0411556	2781218
03UR85	Kalba (Upper)	0429369	2757941
03UR123	Kalba (Upper)	0430248	2765458
03UR140	Kalba (Upper)	0430915	2767528
03UR199	Kalba (Upper)	0429445	2777185
UAE3031	Kalba (Upper)	0428450	2763604
UAE3115	Microgabbro Dyke	0430226	2759046
UAE3183	Microgabbro Dyke	0425883	2754466
03UR150	Microgabbro Dyke	0427736	2770545
UAE450	Bithna (Late)	0418983	2786583
UAE517	Bithna (Late)	0411114	2785117
UAE3969	Bithna (Late)	0411719	2764384
UAE3987	Bithna (Late)	0411625	2761368
04UR30	Fujairah (Late)	0427173	2754558
04UR32	Fujairah (Late)	0426638	2755377
UAE2376	Fujairah (Late)	0421018	2748997
UAE3979	Fujairah (Late)	0411625	2761368

Table D4, Displaying the locations of the Aswad Block gabbro samples

Block	Khawr Fakkan	Khawr Fakkan	Khawr Fakkan	Khawr Fakkan	Khawr Fakkan	Khawr Fakkan	Khawr Fakkan	Khawr Fakkan	Khawr Fakkan	Khawr Fakkan	Khawr Fakkan	Khawr Fakkan	Khawr Fakkan	Khawr Fakkan	Khawr Fakkan
Sample No:	UAE276-2-1	UAE276-2-2	UAE276-2-3	UAE276-2-4	UAE276-3-1	UAE276-3-2	UAE276-3-3	UAE276-4-1	UAE276-4-2	UAE276-4-3	UAE276-4-4	UAE322-1-1	UAE322-1-2	UAE322-1-3	UAE322-1-4
Sample Type:	MTZ Gabbro	MTZ Gabbro	MTZ Gabbro	MTZ Gabbro	MTZ Gabbro	MTZ Gabbro	MTZ Gabbro	MTZ Gabbro	MTZ Gabbro	MTZ Gabbro	MTZ Gabbro	MTZ Gabbro	MTZ Gabbro	MTZ Gabbro	MTZ Gabbro
wt%															
SiO <sub>2</sub>	52.17	52.17	52.17	52.17	51.79	51.79	51.79	51.79	51.79	51.79	51.79	52.16	52.16	52.16	52.16
TiO <sub>2</sub>	0.24	0.24	0.24	0.24	0.28	0.28	0.28	0.23	0.23	0.23	0.23	0.1	0.1	0.1	0.1
Al <sub>2</sub> O <sub>3</sub>	3.12	3.12	3.12	3.12	2.86	2.86	2.86	2.89	2.89	2.89	2.89	2.78	2.78	2.78	2.78
Cr <sub>2</sub> O <sub>3</sub>	0.92	0.92	0.92	0.92	0.51	0.51	0.51	0.45	0.45	0.45	0.45	0.65	0.65	0.65	0.65
Fe <sub>2</sub> O <sub>3</sub>	3.32	3.32	3.32	3.32	3.23	3.23	3.23	3.18	3.18	3.18	3.18	3.64	3.64	3.64	3.64
MnO	0	0	0	0	0	0	0	0	0	0	0	0.02	0.02	0.02	0.02
MgO	16.94	16.94	16.94	16.94	16.73	16.73	16.73	16.47	16.47	16.47	16.47	16.6	16.6	16.6	16.6
CaO	23.53	23.53	23.53	23.53	23.48	23.48	23.48	23.81	23.81	23.81	23.81	23.45	23.45	23.45	23.45
Na <sub>2</sub> O	0.28	0.28	0.28	0.28	0.24	0.24	0.24	0.22	0.22	0.22	0.22	0.29	0.29	0.29	0.29
Total	100.52	100.52	100.52	100.52	99.13	99.13	99.13	99.06	99.06	99.06	99.06	99.67	99.67	99.67	99.67
ppm															
45Sc	107.23	110.44	109.82	109.74	111.39	112.98	111.30	112.02	117.88	111.48	115.08	112.10	117.82	117.27	111.61
47Ti (%)	0.18	0.20	0.19	0.19	0.19	0.19	0.20	0.17	0.19	0.17	0.16	0.10	0.12	0.11	0.07
51V	205.65	221.34	215.63	217.13	221.76	226.55	226.17	219.26	217.26	213.96	220.20	175.52	167.61	175.17	131.80
52Cr	5040.96	3642.48	3707.67	3143.35	2341.43	1604.06	4015.36	1520.99	1682.56	1261.96	2031.11	2658.17	2799.00	3040.57	2431.91
55Mn (%)	0.10	0.10	0.09	0.10	0.11	0.10	0.11	0.10	0.10	0.10	0.10	0.11	0.10	0.11	0.11
88Sr	6.36	5.96	5.49	5.76	6.70	6.94	6.96	7.92	7.15	8.37	8.17	16.92	23.24	17.33	19.10
89Y	7.60	7.75	6.76	7.79	7.67	7.36	7.83	6.67	7.65	6.08	6.39	4.20	6.16	5.05	4.71
90Zr	3.24	3.02	2.89	2.99	3.08	2.94	3.47	2.39	2.83	3.12	2.22	20.02	39.54	19.26	27.68
93Nb	0.18	0.19	0.17	0.18	0.23	0.20	0.20	0.23	0.23	0.21	0.23	0.35	0.49	0.33	0.35
139La	0.07	0.05	0.05	0.06	0.07	0.08	0.05	0.07	0.07	0.07	0.08	0.92	1.71	0.80	1.21
140Ce	0.36	0.37	0.32	0.33	0.38	0.35	0.38	0.37	0.37	0.35	0.33	1.79	3.18	1.73	2.24
141Pr	0.09	0.09	0.08	0.10	0.10	0.10	0.10	0.08	0.09	0.07	0.08	0.24	0.40	0.22	0.27
146Nd	0.77	0.74	0.66	0.70	0.69	0.80	0.91	0.66	0.84	0.72	0.63	1.04	1.96	1.02	1.36
147Sm	0.49	0.46	0.50	0.51	0.49	0.46	0.46	0.43	0.41	0.43	0.41	0.41	0.55	0.39	0.45
153Eu	0.20	0.20	0.17	0.18	0.19	0.20	0.22	0.17	0.18	0.17	0.20	0.20	0.21	0.20	0.18
157Gd	0.89	0.85	0.78	0.81	0.84	0.87	1.03	0.77	0.74	0.60	0.66	0.55	0.67	0.59	0.59
159Tb	0.16	0.17	0.16	0.17	0.15	0.17	0.16	0.16	0.16	0.16	0.17	0.12	0.16	0.12	0.11
163Dy	1.29	1.20	1.26	1.32	1.19	1.30	1.29	1.13	1.26	1.18	1.15	0.65	0.96	0.86	0.79
165Ho	0.30	0.26	0.24	0.30	0.28	0.27	0.28	0.24	0.29	0.24	0.26	0.17	0.22	0.22	0.18
166Er	0.82	0.80	0.69	0.73	0.85	0.77	0.77	0.72	0.79	0.71	0.70	0.46	0.64	0.58	0.47
169Tm	0.14	0.12	0.10	0.12	0.11	0.14	0.14	0.10	0.12	0.10	0.09	0.06	0.08	0.07	0.08
172Yb	0.71	0.66	0.57	0.70	0.63	0.71	0.65	0.58	0.67	0.48	0.53	0.38	0.55	0.48	0.45
178Hf	0.14	0.17	0.13	0.14	0.14	0.14	0.11	0.13	0.17	0.14	0.10	0.48	0.97	0.47	0.72
232Th	0.00	0.00	0.00	0.00	0.00	0.00	0.00	0.00	0.00	0.00	0.00	0.77	0.63	0.31	0.45

Block	Khawr Fakkan	Khawr Fakkan	Khawr Fakkan	Khawr Fakkan	Khawr Fakkan	Khawr Fakkan	Khawr Fakkan	Khawr Fakkan	Khawr Fakkan	Khawr Fakkan	Khawr Fakkan	Khawr Fakkan
Sample No:	UAE419-3-1	UAE419-3-2	UAE419-3-3	UAE419-4-1	UAE419-4-2	UAE419-4-3	UAE419-5-1	UAE419-5-2	UAE419-5-3	UAE419-2-1	UAE419-2-2	UAE419-2-3
Sample Type:	Layered Gabbro	Layered Gabbro	Layered Gabbro	Layered Gabbro	Layered Gabbro	Layered Gabbro	Layered Gabbro	Layered Gabbro	Layered Gabbro	Layered Gabbro	Layered Gabbro	Layered Gabbro
wt%												
SiO2	51.7	51.7	51.7	51.54	51.54	51.54	51.89	51.89	51.89	51.87	51.87	51.87
TiO2	0.44	0.44	0.44	0.44	0.44	0.44	0.43	0.43	0.43	0.43	0.43	0.43
Al2O3	2.42	2.42	2.42	2.47	2.47	2.47	2.41	2.41	2.41	2.37	2.37	2.37
Cr2O3	0.13	0.13	0.13	0.13	0.13	0.13	0.22	0.22	0.22	0.15	0.15	0.15
Fe2O3	7.25	7.25	7.25	7.01	7.01	7.01	7.39	7.39	7.39	7.13	7.13	7.13
MnO	0.14	0.14	0.14	0.12	0.12	0.12	0.11	0.11	0.11	0.17	0.17	0.17
MgO	16.27	16.27	16.27	15.94	15.94	15.94	16.29	16.29	16.29	16.1	16.1	16.1
CaO	21.8	21.8	21.8	22.15	22.15	22.15	21.52	21.52	21.52	22.2	22.2	22.2
Na2O	0.32	0.32	0.32	0.34	0.34	0.34	0.32	0.32	0.32	0.32	0.32	0.32
Total	100.49	100.49	100.49	100.15	100.15	100.15	100.39	100.39	100.39	100.75	100.75	100.75
ppm												
45Sc	99.11	97.87	98.05	113.38	114.25	116.76	91.94	88.18	86.89	88.93	93.67	94.29
47Ti (%)	0.34	0.33	0.34	0.37	0.38	0.38	0.33	0.28	0.29	0.35	0.38	0.35
51V	351.09	362.76	345.48	303.56	325.20	324.81	371.33	340.42	346.82	399.07	440.24	390.38
52Cr	849.42	922.40	809.81	698.83	742.92	752.19	821.95	923.62	1159.94	893.13	1009.73	929.41
56Mn(%)	0.21	0.22	0.20	0.19	0.20	0.19	0.22	0.23	0.23	0.22	0.25	0.23
88Sr	8.44	7.89	7.83	8.74	8.01	8.28	8.14	7.98	8.13	8.52	7.82	8.33
89Y	13.43	12.87	13.19	15.48	15.71	15.72	12.24	10.95	11.43	12.22	11.70	12.12
90Zr	5.72	5.50	5.78	6.90	7.20	7.17	5.07	4.65	4.53	5.49	5.13	4.94
93Nb	0.62	0.60	0.55	0.50	0.47	0.47	0.58	0.55	0.51	0.71	0.65	0.63
139La	0.11	0.11	0.10	0.12	0.11	0.12	0.10	0.10	0.10	0.12	0.11	0.10
140Ce	0.76	0.73	0.78	0.71	0.69	0.69	0.77	0.76	0.79	0.90	0.88	0.87
141Pr	0.22	0.20	0.20	0.22	0.21	0.22	0.21	0.21	0.20	0.22	0.21	0.21
148Nd	1.62	1.54	1.64	1.60	1.61	1.63	1.60	1.42	1.31	1.58	1.61	1.58
147Sm	0.96	0.83	0.93	1.08	1.03	1.11	0.90	0.83	0.82	0.91	0.98	0.80
153Eu	0.36	0.36	0.35	0.38	0.40	0.42	0.38	0.34	0.32	0.38	0.38	0.37
157Gd	1.65	1.59	1.62	1.77	1.89	2.01	1.60	1.43	1.39	1.48	1.51	1.45
159Tb	0.32	0.33	0.29	0.34	0.40	0.39	0.30	0.28	0.28	0.28	0.31	0.29
163Dy	2.27	2.16	2.29	2.82	2.68	2.87	2.05	1.88	1.73	2.02	1.98	1.99
166Ho	0.51	0.50	0.49	0.59	0.62	0.62	0.48	0.41	0.42	0.44	0.44	0.48
168Er	1.38	1.35	1.39	1.79	1.74	1.87	1.33	1.27	1.10	1.26	1.34	1.32
169Tm	0.20	0.21	0.20	0.26	0.25	0.26	0.20	0.19	0.17	0.19	0.17	0.18
172Yb	1.10	1.16	1.15	1.43	1.42	1.43	1.07	1.09	1.08	1.08	1.15	1.13
178Hf	0.30	0.28	0.25	0.34	0.35	0.33	0.27	0.22	0.22	0.28	0.24	0.24
232Th	0.00	0.00	0.00	0.00	0.00	0.00	0.00	0.00	0.00	0.00	0.00	0.00

Block	Khawr Fakkan	Khawr Fakkan	Khawr Fakkan	Khawr Fakkan	Khawr Fakkan	Khawr Fakkan	Khawr Fakkan	Khawr Fakkan	Khawr Fakkan	Khawr Fakkan	Khawr Fakkan	Khawr Fakkan	Khawr Fakkan	Khawr Fakkan	Khawr Fakkan	Khawr Fakkan	Khawr Fakkan
Sample No:	UAE421-1-1	UAE421-1-2	UAE421-1-3	UAE421-2-1	UAE421-2-2	UAE421-2-3	UAE421-3-1	UAE421-3-2	UAE421-3-3	UAE103-2-1	UAE103-2-2	UAE103-2-3	UAE103-2-4	UAE103-3-1	UAE103-3-2	UAE103-3-3	UAE103-3-4
Sample Type:	Layered Gabbro	Layered Gabbro	Layered Gabbro	Layered Gabbro	Layered Gabbro	Layered Gabbro	Layered Gabbro	Layered Gabbro	Layered Gabbro	Upper Gabbro	Upper Gabbro	Upper Gabbro	Upper Gabbro	Upper Gabbro	Upper Gabbro	Upper Gabbro	Upper Gabbro
wt%																	
SiO <sub>2</sub>	53.01	53.01	53.01	53.21	53.21	53.21	53.02	53.02	53.02	50.49	50.49	50.49	50.49	50.37	50.37	50.37	50.37
TiO <sub>2</sub>	0.25	0.25	0.25	0.18	0.18	0.18	0.24	0.24	0.24	0.73	0.73	0.73	0.73	0.75	0.75	0.75	0.75
Al <sub>2</sub> O <sub>3</sub>	2.60	2.60	2.60	2.55	2.55	2.55	2.65	2.65	2.65	2.66	2.66	2.66	2.66	2.67	2.67	2.67	2.67
Cr <sub>2</sub> O <sub>3</sub>	0.73	0.73	0.73	0.70	0.70	0.70	0.74	0.74	0.74	0.02	0.02	0.02	0.02	0.02	0.02	0.02	0.02
Fe <sub>2</sub> O <sub>3</sub>	4.16	4.16	4.16	4.15	4.15	4.15	4.20	4.20	4.20	9.06	9.06	9.06	9.06	8.57	8.57	8.57	8.57
MnO	0.04	0.04	0.04	0.02	0.02	0.02	0.05	0.05	0.05	0.19	0.19	0.19	0.19	0.27	0.27	0.27	0.27
MgO	17.35	17.35	17.35	17.11	17.11	17.11	17.19	17.19	17.19	15.26	15.26	15.26	15.26	14.87	14.87	14.87	14.87
CaO	23.48	23.48	23.48	23.42	23.42	23.42	23.40	23.40	23.40	20.89	20.89	20.89	20.89	21.48	21.48	21.48	21.48
Na <sub>2</sub> O	0.31	0.31	0.31	0.28	0.28	0.28	0.32	0.32	0.32	0.37	0.37	0.37	0.37	0.38	0.38	0.38	0.38
Total	101.94	101.94	101.94	101.60	101.60	101.60	101.62	101.62	101.62	99.69	99.69	99.69	99.69	99.38	99.38	99.38	99.38
ppm																	
45Sc	77.55	80.43	79.59	82.93	85.95	82.26	85.51	83.87	84.98	150.32	145.40	141.80	137.57	138.75	133.76	138.76	128.25
47Ti (%)	0.17	0.17	0.17	0.17	0.16	0.16	0.16	0.16	0.16	0.56	0.59	0.54	0.53	0.59	0.59	0.58	0.58
51V	270.93	282.26	272.40	240.10	234.08	249.71	225.56	238.57	236.80	398.10	440.49	415.22	425.06	441.01	436.42	486.66	470.11
52Cr	4160.96	4804.35	4522.21	3983.71	3223.82	4158.15	3690.28	3937.71	3947.90	12.83	16.84	16.65	16.65	12.95	11.60	14.54	17.19
55Mn (%)	0.16	0.16	0.16	0.13	0.13	0.13	0.13	0.13	0.14	0.23	0.26	0.23	0.24	0.26	0.26	0.30	0.28
86Sr	7.74	7.69	8.48	13.54	15.05	7.80	10.40	10.22	10.03	7.80	8.43	7.38	7.42	8.32	8.87	8.71	7.80
89Y	8.71	7.17	8.80	8.03	8.45	7.43	7.70	7.47	7.94	17.91	17.35	16.76	15.92	16.45	16.31	15.30	15.54
90Zr	5.23	4.66	5.46	14.99	19.33	4.80	8.25	9.54	10.21	7.52	7.88	7.85	7.29	7.44	6.74	6.58	6.92
93Nb	0.54	0.48	0.50	0.59	0.58	0.49	0.54	0.52	0.51	0.22	0.23	0.20	0.20	0.25	0.24	0.23	0.24
139La	0.17	0.16	0.20	0.85	0.82	0.16	0.35	0.38	0.43	0.14	0.14	0.12	0.13	0.12	0.13	0.12	0.12
140Ce	0.82	0.59	0.76	1.47	1.81	0.66	0.89	0.99	0.95	0.73	0.81	0.83	0.80	0.86	0.82	0.82	0.90
141Pr	0.12	0.12	0.13	0.22	0.26	0.12	0.16	0.16	0.16	0.22	0.22	0.21	0.23	0.21	0.22	0.20	0.23
148Nd	0.86	0.82	0.96	1.25	1.55	0.99	1.00	0.95	1.09	1.85	1.97	1.72	1.76	1.73	1.72	1.66	1.78
147Sm	0.44	0.50	0.44	0.81	0.84	0.45	0.48	0.51	0.82	1.05	1.10	1.06	1.12	1.05	1.06	0.87	1.12
153Eu	0.19	0.23	0.20	0.22	0.23	0.21	0.19	0.20	0.20	0.48	0.47	0.42	0.44	0.42	0.47	0.42	0.42
157Gd	0.71	0.71	0.77	0.95	1.04	0.80	0.85	0.95	0.90	2.05	1.95	1.78	1.69	1.80	1.86	1.77	1.80
159Tb	0.15	0.16	0.17	0.18	0.20	0.16	0.16	0.16	0.19	0.43	0.41	0.43	0.38	0.39	0.42	0.33	0.40
163Dy	1.18	1.19	1.18	1.37	1.48	1.19	1.13	1.19	1.38	3.10	2.95	2.91	2.72	2.93	2.78	2.57	2.33
165Ho	0.25	0.28	0.28	0.28	0.28	0.28	0.29	0.28	0.29	0.68	0.67	0.60	0.55	0.65	0.61	0.60	0.60
168Er	0.89	0.76	0.77	0.83	0.91	0.75	0.82	0.74	0.79	1.98	1.85	1.80	1.54	1.78	1.76	1.70	1.79
169Tm	0.11	0.12	0.12	0.13	0.15	0.11	0.12	0.11	0.14	0.30	0.29	0.29	0.23	0.25	0.26	0.22	0.22
172Yb	0.80	0.71	0.71	0.80	0.79	0.63	0.74	0.71	0.74	1.50	1.67	1.45	1.54	1.42	1.43	1.37	1.52
178Hf	0.20	0.17	0.21	0.49	0.55	0.20	0.26	0.26	0.35	0.34	0.31	0.37	0.33	0.35	0.30	0.34	0.36
232Th	0.06	0.04	0.06	0.25	0.29	0.04	0.12	0.12	0.13	0.00	0.01	0.01	0.00	0.01	0.01	0.00	0.00



Block	Khawr Fakkan	Khawr Fakkan	Khawr Fakkan	Khawr Fakkan	Khawr Fakkan	Khawr Fakkan	Khawr Fakkan	Khawr Fakkan	Khawr Fakkan	Khawr Fakkan	Khawr Fakkan	Khawr Fakkan	Khawr Fakkan	Khawr Fakkan	Khawr Fakkan	Khawr Fakkan	Khawr Fakkan	Khawr Fakkan	
Sample No:	UAE314-1-1	UAE314-1-2	UAE314-1-3	UAE314-1-4	UAE314-2-1	UAE314-2-2	UAE314-2-3	UAE314-3-1	UAE314-3-2	UAE314-3-3	UAE552-1-1	UAE552-1-2	UAE552-1-3	UAE552-1-4	UAE552-2-1	UAE552-2-2	UAE552-2-3	UAE552-2-4	
Sample Type:	Upper Gabbro (Foliated)	Upper Gabbro (Foliated)	Upper Gabbro (Foliated)	Upper Gabbro (Foliated)	Upper Gabbro (Foliated)	Upper Gabbro (Foliated)	Upper Gabbro (Foliated)	Upper Gabbro (Foliated)	Upper Gabbro (Foliated)	Upper Gabbro (Foliated)	Upper Gabbro	Upper Gabbro	Upper Gabbro	Upper Gabbro	Upper Gabbro	Upper Gabbro	Upper Gabbro	Upper Gabbro	
wt%																			
SiO <sub>2</sub>	52.42	52.42	52.42	52.42	52.01	52.01	52.01	52.32	52.32	52.32	51.6	51.6	51.6	51.6	51.33	51.33	51.33	51.33	
TiO <sub>2</sub>	0.81	0.81	0.81	0.81	0.84	0.84	0.84	0.58	0.58	0.58	0.75	0.75	0.75	0.75	0.79	0.79	0.79	0.79	
Al <sub>2</sub> O <sub>3</sub>	2.74	2.74	2.74	2.74	2.81	2.81	2.81	2.75	2.75	2.75	2.56	2.56	2.56	2.56	2.73	2.73	2.73	2.73	
Cr <sub>2</sub> O <sub>3</sub>	0.00	0.00	0.00	0.00	0.02	0.02	0.02	0.02	0.02	0.02	0.25	0.25	0.25	0.25	0.31	0.31	0.31	0.31	
Fe <sub>2</sub> O <sub>3</sub>	8.48	8.48	8.48	8.48	8.37	8.37	8.37	8.12	8.12	8.12	8.22	8.22	8.22	8.22	8.4	8.4	8.4	8.4	
MnO	0.29	0.29	0.29	0.29	0.21	0.21	0.21	0.27	0.27	0.27	0.08	0.08	0.08	0.08	0.08	0.08	0.08	0.08	
MgO	15.47	15.47	15.47	15.47	15.05	15.05	15.05	15.27	15.27	15.27	15.59	15.59	15.59	15.59	15.53	15.53	15.53	15.53	
CaO	22.00	22.00	22.00	22.00	22.05	22.05	22.05	22.37	22.37	22.37	22.86	22.86	22.86	22.86	22.63	22.63	22.63	22.63	
Na <sub>2</sub> O	0.44	0.44	0.44	0.44	0.45	0.45	0.45	0.43	0.43	0.43	0.45	0.45	0.45	0.45	0.47	0.47	0.47	0.47	
Total	101.44	101.44	101.44	101.44	101.39	101.39	101.39	101.51	101.51	101.51	100.38	100.38	100.38	100.38	100.28	100.28	100.28	100.28	
ppm																			
45Sc	135.11	136.35	126.81	128.00	132.35	129.21	126.91	157.58	157.43	162.97	138.97	149.09	146.74	144.94	119.55	123.04	121.19	120.84	
47Ti (%)	0.51	0.50	0.48	0.50	0.50	0.50	0.48	0.44	0.42	0.53	0.69	0.71	0.73	0.63	0.60	0.64	0.67	0.68	
51V	336.63	371.17	387.47	374.72	364.06	364.78	350.34	271.27	262.48	298.80	378.33	412.37	407.20	398.10	438.02	464.25	475.86	479.13	
52Cr	158.92	86.64	150.43	167.73	155.56	129.58	139.93	100.64	90.01	102.03	1202.29	1473.11	1397.87	1244.66	1451.34	1200.50	1154.88	1062.53	
55Mn(%)	0.35	0.34	0.33	0.34	0.33	0.33	0.32	0.26	0.26	0.27	0.19	0.19	0.19	0.19	0.20	0.20	0.21	0.21	
85Sr	7.12	8.03	7.75	7.94	8.26	8.37	8.26	7.78	8.00	8.06	11.85	12.55	12.50	12.38	11.89	12.88	13.14	11.49	
89Y	16.01	17.69	17.08	17.70	16.37	17.66	16.25	21.47	20.50	23.36	27.58	27.85	25.87	25.41	21.23	21.33	21.82	18.84	
90Zr	7.52	8.87	8.15	8.48	8.20	8.73	8.12	10.07	9.80	11.83	24.78	24.52	21.25	20.39	16.72	16.56	16.49	16.84	
93Nb	0.41	0.58	0.48	0.53	0.62	0.58	0.59	0.52	0.50	0.47	0.58	0.59	0.57	0.58	0.75	0.71	0.69	0.66	
139La	0.11	0.14	0.14	0.13	0.14	0.14	0.14	0.13	0.14	0.14	0.41	0.44	0.42	0.41	0.40	0.40	0.39	0.40	
140Ce	0.89	1.08	0.94	0.96	1.03	1.04	1.03	0.79	0.74	0.85	2.26	2.39	2.25	2.26	2.55	2.56	2.54	2.57	
141Pr	0.22	0.28	0.27	0.26	0.27	0.27	0.25	0.24	0.24	0.28	0.55	0.60	0.56	0.55	0.59	0.57	0.55	0.54	
146Nd	1.67	2.12	2.02	2.14	2.07	2.04	1.89	1.94	1.96	2.36	4.03	4.52	4.06	3.89	3.76	3.81	3.77	3.86	
147Sm	1.08	1.28	1.30	1.32	1.15	1.22	1.30	1.33	1.25	1.48	1.96	2.13	2.07	2.01	1.80	1.87	1.82	1.89	
153Eu	0.47	0.50	0.51	0.52	0.50	0.52	0.49	0.50	0.48	0.54	0.69	0.67	0.68	0.65	0.63	0.61	0.58	0.65	
157Gd	1.85	2.24	1.92	2.07	2.06	2.07	1.84	2.40	2.48	2.59	3.26	3.58	3.27	3.27	2.83	2.75	2.79	3.11	
159Tb	0.40	0.40	0.38	0.41	0.43	0.43	0.39	0.47	0.45	0.52	0.86	0.88	0.83	0.84	0.82	0.82	0.81	0.86	
163Dy	2.85	2.94	2.96	2.98	2.99	3.13	2.79	3.58	3.31	3.87	4.45	4.87	4.29	4.14	3.46	3.56	3.58	3.86	
165Ho	0.82	0.87	0.87	0.89	0.87	0.92	0.81	0.83	0.79	0.92	1.01	1.00	0.96	0.95	0.75	0.78	0.79	0.82	
166Er	1.67	1.94	1.84	1.95	1.85	1.79	1.72	2.31	2.39	2.57	2.71	2.77	2.78	2.59	2.13	2.09	2.11	2.29	
169Tm	0.26	0.28	0.25	0.26	0.27	0.24	0.24	0.32	0.29	0.33	0.39	0.41	0.38	0.38	0.30	0.35	0.33	0.34	
172Yb	1.73	1.75	1.65	1.83	1.58	1.72	1.54	2.00	1.79	2.28	2.35	2.26	2.43	2.37	1.84	1.95	1.92	2.00	
178Hf	0.32	0.41	0.38	0.38	0.37	0.42	0.38	0.48	0.46	0.55	1.05	1.09	0.91	0.91	0.78	0.67	0.73	0.76	
232Th	0.00	0.00	0.00	0.00	0.00	0.00	0.00	0.00	0.00	0.00	0.03	0.07	0.03	0.01	0.01	0.02	0.02	0.02	

4  
Clinopyroxene major (SEM-EDS) and trace (LA-ICP-MS) element data for Khawr Fakkan Block plutonic samples

Block	Khawr Fakkan	Khawr Fakkan	Khawr Fakkan	Khawr Fakkan	Khawr Fakkan	Khawr Fakkan	Khawr Fakkan	Khawr Fakkan	Khawr Fakkan	Khawr Fakkan	Khawr Fakkan	Khawr Fakkan	Khawr Fakkan	Khawr Fakkan	Khawr Fakkan	Khawr Fakkan	Khawr Fakkan	Khawr Fakkan	
Sample No:	UAE552-3-1	UAE552-3-2	UAE552-3-3	UAE552-3-4	UAE552-3-5	UAE557-1-1	UAE557-1-2	UAE557-1-3	UAE557-2-1	UAE557-2-2	UAE557-2-3	UAE557-3-1	UAE557-3-2	UAE557-3-3	UAE559-1-1	UAE559-1-2	UAE559-1-3	UAE559-2-1	
Sample Type:	Upper Gabbro	Upper Gabbro	Upper Gabbro	Upper Gabbro	Upper Gabbro	Upper Gabbro	Upper Gabbro	Upper Gabbro	Upper Gabbro	Upper Gabbro	Upper Gabbro	Upper Gabbro	Upper Gabbro	Upper Gabbro	Upper Gabbro	Upper Gabbro	Upper Gabbro	Upper Gabbro	
w%																			
SiO <sub>2</sub>	51.41	51.41	51.41	51.41	51.41	52.00	52.00	52.00	51.86	51.86	51.86	52.15	52.15	52.15	51.81	51.81	51.81	52.02	
TiO <sub>2</sub>	0.78	0.78	0.78	0.78	0.78	0.98	0.98	0.98	0.44	0.44	0.44	0.65	0.65	0.65	0.72	0.72	0.72	0.61	
Al <sub>2</sub> O <sub>3</sub>	2.68	2.68	2.68	2.68	2.68	2.71	2.71	2.71	3.51	3.51	3.51	3.10	3.10	3.10	2.40	2.40	2.40	2.17	
Cr <sub>2</sub> O <sub>3</sub>	0.29	0.29	0.29	0.29	0.29	0.83	0.83	0.83	1.52	1.52	1.52	0.24	0.24	0.24	0.45	0.45	0.45	0.17	
Fe <sub>2</sub> O <sub>3</sub>	6.35	6.35	6.35	6.35	6.35	4.87	4.87	4.87	4.60	4.60	4.60	5.17	5.17	5.17	5.32	5.32	5.32	5.68	
MnO	0.08	0.08	0.08	0.08	0.08	0.09	0.09	0.09	0.00	0.00	0.00	0.10	0.10	0.10	0.11	0.11	0.11	0.13	
MgO	15.55	15.55	15.55	15.55	15.55	16.88	16.88	16.88	16.75	16.75	16.75	17.10	17.10	17.10	16.23	16.23	16.23	16.33	
CaO	22.71	22.71	22.71	22.71	22.71	22.89	22.89	22.89	22.70	22.70	22.70	22.54	22.54	22.54	23.06	23.06	23.06	22.74	
Na <sub>2</sub> O	0.46	0.46	0.46	0.46	0.46	0.46	0.46	0.46	0.44	0.44	0.44	0.35	0.35	0.35	0.37	0.37	0.37	0.35	
Total	100.31	100.31	100.31	100.31	100.31	101.52	101.52	101.52	101.82	101.82	101.82	101.40	101.40	101.40	100.48	100.48	100.48	100.21	
ppm																			
45Sc	147.45	150.92	163.12	151.75	163.11	98.87	93.00	89.09	107.84	103.68	97.88	113.08	105.89	103.88	104.18	85.81	102.88	97.10	
47Ti (%)	0.62	0.64	0.71	0.61	0.78	0.48	0.67	0.59	0.34	0.31	0.28	0.48	0.56	0.40	0.68	0.51	0.59	0.42	
51V	345.33	337.37	375.84	321.38	410.00	404.47	341.43	401.05	310.31	307.38	280.38	380.70	431.38	353.37	371.88	370.89	378.44	353.75	
52Cr	1089.18	887.08	1236.34	980.09	1488.11	5682.17	5548.51	6121.80	9937.20	9784.40	8826.77	1634.01	2544.44	708.88	2787.40	2268.08	1785.75	725.72	
55Mn (%)	0.17	0.16	0.17	0.17	0.19	0.20	0.20	0.21	0.15	0.14	0.14	0.19	0.20	0.19	0.21	0.24	0.21	0.21	
88Sr	11.56	11.28	10.18	9.87	11.99	7.84	8.19	7.88	9.32	10.13	9.28	10.07	10.21	9.84	7.40	7.75	7.43	7.34	
89Y	28.86	29.97	31.84	29.43	31.40	34.94	25.81	30.34	14.72	11.18	10.13	22.47	23.84	18.14	29.33	23.05	26.73	21.37	
90Zr	23.40	26.13	30.68	25.15	28.35	33.25	18.32	27.89	7.95	5.54	5.71	10.39	12.90	8.21	35.85	23.67	28.09	16.53	
93Nb	0.55	0.55	0.59	0.58	0.60	0.88	0.83	0.65	0.71	0.83	0.63	0.61	0.69	0.60	0.16	0.16	0.14	0.18	
139La	0.49	0.45	0.40	0.39	0.49	0.39	0.43	0.42	0.27	0.15	0.18	0.26	0.27	0.25	0.37	0.28	0.32	0.34	
140Ce	2.07	2.01	2.11	1.93	2.33	3.08	2.84	3.80	1.33	0.98	0.90	1.51	1.88	1.41	2.33	2.05	2.05	1.84	
141Pr	0.56	0.56	0.57	0.51	0.58	0.78	0.70	0.77	0.32	0.21	0.20	0.37	0.41	0.34	0.59	0.46	0.50	0.45	
148Nd	4.12	4.21	4.37	4.00	4.40	5.80	4.83	5.21	2.18	1.46	1.44	2.89	3.09	2.41	4.44	3.80	3.84	3.01	
147Sm	2.12	2.16	2.28	2.03	2.27	2.87	2.08	2.28	1.12	0.84	0.83	1.60	1.63	1.29	2.32	1.94	1.82	1.55	
153Eu	0.65	0.70	0.70	0.67	0.71	0.59	0.51	0.61	0.43	0.35	0.32	0.48	0.46	0.45	0.66	0.36	0.49	0.45	
157Gd	3.48	3.76	3.78	3.71	3.56	4.04	2.97	3.58	1.73	1.40	1.18	2.64	2.71	2.08	3.56	2.95	3.23	2.35	
159Tb	0.68	0.89	0.75	0.71	0.72	0.83	0.59	0.72	0.35	0.29	0.29	0.52	0.55	0.42	0.74	0.51	0.63	0.50	
163Dy	4.74	4.84	5.35	4.93	5.41	5.85	4.11	5.09	2.59	2.01	1.77	3.53	3.87	3.04	4.94	3.19	4.33	3.26	
165Ho	1.14	1.13	1.17	1.11	1.16	1.26	0.92	1.09	0.56	0.45	0.45	0.83	0.87	0.71	1.18	0.76	1.02	0.78	
166Er	2.97	2.99	3.18	3.05	3.18	3.89	2.88	3.30	1.60	1.11	1.13	2.34	2.49	1.98	3.19	2.82	2.91	2.32	
169Tm	0.43	0.45	0.44	0.45	0.48	0.52	0.40	0.46	0.23	0.17	0.14	0.36	0.37	0.27	0.45	0.38	0.44	0.31	
172Yb	2.59	2.59	2.70	2.57	2.80	3.29	2.54	2.91	1.38	1.02	0.98	2.21	2.15	1.69	2.78	2.74	2.78	2.10	
178Hf	0.95	0.98	1.38	1.18	1.24	0.77	0.38	0.58	0.35	0.32	0.27	0.45	0.55	0.33	1.04	0.82	0.88	0.40	
232Th	0.03	0.04	0.03	0.03	0.03	0.07	0.08	0.10	0.03	0.01	0.01	0.02	0.02	0.03	0.02	0.02	0.02	0.02	

Block	Khawr Fakkan	Khawr Fakkan	Khawr Fakkan	Khawr Fakkan	Khawr Fakkan	Khawr Fakkan	Khawr Fakkan	Khawr Fakkan	Khawr Fakkan	Khawr Fakkan	Khawr Fakkan	Khawr Fakkan
Sample No:	UAE559-2-2	UAE559-2-3	UAE559-3-1	UAE559-3-2	UAE559-3-3	03UR74	03UR74	03UR74	03UR74	03UR74	03UR74	03UR74
Sample Type:	Upper Gabbro	Upper Gabbro	Upper Gabbro	Upper Gabbro	Upper Gabbro	Late Gabbro Pegmatite	Late Gabbro Pegmatite	Late Gabbro Pegmatite	Late Gabbro Pegmatite	Late Gabbro Pegmatite	Late Gabbro Pegmatite	Late Gabbro Pegmatite
wt%												
SiO <sub>2</sub>	52.02	52.02	51.30	51.30	51.30	53.36	53.36	53.36	53.36	53.36	53.36	53.36
TiO <sub>2</sub>	0.61	0.61	0.31	0.31	0.31	0.07	0.07	0.07	0.07	0.07	0.07	0.07
Al <sub>2</sub> O <sub>3</sub>	2.17	2.17	3.22	3.22	3.22	1.96	1.96	1.96	1.96	1.96	1.96	1.96
Cr <sub>2</sub> O <sub>3</sub>	0.17	0.17	1.33	1.33	1.33	0.12	0.12	0.12	0.12	0.12	0.12	0.12
Fe <sub>2</sub> O <sub>3</sub>	5.66	5.66	4.89	4.89	4.89	4.63	4.63	4.63	4.63	4.63	4.63	4.63
MnO	0.13	0.13	0.12	0.12	0.12	0.20	0.20	0.20	0.20	0.20	0.20	0.20
MgO	16.33	16.33	16.34	16.34	16.34	16.39	16.39	16.39	16.39	16.39	16.39	16.39
CaO	22.74	22.74	22.55	22.55	22.55	23.27	23.27	23.27	23.27	23.27	23.27	23.27
Na <sub>2</sub> O	0.35	0.35	0.38	0.38	0.38	0	0	0	0	0	0	0
Total	100.21	100.21	100.43	100.43	100.43	100.00	100.00	100.00	100.00	100.00	100.00	100.00
ppm												
45Sc	96.91	97.15	90.17	81.27	77.95	121.00	122.28	114.40	120.86	113.88	109.69	115.23
47Ti (%)	0.42	0.64	0.31	0.24	0.22	0.07	0.07	0.06	0.06	0.07	0.06	0.07
51V	375.12	428.39	346.01	293.28	319.61	330.65	354.63	322.80	328.13	318.93	335.38	321.58
52Cr	699.14	768.37	10715.68	9088.02	9558.45	679.05	702.45	833.44	632.23	568.89	604.29	642.91
56Mn(%)	0.22	0.23	0.20	0.15	0.16	0.15	0.15	0.15	0.14	0.14	0.15	0.15
88Sr	8.04	6.85	6.93	6.16	6.32	6.14	6.76	6.62	7.00	7.91	8.21	10.00
89Y	22.17	28.06	13.71	7.24	6.89	5.37	6.89	5.88	5.47	5.82	5.44	5.82
90Zr	16.84	31.41	12.25	3.17	3.02	3.19	3.29	2.08	2.52	2.36	2.21	3.17
93Nb	0.17	0.16	0.29	0.22	0.22	0.07	0.07	0.09	0.09	0.07	0.07	0.11
139La	0.32	0.31	0.32	0.11	0.13	0.27	0.26	0.19	0.19	0.14	0.17	0.27
140Ce	2.20	2.35	2.03	0.71	0.66	0.65	0.66	0.69	0.64	0.66	0.71	0.68
141Pr	0.50	0.60	0.41	0.14	0.17	0.15	0.14	0.13	0.14	0.12	0.12	0.17
146Nd	3.51	4.19	2.67	1.06	0.96	0.79	0.85	0.76	0.72	0.71	0.66	0.91
147Sm	1.66	2.36	1.18	0.48	0.42	0.34	0.53	0.41	0.34	0.42	0.40	0.32
153Eu	0.45	0.50	0.39	0.22	0.22	0.14	0.14	0.13	0.11	0.14	0.14	0.13
157Gd	2.58	3.69	1.78	0.89	0.95	0.63	0.69	0.64	0.59	0.56	0.58	0.56
159Tb	0.51	0.70	0.34	0.19	0.18	0.12	0.13	0.12	0.11	0.14	0.11	0.12
163Dy	3.92	4.75	2.17	1.35	1.11	1.02	1.25	1.21	1.12	0.97	1.05	1.23
166Ho	0.65	1.07	0.50	0.32	0.27	0.20	0.24	0.21	0.23	0.21	0.22	0.21
166Er	2.46	2.93	1.51	0.75	0.76	0.55	0.66	0.62	0.54	0.58	0.55	0.57
169Tm	0.35	0.41	0.22	0.11	0.11	0.11	0.11	0.10	0.09	0.10	0.09	0.10
172Yb	2.43	2.52	1.44	0.66	0.71	0.52	0.71	0.68	0.57	0.64	0.57	0.63
178Hf	0.44	1.04	0.26	0.15	0.17	0.14	0.15	0.12	0.12	0.08	0.12	0.16
232Th	0.02	0.02	0.02	0.01	0.01	0.06	0.04	0.00	0.03	0.02	0.01	0.07

Block	Aswad	Aswad	Aswad	Aswad	Aswad	Aswad	Aswad	Aswad	Aswad	Aswad	Aswad	Aswad	Aswad	Aswad	Aswad	Aswad	Aswad	Aswad
Sample No:	04UR44-1-1	04UR44-1-2	04UR44-1-3	04UR44-2-1	04UR44-2-2	04UR44-2-3	04UR44-3-1	04UR44-3-2	04UR44-3-3	UAE644-1-1	UAE644-1-2	UAE644-1-3	UAE644-2-1	UAE644-2-2	UAE644-2-3	UAE644-3-1	UAE644-3-2	UAE644-3-3
Sample Type:	Layered Gabbro	Layered Gabbro	Layered Gabbro	Layered Gabbro	Layered Gabbro	Layered Gabbro	Layered Gabbro	Layered Gabbro	Layered Gabbro	Layered Gabbro	Layered Gabbro	Layered Gabbro	Layered Gabbro	Layered Gabbro	Layered Gabbro	Layered Gabbro	Layered Gabbro	Layered Gabbro
wt%																		
SiO2	52.42	52.42	52.42	52.28	52.28	52.28	52.30	52.30	52.30	52.22	52.22	52.22	52.03	52.03	52.03	51.82	51.92	51.92
TiO2	0.28	0.28	0.28	0.28	0.28	0.28	0.32	0.32	0.32	0.40	0.40	0.40	0.33	0.33	0.33	0.44	0.44	0.44
Al2O3	2.23	2.23	2.23	2.33	2.33	2.33	2.28	2.28	2.28	1.82	1.82	1.82	1.85	1.85	1.85	1.81	1.81	1.81
Cr2O3	0.19	0.19	0.19	0.24	0.24	0.24	0.24	0.24	0.24	0.22	0.22	0.22	0.28	0.28	0.28	0.25	0.25	0.25
Fe2O3	4.95	4.95	4.95	5.02	5.02	5.02	5.20	5.20	5.20	7.00	7.00	7.00	6.87	6.87	6.87	6.93	6.93	6.93
MnO	0.08	0.08	0.08	0.1	0.1	0.1	0.08	0.08	0.08	0.08	0.08	0.08	0.05	0.05	0.05	0.1	0.1	0.1
MgO	18	18	18	17.7	17.7	17.7	18.02	18.02	18.02	18.20	18.20	18.20	18.17	18.17	18.17	18.12	18.12	18.12
CaO	21.71	21.71	21.71	21.72	21.72	21.72	21.28	21.28	21.28	22.09	22.09	22.09	21.89	21.89	21.89	22.09	22.09	22.09
Na2O	0.00	0.00	0.00	0.00	0.00	0.00	0.00	0.00	0.00	0.24	0.24	0.24	0.22	0.22	0.22	0.19	0.19	0.19
Total	99.84	99.84	99.84	99.88	99.88	99.88	99.70	99.70	99.70	100.25	100.25	100.25	99.70	99.70	99.70	99.87	99.87	99.87
ppm																		
45Sc	85.96	98.02	97.34	92.70	100.87	103.50	85.90	95.54	98.80	102.50	105.65	101.19	99.07	110.43	104.28	103.74	101.99	104.49
47Ti (%)	0.19	0.20	0.19	0.19	0.23	0.24	0.23	0.24	0.24	0.31	0.33	0.31	0.22	0.32	0.27	0.31	0.30	0.30
Ti	1132.71	1225.98	1110.07	1124.21	1396.87	1449.52	1361.58	1415.82	1425.26	1887.40	2007.41	1840.70	1322.82	1908.00	1843.48	1879.00	1815.87	1817.18
51V	229.84	259.55	277.96	248.82	302.23	312.94	285.81	285.58	277.75	411.95	409.26	418.99	330.85	380.58	392.05	397.45	389.80	401.11
52Cr	1182.11	712.07	866.08	1226.33	1315.38	700.87	1573.34	739.90	811.53	888.84	929.61	994.55	2653.31	789.93	1018.26	959.40	935.38	987.82
55Mn (%)	0.13	0.16	0.15	0.14	0.17	0.17	0.16	0.16	0.15	0.22	0.23	0.23	0.22	0.21	0.23	0.22	0.21	0.23
86Sr	6.80	5.78	6.46	6.54	6.02	6.39	5.52	5.40	5.40	6.43	7.22	6.40	6.44	6.83	6.83	7.65	6.89	6.53
89Y	8.25	7.73	7.09	6.87	9.08	9.43	7.43	9.22	6.75	14.26	14.17	13.85	13.40	14.82	13.03	14.87	14.37	14.48
90Zr	1.88	2.14	1.89	1.85	2.92	3.14	2.21	2.88	2.91	6.13	5.83	5.77	5.49	6.44	4.44	6.63	5.80	5.93
93Nb	-0.01	-0.01	-0.01	-0.01	-0.01	-0.01	-0.01	-0.01	-0.01	0.95	0.95	0.95	0.83	0.85	0.85	0.88	0.81	0.81
138La	0.04	0.06	0.04	0.05	0.06	0.06	0.05	0.06	0.06	0.15	0.16	0.15	0.14	0.15	0.15	0.16	0.13	0.18
140Ce	0.30	0.37	0.30	0.31	0.44	0.46	0.35	0.38	0.43	0.99	0.95	0.95	0.90	0.92	0.90	0.91	0.91	0.95
141Pr	0.08	0.10	0.08	0.09	0.12	0.12	0.10	0.12	0.11	0.23	0.22	0.22	0.21	0.23	0.20	0.24	0.23	0.23
146Nd	0.66	0.79	0.71	0.73	0.97	1.01	0.76	0.93	0.97	1.68	1.77	1.48	1.59	1.73	1.48	1.89	1.74	1.88
147Sm	0.41	0.48	0.49	0.43	0.68	0.67	0.50	0.62	0.57	0.96	0.97	0.92	0.82	0.98	0.87	1.02	0.92	0.94
153Eu	0.19	0.23	0.20	0.19	0.28	0.25	0.22	0.24	0.26	0.30	0.33	0.33	0.28	0.31	0.30	0.29	0.32	0.30
157Gd	0.70	0.91	0.83	0.75	1.07	1.19	0.89	1.00	1.04	1.38	1.81	1.57	1.38	1.58	1.43	1.64	1.57	1.87
159Tb	0.15	0.18	0.17	0.14	0.22	0.23	0.19	0.21	0.21	0.34	0.38	0.32	0.29	0.37	0.27	0.38	0.37	0.35
163Dy	1.01	1.41	1.22	1.09	1.58	1.61	1.32	1.56	1.58	2.43	2.46	2.38	2.25	2.58	2.05	2.52	2.45	2.43
165Ho	0.25	0.27	0.25	0.25	0.34	0.38	0.28	0.35	0.34	0.58	0.51	0.57	0.53	0.59	0.47	0.59	0.58	0.58
166Er	0.88	0.91	0.74	0.68	0.94	0.95	0.83	0.98	0.95	1.51	1.63	1.58	1.44	1.89	1.40	1.89	1.61	1.85
169Tm	0.11	0.12	0.12	0.09	0.12	0.12	0.12	0.14	0.14	0.22	0.24	0.22	0.24	0.23	0.19	0.23	0.24	0.21
172Yb	0.81	0.82	0.71	0.84	0.88	0.90	0.74	0.84	0.86	1.48	1.47	1.37	1.34	1.45	1.21	1.51	1.40	1.32
178Hf	0.10	0.13	0.12	0.14	0.19	0.20	0.16	0.19	0.18	0.31	0.32	0.27	0.20	0.30	0.20	0.27	0.30	0.27
232Th	0.00	0.00	0.00	0.00	0.00	0.00	0.00	0.00	0.00	0.00	0.00	0.00	0.00	0.00	0.00	0.00	0.00	0.00

*Clinopyroxene major (SEM-EDS) and trace (LA-ICP-MS) element data for Aswad Block plutonic samples*

Block	Aswad	Aswad	Aswad	Aswad	Aswad	Aswad	Aswad	Aswad	Aswad	Aswad	Aswad	Aswad	Aswad	Aswad	Aswad	Aswad	Aswad
Sample No:	03UR85-1-1	03UR85-1-2	03UR85-2-1	03UR85-3-1	03UR85-3-2	03UR85-3-3	03UR123-1-1	03UR123-1-2	03UR123-1-3	03UR123-2-1	03UR123-2-2	03UR123-2-3	03UR123-3-1	03UR123-3-2	03UR123-3-3	03UR140-1-1	03UR140-1-2
Sample Type:	Kalbe (Upper) Gabbro	Kalbe (Upper) Gabbro	Kalbe (Upper) Gabbro	Kalbe (Upper) Gabbro	Kalbe (Upper) Gabbro	Kalbe (Upper) Gabbro	Kalbe (Upper) Gabbro	Kalbe (Upper) Gabbro	Kalbe (Upper) Gabbro	Kalbe (Upper) Gabbro	Kalbe (Upper) Gabbro	Kalbe (Upper) Gabbro	Kalbe (Upper) Gabbro	Kalbe (Upper) Gabbro	Kalbe (Upper) Gabbro	Kalbe (Upper) Gabbro	Kalbe (Upper) Gabbro
wt%																	
SiO2	51.33	51.33	51.45	51.77	51.77	51.77	52.14	52.14	52.14	52.43	52.43	52.43	52.34	52.34	52.34	52.22	52.22
TiO2	0.58	0.58	0.52	0.44	0.44	0.44	0.45	0.45	0.45	0.42	0.42	0.42	0.37	0.37	0.37	0.41	0.41
Al2O3	2.45	2.45	1.75	2.21	2.21	2.21	1.98	1.98	1.98	2.08	2.08	2.08	2.1	2.1	2.1	2.08	2.08
Cr2O3	0.36	0.36	0.05	0.39	0.39	0.39	0.04	0.04	0.04	0.05	0.05	0.05	0.05	0.05	0.05	0.18	0.18
Fe2O3	7.91	7.91	8.06	8.52	8.52	8.52	8.96	8.96	8.96	8.48	8.48	8.48	8.53	8.53	8.53	8.23	8.23
MnO	0.15	0.15	0.21	0.1	0.1	0.1	0.07	0.07	0.07	0.05	0.05	0.05	0.04	0.04	0.04	0.00	0.00
MgO	15.66	15.66	15.44	16.61	16.61	16.61	17.1	17.1	17.1	17.47	17.47	17.47	17.41	17.41	17.41	17.67	17.67
CaO	21.28	21.28	21.62	21.7	21.7	21.7	20.95	20.95	20.95	20.78	20.78	20.78	20.9	20.9	20.9	21.75	21.75
Na2O	0.3	0.3	0.31	0.28	0.28	0.28	0.3	0.3	0.3	0.24	0.24	0.24	0.24	0.24	0.24	0.10	0.10
Total	100	100	100	100	100	100	100	100	100	100	100	100	100	100	100	99.60	99.60
ppm																	
45Sc	113.90	99.60	135.66	113.02	118.53	103.34	99.63	104.16	105.79	105.37	104.16	97.33	97.22	93.76	93.60	110.06	92.02
47Ti (%)	0.45	0.60	0.71	0.33	0.38	0.43	0.35	0.34	0.33	0.33	0.33	0.28	0.33	0.32	0.30	0.40	0.28
Ti	2724.27	3599.99	4266.04	1972.70	2278.45	2590.66	2109.69	2064.22	2006.21	1961.03	1956.42	1683.22	1976.85	1694.11	1615.03	2392.17	1664.62
51V	347.44	380.21	449.78	288.71	285.76	291.58	326.40	323.42	309.89	296.67	303.26	286.31	311.61	301.49	301.44	336.06	249.04
52Cr	2582.40	3319.70	285.01	2111.60	1360.77	2887.67	113.19	97.40	108.77	290.55	189.91	605.87	243.35	473.98	162.66	263.94	2221.94
55Mn (%)	0.19	0.27	0.27	0.16	0.16	0.17	0.18	0.16	0.17	0.17	0.17	0.15	0.16	0.15	0.17	0.17	0.13
68Zn	10.67	8.93	9.99	10.00	11.53	12.59	8.23	7.91	7.74	8.06	8.06	7.09	8.38	8.38	7.90	9.35	9.43
89Y	18.27	46.19	29.73	13.82	14.93	17.72	13.38	13.69	14.34	13.57	13.52	11.72	12.52	12.37	12.32	17.11	9.07
90Zr	10.97	39.75	17.44	7.82	10.08	16.45	5.14	5.28	5.59	5.36	5.17	4.54	4.91	4.87	4.85	7.18	5.04
93Nb	0.41	0.35	0.32	0.31	0.39	0.32	0.42	0.32	0.34	0.28	0.35	0.35	0.42	0.40	0.42	0.30	0.29
139La	0.27	1.16	0.66	0.26	0.41	0.56	0.12	0.11	0.10	0.11	0.10	0.09	0.10	0.12	0.09	0.13	0.11
140Ce	1.23	6.38	2.03	1.00	1.43	2.13	0.70	0.89	0.62	0.64	0.65	0.64	0.71	0.72	0.66	0.87	0.60
141Pr	0.30	1.53	0.49	0.23	0.32	0.45	0.19	0.20	0.19	0.19	0.19	0.19	0.20	0.20	0.16	0.24	0.16
146Nd	2.28	10.31	3.67	1.67	2.25	3.17	1.69	1.42	1.64	1.82	1.61	1.33	1.60	1.71	1.62	1.95	1.28
147Sm	1.24	4.40	2.06	0.98	1.04	1.34	0.61	0.65	0.66	0.64	1.04	0.63	0.90	0.64	0.63	1.20	0.60
153Eu	0.45	0.85	0.62	0.34	0.36	0.41	0.36	0.34	0.35	0.34	0.32	0.28	0.37	0.35	0.34	0.41	0.28
157Gd	1.98	6.18	3.31	1.72	1.82	2.18	1.47	1.65	1.77	1.65	1.63	1.27	1.42	1.55	1.34	1.97	1.15
160Tb	0.41	1.23	0.69	0.35	0.37	0.42	0.31	0.33	0.32	0.33	0.32	0.28	0.30	0.32	0.30	0.41	0.24
163Dy	2.79	8.14	4.95	2.41	2.49	3.00	2.23	2.25	2.47	2.32	2.39	1.90	2.10	2.21	1.95	2.81	1.66
165Ho	0.65	1.79	1.14	0.53	0.59	0.69	0.45	0.48	0.53	0.52	0.60	0.42	0.44	0.48	0.45	0.64	0.36
168Er	1.73	4.85	3.01	1.41	1.55	1.87	1.33	1.37	1.55	1.41	1.32	1.17	1.37	1.31	1.22	1.80	1.03
169Tm	0.26	0.99	0.45	0.22	0.23	0.29	0.18	0.19	0.19	0.20	0.21	0.17	0.19	0.19	0.19	0.26	0.15
172Yb	1.46	4.29	2.68	1.22	1.34	1.72	1.19	1.29	1.34	1.22	1.27	1.06	1.28	1.16	1.16	1.53	0.91
176Hf	0.52	1.34	0.78	0.32	0.43	0.63	0.31	0.26	0.32	0.30	0.27	0.24	0.31	0.27	0.25	0.40	0.22
232Th	0.02	0.04	0.06	0.29	0.06	0.09	0.00	0.00	0.00	-0.01	0.00	0.00	0.00	0.00	0.00	0.00	0.01

Clinopyroxene major (SEM-EDS) and trace (LA-ICP-MS) element data for Aswad Block plutonic samples

Block	Aswad	Aswad	Aswad	Aswad	Aswad	Aswad	Aswad	Aswad	Aswad	Aswad	Aswad	Aswad	Aswad	Aswad	Aswad	Aswad
Sample No:	03UR140-2-1	03UR140-2-2	03UR140-3-1	03UR140-3-2	03UR140-3-3	03UR140-4-1	03UR140-4-2	03UR140-4-3	03UR140-4-4	03UR199-1-1	03UR199-1-2	03UR199-2-1	03UR199-2-2	04UR199-3-1	03UR199-3-2	03UR199-3-3
Sample Type:	Kaliba (Upper) Gabbro	Kaliba (Upper) Gabbro	Kaliba (Upper) Gabbro	Kaliba (Upper) Gabbro	Kaliba (Upper) Gabbro	Kaliba (Upper) Gabbro	Kaliba (Upper) Gabbro	Kaliba (Upper) Gabbro	Kaliba (Upper) Gabbro	Kaliba (Upper) Gabbro	Kaliba (Upper) Gabbro	Kaliba (Upper) Gabbro	Kaliba (Upper) Gabbro	Kaliba (Upper) Gabbro	Kaliba (Upper) Gabbro	Kaliba (Upper) Gabbro
wt%																
SiO <sub>2</sub>	50.87	50.87	51.87	51.87	51.87	52.52	52.52	52.52	52.52	50.92	50.92	52.53	52.53	51.81	51.81	51.81
TiO <sub>2</sub>	0.97	0.97	0.38	0.38	0.38	0.38	0.38	0.38	0.38	0.95	0.95	0.21	0.21	0.39	0.39	0.39
Al <sub>2</sub> O <sub>3</sub>	2.19	2.19	2.46	2.45	2.45	2.17	2.17	2.17	2.17	2.9	2.9	1.77	1.77	2.52	2.52	2.52
Cr <sub>2</sub> O <sub>3</sub>	0.05	0.05	0.49	0.49	0.49	0.31	0.31	0.31	0.31	0.39	0.39	0.61	0.61	0.66	0.66	0.66
Fe <sub>2</sub> O <sub>3</sub>	7.89	7.89	4.49	4.49	4.49	4.99	4.99	4.99	4.99	7.85	7.85	4.84	4.84	5.99	5.99	5.99
MnO	0.20	0.20	0.09	0.09	0.09	0.04	0.04	0.04	0.04	0.23	0.23	0.11	0.11	0.13	0.13	0.13
MgO	15.29	15.29	17.41	17.41	17.41	17.99	17.99	17.99	17.99	15.72	15.72	18.57	18.57	18.99	18.99	18.99
CaO	21.84	21.84	21.85	21.95	21.95	21.81	21.81	21.81	21.81	20.54	20.54	23.1	23.1	21.84	21.84	21.84
Na <sub>2</sub> O	0.28	0.28	0.04	0.04	0.04	0.09	0.09	0.09	0.09	0.6	0.6	0.17	0.17	0.21	0.21	0.21
Total	99.43	99.43	99.14	99.14	99.14	99.72	99.72	99.72	99.72	100	100	100	100	100	100	100
ppm																
48Sc	112.95	110.93	88.83	94.74	97.92	101.29	97.73	94.93	103.42	108.65	97.93	108.34	92.21	91.76	98.24	97.27
47Ti (%)	0.69	0.89	0.27	0.28	0.31	0.31	0.34	0.32	0.28	0.95	0.42	0.42	0.30	0.27	0.32	0.60
Ti	4156.29	5336.03	1800.85	1859.82	1878.98	1895.69	2038.85	1842.89	1983.59	3928.88	2499.87	2487.98	1827.31	1607.65	1939.88	3587.00
51V	505.07	625.02	255.31	284.54	305.11	288.03	284.29	288.35	288.09	348.27	299.18	389.32	291.82	251.75	284.79	388.94
52Cr	75.95	82.86	3019.13	2401.31	2909.41	1272.32	1312.25	1328.20	1999.50	2795.46	2015.25	6613.55	9380.83	8085.34	6483.91	485.09
55Mn (%)	0.27	0.31	0.13	0.15	0.16	0.16	0.16	0.16	0.16	0.22	0.19	0.17	0.16	0.12	0.13	0.22
88Sr	9.53	11.31	9.37	10.49	9.44	9.19	8.84	8.82	8.84	10.50	8.28	11.36	10.27	10.70	7.52	8.64
89Y	25.35	39.78	6.59	9.03	11.10	10.82	11.41	10.82	9.23	38.88	17.84	13.96	10.71	11.21	12.70	48.08
90Zr	12.35	20.37	4.47	5.94	7.14	4.78	5.99	4.95	4.16	35.08	9.88	9.73	5.47	4.96	6.36	51.83
93Nb	0.32	0.38	0.38	0.37	0.34	0.33	0.31	0.30	0.31	0.84	0.28	0.38	0.39	0.40	0.35	0.41
138La	0.27	0.81	0.12	0.18	0.19	0.10	0.12	0.11	0.10	0.80	0.49	0.30	0.18	0.17	0.17	0.88
140Ce	1.85	3.00	0.82	0.84	1.05	0.80	0.73	0.70	0.68	3.04	1.56	1.38	0.85	0.89	0.79	4.95
141Pr	0.42	0.71	0.17	0.21	0.29	0.19	0.20	0.19	0.18	0.68	0.32	0.20	0.20	0.17	0.19	1.19
146Nd	3.39	5.17	1.29	1.94	1.78	1.48	1.56	1.47	1.15	8.06	2.21	2.07	1.47	1.40	1.44	7.95
147Sm	1.87	2.85	0.89	0.96	0.98	0.91	0.92	0.79	0.79	2.82	1.20	1.12	0.79	0.70	0.89	3.78
153Eu	0.59	0.71	0.29	0.29	0.34	0.32	0.31	0.31	0.30	0.55	0.34	0.42	0.30	0.28	0.30	0.73
157Gd	3.07	4.47	1.08	1.32	1.51	1.35	1.80	1.29	1.14	4.19	1.91	1.89	1.30	1.35	1.42	5.42
159Tb	0.84	0.87	0.20	0.23	0.29	0.27	0.29	0.27	0.24	0.83	0.39	0.33	0.28	0.28	0.29	1.11
163Dy	4.28	6.35	1.58	1.81	1.99	1.88	1.95	1.83	1.77	6.08	2.80	2.35	1.80	1.74	2.00	7.93
165Ho	0.88	1.39	0.32	0.38	0.48	0.43	0.42	0.44	0.38	1.40	0.65	0.57	0.39	0.41	0.48	1.71
166Er	2.84	4.09	0.87	0.97	1.20	1.16	1.15	1.17	1.02	3.98	1.84	1.53	1.12	1.08	1.28	4.80
169Tm	0.39	0.59	0.11	0.15	0.18	0.17	0.17	0.18	0.15	0.59	0.29	0.23	0.17	0.17	0.19	0.72
172Yb	2.47	3.73	0.74	0.84	1.08	1.02	1.08	1.03	0.91	3.88	1.84	1.43	1.08	1.07	1.15	4.28
176Hf	0.66	0.84	0.21	0.33	0.36	0.25	0.25	0.26	0.19	1.05	0.41	0.55	0.25	0.29	0.37	2.02
232Th	0.01	0.05	0.01	0.02	0.01	0.00	0.00	0.00	0.00	0.14	0.11	0.02	0.01	0.01	0.01	0.01

Clinopyroxene major (SEM-EDS) and trace (LA-ICP-MS) element data for Aswad Block plutonic samples

Block	Aswad	Aswad	Aswad	Aswad	Aswad	Aswad	Aswad	Aswad	Aswad	Aswad	Aswad	Aswad	Aswad	Aswad	Aswad	Aswad	Aswad	Aswad	
Sample No:	UAE3031-1-1	UAE3031-1-2	UAE3031-1-3	UAE3031-1-4	UAE3031-1-5	UAE3031-2-1	UAE3031-2-2	UAE3031-2-3	UAE3031-3-1	UAE3031-3-2	UAE3031-3-3	UAE450-1-1	UAE450-1-2	UAE450-1-3	UAE450-2-1	UAE450-2-2	UAE450-2-3	UAE450-3-1	
Sample Type:	Kalba (Upper) Gabbro	Kalba (Upper) Gabbro	Kalba (Upper) Gabbro	Kalba (Upper) Gabbro	Kalba (Upper) Gabbro	Kalba (Upper) Gabbro	Kalba (Upper) Gabbro	Kalba (Upper) Gabbro	Kalba (Upper) Gabbro	Kalba (Upper) Gabbro	Kalba (Upper) Gabbro	Blitha Gabbro	Blitha Gabbro	Blitha Gabbro	Blitha Gabbro	Blitha Gabbro	Blitha Gabbro	Blitha Gabbro	
wt%																			
SiO <sub>2</sub>	51.93	51.93	51.93	51.93	51.93	52.10	52.10	52.10	52.08	52.08	52.08	52.17	52.17	52.17	52.04	52.04	52.04	51.99	
TiO <sub>2</sub>	0.30	0.30	0.30	0.30	0.30	0.29	0.29	0.29	0.28	0.28	0.28	0.16	0.16	0.16	0.19	0.19	0.19	0.18	
Al <sub>2</sub> O <sub>3</sub>	2.46	2.46	2.46	2.46	2.46	2.64	2.64	2.64	2.64	2.64	2.64	3.04	3.04	3.04	3.19	3.19	3.19	3.34	
Cr <sub>2</sub> O <sub>3</sub>	0.77	0.77	0.77	0.77	0.77	0.78	0.78	0.78	0.81	0.81	0.81	1.10	1.10	1.10	1.20	1.20	1.20	1.20	
Fe <sub>2</sub> O <sub>3</sub>	6.12	6.12	6.12	6.12	6.12	6.36	6.36	6.36	6.34	6.34	6.34	6.76	6.76	6.76	6.94	6.94	6.94	7.19	
MnO	0.06	0.06	0.06	0.06	0.06	0.10	0.10	0.10	0.09	0.09	0.09	0.00	0.00	0.00	0.00	0.00	0.00	0.02	
MgO	16.97	16.97	16.97	16.97	16.97	16.95	16.95	16.95	16.89	16.89	16.89	16.95	16.95	16.95	17.24	17.24	17.24	16.82	
CaO	21.09	21.09	21.09	21.09	21.09	21.51	21.51	21.51	21.49	21.49	21.49	23.59	23.59	23.59	23.29	23.29	23.29	23.21	
Na <sub>2</sub> O	0.30	0.30	0.30	0.30	0.30	0.37	0.37	0.37	0.37	0.37	0.37	0.16	0.16	0.16	0.02	0.02	0.02	0.19	
Total	100.00	100.00	100.00	100.00	100.00	100.00	100.00	100.00	100.00	100.00	100.00	100.89	100.89	100.89	101.07	101.07	101.07	100.44	
ppm																			
45Sc	62.24	62.01	63.09	62.02	79.99	80.75	83.73	78.01	69.95	76.39	76.84	100.20	100.21	101.62	100.51	105.63	104.01	72.98	
47Ti (%)	0.27	0.25	0.28	0.33	0.25	0.23	0.23	0.23	0.22	0.23	0.23	0.18	0.18	0.17	0.14	0.16	0.16	0.14	
Ti	1802.26	1495.02	1698.70	1970.14	1519.82	1378.70	1564.45	1366.87	1324.09	1336.55	1407.91	1059.42	958.70	1032.84	967.46	963.15	1058.44	866.45	
51V	270.51	265.93	267.39	283.03	275.93	282.85	285.98	271.37	284.26	287.71	287.30	193.44	195.73	171.77	149.96	173.49	176.30	216.52	
52Cr	4125.63	4329.78	4184.44	4320.99	4351.40	4691.16	4502.90	4403.78	4818.90	4930.26	4969.63	5110.92	5626.92	6360.69	5673.94	6920.97	6366.87	7369.17	
56Mn (%)	0.16	0.16	0.14	0.17	0.16	0.16	0.14	0.15	0.15	0.15	0.15	0.10	0.09	0.10	0.08	0.08	0.09	0.11	
88Sr	5.05	4.84	5.42	6.82	5.83	5.51	6.06	5.12	4.73	4.45	4.93	7.87	7.63	24.36	7.03	7.23	6.15	14.09	
89Y	11.20	12.59	12.27	14.36	11.63	10.49	9.65	8.38	7.16	6.47	6.35	6.92	6.72	7.44	7.01	7.22	6.29	4.61	
90Zr	6.52	6.90	6.90	15.99	6.37	5.99	6.06	4.01	2.45	3.25	4.36	2.86	2.86	3.36	2.63	3.58	3.66	2.11	
93Nb	0.07	0.09	0.07	0.11	0.07	0.08	0.04	0.05	0.04	0.05	0.04	0.12	0.11	0.11	0.13	0.12	0.11	0.16	
139La	0.15	0.18	0.20	0.38	0.20	0.18	0.11	0.08	0.07	0.11	0.06	0.06	0.06	0.07	0.05	0.05	0.05	0.06	
140Ce	0.59	0.51	0.72	1.24	0.77	0.71	0.69	0.46	0.34	0.46	0.49	0.24	0.25	0.32	0.24	0.27	0.27	0.39	
141Pr	0.14	0.16	0.19	0.25	0.19	0.16	0.13	0.10	0.12	0.12	0.12	0.06	0.07	0.09	0.09	0.09	0.10	0.09	
148Nd	1.07	1.42	1.34	1.90	1.35	1.15	0.97	0.65	0.51	0.59	0.59	0.37	0.37	0.51	0.37	0.46	0.76	0.70	
147Sm	0.66	0.75	0.71	0.92	0.78	0.69	0.59	0.57	0.49	0.55	0.53	0.42	0.42	0.48	0.45	0.45	0.50	0.32	
153Eu	0.22	0.22	0.22	0.26	0.22	0.22	0.21	0.21	0.20	0.21	0.21	0.16	0.16	0.14	0.16	0.16	0.16	0.13	
157Gd	1.09	1.28	1.24	1.54	1.24	1.14	1.06	0.93	0.76	0.85	0.97	0.62	0.78	0.86	0.75	0.86	0.92	0.52	
169Tb	0.24	0.27	0.27	0.32	0.29	0.22	0.21	0.19	0.16	0.19	0.19	0.17	0.17	0.16	0.16	0.16	0.16	0.12	
183Dy	1.69	1.94	1.88	2.16	1.80	1.67	1.50	1.32	1.21	1.30	1.37	1.27	1.19	1.31	1.26	1.23	1.42	0.83	
185Ho	0.40	0.45	0.45	0.52	0.43	0.38	0.37	0.30	0.27	0.29	0.31	0.26	0.24	0.30	0.29	0.29	0.32	0.19	
166Er	1.15	1.33	1.28	1.55	1.28	1.12	1.02	0.88	0.76	0.84	0.95	0.63	0.73	0.89	0.83	0.78	0.92	0.52	
169Tm	0.16	0.21	0.20	0.24	0.19	0.17	0.15	0.13	0.11	0.13	0.12	0.13	0.10	0.12	0.11	0.13	0.14	0.08	
172Yb	1.10	1.31	1.26	1.52	1.29	1.13	0.97	0.80	0.74	0.89	0.94	0.68	0.80	0.70	0.89	0.83	0.71	0.43	
178Yf	0.25	0.23	0.26	0.41	0.27	0.21	0.24	0.17	0.13	0.16	0.17	0.16	0.15	0.20	0.20	0.27	0.26	0.10	
232Th	0.04	0.04	0.06	0.11	0.06	0.05	0.04	0.03	0.01	0.01	0.02	0.00	0.00	0.00	0.00	0.00	0.00	0.00	

4 Clinopyroxene major (SEM-EDS) and trace (LA-ICP-MS) element data for Aswad Block plutonic samples

Block	Aswad	Aswad	Aswad	Aswad	Aswad	Aswad	Aswad	Aswad	Aswad	Aswad	Aswad	Aswad	Aswad	Aswad	Aswad	Aswad	Aswad	Aswad
Sample No:	UAE450-3-2	UAE450-3-3	UAE517-1-1	UAE517-1-2	UAE517-1-3	UAE517-2-1	UAE517-2-2	UAE517-2-3	UAE517-4-1	UAE517-4-2	UAE517-4-3	UAE3999-1-1	UAE3999-1-2	UAE3999-1-3	UAE3999-2-1	UAE3999-2-2	UAE3999-2-3	UAE3999-3-1
Sample Type:	Bithna Gabbro	Bithna Gabbro	Bithna Gabbro	Bithna Gabbro	Bithna Gabbro	Bithna Gabbro	Bithna Gabbro	Bithna Gabbro	Bithna Gabbro	Bithna Gabbro	Bithna Gabbro	Bithna Gabbro	Bithna Gabbro	Bithna Gabbro	Bithna Gabbro	Bithna Gabbro	Bithna Gabbro	Bithna Gabbro
wt%																		
SiO2	51.66	51.66	52.24	52.24	52.24	52.34	52.34	52.34	52.21	52.21	52.21	51.16	51.16	51.16	50.59	50.59	50.59	51.19
TiO2	0.18	0.18	0.49	0.49	0.49	0.47	0.47	0.47	0.41	0.41	0.41	0.48	0.48	0.48	0.42	0.42	0.42	0.57
Al2O3	3.34	3.34	2.08	2.08	2.08	1.95	1.95	1.95	2.08	2.08	2.08	1.77	1.77	1.77	5.21	5.21	5.21	1.73
Cr2O3	1.20	1.20	0.48	0.48	0.48	0.44	0.44	0.44	0.66	0.66	0.66	0.08	0.08	0.08	0.02	0.02	0.02	0.08
Fe2O3	3.79	3.79	5.53	5.53	5.53	5.44	5.44	5.44	5.45	5.45	5.45	9.88	9.88	9.88	9.11	9.11	9.11	9.78
MnO	0.02	0.02	0.06	0.06	0.06	0.09	0.09	0.09	0.06	0.06	0.06	0.23	0.23	0.23	0.22	0.22	0.22	0.21
MgO	16.82	16.82	16.58	16.58	16.58	16.80	16.80	16.80	16.49	16.49	16.49	14.34	14.34	14.34	12.9	12.9	12.9	14.38
CaO	23.21	23.21	22.82	22.82	22.82	22.83	22.83	22.83	23.06	23.06	23.06	21.74	21.74	21.74	21.07	21.07	21.07	21.8
Na2O	0.19	0.19	0.27	0.27	0.27	0.30	0.30	0.30	0.28	0.28	0.28	0.32	0.32	0.32	0.45	0.45	0.45	0.31
Total	100.44	100.44	100.66	100.66	100.66	100.66	100.66	100.66	100.66	100.66	100.66	100	100	100	100	100	100	100
ppm																		
45Rc	73.86	68.49	118.72	117.29	99.14	106.66	100.52	84.59	113.90	101.61	106.90	177.62	172.63	170.20	163.07	166.80	164.63	161.52
47Ti (%)	0.14	0.13	0.50	0.60	0.35	0.44	0.37	0.35	0.39	0.29	0.31	0.38	0.39	0.38	0.36	0.36	0.36	0.40
Tl	825.40	802.99	2997.73	3593.53	2069.44	2629.43	2216.45	2110.86	2306.00	1736.46	1831.68	2262.08	2340.04	2132.14	2167.41	2136.24	2266.08	2400.63
51V	227.11	218.13	315.82	347.46	249.19	348.80	332.79	302.60	306.07	240.35	243.03	336.94	343.44	324.64	294.90	300.35	311.68	323.20
52Cr	8903.30	8920.98	1812.95	2239.59	3815.91	2249.99	3973.21	2182.89	2079.01	4227.88	4182.88	69.19	66.09	49.76	35.92	41.28	47.84	39.19
55Mn (%)	0.11	0.10	0.18	0.18	0.19	0.19	0.20	0.19	0.18	0.18	0.14	0.23	0.23	0.24	0.24	0.24	0.23	0.23
88Sr	8.25	10.73	7.24	7.98	8.35	8.27	8.24	7.85	8.49	8.09	9.31	4.94	4.94	5.30	5.04	4.73	4.80	4.81
89Y	4.25	4.05	29.19	29.40	20.14	19.79	18.24	17.01	20.40	19.29	19.11	26.99	26.56	24.72	23.18	24.04	23.90	23.28
90Zr	2.08	1.94	29.18	28.88	14.05	19.04	11.77	11.50	14.43	10.86	10.41	9.47	8.47	8.85	7.87	8.83	8.06	7.87
93Nb	0.16	0.15	0.13	0.12	0.13	0.16	0.14	0.14	0.19	0.14	0.12	0.00	0.00	0.00	0.00	0.00	0.00	0.00
139La	0.06	0.06	0.39	0.40	0.35	0.35	0.32	0.30	0.39	0.36	0.32	0.17	0.17	0.16	0.16	0.14	0.15	0.14
140Ce	0.32	0.37	1.97	2.02	1.79	1.98	1.90	1.83	1.92	1.89	1.69	0.84	0.85	0.80	0.86	0.84	0.84	0.87
141Pr	0.07	0.08	0.48	0.53	0.41	0.45	0.44	0.43	0.46	0.44	0.37	0.27	0.27	0.28	0.26	0.26	0.26	0.27
148Nd	0.64	0.67	3.76	4.06	3.01	3.29	3.14	2.68	3.02	2.88	2.54	2.44	2.39	2.20	2.22	2.29	2.28	2.31
147Sm	0.30	0.32	1.84	2.07	1.47	1.65	1.53	1.38	1.52	1.24	1.08	1.41	1.42	1.44	1.44	1.39	1.43	1.45
153Eu	0.13	0.11	0.54	0.61	0.47	0.46	0.45	0.45	0.44	0.42	0.36	0.39	0.42	0.39	0.39	0.39	0.37	0.40
157Gd	0.66	0.47	3.09	3.79	2.62	2.42	2.41	2.30	2.15	1.87	1.80	2.87	2.84	2.89	2.87	2.82	2.73	2.79
159Tb	0.12	0.11	0.69	0.74	0.47	0.48	0.45	0.44	0.50	0.37	0.36	0.62	0.60	0.57	0.56	0.56	0.56	0.57
163Dy	0.65	0.67	4.65	4.99	3.60	3.46	3.13	3.08	3.51	2.86	2.46	4.26	4.31	4.13	4.04	4.05	3.94	4.02
165Ho	0.14	0.17	1.10	1.16	0.82	0.79	0.66	0.70	0.77	0.61	0.59	1.00	1.01	0.97	0.92	0.97	0.90	0.93
166Er	0.47	0.41	2.80	3.42	2.26	2.05	1.92	2.00	2.16	1.76	1.72	3.00	2.80	2.74	2.87	2.84	2.46	2.60
169Tm	0.06	0.06	0.42	0.46	0.33	0.29	0.30	0.28	0.32	0.26	0.25	0.42	0.39	0.41	0.36	0.39	0.36	0.39
172Yb	0.44	0.36	2.30	2.71	2.08	2.07	1.90	1.83	1.91	1.80	1.38	2.43	2.48	2.42	2.26	2.30	2.22	2.24
178Hf	0.14	0.11	1.53	1.16	0.40	0.56	0.36	0.41	0.50	0.38	0.38	0.47	0.45	0.44	0.43	0.46	0.43	0.45
232Th	0.00	0.00	0.01	0.01	0.03	0.01	0.01	0.01	0.01	0.01	0.01	0.00	0.00	0.00	0.00	0.00	0.01	0.00

Clinopyroxene major (SEM-EDS) and trace (LA-ICP-MS) element data for Aswad Block plutonic samples



Block	Aswad	Aswad	Aswad	Aswad	Aswad	Aswad	Aswad	Aswad	Aswad	Aswad	Aswad	Aswad	Aswad	Aswad	Aswad	Aswad	Aswad	Aswad	
Sample No:	UAE3969-3-2	UAE3969-3-3	UAE3967-1-1	UAE3967-1-2	UAE3967-1-3	UAE3967-2-1	UAE3967-2-2	UAE3967-3-1	UAE3967-4-1	UAE3967-4-2	UAE3967-5-1	UAE3967-5-2	UAE3967-5-3	04UR30-1-1	04UR30-1-2	04UR30-2-1	04UR30-2-2	04UR30-3-1	
Sample Type:	Bitlha Gabbro	Bitlha Gabbro	Bitlha Gabbro	Bitlha Gabbro	Bitlha Gabbro	Bitlha Gabbro	Bitlha Gabbro	Bitlha Gabbro	Bitlha Gabbro	Bitlha Gabbro	Bitlha Gabbro	Bitlha Gabbro	Bitlha Gabbro	Fulalrah Gabbro	Fulalrah Gabbro	Fulalrah Gabbro	Fulalrah Gabbro	Fulalrah Gabbro	
w%																			
SiO <sub>2</sub>	51.16	51.16	51.02	51.02	51.02	50.89	50.89	51.56	51.36	51.36	51.4	51.4	51.4	52.31	52.31	52.63	52.63	52.74	
TiO <sub>2</sub>	0.67	0.67	0.41	0.41	0.41	0.45	0.45	0.32	0.31	0.31	0.32	0.32	0.32	0.28	0.28	0.16	0.16	0.40	
Al <sub>2</sub> O <sub>3</sub>	1.73	1.73	1.47	1.47	1.47	1.69	1.69	1.12	1.27	1.27	1.22	1.22	1.22	1.36	1.36	1.84	1.84	1.07	
Cr <sub>2</sub> O <sub>3</sub>	0.06	0.06	0.00	0.00	0.00	0.11	0.11	0	0.06	0.06	0	0	0	0.49	0.49	0.50	0.50	0.49	
Fe <sub>2</sub> O <sub>3</sub>	9.78	9.78	12.03	12.03	12.03	11.08	11.08	9.57	10.83	10.83	10.8	10.8	10.8	5.94	5.94	5.08	5.08	5.85	
MnO	0.21	0.21	0.25	0.25	0.25	0.23	0.23	0.32	0.24	0.24	0.15	0.15	0.15	0.04	0.04	0.04	0.04	0.12	
MgO	14.36	14.36	14.66	14.66	14.66	14.42	14.42	14.43	14.66	14.66	14.76	14.76	14.76	16.12	16.12	16.72	16.72	16.62	
CaO	21.8	21.8	19.67	19.67	19.67	20.82	20.82	22.39	21.37	21.37	21.07	21.07	21.07	22.66	22.66	22.90	22.90	22.87	
Na <sub>2</sub> O	0.31	0.31	0.27	0.27	0.27	0.33	0.33	0.31	0.19	0.19	0.26	0.26	0.26	0.27	0.27	0.15	0.15	0.10	
Total	100	100	100.00	100.00	100.00	100.00	100.00	100	100.00	100.00	100	100	100	99.37	99.37	99.91	99.91	100.16	
ppm																			
46Sc	165.03	171.00	116.67	116.16	116.26	122.20	121.67	135.74	130.47	127.14	164.80	148.69	167.30	87.83	86.46	93.99	84.69	99.32	
47Ti (%)	0.40	0.41	0.32	0.36	0.32	0.36	0.31	0.35	0.36	0.27	0.34	0.34	0.35	0.29	0.25	0.17	0.13	0.28	
Tl	2375.26	2460.83	1940.45	2159.69	1932.16	2136.51	1936.65	2118.86	2177.13	1947.34	2054.67	2013.54	2119.33	1725.43	1617.92	1025.12	808.55	1957.41	
51V	321.23	360.99	394.95	420.05	399.03	429.36	399.09	429.74	476.50	430.30	396.96	393.65	413.71	359.06	325.01	302.46	267.46	322.91	
52Cr	26.43	51.04	129.36	131.77	123.44	248.96	87.52	187.59	149.45	112.69	80.21	86.82	111.07	2468.47	2616.87	1995.44	3448.00	2624.23	
55Mn (%)	0.23	0.26	0.23	0.23	0.24	0.24	0.25	0.26	0.25	0.24	0.23	0.24	0.23	0.16	0.17	0.14	0.14	0.15	
88Sr	5.41	5.13	6.36	4.34	4.77	4.16	8.24	4.87	4.39	4.80	4.10	4.11	4.26	6.69	6.80	6.93	6.29	4.86	
89Y	22.82	24.93	27.19	26.89	27.96	32.59	26.74	31.15	31.72	27.82	39.69	36.99	41.56	12.46	11.29	8.23	6.63	13.26	
90Zr	7.49	6.16	7.64	8.24	7.70	10.32	6.73	8.71	8.62	7.74	10.47	9.62	11.39	9.99	12.66	3.71	3.16	10.48	
93Nb	0.00	0.01	0.01	0.00	0.01	0.01	0.01	0.01	0.01	0.01	0.01	0.00	0.01	0.01	0.01	0.01	0.02	0.01	
138La	0.14	0.15	0.19	0.18	0.21	0.21	0.18	0.21	0.19	0.18	0.21	0.21	0.19	0.21	0.21	0.14	0.19	0.26	
140Ce	0.86	0.94	1.21	1.21	1.19	1.37	1.18	1.39	1.33	1.24	1.19	1.17	1.23	1.19	1.29	0.84	0.83	1.09	
141Pr	0.26	0.27	0.34	0.35	0.34	0.40	0.34	0.40	0.39	0.36	0.37	0.36	0.39	0.26	0.25	0.12	0.13	0.24	
149Nd	2.32	2.30	2.74	2.96	2.85	3.24	2.87	3.26	3.20	2.96	3.39	3.28	3.81	1.70	1.64	0.82	0.66	1.69	
147Sm	1.49	1.60	1.73	1.62	1.67	2.02	1.76	1.96	1.95	1.67	2.13	2.16	2.22	0.63	0.79	0.46	0.44	0.67	
153Eu	0.41	0.41	0.38	0.39	0.38	0.46	0.37	0.42	0.41	0.36	0.42	0.42	0.44	0.27	0.24	0.18	0.17	0.26	
157Gd	2.69	2.82	3.04	3.21	3.07	3.76	2.97	3.66	3.65	3.21	4.17	4.33	4.77	1.31	1.16	0.61	0.66	1.42	
160Tb	0.57	0.60	0.63	0.65	0.64	0.77	0.63	0.73	0.74	0.66	0.69	0.68	0.95	0.27	0.24	0.18	0.15	0.29	
163Dy	3.81	4.20	4.56	4.64	4.57	5.52	4.38	5.27	5.35	4.76	6.41	6.40	7.11	1.90	1.71	1.27	1.06	2.03	
166Ho	0.93	0.99	1.04	1.10	1.07	1.30	1.03	1.20	1.21	1.09	1.49	1.56	1.66	0.44	0.42	0.30	0.26	0.50	
168Er	2.93	2.73	3.09	3.29	3.06	3.60	3.09	3.55	3.65	3.14	4.43	4.50	4.95	1.39	1.23	0.93	0.76	1.51	
169Tm	0.36	0.42	0.46	0.46	0.45	0.54	0.42	0.52	0.52	0.46	0.64	0.66	0.70	0.18	0.14	0.13	0.13	0.23	
172Yb	2.22	2.51	2.81	2.96	2.83	3.34	2.78	3.14	3.26	2.86	3.89	3.92	4.30	1.27	1.11	0.69	0.77	1.37	
178Hf	0.39	0.46	0.41	0.49	0.44	0.60	0.39	0.45	0.47	0.46	0.59	0.60	0.66	0.44	0.46	0.16	0.12	0.60	
232Th	0.00	0.00	0.00	0.00	0.00	0.00	0.00	0.01	0.00	0.00	0.00	0.00	0.00	0.02	0.06	0.01	0.02	0.00	

6 Clinopyroxene major (SEM-EDS) and trace (LA-ICP-MS) element data for Aswad Block plutonic samples

Block	Aswad	Aswad	Aswad	Aswad	Aswad	Aswad	Aswad	Aswad	Aswad	Aswad	Aswad	Aswad	Aswad	Aswad	Aswad	Aswad	Aswad	Aswad
Sample No:	04UR30-4-1	04UR30-5-1	04UR30-6-1	04UR30-6-2	04UR32-1-1	04UR32-2-1	04UR32-2-2	04UR32-3-1	04UR32-3-2	04UR32-4-1	04UR32-5-1	04UR32-6-1	04UR32-7-1	04UR32-8-1	UAE2376-1-1	UAE2376-1-2	UAE2376-1-3	UAE2376-2-1
Sample Type:	Fujairah Gabbro	Fujairah Gabbro	Fujairah Gabbro	Fujairah Gabbro	Fujairah Gabbro	Fujairah Gabbro	Fujairah Gabbro	Fujairah Gabbro	Fujairah Gabbro	Fujairah Gabbro	Fujairah Gabbro	Fujairah Gabbro	Fujairah Gabbro	Fujairah Gabbro	Fujairah Gabbro	Fujairah Gabbro	Fujairah Gabbro	Fujairah Gabbro
w%																		
SiO2	51.77	51.77	52.21	52.21	52.84	53.46	53.46	53.23	53.23	53.24	52.99	53.45	53.25	52.97	52.66	52.66	52.66	52.6
TiO2	0.20	0.20	0.27	0.27	0.32	0.12	0.12	0.24	0.24	0.20	0.30	0.18	0.21	0.28	0.3	0.3	0.3	0.31
Al2O3	1.67	1.67	1.55	1.55	1.25	0.9	0.9	0.91	0.91	0.90	1.37	0.99	0.99	1.34	1.27	1.27	1.27	1.22
Cr2O3	0.76	0.76	0.45	0.45	0.49	0.39	0.39	0.41	0.41	0.39	0.53	0.39	0.31	0.45	0.25	0.25	0.25	0.39
Fe2O3	5.92	5.92	5.43	5.43	6.5	6.39	6.39	6.23	6.23	6.32	6.40	6.12	6.37	6.23	6.47	6.47	6.47	6.23
MnO	0.14	0.14	0.17	0.17	0	0.19	0.19	0.12	0.12	0.20	0.07	0.19	0.14	0.08	0.19	0.19	0.19	0.14
MgO	19.81	19.81	19.21	19.21	19.29	19.17	19.17	19.35	19.35	19.59	19.19	19.41	19.30	19.47	19.12	19.12	19.12	19.37
CaO	22.92	22.92	23.05	23.05	22.79	23.30	23.30	23.27	23.27	23.22	22.93	23.69	23.33	22.94	22.43	22.43	22.43	22.44
Na2O	0.29	0.29	0.29	0.29	0.25	0.09	0.09	0.09	0.09	0.08	0.19	0.06	0.13	0.17	0.32	0.32	0.32	0.3
Total	99.14	99.14	99.89	99.89	100.72	100.99	100.99	100.8	100.8	101.09	100.94	101.22	100.91	100.92	100	100	100	100
ppm																		
46Sc	95.79	95.04	98.11	105.52	97.89	72.47	92.71	117.81	102.65	94.65	117.13	94.55	104.32	104.81	93.13	93.03	90.76	86.97
47Ti (%)	0.23	0.28	0.13	0.16	0.22	0.07	0.17	0.23	0.16	0.12	0.19	0.19	0.21	0.21	0.16	0.16	0.25	0.20
Ti	1379.00	1678.47	778.40	948.98	1311.87	390.22	992.97	1370.83	987.19	707.54	1181.23	1143.22	1240.88	1246.09	1284.66	975.88	1481.11	1211.73
51V	269.53	397.90	235.13	249.09	400.06	194.71	349.14	373.91	274.99	238.21	333.34	358.61	375.33	374.93	274.37	234.81	291.76	295.00
52Cr	3971.55	2751.59	3033.20	2999.59	2393.51	1267.71	2003.90	2233.95	1484.22	1392.97	2354.20	2199.77	2099.97	2091.94	1958.96	1993.94	1991.49	1978.49
55Mn (%)	0.14	0.18	0.15	0.14	0.19	0.23	0.20	0.18	0.17	0.21	0.19	0.20	0.19	0.17	0.13	0.13	0.13	0.13
88Sr	5.25	6.03	5.24	6.00	5.41	3.99	4.71	4.34	5.41	6.99	5.02	5.11	6.91	5.51	5.49	5.31	6.69	3.69
89Y	13.97	12.01	9.89	11.83	11.35	4.70	6.29	12.83	9.90	7.16	11.93	8.73	11.14	10.92	9.80	7.25	9.74	8.75
90Zr	12.80	10.23	4.75	7.39	4.34	7.49	5.45	6.12	6.57	6.39	7.59	6.92	6.89	4.19	12.41	7.09	15.50	6.21
93Nb	0.01	0.01	0.01	0.02	0.01	0.00	0.00	0.00	0.00	0.00	0.01	0.01	0.01	0.01	0.04	0.03	0.10	0.01
139La	0.35	0.28	0.28	0.28	0.14	0.14	0.18	0.14	0.13	0.15	0.18	0.18	0.18	0.15	0.39	0.25	0.51	0.19
140Ce	1.38	1.33	0.93	1.05	0.73	0.53	0.65	0.69	0.70	0.81	0.69	0.75	0.89	0.75	1.14	0.79	1.38	0.78
141Pr	0.30	0.29	0.19	0.21	0.19	0.09	0.14	0.17	0.19	0.12	0.19	0.19	0.19	0.17	0.20	0.14	0.22	0.19
146Nd	1.91	1.86	1.34	1.50	1.15	0.89	0.96	1.32	1.09	0.82	1.19	0.95	1.19	1.20	1.29	0.80	1.39	1.01
147Sm	0.62	0.79	0.69	0.70	0.69	0.30	0.51	0.74	0.84	0.45	0.67	0.57	0.69	0.63	0.69	0.42	0.65	0.63
153Eu	0.29	0.27	0.19	0.23	0.22	0.10	0.15	0.22	0.17	0.14	0.19	0.17	0.23	0.21	0.19	0.19	0.19	0.18
157Gd	1.37	1.33	0.97	1.21	1.07	0.49	0.83	1.20	0.99	0.79	1.19	0.90	1.17	1.05	1.00	0.73	1.01	0.95
159Tb	0.28	0.27	0.20	0.25	0.24	0.09	0.17	0.28	0.19	0.15	0.25	0.18	0.24	0.24	0.22	0.19	0.21	0.19
163Dy	2.14	1.78	1.48	1.87	1.78	0.72	1.28	1.90	1.44	1.17	1.98	1.37	1.60	1.58	1.84	1.16	1.90	1.33
165Ho	0.51	0.43	0.36	0.45	0.42	0.17	0.30	0.45	0.35	0.28	0.43	0.32	0.42	0.39	0.39	0.27	0.39	0.34
168Er	1.51	1.30	1.04	1.30	1.25	0.55	0.91	1.42	1.19	0.83	1.43	1.01	1.29	1.16	1.10	0.81	1.07	0.92
169Tm	0.24	0.20	0.17	0.19	0.20	0.08	0.14	0.20	0.15	0.13	0.22	0.19	0.19	0.19	0.19	0.12	0.17	0.19
172Yb	1.41	1.26	1.16	1.23	1.17	0.63	0.93	1.36	1.09	0.85	1.24	0.99	1.27	1.17	1.02	0.79	1.03	0.91
176Yf	0.41	0.43	0.15	0.22	0.23	0.23	0.25	0.33	0.32	0.31	0.31	0.29	0.25	0.21	0.40	0.24	0.46	0.33
232Th	0.02	0.03	0.02	0.02	0.01	0.02	0.04	0.01	0.02	0.04	0.09	0.03	0.01	0.01	0.07	0.05	0.14	0.01

Clinopyroxene major (SEM-EDS) and trace (LA-ICP-MS) element data for Aswad Block plutonic samples

Block	Aswad	Aswad	Aswad	Aswad	Aswad	Aswad	Aswad	Aswad	Aswad	Aswad	Aswad	Aswad	Aswad	Aswad	Aswad	Aswad	Aswad	Aswad
Sample No:	UAE2376-2-2	UAE2376-2-3	UAE2376-3-1	UAE2376-3-2	UAE2376-3-3	UAE3182-2-1	UAE3182-2-2	UAE3182-3-1	UAE3182-3-2	UAE3182-3-3	UAE3182-4-1	UAE3182-4-2	UAE3182-4-3	UAE3979-1-1	UAE3979-1-2	UAE3979-1-3	UAE3979-3-1	UAE3979-3-2
Sample Type:	Fujairah Gabbro	Fujairah Gabbro	Fujairah Gabbro	Fujairah Gabbro	Fujairah Gabbro	Fujairah Gabbro	Fujairah Gabbro	Fujairah Gabbro	Fujairah Gabbro	Fujairah Gabbro	Fujairah Gabbro	Fujairah Gabbro	Fujairah Gabbro	Fujairah Gabbro	Fujairah Gabbro	Fujairah Gabbro	Fujairah Gabbro	Fujairah Gabbro
wt%																		
SiO <sub>2</sub>	52.6	52.6	52.6	52.6	52.6	51.99	51.99	52.27	52.27	52.27	52.44	52.44	52.44	52.42	52.42	52.42	52.6	52.6
TiO <sub>2</sub>	0.31	0.31	0.31	0.31	0.31	0.43	0.43	0.33	0.33	0.33	0.27	0.27	0.27	0.27	0.27	0.27	0.32	0.32
Al <sub>2</sub> O <sub>3</sub>	1.22	1.22	1.22	1.22	1.22	1.54	1.54	1.21	1.21	1.21	1.24	1.24	1.24	1.8	1.8	1.8	1.65	1.65
Cr <sub>2</sub> O <sub>3</sub>	0.39	0.39	0.39	0.39	0.39	0.39	0.39	0.57	0.57	0.57	0.41	0.41	0.41	0.04	0.04	0.04	0.1	0.1
Fe <sub>2</sub> O <sub>3</sub>	6.23	6.23	6.23	6.23	6.23	7.32	7.32	7.06	7.06	7.06	6.99	6.99	6.99	6.94	6.94	6.94	6.43	6.43
MnO	0.14	0.14	0.14	0.14	0.14	0.13	0.13	0.00	0.00	0.00	0.11	0.11	0.11	0.14	0.14	0.14	0.05	0.05
MgO	16.37	16.37	16.37	16.37	16.37	16.66	16.66	16.83	16.83	16.83	16.41	16.41	16.41	17.07	17.07	17.07	16.96	16.96
CaO	22.44	22.44	22.43	22.43	22.43	22.21	22.21	22.47	22.47	22.47	22.79	22.79	22.79	21.14	21.14	21.14	21.84	21.84
Na <sub>2</sub> O	0.3	0.3	0.3	0.3	0.3	0.34	0.34	0.26	0.26	0.26	0.33	0.33	0.33	0.19	0.19	0.19	0.17	0.17
Total	100	100	100	100	100	100.00	100.00	100.00	100.00	100.00	100.00	100.00	100.00	100	100	100	100	100
ppm																		
45Sc	81.81	80.84	79.04	85.87	75.56	100.84	105.89	105.03	97.72	96.82	111.15	114.80	115.09	115.42	107.28	107.78	115.59	111.39
47Ti (%)	0.14	0.25	0.22	0.24	0.15	0.30	0.30	0.31	0.32	0.28	0.33	0.35	0.36	0.23	0.21	0.19	0.22	0.28
Ti	860.91	1525.72	1322.47	1469.94	878.46	1817.78	1814.99	1836.07	1927.19	1882.78	1099.43	2079.15	2149.27	1950.68	1277.28	1153.46	1304.79	1662.40
51V	220.96	321.04	280.30	305.20	223.60	362.99	367.27	342.66	337.46	337.54	392.14	413.90	439.39	287.61	289.97	280.10	273.69	285.18
52Cr	1391.96	1875.69	1760.81	1807.21	1336.62	2131.11	1824.48	2188.36	2628.27	1912.04	1810.26	2013.91	1933.44	128.28	224.28	174.98	369.51	525.21
55Mn (%)	0.15	0.14	0.15	0.14	0.14	0.14	0.15	0.14	0.15	0.15	0.14	0.16	0.16	0.21	0.20	0.20	0.19	0.19
88Sr	3.47	4.59	7.61	5.10	4.82	6.43	6.15	6.44	6.65	7.95	6.47	6.08	7.20	6.99	6.55	6.79	6.11	12.05
89Y	7.03	9.99	6.02	9.19	7.23	25.30	26.94	27.79	29.78	26.91	32.89	33.94	35.69	10.17	9.13	6.69	11.75	12.92
90Zr	7.90	8.81	11.17	8.69	8.48	16.65	16.45	20.73	22.34	17.33	13.79	19.13	20.27	5.50	4.82	4.92	16.16	24.82
93Nb	0.01	0.03	0.07	0.03	0.02	0.07	0.09	0.06	0.09	0.07	0.07	0.07	0.04	0.03	0.02	0.03	0.10	0.14
139La	0.16	0.27	0.45	0.30	0.27	0.59	0.62	0.59	0.64	0.61	0.31	0.46	0.39	0.18	0.23	0.23	0.62	0.99
140Ce	0.66	1.02	1.41	1.09	1.02	1.89	2.01	1.80	2.18	1.93	1.59	1.89	1.90	0.79	0.85	0.73	1.32	2.09
141Pr	0.13	0.19	0.21	0.19	0.19	0.42	0.42	0.40	0.49	0.43	0.40	0.44	0.43	0.15	0.13	0.21	0.29	0.29
148Nd	0.64	1.31	1.27	1.25	1.17	3.02	3.07	3.07	3.40	3.15	3.39	3.81	3.35	1.06	0.94	0.95	1.32	1.79
147Sm	0.39	0.84	0.56	0.59	0.55	1.59	1.47	1.71	1.79	1.75	1.64	1.61	1.89	0.69	0.67	0.63	0.96	0.92
153Eu	0.15	0.20	0.19	0.20	0.16	0.39	0.40	0.39	0.42	0.42	0.42	0.45	0.41	0.23	0.22	0.22	0.22	0.26
157Gd	0.72	1.09	0.87	0.99	0.82	2.59	2.70	2.93	3.11	3.16	3.21	3.39	3.39	1.14	0.92	1.02	1.31	1.39
159Tb	0.15	0.22	0.18	0.21	0.15	0.55	0.59	0.62	0.67	0.65	0.67	0.70	0.71	0.24	0.21	0.20	0.27	0.31
163Dy	1.09	1.90	1.29	1.49	1.16	4.18	4.20	4.49	4.74	4.88	4.82	4.88	5.18	1.64	1.54	1.43	1.65	2.21
165Ho	0.27	0.40	0.31	0.35	0.29	0.97	0.99	1.09	1.15	1.12	1.17	1.16	1.21	0.39	0.37	0.35	0.45	0.50
166Er	0.76	1.10	0.90	1.04	0.82	2.66	2.99	3.07	3.39	3.26	3.49	3.55	3.49	1.13	1.10	1.02	1.31	1.43
169Tm	0.13	0.17	0.13	0.16	0.12	0.43	0.45	0.48	0.49	0.51	0.52	0.51	0.52	0.16	0.15	0.14	0.20	0.20
172Yb	0.74	1.07	0.89	0.96	0.87	2.62	2.74	2.83	3.00	2.94	3.16	3.22	3.09	1.07	0.91	0.90	1.16	1.31
178Hf	0.29	0.37	0.32	0.30	0.30	0.56	0.63	0.71	0.69	0.67	0.52	0.52	0.71	0.16	0.16	0.16	0.44	0.69
232Th	0.00	0.04	0.09	0.06	0.04	0.11	0.14	0.35	0.15	0.10	0.02	0.07	0.04	0.05	0.04	0.05	0.21	0.34

Block	Aswad	Aswad	Aswad	Aswad	Aswad	Aswad	Aswad	Aswad	Aswad	Aswad	Aswad	Aswad	Aswad	Aswad	Aswad	Aswad	Aswad
Sample No:	UAE3979-3-3	UAE3979-4-1	UAE3979-4-2	UAE3979-4-3	UAE3115-1-1	UAE3115-1-2	UAE3115-3-1	UAE3115-3-2	UAE3115-4-1	UAE3115-5-1	UAE3115-9-1	UAE3183-1-1	UAE3183-2-1	UAE3183-3-1	UAE3183-4-1	UAE3183-5-1	UAE3183-6-1
Sample Type:	Fujairah Gabbro	Fujairah Gabbro	Fujairah Gabbro	Fujairah Gabbro	'Geotimes' Dyke	'Geotimes' Dyke	'Geotimes' Dyke	'Geotimes' Dyke	'Geotimes' Dyke	'Geotimes' Dyke	'Geotimes' Dyke	'Geotimes' Dyke	'Geotimes' Dyke	'Geotimes' Dyke	'Geotimes' Dyke	'Geotimes' Dyke	'Geotimes' Dyke
wt%																	
SiO2	52.5	52.37	52.37	52.37	51.40	51.40	51.48	51.48	51.30	51.43	51.55	51.95	51.54	51.76	51.80	51.71	51.82
TiO2	0.32	0.35	0.35	0.35	0.45	0.45	0.49	0.49	0.49	0.49	0.54	0.39	0.40	0.37	0.33	0.37	0.39
Al2O3	1.65	1.77	1.77	1.77	1.23	1.23	1.16	1.16	1.29	1.23	1.24	1.37	1.24	1.21	1.49	1.26	1.40
Cr2O3	0.1	0.08	0.08	0.08	0.00	0.00	0.00	0.00	0.09	0.02	0.00	0.03	0.00	0.00	0.10	0.00	0.00
Fe2O3	6.43	6.90	6.90	6.90	10.19	10.19	10.28	10.28	10.34	10.27	10.29	9.59	9.87	9.59	9.58	9.04	9.81
MnO	0.05	0.12	0.12	0.12	0.30	0.30	0.29	0.29	0.30	0.29	0.29	0.29	0.29	0.25	0.29	0.30	0.30
MgO	19.95	19.99	19.99	19.99	14.81	14.81	14.84	14.84	14.80	14.81	14.80	14.80	14.80	14.87	14.81	14.84	14.97
CaO	21.84	21.27	21.27	21.27	21.27	21.27	21.19	21.19	21.03	21.13	20.99	21.58	21.76	21.66	21.45	22.08	21.82
Na2O	0.17	0.16	0.16	0.16	0.32	0.32	0.32	0.32	0.41	0.35	0.35	0.33	0.31	0.39	0.33	0.30	0.31
Total	100	100.00	100.00	100.00	100.00	100.00	100.00	100.00	100.00	100.00	100.00	100.00	100.00	100.00	100.00	100.00	100.00
ppm																	
46Bc	114.01	119.29	105.59	94.03	124.54	119.53	133.25	129.24	133.95	126.40	113.52	115.25	119.95	112.59	110.14	138.11	113.49
47Ti (%)	0.35	0.30	0.24	0.22	0.42	0.35	0.44	0.43	0.41	0.39	0.39	0.39	0.34	0.35	0.35	0.35	0.30
Tl	2075.34	1787.34	1421.95	1344.09	2613.57	2108.55	2640.87	2554.95	2450.08	2340.53	2294.82	2132.09	2034.15	2087.99	2123.78	2097.16	1800.29
51V	310.15	275.77	264.65	293.79	174.81	171.10	181.14	176.99	183.19	169.92	180.20	233.90	200.57	223.55	249.07	229.03	224.71
52Cr	633.93	221.93	397.05	302.99	84.84	89.30	40.99	39.79	135.99	95.04	44.15	72.08	85.81	72.31	96.99	80.93	73.70
55Mn (%)	0.19	0.17	0.18	0.19	0.25	0.25	0.24	0.25	0.24	0.24	0.25	0.30	0.33	0.30	0.30	0.28	0.28
58Sr	11.82	7.75	7.93	8.96	14.85	7.95	8.27	7.82	8.50	7.82	7.90	10.19	8.84	8.51	8.76	7.32	9.40
89Y	14.85	12.95	10.67	9.26	97.66	91.62	108.02	104.24	98.38	103.09	90.28	77.12	70.97	81.12	70.09	84.81	70.83
90Zr	22.40	11.02	9.63	11.77	50.52	45.78	64.02	55.87	48.00	49.20	49.91	45.89	38.45	43.91	40.08	47.93	39.51
93Nb	0.12	0.05	0.09	0.08	0.10	0.04	0.09	0.09	0.07	0.05	0.05	0.03	0.01	0.01	0.02	0.01	0.01
138La	0.64	0.36	0.41	0.48	1.12	1.01	1.18	1.07	1.00	1.00	1.04	0.81	0.69	0.73	0.78	0.82	0.71
140Ce	1.69	1.10	1.03	1.27	6.70	6.95	7.14	6.89	6.19	6.12	7.09	6.22	4.99	4.80	6.20	4.62	4.64
141Pr	0.28	0.22	0.17	0.21	1.91	1.85	2.02	1.89	1.81	2.14	1.82	1.41	1.33	1.42	1.39	1.27	1.27
146Nd	1.75	1.86	1.16	1.36	15.31	14.39	16.33	15.83	14.53	17.01	14.65	11.15	10.13	11.14	10.26	10.98	9.70
147Sm	0.95	0.82	0.82	0.65	7.87	7.56	8.49	8.16	7.66	8.48	7.66	6.73	5.26	5.93	6.43	6.01	5.34
153Eu	0.31	0.28	0.24	0.24	1.36	1.31	1.44	1.34	1.35	1.46	1.36	1.16	1.02	1.19	1.10	1.11	0.98
157Gd	1.70	1.42	1.21	1.07	12.34	11.57	13.27	12.50	12.09	13.02	11.52	9.39	6.99	9.57	6.40	10.13	6.39
159Tb	0.32	0.32	0.24	0.22	2.43	2.28	2.62	2.48	2.40	2.57	2.24	1.90	1.64	1.91	1.85	1.91	1.60
183Dy	2.36	2.24	1.70	1.54	18.73	15.38	17.93	17.27	16.35	17.82	15.20	12.77	11.41	13.51	11.84	14.40	11.89
185Ho	0.58	0.49	0.40	0.36	3.78	3.51	4.06	3.88	3.75	3.82	3.48	2.81	2.82	3.06	2.81	3.13	2.58
189Er	1.64	1.43	1.27	1.02	10.44	9.93	11.38	11.01	10.49	11.02	9.70	8.13	7.81	8.61	7.48	8.80	7.43
169Tm	0.22	0.21	0.17	0.15	1.48	1.39	1.60	1.53	1.47	1.59	1.34	1.12	1.06	1.24	1.07	1.32	1.06
172Yb	1.33	1.27	1.12	1.03	9.15	8.55	9.73	9.19	9.09	9.84	8.81	8.92	8.17	7.25	8.35	7.40	8.33
178Hf	0.66	0.35	0.30	0.37	2.33	2.09	3.00	2.99	2.21	2.36	2.42	1.80	1.85	1.87	1.87	2.11	1.84
232Th	0.27	0.09	0.11	0.14	0.00	0.00	0.01	0.00	0.00	0.01	0.00	0.06	0.01	0.01	0.02	0.02	0.02

9 Clinopyroxene major (SEM-EDS) and trace (LA-ICP-MS) element data for Aswad Block plutonic samples

Block	Aswad	Aswad	Aswad	Aswad	Aswad	Aswad	Aswad	Aswad	Aswad
Sample No:	03UR150-1-1	03UR150-1-2	03UR150-1-3	03UR150-2-1	03UR150-2-2	03UR150-2-3	03UR150-3-1	03UR150-3-2	03UR150-3-3
Sample Type:	Lesall Dyke	Lesall Dyke	Lesall Dyke	Lesall Dyke	Lesall Dyke	Lesall Dyke	Lesall Dyke	Lesall Dyke	Lesall Dyke
wt%									
SiO <sub>2</sub>	52.52	52.52	52.52	52.66	52.66	52.66	52.25	52.25	52.25
TiO <sub>2</sub>	0.27	0.27	0.27	0.27	0.27	0.27	0.36	0.36	0.36
Al <sub>2</sub> O <sub>3</sub>	2.29	2.29	2.29	2.19	2.19	2.19	2.48	2.48	2.48
Cr <sub>2</sub> O <sub>3</sub>	0.55	0.55	0.55	0.51	0.51	0.51	0.65	0.65	0.65
Fe <sub>2</sub> O <sub>3</sub>	5.25	5.25	5.25	5.24	5.24	5.24	5.38	5.38	5.38
MnO	0.11	0.11	0.11	0.09	0.09	0.09	0.08	0.08	0.08
MgO	18.07	18.07	18.07	18.14	18.14	18.14	17.95	17.95	17.95
CaO	20.77	20.77	20.77	20.89	20.89	20.89	20.88	20.88	20.88
Na <sub>2</sub> O	0.16	0.16	0.16	0.20	0.20	0.20	0.2	0.2	0.2
Total	100	100	100	100.00	100.00	100.00	100	100	100
ppm									
45Sc	79.04	82.03	86.89	91.31	90.33	85.84	97.42	106.49	85.84
47Ti (%)	0.22	0.23	0.24	0.24	0.25	0.22	0.25	0.31	0.25
Ti	1321.23	1390.45	1449.65	1462.90	1486.03	1313.30	1473.86	1874.76	1615.64
51V	249.84	286.72	280.57	279.29	281.13	283.46	281.85	301.93	310.02
52Cr	2655.02	2890.93	2780.41	2991.91	2999.84	2499.68	4297.13	3451.89	3306.82
55Mn (%)	0.13	0.13	0.13	0.13	0.14	0.14	0.12	0.13	0.13
88Sr	5.41	6.03	6.04	5.81	5.49	5.16	5.30	6.14	6.02
89Y	6.00	9.18	9.02	9.96	10.35	9.38	10.89	13.17	9.96
90Zr	2.85	3.37	3.38	3.81	4.05	3.27	4.10	6.14	3.96
93Nb	0.01	0.00	0.01	0.00	0.00	0.01	0.00	0.00	0.00
139La	0.06	0.08	0.08	0.07	0.08	0.08	0.06	0.10	0.07
140Ce	0.35	0.44	0.44	0.41	0.46	0.41	0.38	0.56	0.49
141Pr	0.10	0.13	0.12	0.12	0.12	0.11	0.11	0.16	0.13
148Nd	0.80	1.05	0.94	1.02	1.04	0.81	0.97	1.37	1.13
147Sm	0.61	0.59	0.56	0.66	0.69	0.65	0.63	0.63	0.74
153Eu	0.19	0.22	0.23	0.24	0.23	0.21	0.21	0.30	0.27
157Gd	0.87	1.07	1.05	1.23	1.11	1.00	1.16	1.50	1.04
159Tb	0.19	0.20	0.21	0.23	0.22	0.22	0.23	0.30	0.22
163Dy	1.31	1.48	1.56	1.66	1.75	1.63	1.87	2.28	1.70
165Ho	0.26	0.33	0.36	0.37	0.39	0.36	0.41	0.49	0.35
169Er	0.86	0.94	0.99	1.12	1.13	1.03	1.19	1.46	1.08
169Tm	0.12	0.14	0.15	0.17	0.16	0.15	0.17	0.21	0.15
172Yb	0.78	0.90	0.90	0.95	1.02	0.81	1.08	1.27	0.99
178Hf	0.15	0.18	0.20	0.24	0.24	0.19	0.25	0.37	0.21
232Th	0.00	0.00	0.00	0.00	0.00	0.00	0.00	0.00	0.00

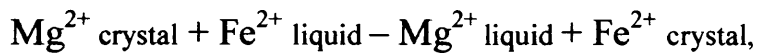
## Appendix E: Partition coefficient modelling

### E1 Partition coefficient theory

Two types of partition coefficient are discussed in this chapter, firstly the ‘exchange coefficient’ (represented by the symbol  $K_D$ ) and secondly, the ‘Nernst partition coefficient’ (represented by the symbol  $D$ ).

#### $K_D$

The exchange coefficient,  $K_D$  can be used for major elements and for trace elements where Henry’s Law no longer applies. In this study it is used to determine how  $Fe^{2+}$  and  $Mg^{2+}$  cations are exchanged between olivine, clinopyroxene and melt. The exchange coefficient is represented by the equation:



and is defined by the expression:

$$K_{D \text{ Fe/Mg}} = [X_{Fe}/X_{Mg}]_{\text{crystal}}/[X_{Fe}/X_{Mg}]_{\text{melt}}$$

Where Fe and Mg are mole fractions (e.g. Beattie et al., 1993).

#### $D$

The Nernst partition coefficient describes the distribution of a trace element between a mineral and a melt and is defined as:

$$D = C_{\text{Cryst } i}/C_{\text{Melt } i}$$

Where  $C_{\text{Cryst } i}$  is the concentration of the trace element  $i$  in the crystal, and  $C_{\text{Melt } i}$  is the concentration of  $i$  in the melt.

Whilst these values describe the behaviour of elements between a given mineral and melt, petrogenetic modelling requires that the trace element is quantified in terms of its equilibrium with all mineral phases present. The trace element is instead discussed in terms of its *bulk partition coefficient*, which is calculated from the Nernst coefficients weighted according to the relative proportions of coexisting phases in the assemblage. For a three-phase assemblage the bulk coefficient  $i$  is defined by:

$$\text{Bulk } D_i = [(\alpha X) + (\beta Y) + (\gamma Z)]$$

where  $\alpha$ ,  $\beta$  and  $\gamma$  are the Nernst partition coefficients of element  $i$  in weight fraction phases X, Y and Z respectively.

Where the behaviour of trace element  $i$  between a single solid phase and melt is governed by its Nernst partition coefficient, bulk  $D_i$  is thus dependent upon estimated modal proportions and Nernst coefficients.

Thomas (2003) proposed that realistic changes to the proportions of the crystallising phases, or to the Nernst partition coefficients significantly alter modelled trends for the clinopyroxenes of the Oman – U.A.E. ophiolite blocks. Thus it is concluded that, although mineral modes vary considerably between gabbro samples, for the purpose of this study these changes can be ignored. Also, the variations in clinopyroxene major element composition, the principal control on Nernst partition coefficients (Wood and Blundy, 1997) are minor. A fixed set of Nernst partition coefficients and fixed cotectic proportions are therefore used throughout this study. The Nernst partition coefficients are from Bédard (1994) (Chapter 5, Table 5.1). The ‘typical’ U.A.E. gabbro assemblage is taken to be 55% plagioclase, 35% clinopyroxene and 10% olivine (Following Browning, 1982), and it is assumed that throughout crystallisation the ideal cotectic proportion remained constant.

## E2 Partition coefficient calculation

The method used the calculations and method of Wood and Blundy (1997) with a spreadsheet program generated by Banks (2004), which calculates  $D$  following the Brice equation (detailed below). Calculations using these  $D$  are compared to the  $D$  used for ophiolitic clinopyroxene from the Bay of Islands ophiolite by Bédard (1994) (Table 5.1).

The partition coefficients for this study (Chapter 5) were calculated following this six step procedure, which follows the calculations of Wood and Blundy (1997).

### 1

Calculating the optimum radius ( $r_o$ ). This is the location of the peak of the parabola, using the number of cations of Al in the clinopyroxene M1 site and the number of cations of Ca in the clinopyroxene M2 site, where:

$$R_o = 0.974 + 0.0067X_{Ca}^{M2} - 0.051X_{Al}^{M1} (\text{Å})$$

$X$  is the number of cations of Ca ( $C_a$ ) and Al ( $A_l$ ) in the clinopyroxene when the clinopyroxene major element oxide composition is re-calculated to a sum of 4 cations.

### 2

Calculating the Young's modulus ( $E$ ) for  $3^+$  ions in the clinopyroxene M2 site (the width of the parabola) (Figure 2 and 3, page 169 in Wood and Blundy, 1997). This is done using the following equation at the specified temperature of interest:

$$E_{M2}^{3+} = 318.6 + 6.9P - 0.036T$$

$P$  is pressure in GPa and has been set at 0.5 (after Bédard, 1994 and Thomas, 2003).



T is temperature in Kelvin and calculated at 1500K (calculated using estimates of the crystallisation temperature of clinopyroxene in oceanic crust).

P and T of the samples modelled in Chapter 5 are taken as 0.5GPa and 1500K. Further studies looking to expand on this research could use different combinations of pressure and temperature, which could offer explanation for the generally lower  $Sm_{(n)}/Yb_{(n)}$  ratios for the Khawr Fakkan and Aswad Block samples presented in Figures 5.6 and 5.13. However, it has been proposed by Bédard (1994) and Thomas (2003) that even significant changes in pressure and temperature do not significantly alter the modelled values (e.g. Figure A-2 and A-3, pages 151 and 152, of Bédard, 1994).

### 3

Calculating  $X^{M1}_{MG}$  in the clinopyroxene

$$X^{M1}_{MG} = M1(Ti + Cr + Al + Mn) - M2(Mg + Fe)$$

To establish the distribution of cations of Mg in the M1 site

### 4

Estimating the Mg# of the melt. The clinopyroxene composition is used to calculate:

$$K^{cpx}_{Fe-Mg} = 0.109 + 0.186 Mg\#_{cpx}$$

Then the Mg# of the melt can be obtained following:

$$Mg\#_{melt} = K^{cpx}_{Fe-Mg} Mg\#_{cpx} / 1 - Mg\#_{cpx} + Mg\#_{cpx} K^{cpx}_{Fe-Mg}$$

## 5

Calculating  $D_o^{3+}$  (optimum radius of the Anuma<sup>3+</sup> curve) by re-arranging equations 3 and 4 on page 178 of Wood and Blundy (1997) to:

$$D_o^{3+} = Mg\#_{\text{melt}} / X_{\text{MG}}^{M1} (\exp(88750 - 65.644T + 7050P - 770P^2)/RT)$$

R = Universal Gas Constant (8.3144JK<sup>-1</sup> mol<sup>-1</sup>)

T = Temperature in K

P = Pressure in GPa

## 6

Knowing  $D_o$  and all other parameters (steps 1-5) it is possible to calculate the D (partition coefficient for an unknown element) from the Brice equation:

$$D = D_o \exp(-4\pi E_{M2} N_A (r_o/2(r_i - r_o)^2 + 1/3(r_i - r_o)^3) / RT)$$

$r_i$  = radius of element of known partition coefficient (REE<sub>i</sub>)

$N_A$  = 6.022<sup>23</sup>

### E3 Calculated partition coefficients

Once the REE partition coefficients for every LA-ICP-MS clinopyroxene sample were determined using steps 1-6, the REE content of the melts in equilibrium with the clinopyroxenes was calculated using:

$$C_{\text{element } i}^{\text{melt}} = C_{\text{element } i}^{\text{cpx}} / Kd_{\text{element } i}$$

C = concentration of trace element i

Kd = calculated Nernst partition coefficient

## **References**

Alabaster T, Pearce JA, Mallick DIJ, Elboushi IM (1980) The volcanic stratigraphy and location of massive sulphide deposits in the Oman ophiolite. *International Ophiolite Symposium*. Cyprus 1979. pp. 751-757

Alabaster T, Pearce JA, Malpas J (1982) The volcanic stratigraphy and petrogenesis of the Oman ophiolite complex. *Contributions Mineral Petrology* **81**, 168-183.

Allerton S, MacLeod CJ (1998) Fault-controlled magma transport through the mantle lithosphere at slow-spreading ridges. In: RA Mills and K Harrison (eds.) *Modern Ocean Floor Processes and the Geological Record*. Geological Society: London.

Alt JC, Teagle DAH (2000) Hydrothermal alteration and fluid fluxes in ophiolites and oceanic crust. *Ophiolites and Oceanic Crust: New Insights from Field Studies and Ocean Drilling Special Paper-Geological Society of America vol. 349 (2000)*,, 273-283.

Anders E, Grevesse N (1989) Abundances of the elements: meteoric and solar. *Geochimica et Cosmochimica Acta* **53**, 197-214.

B.G.S. (2006) *U.A.E. Geological Mapping Project*. Government of the United Arab Emirates, Department of Petroleum and Mineral Resources.

Banks GJ (2004) Accretion of the lower oceanic crust in the Troodos ophiolite: Textural and geochemical constraints from drill core CY-4, Cyprus. PhD, Cardiff University.

Beattie PD (1993) On the occurrence of apparent non-Henry's Law behaviour in experimental partitioning studies. *Geochim Cosmochim Acta* **57 (1)**, 47-55.

Bedard JH (1991) Cumulate recycling and crustal evolution in the Bay of Islands ophiolite. *J. Geology* **99**, 225-249.

Bedard JH (1994) A procedure for calculating the equilibrium distribution of trace elements amongst the minerals of cumulate rocks, and the concentration of the trace elements in co-existing liquids. *Chemical Geology* **118**, 143-153.

Bedard JH (1999) Petrogenesis of boninites from the Betts Cove ophiolite, Newfoundland, Canada: Identification of subducted source components. *Journal of Petrology* **40**, 1853-1889.

Bedard JH, Hebert R (1996) The Lower crust of the Bay of Islands ophiolite, Canada: Petrology, mineralogy, and the importance of syntaxis in magmatic differentiation in ophiolites and at ocean ridges. *Journal of Geophysical Research* **101**, 25,105-25, 124.

Bedard JH, Herbert R, Berclaz A, Varfalvy V (2000) Syntaxis and the genesis of lower oceanic crust. *Ophiolites and Oceanic Crust: New Insights from Field Studies*

and Ocean Drilling Special Paper-Geological Society of America vol. 349 (2000),, 105-121.

Benn K, Nicolas A, Reuber I (1988) Mantle-crust transition zone and origin of wehrlitic magmas: Evidence from the Oman ophiolite. *Tectonophysics* **151**, 75-85.

Bickle MJ, Teagle AH (1992) Strontium alteration in the Troodos ophiolite: implications for fluid fluxes and geochemical transport in mid-ocean ridge hydrothermal systems. *Earth and Planetary Science Letters* **113**, 219-237.

Blundy JD, Wood BJ (1991) Crystallization-chemical controls on the partitioning of Sr and Ba between plagioclase feldspar, silicate melts and hydrothermal solutions. *Geochim Cosmochim Acta* **55**, 193-209.

Blundy JD, Wood BJ (1994) Prediction of crystal-melt partition coefficients from elastic moduli. *Nature* **372**, 452-454.

Boudier F, Ceuleneer G., Nicolas A (1988) Shear zones, thrusts and related magmatism in the Oman ophiolite: Initiation of thrusting on an oceanic ridge. *Tectonophysics* **151**, 275-296.

Boudier F, Coleman RG (1981) Cross section through the peridotite in the Semail ophiolite, southeastern Oman mountains. *Journal of Geophysical Research* **86**, 307-326.

Boudier F, Nicolas A, Ildefonse B (1996) Magma chambers in the Oman ophiolite: fed from the top and the bottom. *Earth and Planetary Science Letters* **144**, 239-250.

Boudier F, Nicolas A, Ildefonse B, Jousset D (1997) EPR microplates, a model for the Oman ophiolite. *Terra Nova* **9**, 79-82.

Braun M, Kelemen P (2002) Dunite distribution in the Oman Ophiolite: Implications for melt flux through porous dunite conduits. *Geochemistry, Geophysics and Geosystems: G3* **3**.

Brown MA (1980) Textural and geochemical evidence for the origin of some chromite deposits in the Oman ophiolite. *Proceedings of the International Ophiolite Symposium. Cyprus*. pp. 714-721

Browning P (1982) The petrology, Geochemistry, and structure of the plutonic rocks of the Oman ophiolite. PhD thesis, Open University.

Browning P, Smewing JD (1981) Processes in magma chambers beneath spreading axis: evidence for magmatic associations in the Oman ophiolite. *Journal of the Geological Society of London* **138**, 279-280.

Buck WR (2000) Can downward flow of dense cumulate slurry through mushy upper gabbros produce lower gabbros at a fast-spreading center. *Ophiolites and*

**Oceanic Crust: New Insights from Field Studies and Ocean Drilling Special Paper-Geological Society of America vol. 349 (2000),, 121-127.**

Buck WR, Delaney PT, Karson A, Lagabriele Y (eds.) (1998) *Faulting and Magmatism at Mid-Ocean Ridges*. American Geophysical Union: Washington D.C.

Cameron WE (1985) Petrology and origin of primitive lavas from the Troodos ophiolite, Cyprus. *Contributions Mineral Petrology* **89**, 239-255.

Cameron WE, McCulloch MT, Walker DA (1983) Boninite petrogenesis: chemical and Nd-Sr isotopic constraints. *Earth and Planetary Science Letters* **65**, 75-89.

Cann JR (1974) A model for oceanic crustal structure developed. *Geophys. J. R. Astron. Soc.* **39**, 169-187.

Cann JR, Strens MR (1982) Black smokers fuelled by freezing magma. *Nature* **298**, 147-149.

Carter HJ (1850) Geological observations on the igneous rocks of Muscat and its neighbourhood, and on limestone formation at their circumference. *Journal of Bombay Branch of the Royal Asiatic Society* III, 118-129.

Casey JF, Dewey JF (1984) Initiation of subduction zones along transform and accreting plate boundaries, triple-junction evolution, and fore-arc spreading centres; implications for ophiolitic geology and obduction. *Ophiolites and oceanic lithosphere: Geological Society of London Special Publication* **13**, 269-297.

Ceuleneer G, Nicolas A, Boudier F (1988) Mantle flow patterns at an oceanic spreading centre: The Oman peridotites record. *Tectonophysics* **151**, 1-26.

Chen YJ (2000) Dependence of crustal accretion and ridge-axis topography on spreading rate, mantle temperature, and hydrothermal cooling. *Ophiolites and Oceanic Crust: New Insights from Field Studies and Ocean Drilling Special Paper-Geological Society of America vol. 349 (2000),, 161-181.*

Coleman RG (1977) *Ophiolites, Ancient Oceanic Lithosphere?* Springer-Verlag.

Coleman RG (2000) Prospecting for ophiolites along the California continental margin. *Ophiolites and Oceanic Crust: New Insights from Field Studies and Ocean Drilling Special Paper-Geological Society of America vol. 349 (2000), 351-365.*

Coogan LA, Banks GJ, Gillis K, MacLeod CJ, Pearce JA (2003) Hidden melting signatures recorded in the Troodos ophiolite plutonic suite: evidence for widespread generation of depleted melts and intra-crustal melt aggregation. *Contributions Mineral Petrology* **144**, 484-505.

Coogan LA, Gillis KM, MacLeod CJ, Thompson GM, Hekinian R (2002) Petrology and geochemistry of the lower ocean crust formed at the East Pacific Rise and

Exposed at Hess Deep: A synthesis and new results. *Geochemistry, Geophysics, Geosystems* **3**.

Coogan LA, Kempton PD, Saunders AD, Norry MJ (2000a) Melt aggregation within the crust beneath the Mid-Atlantic Ridge: Evidence from plagioclase and clinopyroxene major and trace element compositions. *Earth and Planetary Science Letters*, 127-146.

Coogan LA, MacLeod CJ, Dick HJB, Edwards SJ, Kvassnes A, Natland JH, Robinson PT, Thompson GM, O'Hara MJ (2001) Whole-rock geochemistry from the Southwest Indian Ridge: Constraints on geochemical fractionations between the upper and lower oceanic crust and magma chamber processes at (very) slow spreading ridges. *Chemical Geology* **178**, 1-22.

Coogan LA, Saunders AD, Kempton PD, Norry MJ (2000b) Evidence from oceanic gabbros for porous melt migration within a crystal mush beneath the Mid-Atlantic Ridge. *Geochemistry, Geophysics, Geosystems* **1**.

Coogan LA, Thompson G, MacLeod CJ (2002b) A textural and geochemical investigation of high level gabbros from the Oman ophiolite: Implications for the role of the axial magma chamber at fast-spreading ridges. *Lithos* **63**, 67-82.

Cox KG, Bell JD, Pankhurst RJ (1979) *The interpretation of igneous rocks*. George, Allen and Unwin: London.

Crawford AJ, Falloon TJ, Green DH (1989) Classification, petrogenesis and tectonic setting of boninite. In: AJ Crawford (ed.) *Boninites and related rocks*. pp. 1-49. Unwin Hyman: London.

Dewey JF, Bird JM (1971) Origin and emplacement of the ophiolite suite: Appalachian ophiolites in Newfoundland. *Journal of Geophysical Research* **76**, 3179-3206.

Dilek YM, E., Elthon, D., Nicolas, A. (2000) Ophiolites and Oceanic Crust: New insights from field studies and the Ocean Drilling Programme. *Geological Society of America, Special paper 349*.

Dunlop HM, Fouillac WKR (1986) O, H, Sr, Nd isotope systematics of the Oman ophiolite. *Ophiolites 'Through Time'*. Conf. Nantes. p. 25

Edwards S, Pearce JA, Freeman J (2000) New insights concerning the influence of water during the formation of podiform chromitite. *Ophiolites and Oceanic Crust: New Insights from Field Studies and Ocean Drilling Special Paper-Geological Society of America vol. 349 (2000)*, 139-147.

Einaudi F, Pezard PA, Cocheme J, Coulon C, Laverne C, Godard M (2000) Petrography, geochemistry and physical properties of a continuous extrusive section from the Sarami Massif, Semail Ophiolite. *Marine Geophysical Researches* **21**, 387-407.

Ernewein M, Pflumio C, Whitechurch H (1988) The death of an accretion zone as evidenced by the magmatic history of the Semail ophiolite (Oman). *Tectonophysics* **151**, 247-274.

Flower MFJ (2003) Ophiolites, historical contingency, and the Wilson Cycle. *Ophiolite Concept and the Evolution of Geological Thought, Geological Society of America, Special Paper 373*, p.111-135.

Fryer P, Lockwood JP, Becker N, Phipps S, Todd S (2000) Significance of serpentine mud volcanism in convergent margins. *Ophiolites and Oceanic Crust: New Insights from Field Studies and Ocean Drilling Special Paper-Geological Society of America vol. 349 (2000)*,.

Furnes H, Skjerlie KP, Dilek Y (2000) Petrology, tectonics, and hydrothermal alteration of a fossil backarc oceanic crust: Solund-Stavfjord ophiolite complex of the western Norwegian Caledonides - A review. *Ophiolites and Oceanic Crust: New Insights from Field Studies and Ocean Drilling Special Paper-Geological Society of America vol. 349 (2000)*,, 443-460.

Garrido CJ, Keleman P, Hirth G (2001) Variation of cooling rate with depth in lower crust formed at an oceanic spreading ridge: Plagioclase crystal size distributions in gabbros from the Oman ophiolite. *Geochemistry, Geophysics and Geosystems: G3* **2**.

Gass IG (1968) Is the Troodos massif of Cyprus a fragment of the Mesozoic ocean floor? *Nature*, 39-42.

Ghazi AM, Hassanipak AA (2000) Petrology and geochemistry of the Shahr-Babak ophiolite, central Iran. *Ophiolites and Oceanic Crust: New Insights from Field Studies and Ocean Drilling Special Paper-Geological Society of America vol. 349*, 485-498.

Gillis K, Banerjee N (2000) Hydrothermal alteration patterns in supra-subduction zone ophiolites. *Ophiolites and Oceanic Crust: New Insights from Field Studies and Ocean Drilling Special Paper-Geological Society of America vol. 349 (2000)*,, 283.

Gillis K, Coogan LA (2002) Anatectic migmatites from the roof of an ocean ridge magma chamber. *Journal of Petrology* **43**, 2075-2095.

Girardeau J, Monnier C, Launeau P, Quatrevaux F (2002) Kinematics of mantle flow beneath a fossil Overlapping Spreading Center: The Wuqbah massif case, Oman ophiolite. *Geochemistry, Geophysics and Geosystems: G3* **3**.

Glennie KW, Boeuf MGA, Hughs-Clarke MW, Moody-Stuart M, Pillaar WFH, Reinhardt BM (1974) Geology of the Oman Mountains. *Verhandelingen van het Koninklijk Nederlands Geologisch Mijnbouwkundig Genootschap*.



Gnos E, Nicolas A (1996) Structural evolution of the northern end of the Oman ophiolite and enclosed granulites. *Tectonophysics* **254**, 111-137.

Godard M, Dautria J, Perrin M (2003) Geochemical variability of the Oman ophiolite lavas: Relationship with spatial distribution and paleomagnetic directions. *Geochemistry, Geophysics and Geosystems: G<sup>3</sup>* **4**.

Godfrey NJ, Dilek Y (2000) Mesozoic assimilation of oceanic crust and island arc into the North American continental margin in California and Nevada: Insights from geophysical data. *Ophiolites and Oceanic Crust: New Insights from Field Studies and Ocean Drilling Special Paper-Geological Society of America vol. 349 (2000)*,, 365-383.

Grantham GH, Goedhart ML, Wipplinger PE, Thomas RJ, Eglinton BM, Harmer RE, Hartzler FJ (2003) *The geology of the Emirate of Fujairah Sheet explanation for 1: 50 000 geological maps*. Council for Geoscience, South Africa, Cape Town.

Gray DRea (2000) A new structural profile along the Muscat-Ibra transect, Oman: Implications for emplacement of the Samail ophiolite. *Ophiolites and Oceanic Crust: New Insights from Field Studies and Ocean Drilling Special Paper-Geological Society of America vol. 349 349*, 513-523.

Hacker BR, Mosenfelder JL, Gnos E (1996) Rapid emplacement of the Oman Ophiolite; thermal and geochronologic constraints. *Tectonics* **15**, 1230-1247.

Harris R, Long T (2000) The Timor ophiolite, Indonesia: Model or myth? *Ophiolites and Oceanic Crust: New Insights from Field Studies and Ocean Drilling Special Paper-Geological Society of America vol. 349 (2000)*,, 321-331.

Hart SR, Dunn T (1993) Experimental cpx/melt partitioning of 24 trace elements. *Contributions to Mineralogy and Petrology* **113**, 1-8.

Hawkins JW (2003) Geology of supra-subduction zones, Implications for the origins of ophiolites. *geological Society of America, Special paper 373*, 227-268.

Henstock TJ, Woods AW, White RS (1993) The accretion of oceanic crust by episodic sill intrusion. *Journal of Geophysical Research* **98**, 4143-4161.

Hickey RL, Frey FA (1982) Geochemical characteristics of boninite series volcanics: implications for their source. *Geochimica et Cosmochimica Acta* **46**, 2099-2115.

Holtzman B (2000) Gauging stress from mantle chromitite pods in the Oman ophiolite. *Ophiolites and Oceanic Crust: New Insights from Field Studies and Ocean Drilling Special Paper-Geological Society of America vol. 349 (2000)*,, 149-158.

Horn I, Gunther D (2003) The influence of ablation carrier gasses He, Ne and Ar on the particle size distribution and transport efficiencies of laser ablation induced aerosols: Implications for LA-ICP-MS. *Appl. Surf. Sci* **207**, 144-157.

Humph SE (2000) A synthesis of geological and geochemical investigations of the TAG hydrothermal field. *Ophiolites and Oceanic Crust: New Insights from Field Studies and Ocean Drilling Special Paper-Geological Society of America vol. 349 (2000)*,.

Humphris SE (1995) The internal structure of an active sea-floor massive sulphide deposit. *Nature* **377**, 713-716.

Humphris SE, Tivey M (2000) A synthesis of geological and geochemical investigations of the TAG hydrothermal field: Insights into fluid-flow and mixing processes in a hydrothermal system. *Ophiolites and Oceanic Crust: New Insights from Field Studies and Ocean Drilling Special Paper-Geological Society of America vol. 349 (2000)*,, 213-237.

Hunting (1985) Geological Map of the Northern Emirates. Government of the United Arab Emirates, Ministry of Petroleum and Mineral Resources: Abu Dhabi.

Ingersoll RV (2000) Models for origin and emplacement of Jurassic ophiolites of northern California. *Ophiolites and Oceanic Crust: New Insights from Field Studies and Ocean Drilling Special Paper-Geological Society of America vol. 349 (2000)*,, 395-403.

Ishikawa T, Fujisawa S, Nagaishi K, Masuda T (2005) Trace element characteristics of the fluid liberated from amphibolite-facies slab: Inference from the metamorphic sole beneath the Oman ophiolite and implication for boninite genesis. *Earth and Planetary Science Letters in press*, 23.

Ishikawa T, Nagaishi K, Umino S (2002) Boninitic volcanism in the Oman ophiolite: Implications for thermal condition during transition from spreading ridge to arc. *Geology* **30**, 899-902.

Jackson SE (2001) The application of ND:YAG lasers in LA-ICP-MS. In: P Sylvester (ed.) *Laser-Ablation-ICPMS in the Earth Sciences*. pp. 29-47. Mineralogical Association of Canada: St.Johns.

Jackson SE, Longerich HP, Dunning GR, Fryer BJ (1992) The application of laser ablation microprobe-inductively coupled plasma-mass spectrometry (LAM-ICP-MS) to in situ trace element determinations in minerals. *Can. Mineral* **30**, 1049-1064.

Jarvis KE, Williams JG (1989) The analysis of geological samples by slurry nebulisation inductively coupled plasma-mass spectrometry (ICP-MS). *Chemical Geology* **77**, 53-63.

Ji-feng Xu PRC, Xian-hua Li, Xue-yuan Yu,, Ben-ren Zhang Y-wH (2002) MORB-type rocks from the Paleo-Tethyan Mian-Lueyang northern ophiolite in the

Qinling Mountains, central China: implications for the source of the low  $^{206}\text{Pb}$ / $^{204}\text{Pb}$  and high  $^{143}\text{Nd}/^{144}\text{Nd}$  mantle component in the Indian Ocean. *Earth and Planetary Science Letters* **198**, 323-337.

Jones K (2005) The laser ablation ICP-MS analysis of olivine-hosted melt inclusions from the Mull Plateau Group Lavas, Mull, Scotland. PhD, Cardiff University.

Jousselin D, Nicolas A (2000) The Moho transition zone in the Oman ophiolite-relation with wehrlites in the crust and dunites in the mantle. *Marine Geophysical Researches* **21**, 229-241.

Juteau T, Ernwein M, Reuber I, Whitechurch H, Dahl R (1988) Duality of magmatism in the plutonic sequence of the Sumail Nappe, Oman. *Tectonophysics* **151**, 107-135.

Karpoff AM, Walter A-V, Pflumio C (1988) Mealliferous sediments within lava sequences of the Sumail ophiolite (Oman): Mineralogical and geochemical characterisation, origin and evolution. *Tectonophysics* **151**, 223-245.

Kearey P, Vine FJ (1996) *Global Tectonics*. Blackwell Science.

Keleman P, Koga KT, Shimizu N (1997) Geochemistry of gabbro sills in the crust-mantle transition zone of the Oman ophiolite: implications for the origin of the oceanic lower crust. *Earth and Planetary Science Letters* **146**, 475-488.

Kelley DS, Furr-Green MK (2000) Volatiles in mid-ocean ridge environments. *Ophiolites and Oceanic Crust: New Insights from Field Studies and Ocean Drilling Special Paper-Geological Society of America vol. 349 (2000)*,, 237-261.

Keppler H (1996) Constraints from partitioning experiments on the composition of subduction-zone fluids. *Nature* **380**, 237-240.

Kerr AC, Tarney J, Kempton PD, Pringle M, Nivia A (2004) Mafic pegmatites intruding oceanic plateau gabbros and ultramafic cumulates from Bolivar, Columbia: Evidence for a 'wet' mantle plume. *Journal of Petrology* **45**, 1877-1906.

Koga KT, Keleman PB, Shimizu N (2001) Petrogenesis of the crust-mantle transition zone and the origin of lower crustal wehrlite in the Oman ophiolite. *Geochemistry, Geophysics and Geosystems: G<sup>3</sup>* **2**.

Korenaga J, Keleman P (1998) Melt migration through the oceanic lower crust: a constraint from melt percolation modelling with finite solid diffusion. *Earth and Planetary Science Letters* **156**, 1-11.

Kyser TK, Cameron WE, Nisbet EG (1986) Boninite petrogenesis and alteration history: constraints from stable isotope compositions of boninites from Cape Vogel, New Caledonia and Cyprus. *Contributions Mineral Petrology* **93**, 222-226.

Lavis S (2005) Recycling in subduction zones: Evidence from eclogites and blueschists of NW China. PhD, Cardiff University.

Le Maitre RW, Bateman P, *et al.* (1989) *A classification of igneous rocks and glossary of terms*. Blackwell: Oxford.

Lee GM (1928) The geology and tectonics of Oman and parts of southeastern Arabia. *Geological Society of London, Quarterly Journal* **84**, 585-670.

Lippard SJ, Shelton AW, Gass IG (1986) *The Ophiolite of Northern Oman*. The Geological Society, Memoir No.11.

Macdonald KC (1982) Mid-ocean ridges: Fine scale tectonics, volcanic and hydrothermal processes within the plate boundary zone. *Annual review of Earth and Planetary Sciences* **10**, 155-190.

Macdonald KC (1998) Linkages between faulting, volcanism, hydrothermal activity and segmentation on fast spreading centres. In: WR Buck, *et al.* (ed.) *Faulting and Magmatism at Mid-Ocean Ridges*. pp. 27-58. American Geophysical Union: Washington D.C.

MacLeod CJ, Rothery DA (1992) Ridge axial segmentation in the Oman ophiolite: evidence from along-strike variations in the sheeted dyke complex. *Ophiolites and their modern oceanic analogues: Geological Society Special Publication No. 60*, 39-63.

MacLeod CJ, Yaouancq G (2000) A fossil melt lens in the Oman ophiolite: Implications for magma chamber processes at fast spreading ridges. *Earth and Planetary Science Letters* **176**, 357-373.

Manning CE, MacLeod CJ, Weston PE (2000) Lower-crustal cracking front at fast-spreading ridges: Evidence from the East Pacific Rise and the Oman ophiolite. *Ophiolites and Oceanic Crust: New Insights from Field Studies and Ocean Drilling Special Paper-Geological Society of America vol. 349 (2000)*,, 261-273.

Metcalf RV, Wallin ET, Willse KR, Muller ER (2000) Geology and geochemistry of the ophiolitic Trinity terrane, California: Evidence of middle Paleozoic depleted supra-subduction zone magmatism in a proto-arc setting. *Ophiolites and Oceanic Crust: New Insights from Field Studies and Ocean Drilling Special Paper-Geological Society of America vol. 349 (2000)*,, 403-419.

Miyashiro A (1973) The Troodos ophiolitic complex was probably formed in an island arc. *Earth and Planetary Science Letters* **19**, 218-224.

Miyashiro A (1975) Classification, characteristics, and origin of ophiolites. *Journal of Geology* **83**, 249-281.

Moores EM, Kellog LH, Dilek Y (2000) Tethyan ophiolites, mantle convection, and tectonic "historical contingency": A resolution of the "ophiolite conundrum".

***Ophiolites and Oceanic Crust: New Insights from Field Studies and Ocean Drilling Special Paper-Geological Society of America vol. 349 (2000),, 3-12.***

Moore EM, Vine FJ (1971) Troodos Massif, Cyprus and other ophiolites as oceanic crust: evaluation and implications. *Philos.Trans.R.Soc.London Ser A268*, 443-466.

Nedimovic MR, Carbotte SM, Harding AJ, Detrick RS, Canales JP, Diebold JB, Kent GM, Tischer M, Babcock JM (2005) Frozen magma lenses below the oceanic crust *Nature* **436**, 1149-1152.

Nicolas A (1986) A melt extraction model based on structural studies in mantle peridotites. *Journal of Petrology*, 999-1022.

Nicolas A (1992) Kinematics in magmatic rocks with special reference to gabbros. *Journal of Petrology* **33**, 891-915.

Nicolas A (1995) *The Mid-Oceanic Ridges, Mountains below sea level*. Springer.

Nicolas A, Ildefonse B, Boudier F, Lenoir X, Ben Ismail W. (2000) Dike distribution in the Oman-United Arab Emirates ophiolite. *Marine Geophysical Researches* **21**, 269-287.

Nicolas A, Boudier F (2000) Large mantle upwellings and related variations in crustal thickness in the Oman ophiolite. *Ophiolites and Oceanic Crust: New Insights from Field Studies and Ocean Drilling Special Paper-Geological Society of America vol. 349 (2000),, 67-73.*

Nicolas A, Boudier F, Ildefonse B (1996) Variable crustal thickness in the Oman ophiolite: Implication for oceanic crust. *Journal of Geophysical Research* **101**, 17941-17950.

Nicolas A, Boudier F, Michibayashi K, Gerbert-Gaillard L (2000) Aswad massif (United Arab Emirates): Archetype of the Oman-U.A.E ophiolite belt. *Ophiolites and Oceanic Crust: New Insights from Field Studies and Ocean Drilling Special Paper-Geological Society of America vol. 349*, 499-512.

Nicolas A, Ceuleneer F, Boudier F, Misseri M (1988) Structural mapping in the Oman ophiolites: Mantle diapirism along an oceanic ridge. *Tectonophysics* **151**, 27-54.

Nicolas A, Poliakov A (2001) Melt migration and mechanical sterte in the lower crust of oceanic ridges. *Terra Nova* **13**, 64-69.

Nicolas A, Reuber I, Benn K (1988) A new Magma chamber model based on structural studies in the Oman ophiolite. *Tectonophysics* **151**, 87-105.

Norrish K, Chappell BW (1967) X-ray fluorescence spectrography. In: J Zussman (ed.) *Physical methods in determinative mineralogy*. pp. 201-272. Academic Press: New York.

Pallister JS (1981) Structure of the sheeted dyke complex of the Samail ophiolite near Ibra, Oman. *Journal of Geophysical Research* **86**, 2661-2672.

Pallister JS, Hopson CA (1981) Samail ophiolite plutonic suite: field relationships, phase variation, cryptic variation and layering, and a model of a spreading ridge magma chamber. *Journal of Geophysical Research* **86**, 2593-2644.

Pearce JA (1980) Geochemical evidence for the genesis and eruptive setting of lavas from Tehyan ophiolites. In: A Panayiotou (ed.) *Ophiolites, proceedings International Ophiolite Symposium, Cyprus*. pp. 261-272. The Geological Survey of Cyprus, Nicosia.

Pearce JA, Lippard, S.J. and Roberts, S. (1984) Characteristics and tectonic significance of Supra-subduction zone ophiolites. *Geological Society of London, Special Publication* **16**, 77-94.

Pearce JA (1996) A user's guide to basalt discrimination diagrams. In: DA Wyman (ed.) *In: Trace element geochemistry of volcanic rocks: Applications for massive sulphide exploration*. pp. 79-113. Geological Association of Canada, Short course notes.

Pearce JA (2003) Supra-subduction zone ophiolites: the search for modern analogues. *Geological Society of America, Special paper* **373**, 269-295.

Pearce JA, Alabaster T, Shelton AW, Searle MP (1981) The Oman ophiolite as a cretaceous arc-basin complex: Evidence and implications. *Philos.Trans.R.Soc.London Ser A*, 299-317.

Pearce JA, Cann JR (1971) Ophiolite origin investigated by discriminant analysis using Ti, Zr and Y. *Earth and Planetary Science Letters* **12**, 339-349.

Pearce JA, Cann JR (1973) Tectonic setting of basic volcanic rocks determined using trace element analyses. *Earth and Planetary Science Letters* **19**, 290-300.

Pearce JA, Ernewein M, Bloomer SH, Parson LM, Murton BL, Johnson LE (1995) Geochemistry of Lau Basin volcanic rocks: influence of ridge segmentation and arc proximity. *Geological Society Special Publication: Volcanism associated with extension at Consuming Plate Margins* **81**, 53-75.

Pearce JA, Norry MJ (1979) Petrogenetic implications of Ti, Zr, Y and Nb variations in volcanic rocks. *Contributions Mineral Petrology* **69**, 33-47.

Pearce JA, Peate DW (1995) Tectonic implications of the composition of volcanic arc magmas. *Annu. Rev. Earth Planet. Sci* **23**, 251-85.

Pearce JA, Stern RJ, Bloomer SH, Fryer P (2005) Geochemical mapping of the Mariana arc-basin system: Implications for the nature and distribution of subduction components. *Geochemistry, Geophysics and Geosystems: G3* 6.

Pedersen RB, Malpas J, Fallon T (1996) Petrology and geochemistry of gabbroic and related rocks from Site 894, Hess Deep. *Proc. Ocean Drill. Program Sci. Results* 147, 3-19.

Penrose (1972) Penrose Conference Participants. *Penrose field conference on ophiolites*. pp. 24-25. (Geotimes)

Perrin M, Plenier J, Daurtia M, Cocaud E, Prevot M (2000) Rotation of the Semail ophiolite (Oman): Additional paleomagnetic data from the volcanic sequence. *Marine Geophysical Researches* 21, 181-194.

Perrin M, Prevot M, Bruere F (1994) Rotation of the Oman ophiolite and initial location of the ridge in the hotspot reference frame. *Tectonophysics* 229, 31-42.

Pessagno EA, Hull DM, Hopson CA (2000) Tectonostratigraphic significance of sedimentary strata occurring within and above the Coast Range ophiolite (California Coast Ranges) and the Josephine ophiolite (Klamath Mountains), northwest California. *Ophiolites and Oceanic Crust: New Insights from Field Studies and Ocean Drilling Special Paper-Geological Society of America vol. 349 (2000)*,, 383-395.

Peters T (2000) Formation and evolution of the western Indian Ocean as evidenced by the Masirah ophiolite: A review. *Ophiolites and Oceanic Crust: New Insights from Field Studies and Ocean Drilling Special Paper-Geological Society of America vol. 349*, 525-536.

Pezard PA (2000) On the boundary between seismic layers 2 and 3: A stress change? *Ophiolites and Oceanic Crust: New Insights from Field Studies and Ocean Drilling Special Paper-Geological Society of America vol. 349 (2000)*,, 195-203.

Pflumino C (1991) Evidences for polyphased oceanic alteration of the extrusive sequence of the Semail ophiolite from the Salahi Block (Northern Oman). *Peters, T (ed) Ophiolite genesis and evolution of the oceanic lithosphere*, 313-351.

Phipps-Morgan J, Chen YJ (1993) The genesis of oceanic crust: magma injection, hydrothermal circulation and crustal flow. *Journal of Geophysical Research* 98, 6283-6297.

Quick JE, Denlinger RP (1993) Ductile deformation and the origin of layered gabbro in ophiolites. *Journal of Geophysical Research* 98, 14015-14027.

Ramos VA, Escayola M, Mutti DI, Vujovich GI (2000) Proterozoic-early Paleozoic ophiolites of the Andean basement of southern south America. *Ophiolites and Oceanic Crust: New Insights from Field Studies and Ocean Drilling Special Paper-Geological Society of America vol. 349 (2000)*,, 331-351.

Rampone E, Piccardo GB (2000) The ophiolite-lithosphere analogue: New insights from the Northern Apennines (Italy). *Ophiolites and Oceanic Crust: New Insights from Field Studies and Ocean Drilling Special Paper-Geological Society of America* vol. 349 (2000),.

Rassios A, Smith AG (2000) Constraints on the formation and emplacement age of western Greek ophiolites (Vourinos, Pindos, and Othris) inferred from deformation structures in peridotites. *Ophiolites and Oceanic Crust: New Insights from Field Studies and Ocean Drilling Special Paper-Geological Society of America* vol. 349, 473-484.

Ravaut P, Bayer R, Hassani R, Al Yahya'eh A, Rousset D (1997) Structure and evolution of the northern Oman margin: Gravity and seismic constraints over the Zagros-Makram-Oman collision zone. *Tectonophysics* 279, 253-280.

Reinhardt BM (1969) On the genesis and emplacement of ophiolites in the Oman mountains geosyncline. *Schweiz. Mineral. Petrogr. Mitt* 49, 1-30.

Reuber I (1988) Complexity of the crustal sequence in the northern Oman ophiolite (Fitz and southern Aswad blocks): The effect of early slicing? *Tectonophysics* 151, 137-165.

Robinson PT, Dick HJB, Natland JH, party Ols (2000) Lower oceanic crust formed at an ultra-slow-spreading ridge: Ocean Drilling Program Hole 735B Southwest Indian Ridge. *Ophiolites and Oceanic Crust: New Insights from Field Studies and Ocean Drilling Special Paper-Geological Society of America* vol. 349 (2000),, 75-87.

Robinson PTea (1983) Volcanic glass compositions of the Troodos ophiolite, Cyprus. *Geology* 11, 400-406.

Rocci G, Ohnenstetter D, Ohnenstetter M (1975) La dualite des ophiolites tethysiennes. *Petrologie* 1, 172-174.

Rollinson H (1993) *Using geochemical data: evaluation, presentation, interpretation*. Longman Scientific and Technical: New York.

Rosencrantz E (1983) The Structure of sheeted dikes and the associated rocks in North Arm Massif, Bay of Islands ophiolite complex, and the intrusive process at oceanic spreading centers. *Canadian Journal of Earth Science* 20, 787-801.

Rothery DA (1983) The base of the sheeted dyke complex, Oman ophiolite: Implications for magma chambers at oceanic spreading axes. *Journal of the Geological Society of London* 140, 287-296.

S.A.G.S. (2001) *Mapping of Fujairah Emirate*. Government of the United Arab Emirates, Department of petroleum and Mineral Resources.



Sato H, Ogawa Y (2000) Sulfide minerals as an indicator for petrogenesis and serpentinisation of peridotites: An example from the Hayama-Mineoka belt, central Japan. *Ophiolites and Oceanic Crust: New Insights from Field Studies and Ocean Drilling Special Paper-Geological Society of America vol. 349 (2000)*, 419-431.

Saunders AD, Tarney J (1979) The geochemistry of basalts from a back-arc spreading centre in the Scotia Sea. *Geochim Cosmochim Acta* **43**, 555-572.

Schmincke HU, Rautenschlein M (1983) Troodos extrusive series of Cyprus: A comparison with oceanic crust. *Geology* **11**, 405-409.

Schouten H (2000) Comparison of volcanic construction in the Troodos ophiolite and oceanic crust using paleomagnetic inclinations from Cyprus Crustal Study Project (CCSP) CY-1 and CY-1A and Ocean Drilling Programme (ODP) 504B drill cores. *Ophiolites and Oceanic Crust: New Insights from Field Studies and Ocean Drilling Special Paper-Geological Society of America vol. 349 (2000)*, 181-195.

Searle MP, Malpas J (1980) The structure and metamorphism of rocks beneath the Semail ophiolite of Oman, and their significance in ophiolite obduction. *Royal Society of Edinburgh philosophical Transactions* **71**, 213-228.

Shervais JW (1982) Ti-V plots and the petrogenesis of modern and ophiolitic lavas. *Earth and Planetary Science Letters* **59**, 101-118.

Shimizu N (1981) Trace element incorporation into growing augite phenocryst. *Nature*, 575-577.

Singh SC, Kent GM, Collier JS, Harding AJ, Orcutt JA (1998) Melt to mush variations in crustal magma properties along the ridge crest at the southern East Pacific Rise. *Nature* **394 (6696)**, 874-878.

Sinton JM, Detrick RS (1992) Mid-Ocean Ridge magma chambers. *Journal of Geophysical Research* **97**, 197-216.

Sleep NH (1975) Formation of oceanic crust; some thermal constraints. *Journal of Geophysical Research* **97**, 197-216.

Smewing JD (1981) Mixing characteristics and compositional differences in mantle-derived melts beneath spreading axes - evidence from cyclically layered rocks in the ophiolite of North Oman. *Journal of Geophysical Research* **86**, 2645-2659.

Sneeringer M, Hart SR, Shimizu N (1984) Strontium and samarium diffusion in diopside. *Geochim Cosmochim Acta* **48**, 1589-1608.

Spadea P, Scarrow JH (2000) Early Devonian boninites from the Magnitogorsk arc, southern Urals (Russia): Implications for early development of a collisional orogen. *Ophiolites and Oceanic Crust: New Insights from Field Studies and Ocean Drilling Special Paper-Geological Society of America vol. 349*, 461-472.

Stern CR (1980) Geochemistry of Chilean ophiolites:evidence for the compositional evolution of the mantle source of back-arc basin basalts. *Journal of Geophysical Research* **85**, 955-966.

Stern RJ (2002) Subduction Zones. *Reviews of Geophysics* **40**.

Streckeisen A (1976) To each plutonic rock its proper name. *Earth-Science Reviews* **12**, 1-33.

Sturm ME, Klein EM, Karsten J, Karson JA (2000) Evidence for subduction-related contamination of the mantle beneath the southern Chile Ridge: Implications for ambiguous ophiolite compositions. *Ophiolites and Oceanic Crust: New Insights from Field Studies and Ocean Drilling Special Paper-Geological Society of America vol. 349 (2000),.*

Suhr G, Edwards SJ (2000) Contrasting mantle sequences exposed in the Lewis Hills massif: Evidence for the early, arc-related history of the Bay of Islands ophiolite. *Ophiolites and Oceanic Crust: New Insights from Field Studies and Ocean Drilling Special Paper-Geological Society of America vol. 349 (2000),, 433-442.*

Sun SS, McDonough WF (1989) Chemical and isotopic systematics of oceanic basalts: Implications for mantle composition and processes. In: AD Saunders and MJ Norry (eds.) *Magmatism in the Ocean Basins*. pp. 313-345. Geol. Soc. London: London.

Sun SS, McDonough WF (1989) Chemical and isotopic systematics of oceanic basalts: Implications for mantle composition and processes. In: AD Saunders and MJ Norry (eds.).

Sun YF, Goldberg D (2000) Characterization of the upper oceanic crust using high-resolution seismic amplitude modeling. *Ophiolites and Oceanic Crust: New Insights from Field Studies and Ocean Drilling Special Paper-Geological Society of America vol. 349 (2000),, 203-211.*

Sylvester P (2001) *Laser-Ablation-ICP-MS in the Earth Sciences*. Mineralogical Society of Canada: St.Johns.

Taylor RN, Nesbitt RW (1988) Light rare-earth enrichment of supra subduction-zone mantle: Evidence from the Troodos ophiolite, Cyprus. *Geology* **16**, 448-451.

Thomas RM (2003) Processes of lower crustal accretion beneath fast-spreading ocean ridges: constraints from the Wadi Abyad section in the Nakhl-Rustaq massif, south-central Oman ophiolite. PhD thesis, Cardiff University.

Thy P, Dilek Y (2000) Magmatic and tectonic controls on the evolution of oceanic magma chambers at slow-spreading ridges: Perspectives from ophiolitic and continental layered intrusions. *Ophiolites and Oceanic Crust: New Insights from*

*Field Studies and Ocean Drilling Special Paper-Geological Society of America vol. 349 (2000),, 87-104.*

Till R (1974) *Statistical methods for the earth scientist: an introduction*. Macmillan: Oxford.

Tilton GR, Hopson CA, Wright JE (1981) Uranium-lead isotopic ages of the Semail ophiolite, Oman, with applications to Tethyan ocean ridge tectonics. *Journal of Geophysical Research* **86**, 2763-2775.

Tippit PR, Pessagno Jr. EA, Smewing JD (1981) The biostratigraphy of sediments in the volcanic unit of the Semail ophiolite. *J. Geophys. Res.* **86**, 2756-2762.

Tribuzio R, Tiepolo M, Vannucci R (2000) Evolution of gabbroic rocks of the Northern Apennine ophiolites (Italy): Comparison with the lower oceanic crust from modern slow-spreading ridges. *Ophiolites and Oceanic Crust: New Insights from Field Studies and Ocean Drilling Special Paper-Geological Society of America vol. 349 (2000),, 129-139.*

Umino S, Yanai S, Jaman AR, Nakamura Y, Iiyama JT (1990) The transition from spreadin to subduction, evidence from the Semail Ophiolite, northern Oman Mountains. *Ophiolites, oceanic crustal analogues, Proceedings of Troodos 1987: Nicosia, Cyprus, Ministry of Agriculture and Natural Resources*, p. 375-384.

Van Orman JA, Grove TL, Shimizu N (2001) Rare earth element diffusion in diopside: influence of temperature, pressure and ionic radius and an elastic model for diffusion in silicates. *Contributions Mineral Petrology* **141**, 687-703.

Varne R, Brown AV, Fallon T (2000) Maquarie Island: Its geology, structural history, and the timing and tectonic setting of its N-MORB to E-MORB magmatism. *Ophiolites and Oceanic Crust: New Insights from Field Studies and Ocean Drilling Special Paper-Geological Society of America vol. 349 (2000),, 301-321.*

Vetter SK, Stakes DS (1990) Repeated magma injection and the geochemical evolution of the Northern Semail plutonic suite. *Ophiolites, oceanic crustal analogues, Proceedings of Troodos 1987: Nicosia, Cyprus, Ministry of Agriculture and Natural Resources*, 397-413.

Vetter SK, Stakes DS (1990) Repeated magma injection and the geochemical evolution of the Northern Semail plutonic suite.

Wakabayashi J, Dilek Y (2000) Spatial and temporal relationships between ophiolites and their metamorphic soles: A test of models of forearc ophiolite genesis. *Ophiolites and Oceanic Crust: New Insights from Field Studies and Ocean Drilling Special Paper-Geological Society of America vol. 349 (2000),, 53-65.*

Wake CA, Pearce JA (2005) Geochemical mapping of the extrusive sequence of the Troodos Ophiolite, Cyprus: an investigation into the relationship between lava

compositions and proximity to a paleo-subduction zone and a paleo-transform fault. Ph. D Thesis. Cardiff University.

Watson EB (1985) Henry's law behaviour in simple systems and in magmas: Criteria for discerning concentration-dependent partition coefficients in nature. *Geochim Cosmochin Acta* **49**, 917-923.

Watson EB (1996) Surface enrichment and trace-element uptake during crystal growth. *Geochim Cosmochin Acta* **60**, 5013-5060.

Wood BJ, Blundy JD (1997) A predictive model for rare earth element partitioning between clinopyroxene and anhydrous silicate melt. *Contributions to Mineralogy and Petrology* **129** (2-3), 161-181.

Yaouancq G (2001) Structure of the axial magma chamber and magmatic processes at fast-spreading ridges:constraints from the oman ophiolite. PhD, Cardiff University.



JORGE CLAY © 2005